Volume 68A
Number 6
Nov.–Dec. 1964

# Physics and Chemistry

U.S. DEPARTMENT OF COMMERCE

## SECTION A
## JOURNAL OF RESEARCH

NATIONAL BUREAU OF STANDARDS

# Journal of Research

of the

National Bureau of Standards

A. Physics and Chemistry

Nov.–Dec. • 1964

VOLUME • 68A

NUMBER • 6

Editor: C. W. Beckett

Associate Editors: D. D. Wagman
J. M. Richardson

Publication dates:
Feb. 1, Apr. 1, June 1, Aug. 1, Oct. 1, Dec. 1, 1964


JOURNAL OF RESEARCH

The National Bureau of Standards Journal of Research reports research and development in the fields of activity shown at right. Also included from time to time are survey articles on topics closely related to the Bureau's scientific and technical program.

The Journal is published in four separate sections as follows:

**A. Physics and Chemistry**

Contains papers of interest primarily to scientists working in these fields. Issued six times a year. Annual subscription: domestic, $4.00; foreign, $4.75. Single copy, 70c.

**B. Mathematics and Mathematical Physics**

Presents studies and compilations designed mainly for the mathematician and the theoretical physicist. Issued quarterly. Annual subscription: domestic, $2.25; foreign, $2.75. Single copy, 75c.

**C. Engineering and Instrumentation**

Reports research and development results of interest chiefly to the engineer and the applied scientist. Issued quarterly. Annual subscription: domestic, $2.25; foreign, $2.75. Single copy, 75c.

**D. Radio Science (formerly Radio Propagation)**

Published in cooperation with U.S. National Committee of URSI. Presents papers in radio propagation, communications, and radio science generally. Issued monthly. Annual subscription: domestic, $9.00; foreign, $11.50. Single copy, $1.00.

The National Bureau of Standards is a principal focal point in the Federal Government for assuring maximum application of the physical and engineering sciences to the advancement of technology in industry and commerce. Its responsibilities include development and maintenance of the national standards of measurement, and the provisions of means for making measurements consistent with those standards; determination of physical constants and properties of materials; development of methods for testing materials, mechanisms, and structures, and making such tests as may be necessary, particularly for government agencies; cooperation in the establishment of standard practices for incorporation in codes and specifications; advisory service to government agencies on scientific and technical problems; invention and development of devices to serve special needs of the Government; assistance to industry, business and consumers in the development and acceptance of commercial standards and simplified trade practice recommendations; administration of programs in cooperation with United States business groups and standards organizations for the development of international standards of practice; and maintenance of a clearinghouse for the collection and dissemination of scientific, technical, and engineering information.

**Institute for Basic Standards.** Electricity. Metrology. Heat. Radiation Physics. Mechanics. Applied Mathematics. Atomic Physics. Physical Chemistry. Laboratory Astrophysics.* Radio Standards Laboratory: Radio Standards Physics; Radio Standards Engineering.** Office of Standard Reference Data.

**Institute for Materials Research.** Analytical Chemistry. Polymers. Metallurgy. Inorganic Materials. Reactor Radiations. Cryogenics.** Office of Standard Reference Materials.

**Central Radio Propagation Laboratory.*** Ionosphere Research and Propagation. Troposphere and Space Communications. Radio Systems. Upper Atmosphere and Space Physics.

**Institute for Applied Technology.** Textiles and Apparel Technology Center. Building Research. Industrial Equipment. Information Technology. Performance Test Development. Instrumentation. Transport Systems. Office of Technical Services. Office of Weights and Measures. Office of Engineering Standards. Office of Industrial Services.

*JILA Group, Joint Institute for Laboratory Astrophysics of the University of Colorado and the National Bureau of Standards.
**Located at Boulder, Colo.


U.S. DEPARTMENT OF COMMERCE
Luther H. Hodges, Secretary

NATIONAL BUREAU OF STANDARDS
A. V. Astin, Director

Order all publications from the Superintendent of Documents
U.S. Government Printing Office, Washington, D.C., 20402

Use of funds for printing this publication approved by the Director of the Bureau of the Budget (June 19, 1961).

JOURNAL OF RESEARCH of the National Bureau of Standards—A. Physics and Chemistry
Vol. 68A, No. 6, November–December 1964

# The 1962 $He^3$ Scale of Temperatures. I. New Vapor Pressure Comparisons[1]

S. G. Sydoriak and R. H. Sherman

Los Alamos Scientific Laboratory, University of California
Los Alamos, N. Mex.

(June 16, 1964)

A comparison of $He^3$ and $He^4$ vapor pressures, ($P_3$, $P_4$), has been made in an apparatus designed to reduce the number and magnitude of corrections associated with the refluxing film in the $He^4$ pressure sensing tube and the attached bulb. The critical pressure of $He^3$ has been redetermined to be at 873.0 ±1.5 mm Hg at 0° C and standard gravity; the corresponding temperature as measured by a $He^4$ thermometer is 3.3240 ±0.0018° K on the 1958 $He^4$ scale. These ($P_3$, $P_4$) comparisons and the 1958 $He^4$ scale are the basis of the 1962 $He^3$ scale of temperatures derived and evaluated in the papers following this one.

Empirical interpolation equations containing only $P_3$ and $P_4$ are described by means of which existing $P_4$ measurements may be converted to an equivalent $P_3$. A comparison has been made between this interpolation and a conversion in which the 1958 $He^4$ and 1962 $He^3$ scales are used as parameters. Deviations between the two procedures are within the estimated errors of the ($P_3$, $P_4$) measurements.

In subsidiary experiments on techniques for $He^4$ thermometry a typical vapor pressure bulb arrangement was tested. It is shown that the refluxing film introduces a heat flux, $\dot{Q}_f$, and a resulting Kapitza temperature drop, $\Delta T_k$, between the He II and its container, which may amount to many millidegrees.

The feasibility of calculating $\Delta T_k$ for a particular $He^4$ vapor pressure bulb was studied. The necessity of measuring $\Delta T_k/\dot{Q}_f$ at least once *in situ* is pointed out. In addition, it is necessary to redetermine the film flow rate periodically at the same time that $He^4$ vapor pressure measurements are being made.

## 1. Introduction

At the VIIth International Conference of Low Temperature Physics a proposal was made [1][2] to calculate a new $He^3$ vapor pressure-temperature scale based on the 1958 $He^4$ Temperature scale [2], the newly available $He^3$ specific heat data [3, 4], and the $He^3$–$He^4$ vapor pressure comparisons of Abraham, Osborne, and Weinstock (AOW) [5].

This is the first of four papers describing: I. New ($P_3$, $P_4$) data; II. The derivation of a new $He^3$ temperature scale [6]; and III. Its evaluation [7]. Paper IV [8] provides detailed tables of the scale. The 1962 $He^3$ scale is intended to replace the $T_E$ and $T_L$ $He^3$ scales of reference [9].

*A Thermodynamic Inconsistency.* In the course of the attempt to determine a new $He^3$ vapor pressure-temperature scale, it became apparent [10] that there was a thermodynamic inconsistency equivalent to several millidegrees in the temperature interval between 2 and 1 °K. It seemed reasonable to consider that either the 1958 $He^4$ scale or the AOW comparison data was in error, and that the error increased as one approached 1 °K, because the gas thermometer data of Keller [11, 12] on which the 1958 $He^4$ scale is partially based are in reasonable agreement with the 1958 $He^4$ scale near 2 °K and are nonexistent below 1.5 °K; and because unexplained experimental difficulties were encountered by AOW below about 1.7 °K. If the 1958 $He^4$ scale and the AOW data are assumed to be correct at 2 °K, then the thermodynamic inconsistency was such that $P_4$ appeared to be too high (or $P_3$ too low) at 1 °K. A detailed discussion of the inconsistency and of possible errors in the 1958 $He^4$ scale will be given in III [7]. In this paper we shall examine possibilities for error in vapor pressure measurements.

*Techniques of $He^4$ Vapor Pressure Measurement.* In the AOW measurements $He^3$ and $He^4$ were condensed in identical adjacent bulbs drilled in a single block of copper and connected to unjacketed pressure sensing tubes, all being immersed in a liquid $He^4$ bath. The use of a $He^4$ bulb pressure rather than bath pressure has been thoroughly substantiated in subsequent years, for measurements above $T_\lambda$. Extensive studies of hydrostatic head correction to a He I bath pressure measurement of the temperature of an immersed body [13, 14, 15] have shown these

[1] Work performed under the auspices of the U.S. Atomic Energy Commission.
[2] Figures in brackets indicate the literature references at the end of this paper.

corrections to be unreliable. The temperature gradient in the bath liquid is generally less than that calculated from the measured surface temperature and liquid depth. In the thesis of Durieux [15] it is recommended that the need for hydrostatic head corrections be avoided by use of a copper vapor pressure bulb in good thermal contact with the object whose temperature is desired to be known.

Unfortunately, below 1.7 °K, where AOW expected the cryostat and $He^4$ bulb pressures to agree because of the high conductivity of He II, they did not do so. This was attributed by AOW "chiefly to the impracticably long time required for pressure equilibrium in the $He^4$ vapor pressure bulb system. The cryostat pressure was therefore used to determine the temperature of the $He^3$" for $T<T_\lambda$. For their last three data points, all below 1.3 °K, they used a $He^4$ pressure sensing tube ten times larger in diameter and found agreement with cryostat pressures to within 1 millidegree. The agreement may, however, have been fortuitous.

Concern about the qualitative design details of pressure-sensing tubes has been the subject of a great deal of discussion in recent years. A summary has been given by Brickwedde [16]. Some experimenters have favored use of vacuum-jacketed metal tubes, some unjacketed glass tubes, and some jacketed tubes with helium vapor in the jacket. It has been contended by some that, until the problem is better understood, it might be desirable to provide a different temperature scale with the particular arrangement one prefers of the above design details.

In the present paper we propose to show that due to two phenomena associated with film reflux a $He^4$ vapor pressure bulb is not well suited, below $T_\lambda$, for accurately indicating the temperature of the wall of the bulb or of the liquid in which it is immersed, regardless of the type of pressure-sensing tube used. One of these effects is the pressure drop, $\Delta P_f$, between that part of the pressure-sensing tube where the film vaporizes and the parent liquid where it recondenses. The other effect is the temperature drop, $\Delta T_k$, due to heat flow between the He II liquid and the refrigerated wall of the bulb.

A bath pressure measurement provides a more reliable thermometer for the contents of a He II bath because there is no $\Delta T_k$ to consider. However, depending on design details, one may need to make significant $\Delta P_f$ or other types of corrections to a measurement of bath pressure below $P_\lambda$. To make these corrections, it may be necessary to carry out complex subsidiary experiments.

Our principal objective is, of course, to obtain a reliable correlation between $He^3$ and $He^4$ vapor pressure over a broad temperature range to the critical point.

## 2. Calculation of Film Reflux and Recondensation Corrections

*Film Reflux Correction.* The existence of a "driving" pressure, $\Delta P_f$, between the level where the mobile $He^4$ film vaporizes, and the (lower) pressure in the bulb, where the film vapor recondenses, is a well-known correction [17] to He II thermometry based on Poiseuille's Law [17, 18]. If vaporization of the film takes place a distance, $L_f$, above the bottom of a pressure-sensing tube of radius $a$, then, for viscous flow of the refluxing vapor, $\Delta P_f$ (microns)$=6\eta L_f \dot{V}_f/\pi a^4$, where $\eta$ is the viscosity, and $\dot{V}_f$ the volume flow rate of the refluxing vapor. For $\eta$ we can use an empirical equation, $\eta=(1.3T+2.1)\times10^{-6}$, which we fitted to the theoretical calculations of deBoer and Cohen [19] in the temperature range 0.8 to 2.2 °K. (Their theory is in excellent agreement with experiments [20, 21] done between 1.3 and 4.2 °K.)

For $\dot{V}_f$ we can substitute $2\pi a \dot{n}_f v_g$ where $v_g$ is the molar volume of the vapor, for which the ideal gas value is adequate, and $\dot{n}_f$ is the molar flow rate of film per centimeter circumference [22]. With these substitutions we get

$$P\Delta P_f=\frac{(970T+1570)TL_f\dot{n}_f}{a^3} \tag{1}$$

in units of (microns)$^2$ if $L_f$ and $a$ are in centimeters. As an example, for clean glass tubing at 1 °K, $\dot{n}_f\approx3.5\times10^{-6}$ moles cm$^{-1}$ sec$^{-1}$ and eq (1) gives $P\Delta P=0.0089L_f/a^3$. Allowing for the higher values of $\eta$ we used, this is in excellent agreement with the equation of Bleaney and Hull [18].

Figure 1 shows the temperature correction equivalent to $\Delta P_f$ calculated for "clean" tubing of various typical sizes assuming $L_f=10$ cm. The correction is seen to be 1 mdeg at a temperature of the order

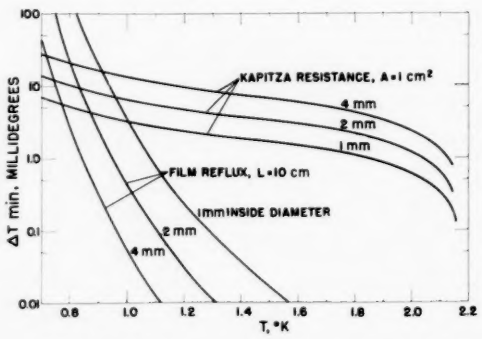


FIGURE 1. *Examples of* minimum *temperature corrections for a* $He^4$ *vapor pressure thermometer bulb based on the minimum superfluid film flux rate for pressure-sensing tubes of the indicated inside diameters.*

For the curves marked film reflux, $\Delta T_{min}$ is the temperature inferred from the pressure *minus* the liquid temperature. In calculating the film reflux pressure drop, the mobile film is assumed to evaporate a distance $L$ from the cold end of the pressure-sensing tube and the vapor to return to the bulb by laminar flow. For the curves marked Kapitza resistance, $\Delta T_{min}$ is the temperature difference between the thermometric fluid and the bulb wall assuming the area of thermal contact to be A. If the bulb is immersed in liquid the temperature of which is being measured, a second $\Delta T_K$ correction will be needed to account for the Kapitza resistance between the bulb wall and the external liquid.

Minute deposits of air on the tubing can increase the film flow and thus cause the required correction to be greater than $\Delta T_{min}$ by as much as a factor of twenty and extraordinary precautions are needed to come within a factor of two of the plotted corrections. Because it is so nonreproducible, the film flow rate should be concurrently determined, for example by a measurement of the recondensation heat leak.

of 1 °K if the tubing is scrupulously clean. If impurities on the walls cause the film flow to be an order of magnitude higher a 1 mdeg correction will be needed at about 1.2 °K.

Unfortunately (1) is difficult to apply to an actual measurement of vapor pressure for many reasons. The transfer rate depends markedly on the condition of the surface which is generally not as smooth as glass. What is worse, insofar as a calculation of $\Delta P_f$ is concerned, is the fact that $\dot{n}_f$ has been found [23] to depend very markedly on traces of impurities, such as solid air, on the wall over which the film passes. If $\dot{n}_{f,\min}$ is the value of $\dot{n}_f$ for perfectly clean tubing and if precautions are taken to clean the tubing wall or to prevent entry of condensable gases into the assembled system, $\dot{n}_f$ may be expected to exceed $\dot{n}_{f,\min}$, and a factor of 2 or more is not unreasonable [24]. A layer of solid air so thin as to be invisible can cause $\dot{n}_f$ to exceed the value measured for clean tubing [22] by as much as a factor of 10 or more [23]. It has been our experience that even though no leaks could be detected in our plumbing by a sensitive mass spectrometer leak detector, still $\dot{n}_f$ gradually increased, over a period of several days, by almost an order of magnitude. We presume the increase to have been due to an undetectable air leak or to migration of adsorbed gases from warm parts of the system to cold parts. In the light of the above observations, it is clearly imperative, for a proper evaluation of $\Delta P_f$, that an experimental determination of $\dot{n}_f$ be made *in situ*. This we have done, in effect, by measuring the heat of recondensation of the refluxing film, $\dot{Q}_f$, since $\dot{n}_f=\dot{Q}_f/(2\pi a\lambda_f)$, where $\lambda_f$ is the heat of transport of the film per mole. Since the mobile part of the film does not carry any entropy, $\lambda_f=TS_G$; and since the heat of vaporization of bulk liquid is $\lambda_{II}=T(S_G-S_l)$, therefore

$$\lambda_f=\lambda_{II}+TS_l. \tag{2}$$

For $\lambda_{II}$ and the entropy of the bulk liquid, $S_l$, we refer the reader to table VI of ref. [25].

Another difficulty in applying eq (1) is that the appropriate value of $L_f$, the height of rise of the mobile film, is very much dependent on the detailed design of the pressure sensing tube, especially on whether or not it is vacuum jacketed. We base the calculation on the assumption that the film will rise to a level at which sufficient heat flux, $\dot{Q}_f$, is available to vaporize the film. For a tube in a vacuum, having total length $L_s$, and if $w$ is the tube wall thickness then

$$L_s-L_f=\frac{2\pi aw}{\dot{Q}_f}\int_{T_f}^{T_s} k dT=\frac{w}{\dot{n}_f\lambda_f}\int_{T_f}^{T_s} k dT \tag{3}$$

where $k$ is the thermal conductivity of the tubing. (It is easy to show that for the practical thermometry case where $\Delta P_f \ll P$, the temperature rise, $\Delta T_f$, of the mobile (saturated) part of the film will also be small; since $\dot{n}_f$ varies but slowly with $T$, it follows that the flow rate will be essentially constant up to the level where vaporization of the entire film is energetically possible. Hence practically all of the vaporization will take place within a narrow band of the tubing, as has been assumed in writing down eq (3).)

Table 1 shows what one might expect $L_f$ to be for a typical "clean" and "dirty" Inconel tube, with $w$=0.01 cm, $L_s$=30 cm, $T$=1.5 °K, and various values of $T_s$. We note that when the tubing is lagged (thermally shorted) at helium temperatures the film will rise almost to the level of the heat source, especially if the tubing wall is "dirty." If the tubing is lagged at liquid nitrogen temperature it is unlikely that the film will rise appreciably in a clean sensing tube, since there will be more than enough heat approaching the liquid to completely vaporize the film. If this happens, the $\Delta P_f$ correction will, of course, vanish, but the additional heat reaching the cell will give rise to temperature gradients throughout the experimental cell whose disposition will need to be considered carefully. More will be said later about the temperature excess of the walls of an immersed bulb transmitting heat to its bath liquid.

TABLE 1.—*Height of rise of film, $L_f$, in a typical pressure-sensing tube held at temperature $T_s$ a distance 30 cm above the bulk liquid.*

The tube is made of inconel having 0.01 cm wall thickness and a mean thermal conductivity, $k$. For "clean" tubing the volume flow rate of film is $7.5\times10^{-3}$ cm (cm perimeter)$^{-1}$ sec$^{-1}$ and the assumed rate for "dirty" tubing is 10 times greater. Negative $L_f$ means more than enough heat reaches the bulb to vaporize the film before it can enter the pressure sensing tube, therefore $L_f=0$.

| Tube environment | $T_s$ | $k$ | Clean wall $L_f$ | Dirty wall $L_f$ |
|---|---|---|---|---|
| | *deg* | *W/cm deg* | *cm* | *cm* |
| Vacuum | 1.6 | 0.007 | 29.98 | 29.998 |
| Vacuum | 4.2 | 0.017 | 28.6 | 29.86 |
| Vacuum | 75 | 0.072 | −130.0→0 | 14.0 |
| Vacuum | 300 | 0.120 | −1050 →0 | −78 →0 |
| Effluent vapor | 300 | 0.120 | −6 →0 | 26.4 |

If the sensing tube is not in a vacuum, as assumed above, but is exposed to effluent $He^4$ vapor, the heat flux down the tube may be greatly diminished. Sydoriak and Sommers show in figure 2 of ref. [26] that for complete heat exchange between effluent vapor and a glass tube the heat flux reaching the bath by conduction down the tube will be reduced by a factor of at least 30 if $T_s$=300 °K. If conduction heat is not the major cause of vaporization the reduction in heat flux will be even greater. As a result $L_s-L_f$ may be so much lower than given by eq (3) that even for $T_s$=300 °K the film may "need" to rise to such high levels that $\Delta P_f$ may be a significant correction.

In view of the many and practically unpredictable factors discussed above which can influence $\Delta P_f$ and the heat conveyed by a pressure sensing tube it is not surprising that agreement has been lacking as to how a $He^4$ vapor pressure measurement should be made.

*Film Recondensation Correction.* If a bulb temperature measurement is being made there will be an additional source of error in He II thermometry. We refer to the temperature jump, $\Delta T_k$, across the boundary between a liquid and its container when a heat flux, $\dot{Q}$, exists between the liquid and the

container wall. The temperature dependence of $\Delta T_k$ for the case of liquid $He^4$ was first studied in some detail by Kapitza [27], whose data for heat transfer from polished copper to He II between 1.6 and 2.1° (his fig. 30) fits the relation $\Delta T_k = 5.9\ \dot{Q}/AT^3$, where $A$ is the immersed surface area of copper across which heat $\dot{Q}$ in watts flows. More recently, Fairbank and Wilks [28] found $\Delta T_k = 45\ \dot{Q}/AT^2$. Using a better defined area of contact, Challis, Dransfeld, and Wilks [29] have found a $T^{2.5}$ power law dependence. Their data yield a coefficient of 19.0 for polished copper and 9.0 for etched copper.

The most complete investigation has been done recently by Kuang Wey-Yen [30], whose measurements extended from 2 to 0.6 °K. He finds $\Delta T_k = 21\ \dot{Q}/AT^{2.6}$, in excellent agreement with the polished copper data of ref. [29]. He also investigated the reversibility of the effect, and found $\Delta T_k$ to be different, but of the same order of magnitude, for heat flow from liquid to solid as for the usually studied case of flow from solid to liquid. Evidently the discrepency was not considered significant, since neither the data nor the sense of the discrepancy are given. This is unfortunate because, we shall see, our results, which also pertain to heat flow from liquid to solid, are also in disagreement, by an order of magnitude, from published data above 1 °K for heat flow from solid to liquid. According to the phonon radiation theory of Khalatnikov [31], $\Delta T_k \propto T^{-3}$, in fair agreement with observed temperature dependences, but the predicted values of $\Delta T_k$ are 10 to 30 times greater than the highest observed values.

Some time ago it was pointed out that this so-called Kapitza resistance is a likely cause of serious error in $He^4$ thermometry [32]. For a closed, vacuum-jacketed tube containing liquid He II at 1 °K to a depth of $h$ cm it was indicated that

$$\Delta T_k \sim (10/h)\ \text{mdeg}, \tag{4}$$

using ref. [28] data. Thus, for $h \sim 1$ cm, which is more or less typical, a temperature error of 1 percent was indicated at 1 °K. Actually, the above equation gives only a minimum value of $\Delta T_k$ since it is based on the same purity assumption often made in a $\Delta P_f$ estimate of error: i.e., that the surface over which the film flows is completely free of traces of impurities. With minute traces of solid air on the tubing wall the effective perimeter for film flow can increase by an order of magnitude. This would cause $\dot{Q}_f$ and hence $\Delta T_k$ to also increase by an order of magnitude. On the other hand, if the tube is not vacuum jacketed, as in the AOW experiments, the appropriate value of $h$ may be comparable to the immersion depth of the pressure sensing tube, since recondensation may take place throughout the immersed parts of the tubing wall. This would tend to bring the expected $\Delta T_k$ down, for a typical geometry and tubing cleanliness, from the order of several tens of millidegrees to the order of several millidegrees at 1 °K. In support of this viewpoint we refer the reader to the thesis of Durieux, ref. [15], figure 44. For example, with a $He^4$ bath temperature of 1.35 °K the temperature of a glass vapor pressure thermometer exceeded the bath temperature by 13 mdeg when vacuum jacketed, but only by 4 mdeg when the (immersed) jacket was filled with gas. He stated the "warming up was probably mainly caused by the heat input due to the film creep."

Figure 1 shows examples of minimum temperature corrections due to the Kapitza resistance, $\Delta T_k$, for three tubing diameters. The wall of the thermometer bulb is assumed to have an area of 1 $cm^2$ and to be at temperature, $T$. For the selected geometries of figure 1 the $\Delta T_k$ correction is seen to be much greater than the $\Delta P_f$ correction, if $T > 1.2°$.

To our knowledge, neither of these possible sources of error, $\Delta P_f$ nor $\Delta T_k$, has been examined experimentally. In their report, AOW stated "there was an uncertain (although probably negligible) correction due to film flow." Because of this uncertainty and our observed thermodynamic inconsistency between the 1958 $He^4$ scale and the AOW data, new ($P_3$, $P_4$) comparisons were undertaken in an apparatus with which $\Delta T_k$ and $\Delta P_f$ could be determined separately and compared with calculations. In view of the uncertainty of film flow rates, it was felt that a simultaneous determination should be made of the film flow rate or, alternatively, of the consequent increase in heat leak, $\dot{Q}_f$, due to recondensation of the vapor. The $\dot{Q}_f$ measurement is feasible with the apparatus described below.

It should be clear by now that calculations of $\Delta P_f$ and $\Delta T_k$ corrections to a He II vapor pressure measurement of temperature may be subject to many serious uncertainties, and with many geometrical arrangements such corrections may be altogether impractical. But by giving sufficient attention to the details of the geometrical arrangements and by making subsidiary measurements it may be possible to make moderately reliable corrections down to, perhaps, 0.9 °K. This we have attempted to do, as described below.

## 3. Cryogenic Apparatus

To accomplish our objectives the apparatus was, in essence, a calorimeter; it is shown in figure 2, where we represent poorly conducting Inconel tubing with fine lines and thick copper walls with crosshatching. Thus the walls of cells A, B, and D are in good thermal contact with each other, but in poor thermal contact with cell C when no helium is present in D. Heat leak from above is reduced to a minimum by maintaining a temperature within a few tenths of a degree of the cell temperatures at tubing levels several centimeters above the cells.

When He II is present in D, there will be some recondensation of the refluxing film on the surface of the bulk liquid, which will therefore be at a temperature, $T_4$, which is greater than that of the refrigerated wall of the cell, by an amount $\Delta T_k$. Since the $He^3$ cell, C, is well insulated, its temperature will be the same as the liquid in which it is immersed. For $He^3$–$He^4$ vapor pressure comparisons, which are the

principal objective of this work, we therefore use the $He^3$ pressure, $P_3$, in cell C and the $He^4$ pressure, $P_4$, in cell D.

Another objective is to show that the film reflux phenomenon is an important source of error in an improperly designed $He^4$ thermometer system. For this we need to determine the temperatures of liquid $He^4$, $T_4$, and the wall of its container, $T_w$, and to compare $T_4 - T_w$ with a calculation of $\Delta T_k$ based on a measurement of the heat leak, $\dot{Q}_f$, due to the refluxing film. We get $T_w$ from one additional measurement, namely, a $He^3$ vapor pressure in cell B, whose wall is in good thermal contact with the wall of the $He^4$ cell, D. Then:

$$T_4 - T_w = (P_C - P_B)(dT/dP), \qquad (5)$$

where the derivative is the slope of any reasonably good $He^3$ temperature-versus-vapor pressure relationship. For $\dot{Q}_f$ we need to determine the total heat leak to ABCD. From the measured evaporation rate of refrigerant $He^3$ condensed in the annulus, A, we can calculate the total heat leak. On subtracting the background heat leak measured (in a few runs) in the absence of He II we obtain $\dot{Q}_f$.

Other details of the Dewar are shown schematically in figure 3 and have been described in some detail elsewhere [33]. We merely wish to point out that the experimental cells are completely surrounded by concentric copper radiation shielding bolted to pots of liquid $He^4$ and liquid $N_2$. Except at the various flanges to which they are lagged, the pressure-sensing tubes are everywhere in vacuum, and hence have a gas retention which is small and independent of the levels of the various refrigerants. This greatly simplifies the filling of a metal vapor pressure bulb to a desired liquid level, once a determination has been made of the gas retention volume for a particular value of $T$. Also, possible inverse temperature gradients in the refrigerant liquids do not introduce the danger of condensation at cold spots, as might occur if the pressure sensing tubes were not vacuum jacketed. As shown, inside diameters of the pressure sensing tubes become progressively larger at higher levels in order that thermomolecular pressure gradients be roughly the same in each section. Couplings used at these joints are designed to block the flow of radiation from higher temperatures (see insert to fig. 3). Several carbon resistors (not shown) are used to monitor temperatures of the various flanges and radiation shields.

## 4. Pressure Measurement

*$He^3$ Pressures.* $He^3$ vapor pressures were observed on oil and mercury manometers having inside diameters of 20 mm and 14.5 mm, respectively. A Wild cathetometer having a 70 cm focal length and read to 0.01 mm Hg was used to read $P_3$ and mercury meniscus heights. For each data point two to three readings of $P_3$ were taken at 10-min

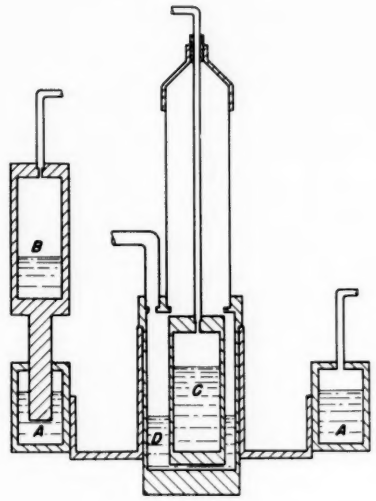


FIGURE 2. *Vapor pressure cells.*

Fine lines represent poorly conducting tubing, while crosshatching represents copper. $He^3$ refrigerant is contained in annulus A. Liquid $He^3$ thermometer bulb, C, measures $P_3$, and is at the same temperature as the liquid $He^4$ in cell D, even when recondensing film warms the liquid $He^4$. The wall temperature of cell D is measured by $He^3$ bulb, B.

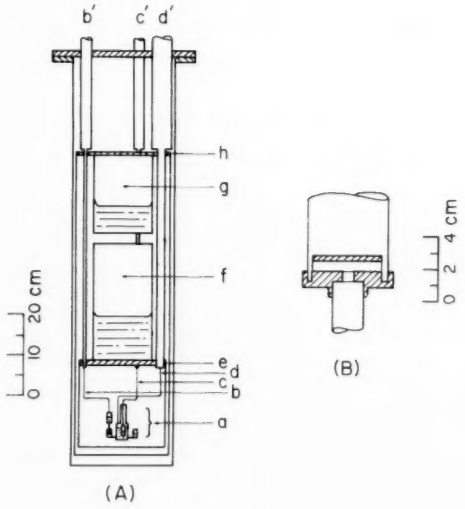


FIGURE 3A. *Dewar.*

The cells shown in figure 2 are shown in brackets at *a*. Stepped pressure-sensing tubes for cells B, C, and D are labeled *bb′*, *cc′*, and *dd′* respectively. The steps are in thermal contact with liquid $He^4$ refrigerant pot, *f*, at flange, *e*, and with liquid $N_2$ pot *g*, at flange, *h*. Copper radiation shields are bolted to *f* at flange, *e*, and to *g* at flange, *h*. To minimize the thermomolecular pressure gradient without unduly increasing heat leaks, tubes *bb′* and *cc′* increase in inside diameter from 0.133 cm to 0.583 cm at *e*, and to 2.49 cm at *h*. Tube *dd′* increases from 0.266 to 1.85 at *e*, and to 4.89 cm at *h*.

FIGURE 3B. *A sectional view shows the details of reducing couplings which also serve as radiation shields in each of the vapor pressure-sensing tubes.*

The couplings are soft soldered to flange, *h*.

intervals. The temperature was held constant to 0.1 mdeg for at least 10 min prior to each reading.

Meniscus corrections for the $He^3$ mercury manometer were taken from Cawood and Patterson [34], who list capillary depressions which are 1.1 to 1.5 times greater than those of Kistemaker [35]. The choice was made on the basis of a number of auxiliary experiments done at several controlled pressures: at each pressure meniscus heights were forcibly altered by tapping the manometer legs. Using Kistemaker's table the average spread in the corrected pressures was reduced to 0.07 mm. With the Cawood and Patterson table the corrected pressures had an average spread of 0.02 mm. The indication was that the Cawood and Patterson table is somewhat preferable for use with our particular manometer tubing and mercury. We do not intend to imply any generality to this conclusion. The surface tension of mercury in glass tubes is known to vary widely even if purified with care [35], and it is necessary, as pointed out by Kistemaker, to adjust published tables of meniscus corrections in accordance with a calibration *in situ* of each particular combination of type of glass and sample of mercury. Should neither ref. [34] or ref. [35] provide suitable tables of the correction, one can refer to the more extensive tables given in the NBS Monograph 8 [36].

The cathetometer scale was calibrated against an Invar meter bar. The net reading, meniscus correction and scale errors were estimated to amount to 27 $\mu$ in a measurement of $P_3$.

*$He^4$ Pressures—Brief Description of a Special Manometer.* For $He^4$ vapor pressure readings the mercury manometer tubing diameter used was 22 mm and menisci in the two arms were found to be sufficiently flat and equal to render meniscus corrections neglible.

At 1 °K, $P_4$ is so small that a cathetometer would not provide adequate accuracy. A special high-sensitivity manometer system containing oil and mercury U tubes of 25 mm bore was therefore designed to read $P_4$. This is capable of an accuracy of a few microns of mercury and requires less time and eyestrain than is required in reading a cathetometer to tens of microns or an ordinary mirror-scale manometer to a few hundred microns. Because of its general usefulness a brief description will be given. A separate traveling microscope comparator is used to view each arm of the manometer. The travel of each comparator is 10 cm and a vernier gives direct readings to 1 micron. For several readings at more or less the same pressure it is therefore not necessary to reposition the frame of either comparator. Hence successive readings at more or less the same pressure can be taken rapidly. An illuminator attached to each microscope barrel projects a collimated beam of light from behind the meniscus into the telescope. With this arrangement parallax effects are virtually eliminated.

The manometer temperature was monitored by standardized mercury thermometers marked every 0.1 °C. In order that they have approximately the same response time as the oil manometer, the monitoring thermometers were immersed in oil-filled test tubes of the same diameter as the manometer tubing to which they were fastened. Room temperature was controlled to a fraction of a degree by forced-air circulation and a sensitive thermostat. With this system and a box of heavy walled aluminum surrounding the manometers the two monitoring thermometers differed by less than 0.1 °C. Calibrations against a standard Invar meter bar were made for each comparator. They were found to be correct in the measurement of several lengths on the meter bar ranging from 1 to 10 cm with standard deviations of $\pm 2.4$ and $\pm 1.9$ $\mu$. For a pressure measurement the net standard deviation due to errors in the scales was therefore $\pm 3.1$ $\mu$. In a series of 23 static pressure measurements with three readings of each pressure, the average deviation was found to be $\pm 1.7$ $\mu$. The net reading and scale errors for mercury pressure, $P_4$, were therefore $\sqrt{3.1^2+1.7^2}=\pm 3.5$ $\mu$ of mercury.

In an experimental comparison of vapor pressures there is an additional source of error associated with differing equilibration times for the $He^3$ and $He^4$ systems and slow variations in cell temperature. This was minimized by controlling the temperature to a tenth of a millidegree for several minutes prior to each set of readings of $P_3$ and $P_4$, using a suitable carbon resistor or a Consolidated Engineering Corporation Micromanometer, which is a capacity-sensing differential pressure gage having a sensitivity of 0.20 $\mu$ at any pressure.

*Conversion of Millimeters Oil to Standard Millimeters Mercury.* *n*-Dibutyl phthalate was used in both oil manometers. The conversion factor, $F$, in microns of mercury at 0 °C per millimeter of oil at t °C, was determined by two different methods: first, by means of a pycnometer, using both water and mercury in standard procedures for determining the volumes of the pycnometer bulb and capillary; and second, by a direct comparison *in situ* of the mercury and oil manometers. The oil was outgassed by refluxing under vacuum while stirring; the manometers were evacuated when not in use.

In the region of temperatures occuring in our $P_3$-versus-$P_4$ measurements, the above oil density and direct determinations of $F$ are in agreement to 0.012 percent or better.

*McLeod Gage.* The McLeod gage had an extra-long Truebore tubing capillary, about 500 mm long $\times$ 1 mm bore. It was calibrated by means of an oil manometer read with a traveling microscope and used as a $P=h^2K(h)$ instrument, where $h$ is both the height of the compressed gas column and the mercury pressure head on it and $K(h)$ is the gage "constant" which may have a slight variation with $h$ due to a tapering capillary or for a reason given in the following paragraph.

An important procedural detail when taking a group of McLeod gage readings is to isolate the Dewar from the gage prior to each reading. If this is not done, warm gas will be pushed into the vapor pressure bulb as the mercury rises in the gage, and

several minutes will be required to restore an equilibrium temperature prior to the next reading. As a consequence of closing the valve the McLeod factor, $K$, will deviate from a constant more than would otherwise be the case. Naturally the same valve should be closed during calibration as is closed during subsequent vapor pressure measurements. In our apparatus the variation in $K(h)$ amounted to a fraction of a percent. For the function $K(h)$ a smooth curve was drawn through the calibration data. For the average of three readings at each of 17 calibration pressures, ranging from 40 to 2600 $\mu$, the standard deviation from $K(h)$ was $\pm 0.38$ percent.

*Thermomolecular Pressure Ratio.* Despite the large tubing sizes used, it was necessary at $T \leq 1.2$ °K to make thermomolecular pressure corrections of $He^4$ pressures. With stepped tubing this is a tedious calculation, even when graphs of $P_{cold}/P_{warm}$ of adequate sensitivity are available [37] for each section of tubing. For this reason we recommend to others use of a graph of the form of figure 4, in which the thermomolecular correction is expressed in terms of a correction in millidegrees to a scale temperature read from uncorrected pressures. Once the graph has been prepared for a particular geometry and isotope, no further calculations are required, beyond a simple subtraction.

For the stepped tubing used in the present measurements, the equivalent temperature correction was 4.5 mdeg at 0.90 °K.

*Gravity Correction.* The measured pressures have been reduced to standard gravity by multiplying by the ratio of local gravity, 979.125 cm/sec$^2$, to standard gravity, 980.665 cm/sec$^2$.

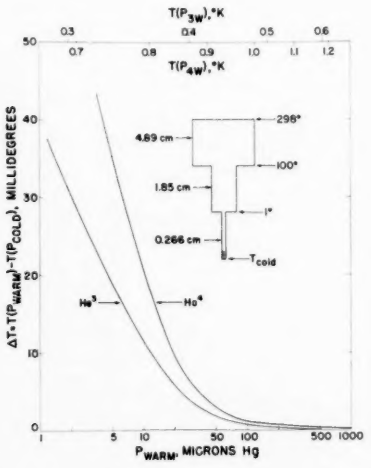


FIGURE 4. *A convenient method of correcting for thermal transpiration.*

The observed pressure at the warm end of the vapor pressure sensing tube, $P_{warm}$, plus a vapor pressure scale of temperatures, yield a first approximation to the liquid temperature, $T(P_{warm})$. The figure shows the correction, $\Delta T$, to be subtracted from $T(P_{warm})$ to account for thermal transpiration in the pressure sensing tubes shown in the insert. Although the ratio of $P_{cold}$ to $P_{warm}$ is the same for $He^4$ and $He^3$, $dT/dP$ is not the same for the two isotopes and the function $\Delta T(P_{warm})$ is therefore not the same.

*Hydrostatic Pressure Correction.* A small correction was made for the hydrostatic head of the gas column. This was appreciable only for the region below the flange $h$ shown in figure 3, and most of the correction (80%) applied to the 18 cm high column between the $He^3$ and $He^4$ refrigerants. In equivalent millidegrees the total correction ranged from 0.14 to 0.67 mdeg for $He^3$ between 1° and 3.323° respectively and from 0.08 to 0.30 mdeg for $He^4$ over the same temperatures.

*$He^4$ Impurity Correction.* The $He^4$ impurity in the stored $He^3$ was measured several times in the course of these experiments, using a mass spectrometer readable to 0.003 percent $He^4$ in $He^3$. The measured $He^4$ impurity was 0.041 mole percent. The correction was calculated from a smoothed curve obtained from the data of Sydoriak and Roberts [32] and of Esel'son and Berezniak [38] for 90 percent $He^3$ solutions. Since the liquid phase diagrams for both these sets of data show that mixture vapor pressure, $P_X$, varies linearly with $He^3$ mole fraction, X, between 90 and 100 percent, we assume that $(dP_X/dX)_{T,\,X=1} \approx (P_3 - P_X)/(1-X)$.

The correction raised $P_3$ by 0.037 and 0.030 percent at temperatures of 0.9 and 3.0 °K respectively. A more complete discussion and a table of this correction are given in paper III of this series.

*$\Delta P_f$ Correction.* The considerations on which $\Delta P_f$, the film reflux pressure correction is based, have already been discussed. Using eqs (1), (2), and (3) we found $\Delta P_f$ to be equivalent to temperature corrections ranging from 3.7 mdeg at 0.9 °K, to 0.18 mdeg at 1.1 °K, and to negligible ($<0.02$ mdeg) at 1.2 °K and at higher temperatures.

## 5. Results

*Corrected $(P_3, P_4)$ Data.* Table 2 shows results of measurements of $P_4$ and $P_3$, corrected as described above. Since $P_3$ is the pressure observed in cell C, which is immersed in a "bath" of $He^4$ in cell D, no $\Delta T_k$ correction was needed with these data. The error columns, whose inverse was used as a weighting factor in subsequent calculations of a temperature scale (part II of this series), are the arithmetic sum of the estimates of probable error in the meniscus correction, manometer readings, mercury density, impurity correction, thermomolecular correction, and $\Delta P_f$.

We defer until later a discussion of data point 44, which represents a redetermination of the critical point of $He^3$. We only wish to point out that the indicated estimates of error for this point are large because of the inherent difficulty of any vapor pressure measurements near a critical pressure. Actually, the effort put into data point 44 was several times greater than the effort put into any other data point in the table.

In the sixth column $\delta P_3$ and $\delta P_4$ have been combined to show the effect on $P_3$ of errors in both $P_3$ and $P_4$: $\delta P_3' = \delta P_3 + \delta P_4 (dP_3/dP_4)$, the derivative being calculated from existing $He^3$ and $He^4$ temperature scale tables, $T_L$ [9] and $T_{L55}$ [25], respectively.

The entries in this column will be appreciably exceeded by deviations of the data from an interpolation table, calculated as described below, only if an important source of random error has been underestimated or overlooked.

*Direct Interpolation Equations.* For various reasons it was felt desirable to derive interpolation equations by which any $He^4$ vapor pressure could be converted to an equivalent $He^3$ vapor pressure in one step, i.e., without the intervention of any vapor pressure-*versus*-temperature scales. A table calculated from interpolation equations has been used, for example, to compare the 1962 $He^3$ vapor pressure-temperature scale with absolute gas thermometer temperatures taken in conjunction with $He^4$ vapor pressure measurements. The results of the comparison will be given in paper II of this series. Similarly, existing paramagnetic salt data taken in conjunction with $He^4$ vapor pressure measurements can be compared with a $He^3$ temperature scale by the use of such direct $P_4 \rightarrow P_3$ interpolation equations.

Another use, of more immediate interest to us, is an examination of the data of table 2 for excessive scatter or for unrealistic assignment of probable errors. Of course, a two-step comparison is always possible, using any two smooth $He^4$ and $He^3$ temperature scales. This, however, introduces an added uncertainty in that the temperature scales used as interpolation devices may not themselves be completely smooth or may have an incorrect "shape" in certain regions such as, for example, the region of the $He^4$ lambda temperature.

It was not possible to obtain a single equation $f(P_3)=g(P_4)$. Therefore, the interpolation equations were obtained as follows: successive groups of eight adjacent data points in table 2 were fitted by the method of least squares to equations of the forms

$$P_3=a+bP_4+cP_4^2 \tag{5}$$

and

$$\ln P_3=a+b \ln P_4+c (\ln P_4)^2. \tag{6}$$

TABLE 2. *Results*

$P_3$ and $P_4$ are the corrected $He^3$ and $He^4$ vapor pressures and $\delta P_3$ and $\delta P_4$ the estimated errors in $P_3$ and $P_4$ respectively. If the function $P_3$ $(P_4)$ is properly deduced from the table the estimated error in $P_3$ for a given $P_4$ is assumed to be $\delta P_3'=P_3+\delta P_4(dP_3/dP_4)$. The equations used are actually quadratic in $P_4$ or ln $P_4$. See p. 554 (eqs 5&6). The seventh column shows the fit of a direct (one-step) interpolation table giving ${}_1P_3$ as a function of $P_4$. ${}_1P_3$ was obtained from a series of quadratic equations in $P_3$ and $P_4$ fitted to successive groups of eight consecutive data points in the table. The eighth cloumn shows the fit of a two-step "conversion" of a $P_4$ to a $P_3$ at the same temperature, using temperature as an interpolation parameter; i.e., ${}_2P_3$ was obtained from $P_4$ by way of the 1958 $He^4$ and 1962 $He^3$ temperature scales. The broad similarities between the last three columns give evidence of the adequacy of the error estimates and of the various curve and equation fitting procedures used to construct the above-mentioned tables.

Error estimates for point 44, which is at the critical pressure and temperature of $He^3$, refer only to the error in the measurement of $P_3$ and $P_4$. That is, they do not include the error in the decision that this is the critical point. Units of all columns in the table are microns of mercury at 0 °C and standard gravity.

| Point | $P_4$ | $\pm\delta P_4$ | $P_3$ | $\pm\delta P_3$ | $\pm\delta P_3'$ | $P_3-{}_1P_3$ | $P_3-{}_2P_3$ |
|---|---|---|---|---|---|---|---|
| 1 | 40.85 | 0.34 | 5254 | 3 | 26 | −1.6 | −4.3 |
| 2 | 67.27 | 0.39 | 6671 | 3 | 22 | −3.7 | −7.6 |
| 3 | 115.56 | 0.45 | 8692 | 4 | 20 | 10.5 | 10.5 |
| 4 | 159.41 | 0.70 | 10176 | 4 | 26 | 8.1 | 13.6 |
| 5 | 188.19 | 0.69 | 11041 | 4 | 24 | 5.4 | 10.5 |
| 6 | 282.08 | 1.00 | 13487 | 5 | 29 | −5.7 | 1.5 |
| 7 | 615.05 | 1.20 | 20001 | 8 | 28 | 5.5 | 3.4 |
| 8 | 1210.3 | 0.7 | 28395 | 11 | 19 | 4.0 | 12.9 |
| 9 | 2154.7 | 0.8 | 38512 | 14 | 22 | −21 | 3 |
| 10 | 3521.6 | 1.0 | 50234 | 18 | 26 | −26 | 11 |
| 11 | 5791.8 | 1.3 | 66069 | 27 | 35 | −37 | −48 |
| 12 | 8490.2 | 1.6 | 81978 | 60 | 69 | −75 | −112 |
| 13 | 8583.6 | 1.6 | 82515 | 28 | 37 | −22 | −85 |
| 14 | 12516 | 8 | 102750 | 60 | 108 | 41 | −7 |
| 15 | 12706 | 8 | 103650 | 60 | 108 | 34 | −38 |
| 16 | 12745 | 2 | 103810 | 60 | 71 | 17 | −47 |
| 17 | 17263 | 3 | 124230 | 70 | 85 | −36 | −122 |
| 18 | 17647 | 3 | 125860 | 60 | 72 | −29 | −151 |
| 19 | 23972 | 8 | 151880 | 70 | 100 | −22 | −37 |
| 20 | 24361 | 8 | 153490 | 35 | 65 | 54 | 89 |
| 21 | 31791 | 9 | 181580 | 48 | 82 | 56 | 64 |
| 22 | 35937 | 9 | 196610 | 45 | 77 | 36 | 54 |
| 23 | 37807 | 9 | 203290 | 55 | 88 | 0 | 45 |
| 24 | 38498 | 9 | 205830 | 55 | 89 | 59 | 121 |
| 25 | 40975 | 9 | 214470 | 80 | 111 | −48 | 7 |
| 26 | 44635 | 9 | 227210 | 59 | 91 | 3 | 30 |
| 27 | 51023 | 9 | 248770 | 80 | 110 | −5 | −25 |
| 28 | 63396 | 9 | 288860 | 90 | 119 | −30 | −41 |
| 29 | 77731 | 10 | 333140 | 90 | 118 | −13 | −6 |
| 30 | 94167 | 10 | 381810 | 110 | 140 | 136 | 173 |
| 31 | 112412 | 10 | 433390 | 106 | 127 | −21 | 64 |
| 32 | 133810 | 11 | 491850 | 110 | 140 | −110 | −6 |
| 33 | 157652 | 11 | 555000 | 110 | 136 | 9 | 16 |
| 34 | 181836 | 12 | 617090 | 130 | 161 | −164 | −214 |
| 35 | 197613 | 22 | 657110 | 109 | 164 | −43 | −94 |
| 36 | 197852 | 19 | 657780 | 110 | 161 | 34 | −25 |
| 37 | 198314 | 19 | 658950 | 110 | 161 | 54 | −14 |
| 38 | 223380 | 22 | 721410 | 114 | 168 | 35 | 82 |
| 39 | 226755 | 22 | 729700 | 114 | 168 | −21 | 50 |
| 40 | 230422 | 23 | 738630 | 116 | 171 | 29 | −31 |
| 41 | 257649 | 19 | 804980 | 120 | 170 | −162 | −59 |
| 42 | 258223 | 19 | 806350 | 120 | 170 | −198 | −108 |
| 43 | 277744 | 21 | 853730 | 140 | 192 | −52 | 253 |
| 44 | 285660 | 170 | 873000 | 300 | 710 | 174 | 448 |

Because of the specific heat anomaly of the liquid $He^4$ we excluded groups of data points which overlapped the lambda temperature. Point 23 is very close to the lambda point vapor pressure, $P_\lambda$, and was used as a terminal point for the last equation below $P_\lambda$ and the first equation above $P_\lambda$.

Except for the last five equations, the fit of the logarithmic equation was much better than the fit of eq (5), by a factor of 2 to 5 times. For the five equations of highest pressures the fit of equation (5) was best, by an average factor of 3 times. In accord with these observations the most appropriate of the derived equations were retained.

The coefficients of the selected equations and the detailed $P_3(P_4)$ interpolation table are available from the authors on request. The seventh column of table 2 shows how the interpolation table fits the data.

We note that, in general, the deviations of the data points from the direct interpolation table are comparable to and usually less than the quantity $\delta P'_3$, which is representative of the combined estimated random errors in $P_3$ and $P_4$. That is to say, each data point lies on a smooth curve with its neighbors, with a deviation comparable to the estimated random errors in the measurements. For the four entries at which $P_3 - {}_1P_3$, exceeds $\delta P'_3$, the average value of $(P_3 - {}_1P_3)/\delta P'_3$ is 1.08. We conclude that the error estimates are probably satisfactory for use as weighting factors in deriving a vapor pressure equation from these data.

The last column shows the results of a two-step interpolation using the temperature as a parameter: from $P_4$ and the 1958 $He^4$ scale we get $T_{58}$ and from this temperature and the 1962 $He^3$ scale (paper II of this series) we get ${}_2P_3$. The table shows that the deviation from the observed $He^3$ pressure of the two-step conversion from $P_4$ to an equivalent $P_3$ are, on average, 1.5 times as great as the deviations of the one-step conversion, but they are nowhere excessively greater than the "expected" deviations $\delta P'_3$. For the 10 points which exceed $\delta P'_3$ the average ratio of $P_3 - {}_2P_3$ with respect to $\delta P'_3$ is 1.40. It appears from this that the procedures employed in the establishment of the 1958 $He^4$ scale did not introduce irregularities capable of preventing calculation of an adequate $He^3$ temperature scale equation.

The general similarity of the last three columns also suggests that an adequate number of floating coefficients were used to fit the data to the $P_3(P_4)$ and the $P_3(T_{62})$ equations. For information as to whether an *excessive* number of floating coefficients had been used it is necessary to compare ${}_1P_3$ and ${}_2P_3$ in regions between the fitted points. If, for example, $N$ data points were fitted to equations of different form each of which contained a number of floating coefficients approaching $N$ the fit would be excellent at the data points but very poor elsewhere. We have compared ${}_1P_3$ and ${}_2P_3$ at 63 values of $P_4$ selected at random and find the average deviation between them to be 0.026 percent of ${}_1P_3$ with a maximum deviation of 0.10 percent of ${}_1P_3$. (In terms of equivalent millidegrees the average deviation between the two conversion procedures is 0.14 mdeg, with a maximum deviation of 0.5 mdeg.) By comparison, for $P_4$'s at the fitted data points we find from table 2 that ${}_1P_3$ and ${}_2P_3$ differ by an average of 0.030 percent of ${}_1P_3$. We conclude that an excessive number of fitted coefficients have not been used in deriving the $P_3(P_4)$ and $P_3$ $(T_{62})$ equations.

*Redetermination of the Critical Point.* Point 44 of table 2 represents a redetermination of the critical pressure and temperature by the method of pseudo-isotherms [9, 5] from data shown in figure 5. Below the critical point, the presence of a liquid level within cell A (cf. fig. 2) is recognized by the fact that for a portion of an isotherm the observed cell pressure is independent of the amount of $He^3$ taken out of the storage container and admitted into the Dewar and pressure gauge system. A sensitive bellows type gage marked every mm Hg was used in these measurements. It was calibrated against the same sensitive $He^4$ mercury manometer described above.

For isotherms approaching the critical isotherm from lower temperatures the liquid and vapor densities approach the same value and the width of the flat for an "isotherm" approaches zero. The dashed line in the figure is an estimate of the loci of points at which liquefaction within the copper cell began or ended. The top of the dashed line therefore lies on the critical isotherm and the value of the ordinate equals the critical pressure. We estimate the uncertainty in choice of the ordinate

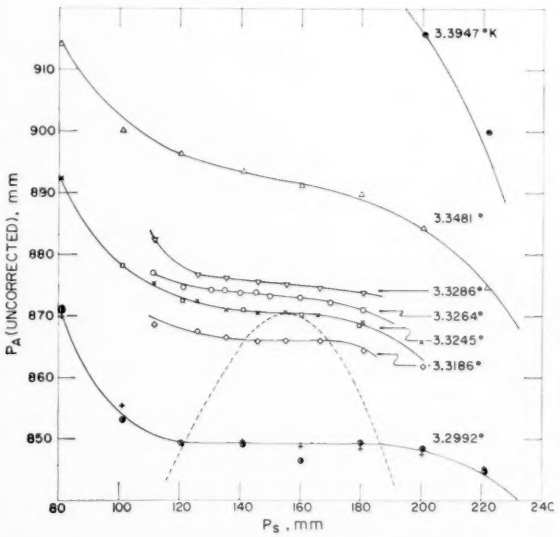


FIGURE 5. *Data for critical pressure determination.*

The equilibrium pressure, $P_A$, in cell A (fig. 2) as a function of pressure of $He^3$ in storage, $P_S$, at a number of temperatures controlled by pumping on $He^3$ in cell B and measured by a liquid $He^4$ pressure in cell D. $P_A$ represents a vapor pressure when $P_A$ is independent of $P_S$. The dashed line therefore encloses the region in which cell A is partly full of liquid and the top of the dashed line is at the pressure and temperature of the critical point. The corrected critical pressure is found to be 873.0±1.5 mm Hg at 0 °C and standard gravity. The error estimate includes the uncertainty in location of the peak of the coexistence curve. The critical temperature is 3.3240 °K on the 1958 $He^4$ scale.

of the top of the dome to be $\pm 1.2$ mm Hg. As drawn in the figure the top occurs at a corrected pressure of 873.00 $\pm 0.30$ mm Hg. The critical pressure is therefore 873.00 $\pm 1.50$ mm Hg. The corrected temperature of the chosen "critical isotherm" is 3.3240 $\pm 0.0005$ °K. If we add on the uncertainty in locating the top of the dome the critical temperature is 3.3240 $\pm 0.0018$ °K.

The first determinations of the critical pressure were by Abraham, Osborne, and Weinstock [5], who obtained 890 mm Hg by the above method and 860 mm Hg by the visual method of detecting disappearance of the liquid meniscus. Next, by the above pseudo-isotherm method, Sydoriak, Grilly, and Hammel (39) found $P_c = 875$ mm Hg. From measurements of density by an optical method, Peshkov [40] obtained $T_c = 3.38 \pm 0.03$ °K and $930 \pm 20$ mm Hg. Our correction for $He^4$ impurity was made by direct linear extrapolation from the $He^4$ critical point through the observed point (0.031% $He^4$) to 0.0 percent $He^4$.

*Demonstration of $\Delta T_k$ Errors in a $He^4$ Bulb Thermometer Below $T_\lambda$.* The ($P_3$, $P_4$) data of table 2 were taken with a $He^3$ bulb (cell C, fig. 2) immersed in a bath of $He^4$ (cell D, fig. 2). Since all of the heat of condensation of the refluxing film was taken up in the refrigerated walls of cell D, there was no need for a $\Delta T_k$ correction between the liquids in C and D.

In many experiments a $He^4$ vapor pressure bulb is used to determine the temperature of an object to which it is attached. To demonstrate the need for a $\Delta T_k$ correction to such a measurement when $T < T_\lambda$, we also made some comparisons between $T_C$ and temperatures, $T_B$, calculated from the $He^3$ vapor pressure in cell B, which is in good thermal contact with the walls of the $He^4$ cell. Some of the results are shown in table 3. We note that above $T_\lambda$ the two $He^3$ bulbs read the same temperature but below $T_\lambda$ they are in serious disagreement, by an amount which increases rapidly as the temperature is progressively reduced below 2 °K.

From the concurrently measured boil-off of the $He^3$ refrigerant we were able to estimate the heat of recondensation, $\dot{Q}_f$, of the refluxing film in cell D. From this it should be possible, in principle, to calculate $\Delta T_k$ and to decide, by comparison with ($T_C - T_B$), whether we have a valid explanation of the origin of the discrepancy and a means of correcting from a measured $He^4$ bulb pressure to the temperature of the bulb wall.

Unfortunately, as we have seen in the introduction, experimental values of $\dot{Q}/\Delta T_k$ for copper are not reproducible from one sample to another, so a quantitative check against our measured $\Delta T_k$ is not possible. Qualitatively, however, our results are similar to experimental and theoretical values appearing in the literature. Figure 6 shows our data, Khalatnikov's theoretical curve as interpreted by Challis et al. [29], and the results of various experimenters. The fact that none of the reported measurements overlaps our data does not appear to be too significant, in view of the very large differences between the various experiments. Kuang Wey-Yen has clearly demonstrated the large effect that the condition of the surface (the Beilby layer) has on $\Delta T_k$. Quite possibly our $He^4$ cell surface, which was thoroughly annealed when being silver-soldered, was altogether different from the surfaces on which the other $\Delta T_k$ measurements were made (if these other cells or surfaces were soft soldered, as appears likely from the description of the various experiments). It is also possible that the direction of heat flow, from liquid to solid in our experiments and from solid to liquid in all the others, affects the magnitude of $\Delta T_k$.

TABLE 3.—*The Kapitza resistance, $\Delta T_K$, due to film recondensation heat flux, $\dot{Q}_f$, to the $He^4$ cell;* $\Delta T_K = T_C - T_B$

| $T$ | $\Delta T_K$ | $\dot{Q}_f$ |
|---|---|---|
| *deg* | *mdeg* | *mW* |
| 0.82 | 7.2 | 0.44 |
| 0.85 | 9.0 | 0.42 |
| 0.90 | 2.4 | 0.31 |
| 0.94 | 2.1 | 0.31 |
| 0.98 | 4.6 | 0.53 |
| 0.99 | 9.2 | 1.19 |
| 0.99 | 9.1 | 1.50 |
| 1.00 | 1.9 | 0.26 |
| 1.05 | 1.4 | 0.29 |
| 1.09 | 3.5 | 0.50 |
| 1.10 | 1.0 | 0.28 |
| 1.30 | 1.2 | 0.39 |
| 1.40 | 1.5 | 0.64 |
| 1.50 | 2.3 | 0.77 |
| 1.81 | 0.5 | 0.52 |
| 2.00 | 0.4 | 0.36 |
| 2.01 | 0.4 | 0.24 |
| 2.23 | 0.1 | None |
| 2.60 | −0.3 | Do. |
| 2.80 | −0.1 | Do. |
| 2.91 | −0.1 | Do. |
| 3.00 | −0.1 | Do. |
| 3.00 | −0.2 | Do. |
| 3.10 | −0.3 | Do. |
| 3.15 | 0.0 | Do. |

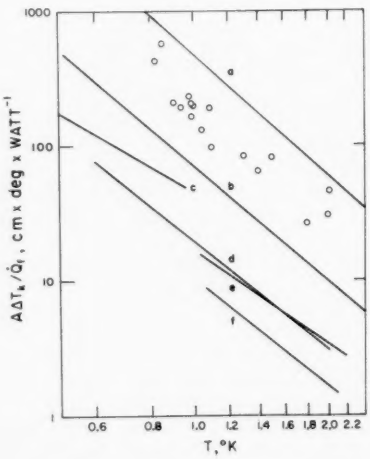


FIGURE 6. *The Kapitza resistance,* A $\Delta T_K/\dot{Q}_f$, *where* $\Delta T_K = T_C - T_B$.

$\dot{Q}_f$ is obtained from the increase in evaporation rate due to the presence of He II in cell D, and A is the total inside surface area of cell D. Curves *a* and *b* are from Khalatnikov's theoretical result [31] as calculated for copper by Challis, et al. (ref. [29]) and Kuang Wey-Yen (ref. [30]).

Curves *c* and *d* are experimental results for copper, refs. [28] and [30] respectively. Curves *e* and *f* are experimental results on polished and etched copper respectively, as given in ref. [29].

As noted earlier, Kuang Wey-Yen looked for such a directional dependence and found a difference of less than an order of magnitude, but unfortunately he does not state which direction gave a higher $\Delta T_k$, so no conclusion can be drawn. Finally, it may possibly be significant that our liquid to solid ($T_C - T_B$) values lie between $\Delta T_k$'s based on solid to liquid measurements and $\Delta T_k$ as given by Khalatnikov's theory. Perhaps the properties of bulk material used [29] in making calculations from the theory are more applicable to our well-annealed surface than to the surfaces studied by the other experimenters.

In any case, it is clearly impossible, in the present state of knowledge of the Kapitza temperature discontinuity, to correct properly a measured $He^4$ vapor pressure bulb measurement below $T_\lambda$ to obtain the temperature of the bulb wall. Even if the conversion from $\dot{Q}$ to $\Delta T_k$ were established experimentally for a particular bulb, as we have done, it would be impractical, in most cases, to meet the requirement of measuring $\dot{Q}_f$ frequently. Nor, in our experience, can the measurement of $\dot{Q}_f$ be justifiably avoided by using known film flow rates for clean tubing, $\dot{n}_{f,\min}$, or a predetermined multiple of $\dot{n}_{f,\min}$. As noted earlier, we have found that, although no leaks were detectable into our $He^4$ cell system, using a mass spectrometer leak detector sensitive to $10^{-10}$ cm$^3$/sec, yet our measured $\dot{Q}_f$ was not reproducible from day to day. During an early series of runs $\dot{Q}_f$ steadily increased from a value corresponding to 1.2 $\dot{n}_{f,\min}$ immediately after cooling the Dewar off to 11 $\dot{n}_{f,\min}$ during the ensuing 7 days of experimentation at liquid helium temperatures. It is possible that the increase was attributable to impurities present in the $He^4$ storage can although this was filled from vapor drawn off the large liquid $He^4$ pot. In later runs the ratio $\dot{n}_{f,\text{obs}}/\dot{n}_{f,\min}$ averaged 2.9 and ranged no higher than 4.2.

*Possibility of Gas Oscillations.* Resonant oscillations of a gas column between warm and cold portions of a tube are a possible cause of error in vapor pressure bulb thermometry for two reasons: The pressure measured at the warm end may differ from the vapor pressure; and heating of the liquid by the downward surges of warm gas will occur.

We believe gas oscillations were not a significant cause of error in the present measurements for two reasons: During the measurements no pressure fluctuations were detected on a Consolidated Micromanometer which was capable of detecting fluctuations of 0.2 $\mu$ at any pressure and at frequencies up to about 30 c/s; and pressures above the lambda point measured simultaneously in cells B and C gave no evidence of the existence of gas oscillations. In support of the latter statement we note in table 3 measurements of $P_B$ and $P_C$ made at seven different pressures above $P_\lambda$. Since bulbs B and C and their pressure sensing tubes are identical, it is reasonable to assume that the heat leak to bulbs B and C due to gas oscillations would be the same. Since bulb B is in much better thermal contact with the refrigerant than is bulb C, one would expect B to be appreciably colder than C if significant gas oscillations were occurring. Actually we found $T_C - T_B$ to average $-0.14$ mdeg for the seven measured temperatures above $T_\lambda$. We conclude that gas oscillations were not a significant cause of error above $P_\lambda$.

For temperatures below $T_\lambda$ we have no such evidence because $T_C - T_B$ is predominantly a measure of the film reflux phenomenon. However, the absence of detectable pressure oscillations provides some assurance that gas oscillations were not occurring below $T_\lambda$.

## 6. Conclusion

The data of table 2 appear to be suitable for derivation of a $He^3$ scale of temperatures. The paper which follows this one describes this derivation. A $He^4$ vapor pressure bulb is found to be impractical for accurate thermometry below $T_\lambda$ because of the difficulty of correcting for the pressure gradient heating effects due to the refluxing film.

---

We acknowledge the participation of T. R. Roberts in some of the measurements, his help with impurity correction calculations, and his critical reading of this manuscript; and D. H. Liebenberg for assistance in some of the measurements.

## References*

[1] S. G. Sydoriak, T. R. Roberts, and R. H. Sherman, Proc. 7th Intern. Conf. Low Temperature Physics, ed. G. M. Graham and A. C. Hollis-Hallett (Univ. of Toronto Press, Toronto, 1961), ch. 30, p. 717.
[2] F. G. Brickwedde, H. van Dijk, M. Durieux, J. R. Clement, and J. K. Logan, J. Res. NBS **64A** (Phys. & Chem.), 1 (1960).
[3] D. F. Brewer, A. K. Sreedhar, H. C. Kramers, and J. G. Daunt, Phys. Rev. **115,** 836 (1959).
[4] B. Weinstock, B. M. Abraham, and D. W. Osborne, Nuovo Cimento Suppl. **9,** 310 (1958).
[5] B. M. Abraham, D. W. Osborne, and B. Weinstock, Phys. Rev. **80,** 366 (1950).
[6] S. G. Sydoriak, T. R. Roberts, and R. H. Sherman, Paper II of this series.
[7] T. R. Roberts, R. H. Sherman, and S. G. Sydoriak, Paper III of this series.
[8] R. H. Sherman, S. G. Sydoriak, and T. R. Roberts, Paper IV of this series. See also Los Alamos Scientific Lab. Rept. LAMS 2701 (July 1962).
[9] S. G. Sydoriak and T. R. Roberts, Phys. Rev. **106,** 175 (1957).
[10] T. R. Roberts, S. G. Sydoriak, and R. H. Sherman, Proc. 4th Symp. Temperature, Its Measurement and Control in Science and Industry, ed. C. M. Herzfeld (Reinhold Publ. Corp., New York, 1962), Vol. 3, pt. 1, p. 75.
[11] W. E. Keller, Phys. Rev. **97,** 1 (1955); **100,** 1790 (1955).
[12] W. E. Keller, Phys. Rev. **98,** 1571 (1955).
[13] F. E. Hoare and J. E. Zimmerman, Rev. Sci. Instr. **30,** 184 (1959); R. T. Swim, Advances in Cryogenic Engineering, ed. K. D. Timmerhaus (Plenum Press, Inc., New York, 1960), Vol. 5, pp. 498–504.
[14] H. H. Plumb, Proc. 10th Intern. Congr. Refrigeration, Copenhagen, 1959, ed. M. Jul and A. M. S. Jul (Pergamon Press, Paris, 1960), Vol. 1, pp. 184–187.

*This list of references applies to papers I, II, III, and IV of this series. For completeness and convenience, it is reproduced in its entirety at the end of each paper.

[15] M. Durieux, Thermometry at Liquid Helium and Liquid Hydrogen Temperatures, Thesis, Leiden Univ. (16 Mar. 1960).
[16] F. G. Brickwedde, Report on the Conference Agreement on the Helium Vapor-Pressure Scale of Temperatures, Conf. Physique des Basses Temperatures, Paris, 2–8 Septembre 1955, pp. 608–610.
[17] B. Bleaney and F. Simon, Trans. Faraday Soc. **35,** 1205 (1939).
[18] B. Bleaney and R. A. Hull, Proc. Roy. Soc. (London) **178A,** 74 (1941).
[19] J. de Boer and E. G. D. Cohen, Physica **17,** 993 (1951).
[20] E. W. Becker and R. Misenta, Phys. Rev. **93,** 244 (1954).
[21] E. W. Becker, R. Misenta, and F. Schmeissner, Z. Physik **137,** 126 (1954).
[22] K. Mendelssohn and G. K. White, Proc. Phys. Soc. (London) **A63,** 1328 (1950).
[23] R. Bowers and K. Mendelssohn, Nature **163,** 870 (1949); Proc. Phys. Soc. (London) **A63,** 1318 (1950).
[24] K. W. Taconis, Progress in Low Temperature Physics, ed. C. J. Gorter (North Holland Publ. Co., Amsterdam, The Netherlands, 1961), Vol. 3, p. 154.
[25] H. van Dijk and M. Durieux, Physica **24,** 1 (1958).
[26] S. G. Sydoriak and H. S. Sommers, Jr., Rev. Sci. Instr. **22,** 915 (1951).
[27] P. Kapitza, J. Phys. (U.S.S.R.) **4,** 181 (1941).
[28] H. A. Fairbank and J. Wilks, Proc. Roy. Soc. (London) **A231,** 545 (1955).
[29] L. J. Challis, K. Dransfeld, and J. Wilks, Proc. Roy. Soc. (London) **A260,** 31 (1961).
[30] Kuang Wey-Yen, Zh. Experim. i Teor. Fiz. (U.S.S.R.) **42,** 921 (1962); Soviet Phys. JETP (English Transl.) **15,** 635 (1962).
[31] I.M. Khalatnikov, Zh. Experim. i Teor. Fiz. (U.S.S.R.) **22,** 687 (1952).
[32] S. G. Sydoriak and T. R. Roberts, Phys. Rev. **118,** 901 (1960).
[33] R. L. Mills, E.R. Grilly, and S. G. Sydoriak, Ann. Phys. **12,** 41 (1961).
[34] W. Cawood and H. S. Patterson, Trans. Faraday Soc. **29,** 522 (1933).
[35] J. Kistemaker, Leiden Commun. **268d** (1944); Physica **11,** 277 (1944–1946); B. E. Blaisdell, J. Math. Phys. **19,** 186 (1940).
[36] W. G. Brombacher, D. P. Johnson, and J. L. Cross, Mercury Barometers and Manometers, NBS Mono. 8 (U.S. Govt. Printing Office, Washington, 1960).
[37] T. R. Roberts and S. G. Sydoriak, Phys. Rev. **102,** 304 (1956).
[38] B. N. Esel'son and N. G. Berezniak, Zh. Experim. i Teor. Fiz. (U.S.S.R.) **30,** 628 (1956); Soviet Phys. JETP (English Transl.) **3,** 568 (1956).
[39] S. G. Sydoriak, E. R. Grilly, and E. F. Hammel, Phys. Rev. **75,** 303 (1949).
[40] V. P. Peshkov, Zh. Experim. i Teor. Fiz. (U.S.S.R.) **33,** 833 (1957); Soviet Phys. JETP (English Transl.) **4,** 645 (1958).
[41] H. van Dijk and D. Shoenberg, Nature **164,** 151 (1949).
[42] T. C. Chen and F. London, Phys. Rev. **89,** 1038 (1953).
[43] W. E. Keller, Nature **178,** 883 (1956); J. R. Clement, Low Temperature Physics and Chemistry (Univ. of Wisconsin Press, Madison, 1958), p. 187 (Proc. 5th Intern. Conf. Low Temperature Physics and Chemistry, Madison, Wis., 1957).
[44] L. Goldstein, Phys. Rev. **96,** 1455 (1954); Phys. Rev. **102,** 1205 (1956).
[45] R. H. Sherman, T. R. Roberts, and S. G. Sydoriak, Supplement au Bulletin de l'Institut International du Froid, Annexe 1961–5, p. 125 (Proc. Meeting of Commission I of the International Institute of Refrigeration, London, 1961).
[46] S. G. Sydoriak and R. H. Sherman, Paper I of this series.
[47] W. E. Deming, Statistical Adjustment of Data (John Wiley & Sons, New York, 1943).
[48] T. R. Roberts, S. G. Sydoriak, and R. H. Sherman, see ref. [45], p. 115.
[49] E. R. Grilly and E. F. Hammel, Progress in Low Temperature Physics III (1961), pp. 113–152.
[50] E. C. Kerr and R. D. Taylor, Proc. 7th Intern. Conf. Low Temperature Physics, ch. 24, pp. 605–608, ed. G. M. Graham and A. C. Hollis-Hallett (Univ. of Toronto Press, Toronto, 1961).
[51] R. H. Sherman and F. J. Edeskuty, Ann. Phys. **9,** 522 (1960).
[52] T. R. Roberts, R. H. Sherman, S. G. Sydoriak, and F. G. Brickwedde, Progress in Low Temperature Physics IV, ch. 10 (North Holland Publ. Co., Amsterdam, The Netherlands, 1964), p. 480.
[53] A. M. Mood, Introduction to the Theory of Statistics, p. 299 (McGraw-Hill, New York, N.Y., 1950).
[54] M. Durieux, Procès-Verbaux du Comité Consultatif de Thermométrie auprès du Comité International des Poids et Mesures, 6e Session, 1962 (Gauthier-Villars, Paris, France, 1964), p. 190.
[55] D. W. Osborne, private communication.
[56] R. Berman and C. F. Mate, Phil. Mag. **3,** 461 (1958).
[57] H. van Dijk, Progr. Cryog. **2,** p. 125 (Academic Press, Inc., New York, N.Y., 1962).
[58] G. Cataland and H. H. Plumb, Proc. 8th Intern. Conf. Low Temperature Physics, London, Sept. 16–22, 1962, ed. R. O. Davies (Butterworths, Washington, D. C., 1963), pp. 439–40.
[59] E. C. Kerr, Phys. Rev. **96,** 551 (1954).
[60] E. C. Kerr and R. D. Taylor, Ann. Phys. **20,** 450 (1962).
[61] A. C. Anderson, G. L. Salinger, W. A. Steyert, and J. C. Wheatley, Phys. Rev. Letters **6,** 331 (1961); A. C. Anderson, W. Reese, and J. C. Wheatley, Phys. Rev. **130,** 495 (1963).
[62] M. Strongin, G. O. Zimmerman, and H. A. Fairbank, Phys. Rev. **128,** 1983 (1962).
[63] B. M. Abraham, D. W. Osborne, and B. Weinstock, Phys. Rev. **98,** 551 (1955).
[64] G. R. Grove and W. J. Haubach, Jr.; see ref. [58], p. 441. For further information, write Gaseous Isotope Sales, Montsanto Research Corporation, Mound Laboratory, Miamisburg, Ohio.
[65] D. O. Edwards and J. G. Daunt, Phys. Rev. **124,** 640 (1961).
[66] S. G. Sydoriak, T. R. Roberts, and R. H. Sherman; see ref. [58], pp. 437–8.
[67] J. A. Hall, Sixième Rapport du Comité Consultatif de Thermométrie au Comité International des Poids et Mesures; see ref. [54].
[68] H. F. Stimson, NBS Tech. News Bull. **47,** No. 2, 30 (Feb. 1963); Nature **197,** 1055 (1963).
[69] F. G. Brickwedde, Phys. Today **16,** 24 (1963).
[70] S. Weber, Commun. Kamerlingh Onnes Lab. Univ. Leiden Suppl. **71b** (1932), **264b** and **264d** (1936).
[71] S. Weber and G. Schmidt, Commun. Kamerlingh Onnes Lab. Univ. Leiden **264c** (1936).
[72] C. E. Chase, E. Maxwell, and W. M. Whitney, Physica **26,** 160 (1960); C. E. Chase, E. Maxwell, and W. E. Millett, Physica **27,** 1129 (1961).
[73] R. H. Moore and R. K. Zeigler, Trans. Am. Nuclear Soc. **1,** 128–9 (1958); The Solution of the General Least Squares Problem with Special Reference to High-Speed Computers, Los Alamos Scientific Lab. Rept. LA–2367 (Mar. 4, 1960).
[74] T. R. Roberts and B. K. Swartz, Proc. 2d Symp. Liquid and Solid Helium Three, ed. J. G. Daunt (Ohio State Univ. Press, Columbus, 1960), p. 163.

(Paper 68A6–301)

JOURNAL OF RESEARCH of the National Bureau of Standards—A. Physics and Chemistry
Vol. 68A, No. 6, November–December 1964

# The 1962 $He^3$ Scale of Temperatures
# II. Derivation[1]

S. G. Sydoriak, T. R. Roberts, and R. H. Sherman

Los Alamos Scientific Laboratory, University of California
Los Alamos, N. Mex.

(July 16, 1964)

An Experimental Thermodynamic Equation (ETE) temperature scale valid from 0.2 to 2.0 °K has been calculated for $He^3$. The scale is based on new comparisons, ($P_3$, $P_4$), of $He^3$ and $He^4$ vapor pressures above 0.9 °K; on the 1958 $He^4$ temperature scale; and on the best available data for several thermodynamic properties of $He^3$ from 0.2 to 2.0 °K.

The $T_{62}$ Full-Range Working Equation (FWE) scale,

$$\ln P_3 = -2.49174/T + 4.80386 - 0.286001\ T + 0.198608\ T^2 - 0.0502237\ T^3 + 0.00505486\ T^4 + 2.24846 \ln T$$

fits the ETE scale and the ($P_3$, $T_{58}$) data and is therefore valid for use from 0.2 to the critical point, 3.324 °K. The maximum deviation from the ETE scale is 0.4 mdeg and the standard deviation from the input data is 0.25 mdeg. The fit to the seven recalculated isotherms of Keller in the range of the 1962 $He^3$ scale can be determined by converting Keller's $P_4$'s to equivalent $P_3$'s, using direct $P_4$ to $P_3$ interpolation equations. The fit of the 1962 $He^3$ scale is as good as the fit of the 1958 $He^4$ scale to the same isotherms, the average displacements of the two scales both being 1.5 mdeg below the isotherms. The average standard deviations for ($T_{62} - T_{1958}$) and for ($T_{58} - T_{1958}$) are 1.2 and 1.0 mdeg, respectively, for these seven isotherms.

## 1. Introduction

At the time $He^3$ was first liquified [39][2] a comparison of its vapor pressures, $P_3$, with those of $He^4$, $P_4$, was given, along with a careful determination of its critical pressure, $P_c$, which was found to be 875 mm Hg. Subsequently, Abraham, Osborne, and Weinstock (AOW) presented [5] more accurate ($P_3$, $P_4$) comparisons, additional critical point data in agreement with ref. [1], and an empirical temperature scale, $T_K$, based on a modification [5] of the 1948 $He^4$ scale [41]. They found it possible to fit all their data, ranging from 0.011 $P_c$ (1.02 °K) up to $P_c$, to an equation for log ($P/T^{5/2}$) having only three fitted powers of $T$.

In 1953, Chen and London [42] criticised the form of the $T_K$ equation and attempted to fit the same ($P_3$, $P_4$) data of AOW to an equation having a proper theoretical form for extrapolation to 0 °K. Although they fitted coefficients of five powers of $T$, and omitted data at pressures above 0.4 $P_c$, the fit of their equation was not satisfactory above 0.1 $P_c$.

In 1957 Sydoriak and Roberts [9] extended the measured range of pressures and temperatures down to 0.000074 $P_c$ and 0.45 °K using two different paramagnetic salts calibrated against $He^3$ above 1° for the temperature measurement. At that time two newer $He^4$ temperature scales were in use, so two $He^3$ scales were calculated: the $T_E$ $He^3$ scale, based on the 1955E $He^4$ scale [43], and the $T_L$ $He^3$ scale, based on the 1955L $He^4$ scale [25].

[1] Work performed under the auspices of the United States Atomic Energy Commission.
[2] Figures in brackets indicate the literature references at the end of thir paper.

Only by abandoning attempts to retain an analytical expression of proper theoretical form for extrapolation to 0 °K did Sydoriak and Roberts find it possible to get a good fit to their data in combination with those of AOW. To cover the four orders of magnitude range in $P_3$ only four fitted powers of $T$ were needed.

Following the adoption of the 1958 $He^4$ scale [2] the present authors made a proposal [1] to the Seventh International Conference of Low Temperature Physics held at the University of Toronto in 1960 for a new $He^3$ vapor pressure scale to be based on the 1958 $He^4$ scale and on various thermodynamic properties of $He^3$. The proposed procedure was similar to that used for the existing $T_E$ and $T_L$ scales except that newly available specific heat data [3, 4] could now be included instead of using a calculated "spin entropy" [44] term. In addition, a different magnetic temperature conversion was being studied for the paramagnetic salt data [9] intended to be used to extend the scale below 1 °K.

The proposal was favorably received by members of the conference, with some reservations as to the feasibility of including vapor pressure data obtained with an iron alum thermometer.

We have subsequently abandoned incorporation of any paramagnetic salt data into the scale derivation except for measurements of specific heat using a cerium magnesium nitrate thermometer [3].

An alternative procedure for establishment of the low-temperature end of the new $He^3$ scale has been thoroughly discussed [10] in a report to the Fourth Symposium on Temperature, its Measurement and Control in Science and Industry, Columbus, Ohio, March 1961. In this method the thermodynamic consistency of the $(P,T)$ data can be examined point by point. The method showed [45] that the AOW data could not be combined with the 1958 $He^4$ scale to yield a thermodynamically consistent scale in the range from 1 to 2 °K. A detailed discussion of the inconsistency, which is equivalent to several millidegrees, is given in a companion paper [7] to this one, hereafter referred to as Part III. Because of this inconsistency new $(P_3,P_4)$ comparisons were undertaken [45] in an improved apparatus designed to mininize errors due to $He^4$ film reflux. The results are reported in detail in another companion paper [46] to this one, hereafter referred to as Part I.

Since the measurements reported in Part I provide an explanation for the thermodynamic inconsistency, below $T_\lambda$, of a scale based on the AOW data, we have used only $(P_3,P_4)$ data given in Part I in deriving the 1962 $He^3$ scale, reserving the AOW data above $T_\lambda$ for the purpose of checking the final scale.

The second and third virial coefficients of $He^3$ are needed to establish the low-temperature end of the present scale. For this purpose Keller's isotherm data [12] has been reanalyzed, using the method of multiple variable least squares [47, 48]. For a further discussion of the method and results we refer to Part III, in which the scale derived below is examined for consistency with isotherm, paramagnetic salt, and latent heat data.

## 2. The High-Temperature Working Equation Scale

The three steps required to arrive at a full range equation are those discussed in detail for a Method I derivation in ref. [10].

The first step is to derive a working equation scale by which one can interpolate between the $(P_3, P_4)$ data points of Part I converted to a $(P_3, T_{58})$ table of data. The primary use of this scale is for making small corrections to experimental quantities of second order importance which enter into the thermodynamic treatment of the $(P_3, T_{58})$ data. It will suffice to state that we used a working equation scale which fits the $(P_3, T_{58})$ data with a variance of 0.25 mdeg and a maximum deviation of 0.6 mdeg. (In other $He^3$ scale derivations a high-temperature working scale was considerably more important, since it was also used in the determination of paramagnetic salt calibration equations [9] and to assign temperatures to $He^3$ latent heat data [10].)

## 3. The Experimental Thermodynamic Scale

The second step is to derive an analytical expression for the thermodynamic vapor pressure equation (see eqs (2) and (4) of ref. [10]) which can be written as follows, putting on the left those terms which can be evaluated from existing thermodynamic data:

$$\ln P_3+f(T)+f(C_{sat}, T)-\epsilon+f(V_L, P_3, T)=-\frac{a}{RT}-\frac{b}{R}. \tag{1}$$

The values of $P_3$ and $T_{58}$ used are given in table 1, which is a portion of the data of Part I, excluding the lowest three data points, at $P_4<40\mu$, because the calculated $He^4$ film reflux pressure drop was excessive.

The second term is

$$f(T)=-i-(5/2)\ln T \tag{2}$$

where $i$ is the chemical constant, $i=5.31733$.

For the remaining terms on the left we write the thermodynamic function and its empirical equivalent as follows. The calculable part of the specific heat term is

$$f(C_{sat}, T)=\frac{1}{RT}\int_{T_m}^{T} dT' \int_{T_m}^{T'} (C_{sat}/T'')dT'', \tag{3a}$$

where $C_{sat}$ is the specific heat of saturated liquid $He^3$. Smoothed values of the $C_{sat}$ data of Brewer, Sreedhar, Kramers, and Daunt [3] and data points of Weinstock, Abraham, and Osborne [4] are shown in table 2, and are used to obtain an empirical equation for $C_{sat}$,

$$C_{sat,\,x}/R=0.25154+0.47485T-0.54064T^2 +0.406356T^3-0.082729T^4 \tag{3b}$$

for $0.2<T<2°$. In this and the following equations and tables the subscript, $x$, is used to designate either an empirical function of $T$ fitted to a thermodynamic quantity or an experimental interpolation equation.

The lower limit of the fit, 0.2 °K, was arbitrarily selected within the range of measured values of $C_{sat}$. By this choice the lower limit of reliability of the 1962 $He^3$ scale is chosen to be 0.2 °K. By inserting eq (3b), the exact theoretical expression (3a) is converted to the experimental interpolation equation for $T_m=1.0°$ and $0.2<T<2°$:

$$f_x(C_{sat}, T)=\frac{0.39332}{T}-0.57013+0.237426T$$
$$-0.090344T^2+0.033863T^3-0.0041364T^4$$
$$+0.25154 \ln T. \quad (3c)$$

TABLE 1. $He^3$ *vapor pressure data* [a] *used in deriving the 1962* $He^3$ *scale*

$P_3$ is the measured $He^3$ vapor pressure in mm Hg at 0 °C and standard gravity, $\delta P_3$ the estimated maximum error in $P_3$, and $\delta T_{62}$ the temperature error equivalent to $\delta P_3$. Temperature $T_{58}$ is obtained from the measured $He^4$ vapor pressure, $P_4$, and the 1958 $He^4$ temperature scale. $\delta T_{58}$ is the estimated maximum error in $T_{58}$ equivalent to the maximum estimated error in our measurement of $P_4$, excluding possible errors in the 1958 $He^4$ scale itself. The last column showing the deviations of the 1962 $He^3$ scale from the input data, exhibits a random scatter above 2 °K. At lower temperatures there appears to be some small regularity in the misfit.

In fitting the coefficients of the equation for the 1962 $He^3$ scale, the weight given to each data point was a function of both $\delta P_3$ and $\delta T_{58}$.[b] As expected, for almost all of the data points $(T_{62}-T_{58})<(\delta T_{62}+\delta T_{58})$, since the right side of the inequality is the estimated maximum error. On average $(\delta T_{62}+\delta T_{58})$ was 1.7 times $(T_{62}-T_{58})$.

The last entry in the table is the measured value of the critical point.[a] In addition to the pressure measurement error listed, there is an uncertainty of ±1.5 mm Hg in the location of the critical point.

| $P_3$ | $\pm\delta P_3$ | $\pm\delta T_{62}$ | $T_{58}$ | $\pm\delta T_{58}$ | $T_{62}-T_{58}$ |
|---|---|---|---|---|---|
| *mm Hg* | *mm Hg* | *mdeg* | *deg* | *mdeg* | *mdeg* |
| 5.254 | 0.003 | 0.11 | 0.89848 | 0.78 | −0.2 |
| 6.671 | .003 | .09 | .94311 | .56 | −.2 |
| 8.692 | .004 | .10 | .99612 | .39 | .3 |
| 10.176 | .004 | .09 | 1.03014 | .48 | .3 |
| 11.041 | .004 | .08 | 1.04850 | .41 | .2 |
| 13.487 | .005 | .09 | 1.09572 | .42 | .0 |
| 20.001 | .008 | .11 | 1.19772 | .27 | .0 |
| 28.395 | .011 | .12 | 1.30024 | .09 | .1 |
| 38.512 | .014 | .13 | 1.39994 | .68 | .0 |
| 50.234 | .018 | .13 | 1.49553 | .58 | .1 |
| 66.069 | .027 | .17 | 1.60410 | .53 | −.3 |
| 81.978 | .060 | .32 | 1.69703 | .48 | −.6 |
| 82.515 | .028 | .15 | 1.69980 | .48 | −.5 |
| 102.75 | .060 | .28 | 1.80113 | .18 | −.0 |
| 103.65 | .060 | .28 | 1.80548 | .18 | −.2 |
| 103.81 | .060 | .28 | 1.80627 | .05 | −.2 |
| 124.23 | .070 | .29 | 1.89616 | .06 | −.5 |
| 125.86 | .060 | .25 | 1.90300 | .05 | −.6 |
| 151.88 | .070 | .26 | 2.00293 | .11 | −.1 |
| 153.49 | .035 | .13 | 2.00845 | .11 | .2 |
| 181.58 | .048 | .16 | 2.10432 | .11 | .2 |
| 196.61 | .045 | .14 | 2.15174 | .10 | .2 |
| 203.29 | .055 | .17 | 2.17207 | .10 | .1 |
| 205.83 | .055 | .16 | 2.17945 | .10 | .4 |
| 214.47 | .080 | .23 | 2.20521 | .09 | .0 |
| 227.21 | .059 | .17 | 2.24144 | .09 | .1 |
| 248.77 | .080 | .21 | 2.30010 | .08 | −.1 |
| 288.86 | .090 | .22 | 2.40069 | .07 | −.1 |
| 333.14 | .090 | .20 | 2.50157 | .06 | .0 |
| 381.81 | .110 | .22 | 2.60250 | .06 | .3 |
| 433.39 | .100 | .18 | 2.70121 | .05 | .1 |
| 491.85 | .110 | .19 | 2.80389 | .05 | .0 |
| 555.00 | .110 | .17 | 2.90588 | .04 | .0 |
| 617.09 | .130 | .19 | 2.99913 | .04 | −.3 |
| 657.11 | .109 | .16 | 3.05549 | .08 | −.1 |
| 657.78 | .110 | .16 | 3.05632 | .07 | .0 |
| 658.95 | .110 | .16 | 3.05792 | .07 | .0 |
| 721.41 | .114 | .15 | 3.14129 | .07 | .1 |
| 729.70 | .114 | .15 | 3.15203 | .07 | .1 |
| 738.63 | .116 | .15 | 3.16356 | .07 | .0 |
| 804.98 | .120 | .14 | 3.24556 | .06 | −.1 |
| 806.35 | .120 | .14 | 3.24724 | .06 | −.1 |
| 853.73 | .140 | .16 | 3.30238 | .06 | .3 |
| 873.00 | .300 | .34 | 3.3240 | .47 | .6 |

[a] Ref. [46] (Paper I of this series).
[b] Ref. [7] (Paper III of this series).

TABLE 2. *Values at selected temperatures, T, of the specific heat function* [a], $f(C_{sat},T)$ *appearing in the thermodynamic equation for* $\ln P_3$

The fun ction is evaluated by means of an explicit equation [b], $C_{sat,x}$, fitted to smoothed $C_{sat}$ data of Brewer, Sreedhar, Kramers, and Daunt [c] below 1 °K and plotted data points of Weinstock, Abraham, and Osborne [d] above 1 °K. The misfit of the equation, $\Delta C=C_{sat,x}-C_{sat,obs}$, is seen to have a random scatter.

| $T$ | $C_{sat,x}$ | $\Delta C_{sat}$ | $f_x(C_{sat},T)$ |
|---|---|---|---|
| *deg* | *cal mole*$^{-1}$ *deg*$^{-1}$ | *mcal mole*$^{-1}$ *deg*$^{-1}$ | |
| 0.2 | 0.652 [b] | 8 [e] | 0.000 |
| .3 | .706 | −8 | .0243 |
| .4 | .752 | −5 | .0665 |
| .5 | .793 | 0 | .1109 |
| .6 | .831 | 8 | .1539 |
| .7 | .870 | 3 | .1946 |
| .8 | .911 | ---------- | .2329 |
| .9 | .957 | ---------- | .2691 |
| 1.0 | 1.009 | ---------- | .3034 |
| 1.1 | 1.069 | −4, −9 [d,e] | .3362 |
| 1.2 | 1.136 | +1, −9, +4 | .3675 |
| 1.3 | 1.211 | +6, +4 | .3977 |
| 1.4 | 1.294 | +5, −1 | .4269 |
| 1.5 | 1.385 | −6 | .4553 |
| 1.6 | 1.482 | −13, +14 | .4831 |
| 1.7 | 1.585 | +2 | .5104 |
| 1.8 | 1.692 | +16, −4 | .5372 |
| 1.9 | 1.800 | −20, +2 | .5637 |
| 2.0 | 1.908 | +5 | .5899 |

[a] Eq (3a)
[b] Eq (3b)
[c] Ref. [3]
[d] Ref. [4]. Both $T$ and $C_{sat}$ were adjusted to the $T_{58}$ scale; e.g., $C_{sat}$ was multiplied by the value of $dT_{58}/dT_K$ at each data point.
[e] Where multiple entries appear they refer to data points nearest to the indicated temperatures.

TABLE 3. *The vapor volume term* [a], $\epsilon$, *in the equation for* $\ln P_3$, *as evaluated by an iterative procedure, using a high-speed digital computer*

For their general usefulness the table also shows solutions of the cubic equation [b] for the vapor volume $V_G$, and values of the second [c] and third [d] virial coefficients, $B$ and $C$, based on reanalysis [e] of the isotherms of Keller [f].

| $T$ | $V_G$ | $B$ | $C$ | $\epsilon$ |
|---|---|---|---|---|
| *deg* | *cm*$^3$*/mole* | *cm*$^3$*/mole* | (*cm*$^3$*/mole*)$^2$ | |
| 0.2 | $1.03\times10^9$ | −1350 | 6409 | 0.0000 |
| .3 | $9.97\times10^6$ | −898.3 | 5233 | .0001 |
| .4 | $8.87\times10^5$ | −672.5 | 4532 | .0008 |
| .5 | $1.95\times10^5$ | −537.0 | 4053 | .0027 |
| .6 | $6.83\times10^4$ | −446.7 | 3700 | .0065 |
| .7 | $3.123\times10^4$ | −382.2 | 3426 | .0122 |
| .8 | $1.692\times10^4$ | −333.8 | 3204 | .0195 |
| .9 | $1.028\times10^4$ | −296.2 | 3021 | .0284 |
| 1.0 | 6780 | −266.0 | 2866 | .0384 |
| 1.1 | 4747 | −241.4 | 2732 | .0495 |
| 1.2 | 3478 | −220.9 | 2616 | .0613 |
| 1.3 | 2640 | −203.5 | 2513 | .0738 |
| 1.4 | 2061 | −188.6 | 2422 | .0868 |
| 1.5 | 1646 | −175.7 | 2340 | .1003 |
| 1.6 | 1339 | −164.4 | 2266 | .1141 |
| 1.7 | 1106 | −154.5 | 2198 | .1282 |
| 1.8 | 925.6 | −145.6 | 2136 | .1427 |
| 1.9 | 782.8 | −137.7 | 2079 | .1574 |
| 2.0 | 667.9 | −130.6 | 2027 | .1723 |

[a] Eq (4a)
[b] Eq (4b)
[c] Eq (4c)
[d] Eq (4d)
[e] Ref. [7]
[f] Ref. [12]

For convenience we have taken $T_m$ to be 1.0 °K, although any other temperature in the range of eq (3b) could as well have been selected. The effect of the specific heat term on the ETE scale below 1 °K is easier to identify with this choice of $T_m$.

The vapor volume term is

$$\epsilon = \ln(P_3 V_G/RT) - \frac{2B}{V_G} - \frac{3C}{2V_G^2}. \quad (4a)$$

For the vapor volume, $V_G$, we used the inverse volume expansion form of the equation of state

$$PV_G = RT\left(1 + \frac{B}{V_G} + \frac{C}{V_G^2}\right). \quad (4b)$$

For the second and third virial coefficients of $He^3$ we used the equations found in Part III in the multiple parameter least squares analysis of Keller's isotherm data [12],

$$B = 4.942 - \frac{270.986}{T} \text{ cm}^3/\text{mole} \quad (4c)$$

and

$$C = 2866/\sqrt{T} \text{ cm}^6/\text{mole}^2. \quad (4d)$$

Since a high-speed calculator was available, it was possible to use the implicit form (4a), with $P_3$ being taken from the $(P_3, T_{58})$ data of table 1. Table 3 shows values of the term and of its component parts.

The liquid volume term is

$$f(V_L, P_3, T) = -\frac{1}{RT}\int_0^{P_3} V_L dP_3 \quad (5a)$$

or

$$f_x(V_L, P_3, T) = -0.005554T^3 - 0.000163T^4, \quad T < 2°\text{K}. \quad (5b)$$

The coefficients of (5b) were evaluated by fitting the next to last column of table 4, which is calculated from the smoothed [49] $V_L$ data of Taylor and Kerr [50] and of Sherman and Edeskuty [51] and from the working equation (for $\Delta P_3$).

TABLE 4. *The liquid volume term,* $f(V_L, P_3, T)$, *in the equation for* $\ln P_3$ *is calculated by numerical integration at selected temperatures,* T, *using smoothed values* [a], $V_L$, *of liquid volume data of Kerr and Taylor* [b] *and Sherman and Edeskuty* [c]

For $P_3$ the high-temperature working equation is used. Column 3 shows values [d] calculated from a power series in $T^n$ fitted to column 2. The last two columns show the mismatch and its equivalent in millidegrees.

| $T$ | $f(V_L, P_3, T)$ | $f_x(V_L, P_3, T)$ | $f_x - f$ | $\Delta T$ |
|---|---|---|---|---|
| *deg* | | | | *mdeg* |
| 0.2 | 0.0000 | 0.0000 | 0.0000 | 0.0 |
| .4 | .0000 | .0004 | .0004 | .0 |
| .6 | .0005 | .0012 | .0007 | .1 |
| .8 | .0021 | .0029 | .0008 | .1 |
| 1.0 | .0052 | .0057 | .0005 | .1 |
| 1.2 | .0099 | .0099 | −.0000 | −.0 |
| 1.4 | .0163 | .0158 | −.0005 | −.2 |
| 1.6 | .0244 | .0238 | −.0006 | −.2 |
| 1.8 | .0342 | .0341 | −.0001 | −.0 |
| 2.0 | .0459 | .0470 | .0011 | .6 |

[a] Ref. (49)
[b] Ref. (50)
[c] Ref. (51)
[d] Eq. (5b)

On the right side of eq (1) we have those terms of the thermodynamic equation which cannot be adequately calculated from existing data on $He^3$:

$$a = L_o - \int_0^{T_m} C_{sat} dT \quad (6)$$

and

$$b = S_L(T_m) \quad (7)$$

where $L_o$ is the value of the latent heat of vaporization at absolute zero, and $S_L(T_m)$ is the liquid entropy at $T_m$.

Using the ordinary method of least squares analysis and weighting each data point equally in this step of the derivation of the 1962 $He^3$ scale, we find

$$a/R = 2.09842 \pm 0.00070 \text{ for } T_m = 1.0° \quad (8a)$$

and

$$b/R = 1.08360 \pm 0.00046 \text{ for } T_m = 1.0°. \quad (8b)$$

By combining all the above functions we obtain an experimental thermodynamic equation scale (ETE) which is valid from 0.2 to 2.0 °K.

Because of the complexity of the ETE equation, and the fact that it is implicit in the pressure, iterative solutions were obtained with the aid of an electronic digital computer. A table in steps of 1 mdeg was prepared for comparison with the working equation scale.

## 4. The 1962 $He^3$ Full-Range Working Equation Scale

To obtain an expression valid over the full range from 0.2 °K to the critical point we now fit selected portions of eq (1) to a power series in $T^n$, using as input pressures all of the $(P_3, T_{58})$ data of table 1. Using the method of multiple variable least squares analysis [47, 48] we fit

$$\ln P_3 + f(T) + f_x(C_{sat}, T) + \frac{a}{RT} + \frac{b}{R} = \sum_{n=1}^{4} d_n T^n. \quad (9a)$$

Note that in this fitting the vapor and liquid volume terms are expected to be fitted by the power series. To be acceptable it will therefore be necessary to demonstrate not only that the scale fits the input data but also that the scale of (9a) agrees with the ETE scale below the range of the input data, i.e., below $P_3 = 5.254$ mm.

The solution of the analysis, combining coefficients of identical powers of $T$, is the full range working equation scale, FWE,

$$\ln P_3 = -2.49174/T + 4.80386 - 0.286001T + 0.198608T^2 - 0.0502237T^3 + 0.00505486T^4 + 2.24846 \ln T \quad 0.2 < T < 3.324°\text{K}. \quad (9b)$$

The upper limit is the critical point temperature consistent with the redetermination of the critical pressure found in Part I to be at 873.0 mm Hg.

As shown in figure 1, a comparison of the two tables we generate from the ETE scale and the FWE scale shows excellent agreement: nowhere below 2 °K do the scales differ by more than 0.4 mdeg. Equation (9b) is therefore in effect an experimental thermodynamic scale from 0.2 to 2.0 °K and an empirical scale above 2 °K.

A comparison of the fit of the 1962 $He^3$ scale to the input ($P_3$, $T_{58}$) data is given in table 1 and figure 1. The standard deviation of the data from the scale is 0.25 mdeg.

The $He^4$ lambda point occurs at $P_{4,\lambda}=37.80$ mm Hg (corrected to 0 °C and standard gravity). On the 1958 $He^4$ scale this corresponds to 2.1720 °K. In Part I a direct interpolation procedure is described by which the value of $P_3$ which corresponds to $P_{4,\lambda}$ is 203.25 mm Hg. Hence $T_{62,\lambda}=2.1721$ °K, for $P_3=203.25$ in good agreement with the value of this fixed point on the 1958 $He^4$ scale of temperatures.

The most fundamental test which can be given to the 1962 $He^3$ scale is its fit to $He^3$ and $He^4$ isotherm data, of which those of Keller [11, 12] are the most complete and accurate. Although Keller used a $He^4$ thermometer in most of his isotherms, his observed $P_4$'s can be related to $P_3$'s by the direct interpolation equations described in Part I. In Part III Keller's isotherms have been reanalyzed by the method of multiple variable least squares. Results

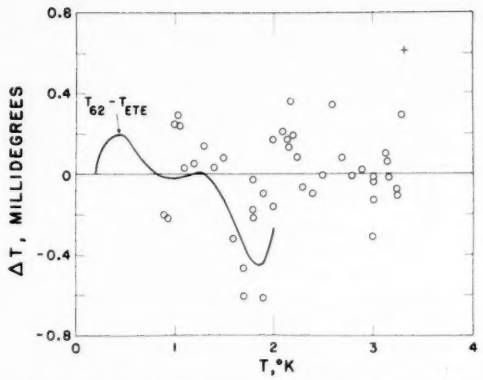


FIGURE 1. *The solid line is the deviation of the 1962 $He^3$ scale (i.e., the Full-range Working Equation, eq 9b) from the Experimental Thermodynamic Equation (ETE) scale in the range of validity of the ETE scale.*

Plotted points are deviations of the 1962 $He^3$ scale from the ($P_3$,$P_4$) input data: $T_{62}(P_3)-T_{58}(P_4)$. The + represents data at the critical point.

of the comparison with the 1962 $He^3$ and with the 1958 $He^4$ scales are shown in figure 2. We note that the weighted average of $T_{N,62}$ is 1.52 mdeg below $T_{1so}$, whereas for the same isotherms $T_{N,58}$ averages 1.50 mdeg below $T_{1so}$. Since for these isotherms $T_{N,62}-T_{1so}$ and $T_{N,58}-T_{1so}$ have average standard deviations of 1.2 mdeg and 1.0 mdeg, respectively, we conclude that not much would be gained by basing a $He^3$ scale more directly on the isotherm data. In other words, the 1958 $He^4$ scale, which is

TABLE 5. $He^3$ *vapor pressures on the 1962* $He^3$ *scale at 0 °C and standard gravity, 980.665 cm/sec²*

The units of pressure are microns ($10^{-3}$ mm) of mercury below 1 °K and millimeters of mercury at higher temperatures

| $T$ | 0.00 | 0.01 | 0.02 | 0.03 | 0.04 | 0.05 | 0.06 | 0.07 | 0.08 | 0.09 |
|---|---|---|---|---|---|---|---|---|---|---|
| 0.20 | 0.012 | 0.024 | 0.046 | 0.084 | 0.144 | 0.239 | 0.382 | 0.592 | 0.891 | 1.308 |
| 0.30 | 1.877 | 2.636 | 3.633 | 4.921 | 6.561 | 8.619 | 11.173 | 14.304 | 18.105 | 22.673 |
| 0.40 | 28.11 | 34.54 | 42.08 | 50.86 | 61.01 | 72.68 | 86.02 | 101.17 | 118.31 | 137.61 |
| 0.50 | 159.2 | 183.3 | 210.1 | 239.8 | 272.5 | 308.5 | 347.9 | 391.1 | 438.0 | 489.1 |
| 0.60 | 544.4 | 604.3 | 668.9 | 738.4 | 813.0 | 893.0 | 978.7 | 1070.1 | 1167.6 | 1271.4 |
| 0.70 | 1381 | 1498 | 1622 | 1753 | 1892 | 2038 | 2192 | 2355 | 2525 | 2704 |
| 0.80 | 2892 | 3089 | 3295 | 3511 | 3736 | 3971 | 4216 | 4472 | 4739 | 5016 |
| 0.90 | 5304 | 5603 | 5914 | 6237 | 6572 | 6918 | 7277 | 7649 | 8034 | 8431 |
| 1.00 | 8.842 | 9.267 | 9.704 | 10.156 | 10.622 | 11.102 | 11.597 | 12.106 | 12.631 | 13.170 |
| 1.10 | 13.725 | 14.295 | 14.881 | 15.484 | 16.102 | 16.737 | 17.388 | 18.056 | 18.741 | 19.443 |
| 1.20 | 20.163 | 20.900 | 21.655 | 22.428 | 23.220 | 24.029 | 24.857 | 25.704 | 26.571 | 27.456 |
| 1.30 | 28.360 | 29.285 | 30.229 | 31.193 | 32.177 | 33.181 | 34.206 | 35.252 | 36.319 | 37.407 |
| 1.40 | 38.516 | 39.646 | 40.799 | 41.973 | 43.169 | 44.388 | 45.629 | 46.893 | 48.179 | 49.489 |
| 1.50 | 50.822 | 52.178 | 53.558 | 54.961 | 56.389 | 57.840 | 59.316 | 60.817 | 62.342 | 63.892 |
| 1.60 | 65.467 | 67.068 | 68.694 | 70.345 | 72.022 | 73.726 | 75.455 | 77.211 | 78.993 | 80.802 |
| 1.70 | 82.638 | 84.501 | 86.391 | 88.309 | 90.254 | 92.228 | 94.229 | 96.258 | 98.315 | 100.402 |
| 1.80 | 102.516 | 104.660 | 106.833 | 109.035 | 111.266 | 113.527 | 115.818 | 118.138 | 120.489 | 122.870 |
| 1.90 | 125.282 | 127.724 | 130.197 | 132.701 | 135.236 | 137.803 | 140.401 | 143.031 | 145.692 | 148.386 |
| 2.00 | 151.112 | 153.870 | 156.661 | 159.485 | 162.342 | 165.232 | 168.155 | 171.112 | 174.102 | 177.126 |
| 2.10 | 180.184 | 183.276 | 186.403 | 189.564 | 192.760 | 195.990 | 199.256 | 202.557 | 205.894 | 209.266 |
| 2.20 | 212.673 | 216.117 | 219.597 | 223.113 | 226.665 | 230.255 | 233.881 | 237.544 | 241.244 | 244.982 |
| 2.30 | 248.757 | 252.570 | 256.420 | 260.309 | 264.236 | 268.202 | 272.206 | 276.249 | 280.331 | 284.452 |
| 2.40 | 288.613 | 292.813 | 297.053 | 301.333 | 305.653 | 310.013 | 314.414 | 318.855 | 323.337 | 327.861 |
| 2.50 | 332.425 | 337.031 | 341.679 | 346.368 | 351.100 | 355.874 | 360.690 | 365.549 | 370.450 | 375.395 |
| 2.60 | 380.383 | 385.414 | 390.489 | 395.608 | 400.771 | 405.978 | 411.230 | 416.526 | 421.868 | 427.254 |
| 2.70 | 432.686 | 438.164 | 443.687 | 449.256 | 454.872 | 460.534 | 466.242 | 471.998 | 477.801 | 483.651 |
| 2.80 | 489.549 | 495.495 | 501.488 | 507.531 | 513.622 | 519.762 | 525.951 | 532.189 | 538.477 | 544.815 |
| 2.90 | 551.203 | 557.642 | 564.131 | 570.672 | 577.264 | 583.907 | 590.602 | 597.349 | 604.149 | 611.002 |
| 3.00 | 617.907 | 624.866 | 631.879 | 638.945 | 646.066 | 653.241 | 660.472 | 667.757 | 675.098 | 682.496 |
| 3.10 | 689.949 | 697.459 | 705.026 | 712.650 | 720.332 | 728.072 | 735.871 | 743.728 | 751.644 | 759.620 |
| 3.20 | 767.656 | 775.753 | 783.910 | 792.128 | 800.408 | 808.750 | 817.155 | 825.622 | 834.153 | 842.747 |
| 3.30 | 851.406 | 860.130 | 868.918 | 877.773 | | | | | | |

itself fundamentally based on these isotherm data, has evidently been an adequate interpolation parameter for fitting the $He^3$ data to these isotherms.

Table 5 shows vapor pressures calculated from eq (9b) in steps of 10 mdeg. In table 6 we show $dP/dT$ and $T_{62}-T_x$ in 0.1 deg steps, where $T_{62}$ corresponds to eq (9b) and $T_x$ to the various $He^3$ scales in use in the past. We also have included on the far right the two $He^4$ scale differences $(T_{L55}-T_{58})$ and $(T_{55E}-T_{58})$, as given in the NBS Monograph 10 "The 1958 $He^4$ Scale of Temperatures" [2]. In a few recent publications an attempt has been made to "correct" the $T_L$ and $T_E$ $He^3$ scales by adding these $He^4$ scale "correction" terms. To convert these temperatures to the 1962 $He^3$ scale it is necessary to apply the sum of columns 3 and 6 (or 4 and 7) to the "corrected $T_L$" or "corrected $T_E$" scales.

Detailed $(P,T)$ and $(T,P)$ tables have been published [8] by the Los Alamos Scientific Laboratory and in Part IV of this series.

In order to make the advantages of $He^3$ as a vapor pressure thermometer more widely accessible, specially purified $He^3$ is being made available for purchase[3] for thermometry through the United States Atomic Energy Commission isotopes program.

[3] Information may be obtained from Gaseous Isotopes Sales, Monsanto Research Corporation, Mound Laboratory, Miamisburg, Ohio.

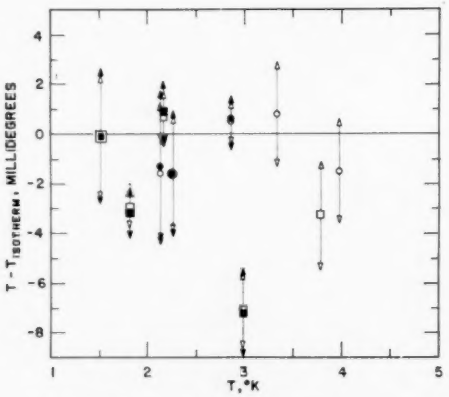


FIGURE 2. *Deviations of temperature scales from Keller's (ref. [11, 12]) isotherm temperatures.*

$T_{iso}$, *as reanalyzed in Part III (ref. [7]).* ● $(T_{62}-T_{iso})$ for $He^4$ isotherms; ■ $(T_{62}-T_{iso})$ for $He^3$ isotherms; ○,□ $(T_{58}-T_{iso})$ for $He^4$ and $He^3$ isotherms, respectively. To get $T_{62}$, Keller's $He^4$ vapor pressure thermometer readings are converted to equivalent $P_3$'s by means of direct $P_4$-to-$P_3$ interpolation equations derived in Part I (ref. [46]). Lengths of bars for the 1958 $He^4$ scale deviations are equal to the standard deviation for $T_{iso}$ as calculated in the analysis of the isotherm data. For 1962 $He^3$ scale deviations we add on the standard deviation of the conversion from $P_3$ to equivalent $P_4$. The $T_{62}$ and $T_{58}$ bars terminate in solid and open triangles respectively.

If it were possible the authors would acknowledge in detail the aid given by numerous cryogenists in the course of the development and evaluation of the 1962 $He^3$ scale of temperatures and the discussions concerning the scale by the Advisory Committee on Thermometry of the International Committee on Weights and Measures. We are especially indebted to F. G. Brickwedde, B. M. Abraham, H. van Dijk, M. Durieux, R. I. Joseph, W. E. Keller, D. W. Osborne, and J. H. van Vleck. Since our correspondence ran to several dozen letters it would be impractical to specify all of the participants and to elaborate on their various contributions.

TABLE 6. *The temperature derivative* $dP_3/dT_{62}$ *and deviations of various* $He^3$ *temperature scales from the present 1962* $He^3$ *scale*

Columns 3, 4, and 5 give differences of the $T_E$, $T_L$, and $T_K$ $He^3$ scales respectively from the 1962 $He^4$ scale in the form $(T_{62}-T_x)$ expressed in millidegrees. In Columns 6 and 7 are reproduced the deviations of the 1955 $He^4$ scales from the accepted 1958 $He^4$ scale as these deviations have been utilized by some investigators in an attempt to "update" the $T_E$ and $T_L$ $He^3$ scales.

| $T$ | $dP_3/dT_{62}$ | $T_{62}-T_L$ [a] | $T_{62}-T_E$ [a] | $T_{62}-T_K$ [b] | $(T_{L55}-T_{58})$ [c] | $(T_{55E}-T_{58})$ [c] |
|---|---|---|---|---|---|---|
| °K | mm Hg/°K | mdeg | mdeg | mdeg | mdeg | mdeg |
| 0.2 | 0.001 | | | | | |
| .3 | .066 | −5.0 | −6.3 | | | |
| .4 | .592 | −5.8 | −7.4 | | | |
| .5 | 2.283 | −6.2 | −8.1 | | | |
| .6 | 5.756 | −6.2 | −8.3 | | | |
| .7 | 11.362 | −5.8 | −8.2 | | −1.1 | 1.0 |
| .8 | 19.234 | −5.2 | −7.8 | | −1.2 | 1.1 |
| .9 | 29.379 | −4.4 | −7.3 | | −1.3 | 1.2 |
| 1.0 | 41.745 | −3.6 | −6.7 | −4.0 | −1.5 | 1.3 |
| 1.1 | 56.26 | −2.9 | −6.1 | −3.7 | −1.6 | 1.4 |
| 1.2 | 72.84 | −2.1 | −5.4 | −3.2 | −1.7 | 1.5 |
| 1.3 | 91.44 | −1.5 | −4.9 | −2.5 | −1.8 | 1.5 |
| 1.4 | 111.99 | −0.9 | −4.4 | −1.6 | −1.9 | 1.6 |
| 1.5 | 134.45 | −.4 | −3.9 | −0.7 | −2.0 | 1.6 |
| 1.6 | 158.78 | .0 | −3.4 | 0.2 | −2.1 | 1.5 |
| 1.7 | 184.94 | .3 | −3.1 | 1.1 | −2.1 | 1.4 |
| 1.8 | 212.92 | .5 | −2.8 | 2.0 | −2.2 | 1.1 |
| 1.9 | 242.68 | .7 | −2.4 | 2.7 | −2.2 | 0.8 |
| 2.0 | 274.22 | .9 | −2.0 | 3.4 | −2.2 | 0.6 |
| 2.1 | 307.51 | 1.1 | −1.6 | 3.9 | −2.2 | 0.6 |
| 2.2 | 342.57 | 1.4 | −1.1 | 4.3 | −2.2 | 0.8 |
| 2.3 | 379.40 | 1.6 | −0.6 | 4.5 | −2.1 | 0.5 |
| 2.4 | 418.03 | 1.9 | 0.0 | 4.5 | −2.0 | 0.0 |
| 2.5 | 458.53 | 2.2 | 0.6 | 4.4 | −1.9 | −0.4 |
| 2.6 | 500.96 | 2.5 | 1.3 | 4.1 | −1.8 | −0.7 |
| 2.7 | 545.46 | 2.7 | 1.9 | 3.5 | −1.5 | −0.9 |
| 2.8 | 592.18 | 2.9 | 2.4 | 2.7 | −1.3 | −1.1 |
| 2.9 | 641.34 | 2.8 | 2.7 | 1.5 | −0.9 | −1.1 |
| 3.0 | 693.22 | 2.5 | 2.9 | 0.0 | −0.6 | −1.1 |
| 3.1 | 748.16 | 1.9 | 2.6 | −2.0 | −0.2 | −1.1 |
| 3.2 | 806.61 | 0.6 | 1.7 | −4.7 | 0.2 | −0.9 |
| 3.3 | 869.11 | −1.3 | 0.1 | −8.0 | 0.7 | −0.7 |

[a] Ref. [9]
[b] Refs. [5, 41]
[c] Ref. [2]

## References*

[1] S. G. Sydoriak, T. R. Roberts, and R. H. Sherman, Proc. 7th Intern. Conf. Low Temperature Physics, ed. G. M. Graham and A. C. Hollis-Hallett (Univ. of Toronto Press, Toronto, 1961), ch. 30, p. 717.
[2] F. G. Brickwedde, H. van Dijk, M. Durieux, J. R. Clement, and J. K. Logan, J. Res. NBS **64A** (Phys. & Chem.), 1 (1960).
[3] D. F. Brewer, A. K. Sreedhar, H. C. Kramers, and J. G. Daunt, Phys. Rev. **115,** 836 (1959).
[4] B. Weinstock, B. M. Abraham, and D. W. Osborne, Nuovo Cimento Suppl. **9,** 310 (1958).
[5] B. M. Abraham, D. W. Osborne, and B. Weinstock, Phys. Rev. **80,** 366 (1950).
[6] S. G. Sydoriak, T. R. Roberts, and R. H. Sherman, Paper II of this series.
[7] T. R. Roberts, R. H. Sherman, and S. G. Sydoriak, Paper III of this series.
[8] R. H. Sherman, S. G. Sydoriak, and T. R. Roberts, Paper IV of this series. See also Los Alamos Scientific Lab. Rept. LAMS 2701 (July 1962).

*This list of references applies to papers I, II, III, and IV of this series. For completeness and convenience, it is reproduced in its entirety at the end of each paper.

[9] S. G. Sydoriak and T. R. Roberts, Phys. Rev. **106,** 175 (1957).
[10] T. R. Roberts, S. G. Sydoriak, and R. H. Sherman, Proc. 4th Symp. Temperature, Its Measurement and Control in Science and Industry, ed. C. M. Herzfeld (Reinhold Publ. Corp., New York, 1962), Vol. 3, pt. 1, p. 75.
[11] W. E. Keller, Phys. Rev. **97,** 1 (1955); **100,** 1790 (1955).
[12] W. E. Keller, Phys. Rev. **98,** 1571 (1955).
[13] F. E. Hoare and J. E. Zimmerman, Rev. Sci. Instr. **30,** 184 (1959); R. T. Swim, Advances in Cryogenic Engineering, ed. K. D. Timmerhaus (Plenum Press, Inc., New York, 1960), Vol. 5, pp. 498–504.
[14] H. H. Plumb, Proc. 10th Intern. Congr. Refrigeration, Copenhagen, 1959, ed. M. Jul and A. M. S. Jul (Pergamon Press, Paris, 1960), Vol. 1, pp. 184–187.
[15] M. Durieux, Thermometry at Liquid Helium and Liquid Hydrogen Temperatures, Thesis, Leiden Univ. (16 Mar. 1960).
[16] F. G. Brickwedde, Report on the Conference Agreement on the Helium Vapor-Pressure Scale of Temperatures, Conf. Physique des Basses Temperatures, Paris, 2–8 Septembre 1955, pp. 608–610.
[17] B. Bleaney and F. Simon, Trans. Faraday Soc. **35,** 1205 (1939).
[18] B. Bleaney and R. A. Hull, Proc. Roy. Soc. (London) **178A,** 74 (1941).
[19] J. de Boer and E. G. D. Cohen, Physica **17,** 993 (1951).
[20] E. W. Becker and R. Misenta, Phys. Rev. **93,** 244 (1954).
[21] E. W. Becker, R. Misenta, and F. Schmeissner, Z. Physik **137,** 126 (1954).
[22] K. Mendelssohn and G. K. White, Proc. Phys. Soc. (London) **A63,** 1328 (1950).
[23] R. Bowers and K. Mendelssohn, Nature **163,** 870 (1949); Proc. Phys. Soc. (London) **A63,** 1318 (1950).
[24] K. W. Taconis, Progress in Low Temperature Physics, ed. C. J. Gorter (North Holland Publ. Co., Amsterdam, The Netherlands, 1961), Vol. 3, p. 154.
[25] H. van Dijk and M. Durieux, Physica **24,** 1 (1958).
[26] S. G. Sydoriak and H. S. Sommers, Jr., Rev. Sci. Instr. **22,** 915 (1951).
[27] P. Kapitza, J. Phys. (U.S.S.R.) **4,** 181 (1941).
[28] H. A. Fairbank and J. Wilks, Proc. Roy. Soc. (London) **A231,** 545 (1955).
[29] L. J. Challis, K. Dransfeld, and J. Wilks, Proc. Roy. Soc. (London) **A260,** 31 (1961).
[30] Kuang Wey-Yen, Zh. Experim. i Teor. Fiz. (U.S.S.R.) **42,** 921 (1962); Soviet Phys. JETP (English Transl.) **15,** 635 (1962).
[31] I.M. Khalatnikov, Zh. Experim. i Teor. Fiz. (U.S.S.R.) **22,** 687 (1952).
[32] S. G. Sydoriak and T. R. Roberts, Phys. Rev. **118,** 901 (1960).
[33] R. L. Mills, E.R. Grilly, and S. G. Sydoriak, Ann. Phys. **12,** 41 (1961).
[34] W. Cawood and H. S. Patterson, Trans. Faraday Soc. **29,** 522 (1933).
[35] J. Kistemaker, Leiden Commun. **268d** (1944); Physica **11,** 277 (1944–1946); B. E. Blaisdell, J. Math. Phys. **19,** 186 (1940).
[36] W. G. Brombacher, D. P. Johnson, and J. L. Cross, Mercury Barometers and Manometers, NBS Mono. 8 (U.S. Govt. Printing Office, Washington, 1960).
[37] T. R. Roberts and S. G. Sydoriak, Phys. Rev. **102,** 304 (1956).
[38] B. N. Esel'son and N. G. Berezniak, Zh. Experim. i Teor. Fiz. (U.S.S.R.) **30,** 628 (1956); Soviet Phys. JETP (English Transl.) **3,** 568 (1956).
[39] S. G. Sydoriak, E. R. Grilly, and E. F. Hammel, Phys. Rev. **75,** 303 (1949).
[40] V. P. Peshkov, Zh. Experim. i Teor. Fiz. (U.S.S.R.) **33,** 833 (1957); Soviet Phys. JETP (English Transl.) **4,** 645 (1958).
[41] H. van Dijk and D. Shoenberg, Nature **164,** 151 (1949).
[42] T. C. Chen and F. London, Phys. Rev. **89,** 1038 (1953).
[43] W. E. Keller, Nature **178,** 883 (1956); J. R. Clement, Low Temperature Physics and Chemistry (Univ. of Wisconsin Press, Madison, 1958), p. 187 (Proc. 5th Intern. Conf. Low Temperature Physics and Chemistry, Madison, Wis., 1957).
[44] L. Goldstein, Phys. Rev. **496,** 155 (1954); Phys. Rev. **102,** 1205 (1956).
[45] R. H. Sherman, T. R. Roberts, and S. G. Sydoriak, Supplement au Bulletin de l'Institut International du Froid, Annexe 1961–5, p. 125 (Proc. Meeting of Commission I of the International Institute of Refrigeration, London, 1961).
[46] S. G. Sydoriak and R. H. Sherman, Paper I of this series.
[47] W. E. Deming, Statistical Adjustment of Data (John Wiley & Sons, New York, 1943).
[48] T. R. Roberts, S. G. Sydoriak, and R. H. Sherman, see ref. [45], p. 115.
[49] E. R. Grilly and E. F. Hammel, Progress in Low Temperature Physics III (1961), pp. 113–152.
[50] E. C. Kerr and R. D. Taylor, Proc. 7th Intern. Conf. Low Temperature Physics, ch. 24, pp. 605–608, ed. G. M. Graham and A. C. Hollis-Hallett (Univ. of Toronto Press, Toronto, 1961).
[51] R. H. Sherman and F. J. Edeskuty, Ann. Phys. **9,** 522 (1960).
[52] T. R. Roberts, R. H. Sherman, S. G. Sydoriak, and F. G. Brickwedde, Progress in Low Temperature Physics IV, ch. 10 (North Holland Publ. Co., Amsterdam, The Netherlands, 1964), p. 480
[53] A. M. Mood, Introduction to the Theory of Statistics, p. 299 (McGraw-Hill, New York, N.Y., 1950).
[54] M. Durieux, Procès-Verbaux du Comité Consultatif de Thermométrie auprès du Comité International des Poids et Mesures, 6e Session, 1962 (Gauthier-Villars, Paris, France, 1964), p. 190.
[55] D. W. Osborne, private communication.
[56] R. Berman and C. F. Mate, Phil. Mag. **3,** 461 (1958).
[57] H. van Dijk, Progr. Cryog. **2,** p. 125 (Academic Press, Inc., New York, N.Y., 1962).
[58] G. Cataland and H. H. Plumb, Proc. 8th Intern. Conf. Low Temperature Physics, London, Sept. 16–22, 1962, ed. R. O. Davies (Butterworths, Washington, D.C., 1963), pp. 439–40.
[59] E. C. Kerr, Phys. Rev. **96,** 551 (1954).
[60] E. C. Kerr and R. D. Taylor, Ann. Phys. **20,** 450 (1962).
[61] A. C. Anderson, G. L. Salinger, W. A. Steyert, and J. C. Wheatley, Phys. Rev. Letters **6,** 331 (1961); A. C. Anderson, W. Reese, and J. C. Wheatley, Phys. Rev. **130,** 495 (1963).
[62] M. Strongin, G. O. Zimmerman, and H. A. Fairbank, Phys. Rev. **128,** 1983 (1962).
[63] B. M. Abraham, D. W. Osborne, and B. Weinstock, Phys. Rev. **98,** 551 (1955).
[64] G. R. Grove and W. J. Haubach, Jr.; see ref. [58], p. 441. For further information, write Gaseous Isotope Sales, Montsanto Research Corporation, Mound Laboratory, Miamisburg, Ohio.
[65] D. O. Edwards and J. G. Daunt, Phys. Rev. **124,** 640 (1961).
[66] S. G. Sydoriak, T. R. Roberts, and R. H. Sherman; see ref. [58], pp. 437–8.
[67] J. A. Hall, Sixième Rapport du Comité Consultatif de Thermométrie au Comité International des Poids et Mesures; see ref. [54].
[68] H. F. Stimson, NBS Tech. News Bull. **47,** No. 2, 30 (Feb. 1963); Nature **197,** 1055 (1963).
[69] F. G. Brickwedde, Phys. Today **16,** 24 (1963).
[70] S. Weber, Commun. Kamerlingh Onnes Lab. Univ. Leiden Suppl. **71b** (1932), **264b** and **264d** (1936).
[71] S. Weber and G. Schmidt, Commun. Kamerlingh Onnes Lab. Univ. Leiden **264c** (1936).
[72] C. E. Chase, E. Maxwell, and W. M. Whitney, Physica **26,** 160 (1960); C. E. Chase, E. Maxwell, and W. E. Millett, Physica **27,** 1129 (1961).
[73] R. H. Moore and R. K. Zeigler, Trans. Am. Nuclear Soc. **1,** 128–9 (1958); The Solution of the General Least Squares Problem with Special Reference to High-Speed Computers, Los Alamos Scientific Lab. Rept. LA–2367 (Mar. 4, 1960).
[74] T. R. Roberts and B. K. Swartz, Proc. 2d Symp. Liquid and Solid Helium Three, ed. J. G. Daunt (Ohio State Univ. Press, Columbus, 1960), p. 163.

(Paper 68A6–302)

JOURNAL OF RESEARCH of the National Bureau of Standards—A. Physics and Chemistry
Vol. 68A, No. 6, November–December 1964

# The 1962 $He^3$ Scale of Temperatures[1] III. Evaluation and Status[2]

T. R. Roberts, R. H. Sherman, and S. G. Sydoriak

Los Alamos Scientific Laboratory, University of California
Los Alamos, N. Mex.

(June 16, 1964)

In this third paper the 1962 $He^3$ Scale of Temperatures is evaluated both as to its precision and its deviations from the thermodynamic Kelvin Scale. Various thermodynamic quantities of $He^3$ consistent with the 1962 $He^3$ Scale are derived and listed. The correction to an observed vapor pressure for small amounts of $He^4$ is discussed and tabulated. A description is given of the method of multiple variable least squares analysis used for deriving the final scale equation and for re-analysis of isotherm data. Finally the present status of the 1962 $He^3$ Scale is discussed along with some considerations for the future.

## 1. An Evaluation of the 1962 $He^3$ Scale

### 1.1. Fit of the Input 1961 L.A.S.L. Vapor-Pressure Data

One factor in evaluating the 1962 $He^3$ Scale is the fit of the input vapor-pressure data of Part I [46] to the Scale. Figure 1 and table 1 of Part II [6] show the deviations of the observed data from the final scale as $T_{62}(P_3)-T_{58}(P_4)$. The symbol $T_{62}$ is the temperature on the 1962 $He^3$ Scale corresponding to a $He^3$ vapor pressure, $P_3$, while $T_{58}$ is the temperature on the 1958 $He^4$ Scale [2] corresponding to the experimentally determined isothermal $He^4$ vapor pressure, $P_4$. The standard deviation of the data from the scale is 0.25 mdeg and the maximum deviation over the full range is 0.6 mdeg. The data may not scatter completely randomly. For example, the data points just below 2 °K are all below the 1958 $He^4$ Scale and the points just above 2 °K are all above the 1958 $He^4$ Scale. Hence, if one wished to obtain the vapor pressure of $He^3$ which is most probably isothermal with a given $He^4$ vapor pressure, a slightly better value (in terms of consistency with the observed data) may be obtained by drawing a smooth curve through these data points or by using direct interpolation equations as discussed in Part I. However, the overall fit of the Scale to the input data is very satisfactory in comparison with the errors of measurement of the two vapor pressures.

### 1.2. Fit of the Experimental Thermodynamic Equation (ETE) Scale

Below 0.9 °K the 1962 $He^3$ Scale was evaluated by examining its fit to the ETE Scale described in Part II. The ETE Scale is defined by a linear equation fitted to an empirical function, $F_x(P_3,T)$, of $He^3$ vapor pressure and temperature,

$$F_x(P_3,T)=(a+bT)/R. \qquad (1)$$

As shown by the full line curve in figure 1 of Part II, temperatures calculated from eq (1) are in good agreement with the 1962 $He^3$ Scale; nowhere below 2 °K do the scales differ by more than 0.4 mdeg. the 1962 $He^3$ Scale, defined by eq (9b) of Part II, is therefore in effect an ETE scale from 0.2 to 2° and an empirical scale above 2 °K.

The effect of possible errors in the various terms of the equation for the ETE scale, over the temperature range from 0.2 to 1.0 °K, should also be considered in evaluating the 1962 $He^3$ Scale. The ETE scale was obtained from a least squares fit of the $He^3$–$He^4$ vapor-pressure intercomparisons between 0.9 and 2.0 °K to eq (1). The function $F_x(P_3,T)$ is calculated for each experimental $P_3,T_{58}$-observation; deviations of this "observed" value of $F_x(P_3,T)$ from the fitted value, $[(a+bT_{58})/R]$, from eq (1) are shown as circles in figure 1. The function $F_x\ (P_3,T)$ is derived in Part II and in ref. [10] as

$$F_x(P_3,T)=T[(5/2)\ \ln\ T-\ln\ P_3+i_0 +f_x(V_L)-f_x(C_{sat})+\epsilon] \qquad (2)$$

[1] Much of the material in this paper III has been included in a review chapter [52] on the development of the scale.
[2] Work performed under the auspices of the U.S. Atomic Energy Commission.

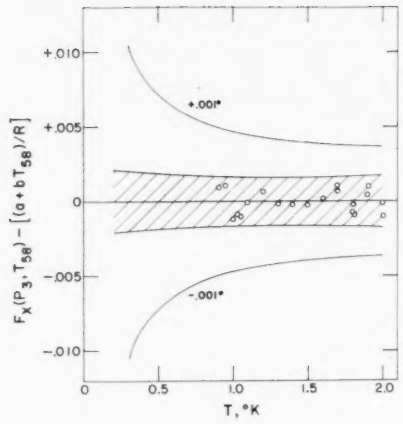


FIGURE 1.—*Deviations from the ETE Scale, eq (1).*

The circles are deviations from the fitted equation of the function $F_x(P_3,T_{58})$ calculated from eq (2) for each input $(P_3,T_{58})$ data point. The central cross-hatched area is the 95 percent prediction interval [53] for a prediction of $F_x(P_3,T)$ from eq (1) as calculated from the ± values for $a$ and $b$ given in eqs (3) and (4). The outermost solid curves represent a change in $F_x(P_3,T)$ corresponding to a 1 mdeg change in temperature and are calculated as $0.001\ T(d\ln P_3/dT)_{sat}$.

where $i_0$ is the chemical constant including the nuclear spin degeneracy; $f_x(V_L)$ is an empirical power series representing the theoretical and exact integral term,

$$f(V_L) \equiv (1/RT)\int_0^T V_L(dP_3/dT)_{sat}dT$$

involving the molar liquid volume, $V_L$; $f_x(C_{sat})$ is an equation for the theoretical and exact double integral term of eq (3a) of Part II, $f(C_{sat}) \equiv (1/RT)\int_1^T dT' \int_1^{T'} (C_{sat}/T'')dT''$, based on an empirical power series fitted between 0.2 and 2.0 °K to data for $C_{sat}$, the specific heat of the saturated liquid; and $\epsilon$ is the gas imperfection term, eq (4a) of Part II.

The least squares values for the coefficients $a$ and $b$ of eq (1), and their equivalent expressions from eqs (6) and (7) of Part II are

$$a = L_0 - \int_0^1 C_{sat}dT = 17.4459 \pm 0.0058 \text{ joule mole}^{-1} \quad (3)$$

and

$$b = S_L(1.0°) = 9.0098 \pm 0.0038 \text{ joule mole}^{-1} \text{ deg}^{-1}. \quad (4)$$

The *plus-or-minus* values for $a$ and $b$ were found from the fit of the data points to the straight line, $a+bT$. Mood [53] has given an equation for the prediction interval for a single prediction of $F_x(P_3,T)$ from eq (1) for any value of $T$. The ETE Scale is just the set of $P_3$ values obtained by solving eq (2) for ln $P_3$ at any given temperature using the predicted value of $F_x(P_3,T)$. Hence a prediction interval for $F_x(P_3,T)$ can be expressed as an equivalent prediction interval in $P_3$ by neglecting the contribution of possible errors in the other terms on the right hand side of eq (2).

The 95 percent prediction interval for a single prediction of $F_x(P_3,T)$ [with a 95 percent probability of containing the statistically "true" value of $F_x(P_3,T)$] is shown as the central cross-hatched area in figure 1. The outermost curves in this figure show the change in $F_x(P_3, T)$ corresponding to a one millidegree change in temperature. The same prediction intervals have been converted to equivalent temperature scale errors as listed in table 1.

The effects of random errors of ±3 percent in $f_x$ $(C_{sat})$ and $\epsilon$ on individual temperatures below 1° are also shown in table 1.

Systematic errors in $f_x(C_{sat})$, $\epsilon$ and in $f_x(V_L)$ would be compensated between 0.9° and 2.0° by the least squares process of fitting the $(P_3,T_{58})$ data to eq (1). The scale below 1° would be skewed by such errors as is shown in table 1 for assumed 3 percent systematic errors in all values of $C_{sat}$ or $\epsilon$. Table 1 also shows the systematic errors below 1° resulting from use of the approximate empirical function, $f_x(V_L)$, instead of the graphically integrated values of the true thermodynamic function, $f(V_L)$ [see table 4 of Part II].

Another possible source of systematic error is a smooth deviation of the 1958 $He^4$ Scale from the thermodynamic Kelvin Scale. The effect on the ETE scale of adding 2 mdeg to each scale input temperature is listed in table 1.

TABLE 1. *Effect of possible systematic or random errors on the ETE scale, eq (1)*

Systematic or random changes in the constants $a$ and $b$ of eqs (3) and (4) and of temperatures on the ETE scale below 1 °K are listed for the following arbitrary, but plausible, cases:

Case 1. the fit of the input $(P_3,T_{58})$ data expressed as the 95 percent confidence limit [53] for the prediction of a value of ln $P$ at any single temperature (see fig. 1);
Case 2. random errors of ±3 percent in $f_x$ $(C_{sat})$;
Case 3. random errors of ±3 percent in $\epsilon$, eq (4a) of Part II;
Case 4. a systematic error of −3 percent in all $C_{sat}$ values, and hence in $f_x(C_{sat})$;
Case 5. a systematic error of +3 percent in all values of $\epsilon$;
Case 6. the difference between the empirical function, $f_x(V_L)$, and the numerically integrated values of the thermodynamic term, $f(V_L) = \int_0^T V_L(dP/dT)_{sat}\,dT$; and
Case 7. the increase of all values of input temperatures between 0.9 and 2.0 °K by adding 0.002 deg to each $T_{58}$.

| Case | $\Delta a$ | $\Delta b$ | $\Delta T$ | | | | |
|---|---|---|---|---|---|---|---|
| | | | 1.0 °K | 0.8 °K | 0.6 °K | 0.4 °K | 0.2 °K |
| | *J/mole* | *J/mole deg* | *mdeg* | *mdeg* | *mdeg* | *mdeg* | *mdeg* |
| 1 | ±0.006 | ±0.004 | ±0.4 | ±0.3 | ±0.2 | ±0.2 | ±0.1 |
| 2 | | | 0.0 | ±0.1 | ±0.2 | ±0.4 | ±0.4 |
| 3 | | | ±0.2 | ±0.1 | 0.0 | 0.0 | 0.0 |
| 4 | 0.069 | −0.060 | 0.2 | 0.5 | 0.8 | 1.0 | 1.0 |
| 5 | 0.073 | −0.076 | 0.2 | 0.4 | 0.5 | 0.6 | 0.5 |
| 6 | | | −0.1 | −0.1 | −0.1 | 0.0 | 0.0 |
| 7 | 0.094 | −0.026 | | 1.7 | 1.5 | 1.2 | 0.7 |

The overall effect on the 1962 $He^3$ Scale of random errors in the specific heat of liquid $He^3$, the virial coefficient equations, and the 1958 $He^4$ Scale might amount to as much as three millidegrees. Durieux [54] has analyzed the 1962 $He^3$ Scale for the effects of possible errors and has reached similar conclusions.

### 1.3. Fit of the Argonne Laboratory Vapor-Pressure Data

The $He^3$–$He^4$ vapor-pressure intercomparisons of Abraham, Osborne, and Weinstock [5] have been used in deriving all previous $He^3$ temperature scales, but these were rejected for the 1962 $He^3$ Scale because of apparent thermodynamic inconsistency (see refs. [10 and 45]) with recent precise measurements of the latent heat of vaporization of $He^3$ by the same workers [4, 55]. The fit of the AOW vapor-pressure data to the 1962 $He^3$ Scale is shown in figure 2. Above 1.9° the agreement is within 0.5 mdeg. Below 1.5° the AOW data deviate systematically from the 1962 Scale indicating either that their $He^3$ vapor pressures were lower or that their $He^4$ pressures were higher than the data of Sydoriak and Sherman (Part I). For encircled points in figure 2, a $He^4$ vapor pressure bulb was fastened to the $He^3$ bulb. The $He^4$ pressure may have been high because of insufficient correction for effects due to the refluxing superfluid film. For the uncircled crosses and dots, the $He^4$ bath pressure was measured in the pumping line in a warm part of the apparatus. The corrected $He^4$ pressures as published may have been high because the effluent gas was significantly colder than the tip of the pressure-sensing tube, thus increasing the actual thermomolecular pressure difference.

### 1.4. Fit of Heat-of-Vaporization Data

Heat-of-vaporization, $L$, data may be used to test the thermodynamic consistency of the temperature scale. The equations used may be either

$$L=T(S_G-S_L) \tag{5}$$

with the vapor entropy, $S_G$, calculated from the Sackur-Tetrode equation, or

$$L=T(V_G-V_L)(dP/dT)_{sat} \tag{6}$$

from the Clausius-Clapeyron equation. The use of these equations for testing $He^4$ scales of temperature has been discussed extensively; see van Dijk and Durieux [25], Durieux [15], Berman and Mate [56], and Keller [43].

The liquid entropy at 1.0 °K (or any other temperature) may be calculated from eq (5) and data for $C_{sat}$ as

$$S_L(1.0°)=S_G(T)-(L/T)-\int_{1.0}^{T}(C_{sat}/T')dT'. \tag{7}$$

The Argonne (WAO) heat-of-vaporization measurements [4] were undertaken in order to determine the entropy of liquid $He^3$ in this way.

At one stage of the derivation of the 1962 $He^3$ Scale, it was proposed [10] to use all the WAO heat-of-vaporization data and eq (7) to get an average value for $S_L(1.0°)$, which is just the coefficient, $b$, in eqs (1) and (4). Then, values of $(a/R)=F_x(P_3,T)-(bT/R)$ from eq (1) were computed for every vapor-pressure datum point between 0.9 and 2.0 °K. This two-step method failed to converge on a stable, consistent pair of constants $a$ and $b$, and led to the decision to undertake the new L.A.S.L. intercomparisons of the vapor pressures of $He^3$ and $He^4$. Analysis of the new intercomparisons [45] by this same two-step method also failed to yield a consistent set of $a$ and $b$ values, although these data showed much less scatter, as shown in figure 3. The heat-of-vaporization data were not used to determine the 1962 $He^3$ Scale; instead $a$ and $b$ values were obtained by a least squares fit of the $He^3$ vapor-pressure data to eq (1) using for $T$ the $T_{58}$

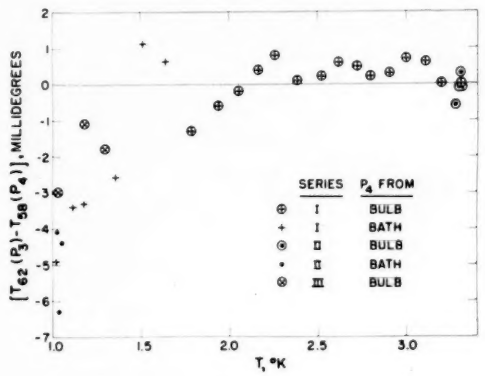


FIGURE 2.—*The deviation in millidegrees of the 1950 Abraham, Osborne, and Weinstock* [5] ($P_3$, $P_4$) *data from the 1962* $He^3$ *Scale:* $T_{62}(P_3)-T_{58}(P_4)$.

The uncircled crosses and small dots are data points below the λ-point for which the $He^4$ cryostat bath pressure was published as $P_4$. For the encircled points a $He^4$ vapor pressure bulb was fastened to the $He^3$ bulb.

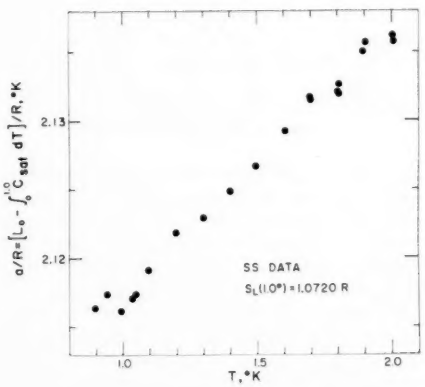


FIGURE 3.—*Demonstration of the remaining thermodynamic inconsistency between eqs (1) and (7) involving the* $He^3$ *latent-heat data,* ($L$, $P_3$)*, of Weinstock, Abraham, and Osborne* [4], [55]*; the* ($P_3$, $P_4$) *intercomparisons of Sydoriak and Sherman* [46]*; and the 1958* $He^4$ *Scale* [2], $T_{58}(P_4)$.

The indicated value of $S_L(1.0°)$ is the average of nine values calculated from eq (7) for the WAO ($L$,$P_3$) data and is about 1 percent lower than the 1962 $He^3$ Scale value for that entropy, eq (4). The solid circles are the individual values of the theoretical constant, $(a/R)$, in eq (1) calculated for each ($P_3$,$T_{58}$) data point as $F_x(P_3,T_{58})-[S_L(1.0°)\,T_{58}/R]$ using the indicated average value of $S_L(1.0°)$.

values that corresponded to the $He^4$ vapor pressures observed concurrently with the $He^3$ vapor pressures.

The 1958 WAO heat-of-vaporization data may be used to test the 1962 $He^3$ Scale in the manner explained by Durieux [15]. In terms of an apparent heat of vaporization, $L_a$ (defined as the heat necessary to evolve a mole of gas outside of a calorimeter), eq (6) becomes

$$L_a = TV_G(dP/dT)_{sat}$$
$$= -R(1+B/V_G+C/V_G^2)[d\ln P/d(1/T)]_{sat}$$
$$= RT^2Z(d\ln P/dT)_{sat} \quad (8)$$

where the compressibility coefficient, $Z \equiv (PV_G/RT) = (1+B/V_G+C/V_G^2)$ from the density virial form of the equation of state.

As shown in figure 4, the observed values of $L_a$ average about 0.5 percent higher than the values calculated from the 1962 $He^3$ Scale using eq (8), a deviation considerably in excess of the estimated 0.1 percent accuracy [55] of the $L_a$ measurements. Durieux [15] calculates that the $L_a$ values of Berman and Mate [56] for $He^4$ average 0.76 percent higher than the values calculated from the 1958 $He^4$ Scale between 2.2 and 3.0 °K. These differences may be due in part to a deviation of the 1962 $He^3$ and 1958 $He^4$ Scales from the true thermodynamic temperature scale. An estimate of such a difference may be obtained by neglecting the variation of $(d\ln P/dT)_{sat}$ and $Z$ in eq (8). In this case $\delta T/T \approx (1/2)(\delta L_a)/L_a$. From the dashed curve drawn through the $He^3$ data of figure 4 this estimate of $\delta T$ varies from 3 mdeg at 1.2 °K to 1 mdeg at 2.0 °K, a not unreasonable range of deviations. For the $He^4$ data, this approximation yields values from 8 mdeg at 2.2 °K up to 11 mdeg at 3.0 °K which are much larger than appears reasonable for the departure of the 1958 $He^4$ Scale from the thermodynamic scale. An error in the temperature scale also would cause both $(d\ln P/dT)_{sat}$ and $Z$ to change.

### 1.5. Fit of Gas Thermometer, Isotherm, and Acoustic Interferometer Measurements

In principle, gas thermometer, isotherm and acoustic interferometer measurements of the absolute temperature associated with a $He^4$ vapor pressure may be used to check the 1962 $He^3$ Scale by directly interpolating the $He^4$ vapor pressure to an isothermal $He^3$ vapor pressure. The direct interpolation equations and table described in Part I are usable for this interpolation of $He^4$ vapor pressures. Since the 1962 $He^3$ Scale has been made to agree so closely with the 1958 $He^4$ Scale, at least in terms of the $(P_3, P_4)$ data of Part I, little really significant new information would be expected from this kind of comparison.

Van Dijk [57] has critically reanalyzed all published gas thermometer and isotherm measurements and compared them with the 1958 $He^4$ Scale. The majority of these measurements between 1.5 and 3.3 °K seem to indicate that the thermodynamic

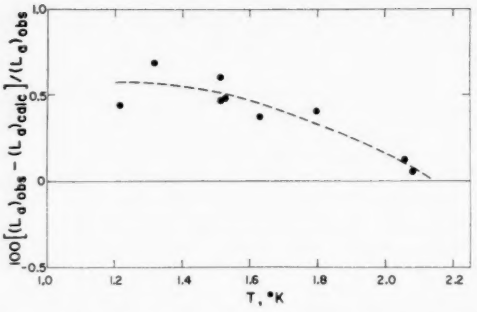


FIGURE 4.—*Deviations of the values of* $L_a$, *the apparent latent heat of vaporization (see sec. 1.4), observed by Weinstock, Abraham, and Osborne [4, 55] from values of* $L_a$ *calculated for the 1962* $He^3$ *Scale from eq (8) using eqs (10) and (11).*

temperature may be several millidegrees higher than $T_{58}$, although the data scatter over a range of about ±10 mdeg from $T_{58}$.

Two preliminary acoustic interferometer results of Cataland and Plumb [58] indicate thermodynamic temperatures that are 3±2 mdeg higher than $T_{58}$ at 2.0 and 2.2 °K.

The isotherm measurements of Keller [11, 12] are generally conceded to be the most accurate in the liquid helium temperature range, and are the only data for gaseous $He^3$. During the derivation of the 1962 $He^3$ Scale, the isotherm data of Keller were reanalyzed [10, 48] by Deming's method [47] of least squares adjustment with errors in more than one measured variable (see appendix A). For the isotherm measurements the observed pressures for each data point were corrected or normalized to a calculated value which would have been observed if the cell volume were at the normalized temperature for the set of data points. This normalized temperature, $T_{N,58}$, was taken as the temperature on the 1958 $He^4$ Scale corresponding to $\bar{P}_4$, the average $He^4$ vapor pressure for the set of data. The values of $\bar{P}_4$ and $T_{N,58}$ are listed in tables 2 and 3. The method of normalization was essentially the same as that described in detail by Keller [11].

For the isotherm measurements the quantity minimized by the least squares adjustment was $\sum[W_p(P_0-P_c)^2+W_n(N_0-N_c)^2]$ where the independently observed variables are $P_0$, the normalized helium gas pressure, and $N_0$, the molar density. The fitted function was

$$F(P_c, N_c) = P_c - N_cRT(1+BN_c+CN_c^2) = 0 \quad (9)$$

where $B$ and $C$ are the second and third virial coefficients, $T$ is the isotherm temperature for a normalized set of data, and $P_c$ and $N_c$ are the calculated or adjusted values of $P$ and $N$. The individual weights, $W_p$ and $W_n$, were calculated from Keller's assignment of errors in the various observed quantities.

TABLE 2. *Summary of reanalysis of Keller's gaseous* $He^3$ *isotherms [12]*

The isotherm designations, the data points, and the method of normalization for each isotherm are the same as those used by Keller. $\overline{P}_4$ is the average $He^4$ vapor pressure for each isotherm and $\overline{P}_3$ is the average $He^3$ vapor pressure for the $\alpha$ isotherm. $T_{58}(\overline{P}_4)$ is the normalized temperature for each isotherm and is the 1958 $He^4$ Scale temperature corresponding to $\overline{P}_4$. $P_3(\overline{P}_4)$ is the directly interpolated $He^3$ vapor pressure corresponding to $\overline{P}_4$, using the direct interpolation equations described in Part I, and $T_{62}[P_3(\overline{P}_4)]$ is the 1962 $He^3$ Scale temperature corresponding to $P_3(\overline{P}_4)$. The values of $T_{iso}$, $B$, and $C$ listed under the heading "Three-constant fit" were obtained by solving eq (9) using Deming's method of least squares adjustment with errors in two measured variables (see appendix A). The standard errors and the weighted variance are calculated in accordance with the statistical formulas given by Deming [47]. The two constant fit values of $T_{iso}$ and $B$ were obtained by solving eq (9) assuming $C=0$. For the For the $\gamma$, $\delta$, and $\epsilon$ isotherms the variance of the three-constant fit is lower and the values of $C$ are greater than the magnitude of their statistically assigned errors. Therefore the three constant fit solutions were used for fitting $He^3$ virial coefficient equations, eqs (10) and (11), and for the temperature differences shown in figure 2 of Part II.

| Isotherm | Units | $\gamma$ | $\delta$ | $\alpha$ | $\epsilon$ | $\beta$ |
|---|---|---|---|---|---|---|
| No. of points | | 18 | 18 | 11 | 10 | 8 |
| $\overline{P}_4$ | mm Hg | 489.52 | 178.09 | 36.16 | 13.070 | 3.782 |
| $T_{58}(\overline{P}_4)$ | mdeg | 3779.1 | 2985.3 | 2154.2 | 1813.4 | 1510.3 |
| $P_3(\overline{P}_4)$ | mm Hg | | 607.70 | 197.43 | 105.33 | 52.21 |
| $\overline{P}_3$ | mm Hg | | | 197.62 | | |
| $T_{62}[P_3(\overline{P}_4)]$ | mdeg | | 2985.2±0.2 | 2154.4±0.2 | 1813.1±0.2 | 1510.2±0.2 |
| $T_{62}(\overline{P}_3)$ | mdeg | | | 2.1550 | | |
| THREE-CONSTANT FIT | | | | | | |
| $T_{iso}$ | mdeg | 3782.3±2.2 | 2992.4±1.6 | 2153.7±1.0 | 1816.4±0.8 | 1510.4±2.5 |
| $B$ | $cm^3$/mole | −65.50±0.86 | −86.31±0.52 | −118.81±1.35 | −145.08±1.61 | −162.15±10.7 |
| $C$ | $cm^6$/$mole^2$ | 1192±306 | 1746±136 | 548±822 | 2611±1289 | −11,069±16,390 |
| Variance | | 7.0 | 13.8 | 6.1 | 0.86 | 4.8 |
| $(T_{58}-T_{iso})$ | mdeg | −3.3±2.2 | −7.1±1.6 | 0.5±1.0 | −3.0±0.8 | −0.1±2.5 |
| $(T_{62}-T_{iso})$ | mdeg | | −7.2±1.8 | 0.7±1.2 | −3.2±1.0 | −0.2±2.7 |
| $(T_{62}(\overline{P}_3)-T_{iso})$ | mdeg | | | 1.3±1.0 | | |
| TWO-CONSTANT FIT | | | | | | |
| $T_{iso}$ | mdeg | 3774.4±1.3 | 2974.4±2.8 | 2153.2±0.6 | 1814.9±0.4 | 1512.0±0.7 |
| $B$ | $cm^3$/mole | −62.18±0.19 | −79.66±0.33 | −117.92±0.26 | −141.87±0.29 | −169.30±1.15 |
| Variance | | 13.2 | 156 | 5.7 | 1.20 | 4.4 |

TABLE 3. *Summary of reanalysis of Keller's gaseous* $He^4$ *isotherms [11]*

The various quantities have the same meaning as in table 2. The three constant fits gave a statistically better fit for only one isotherm, so the results of the two constant fits have been accepted as being more meaningful and have been used for figure 2 of Part II.

| Isotherm | Units | A | B | C | D | E |
|---|---|---|---|---|---|---|
| No. of points | | 12 | 14 | 12 | 17 | 9 |
| $\overline{P}_4$ | mm Hg | 588.55 | 291.31 | 147.55 | 52.758 | 35.541 |
| $T_{58}(\overline{P}_4)$ | mdeg | 3954.2 | 3339.2 | 2864.0 | 2315.1 | 2147.3 |
| $P_3(\overline{P}_4)$ | mm Hg | | | 528.42 | 254.50 | 195.21 |
| $T_{62}[P_3(\overline{P}_4)]$ | mdeg | | | 2864.0±0.2 | 2315.0±0.2 | 2147.6±0.2 |
| TWO-CONSTANT FIT | | | | | | |
| $T_{iso}$ | mdeg | 3953.7±2.1 | 3338.4±2.1 | 2863.5±0.9 | 2316.7±2.3 | 2148.9±0.9 |
| $B$ | $cm^3$/mole | −83.97±0.66 | −103.60±0.78 | −124.16±0.63 | −153.38±4.21 | −176.04±2.04 |
| Variance | | 8.7 | 17.8 | 3.6 | 23.4 | 1.69 |
| $(T_{58}-T_{iso})$ | mdeg | −1.5±2.1 | 0.8±2.1 | 0.5±0.9 | −1.6±2.3 | −1.6±0.9 |
| $(T_{62}-T_{iso})$ | mdeg | | | 0.5±1.1 | −1.7±2.5 | −1.3±1.1 |
| THREE-CONSTANT FIT | | | | | | |
| $T_{iso}$ | mdeg | 3953.8±4.3 | 3335.3±3.7 | 2860.9±1.5 | 2311.9±6.1 | 2146.5±2.8 |
| $B$ | $cm^3$/mole | −82.16±3.52 | −99.80±3.78 | −118.47±2.86 | −132.1±25.7 | −162.6±15.8 |
| $C$ | $cm^6$/$mole^2$ | −1452±2773 | −3133±3042 | −6741±3331 | −50,490±60,020 | −38,900±45,160 |
| Variance | | 9.4 | 17.7 | 2.8 | 23.9 | 1.75 |

The results of the reanalysis of Keller's gaseous $He^3$ data [12] were fitted to empirical equations for the $He^3$ second and third virial coefficients. These equations are

$$B=(4.942-270.976/T) \text{ cm}^3/\text{mole} \quad (10)$$

and

$$C=(2866/\sqrt{T}) \text{ cm}^6/\text{mole}^2. \quad (11)$$

The deviations of both $He^3$ and $He^4$ isotherm temperatures from the 1962 $He^3$ and 1958 $He^4$ Scales are shown in figure 2 of Part II. Keller used a $He^4$ vapor-pressure thermometer for all but one of his isotherms, but his observed $P_4$'s have been interpolated to $P_3$'s by use of the direct interpolation equations of Part I. The weighted average of the isotherm temperatures is $1.50 \pm 1.0$ mdeg above the corresponding $T_{58}$ values and $1.52 \pm 1.2$ mdeg above the $T_{62}$ values. For one isotherm $He^3$ containing about 0.25 percent $He^4$ was condensed in the vapor-pressure bulb. The corrected average pressure for pure $He^3$ was $197.62 \pm 0.02$ mm Hg ($T_{62}=2.1550$ °K) at an isotherm temperature of $2.1537 \pm 0.0010$ °K. It was concluded that nothing would be gained by trying to base a $He^3$ scale more directly on these isotherm temperatures since the 1958 $He^4$ Scale is based on these data. Moreover, the 1962 $He^3$ Scale, as it has been set up to agree with the 1958 $He^4$ Scale, adequately expresses the experimental $He^3-He^4$ vapor-pressure relation for most practical purposes.

## 2. Thermodynamic Properties of $He^3$ Consistent with the 1962 $He^3$ Scale

Two temperatures which are frequently given in discussing helium vapor pressure scales are the boiling point and the critical point. The boiling point of $He^3$ on the 1962 $He^3$ Scale, at a vapor pressure of 760 mm Hg at 0 °C and standard gravity, is 3.1905 °K. The temperature at the critical point for $He^3$ was measured by Sydoriak and Sherman [46] by observing the $He^4$ vapor pressure. This measured critical temperature on the 1958 $He^4$ Scale was $3.3240 \pm 0.0018$ °K at a $He^3$ critical pressure, $P_c$, of $873.0 \pm 1.5$ mm Hg. The calculated critical temperature on the 1962 $He^3$ Scale is the temperature given by eq (9b) of Part II [6] corresponding to $P_c$ and is $3.3246 \pm 0.0017$ °K. This close agreement with the directly measured temperature is quite gratifying and somewhat unexpected since the scale-defining equation was fitted over the full range of the vapor-pressure intercomparisons.

Table 4 gives a number of quantities which are consistent with the 1962 $He^3$ Scale, including, for comparison, values of $He^4$ vapor pressures from the 1958 $He^4$ Scale. The concentration derivative of $\ln P_X$, $(d \ln P_X/dX)_{T,X=1}$, where $X$ is the mole fraction of $He^3$ and $P_X$ is the corresponding mixture vapor pressure, is useful for correcting for the $He^4$ impurity in a $He^3$ vapor-pressure thermometer. This correction is discussed in section 3.

The table values for $C_{sat}$, the specific heat of the saturated liquid, were calculated from the empirical equation, eq (3b) of Part II, fitted to specific-heat data for the derivation of the 1962 $He^3$ Scale. The calculated values agree with the experimental data to $\pm 1$ percent; the deviations are given in table 2 of Part II. Values for $S_L$, the entropy of the saturated liquid, were calculated from the relation

$$S_L(T)=S_L(1.0°)+\int_{1.0}^{T}(C_{sat}/T')dT' \quad (12)$$

using the above-mentioned $C_{sat}$ equation and the 1962 $He^3$ Scale value of $S_L(1.0°)$, given in eq (4).

Values for the second and third virial coefficient were calculated from eqs (10) and (11) while $V_G$, the molar volume of the saturated vapor, was calculated from the equation given for $Z$ in eq (8). These calculated values of $V_G$ agree to within 1 percent with the smoothed fit to the experimental data of Kerr [59] up to 2.8 °K. The values of $V_L$, the molar volume of the saturated liquid, are taken from the table of Kerr and Taylor [60]. The values of $L$, the heat of vaporization, are calculated from eq (6).

TABLE 4. *Thermodynamic properties of* $He^3$ *and vapor pressures of* $He^4$ *consistent with the 1962* $He^3$ *Scale*

| $T$ | $P_3$ | $P_4(T_{58})$ | $\left(\frac{d \ln P_3}{dT}\right)$ | $\left(\frac{d \ln P_X}{dX}\right)_T$ at $X=1$ (see note†) | $C_{sat}$ | $S_L$ | Virial coeff. B | Virial coeff. C | $V_G$ | $V_L$ | $L$ |
|---|---|---|---|---|---|---|---|---|---|---|---|
| °K | microns Hg at 0 °C and std. g | | deg$^{-1}$ | | J/deg mole | J/deg mole | cm$^3$/mole | cm$^6$/mole$^2$ | cm$^3$/mole | cm$^3$/mole | J/mole |
| 0 | | | | 0 | | 0 | | | | 36.8346 | 20.56 |
| 0.2 | 0.0121 | | 73.32 | 0.23 | 2.728 | 3.703 | −1350 | 6409 | $103 \times 10^7$ | 36.7809 | 24.29 |
| 0.4 | 28.115 | | 21.04 | 0.47 | 3.146 | 5.731 | −672.5 | 4532 | $887 \times 10^3$ | 36.7203 | 27.97 |
| 0.6 | 544.49 | 6.2812 | 10.57 | 0.70 | 3.477 | 7.071 | −446.7 | 3700 | 68274 | 36.7197 | 31.42 |
| 0.8 | 2892.5 | 11.445 | 6.650 | 0.88 | 3.812 | 8.117 | −233.8 | 3204 | 16909 | 36.7849 | 34.61 |
| 1.0 | 8842.4 | 120.00 | 4.721 | 0.92 | 4.222 | 9.010 | −266.0 | 2866 | 6776.6 | 36.9073 | 37.51 |
| 1.2 | 20163 | 625.02 | 3.613 | 0.92 | 4.753 | 9.824 | −220.9 | 2616 | 3476.7 | 37.0897 | 40.08 |
| 1.4 | 38516 | 2155.4 | 2.908 | 0.91 | 5.414 | 10.605 | −188.6 | 2422 | 2060.7 | 37.3517 | 42.29 |
| 1.6 | 65467 | 5689.9 | 2.425 | 0.89 | 6.201 | 11.378 | −164.4 | 2266 | 1338.9 | 37.7151 | 44.07 |
| 1.8 | 102516 | 12466 | 2.077 | 0.88 | 7.079 | 12.159 | −145.6 | 2136 | 925.5 | 38.201 | 45.34 |
| 2.0 | 151112 | 23767 | 1.815 | 0.86 | 7.983 | 12.951 | −130.6 | 2027 | 667.8 | 38.854 | 45.99 |
| 2.2 | 212673 | 40466 | 1.611 | 0.810 | | | −118.2 | 1932 | 496.6 | 39.680 | 45.91 |
| 2.4 | 288613 | 63304 | 1.448 | 0.781 | | | −108.0 | 1850 | 376.7 | 40.734 | 44.94 |
| 2.6 | 380383 | 93733 | 1.317 | 0.754 | | | −99.3 | 1777 | 288.8 | 42.124 | 42.84 |
| 2.8 | 489549 | 132952 | 1.210 | 0.728 | | | −91.8 | 1713 | 221.0 | 44.049 | 39.11 |
| 3.0 | 617907 | 182073 | 1.122 | 0.705 | | | −85.4 | 1655 | 163.1 | 46.818 | 32.25 |

†Here X is the $He^3$ mole fraction. The $He^4$ mole fraction, (1−X), is used to make the impurity correction.

The heat of vaporization at absolute zero, $L_0$, can be obtained from the fitted constant, $a$, of eq (3) if the specific heat integral is evaluated. The specific heat of liquid $He^3$ under a pressure of a few centimeters of mercury has been measured by Anderson, Wheatley, and coworkers [61] down to a temperature of 0.015 °K. Their empirical equation for $C_p$, the specific heat at a constant pressure of 0.12 atm, is $(C_p/R)=2.89T-7.80T^2+7.09T^3$ for $0<T<0.3°$. Integration of this equation yields $\int_0^{0.2} C_{sat}dT \approx \int_0^{0.2} C_p dT=0.331\pm0.013$ J/mole. This value is in excellent agreement with the value $0.333\pm0.010$ J/mole obtained by graphical integration of the smooth curve through recent specific heat data given by Strongin, Zimmerman, and Fairbank [62]. From the empirical equation for $C_{sat}$ used for the $T_{62}$ scale, $\int_{0.2}^{1.0} C_{sat}dT=2.784\pm0.056$ $J$/mole. Our corresponding value of $L_0$ is $20.56\pm0.07$ $J$/mole.

The entropy of the saturated liquid can be assumed to be approximately equal to $\int_0^T (C_p/T')dT'$ from the 0.12 atm $C_p$ equation of Anderson et al. [61] given above. From this approximation $S_L(0.23$ °K) is $4.05\pm0.17$ J/mole deg. Strongin et al. [62] also have computed the entropy from their extrapolation of specific heat data to 0 °K. Their value for the entropy at 0.23 °K is $3.97\pm0.17$ J/mole deg. These values are in good agreement with the value $4.02\pm0.25$ J/mole deg obtained by Weinstock, Abraham and Osborne [4], who used eq (5) to calculate $S_L(1.5°)$ from their three separate latent heat measurements at that temperature. The equivalent of eq (12) was used by WAO to compute other entropies in the range of the then available specific heat data. The value of $S_L(0.23°)$ consistent with the 1962 $He^3$ Scale, calculated from eq (12), is $S_L(0.23°)=4.09\pm0.10$ J/mole deg, estimating a $\pm2$ percent limit of error for the specific heat integral term. The good agreement among these values is gratifying but it may be fortuitous. For example, the $He^3$ temperature scale used by Weinstock et al. [4] to assign temperatures to observed $He^3$ vapor pressures was the $T_L$ Scale, eq (9) of ref. [9]. The deviations of the $T_L$ Scale from the 1962 $He^3$ Scale are shown in figure 5 and range from $+6$ to $-3$ mdeg. At 1.5 °K, however, the two scales are in good agreement as to *the temperature*. Thus the value of $T$ used in computing both $S_G$ and $L/T$ in eq (7) would give essentially the same value for liquid entropy at $T\approx1.5$ °K on the $T_L$ and 1962 $He^3$ Scales. If, however, a value of $L$ calculated from eq (6) is used in eq (7) instead of a WAO experimental value of $L$, significantly different values are obtained for $S_L$ depending upon which of the two scales, $T_L$ or 1962 $He^3$, is used for the calculation of $(dP_3/dT)_{sat}$ since there is a difference of about 0.4 percent in these derivatives on the two scales as inferred from the slope of the $\Delta T$ curve in figure 5 (see, for example, ref. [63]).

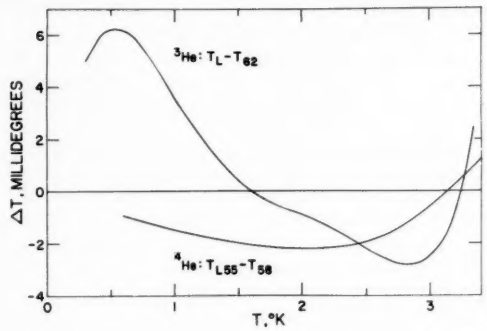


FIGURE 5.—*Graphs of differences between old and new* $He^3$ *and* $He^4$ *temperature scales.*

The $He^3$ curve, $T_L(P_3)-T_{62}(P_3)$, is a graph of the difference between the $T_L$ Scale [9] and the 1962 $He^3$ Scale. The $He^4$ curve is the difference between the $T_{L55}$ Scale [25] and the 1958 $He^4$ Scale given in table 6 of ref [2]. It was intended in their derivations that the $T_L$ Scale would reproduce the $T_{L55}$ Scale, and that the 1962 $He^3$ Scale would reproduce the 1958 $He^4$ Scale. The difference between the two curves is explained principally by the new $(P_3,P_4)$ intercomparison data of Sydoriak and Sherman [46] used in deriving the 1962 $He^3$ Scale.

## 3. Corrections to the Measured Pressure of a $He^3$ Vapor-Pressure Thermometer for the $He^4$ Impurity

Sydoriak and Sherman have discussed in Part I corrections to be applied to an observed pressure as measured in the laboratory in order to obtain the vapor pressure at the surface of liquid $He^3$. The correction for a small $He^4$ impurity will be discussed in more detail here.

The presence of $He^4$ in liquid $He^3$ thermometers lowers the vapor pressure below that of pure $He^3$. Much of the $He^3$ available for purchase up to the present has contained significant quantities of $He^4$; even the $He^3$ used for the 1962 $He^3$ Scale input data measurements [46] contained about 0.04 percent $He^4$. Specially purified $He^3$ containing less than 0.01 percent is being made available for purchase through the Division of Research of the United States Atomic Energy Commission [64].

The correction for small amounts of $He^4$ may be calculated from the approximate relation

$$P_3-P_x\approx(1-X)\,(dP_x/dX)_{T,X=1} \qquad (13)$$

where $P_x$ is the observed vapor pressure for mole fraction, $X$, of $He^3$. Although very little data has been published for the vapor pressures of dilute solutions of $He^4$ in $He^3$, the liquid phase diagrams of Sydoriak and Roberts [32] and Esel'son and Berezniak [38] indicate that $(dP_x/dX)_T$ is probably a constant for $X\geq0.9$ and hence eq (13) may be valid for concentrations of up to 10 percent $He^4$.

Smooth values of this derivative in reduced form,

$$(d\ln P_x/dX)_{T,X=1}=(1/P_3)(dP_x/dX)_{T,X=1}$$
$$\approx\left[1-\left(\frac{P_x}{P_3}\right)\right]/(1-X), \qquad (14)$$

are listed in table 4 and are compared with the raw data of Sydoriak and Roberts [32] in figure 6. Between 0.6 and 2.0 °K the table 4 entries and the solid curve in figure 6 were calculated from eq (14) using the $X=0.9$ values from the smoothed table of ref. [32]. Below 0.6 °K the derivative has been assumed to go linearly to zero at 0 °K mainly because such an extrapolation is consistent with the data below 1 °K, as shown in figure 6. Actually for all practical purposes this derivative may be zero below about 0.2 °K since at these temperatures liquid $He^3$—$He^4$ mixtures with very small amounts of $He^4$ undergo phase separation [65] and, when this happens, the vapor pressure becomes independent of further decreases in $X$. Above 2.0 °K, the table 4 values were calculated from Raoult's law,

$$(d \ln P_x/dX)_{T,X=1}=1-(P_4/P_3), \qquad (15)$$

shown as the dashed curve in figure 6. That law is in fairly good agreement with all existing vapor-pressure data for $X \geq 0.89$ and $T \geq 1.7$ °K.

The concentration of $He^4$ in the saturated vapor will be much less than that of the liquid. This fact can cause fractionation and may require further correction in precise thermometry if much of the $He^3$ in the thermometer system is not condensed.

The correction to a temperature measurement made with a $He^3$ sample containing 0.1 percent $He^4$ in the liquid phase ranges from 0.02 mdeg at 0.4 °K to 0.71 mdeg at 3.2 °K. For most purposes the correction may be calculated from the approximate relation

$$P_3-P_x \approx (1-X)\ P_x(d \ln P_x/dX)_{T,X=1}. \qquad (16)$$

The derivative below 2 °K may be interpolated from a curve through the values listed in table 4 or from figure 6. Above 2 °K the derivative can be easily calculated from eq (15). A careful experimental determination of the correction above 2 °K would improve the accuracy of this correction.

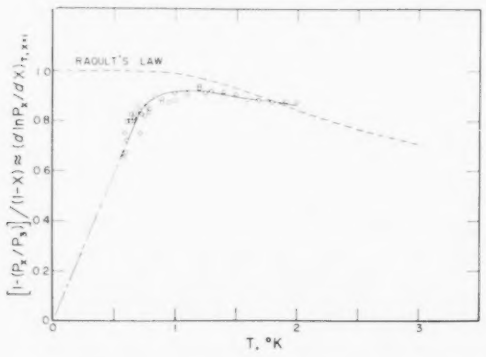


FIGURE 6.—*The correction factor for* $He^4$ *impurity.*

The circles are the data points of Sydoriak and Roberts [32] for $He^3$ mole fraction, $X$, of 0.897. The solid curve from 0.6 to 2.0 °K is drawn through the smoothed table values of ref. [32] for $X=0.9$. The long and short dashed curve is an arbitrary extrapolation to 0 °K. The dashed curve is Raoult's Law, eq (15).

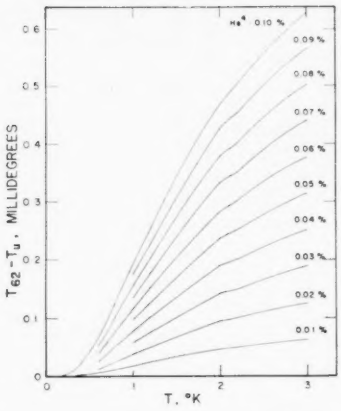


FIGURE 7.—*Correction for* $He^4$ *impurity,* $(T_{62}-T_u)$, *to be added to the uncorrected temperatures,* $T_u$, *calculated from the observed vapor pressure and the 1962* $He^3$ *Scale.*

The correction is calculated as $T_{62}-T_u=(1-X)(d\ln P_x/dX)_{T,X=1}/(d\ln P_3/dT)$ based on eqs (13) and (14) and using the derivative values listed in table 4. The curves can be used for ten times the indicated percent of $He^4$ in the liquid if the ordinate is multiplied by ten.

Figure 7 may be used to read the temperature correction directly for known $He^4$ concentrations in the liquid.

## 4. Status of the 1962 $He^3$ Scale of Temperatures

The 1962 $He^3$ Scale was presented [66] at the Eighth International Conference on Low Temperature Physics in London, September 17–21, 1962. During the next week the new scale was discussed in detail by the Advisory Committee on Thermometry of the International Committee on Weights and Measures. A scale proposal along with ref. [54] has been published along with the minutes of the meeting of the Advisory Committee in Sèvres, France, September 26 and 27, 1962. Quoting from the draft of those minutes [67]:

"Il a estimé que l'*Échelle* $^3$*He 1962* doit également être recommandée pour l'usage général, avec la désignation $T_{62}$.

"Les deux échelles $T_{58}$ (*l'Échelle* $^4$*He 1958*) et $T_{62}$ peuvent être utilisées concurremment dans le domaine où elles sont valables. Cependant, quand il s'agit de l'adoption de cette nouvelle échelle $^3$He comme partie de l'E.I.P.T., on doit prendre soin d'éviter toute ambiguité dans le domaine de recouvrement avec l'échelle $^4$He." [3]

The recommendation by the Advisory Committee of the 1962 $He^3$ Scale was approved in October 1962, by the International Committee on Weights and

[3] "It (the Advisory Committee) has deemed that the 1962 $He^3$ Scale ought equally to be recommended for general usage with designation $T_{62}$.

"The two scales $T_{58}$ and $T_{62}$ can be used concurrently in the range where they are valid. However, when it is a question of adopting this new $He^3$ scale as a part of the I.P.T.S. (International Practical Temperature Scale), care should be taken to avoid any ambiguity in the region of overlap with the $He^4$ scale.

Measures meeting in Sèvres. The International Committee requested the United States and Russian Governments to take steps to make high-purity $He^3$ available internationally for vapor-pressure thermometry, and to prepare and distribute known mixtures of $He^3$ and $He^4$ for the calibration of or the checking of the calibration of apparatus for measuring the isotopic purity of $He^3$.

The status of the 1962 $He^3$ Scale and proposed changes in the International Practical Temperature Scale have been discussed by Stimson [68] and Brickwedde [69].

## 5. Practical Lower Limits for $He^3$ and $He^4$ Vapor-Pressure Thermometry

Practical lower limits for helium vapor-pressure thermometry are determined by the desired precision of temperature determination, the accuracy with which the vapor pressure can be measured, and by how small or how well known the temperature difference is between the thermometric fluid and the object of the measurement.

Below about 2.2 °K, $He^3$ can much more easily be made isothermal with an object the temperature of which is being measured than can $He^4$, for the reasons discussed in Part I. A major factor in fixing a practical lower limit for $He^3$ thermometry is the time necessary to achieve an equilibrium thermomolecular ratio, $P_c/P_w$, of cold pressure, $P_c$, to warm pressure, $P_w$, and more importantly, of sufficient data to permit accurate calculation of that ratio.

To measure temperatures from 0.3 to 0.25 °K to a millidegree precision using $He^3$, vapor pressures from 1.9 to 0.24 $\mu$ would have to be measured to 4 or 5 percent accuracy. This accuracy in the pressure system is relatively easy to achieve. However, the error in $P_c/P_w$ may amount to several percent because of marked quantum effects in the gas viscosity and because no $He^3$ measurements have been made of the empirical thermal transpiration coefficients postulated by Weber [70]. The $He^3$ thermomolecular pressure measurements made by Roberts and Sydoriak [37] showed that for a cold temperature of 2 °K observed $He^3$ $P_c/P_w$ ratios from 1.0 to 0.5 agreed within 1 percent with ratios calculated for $He^4$ using the Weber-Schmidt equation [71].

Roberts and Sydoriak also discuss the possible effect of the low-temperature viscosity on pressure ratios in the tubing at liquid helium temperatures. For warm and cold temperatures, $T_w$ and $T_c$, below 5 °K and pressure ratios close to 1, eq (5) of ref. [37] is $(p_c/p_w)^2=1-0.005642\ (T_w^2-T_c^2)/(Rp_w)^2$ where $R$ is the tubing radius in centimeters and $p_w$ is in microns of mercury. In order to be reasonably sure that the calculated thermomolecular ratio is within 4 or 5 percent of the true ratio for $He^3$ it is suggested that the calculated $(p_c/p_w)$ be kept greater than 0.5 in the rest of the pressure sensing tube. For the stepped pressure sensing tube used by Sydoriak and Sherman with dimensions shown in figure 4 of Part I [46], this suggests a practical lower limit of $Rp_c=0.155$ cm microns or a vapor pressure of 1.16 $\mu$ ($T_{62}=0.287°$).

The practical lower limit for $He^4$ vapor-pressure thermometry is strongly dependent on numerous details of the particular technique and apparatus used. In many cases experimental temperatures are determined from the vapor pressure of the bath in which the experimental apparatus is immersed. For *bath* temperatures and with proper corrections for pressure drops associated with film reflux and/or motion of effluent vapor from the bath, temperatures may be determined down to about 1 °K. Figure 1 of Part I shows errors due to film reflux pressure drops for typical sizes of pressure sensing tubing. However, for temperatures determined by thermal contact with a *closed-bulb* $He^4$ vapor-pressure thermometer the practical lower limit is raised to just below the λ point, because of the large and variable temperature discontinuity at the bulb wall associated with recondensation of the refluxing film. Figure 1 of Part I also shows this "correction" for a variety of conditions.

If the bulb wall is a poor thermal conductor, a still higher limit is imposed due to the effects of the density maximum at about 2.18 °K, discussed by Chase, Maxwell, and coworkers [72].

In the case of precision measurements using $He^3$ thermometry, the publication of only a few pertinent details, such as the diameters and temperatures of any stepped junctions in the pressure sensing tube, will enable future correction of data as improved thermal transpiration corrections become possible.

## 6. Conclusion and Considerations for the Future

These papers on the development of the 1962 $He^3$ Temperature Scale have emphasized marked differences between liquid $He^3$ and $He^4$. One is in the low-temperature variation of the liquid entropy. The quantum mechanical exchange forces in liquid $He^3$ lead to appreciable correlation of the nuclear spins in the liquid at temperatures as high as 1 °K. The difficulty in fitting the entropy curve with a simple analytical expression has led to difficulty in attaching theoretical significance to certain terms in empirical vapor-pressure equations at temperatures below the temperature of fitted data.

The superfluid transition of liquid $He^4$ makes accurate isothermal intercomparisons of $He^3$ and $He^4$ vapor pressures difficult below the $He^4$ λ-point. The 1961 intercomparison data of Sydoriak and Sherman [46], however, are considered to be valid to a few tenths of a millidegree. The 1962 $He^3$ Scale, which is based on these intercomparisons, is believed to be in agreement with the 1958 $He^4$ Scale to within two or three tenths of a millidegree over the full range of the intercomparison data, from 0.9 °K to the critical point, 3.324 °K. A lower limit for practical $He^3$ vapor-pressure thermometry is 0.25 °K corresponding to a $He^3$ vapor pressure of 0.24 $\mu$ Hg.

A number of independent measurements, including measurements of the latent heats of vaporization of $He^3$ and $He^4$, precise isotherm measurements, and preliminary acoustical interferometer measurements,

indicate that both the 1962 $He^3$ Scale and the 1958 $He^4$ Scale may be 2 or 3 mdeg lower than true thermodynamic temperatures between 1 and 3.3 °K. When more accurate data on the thermodynamic properties of $He^3$ and $He^4$ are available, together with better determinations of absolute thermodynamic temperatures, the precise intercomparison data will allow both the $He^3$ and the $He^4$ scales to be adjusted consistently and simultaneously. $He^3$ and $He^4$ scales, thermodynamically consistent between 1 and 3 °K, may be extended by precision paramagnetic salt thermometry above 3 °K using $He^4$ and below 1 °K using $He^3$. Also, the scales may be extended downward by thermodynamic calculations, using coefficients evaluated between 1 and 3 °K as in the development of the 1962 $He^3$ Scale and the $T_{L55}$ $He^4$ Scale [25]. Further measurements on $He^3$ that would be helpful in improving the Scale are measurements of the vapor pressure and thermomolecular pressure ratio down to temperatures of 0.25 °K, more accurate specific heat measurements on the liquid below 2 °K, and specific heat, latent heat, and high-precision vapor-density measurements above 2 °K.

## 7. Appendix A. Method of Multiple Variable Least Squares Analysis

In the usual least squares adjustment of experimental data the implicit assumption is made that only one measured quantity, often called the dependent variable, is in error. This dependent variable is measured as a function of one or more independent variables. The usual procedures for the adjusting of sets of observations to an empirical or theoretical equation assume no error in the independent variables. Frequently, however, the "independent variable" is also determined by a physical measurement and is just as subject to error as the dependent variable.

Deming [47] has discussed a method of adjustment of sets of observations of two or more variables when all variables are subject to error. His method is essentially equivalent to statistical weighting of the data. The method has been coded by P. McWilliams of the Los Alamos laboratory for use with the Gaussian method of iterative least squares analysis adapted by Moore and Zeigler [73] for high-speed computers. We will give a simple example of the method of analysis with exaggerated scatter and uncertainty.

### 7.1. Simple Example

As a simple illustration consider fitting the best straight line to the following three points:

| $X$ | $Y$ |
|---|---|
| $1\pm1$ | $1\pm1$ |
| $4\pm1$ | $5\pm1$ |
| $5\pm1$ | $4\pm1$ |

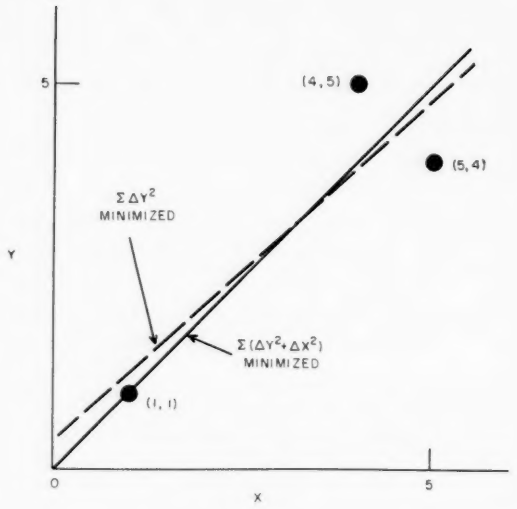


FIGURE 8.—*Simple example of the least squares fit of a straight line to the three observed points shown as dots.*

The dashed line is the usual least squares solution of $Y=a+bX$ which minimizes $\Sigma(Y_o-Y_c)^2$. The solid line is the solution assuming both $X$ and $Y$ are subject to equal absolute errors.

The dashed line in figure 8 shows the fit of the usual least squares solution of $Y=a+bX$ assuming that only $Y$ is in error and equally weighting the points. The solid line, $Y=X$, is the solution assuming that the $X$ and $Y$ values are all equally subject to equal absolute errors. The general case of fitting to a straight line is discussed in detail by Deming. For our special case of equal weighting, the two solutions go through the centroid but have different slopes.

Actually the quantity which is minimized by the least squares solution is

$$S=\sum_{i=1}^{M}[w_{y,i}(Y_{o,i}-Y_{c,i})^2+w_{x,i}(X_{o,i}-X_{c,i})^2] \quad (17)$$

where the subscript $o$ indicates the observed value; subscript $c$ indicates the calculated or adjusted value; and $w_{y,i}$ and $w_{x,i}$ are the weights of the $i$th of $M$ sets of observations. Thus in figure 8 the solid line is identified as minimizing

$$S=\sum[(\Delta Y)^2+(\Delta X)^2]$$

since all the individual weights are equal. $\Delta Y$ is defined as $(Y_o-Y_c)$ and $\Delta X=(X_o-X_c)$.

The geometrical relation between $\Delta Y$ and $\Delta X$ that is assumed in Deming's method of solution is illustrated in figure 18 of ref. [47]. The relation for each point depends on the individual weights for that point.

If $w_x=w_y$, this condition requires that the line from the observed point, $(X, Y_o)$, to the calculated point, $(X_c, Y_c)$, be perpendicular to the calculated curve.

### 7.2. General Discussion of Method

In many cases the least squares problem can be expressed as minimizing eq (17) subject to $M$ equations:

$$F(X_{c,i}, Y_{c,i})=0. \tag{18}$$

As an example consider a case in which three coefficients, $a$, $b$, and $c$, are to be fitted by least squares to the relation $Y=f(X, a, b, c)$. We take

$$F(X, Y)=Y-f(X, a, b, c). \tag{19}$$

Using his geometrical relation between $\Delta Y$ and $\Delta X$, and using the Gaussian method of linearization of the problem by a truncated Taylor's Series expansion of the function, Deming derives a typical least squares solution "normal" equation as

$$\Delta a\sum_{i=1}^{M} W_i F_{a,i}^2+\Delta b\sum_{i=1}^{M} W_i F_{a,i}F_{c,i} +\Delta c\sum_{i=1}^{M} W_i F_{a,i}F_{c,i}=\sum_{i=1}^{M} W_i F_{a,i}F_{o,i}. \tag{20}$$

In this equation, the subscripts $a$,$b$, and $c$ designate the partial derivatives of $F$ with respect to the respective coefficients; $\Delta a=a_1-a_c$, the difference between the initial value, $a_1$, and the calculated or adjusted value, $a_c$; $F_{o,i}=F(X_{o,i}, Y_{o,i}, a_1, b_1, c_1)$; and the weights are

$$W_i=(F_{x,i}^2/w_{x,i}+F_{y,i}^2/w_{y,i})^{-1}. \tag{21}$$

$F_{x,i}$ and $F_{y,i}$ are the partial derivatives of $F$ with respect to $X$ and $Y$, respectively. Where a set of observations, $X_{o,i}$ and $Y_{o,i}$, can be assigned respective standard deviations $\sigma_{x,i}$ and $\sigma_{y,i}$, we take the weights as:

$$w_{x,i}=1/\sigma_{x,i}^2;\ w_{y,i}=1/\sigma_{y,i}^2. \tag{22}$$

If variations in $X$ and $Y$ are independent, substitution of eq (22) in eq (21) yields

$$W_i=1/\sigma_{F,i}^2 \tag{23}$$

and hence the method is equivalent to statistical weighting of the individual sets of observations.

Using the Gaussian method, several iterations using the successively improved values of the coefficients may be used. The partial derivatives are usually evaluated using the observed values of $X$ and $Y$ in each iteration.

As pointed out by Deming, an advantage of the method is that the solution is unequivocal; i.e., the coefficients are independent of variations in the way of writing the equation. Thus a straight line can be written as either $Y=a+bX$ or $X=-a/b+Y/b$ and correspondingly $F$ would be $(Y-a-bX)$ or $(X+a/b-Y/b)$. The values of $a$ and $b$ and the adjusted points will be the same to within higher powers of the residuals, $\Delta X$ and $\Delta Y$.

The least squares code used computes standard deviations of the fitted parameters based on the fit of the observed points to the calculated points. The code also permits computation of standard deviations of points calculated at interpolated or extrapolated points as well as at data points.

---

We are indebted to R. K. Zeigler and P. McWilliams for many discussions and for the development of the computer code.

## References*

[1] S. G. Sydoriak, T. R. Roberts, and R. H. Sherman, Proc. 7th Intern. Conf. Low Temperature Physics, ed. G. M. Graham and A. C. Hollis-Hallett (Univ. of Toronto Press, Toronto, 1961), ch. 30, p. 717.
[2] F. G. Brickwedde, H. van Dijk, M. Durieux, J. R. Clement, and J. K. Logan, J. Res. NBS **64A** (Phys. & Chem.), 1 (1960).
[3] D. F. Brewer, A. K. Sreedhar, H. C. Kramers, and J. G. Daunt, Phys. Rev. **115,** 836 (1959).
[4] B. Weinstock, B. M. Abraham, and D. W. Osborne, Nuovo Cimento Suppl. **9,** 310 (1958).
[5] B. M. Abraham, D. W. Osborne, and B. Weinstock, Phys. Rev. **80,** 366 (1950).
[6] S. G. Sydoriak, T. R. Roberts, and R. H. Sherman, Paper II of this series.
[7] T. R. Roberts, R. H. Sherman, and S. G. Sydoriak, Paper III of this series.
[8] R. H. Sherman, S. G. Sydoriak, and T. R. Roberts, Paper IV of this series. See also Los Alamos Scientific Lab. Rept. LAMS 2701 (July 1962).
[9] S. G. Sydoriak and T. R. Roberts, Phys. Rev. **106,** 175 (1957).
[10] T. R. Roberts, S. G. Sydoriak, and R. H. Sherman, Proc. 4th Symp. Temperature, Its Measurement and Control in Science and Industry, ed. C. M. Herzfeld (Reinhold Publ. Corp., New York, 1962), Vol. 3, pt. 1, p. 75.
[11] W. E. Keller, Phys. Rev. **97,** 1 (1955); **100,** 1790 (1955).
[12] W. E. Keller, Phys. Rev. **98,** 1571 (1955).
[13] F. E. Hoare and J. E. Zimmerman, Rev. Sci. Instr. **30,** 184 (1959); R. T. Swim, Advances in Cryogenic Engineering, ed. K. D. Timmerhaus (Plenum Press, Inc., New York, 1960), Vol. 5, pp. 498–504.
[14] H. H. Plumb, Proc. 10th Intern. Congr. Refrigeration, Copenhagen, 1959, ed. M. Jul and A. M. S. Jul (Pergamon Press, Paris, 1960), Vol. 1, pp. 184–187.
[15] M. Durieux, Thermometry at Liquid Helium and Liquid Hydrogen Temperatures, Thesis, Leiden Univ. (16 Mar. 1960).
[16] F. G. Brickwedde, Report on the Conference Agreement on the Helium Vapor-Pressure Scale of Temperatures, Conf. Physique des Basses Temperatures, Paris, 2–8 Septembre 1955, pp. 608–610.
[17] B. Bleaney and F. Simon, Trans. Faraday Soc. **35,** 1205 (1939).
[18] B. Bleaney and R. A. Hull, Proc. Roy. Soc. (London) **178A,** 74 (1941).
[19] J. de Boer and E. G. D. Cohen, Physica **17,** 993 (1951).
[20] E. W. Becker and R. Misenta, Phys. Rev. **93,** 244 (1954).
[21] E. W. Becker, R. Misenta, and F. Schmeissner, Z. Physik **137,** 126 (1954).
[22] K. Mendelssohn and G. K. White, Proc. Phys. Soc. (London) **A63,** 1328 (1950).
[23] R. Bowers and K. Mendelssohn, Nature **163,** 870 (1949); Proc. Phys. Soc. (London) **A63,** 1318 (1950).

*This list of references applies to papers I, II, III, and IV of this series. For completeness and convenience, it is reproduced in its entirety at the end of each paper.

[24] K. W. Taconis, Progress in Low Temperature Physics, ed. C. J. Gorter (North Holland Publ. Co., Amsterdam, The Netherlands, 1961), Vol. 3, p. 154.
[25] H. van Dijk and M. Durieux, Physica **24,** 1 (1958).
[26] S. G. Sydoriak and H. S. Sommers, Jr., Rev. Sci. Instr. **22,** 915 (1951).
[27] P. Kapitza, J. Phys. (U.S.S.R.) **4,** 181 (1941).
[28] H. A. Fairbank and J. Wilks, Proc. Roy. Soc. (London) **A231,** 545 (1955).
[29] L. J. Challis, K. Dransfeld, and J. Wilks, Proc. Roy. Soc. (London) **A260,** 31 (1961)
[30] Kuang Wey-Yen, Zh. Experim. i Teor. Fiz. (U.S.S.R.) **42,** 921 (1962); Soviet Phys. JETP (English Transl.) **15,** 635 (1962).
[31] I.M. Khalatnikov, Zh. Experim. i Teor. Fiz. (U.S.S.R.) **22,** 687 (1952).
[32] S. G. Sydoriak and T. R. Roberts, Phys. Rev. **118,** 901 (1960).
[33] R. L. Mills, E.R. Grilly, and S. G. Sydoriak, Ann. Phys. **12,** 41 (1961).
[34] W. Cawood and H. S. Patterson, Trans. Faraday Soc. **29,** 522 (1933).
[35] J. Kistemaker, Leiden Commun. **268d** (1944); Physica **11,** 277 (1944–1946); B. E. Blaisdell, J. Math. Phys. **19,** 186 (1940).
[36] W. G. Brombacher, D. P. Johnson, and J. L. Cross, Mercury Barometers and Manometers, NBS Mono. 8 (U.S. Govt. Printing Office, Washington, 1960).
[37] T. R. Roberts and S. G. Sydoriak, Phys. Rev. **102,** 304 (1956).
[38] B. N. Esel'son and N. G. Berezniak, Zh. Experim. i Teor. Fiz. (U.S.S.R.) **30,** 628 (1956); Soviet Phys. JETP (English Transl.) **3,** 568 (1956).
[39] S. G. Sydoriak, E. R. Grilly, and E. F. Hammel, Phys. Rev. **75,** 303 (1949).
[40] V. P. Peshkov, Zh. Experim. i Teor. Fiz. (U.S.S.R.) **33,** 833 (1957); Soviet Phys. JETP (English Transl.) **4,** 645 (1958).
[41] H. van Dijk and D. Shoenberg, Nature **164,** 151 (1949).
[42] T. C. Chen and F. London, Phys. Rev. **89,** 1038 (1953).
[43] W. E. Keller, Nature **178,** 883 (1956); J. R. Clement, Low Temperature Physics and Chemistry (Univ. of Wisconsin Press, Madison, 1958), p. 187 (Proc. 5th Intern. Conf. Low Temperature Physics and Chemistry, Madison, Wis., 1957).
[44] L. Goldstein, Phys. Rev. **96,** 1455 (1954); Phys. Rev. **102,** 1205 (1956).
[45] R. H. Sherman, T. R. Roberts, and S. G. Sydoriak, Supplement au Bulletin de l'Institut International du Froid, Annexe 1961–5, p. 125 (Proc. Meeting of Commission I of the International Institute of Refrigeration, London, 1961).
[46] S. G. Sydoriak and R. H. Sherman, Paper I of this series.
[47] W. E. Deming, Statistical Adjustment of Data (John Wiley & Sons, New York, 1943).
[48] T. R. Roberts, S. G. Sydoriak, and R. H. Sherman, see ref. [45], p. 115.
[49] E. R. Grilly and E. F. Hammel, Progress in Low Temperature Physics III (1961), pp. 113–152.
[50] E. C. Kerr and R. D. Taylor, Proc. 7th Intern. Conf. Low Temperature Physics, ch. 24, pp. 605–608, ed. G. M. Graham and A. C. Hollis-Hallett (Univ. of Toronto Press, Toronto, 1961).
[51] R. H. Sherman and F. J. Edeskuty, Ann. Phys. **9,** 522 (1960).
[52] T. R. Roberts, R. H. Sherman, S. G. Sydoriak, and F. G. Brickwedde, Progress in Low Temperature Physics IV, ch. 10 (North Holland Publ. Co., Amsterdam, The Netherlands, 1964), p. 480.
[53] A. M. Mood, Introduction to the Theory of Statistics, p. 299 (McGraw-Hill, New York, N.Y., 1950).
[54] M. Durieux, Procès-Verbaux du Comité Consultatif de Thermométrie auprès du Comité International des Poids et Mesures, 6e Session, 1962 (Gauthier-Villars, Paris, France, 1964), p. 190.
[55] D. W. Osborne, private communication.
[56] R. Berman and C. F. Mate, Phil. Mag. **3,** 461 (1958).
[57] H. van Dijk, Progr. Cryog. **2,** p. 125 (Academic Press, Inc., New York, N.Y., 1962).
[58] G. Cataland and H. H. Plumb, Proc. 8th Intern. Conf. Low Temperature Physics, London, Sept. 16–22, 1962, ed. R. O. Davies (Butterworths, Washington, D.C., 1963), pp. 439–40
[59] E. C. Kerr, Phys. Rev. **96,** 551 (1954).
[60] E. C. Kerr and R. D. Taylor, Ann. Phys. **20,** 450 (1962).
[61] A. C. Anderson, G. L. Salinger, W. A. Steyert, and J. C. Wheatley, Phys. Rev. Letters **6**, 331 (1961); A. C. Anderson, W. Reese, and J. C. Wheatley, Phys. Rev. **130,** 495 (1963).
[62] M. Strongin, G. O. Zimmerman, and H. A. Fairbank, Phys. Rev. **128,** 1983 (1962).
[63] B. M. Abraham, D. W. Osborne, and B. Weinstock, Phys. Rev. **98,** 551 (1955).
[64] G. R. Grove and W. J. Haubach, Jr.; see ref. [58], p. 441. For further information, write Gaseous Isotope Sales, Montsanto Research Corporation, Mound Laboratory, Miamisburg, Ohio.
[65] D. O. Edwards and J. G. Daunt, Phys. Rev. **124,** 640 (1961).
[66] S. G. Sydoriak, T. R. Roberts, and R. H. Sherman; see ref. [58], pp. 437–8.
[67] J. A. Hall, Sixième Rapport du Comité Consultatif de Thermométrie au Comité International des Poids et Mesures; see ref. [54].
[68] H. F. Stimson, NBS Tech. News Bull. **47,** No. 2, 30 (Feb. 1963); Nature **197,** 1055 (1963).
[69] F. G. Brickwedde, Phys. Today **16,** 24 (1963).
[70] S. Weber, Commun. Kamerlingh Onnes Lab. Univ. Leiden Suppl. **71b** (1932), **264b** and **264d** (1936).
[71] S. Weber and G. Schmidt, Commun. Kamerlingh Onnes Lab. Univ. Leiden **264c** (1936).
[72] C. E. Chase, E. Maxwell, and W. M. Whitney, Physica **26,** 160 (1960); C. E. Chase, E. Maxwell, and W. E. Millett, Physica **27,** 1129 (1961).
[73] R. H. Moore and R. K. Zeigler, Trans. Am. Nuclear Soc. **1,** 128–9 (1958); The Solution of the General Least Squares Problem with Special Reference to High-Speed Computers, Los Alamos Scientific Lab. Rept. LA–2367 (Mar. 4, 1960).
[74] T. R. Roberts and B. K. Swartz, Proc. 2d Symp. Liquid and Solid Helium Three, ed. J. G. Daunt (Ohio State Univ. Press, Columbus, 1960), p. 163.

(Paper 68A6–303)

JOURNAL OF RESEARCH of the National Bureau of Standards—A. Physics and Chemistry
Vol. 68A, No. 6, November–December 1964

# The 1962 $He^3$ Scale of Temperatures IV. Tables[1,2]

R. H. Sherman, S. G. Sydoriak, and T. R. Roberts

Los Alamos Scientific Laboratory, University of California
Los Alamos, N. Mex.

(June 16, 1964)

The detailed tables of the 1962 $He^3$ Scale of Temperatures are presented. The vapor pressure of $He^3$ is tabulated in steps of 1 millidegree from 0.2 to 3.324 °K, the critical temperature. A table giving temperature, to 0.1 millidegree, as a function of pressure is included, as well as the temperature derivative of the vapor pressure.

## 1. Introduction

It is the purpose of this paper to present the detailed tables which comprise the 1962 $He^3$ Scale of Temperatures. The reader is referred to the other publications in this series for discussions of the apparatus and input vapor pressure data [45, 46];[3] the derivation of the scale [6, 66]; and the evaluation of the scale with gas isotherm and other data [7, 10].

## 2. Description of the Tables

In tables 1a and 1b, $He^3$ vapor pressures are given as a function of the temperature, designated as $T_{62}$. Tables 1a and 1b contain entries every millidegree from 0.2 to 3.324 °K, the critical temperature. The pressure, in millimeters of mercury at 0 °C, and standard gravity (980.665 cm/sec.$^2$), is given by the following equation, which defines the 1962 $He^3$ Scale:

$$\ln P_3 = -2.49174/T + 4.80386 - 0.286001\,T + 0.198608\,T^2 - 0.0502237\,T^3 + 0.00505486\,T^4 + 2.24846 \ln T \qquad 0.2 < T < 3.324\ °\mathrm{K}. \quad (1)$$

Tables 2a and 2b are inverted tables giving the temperature as a function of the vapor pressure of $He^3$. The entries were evaluated by solving eq (1) implicitly by a process of successive iterations. The convergence criterion was set at 0.01 mdeg after which the entries were rounded to the nearest 0.1 mdeg (a 5 was always rounded up). Thus tables 1 and 2 should never show more than a 0.1 mdeg deviation from one another.

Table 3, giving values of the derivative $dP_3/dT_{62}$ at intervals of 0.01 deg from 0.2 to 3.33 °K, was computed analytically from eq (1) and its first temperature derivative, i.e.,

$$\frac{dP}{dT} = P\frac{d\ln P}{dT}. \quad (2)$$

Certain portions of parts I, II, and III of this series might be particularly useful to users of these tables. For example, a shortened version of tables 1a and 1b appears as table 5 of Part II.

Deviations of the 1962 $He^3$ Scale from various previous $He^3$ temperature scales are given in table 6 of Part II.

A compliation of thermodynamic properties of $He^3$ consistent with the 1962 $He^3$ Scale is given in table 4 of Part III.

General remarks concerning various needed corrections to a vapor-pressure measurement are given in the section of Part I entitled "Pressure Measurement." Figure 4 of Part I depicts a convenient procedure for making the important thermal transpiration correction. Additional remarks on this latter correction factor are given in section 5 of Part III.

[1] Work performed under the auspices of the United States Atomic Energy Commission.
[2] These tables are the same as those issued as Los Alamos Scientific Laboratory Report LAMS-2701 (July, 1962).
[3] Figures in brackets indicate the literature references at the end of this paper.



743-261—64——3

TABLE 1a. *Vapor pressure of* $He^3$ *(1962 Scale) in microns ($10^{-3}$ mm) of mercury at 0 °C and standard gravity, 980.665 cm/sec²*

| $T_{62}$, °K | 0.000 | 0.001 | 0.002 | 0.003 | 0.004 | 0.005 | 0.006 | 0.007 | 0.008 | 0.009 |
|---|---|---|---|---|---|---|---|---|---|---|
| 0.200 | 0.0121 | 0.0130 | 0.0140 | 0.0150 | 0.0161 | 0.0173 | 0.0185 | 0.0199 | 0.0213 | 0.0228 |
| .210 | .0244 | .0260 | .0278 | .0297 | .0317 | .0338 | .0360 | .0384 | .0409 | .0435 |
| .220 | .0463 | .0492 | .0523 | .0555 | .0590 | .0626 | .0664 | .0703 | .0745 | .0789 |
| .230 | .0835 | .0884 | .0935 | .0988 | .1044 | .1103 | .1165 | .1229 | .1296 | .1367 |
| .240 | .1441 | .1518 | .1599 | .1683 | .1772 | .1864 | .1960 | .2060 | .2165 | .2274 |
| .250 | .2388 | .2506 | .2630 | .2759 | .2893 | .3032 | .3178 | .3329 | .3486 | .3649 |
| .260 | .3819 | .3995 | .4179 | .4369 | .4566 | .4771 | .4984 | .5205 | .5434 | .5671 |
| .270 | .5917 | .6172 | .6436 | .6710 | .6993 | .7286 | .7589 | .7903 | .8228 | .8564 |
| .280 | .8911 | .9270 | .9642 | 1.0025 | 1.0421 | 1.0830 | 1.1253 | 1.1689 | 1.2139 | 1.2603 |
| .290 | 1.3082 | 1.3576 | 1.4086 | 1.4612 | 1.5153 | 1.5712 | 1.6287 | 1.6880 | 1.7490 | 1.8119 |
| .300 | 1.877 | 1.943 | 2.012 | 2.082 | 2.155 | 2.230 | 2.307 | 2.386 | 2.467 | 2.550 |
| .310 | 2.636 | 2.724 | 2.815 | 2.908 | 3.004 | 3.102 | 3.203 | 3.306 | 3.413 | 3.522 |
| .320 | 3.633 | 3.748 | 3.866 | 3.987 | 4.111 | 4.237 | 4.368 | 4.501 | 4.638 | 4.778 |
| .330 | 4.921 | 5.069 | 5.219 | 5.373 | 5.531 | 5.693 | 5.859 | 6.028 | 6.202 | 6.379 |
| .340 | 6.561 | 6.747 | 6.937 | 7.131 | 7.330 | 7.533 | 7.741 | 7.954 | 8.171 | 8.393 |
| .350 | 8.619 | 8.851 | 9.088 | 9.330 | 9.577 | 9.829 | 10.087 | 10.350 | 10.619 | 10.893 |
| .360 | 11.173 | 11.459 | 11.750 | 12.048 | 12.351 | 12.661 | 12.977 | 13.299 | 13.628 | 13.963 |
| .370 | 14.304 | 14.653 | 15.008 | 15.370 | 15.739 | 16.115 | 16.498 | 16.889 | 17.287 | 17.692 |
| .380 | 18.105 | 18.525 | 18.954 | 19.390 | 19.834 | 20.286 | 20.747 | 21.216 | 21.693 | 22.179 |
| .390 | 22.673 | 23.176 | 23.688 | 24.209 | 24.739 | 25.278 | 25.826 | 26.384 | 26.952 | 27.529 |
| .400 | 28.115 | 28.712 | 29.319 | 29.935 | 30.562 | 31.200 | 31.847 | 32.506 | 33.175 | 33.855 |
| .410 | 34.546 | 35.248 | 35.961 | 36.686 | 37.422 | 38.169 | 38.929 | 39.700 | 40.483 | 41.278 |
| .420 | 42.086 | 42.906 | 43.738 | 44.583 | 45.441 | 46.312 | 47.196 | 48.093 | 49.003 | 49.927 |
| .430 | 50.864 | 51.815 | 52.780 | 53.759 | 54.753 | 55.760 | 56.782 | 57.818 | 58.870 | 59.936 |
| .440 | 61.017 | 62.113 | 63.225 | 64.352 | 65.494 | 66.653 | 67.827 | 69.017 | 70.224 | 71.447 |
| .450 | 72.686 | 73.942 | 75.215 | 76.505 | 77.812 | 79.136 | 80.478 | 81.837 | 83.214 | 84.609 |
| .460 | 86.022 | 87.453 | 88.902 | 90.370 | 91.857 | 93.362 | 94.887 | 96.431 | 97.994 | 99.576 |
| .470 | 101.179 | 102.801 | 104.443 | 106.105 | 107.787 | 109.490 | 111.214 | 112.959 | 114.724 | 116.511 |
| .480 | 118.319 | 120.148 | 121.999 | 123.872 | 125.768 | 127.685 | 129.624 | 131.586 | 133.571 | 135.579 |
| .490 | 137.610 | 139.664 | 141.741 | 143.842 | 145.967 | 148.115 | 150.288 | 152.485 | 154.707 | 156.953 |
| .500 | 159.224 | 161.520 | 163.841 | 166.188 | 168.560 | 170.958 | 173.381 | 175.831 | 178.308 | 180.810 |
| .510 | 183.339 | 185.896 | 188.479 | 191.089 | 193.727 | 196.392 | 199.085 | 201.806 | 204.556 | 207.333 |
| .520 | 210.139 | 212.974 | 215.838 | 218.731 | 221.653 | 224.604 | 227.586 | 230.597 | 233.638 | 236.709 |
| .530 | 239.811 | 242.943 | 246.107 | 249.301 | 252.526 | 255.783 | 259.072 | 262.392 | 265.745 | 269.129 |
| .540 | 272.546 | 275.995 | 279.478 | 282.993 | 286.541 | 290.123 | 293.739 | 297.388 | 301.071 | 304.788 |
| .550 | 308.540 | 312.326 | 316.147 | 320.003 | 323.895 | 327.821 | 331.784 | 335.782 | 339.816 | 343.886 |
| .560 | 347.992 | 352.136 | 356.316 | 360.533 | 364.787 | 369.079 | 373.408 | 377.775 | 382.181 | 386.624 |
| .570 | 391.106 | 395.627 | 400.187 | 404.785 | 409.423 | 414.100 | 418.818 | 423.575 | 428.372 | 433.209 |
| .580 | 438.087 | 443.006 | 447.966 | 452.967 | 458.009 | 463.093 | 468.219 | 473.387 | 478.597 | 483.850 |
| .590 | 489.145 | 494.483 | 499.864 | 505.288 | 510.756 | 516.268 | 521.824 | 527.423 | 533.068 | 538.756 |
| .600 | 544.490 | 550.268 | 556.092 | 561.961 | 567.876 | 573.837 | 579.844 | 585.897 | 591.997 | 598.143 |
| .610 | 604.337 | 610.577 | 616.865 | 623.201 | 629.584 | 636.016 | 642.496 | 649.024 | 655.601 | 662.227 |
| .620 | 668.902 | 675.626 | 682.400 | 689.224 | 696.097 | 703.021 | 709.996 | 717.021 | 724.097 | 731.224 |
| .630 | 738.402 | 745.633 | 752.914 | 760.248 | 767.634 | 775.073 | 782.564 | 790.108 | 797.705 | 805.355 |
| .640 | 813.059 | 820.817 | 828.629 | 836.495 | 844.416 | 852.391 | 860.421 | 868.506 | 876.646 | 884.842 |
| .650 | 893.094 | 901.402 | 909.766 | 918.186 | 926.663 | 935.197 | 943.789 | 952.437 | 961.143 | 969.907 |
| .660 | 978.729 | 987.609 | 996.548 | 1005.545 | 1014.601 | 1023.717 | 1032.891 | 1042.126 | 1051.420 | 1060.774 |
| .670 | 1070.189 | 1079.664 | 1089.199 | 1098.796 | 1108.454 | 1118.173 | 1127.954 | 1137.796 | 1147.701 | 1157.668 |
| .680 | 1167.698 | 1177.790 | 1187.946 | 1198.164 | 1208.446 | 1218.792 | 1229.202 | 1239.675 | 1250.213 | 1260.816 |
| .690 | 1271.483 | 1282.216 | 1293.013 | 1303.877 | 1314.805 | 1325.800 | 1336.861 | 1347.989 | 1359.183 | 1370.443 |
| .700 | 1381.771 | 1393.167 | 1404.629 | 1416.160 | 1427.758 | 1439.425 | 1451.160 | 1462.964 | 1474.836 | 1486.778 |
| .710 | 1498.789 | 1510.870 | 1523.021 | 1535.241 | 1547.532 | 1559.894 | 1572.326 | 1584.829 | 1597.403 | 1610.048 |
| .720 | 1622.766 | 1635.555 | 1648.416 | 1661.350 | 1674.356 | 1687.434 | 1700.586 | 1713.811 | 1727.110 | 1740.482 |
| .730 | 1753.928 | 1767.449 | 1781.043 | 1794.713 | 1808.457 | 1822.276 | 1836.171 | 1850.141 | 1864.186 | 1878.308 |
| .740 | 1892.506 | 1906.780 | 1921.132 | 1935.559 | 1950.065 | 1964.647 | 1979.307 | 1994.045 | 2008.861 | 2023.755 |
| .750 | 2038.728 | 2053.779 | 2068.909 | 2084.119 | 2099.408 | 2114.776 | 2130.225 | 2145.753 | 2161.362 | 2177.051 |
| .760 | 2192.821 | 2208.673 | 2224.605 | 2240.619 | 2256.715 | 2272.892 | 2289.152 | 2305.494 | 2321.919 | 2338.426 |
| .770 | 2355.017 | 2371.691 | 2388.448 | 2405.289 | 2422.215 | 2439.224 | 2456.318 | 2473.496 | 2490.760 | 2508.108 |
| .780 | 2525.542 | 2543.061 | 2560.667 | 2578.358 | 2596.136 | 2614.000 | 2631.951 | 2649.988 | 2668.113 | 2686.326 |
| .790 | 2704.626 | 2723.014 | 2741.490 | 2760.054 | 2778.707 | 2797.448 | 2816.279 | 2835.199 | 2854.208 | 2873.307 |
| .800 | 2892.496 | 2911.775 | 2931.145 | 2950.605 | 2970.156 | 2989.798 | 3009.531 | 3029.356 | 3049.272 | 3069.280 |
| .810 | 3089.381 | 3109.574 | 3129.860 | 3150.239 | 3170.710 | 3191.275 | 3211.934 | 3232.686 | 3253.533 | 3274.474 |
| .820 | 3295.508 | 3316.638 | 3337.863 | 3359.183 | 3380.598 | 3402.109 | 3423.716 | 3445.419 | 3467.217 | 3489.113 |
| .830 | 3511.105 | 3533.194 | 3555.381 | 3577.665 | 3600.046 | 3622.525 | 3645.103 | 3667.779 | 3690.553 | 3713.426 |
| .840 | 3736.398 | 3759.469 | 3782.640 | 3805.910 | 3829.281 | 3852.751 | 3876.322 | 3899.993 | 3923.765 | 3947.639 |
| .850 | 3971.613 | 3995.689 | 4019.866 | 4044.146 | 4068.528 | 4093.012 | 4117.598 | 4142.288 | 4167.080 | 4191.976 |
| .860 | 4216.976 | 4242.079 | 4267.286 | 4292.597 | 4318.012 | 4343.533 | 4369.158 | 4394.888 | 4420.723 | 4446.664 |
| .870 | 4472.711 | 4498.864 | 4525.123 | 4551.488 | 4577.960 | 4604.539 | 4631.225 | 4658.018 | 4684.919 | 4711.928 |
| .880 | 4739.044 | 4766.269 | 4793.602 | 4821.044 | 4848.595 | 4876.255 | 4904.024 | 4931.903 | 4959.891 | 4987.990 |
| .890 | 5016.198 | 5044.517 | 5072.947 | 5101.488 | 5130.140 | 5158.903 | 5187.778 | 5216.764 | 5245.863 | 5275.073 |
| .900 | 5304.397 | 5333.832 | 5363.381 | 5393.043 | 5422.818 | 5452.707 | 5482.709 | 5512.826 | 5543.057 | 5573.402 |
| .910 | 5603.862 | 5634.436 | 5665.126 | 5695.931 | 5726.852 | 5757.889 | 5789.041 | 5820.310 | 5851.695 | 5883.196 |
| .920 | 5914.815 | 5946.551 | 5978.404 | 6010.374 | 6042.463 | 6074.669 | 6106.994 | 6139.436 | 6171.998 | 6204.679 |
| .930 | 6237.478 | 6270.397 | 6303.435 | 6336.593 | 6369.871 | 6403.269 | 6436.788 | 6470.427 | 6504.187 | 6538.068 |
| .940 | 6572.071 | 6606.195 | 6640.440 | 6674.808 | 6709.297 | 6743.909 | 6778.644 | 6813.502 | 6848.482 | 6883.586 |
| .950 | 6918.813 | 6954.164 | 6989.639 | 7025.238 | 7060.961 | 7096.809 | 7132.781 | 7168.879 | 7205.101 | 7241.450 |
| .960 | 7277.923 | 7314.523 | 7351.249 | 7388.101 | 7425.079 | 7462.185 | 7499.417 | 7536.776 | 7574.263 | 7611.878 |
| .970 | 7649.620 | 7687.490 | 7725.489 | 7763.616 | 7801.872 | 7840.256 | 7878.770 | 7917.413 | 7956.186 | 7995.088 |
| .980 | 8034.121 | 8073.283 | 8112.576 | 8152.000 | 8191.554 | 8231.240 | 8271.057 | 8311.005 | 8351.085 | 8391.297 |
| .990 | 8431.641 | 8472.118 | 8512.727 | 8553.469 | 8594.343 | 8635.352 | 8676.493 | 8717.768 | 8759.177 | 8800.720 |

TABLE 1b. *Vapor pressure of* $He^3$ *(1962 Scale) in millimeters of mercury at 0 °C and standard gravity, 980.665 cm/sec²*

| $T_{62}$, °K | 0.000 | 0.001 | 0.002 | 0.003 | 0.004 | 0.005 | 0.006 | 0.007 | 0.008 | 0.009 |
|---|---|---|---|---|---|---|---|---|---|---|
| 1.000 | 8.842 | 8.884 | 8.926 | 8.968 | 9.010 | 9.053 | 9.095 | 9.138 | 9.181 | 9.224 |
| 1.010 | 9.267 | 9.310 | 9.353 | 9.397 | 9.440 | 9.484 | 9.528 | 9.572 | 9.616 | 9.660 |
| 1.020 | 9.704 | 9.749 | 9.794 | 9.839 | 9.884 | 9.929 | 9.974 | 10.019 | 10.065 | 10.110 |
| 1.030 | 10.156 | 10.202 | 10.248 | 10.294 | 10.341 | 10.387 | 10.434 | 10.481 | 10.528 | 10.575 |
| 1.040 | 10.622 | 10.669 | 10.717 | 10.765 | 10.812 | 10.860 | 10.908 | 10.957 | 11.005 | 11.054 |
| 1.050 | 11.102 | 11.151 | 11.200 | 11.249 | 11.298 | 11.348 | 11.397 | 11.447 | 11.497 | 11.547 |
| 1.060 | 11.597 | 11.647 | 11.698 | 11.748 | 11.799 | 11.850 | 11.901 | 11.952 | 12.003 | 12.055 |
| 1.070 | 12.106 | 12.158 | 12.210 | 12.262 | 12.314 | 12.367 | 12.419 | 12.472 | 12.525 | 12.577 |
| 1.080 | 12.631 | 12.684 | 12.737 | 12.791 | 12.845 | 12.898 | 12.952 | 13.007 | 13.061 | 13.115 |
| 1.090 | 13.170 | 13.225 | 13.280 | 13.335 | 13.390 | 13.446 | 13.501 | 13.557 | 13.613 | 13.669 |
| 1.100 | 13.725 | 13.781 | 13.838 | 13.894 | 13.951 | 14.008 | 14.065 | 14.123 | 14.180 | 14.238 |
| 1.110 | 14.295 | 14.353 | 14.411 | 14.469 | 14.528 | 14.586 | 14.645 | 14.704 | 14.763 | 14.822 |
| 1.120 | 14.881 | 14.941 | 15.001 | 15.060 | 15.120 | 15.180 | 15.241 | 15.301 | 15.362 | 15.423 |
| 1.130 | 15.484 | 15.545 | 15.606 | 15.667 | 15.729 | 15.791 | 15.853 | 15.915 | 15.977 | 16.039 |
| 1.140 | 16.102 | 16.165 | 16.227 | 16.291 | 16.354 | 16.417 | 16.481 | 16.544 | 16.608 | 16.672 |
| 1.150 | 16.737 | 16.801 | 16.865 | 16.930 | 16.995 | 17.060 | 17.125 | 17.191 | 17.256 | 17.322 |
| 1.160 | 17.388 | 17.454 | 17.520 | 17.586 | 17.653 | 17.720 | 17.787 | 17.854 | 17.921 | 17.988 |
| 1.170 | 18.056 | 18.124 | 18.192 | 18.260 | 18.328 | 18.396 | 18.465 | 18.534 | 18.603 | 18.672 |
| 1.180 | 18.741 | 18.810 | 18.880 | 18.950 | 19.020 | 19.090 | 19.160 | 19.231 | 19.301 | 19.372 |
| 1.190 | 19.443 | 19.514 | 19.586 | 19.657 | 19.729 | 19.801 | 19.873 | 19.945 | 20.018 | 20.090 |
| 1.200 | 20.163 | 20.236 | 20.309 | 20.382 | 20.456 | 20.529 | 20.603 | 20.677 | 20.751 | 20.826 |
| 1.210 | 20.900 | 20.975 | 21.050 | 21.125 | 21.200 | 21.275 | 21.351 | 21.427 | 21.503 | 21.579 |
| 1.220 | 21.655 | 21.732 | 21.808 | 21.885 | 21.962 | 22.039 | 22.117 | 22.194 | 22.272 | 22.350 |
| 1.230 | 22.428 | 22.507 | 22.585 | 22.664 | 22.743 | 22.822 | 22.901 | 22.980 | 23.060 | 23.140 |
| 1.240 | 23.220 | 23.300 | 23.380 | 23.460 | 23.541 | 23.622 | 23.703 | 23.784 | 23.866 | 23.947 |
| 1.250 | 24.029 | 24.111 | 24.193 | 24.276 | 24.358 | 24.441 | 24.524 | 24.607 | 24.690 | 24.774 |
| 1.260 | 24.857 | 24.941 | 25.025 | 25.110 | 25.194 | 25.279 | 25.363 | 25.448 | 25.534 | 25.619 |
| 1.270 | 25.704 | 25.790 | 25.876 | 25.962 | 26.049 | 26.135 | 26.222 | 26.309 | 26.396 | 26.483 |
| 1.280 | 26.571 | 26.658 | 26.746 | 26.834 | 26.922 | 27.011 | 27.099 | 27.188 | 27.277 | 27.366 |
| 1.290 | 27.456 | 27.545 | 27.635 | 27.725 | 27.815 | 27.906 | 27.996 | 28.087 | 28.178 | 28.269 |
| 1.300 | 28.360 | 28.452 | 28.544 | 28.636 | 28.728 | 28.820 | 28.913 | 29.005 | 29.098 | 29.191 |
| 1.310 | 29.285 | 29.378 | 29.472 | 29.566 | 29.660 | 29.754 | 29.849 | 29.943 | 30.038 | 30.133 |
| 1.320 | 30.229 | 30.324 | 30.420 | 30.516 | 30.612 | 30.708 | 30.805 | 30.901 | 30.998 | 31.095 |
| 1.330 | 31.193 | 31.290 | 31.388 | 31.486 | 31.584 | 31.682 | 31.781 | 31.879 | 31.978 | 32.077 |
| 1.340 | 32.177 | 32.276 | 32.376 | 32.476 | 32.576 | 32.676 | 32.777 | 32.878 | 32.979 | 33.080 |
| 1.350 | 33.181 | 33.283 | 33.385 | 33.486 | 33.589 | 33.691 | 33.794 | 33.897 | 34.000 | 34.103 |
| 1.360 | 34.206 | 34.310 | 34.414 | 34.518 | 34.622 | 34.726 | 34.831 | 34.936 | 35.041 | 35.146 |
| 1.370 | 35.252 | 35.358 | 35.464 | 35.570 | 35.676 | 35.783 | 35.889 | 35.996 | 36.104 | 36.211 |
| 1.380 | 36.319 | 36.427 | 36.535 | 36.643 | 36.751 | 36.860 | 36.969 | 37.078 | 37.187 | 37.297 |
| 1.390 | 37.407 | 37.516 | 37.627 | 37.737 | 37.848 | 37.958 | 38.069 | 38.181 | 38.292 | 38.404 |
| 1.400 | 38.516 | 38.628 | 38.740 | 38.853 | 38.965 | 39.078 | 39.191 | 39.305 | 39.418 | 39.532 |
| 1.410 | 39.646 | 39.761 | 39.875 | 39.990 | 40.105 | 40.220 | 40.335 | 40.451 | 40.566 | 40.682 |
| 1.420 | 40.799 | 40.915 | 41.032 | 41.149 | 41.266 | 41.383 | 41.501 | 41.618 | 41.736 | 41.855 |
| 1.430 | 41.973 | 42.092 | 42.210 | 42.330 | 42.449 | 42.568 | 42.688 | 42.808 | 42.928 | 43.049 |
| 1.440 | 43.169 | 43.290 | 43.411 | 43.533 | 43.654 | 43.776 | 43.898 | 44.020 | 44.142 | 44.265 |
| 1.450 | 44.388 | 44.511 | 44.634 | 44.758 | 44.882 | 45.006 | 45.130 | 45.254 | 45.379 | 45.504 |
| 1.460 | 45.629 | 45.754 | 45.880 | 46.006 | 46.132 | 46.258 | 46.385 | 46.511 | 46.638 | 46.765 |
| 1.470 | 46.893 | 47.020 | 47.148 | 47.276 | 47.405 | 47.533 | 47.662 | 47.791 | 47.920 | 48.050 |
| 1.480 | 48.179 | 48.309 | 48.439 | 48.570 | 48.700 | 48.831 | 48.962 | 49.094 | 49.225 | 49.357 |
| 1.490 | 49.489 | 49.621 | 49.754 | 49.886 | 50.019 | 50.152 | 50.286 | 50.419 | 50.553 | 50.687 |
| 1.500 | 50.822 | 50.956 | 51.091 | 51.226 | 51.361 | 51.497 | 51.633 | 51.769 | 51.905 | 52.041 |
| 1.510 | 52.178 | 52.315 | 52.452 | 52.589 | 52.727 | 52.865 | 53.003 | 53.141 | 53.280 | 53.419 |
| 1.520 | 53.558 | 53.697 | 53.837 | 53.976 | 54.116 | 54.257 | 54.397 | 54.538 | 54.679 | 54.820 |
| 1.530 | 54.961 | 55.103 | 55.245 | 55.387 | 55.529 | 55.672 | 55.815 | 55.958 | 56.101 | 56.245 |
| 1.540 | 56.389 | 56.533 | 56.677 | 56.822 | 56.967 | 57.112 | 57.257 | 57.402 | 57.548 | 57.694 |
| 1.550 | 57.840 | 57.987 | 58.134 | 58.281 | 58.428 | 58.575 | 58.723 | 58.871 | 59.019 | 59.168 |
| 1.560 | 59.316 | 59.465 | 59.615 | 59.764 | 59.914 | 60.064 | 60.214 | 60.364 | 60.515 | 60.666 |
| 1.570 | 60.817 | 60.968 | 61.120 | 61.272 | 61.424 | 61.576 | 61.729 | 61.882 | 62.035 | 62.189 |
| 1.580 | 62.342 | 62.496 | 62.650 | 62.805 | 62.959 | 63.114 | 63.269 | 63.425 | 63.580 | 63.736 |
| 1.590 | 63.892 | 64.049 | 64.205 | 64.362 | 64.519 | 64.677 | 64.834 | 64.992 | 65.150 | 65.309 |
| 1.600 | 65.467 | 65.626 | 65.785 | 65.945 | 66.105 | 66.264 | 66.425 | 66.585 | 66.746 | 66.907 |
| 1.610 | 67.068 | 67.229 | 67.391 | 67.553 | 67.715 | 67.878 | 68.040 | 68.203 | 68.366 | 68.530 |
| 1.620 | 68.694 | 68.858 | 69.022 | 69.186 | 69.351 | 69.516 | 69.682 | 69.847 | 70.013 | 70.179 |
| 1.630 | 70.345 | 70.512 | 70.679 | 70.846 | 71.013 | 71.181 | 71.348 | 71.517 | 71.685 | 71.854 |
| 1.640 | 72.022 | 72.192 | 72.361 | 72.531 | 72.701 | 72.871 | 73.041 | 73.212 | 73.383 | 73.554 |
| 1.650 | 73.726 | 73.897 | 74.070 | 74.242 | 74.414 | 74.587 | 74.760 | 74.934 | 75.107 | 75.281 |
| 1.660 | 75.455 | 75.630 | 75.804 | 75.979 | 76.154 | 76.330 | 76.505 | 76.681 | 76.858 | 77.034 |
| 1.670 | 77.211 | 77.388 | 77.565 | 77.743 | 77.921 | 78.099 | 78.277 | 78.456 | 78.635 | 78.814 |
| 1.680 | 78.993 | 79.173 | 79.353 | 79.533 | 79.714 | 79.894 | 80.075 | 80.257 | 80.438 | 80.620 |
| 1.690 | 80.802 | 80.985 | 81.167 | 81.350 | 81.533 | 81.717 | 81.901 | 82.085 | 82.269 | 82.453 |
| 1.700 | 82.638 | 82.823 | 83.009 | 83.194 | 83.380 | 83.566 | 83.753 | 83.939 | 84.126 | 84.314 |
| 1.710 | 84.501 | 84.689 | 84.877 | 85.065 | 85.254 | 85.443 | 85.632 | 85.821 | 86.011 | 86.201 |
| 1.720 | 86.391 | 86.582 | 86.773 | 86.964 | 87.155 | 87.347 | 87.539 | 87.731 | 87.923 | 88.116 |
| 1.730 | 88.309 | 88.502 | 88.696 | 88.890 | 89.084 | 89.278 | 89.473 | 89.668 | 89.863 | 90.059 |
| 1.740 | 90.254 | 90.450 | 90.647 | 90.843 | 91.040 | 91.238 | 91.435 | 91.633 | 91.831 | 92.029 |
| 1.750 | 92.228 | 92.426 | 92.626 | 92.825 | 93.025 | 93.225 | 93.425 | 93.625 | 93.826 | 94.027 |
| 1.760 | 94.229 | 94.430 | 94.632 | 94.834 | 95.037 | 95.240 | 95.443 | 95.646 | 95.850 | 96.054 |
| 1.770 | 96.258 | 96.462 | 96.667 | 96.872 | 97.077 | 97.283 | 97.489 | 97.695 | 97.902 | 98.108 |
| 1.780 | 98.315 | 98.523 | 98.730 | 98.938 | 99.146 | 99.355 | 99.564 | 99.773 | 99.982 | 100.192 |
| 1.790 | 100.402 | 100.612 | 100.822 | 101.033 | 101.244 | 101.455 | 101.667 | 101.879 | 102.091 | 102.304 |

TABLE 1b. *Vapor pressure of* $He^3$ *(1962 Scale) in millimeters of mercury at 0 °C and standard gravity, 980.665 cm/sec²*—Con.

| $T_{62}$, °K | 0.000 | 0.001 | 0.002 | 0.003 | 0.004 | 0.005 | 0.006 | 0.007 | 0.008 | 0.009 |
|---|---|---|---|---|---|---|---|---|---|---|
| 1.800 | 102.516 | 102.729 | 102.943 | 103.156 | 103.370 | 103.585 | 103.799 | 104.014 | 104.229 | 104.444 |
| 1.810 | 104.660 | 104.876 | 105.092 | 105.309 | 105.526 | 105.743 | 105.960 | 106.178 | 106.396 | 106.614 |
| 1.820 | 106.833 | 107.052 | 107.271 | 107.490 | 107.710 | 107.930 | 108.150 | 108.371 | 108.592 | 108.813 |
| 1.830 | 109.035 | 109.256 | 109.479 | 109.701 | 109.924 | 110.147 | 110.370 | 110.593 | 110.817 | 111.042 |
| 1.840 | 111.266 | 111.491 | 111.716 | 111.941 | 112.167 | 112.393 | 112.619 | 112.846 | 113.072 | 113.300 |
| 1.850 | 113.527 | 113.755 | 113.983 | 114.211 | 114.440 | 114.669 | 114.898 | 115.127 | 115.357 | 115.587 |
| 1.860 | 115.818 | 116.048 | 116.279 | 116.511 | 116.742 | 116.974 | 117.206 | 117.439 | 117.672 | 117.905 |
| 1.870 | 118.138 | 118.372 | 118.606 | 118.840 | 119.075 | 119.310 | 119.545 | 119.781 | 120.016 | 120.253 |
| 1.880 | 120.489 | 120.726 | 120.963 | 121.200 | 121.438 | 121.676 | 121.914 | 122.153 | 122.391 | 122.631 |
| 1.890 | 122.870 | 123.110 | 123.350 | 123.590 | 123.831 | 124.072 | 124.313 | 124.555 | 124.797 | 125.039 |
| 1.900 | 125.282 | 125.525 | 125.768 | 126.011 | 126.255 | 126.499 | 126.743 | 126.988 | 127.233 | 127.478 |
| 1.910 | 127.724 | 127.970 | 128.216 | 128.463 | 128.709 | 128.957 | 129.204 | 129.452 | 129.700 | 129.948 |
| 1.920 | 130.197 | 130.446 | 130.695 | 130.945 | 131.195 | 131.445 | 131.696 | 131.946 | 132.198 | 132.449 |
| 1.930 | 132.701 | 132.953 | 133.205 | 133.458 | 133.711 | 133.965 | 134.218 | 134.472 | 134.727 | 134.981 |
| 1.940 | 135.236 | 135.491 | 135.747 | 136.003 | 136.259 | 136.515 | 136.772 | 137.029 | 137.287 | 137.545 |
| 1.950 | 137.803 | 138.061 | 138.320 | 138.579 | 138.838 | 139.098 | 139.358 | 139.618 | 139.879 | 140.140 |
| 1.960 | 140.401 | 140.662 | 140.924 | 141.186 | 141.449 | 141.712 | 141.975 | 142.238 | 142.502 | 142.766 |
| 1.970 | 143.031 | 143.295 | 143.560 | 143.826 | 144.091 | 144.357 | 144.624 | 144.890 | 145.157 | 145.425 |
| 1.980 | 145.692 | 145.960 | 146.228 | 146.497 | 146.766 | 147.035 | 147.305 | 147.575 | 147.845 | 148.115 |
| 1.990 | 148.386 | 148.657 | 148.929 | 149.200 | 149.473 | 149.745 | 150.018 | 150.291 | 150.564 | 150.838 |
| 2.000 | 151.112 | 151.386 | 151.661 | 151.936 | 152.212 | 152.487 | 152.763 | 153.040 | 153.316 | 153.593 |
| 2.010 | 153.870 | 154.148 | 154.426 | 154.704 | 154.983 | 155.262 | 155.541 | 155.821 | 156.101 | 156.381 |
| 2.020 | 156.661 | 156.942 | 157.224 | 157.505 | 157.787 | 158.069 | 158.352 | 158.635 | 158.918 | 159.201 |
| 2.030 | 159.485 | 159.769 | 160.054 | 160.339 | 160.624 | 160.910 | 161.195 | 161.482 | 161.768 | 162.055 |
| 2.040 | 162.342 | 162.629 | 162.917 | 163.205 | 163.494 | 163.783 | 164.072 | 164.361 | 164.651 | 164.941 |
| 2.050 | 165.232 | 165.523 | 165.814 | 166.105 | 166.397 | 166.689 | 166.982 | 167.275 | 167.568 | 167.861 |
| 2.060 | 168.155 | 168.449 | 168.744 | 169.038 | 169.334 | 169.629 | 169.925 | 170.221 | 170.518 | 170.814 |
| 2.070 | 171.112 | 171.409 | 171.707 | 172.005 | 172.304 | 172.602 | 172.902 | 173.201 | 173.501 | 173.801 |
| 2.080 | 174.102 | 174.403 | 174.704 | 175.005 | 175.307 | 175.610 | 175.912 | 176.215 | 176.518 | 176.822 |
| 2.090 | 177.126 | 177.430 | 177.735 | 178.040 | 178.345 | 178.651 | 178.957 | 179.263 | 179.570 | 179.877 |
| 2.100 | 180.184 | 180.492 | 180.800 | 181.108 | 181.417 | 181.726 | 182.035 | 182.345 | 182.655 | 182.965 |
| 2.110 | 183.276 | 183.587 | 183.899 | 184.211 | 184.523 | 184.835 | 185.148 | 185.461 | 185.775 | 186.089 |
| 2.120 | 186.403 | 186.717 | 187.032 | 187.348 | 187.663 | 187.979 | 188.295 | 188.612 | 188.929 | 189.246 |
| 2.130 | 189.564 | 189.882 | 190.200 | 190.519 | 190.838 | 191.158 | 191.477 | 191.797 | 192.118 | 192.439 |
| 2.140 | 192.760 | 193.081 | 193.403 | 193.725 | 194.048 | 194.371 | 194.694 | 195.018 | 195.342 | 195.666 |
| 2.150 | 195.990 | 196.315 | 196.641 | 196.967 | 197.293 | 197.619 | 197.946 | 198.273 | 198.600 | 198.928 |
| 2.160 | 199.256 | 199.585 | 199.914 | 200.243 | 200.572 | 200.902 | 201.233 | 201.563 | 201.894 | 202.226 |
| 2.170 | 202.557 | 202.889 | 203.222 | 203.554 | 203.888 | 204.221 | 204.555 | 204.889 | 205.223 | 205.558 |
| 2.180 | 205.894 | 206.229 | 206.565 | 206.901 | 207.238 | 207.575 | 207.913 | 208.250 | 208.588 | 208.927 |
| 2.190 | 209.266 | 209.605 | 209.944 | 210.284 | 210.624 | 210.965 | 211.306 | 211.647 | 211.989 | 212.331 |
| 2.200 | 212.673 | 213.016 | 213.359 | 213.703 | 214.046 | 214.391 | 214.735 | 215.080 | 215.425 | 215.771 |
| 2.210 | 216.117 | 216.463 | 216.810 | 217.157 | 217.505 | 217.852 | 218.201 | 218.549 | 218.898 | 219.247 |
| 2.220 | 219.597 | 219.947 | 220.297 | 220.648 | 220.999 | 221.350 | 221.702 | 222.054 | 222.407 | 222.760 |
| 2.230 | 223.113 | 223.467 | 223.821 | 224.175 | 224.530 | 224.885 | 225.240 | 225.596 | 225.952 | 226.309 |
| 2.240 | 226.665 | 227.023 | 227.380 | 227.738 | 228.097 | 228.455 | 228.815 | 229.174 | 229.534 | 229.894 |
| 2.250 | 230.255 | 230.616 | 230.977 | 231.339 | 231.701 | 232.063 | 232.426 | 232.789 | 233.153 | 233.516 |
| 2.260 | 233.881 | 234.245 | 234.610 | 234.976 | 235.342 | 235.708 | 236.074 | 236.441 | 236.808 | 237.176 |
| 2.270 | 237.544 | 237.912 | 238.281 | 238.650 | 239.019 | 239.389 | 239.759 | 240.130 | 240.501 | 240.872 |
| 2.280 | 241.244 | 241.616 | 241.989 | 242.361 | 242.735 | 243.108 | 243.482 | 243.856 | 244.231 | 244.606 |
| 2.290 | 244.982 | 245.357 | 245.734 | 246.110 | 246.487 | 246.864 | 247.242 | 247.620 | 247.999 | 248.378 |
| 2.300 | 248.757 | 249.136 | 249.516 | 249.897 | 250.277 | 250.658 | 251.040 | 251.422 | 251.804 | 252.187 |
| 2.310 | 252.570 | 252.953 | 253.337 | 253.721 | 254.105 | 254.490 | 254.876 | 255.261 | 255.647 | 256.034 |
| 2.320 | 256.420 | 256.808 | 257.195 | 257.583 | 257.971 | 258.360 | 258.749 | 259.139 | 259.528 | 259.919 |
| 2.330 | 260.309 | 260.700 | 261.092 | 261.483 | 261.876 | 262.268 | 262.661 | 263.054 | 263.448 | 263.842 |
| 2.340 | 264.236 | 264.631 | 265.026 | 265.422 | 265.818 | 266.214 | 266.611 | 267.008 | 267.406 | 267.804 |
| 2.350 | 268.202 | 268.601 | 269.000 | 269.399 | 269.799 | 270.199 | 270.600 | 271.001 | 271.402 | 271.804 |
| 2.360 | 272.206 | 272.609 | 273.012 | 273.415 | 273.819 | 274.223 | 274.627 | 275.032 | 275.437 | 275.843 |
| 2.370 | 276.249 | 276.656 | 277.062 | 277.470 | 277.877 | 278.285 | 278.694 | 279.103 | 279.512 | 279.921 |
| 2.380 | 280.331 | 280.742 | 281.152 | 281.563 | 281.975 | 282.387 | 282.799 | 283.212 | 283.625 | 284.039 |
| 2.390 | 284.452 | 284.867 | 285.281 | 285.696 | 286.112 | 286.528 | 286.944 | 287.361 | 287.778 | 288.195 |
| 2.400 | 288.613 | 289.031 | 289.450 | 289.869 | 290.288 | 290.708 | 291.128 | 291.549 | 291.970 | 292.391 |
| 2.410 | 292.813 | 293.235 | 293.658 | 294.081 | 294.504 | 294.928 | 295.352 | 295.777 | 296.202 | 296.627 |
| 2.420 | 297.053 | 297.479 | 297.906 | 298.333 | 298.760 | 299.188 | 299.616 | 300.045 | 300.474 | 300.903 |
| 2.430 | 301.333 | 301.763 | 302.194 | 302.625 | 303.056 | 303.488 | 303.920 | 304.353 | 304.786 | 305.219 |
| 2.440 | 305.653 | 306.087 | 306.522 | 306.957 | 307.392 | 307.828 | 308.264 | 308.701 | 309.138 | 309.575 |
| 2.450 | 310.013 | 310.451 | 310.890 | 311.329 | 311.768 | 312.208 | 312.648 | 313.089 | 313.530 | 313.972 |
| 2.460 | 314.414 | 314.856 | 315.299 | 315.742 | 316.185 | 316.629 | 317.074 | 317.518 | 317.963 | 318.409 |
| 2.470 | 318.855 | 319.301 | 319.748 | 320.195 | 320.643 | 321.091 | 321.539 | 321.988 | 322.438 | 322.887 |
| 2.480 | 323.337 | 323.788 | 324.239 | 324.690 | 325.142 | 325.594 | 326.046 | 326.499 | 326.953 | 327.406 |
| 2.490 | 327.861 | 328.315 | 328.770 | 329.226 | 329.681 | 330.138 | 330.594 | 331.051 | 331.509 | 331.967 |
| 2.500 | 332.425 | 332.884 | 333.343 | 333.803 | 334.263 | 334.723 | 335.184 | 335.645 | 336.107 | 336.569 |
| 2.510 | 337.031 | 337.494 | 337.957 | 338.421 | 338.885 | 339.350 | 339.815 | 340.280 | 340.746 | 341.212 |
| 2.520 | 341.679 | 342.146 | 342.613 | 343.081 | 343.550 | 344.018 | 344.487 | 344.957 | 345.427 | 345.897 |
| 2.530 | 346.368 | 346.840 | 347.311 | 347.783 | 348.256 | 348.729 | 349.202 | 349.676 | 350.150 | 350.625 |
| 2.540 | 351.100 | 351.575 | 352.051 | 352.527 | 353.004 | 353.481 | 353.959 | 354.437 | 354.915 | 355.394 |
| 2.550 | 355.874 | 356.353 | 356.833 | 357.314 | 357.795 | 358.276 | 358.758 | 359.240 | 359.723 | 360.206 |
| 2.560 | 360.690 | 361.174 | 361.658 | 362.143 | 362.628 | 363.114 | 363.600 | 364.086 | 364.573 | 365.061 |
| 2.570 | 365.549 | 366.037 | 366.526 | 367.015 | 367.504 | 367.994 | 368.484 | 368.975 | 369.466 | 369.958 |
| 2.580 | 370.450 | 370.943 | 371.436 | 371.929 | 372.423 | 372.917 | 373.412 | 373.907 | 374.403 | 374.899 |
| 2.590 | 375.395 | 375.892 | 376.389 | 376.887 | 377.385 | 377.884 | 378.383 | 378.882 | 379.382 | 379.882 |

TABLE 1b. *Vapor pressure of* $He^3$ *(1962 Scale) in millimeters of mercury at 0 °C and standard gravity, 980.665 cm/sec²*—Con.

| $T_{62}$, °K | 0.000 | 0.001 | 0.002 | 0.003 | 0.004 | 0.005 | 0.006 | 0.007 | 0.008 | 0.009 |
|---|---|---|---|---|---|---|---|---|---|---|
| 2.600 | 380.383 | 380.884 | 381.386 | 381.888 | 382.390 | 382.893 | 383.396 | 383.900 | 384.404 | 384.909 |
| 2.610 | 385.414 | 385.920 | 386.426 | 386.932 | 387.439 | 387.946 | 388.454 | 388.962 | 389.471 | 389.980 |
| 2.620 | 390.489 | 390.999 | 391.510 | 392.020 | 392.532 | 393.043 | 393.555 | 394.068 | 394.581 | 395.094 |
| 2.630 | 395.608 | 396.122 | 396.637 | 397.152 | 397.668 | 398.184 | 398.701 | 399.218 | 399.735 | 400.253 |
| 2.640 | 400.771 | 401.290 | 401.809 | 402.329 | 402.849 | 403.369 | 403.890 | 404.412 | 404.933 | 405.456 |
| 2.650 | 405.978 | 406.502 | 407.025 | 407.549 | 408.074 | 408.599 | 409.124 | 409.650 | 410.176 | 410.703 |
| 2.660 | 411.230 | 411.758 | 412.286 | 412.814 | 413.343 | 413.873 | 414.403 | 414.933 | 415.464 | 415.995 |
| 2.670 | 416.526 | 417.059 | 417.591 | 418.124 | 418.658 | 419.192 | 419.726 | 420.261 | 420.796 | 421.332 |
| 2.680 | 421.868 | 422.404 | 422.942 | 423.479 | 424.017 | 424.555 | 425.094 | 425.634 | 426.173 | 426.714 |
| 2.690 | 427.254 | 427.795 | 428.337 | 428.879 | 429.422 | 429.965 | 430.508 | 431.052 | 431.596 | 432.141 |
| 2.700 | 432.686 | 433.232 | 433.778 | 434.325 | 434.872 | 435.419 | 435.967 | 436.516 | 437.064 | 437.614 |
| 2.710 | 438.164 | 438.714 | 439.265 | 439.816 | 440.367 | 440.919 | 441.472 | 442.025 | 442.578 | 443.132 |
| 2.720 | 443.687 | 444.242 | 444.797 | 445.353 | 445.909 | 446.466 | 447.023 | 447.580 | 448.138 | 448.697 |
| 2.730 | 449.256 | 449.816 | 450.375 | 450.936 | 451.497 | 452.058 | 452.620 | 453.182 | 453.745 | 454.308 |
| 2.740 | 454.872 | 455.436 | 456.000 | 456.565 | 457.131 | 457.697 | 458.263 | 458.830 | 459.379 | 459.965 |
| 2.750 | 460.534 | 461.102 | 461.671 | 462.241 | 462.811 | 463.382 | 463.953 | 464.525 | 465.097 | 465.669 |
| 2.760 | 466.242 | 466.816 | 467.390 | 467.964 | 468.539 | 469.114 | 469.690 | 470.266 | 470.843 | 471.420 |
| 2.770 | 471.998 | 472.576 | 473.155 | 473.734 | 474.313 | 474.893 | 475.474 | 476.055 | 476.636 | 477.218 |
| 2.780 | 477.801 | 478.384 | 478.967 | 479.551 | 480.135 | 480.720 | 481.305 | 481.891 | 482.477 | 483.064 |
| 2.790 | 483.651 | 484.239 | 484.827 | 485.415 | 486.004 | 486.594 | 487.184 | 487.774 | 488.365 | 488.957 |
| 2.800 | 489.549 | 490.141 | 490.734 | 491.327 | 491.921 | 492.516 | 493.110 | 493.706 | 494.302 | 494.898 |
| 2.810 | 495.495 | 496.092 | 496.689 | 497.288 | 497.886 | 498.486 | 499.085 | 499.685 | 500.286 | 500.887 |
| 2.820 | 501.488 | 502.091 | 502.693 | 503.296 | 503.900 | 504.504 | 505.108 | 505.713 | 506.318 | 506.924 |
| 2.830 | 507.531 | 508.138 | 508.745 | 509.353 | 509.961 | 510.570 | 511.180 | 511.789 | 512.400 | 513.010 |
| 2.840 | 513.622 | 514.234 | 514.846 | 515.459 | 516.072 | 516.686 | 517.300 | 517.915 | 518.530 | 519.145 |
| 2.850 | 519.762 | 520.378 | 520.996 | 521.613 | 522.231 | 522.850 | 523.469 | 524.089 | 524.709 | 525.330 |
| 2.860 | 525.951 | 526.572 | 527.194 | 527.817 | 528.440 | 529.064 | 529.688 | 530.312 | 530.937 | 531.563 |
| 2.870 | 532.189 | 532.816 | 533.443 | 534.070 | 534.698 | 535.327 | 535.956 | 536.585 | 537.216 | 537.846 |
| 2.880 | 538.477 | 539.109 | 539.741 | 540.373 | 541.006 | 541.640 | 542.274 | 542.909 | 543.544 | 544.179 |
| 2.890 | 544.815 | 545.452 | 546.089 | 546.726 | 547.364 | 548.003 | 548.642 | 549.282 | 549.922 | 550.562 |
| 2.900 | 551.203 | 551.845 | 552.487 | 553.130 | 553.773 | 554.416 | 555.061 | 555.705 | 556.350 | 556.996 |
| 2.910 | 557.642 | 558.289 | 558.936 | 559.584 | 560.232 | 560.880 | 561.530 | 562.179 | 562.830 | 563.480 |
| 2.920 | 564.131 | 564.783 | 565.435 | 566.088 | 566.742 | 567.395 | 568.050 | 568.704 | 569.360 | 570.016 |
| 2.930 | 570.672 | 571.329 | 571.986 | 572.644 | 573.302 | 573.961 | 574.621 | 575.281 | 575.941 | 576.602 |
| 2.940 | 577.264 | 577.926 | 578.588 | 579.251 | 579.915 | 580.579 | 581.243 | 581.909 | 582.574 | 583.240 |
| 2.950 | 583.907 | 584.574 | 585.242 | 585.910 | 586.579 | 587.248 | 587.918 | 588.588 | 589.259 | 589.930 |
| 2.960 | 590.602 | 591.275 | 591.947 | 592.621 | 593.295 | 593.969 | 594.644 | 595.320 | 595.996 | 596.672 |
| 2.970 | 597.349 | 598.027 | 598.705 | 599.384 | 600.063 | 600.743 | 601.423 | 602.104 | 602.785 | 603.467 |
| 2.980 | 604.149 | 604.832 | 605.515 | 606.199 | 606.884 | 607.569 | 608.254 | 608.940 | 609.627 | 610.314 |
| 2.990 | 611.002 | 611.690 | 612.379 | 613.068 | 613.758 | 614.448 | 615.139 | 615.830 | 616.522 | 617.214 |
| 3.000 | 617.907 | 618.601 | 619.295 | 619.989 | 620.684 | 621.380 | 622.076 | 622.773 | 623.470 | 624.168 |
| 3.010 | 624.866 | 625.565 | 626.264 | 626.964 | 627.665 | 628.366 | 629.067 | 629.769 | 630.472 | 631.175 |
| 3.020 | 631.879 | 632.583 | 633.288 | 633.993 | 634.699 | 635.405 | 636.112 | 636.820 | 637.528 | 638.236 |
| 3.030 | 638.945 | 639.655 | 640.365 | 641.076 | 641.787 | 642.499 | 643.211 | 643.924 | 644.638 | 645.351 |
| 3.040 | 646.066 | 646.781 | 647.497 | 648.213 | 648.930 | 649.647 | 650.365 | 651.083 | 651.802 | 652.521 |
| 3.050 | 653.241 | 653.962 | 654.683 | 655.405 | 656.127 | 656.850 | 657.573 | 658.297 | 659.021 | 659.746 |
| 3.060 | 660.472 | 661.198 | 661.924 | 662.652 | 663.379 | 664.108 | 664.836 | 665.566 | 666.296 | 667.026 |
| 3.070 | 667.757 | 668.489 | 669.221 | 669.954 | 670.687 | 671.421 | 672.155 | 672.890 | 673.626 | 674.362 |
| 3.080 | 675.098 | 675.836 | 676.573 | 677.312 | 678.051 | 678.790 | 679.530 | 680.271 | 681.012 | 681.753 |
| 3.090 | 682.496 | 683.238 | 683.982 | 684.726 | 685.470 | 686.215 | 686.961 | 687.707 | 688.454 | 689.201 |
| 3.100 | 689.949 | 690.697 | 691.446 | 692.196 | 692.946 | 693.697 | 694.448 | 695.200 | 695.952 | 696.705 |
| 3.110 | 697.459 | 698.213 | 698.968 | 699.723 | 700.479 | 701.235 | 701.992 | 702.750 | 703.508 | 704.267 |
| 3.120 | 705.026 | 705.786 | 706.546 | 707.307 | 708.069 | 708.831 | 709.594 | 710.357 | 711.121 | 711.885 |
| 3.130 | 712.650 | 713.416 | 714.182 | 714.949 | 715.716 | 716.484 | 717.252 | 718.021 | 718.791 | 719.561 |
| 3.140 | 720.332 | 721.104 | 721.875 | 722.648 | 723.421 | 724.195 | 724.969 | 725.744 | 726.520 | 727.296 |
| 3.150 | 728.072 | 728.849 | 729.627 | 730.406 | 731.184 | 731.964 | 732.744 | 733.525 | 734.306 | 735.088 |
| 3.160 | 735.871 | 736.654 | 737.437 | 738.222 | 739.006 | 739.792 | 740.578 | 741.364 | 742.152 | 742.939 |
| 3.170 | 743.728 | 744.517 | 745.306 | 746.097 | 746.887 | 747.679 | 748.471 | 749.263 | 750.056 | 750.850 |
| 3.180 | 751.644 | 752.439 | 753.235 | 754.031 | 754.828 | 755.625 | 756.423 | 757.221 | 758.020 | 758.820 |
| 3.190 | 759.620 | 760.421 | 761.223 | 762.025 | 762.828 | 763.631 | 764.435 | 765.239 | 766.044 | 766.850 |
| 3.200 | 767.656 | 768.463 | 769.271 | 770.079 | 770.888 | 771.697 | 772.507 | 773.317 | 774.129 | 774.940 |
| 3.210 | 775.753 | 776.566 | 777.379 | 778.193 | 779.008 | 779.824 | 780.640 | 781.456 | 782.274 | 783.091 |
| 3.220 | 783.910 | 784.729 | 785.549 | 786.369 | 787.190 | 788.011 | 788.833 | 789.656 | 790.480 | 791.304 |
| 3.230 | 792.138 | 792.953 | 793.779 | 794.606 | 795.433 | 796.260 | 797.089 | 797.918 | 798.747 | 799.577 |
| 3.240 | 800.408 | 801.240 | 802.072 | 802.904 | 803.738 | 804.571 | 805.406 | 806.241 | 807.077 | 807.913 |
| 3.250 | 808.750 | 809.588 | 810.426 | 811.265 | 812.104 | 812.945 | 813.785 | 814.627 | 815.469 | 816.311 |
| 3.260 | 817.155 | 817.999 | 818.843 | 819.688 | 820.534 | 821.380 | 822.228 | 823.075 | 823.923 | 824.772 |
| 3.270 | 825.622 | 826.472 | 827.323 | 828.175 | 829.027 | 829.879 | 830.733 | 831.587 | 832.442 | 833.297 |
| 3.280 | 834.153 | 835.009 | 835.867 | 836.724 | 837.583 | 838.442 | 839.302 | 840.162 | 841.023 | 841.885 |
| 3.290 | 842.747 | 843.610 | 844.474 | 845.388 | 846.203 | 847.069 | 847.935 | 848.802 | 849.669 | 850.537 |
| 3.300 | 851.406 | 852.276 | 853.146 | 854.016 | 854.888 | 855.760 | 856.632 | 857.506 | 858.380 | 859.254 |
| 3.310 | 860.130 | 861.006 | 861.882 | 862.759 | 863.637 | 864.516 | 865.395 | 866.275 | 867.155 | 868.037 |
| 3.320 | 868.918 | 869.801 | 870.684 | 871.568 | 872.452 | 873.337 | | | | |

TABLE 2a. $T_{62}$ $He^3$ *temperatures in °K as a function of vapor pressure,* P, *in microns* ($10^{-3}$ *mm*) *of mercury at 0 °C and standard gravity, 980.665 cm/sec²*

| P | 0 | 1 | 2 | 3 | 4 | 5 | 6 | 7 | 8 | 9 |
|---|---|---|---|---|---|---|---|---|---|---|
| 0.01 | 0.1974 13 | 1987 12 | 1999 11 | 2010 10 | 2020 10 | 2030 9 | 2039 9 | 2048 8 | 2056 7 | 2063 8 |
| .02 | .2071 7 | 2078 7 | 2085 6 | 2091 7 | 2098 6 | 2104 6 | 2110 5 | 2115 6 | 2121 5 | 2126 5 |
| .03 | .2131 6 | 2137 4 | 2141 5 | 2146 5 | 2151 4 | 2155 5 | 2160 4 | 2164 4 | 2168 4 | 2172 4 |
| .04 | .2176 4 | 2180 4 | 2184 4 | 2188 4 | 2192 3 | 2195 4 | 2199 3 | 2202 4 | 2206 3 | 2209 4 |
| .05 | .2213 3 | 2216 3 | 2219 3 | 2222 3 | 2225 3 | 2228 3 | 2231 3 | 2234 3 | 2237 3 | 2240 3 |
| .06 | .2243 3 | 2246 2 | 2248 3 | 2251 3 | 2254 3 | 2257 2 | 2259 3 | 2262 2 | 2264 3 | 2267 2 |
| .07 | .2269 3 | 2272 2 | 2274 2 | 2276 3 | 2279 2 | 2281 2 | 2283 3 | 2286 2 | 2288 2 | 2290 2 |
| .08 | .2292 3 | 2295 2 | 2297 2 | 2299 2 | 2301 2 | 2303 2 | 2305 2 | 2307 2 | 2309 2 | 2311 2 |
| .09 | .2313 2 | 2315 2 | 2317 2 | 2319 2 | 2321 2 | 2323 2 | 2325 2 | 2327 1 | 2328 2 | 2330 2 |
| .10 | .2332 18 | 2350 16 | 2366 15 | 2381 14 | 2395 13 | 2408 12 | 2420 12 | 2432 11 | 2443 11 | 2454 10 |
| .20 | .2464 10 | 2474 9 | 2483 9 | 2492 9 | 2501 8 | 2509 9 | 2518 8 | 2526 7 | 2533 8 | 2541 7 |
| .30 | .2548 7 | 2555 7 | 2562 6 | 2568 7 | 2575 6 | 2581 6 | 2587 6 | 2593 6 | 2599 6 | 2605 5 |
| .40 | .2610 6 | 2616 5 | 2621 5 | 2626 6 | 2632 5 | 2637 5 | 2642 5 | 2647 4 | 2651 5 | 2656 5 |
| .50 | .2661 4 | 2665 5 | 2670 4 | 2674 5 | 2679 4 | 2683 4 | 2687 4 | 2691 4 | 2695 4 | 2699 4 |
| .60 | .2703 4 | 2707 4 | 2711 4 | 2715 4 | 2719 3 | 2722 4 | 2726 4 | 2730 3 | 2733 4 | 2737 3 |
| .70 | .2740 4 | 2744 3 | 2747 3 | 2750 4 | 2754 3 | 2757 3 | 2760 4 | 2764 3 | 2767 3 | 2770 3 |
| .80 | .2773 3 | 2776 3 | 2779 3 | 2782 3 | 2785 3 | 2788 3 | 2791 3 | 2794 3 | 2797 3 | 2800 3 |
| .90 | .2803 2 | 2805 3 | 2808 3 | 2811 3 | 2814 2 | 2816 3 | 2819 3 | 2822 2 | 2824 3 | 2827 2 |
| 1 | .2829 25 | 2854 23 | 2877 21 | 2898 20 | 2918 19 | 2937 18 | 2955 17 | 2972 16 | 2988 16 | 3004 14 |
| 2 | .3018 14 | 3032 14 | 3046 13 | 3059 13 | 3072 12 | 3084 12 | 3096 11 | 3107 11 | 3118 11 | 3129 11 |
| 3 | .3140 10 | 3150 10 | 3160 9 | 3169 10 | 3179 9 | 3188 9 | 3197 9 | 3206 8 | 3214 9 | 3223 8 |
| 4 | .3231 8 | 3239 8 | 3247 8 | 3255 7 | 3262 8 | 3270 7 | 3277 7 | 3284 8 | 3292 7 | 3299 6 |
| 5 | .3305 7 | 3312 7 | 3319 6 | 3325 7 | 3332 6 | 3338 6 | 3344 6 | 3350 6 | 3356 6 | 3362 6 |
| 6 | .3368 6 | 3374 6 | 3380 6 | 3386 5 | 3391 6 | 3397 5 | 3402 6 | 3408 5 | 3413 5 | 3418 5 |
| 7 | .3423 5 | 3428 6 | 3434 5 | 3439 4 | 3443 5 | 3448 5 | 3453 5 | 3458 5 | 3463 5 | 3468 4 |
| 8 | .3472 5 | 3477 4 | 3481 5 | 3486 4 | 3490 5 | 3495 4 | 3499 5 | 3504 4 | 3508 4 | 3512 4 |
| 9 | .3516 5 | 3521 4 | 3525 4 | 3529 4 | 3533 4 | 3537 4 | 3541 4 | 3545 4 | 3549 4 | 3553 4 |
| 10 | .3557 37 | 3594 34 | 3628 33 | 3661 30 | 3691 29 | 3720 27 | 3747 26 | 3773 24 | 3797 24 | 3821 23 |
| 20 | .3844 21 | 3865 21 | 3886 21 | 3907 19 | 3926 19 | 3945 18 | 3963 18 | 3981 17 | 3998 17 | 4015 16 |
| 30 | .4031 16 | 4047 15 | 4062 15 | 4077 15 | 4092 15 | 4107 14 | 4121 13 | 4134 14 | 4148 13 | 4161 13 |
| 40 | .4174 13 | 4187 12 | 4199 12 | 4211 12 | 4223 12 | 4235 11 | 4246 12 | 4258 11 | 4269 11 | 4280 11 |
| 50 | .4291 10 | 4301 11 | 4312 10 | 4322 10 | 4332 10 | 4342 10 | 4352 10 | 4362 10 | 4372 9 | 4381 10 |
| 60 | .4391 9 | 4400 9 | 4409 9 | 4418 9 | 4427 9 | 4436 8 | 4444 9 | 4453 8 | 4461 9 | 4470 8 |
| 70 | .4478 8 | 4486 9 | 4495 8 | 4503 7 | 4510 8 | 4518 8 | 4526 8 | 4534 7 | 4541 8 | 4549 7 |
| 80 | .4556 8 | 4564 7 | 4571 7 | 4578 8 | 4586 7 | 4593 7 | 4600 7 | 4607 7 | 4614 7 | 4621 7 |
| 90 | .4628 6 | 4634 7 | 4641 7 | 4648 6 | 4654 7 | 4661 6 | 4667 7 | 4674 6 | 4680 6 | 4686 7 |

TABLE 2b. $T_{62}$ $He^3$ *temperatures in °K as a function of vapor pressure,* P, *in millimeters of mercury at 0 °C and standard gravity, 980.665 cm/sec²*

| P | 0 | 1 | 2 | 3 | 4 | 5 | 6 | 7 | 8 | 9 |
|---|---|---|---|---|---|---|---|---|---|---|
| 0.1 | 0.4693 60 | 4753 56 | 4809 53 | 4862 50 | 4912 47 | 4959 44 | 5003 43 | 5046 41 | 5087 39 | 5126 37 |
| .2 | .5163 37 | 5200 34 | 5234 34 | 5268 33 | 5301 31 | 5332 31 | 5363 30 | 5393 29 | 5422 28 | 5450 27 |
| .3 | .5477 27 | 5504 26 | 5530 26 | 5556 24 | 5580 25 | 5605 24 | 5629 23 | 5652 23 | 5675 23 | 5698 22 |
| .4 | .5720 21 | 5741 22 | 5763 20 | 5783 21 | 5804 20 | 5824 20 | 5844 19 | 5863 20 | 5883 19 | 5902 18 |
| .5 | .5920 19 | 5939 18 | 5957 18 | 5975 17 | 5992 18 | 6010 17 | 6027 17 | 6044 16 | 6060 17 | 6077 16 |
| .6 | .6093 16 | 6109 16 | 6125 16 | 6141 15 | 6156 16 | 6172 15 | 6187 15 | 6202 14 | 6216 15 | 6231 15 |
| .7 | .6246 14 | 6260 14 | 6274 14 | 6288 14 | 6302 14 | 6316 14 | 6330 13 | 6343 14 | 6357 13 | 6370 13 |
| .8 | .6383 13 | 6396 13 | 6409 13 | 6422 12 | 6434 13 | 6447 12 | 6459 13 | 6472 12 | 6484 12 | 6496 12 |
| .9 | .6508 12 | 6520 12 | 6532 12 | 6544 12 | 6556 11 | 6567 12 | 6579 11 | 6590 11 | 6601 12 | 6613 11 |
| 1.0 | .6624 11 | 6635 11 | 6646 11 | 6657 11 | 6668 10 | 6678 11 | 6689 11 | 6700 10 | 6710 11 | 6721 10 |
| 1.1 | .6731 11 | 6742 10 | 6752 10 | 6762 10 | 6772 10 | 6782 10 | 6792 10 | 6802 10 | 6812 10 | 6822 10 |
| 1.2 | .6832 10 | 6842 9 | 6851 10 | 6861 9 | 6870 10 | 6880 9 | 6889 10 | 6899 9 | 6908 9 | 6917 9 |
| 1.3 | .6926 10 | 6936 9 | 6945 9 | 6954 9 | 6963 9 | 6972 9 | 6981 9 | 6990 8 | 6998 9 | 7007 9 |
| 1.4 | .7016 9 | 7025 8 | 7033 9 | 7042 9 | 7051 8 | 7059 9 | 7068 8 | 7076 8 | 7084 9 | 7093 8 |
| 1.5 | .7101 8 | 7109 9 | 7118 8 | 7126 8 | 7134 8 | 7142 8 | 7150 8 | 7158 8 | 7166 8 | 7174 8 |
| 1.6 | .7182 8 | 7190 8 | 7198 8 | 7206 7 | 7213 8 | 7221 8 | 7229 8 | 7237 7 | 7244 8 | 7252 8 |
| 1.7 | .7260 7 | 7267 8 | 7275 7 | 7282 8 | 7290 7 | 7297 8 | 7305 7 | 7312 7 | 7319 8 | 7327 7 |
| 1.8 | .7334 7 | 7341 7 | 7348 8 | 7356 7 | 7363 7 | 7370 7 | 7377 7 | 7384 7 | 7391 7 | 7398 7 |
| 1.9 | .7405 7 | 7412 7 | 7419 7 | 7426 7 | 7433 7 | 7440 7 | 7447 7 | 7454 6 | 7460 7 | 7467 7 |
| 2.0 | .7474 7 | 7481 7 | 7488 6 | 7494 7 | 7501 7 | 7508 6 | 7514 7 | 7521 6 | 7527 7 | 7534 6 |
| 2.1 | .7540 7 | 7547 6 | 7553 7 | 7560 6 | 7566 7 | 7573 6 | 7579 7 | 7586 6 | 7592 6 | 7598 7 |
| 2.2 | .7605 6 | 7611 6 | 7617 6 | 7623 7 | 7630 6 | 7636 6 | 7642 6 | 7648 6 | 7654 7 | 7661 6 |
| 2.3 | .7667 6 | 7673 6 | 7679 6 | 7685 6 | 7691 6 | 7697 6 | 7703 6 | 7709 6 | 7715 6 | 7721 6 |
| 2.4 | .7727 6 | 7733 6 | 7739 6 | 7745 5 | 7750 6 | 7756 6 | 7762 6 | 7768 6 | 7774 6 | 7780 5 |
| 2.5 | .7785 6 | 7791 6 | 7797 6 | 7803 5 | 7808 6 | 7814 6 | 7820 5 | 7825 6 | 7831 6 | 7837 5 |
| 2.6 | .7842 6 | 7848 5 | 7853 6 | 7859 5 | 7864 6 | 7870 6 | 7876 5 | 7881 6 | 7887 5 | 7892 5 |
| 2.7 | .7897 6 | 7903 5 | 7908 6 | 7914 5 | 7919 6 | 7925 5 | 7930 5 | 7935 6 | 7941 5 | 7946 5 |
| 2.8 | .7951 6 | 7957 5 | 7962 5 | 7967 6 | 7973 5 | 7978 5 | 7983 5 | 7988 6 | 7994 5 | 7999 5 |
| 2.9 | .8004 5 | 8009 5 | 8014 5 | 8019 6 | 8025 5 | 8030 5 | 8035 5 | 8040 5 | 8045 5 | 8050 5 |

TABLE 2b. $T_{62}$ $He^3$ *temperatures in °K as a function of vapor pressure,* P, *in millimeters of mercury at 0 °C and standard gravity 980.665 cm/sec²*—Continued

| P | 0 | 1 | 2 | 3 | 4 | 5 | 6 | 7 | 8 | 9 |
|---|---|---|---|---|---|---|---|---|---|---|
| 3 | 0.8055 50 | 8105 49 | 8154 48 | 8202 47 | 8249 46 | 8295 45 | 8340 44 | 8384 43 | 8427 43 | 8470 42 |
| 4 | .8512 41 | 8553 40 | 8593 40 | 8633 39 | 8672 38 | 8710 38 | 8748 38 | 8786 36 | 8822 37 | 8859 35 |
| 5 | .8894 36 | 8930 34 | 8964 35 | 8999 33 | 9032 34 | 9066 33 | 9099 32 | 9131 33 | 9164 31 | 9195 32 |
| 6 | .9227 31 | 9258 31 | 9289 30 | 9319 30 | 9349 30 | 9379 29 | 9408 29 | 9437 29 | 9466 29 | 9495 28 |
| 7 | .9523 28 | 9551 28 | 9579 27 | 9606 27 | 9633 27 | 9660 27 | 9687 26 | 9713 27 | 9740 26 | 9766 25 |
| 8 | .9791 26 | 9817 25 | 9842 25 | 9867 25 | 9892 25 | 9917 24 | 9941 25 | 9966 24 | 9990 24 | 0014 24 |
| 9 | 1.0038 23 | 0061 24 | 0085 23 | 0108 23 | 0131 23 | 0154 22 | 0176 23 | 0199 22 | 0221 23 | 0244 22 |
| 10 | 1.0266 22 | 0288 22 | 0310 21 | 0331 22 | 0353 21 | 0374 21 | 0395 21 | 0416 21 | 0437 21 | 0458 21 |
| 11 | 1.0479 21 | 0500 20 | 0520 20 | 0540 21 | 0561 20 | 0581 20 | 0601 19 | 0620 20 | 0640 20 | 0660 19 |
| 12 | 1.0679 20 | 0699 19 | 0718 19 | 0737 19 | 0756 19 | 0775 19 | 0794 19 | 0813 19 | 0832 18 | 0850 19 |
| 13 | 1.0869 18 | 0887 18 | 0905 19 | 0924 18 | 0942 18 | 0960 18 | 0978 18 | 0996 17 | 1013 18 | 1031 18 |
| 14 | 1.1049 17 | 1066 17 | 1083 18 | 1101 17 | 1118 17 | 1135 17 | 1152 17 | 1169 17 | 1186 17 | 1203 17 |
| 15 | 1.1220 17 | 1237 16 | 1253 17 | 1270 16 | 1286 17 | 1303 16 | 1319 16 | 1335 17 | 1352 16 | 1368 16 |
| 16 | 1.1384 16 | 1400 16 | 1416 16 | 1432 15 | 1447 16 | 1463 16 | 1479 15 | 1494 16 | 1510 15 | 1525 16 |
| 17 | 1.1541 15 | 1556 15 | 1571 16 | 1587 15 | 1602 15 | 1617 15 | 1632 15 | 1647 15 | 1662 15 | 1677 15 |
| 18 | 1.1692 15 | 1707 14 | 1721 15 | 1736 15 | 1751 14 | 1765 15 | 1780 14 | 1794 15 | 1809 14 | 1823 14 |
| 19 | 1.1837 14 | 1851 15 | 1866 14 | 1880 14 | 1894 14 | 1908 14 | 1922 14 | 1936 14 | 1950 14 | 1964 14 |
| 20 | 1.1978 13 | 1991 14 | 2005 14 | 2019 13 | 2032 14 | 2046 14 | 2060 13 | 2073 14 | 2087 13 | 2100 13 |
| 21 | 1.2113 14 | 2127 13 | 2140 13 | 2153 13 | 2166 14 | 2180 13 | 2193 13 | 2206 13 | 2219 13 | 2232 13 |
| 22 | 1.2245 13 | 2258 13 | 2271 13 | 2284 12 | 2296 13 | 2309 13 | 2322 13 | 2335 12 | 2347 13 | 2360 13 |
| 23 | 1.2373 12 | 2385 13 | 2398 12 | 2410 13 | 2423 12 | 2435 12 | 2447 13 | 2460 12 | 2472 12 | 2484 12 |
| 24 | 1.2496 13 | 2509 12 | 2521 12 | 2533 12 | 2545 12 | 2557 12 | 2569 12 | 2581 12 | 2593 12 | 2605 12 |
| 25 | 1.2617 12 | 2629 12 | 2641 12 | 2653 11 | 2664 12 | 2676 12 | 2688 12 | 2700 11 | 2711 12 | 2723 11 |
| 26 | 1.2734 12 | 2746 12 | 2758 11 | 2769 12 | 2781 11 | 2792 11 | 2803 12 | 2815 11 | 2826 12 | 2838 11 |
| 27 | 1.2849 11 | 2860 11 | 2871 12 | 2883 11 | 2894 11 | 2905 11 | 2916 11 | 2927 11 | 2938 11 | 2949 11 |
| 28 | 1.2960 11 | 2971 11 | 2982 11 | 2993 11 | 3004 11 | 3015 11 | 3026 11 | 3037 11 | 3048 11 | 3059 10 |
| 29 | 1.3069 11 | 3080 11 | 3091 11 | 3102 10 | 3112 11 | 3123 11 | 3134 10 | 3144 11 | 3155 10 | 3165 11 |
| 30 | 1.3176 11 | 3187 10 | 3197 10 | 3207 11 | 3218 10 | 3228 11 | 3239 10 | 3249 11 | 3260 10 | 3270 10 |
| 31 | 1.3280 10 | 3290 11 | 3301 10 | 3311 10 | 3321 10 | 3331 11 | 3342 10 | 3352 10 | 3362 10 | 3372 10 |
| 32 | 1.3382 10 | 3392 10 | 3402 10 | 3412 10 | 3422 10 | 3432 10 | 3442 10 | 3452 10 | 3462 10 | 3472 10 |
| 33 | 1.3482 10 | 3492 10 | 3502 10 | 3512 10 | 3522 9 | 3531 10 | 3541 10 | 3551 10 | 3561 9 | 3570 10 |
| 34 | 1.3580 10 | 3590 9 | 3599 10 | 3609 10 | 3619 9 | 3628 10 | 3638 9 | 3647 10 | 3657 10 | 3667 9 |
| 35 | 1.3676 10 | 3686 9 | 3695 10 | 3705 9 | 3714 9 | 3723 10 | 3733 9 | 3742 10 | 3752 9 | 3761 9 |
| 36 | 1.3770 10 | 3780 9 | 3789 9 | 3798 10 | 3808 9 | 3817 9 | 3826 9 | 3835 9 | 3844 10 | 3854 9 |
| 37 | 1.3863 9 | 3872 9 | 3881 9 | 3890 9 | 3899 10 | 3909 9 | 3918 9 | 3927 9 | 3936 9 | 3945 9 |
| 38 | 1.3954 9 | 3963 9 | 3972 9 | 3981 9 | 3990 9 | 3999 9 | 4008 8 | 4016 9 | 4025 9 | 4034 9 |
| 39 | 1.4043 9 | 4052 9 | 4061 9 | 4070 8 | 4078 9 | 4087 9 | 4096 9 | 4105 8 | 4113 9 | 4122 9 |
| 40 | 1.4131 9 | 4140 8 | 4148 9 | 4157 9 | 4166 8 | 4174 9 | 4183 9 | 4192 8 | 4200 9 | 4209 8 |
| 41 | 1.4217 9 | 4226 8 | 4234 9 | 4243 8 | 4251 9 | 4260 8 | 4268 9 | 4277 8 | 4285 9 | 4294 8 |
| 42 | 1.4302 9 | 4311 8 | 4319 9 | 4328 8 | 4336 8 | 4344 9 | 4353 8 | 4361 8 | 4369 9 | 4378 8 |
| 43 | 1.4386 8 | 4394 9 | 4403 8 | 4411 8 | 4419 8 | 4427 9 | 4436 8 | 4444 8 | 4452 8 | 4460 8 |
| 44 | 1.4468 9 | 4477 8 | 4485 8 | 4493 8 | 4501 8 | 4509 8 | 4517 8 | 4525 8 | 4533 8 | 4541 9 |
| 45 | 1.4550 8 | 4558 8 | 4566 8 | 4574 8 | 4582 8 | 4590 8 | 4598 8 | 4606 8 | 4614 8 | 4622 8 |
| 46 | 1.4630 7 | 4637 8 | 4645 8 | 4653 8 | 4661 8 | 4669 8 | 4677 8 | 4685 8 | 4693 8 | 4701 7 |
| 47 | 1.4708 8 | 4716 8 | 4724 8 | 4732 8 | 4740 7 | 4747 8 | 4755 8 | 4763 8 | 4771 7 | 4778 8 |
| 48 | 1.4786 8 | 4794 8 | 4802 7 | 4809 8 | 4817 8 | 4825 7 | 4832 8 | 4840 8 | 4848 7 | 4855 8 |
| 49 | 1.4863 7 | 4870 8 | 4878 8 | 4886 7 | 4893 8 | 4901 7 | 4908 8 | 4916 8 | 4924 7 | 4931 8 |
| 50 | 1.4939 74 | 5013 74 | 5087 73 | 5160 72 | 5232 71 | 5303 70 | 5373 69 | 5442 69 | 5511 68 | 5579 67 |
| 60 | 1.5646 66 | 5712 66 | 5778 65 | 5843 64 | 5907 64 | 5971 62 | 6033 63 | 6096 62 | 6158 61 | 6219 60 |
| 70 | 1.6279 60 | 6339 60 | 6399 59 | 6458 58 | 6516 58 | 6574 57 | 6631 57 | 6688 56 | 6744 56 | 6800 56 |
| 80 | 1.6856 55 | 6911 54 | 6965 55 | 7020 53 | 7073 54 | 7127 52 | 7179 53 | 7232 52 | 7284 52 | 7336 51 |
| 90 | 1.7387 51 | 7438 51 | 7489 50 | 7539 50 | 7589 49 | 7638 49 | 7687 49 | 7736 49 | 7785 48 | 7833 48 |
| 100 | 1.7881 47 | 7928 48 | 7976 47 | 8023 46 | 8069 47 | 8116 46 | 8162 46 | 8208 45 | 8253 45 | 8298 45 |
| 110 | 1.8343 45 | 8388 45 | 8433 44 | 8477 44 | 8521 43 | 8564 44 | 8608 43 | 8651 43 | 8694 43 | 8737 42 |
| 120 | 1.8779 43 | 8822 42 | 8864 41 | 8905 42 | 8947 41 | 8988 42 | 9030 41 | 9071 40 | 9111 41 | 9152 40 |
| 130 | 1.9192 40 | 9232 40 | 9272 40 | 9312 39 | 9351 40 | 9391 39 | 9430 39 | 9469 39 | 9508 38 | 9546 39 |
| 140 | 1.9585 38 | 9623 38 | 9661 38 | 9699 38 | 9737 37 | 9774 38 | 9812 37 | 9849 37 | 9886 37 | 9923 36 |
| 150 | 1.9959 37 | 9996 36 | 0032 37 | 0069 36 | 0105 36 | 0141 35 | 0176 36 | 0212 36 | 0248 35 | 0283 35 |
| 160 | 2.0318 35 | 0353 35 | 0388 35 | 0423 35 | 0458 34 | 0492 34 | 0526 35 | 0561 34 | 0595 34 | 0629 34 |
| 170 | 2.0663 33 | 0696 34 | 0730 33 | 0763 34 | 0797 33 | 0830 33 | 0863 33 | 0896 33 | 0929 32 | 0961 33 |
| 180 | 2.0994 33 | 1027 32 | 1059 32 | 1091 32 | 1123 32 | 1155 32 | 1187 32 | 1219 32 | 1251 31 | 1282 32 |
| 190 | 2.1314 31 | 1345 31 | 1376 32 | 1408 31 | 1439 30 | 1469 31 | 1500 31 | 1531 31 | 1562 30 | 1592 31 |
| 200 | 2.1623 30 | 1653 30 | 1683 30 | 1713 30 | 1743 30 | 1773 30 | 1803 30 | 1833 30 | 1863 29 | 1892 30 |
| 210 | 2.1922 29 | 1951 29 | 1980 30 | 2010 29 | 2039 29 | 2068 29 | 2097 29 | 2126 28 | 2154 29 | 2183 29 |
| 220 | 2.2212 28 | 2240 28 | 2268 29 | 2297 28 | 2325 28 | 2353 28 | 2381 28 | 2409 28 | 2437 28 | 2465 28 |
| 230 | 2.2493 28 | 2521 27 | 2548 28 | 2576 27 | 2603 28 | 2631 27 | 2658 27 | 2685 27 | 2712 28 | 2740 27 |
| 240 | 2.2767 26 | 2793 27 | 2820 27 | 2847 27 | 2874 27 | 2901 26 | 2927 27 | 2954 26 | 2980 26 | 3006 27 |
| 250 | 2.3033 26 | 3059 26 | 3085 26 | 3111 26 | 3137 26 | 3163 26 | 3189 26 | 3215 26 | 3241 25 | 3266 26 |
| 260 | 2.3292 26 | 3318 25 | 3343 26 | 3369 25 | 3394 25 | 3419 26 | 3445 25 | 3470 25 | 3495 25 | 3520 25 |
| 270 | 2.3545 25 | 3570 25 | 3595 25 | 3620 25 | 3645 24 | 3669 25 | 3694 24 | 3718 25 | 3743 25 | 3768 24 |
| 280 | 2.3792 24 | 3816 25 | 3841 24 | 3865 24 | 3889 24 | 3913 24 | 3937 24 | 3961 24 | 3985 24 | 4009 24 |
| 290 | 2.4033 24 | 4057 24 | 4081 23 | 4104 24 | 4128 24 | 4152 23 | 4175 24 | 4199 23 | 4222 24 | 4246 23 |
| 300 | 2.4269 23 | 4292 24 | 4316 23 | 4339 23 | 4362 23 | 4385 23 | 4408 23 | 4431 23 | 4454 23 | 4477 23 |
| 310 | 2.4500 23 | 4523 22 | 4545 23 | 4568 23 | 4591 22 | 4613 23 | 4636 22 | 4658 23 | 4681 22 | 4703 23 |
| 320 | 2.4726 22 | 4748 22 | 4770 23 | 4793 22 | 4815 22 | 4837 22 | 4859 22 | 4881 22 | 4903 22 | 4925 22 |
| 330 | 2.4947 22 | 4969 22 | 4991 22 | 5013 21 | 5034 22 | 5056 22 | 5078 21 | 5099 22 | 5121 22 | 5143 21 |
| 340 | 2.5164 21 | 5185 22 | 5207 21 | 5228 22 | 5250 21 | 5271 21 | 5292 21 | 5313 22 | 5335 21 | 5356 21 |

TABLE 2b. $T_{62}$ $He^3$ *temperatures in °K as a function of vapor pressure,* P, *in millimeters of mercury at 0 °C and standard gravity, 980.665 cm/sec²*—Continued

| P | 0 | 1 | 2 | 3 | 4 | 5 | 6 | 7 | 8 | 9 |
|---|---|---|---|---|---|---|---|---|---|---|
| 350 | 2.5377 21 | 5398 21 | 5419 21 | 5440 21 | 5461 21 | 5482 21 | 5503 21 | 5524 20 | 5544 21 | 5565 21 |
| 360 | 2.5586 20 | 5606 21 | 5627 21 | 5648 20 | 5668 21 | 5689 20 | 5709 21 | 5730 20 | 5750 21 | 5771 20 |
| 370 | 2.5791 20 | 5811 20 | 5831 21 | 5852 20 | 5872 20 | 5892 20 | 5912 20 | 5932 20 | 5952 20 | 5972 20 |
| 380 | 2.5992 20 | 6012 20 | 6032 20 | 6052 20 | 6072 20 | 6092 20 | 6112 19 | 6131 20 | 6151 20 | 6171 19 |
| 390 | 2.6190 20 | 6210 20 | 6230 19 | 6249 20 | 6269 19 | 6288 20 | 6308 19 | 6327 19 | 6346 20 | 6366 19 |
| 400 | 2.6385 19 | 6404 20 | 6424 19 | 6443 19 | 6462 19 | 6481 19 | 6500 20 | 6520 19 | 6539 19 | 6558 19 |
| 410 | 2.6577 19 | 6596 19 | 6615 19 | 6634 18 | 6652 19 | 6671 19 | 6690 19 | 6709 19 | 6728 18 | 6746 19 |
| 420 | 2.6765 19 | 6784 18 | 6802 19 | 6821 19 | 6840 18 | 6858 19 | 6877 18 | 6895 19 | 6914 18 | 6932 19 |
| 430 | 2.6951 18 | 6969 18 | 6987 19 | 7006 18 | 7024 18 | 7042 19 | 7061 18 | 7079 18 | 7097 18 | 7115 18 |
| 440 | 2.7133 18 | 7151 19 | 7170 18 | 7188 18 | 7206 18 | 7224 18 | 7242 18 | 7260 18 | 7278 17 | 7295 18 |
| 450 | 2.7313 18 | 7331 18 | 7349 18 | 7367 18 | 7385 17 | 7402 18 | 7420 18 | 7438 17 | 7455 18 | 7473 18 |
| 460 | 2.7491 17 | 7508 18 | 7526 17 | 7543 18 | 7561 17 | 7578 18 | 7596 17 | 7613 18 | 7631 17 | 7648 17 |
| 470 | 2.7665 18 | 7683 17 | 7700 17 | 7717 18 | 7735 17 | 7752 17 | 7769 17 | 7786 17 | 7803 18 | 7821 17 |
| 480 | 2.7838 17 | 7855 17 | 7872 17 | 7889 17 | 7906 17 | 7923 17 | 7940 17 | 7957 17 | 7974 17 | 7991 17 |
| 490 | 2.8008 17 | 8025 16 | 8041 17 | 8058 17 | 8075 17 | 8092 16 | 8108 17 | 8125 17 | 8142 17 | 8159 16 |
| 500 | 2.8175 17 | 8192 17 | 8209 16 | 8225 17 | 8242 16 | 8258 17 | 8275 16 | 8291 17 | 8308 16 | 8324 17 |
| 510 | 2.8341 16 | 8357 16 | 8373 17 | 8390 16 | 8406 17 | 8423 16 | 8439 16 | 8455 16 | 8471 17 | 8488 16 |
| 520 | 2.8504 16 | 8520 16 | 8536 16 | 8552 17 | 8569 16 | 8585 16 | 8601 16 | 8617 16 | 8633 16 | 8649 16 |
| 530 | 2.8665 16 | 8681 16 | 8697 16 | 8713 16 | 8729 16 | 8745 16 | 8761 16 | 8777 15 | 8792 16 | 8808 16 |
| 540 | 2.8824 16 | 8840 16 | 8856 15 | 8871 16 | 8887 16 | 8903 16 | 8919 15 | 8934 16 | 8950 16 | 8966 15 |
| 550 | 2.8981 16 | 8997 15 | 9012 16 | 9028 16 | 9044 15 | 9059 16 | 9075 15 | 9090 16 | 9106 15 | 9121 15 |
| 560 | 2.9136 16 | 9152 15 | 9167 16 | 9183 15 | 9198 15 | 9213 16 | 9229 15 | 9244 15 | 9259 16 | 9275 15 |
| 570 | 2.9290 15 | 9305 15 | 9320 15 | 9335 16 | 9351 15 | 9366 15 | 9381 15 | 9396 15 | 9411 15 | 9426 15 |
| 580 | 2.9441 15 | 9456 15 | 9471 15 | 9486 15 | 9501 15 | 9516 15 | 9531 15 | 9546 15 | 9561 15 | 9576 15 |
| 590 | 2.9591 15 | 9606 15 | 9621 15 | 9636 14 | 9650 15 | 9665 15 | 9680 15 | 9695 15 | 9710 14 | 9724 15 |
| 600 | 2.9739 15 | 9754 15 | 9769 14 | 9783 15 | 9798 14 | 9812 15 | 9827 15 | 9842 14 | 9856 15 | 9871 14 |
| 610 | 2.9885 15 | 9900 15 | 9915 14 | 9929 15 | 9944 14 | 9958 14 | 9972 15 | 9987 14 | 0001 15 | 0016 14 |
| 620 | 3.0030 15 | 0045 14 | 0059 14 | 0073 15 | 0088 14 | 0102 14 | 0116 15 | 0131 14 | 0145 14 | 0159 14 |
| 630 | 3.0173 15 | 0188 14 | 0202 14 | 0216 14 | 0230 14 | 0244 14 | 0258 15 | 0273 14 | 0287 14 | 0301 14 |
| 640 | 3.0315 14 | 0329 14 | 0343 14 | 0357 14 | 0371 14 | 0385 14 | 0399 14 | 0413 14 | 0427 14 | 0441 14 |
| 650 | 3.0455 14 | 0469 14 | 0483 14 | 0497 14 | 0511 13 | 0524 14 | 0538 14 | 0552 14 | 0566 14 | 0580 14 |
| 660 | 3.0594 13 | 0607 14 | 0621 14 | 0635 14 | 0649 13 | 0662 14 | 0676 14 | 0690 13 | 0703 14 | 0717 14 |
| 670 | 3.0731 13 | 0744 14 | 0758 14 | 0772 13 | 0785 14 | 0799 13 | 0812 14 | 0826 13 | 0839 14 | 0853 13 |
| 680 | 3.0866 14 | 0880 13 | 0893 14 | 0907 13 | 0920 14 | 0934 13 | 0947 14 | 0961 13 | 0974 13 | 0987 14 |
| 690 | 3.1001 13 | 1014 13 | 1027 14 | 1041 13 | 1054 13 | 1067 14 | 1081 13 | 1094 13 | 1107 13 | 1120 14 |
| 700 | 3.1134 13 | 1147 13 | 1160 13 | 1173 14 | 1187 13 | 1200 13 | 1213 13 | 1226 13 | 1239 13 | 1252 13 |
| 710 | 3.1265 13 | 1278 14 | 1292 13 | 1305 13 | 1318 13 | 1331 13 | 1344 13 | 1357 13 | 1370 13 | 1383 13 |
| 720 | 3.1396 13 | 1409 13 | 1422 13 | 1435 13 | 1448 12 | 1460 13 | 1473 13 | 1486 13 | 1499 13 | 1512 13 |
| 730 | 3.1525 13 | 1538 12 | 1550 13 | 1563 13 | 1576 13 | 1589 13 | 1602 12 | 1614 13 | 1627 13 | 1640 13 |
| 740 | 3.1653 12 | 1665 13 | 1678 13 | 1691 12 | 1703 13 | 1716 13 | 1729 12 | 1741 13 | 1754 13 | 1767 12 |
| 750 | 3.1779 13 | 1792 12 | 1804 13 | 1817 13 | 1830 12 | 1842 13 | 1855 12 | 1867 13 | 1880 12 | 1892 13 |
| 760 | 3.1905 12 | 1917 13 | 1930 12 | 1942 13 | 1955 12 | 1967 12 | 1979 13 | 1992 12 | 2004 13 | 2017 12 |
| 770 | 3.2029 12 | 2041 13 | 2054 12 | 2066 12 | 2078 13 | 2091 12 | 2103 12 | 2115 13 | 2128 12 | 2140 12 |
| 780 | 3.2152 12 | 2164 13 | 2177 12 | 2189 12 | 2201 12 | 2213 13 | 2226 12 | 2238 12 | 2250 12 | 2262 12 |
| 790 | 3.2274 12 | 2286 12 | 2298 13 | 2311 12 | 2323 12 | 2335 12 | 2347 12 | 2359 12 | 2371 12 | 2383 12 |
| 800 | 3.2395 12 | 2407 12 | 2419 12 | 2431 12 | 2443 12 | 2455 12 | 2467 12 | 2479 12 | 2491 12 | 2503 12 |
| 810 | 3.2515 12 | 2527 12 | 2539 12 | 2551 12 | 2563 11 | 2574 12 | 2586 12 | 2598 12 | 2610 12 | 2622 12 |
| 820 | 3.2634 12 | 2646 11 | 2657 12 | 2669 12 | 2681 12 | 2693 11 | 2704 12 | 2716 12 | 2728 12 | 2740 11 |
| 830 | 3.2751 12 | 2763 12 | 2775 12 | 2787 11 | 2798 12 | 2810 12 | 2822 11 | 2833 12 | 2845 12 | 2857 11 |
| 840 | 3.2868 12 | 2880 11 | 2891 12 | 2903 12 | 2915 11 | 2926 12 | 2938 11 | 2949 12 | 2961 11 | 2972 12 |
| 850 | 3.2984 11 | 2995 12 | 3007 11 | 3018 12 | 3030 11 | 3041 12 | 3053 11 | 3064 12 | 3076 11 | 3087 12 |
| 860 | 3.3099 11 | 3110 11 | 3121 12 | 3133 11 | 3144 12 | 3156 11 | 3167 11 | 3178 12 | 3190 11 | 3201 11 |
| 870 | 3.3212 12 | 3224 11 | 3235 11 | 3246 | | | | | | |

The correction for $He^4$ impurity is mentioned briefly in Part I and in more detail in section 3 of Part III. In figure 7 of Part III several correction curves are given which may be used to adjust an uncorrected temperature for the effect of the $He^4$ impurity content in the liquid. In this connection the experimenter is cautioned that, due to fractionation between vapor and liquid, the actual concentration of $He^4$ in the liquid probably will be greater than the average concentration of the total gas in the vapor-pressure system by an amount depending on the volume of the vapor space and the experimental technique. For example, if most of the gas is first condensed at very low temperature into the vapor-pressure bulb and then most of that liquid subsequently is evaporated into the vapor space, a large fraction of the $He^4$ will remain in the liquid state and a corresponding high value of the impurity correction will be needed. Such considerations may become particularly important if temperature is being measured as the vapor pressure of a bath of $He^3$. Tables of equilibrium vapor/liquid concentration ratios, if unavoidably needed, are given in references [38] and [74]. The best technique, of course, is to use only very high purity $He^3$. As explained in section 3 of Part III, steps have been undertaken to make $He^3$ of very high purity available for thermometry.

Remarks concerning the possibility and detection of errors due to gas oscillations are given at the end of Part I.

TABLE 3. *The temperature derivative,* $dP_3/dT_{62}$, *in millimeters of mercury per degree Kelvin, for the 1962* $He^3$ *Scale of Temperatures*

| $T_{62}$, °K | 0.00 | 0.01 | 0.02 | 0.03 | 0.04 | 0.05 | 0.06 | 0.07 | 0.08 | 0.09 |
|---|---|---|---|---|---|---|---|---|---|---|
| 0.20 | 0.001 | 0.002 | 0.003 | 0.005 | 0.008 | 0.012 | 0.017 | 0.025 | 0.035 | 0.049 |
| .30 | .066 | .087 | .113 | .145 | .184 | .229 | .283 | .345 | .417 | .499 |
| .40 | .592 | .696 | .814 | .944 | 1.089 | 1.248 | 1.422 | 1.612 | 1.819 | 2.042 |
| .50 | 2.283 | 2.543 | 2.820 | 3.117 | 3.433 | 3.769 | 4.125 | 4.501 | 4.898 | 5.317 |
| .60 | 5.756 | 6.217 | 6.700 | 7.204 | 7.731 | 8.280 | 8.851 | 9.445 | 10.061 | 10.700 |
| .70 | 11.362 | 12.046 | 12.753 | 13.483 | 14.236 | 15.012 | 15.811 | 16.632 | 17.477 | 18.344 |
| .80 | 19.234 | 20.147 | 21.082 | 22.041 | 23.022 | 24.025 | 25.051 | 26.100 | 27.171 | 28.264 |
| .90 | 29.379 | 30.517 | 31.677 | 32.859 | 34.063 | 35.289 | 36.537 | 37.806 | 39.097 | 40.410 |
| 1.00 | 41.745 | 43.100 | 44.478 | 45.876 | 47.296 | 48.737 | 50.199 | 51.682 | 53.186 | 54.711 |
| 1.10 | 56.257 | 57.823 | 59.410 | 61.018 | 62.646 | 64.295 | 65.964 | 67.653 | 69.363 | 71.093 |
| 1.20 | 72.843 | 74.613 | 76.403 | 78.213 | 80.043 | 81.893 | 83.763 | 85.652 | 87.561 | 89.490 |
| 1.30 | 91.438 | 93.406 | 95.394 | 97.400 | 99.427 | 101.472 | 103.537 | 105.621 | 107.724 | 109.847 |
| 1.40 | 111.988 | 114.149 | 116.329 | 118.528 | 120.745 | 122.982 | 125.237 | 127.512 | 129.805 | 132.117 |
| 1.50 | 134.447 | 136.796 | 139.164 | 141.551 | 143.956 | 146.380 | 148.822 | 151.283 | 153.762 | 156.260 |
| 1.60 | 158.776 | 161.311 | 163.863 | 166.435 | 169.024 | 171.632 | 174.257 | 176.902 | 179.564 | 182.244 |
| 1.70 | 184.943 | 187.659 | 190.394 | 193.147 | 195.918 | 198.706 | 201.513 | 204.338 | 207.181 | 210.041 |
| 1.80 | 212.920 | 215.816 | 218.730 | 221.662 | 224.612 | 227.579 | 230.565 | 233.568 | 236.589 | 239.627 |
| 1.90 | 242.684 | 245.758 | 248.849 | 251.959 | 255.086 | 258.230 | 261.393 | 264.573 | 267.770 | 270.985 |
| 2.00 | 274.218 | 277.468 | 280.736 | 284.022 | 287.325 | 290.646 | 293.984 | 297.340 | 300.713 | 304.104 |
| 2.10 | 307.513 | 310.939 | 314.383 | 317.844 | 321.323 | 324.820 | 328.334 | 331.866 | 335.416 | 338.983 |
| 2.20 | 342.568 | 346.171 | 349.792 | 353.430 | 357.086 | 360.760 | 364.451 | 368.161 | 371.889 | 375.634 |
| 2.30 | 379.398 | 383.179 | 386.979 | 390.796 | 394.632 | 398.486 | 402.359 | 406.250 | 410.159 | 414.086 |
| 2.40 | 418.032 | 421.997 | 425.980 | 429.982 | 434.003 | 438.042 | 442.101 | 446.178 | 450.275 | 454.391 |
| 2.50 | 458.526 | 462.680 | 466.854 | 471.048 | 475.261 | 479.495 | 483.748 | 488.021 | 492.314 | 496.628 |
| 2.60 | 500.962 | 505.317 | 509.692 | 514.088 | 518.505 | 522.944 | 527.404 | 531.885 | 536.388 | 540.912 |
| 2.70 | 545.459 | 550.028 | 554.619 | 559.233 | 563.870 | 568.530 | 573.212 | 577.919 | 582.649 | 587.402 |
| 2.80 | 592.180 | 596.982 | 601.809 | 606.661 | 611.537 | 616.440 | 621.367 | 626.321 | 631.301 | 636.307 |
| 2.90 | 641.340 | 646.401 | 651.488 | 656.604 | 661.747 | 666.919 | 672.120 | 677.349 | 682.609 | 687.898 |
| 3.00 | 693.217 | 698.567 | 703.948 | 709.360 | 714.804 | 720.281 | 725.790 | 731.332 | 736.908 | 742.517 |
| 3.10 | 748.162 | 753.841 | 759.556 | 765.306 | 771.093 | 776.918 | 782.779 | 788.679 | 794.617 | 800.595 |
| 3.20 | 806.612 | 812.670 | 818.768 | 824.909 | 831.091 | 837.316 | 843.585 | 849.898 | 856.255 | 862.658 |
| 3.30 | 869.108 | 875.604 | 882.148 | 888.740 | | | | | | |

The fit of the 1962 $He^3$ Scale to the intercomparison $He^3$ and $He^4$ vapor-pressure data of Part I and to the 1958 $He^4$ Scale is given in table 1 and figure 1 of Part II and is discussed in detail in subsection 1.1 of Part III. The fit of the 1962 $He^3$ Scale to Keller's isotherms is given in figure 2 of Part II and is discussed in detail in subsection 1.5 of Part III.

The 1962 $He^3$ Scale of Temperatures has been given status similar to that of the 1958 $He^4$ Scale of Temperatures by the International Committee on Weights and Measures [68, 69]. The pertinent portion of the minutes of that committee's Advisory Committee on Thermometry [67] is given in section 4 of Part III.

## References*


[1] S. G. Sydoriak, T. R. Roberts, and R. H. Sherman, Proc. 7th Intern. Conf. Low Temperature Physics, ed. G. M. Graham and A. C. Hollis-Hallett (Univ. of Toronto Press, Toronto, 1961), ch. 30, p. 717.

[2] F. G. Brickwedde, H. van Dijk, M. Durieux, J. R. Clement, and J. K. Logan, J. Res. NBS **64A** (Phys. & Chem.), 1 (1960).

[3] D. F. Brewer, A. K. Sreedhar, H. C. Kramers, and J. G. Daunt, Phys. Rev. **115,** 836 (1959).

[4] B. Weinstock, B. M. Abraham, and D. W. Osborne, Nuovo Cimento Suppl. **9,** 310 (1958).

[5] B. M. Abraham, D. W. Osborne, and B. Weinstock, Phys. Rev. **80,** 366 (1950).

[6] S. G. Sydoriak, T. R. Roberts, and R. H. Sherman, Paper II of this series.

[7] T. R. Roberts, R. H. Sherman, and S. G. Sydoriak, Paper III of this series.

[8] R. H. Sherman, S. G. Sydoriak, and T. R. Roberts, Paper IV of this series. See also Los Alamos Scientific Lab. Rept. LAMS 2701 (July 1962).

[9] S. G. Sydoriak and T. R. Roberts, Phys. Rev. **106,** 175 (1957).

[10] T. R. Roberts, S. G. Sydoriak, and R. H. Sherman, Proc. 4th Symp. Temperature, Its Measurement and Control in Science and Industry, ed. C. M. Herzfeld (Reinhold Publ. Corp., New York, 1962), Vol. 3, pt. 1, p. 75.

[11] W. E. Keller, Phys. Rev. **97,** 1 (1955); **100,** 1790 (1955).

[12] W. E. Keller, Phys. Rev. **98,** 1571 (1955).

[13] F. E. Hoare and J. E. Zimmerman, Rev. Sci. Instr. **30,** 184 (1959); R. T. Swim, Advances in Cryogenic Engineering, ed. K. D. Timmerhaus (Plenum Press, Inc., New York, 1960), Vol. 5, pp. 498–504.

[14] H. H. Plumb, Proc. 10th Intern. Congr. Refrigeration, Copenhagen, 1959, ed. M. Jul and A. M. S. Jul (Pergamon Press, Paris, 1960), Vol. 1, pp. 184–187.

[15] M. Durieux, Thermometry at Liquid Helium and Liquid Hydrogen Temperatures, Thesis, Leiden Univ. (16 Mar. 1960).

[16] F. G. Brickwedde, Report on the Conference Agreement on the Helium Vapor-Pressure Scale of Temperatures, Conf. Physique des Basses Temperatures, Paris, 2–8 Septembre 1955, pp. 608–610.

[17] B. Bleaney and F. Simon, Trans. Faraday Soc. **35,** 1205 (1939).

[18] B. Bleaney and R. A. Hull, Proc. Roy. Soc. (London) **178A,** 74 (1941).

[19] J. de Boer and E. G. D. Cohen, Physica **17,** 993 (1951).

[20] E. W. Becker and R. Misenta, Phys. Rev. **93,** 244 (1954).

[21] E. W. Becker, R. Misenta, and F. Schmeissner, Z. Physik **137,** 126 (1954).

[22] K. Mendelssohn and G. K. White, Proc. Phys. Soc. (London) **A63,** 1328 (1950).


*This list of references applies to papers I, II, III, and IV of this series. For completeness and convenience, it is reproduced in its entirety at the end of each paper.

[23] R. Bowers and K. Mendelssohn, Nature **163,** 870 (1949); Proc. Phys. Soc. (London) **A63,** 1318 (1950).
[24] K. W. Taconis, Progress in Low Temperature Physics, ed. C. J. Gorter (North Holland Publ. Co., Amsterdam, The Netherlands, 1961), Vol. 3, p. 154.
[25] H. van Dijk and M. Durieux, Physica **24,** 1 (1958).
[26] S. G. Sydoriak and H. S. Sommers, Jr., Rev. Sci. Instr. **22,** 915 (1951).
[27] P. Kapitza, J. Phys. (U.S.S.R.) **4,** 181 (1941).
[28] H. A. Fairbank and J. Wilks, Proc. Roy. Soc. (London) **A231,** 545 (1955).
[29] L. J. Challis, K. Dransfeld, and J. Wilks, Proc. Roy. Soc. (London) **A260,** 31 (1961).
[30] Kuang Wey-Yen, Zh. Experim. i Teor. Fiz. (U.S.S.R.) **42,** 921 (1962); Soviet Phys. JETP (English Transl.) **15,** 635 (1962).
[31] I.M. Khalatnikov, Zh. Experim. i Teor. Fiz. (U.S.S.R.) **22,** 687 (1952).
[32] S. G. Sydoriak and T. R. Roberts, Phys. Rev. **118.** 901 (1960).
[33] R. L. Mills, E.R. Grilly, and S. G. Sydoriak, Ann. Phys. **12,** 41 (1961).
[34] W. Cawood and H. S. Patterson, Trans. Faraday Soc. **29,** 522 (1933).
[35] J. Kistemaker, Leiden Commun. **268d** (1944); Physica **11,** 277 (1944–1946); B. E. Blaisdell, J. Math. Phys. **19,** 186 (1940).
[36] W. G. Brombacher, D. P. Johnson, and J. L. Cross, Mercury Barometers and Manometers, NBS Mono. 8 (U.S. Govt. Printing Office, Washington, 1960).
[37] T. R. Roberts and S. G. Sydoriak, Phys. Rev. **102,** 304 (1956).
[38] B. N. Esel'son and N. G. Berezniak, Zh. Experim. i Teor. Fiz. (U.S.S.R.) **30,** 628 (1956); Soviet Phys. JETP (English Transl.) **3,** 568 (1956).
[39] S. G. Sydoriak, E. R. Grilly, and E. F. Hammel, Phys. Rev. **75,** 303 (1949).
[40] V. P. Peshkov, Zh. Experim. i Teor. Fiz. (U.S.S.R.) **33,** 833 (1957); Soviet Phys. JETP (English Transl.) **4,** 645 (1958).
[41] H. van Dijk and D. Shoenberg, Nature **164,** 151 (1949).
[42] T. C. Chen and F. London, Phys. Rev. **89,** 1038 (1953).
[43] W. E. Keller, Nature **178,** 883 (1956); J. R. Clement, Low Temperature Physics and Chemistry (Univ. of Wisconsin Press, Madison, 1958), p. 187 (Proc. 5th Intern. Conf. Low Temperature Physics and Chemistry, Madison, Wis., 1957).
[44] L. Goldstein, Phys. Rev. **96,** 1455 (1954); Phys. Rev. **102,** 1205 (1956).
[45] R. H. Sherman, T. R. Roberts, and S. G. Sydoriak, Supplement au Bulletin de l'Institut International du Froid, Annexe 1961–5, p. 125 (Proc. Meeting of Commission I of the International Institute of Refrigeration, London, 1961).
[46] S. G. Sydoriak and R. H. Sherman, Paper I of this series.
[47] W. E. Deming, Statistical Adjustment of Data (John Wiley & Sons, New York, 1943).
[48] T. R. Roberts, S. G. Sydoriak, and R. H. Sherman, see ref. [45], p. 115.
[49] E. R. Grilly and E. F. Hammel, Progress in Low Temperature Physics III (1961), pp. 113–152.
[50] E. C. Kerr and R. D. Taylor, Proc. 7th Intern. Conf. Low Temperature Physics, ch. 24, pp. 605–608, ed. G. M. Graham and A. C. Hollis-Hallett (Univ. of Toronto Press, Toronto, 1961).
[51] R. H. Sherman and F. J. Edeskuty, Ann. Phys. **9,** 522 (1960).
[52] T. R. Roberts, R. H. Sherman, S. G. Sydoriak, and F. G. Brickwedde, Progress in Low Temperature Physics IV, ch. 10 (North Holland Publ. Co., Amsterdam, The Netherlands, 1964), p. 480.
[53] A. M. Mood, Introduction to the Theory of Statistics, p. 299 (McGraw-Hill, New York, N.Y., 1950).
[54] M. Durieux, Procès-Verbaux du Comité Consultatif de Thermométrie auprès du Comité International des Poids et Mesures, 6e Session, 1962 (Gauthier-Villars, Paris, France, 1964), p. 190.
[55] D. W. Osborne, private communication.
[56] R. Berman and C. F. Mate, Phil. Mag. **3,** 461 (1958).
[57] H. van Dijk, Progr. Cryog. **2,** p. 125 (Academic Press, Inc., New York, N.Y., 1962).
[58] G. Cataland and H. H. Plumb, Proc. 8th Intern. Conf. Low Temperature Physics, London, Sept. 16–22, 1962, ed R. O. Davies (Butterworths, Washington, D.C., 1963), pp. 439–40.
[59] E. C. Kerr, Phys. Rev. **96,** 551 (1954).
[60] E. C. Kerr and R. D. Taylor, Ann. Phys. **20,** 450 (1962).
[61] A. C. Anderson, G. L. Salinger, W. A. Steyert, and J. C. Wheatley, Phys. Rev. Letters **6,** 331 (1961); A. C. Anderson, W. Reese, and J. C. Wheatley, Phys. Rev. **130,** 495 (1963).
[62] M. Strongin, G. O. Zimmerman, and H. A. Fairbank, Phys. Rev. **128,** 1983 (1962).
[63] B. M. Abraham, D. W. Osborne, and B. Weinstock, Phys. Rev. **98,** 551 (1955).
[64] G. R. Grove and W. J. Haubach, Jr.; see ref. [58], p. 441. For further information, write Gaseous Isotope Sales, Monsanto Research Corporation, Mound Laboratory, Miamisburg, Ohio.
[65] D. O. Edwards and J. G. Daunt, Phys. Rev. **124,** 640 (1961).
[66] S. G. Sydoriak, T. R. Roberts, and R. H. Sherman; see ref. [58], pp. 437–8.
[67] J. A. Hall, Sixième Rapport du Comité Consultatif de Thermométrie au Comité International des Poids et Mesures; see ref. [54].
[68] H. F. Stimson, NBS Tech. News Bull. **47,** No. 2, 30 (Feb. 1963); Nature **197,** 1055 (1963).
[69] F. G. Brickwedde, Phys. Today **16,** 24 (1963).
[70] S. Weber, Commun. Kamerlingh Onnes Lab. Univ. Leiden Suppl. **71b** (1932), **264b** and **264d** (1936).
[71] S. Weber and G. Schmidt, Commun. Kamerlingh Onnes Lab. Univ. Leiden **264c** (1936).
[72] C. E. Chase, E. Maxwell, and W. M. Whitney, Physica **26,** 160 (1960); C. E. Chase, E. Maxwell, and W. E. Millett, Physica **27,** 1129 (1961).
[73] R. H. Moore and R. K. Zeigler, Trans. Am. Nuclear Soc. **1,** 128–9 (1958); The Solution of the General Least Squares Problem with Special Reference to High-Speed Computers, Los Alamos Scientific Lab. Rept. LA–2367 (Mar. 4, 1960).
[74] T. R. Roberts and B. K. Swartz, Proc. 2d Symp. Liquid and Solid Helium Three, ed. J. G. Daunt (Ohio State Univ. Press, Columbus, 1960), p. 163.

(Paper 68A6–304)

JOURNAL OF RESEARCH of the National Bureau of Standards—A. Physics and Chemistry
Vol. 68A, No. 6, November–December 1964

# Absolute Isotopic Abundance Ratio and the Atomic Weight of a Reference Sample of Copper

William R. Shields, Thomas J. Murphy, and Ernest L. Garner

(August 6, 1964)

An absolute value for the isotopic abundance ratio of a reference sample of copper has been obtained by thermal emission mass spectrometry. Samples of known abundance ratio, prepared from nearly pure separated copper isotopes, were used to calibrate the mass spectrometers. The results yield an absolute value of $Cu^{63}/Cu^{65}=2.2440\pm0.0021$ and an atomic weight of $63.54555\pm0.00040$ ($C^{12}=12$). The indicated uncertainties are overall limits of error based on 95 percent confidence limits for the mean and on allowances for the effects of known sources of possible systematic error.

A companion study of the $Cu^{63}/Cu^{65}$ ratio in natural materials has shown that there is significant variation in some rare secondary minerals.

## 1. Introduction

The presently accepted value for the atomic weight of copper [1] [1] (63.54) is based on the revised chemical determinations by Hönigschmid and Johannsen [2] in 1944, and by Ruer and Bode [3] in 1924. The abundance ratios determined by many mass spectroscopists were not used because the instruments had not been calibrated adequately. In the present work, this difficulty is resolved by the use of calibration samples of known isotopic composition prepared from nearly pure separated copper isotopes. A companion study [4] of terrestrial and meteoritic samples showed that there are no significant isotopic variations in meteorites and primary copper ores, which constitute the bulk of the recoverable copper in the earth's crust. However, some rare secondary copper minerals show gross isotopic variation. The observed range is from 0.3 percent enrichment to 1.0 percent depletion in $Cu^{63}$.

## 2. Experimental Procedure

### 2.1. Instrumentation

The thermal ionization mass spectrometers used to compare the isotopic abundance ratios of the reference and terrestrial samples with those of the calibration samples are two nearly identical 12-in. radius of curvature, single-focusing instruments with 68-deg analyser tubes and 60-deg magnet pole pieces. The measuring circuit of instrument No. 4 was a d-c collector into a Cary V.R.E. that drove an expanded-scale recorder. The measuring circuit of instrument No. 3 included a 12-stage ion multiplier, which was necessary to do the analysis on the separated isotopes. The ion source used was a triple filament source with approximately 200 $\mu g$ of copper electroplated on each side filament. The $Cu^{+}(63)$ ion current was nominally adjusted to $5\times10^{-13}$ A, and data were taken only on a growing or constant ion signal. Tests showed that, in such cases, the ratio was independent of time. However, decaying signals showed a strong ratio variation with time and all such runs were rejected.

### 2.2. Purification of the Separated Isotopes

Electromagnetically separated copper isotopes in the form of copper oxide were obtained from the Isotopes Division, Oak Ridge National Laboratory of the Union Carbide Nuclear Company. The $Cu^{63}O$ and the $Cu^{65}O$ were designated Series IW, Lot Number 1064(a) and Series IW, Lot Number 1065(a), respectively. The certificate of analysis accompanying each sample indicated a high degree of chemical purity. They were further purified at the National Bureau of Standards by electrodeposition to insure removal of impurities except those which are deposited with copper.

Each isotope sample was treated as follows: The copper oxide (about 1.2 g) was dissolved in 100 ml of a solution containing 2 ml of concentrated sulfuric acid and 2 ml of concentrated nitric acid. The copper was slowly electrodeposited from an unstirred solution onto a small platinum-gauze electrode. The deposit was then stripped from the electrode with dilute nitric acid and analyzed by quantitative emission spectrography for the elements which could have electrodeposited with copper [5] or which are common impurities in copper. Quantitative values or limits of detection were determined for 18 elements. On this basis the $Cu^{63}$ was estimated to be 99.999 percent pure Cu and the $Cu^{65}$ was estimated to be 99.996 percent pure Cu, the principal impurities being silver and platinum in each case.

[1] Figures in brackets indicate the literature references at the end of this paper.

### 2.3. Copper Concentration of the Separated Isotope Solutions

The solutions of $Cu^{63}$ and $Cu^{65}$ were each transferred to 50 ml Erlenmeyer flasks, diluted to 45 ml, and thoroughly mixed by swirling for several minutes. Each flask was then sealed with a No. 35 rubber serum septum and allowed to stand overnight in the case of a semi-microbalance to insure thermal equilibrium. The flask and contents were then weighed on the semi-microbalance with an accuracy of $\pm 0.02$ mg. Samples were taken by inserting a stainless steel needle attached to a glass hypodermic syringe through the rubber septum and withdrawing the desired amount of solution. A second needle which just punctured the septum served as a vent. The syringe and needle were washed with distilled water and the washings were combined with the bulk of the sample. The weight of the sample withdrawn was determined from the weight of the flask before and after removal of the sample.

Four samples of from 5 to 6 g each were withdrawn from each solution of the separated isotopes and transferred to 22-ml vials by this method. After reduction of the volume to about 10 ml by evaporation on a steam bath, the bulk of the copper content was determined by the following procedure, which is a modification of the electrolytic method described by Wilson and Wilson [6]. One-half milliliter of a diluted acid mixture containing 0.1 ml of $HNO_3$ and 0.1 ml of $H_2SO_4$ was added to the solution in the vial which also served as the electrolysis cell. A stopper for the vial was prepared from an inverted rubber serum septum; a small glass tube, which served as a vent, was inserted through a hole in the septum. The lead of a small platinum-gauze cathode was inserted through the vent tube and a platinum-wire anode was inserted at the edge of the stopper. The copper in each solution was electrodeposited from the unstirred solutions onto the cathode by adjusting the voltage so that the current was about 0.1 A and allowing the electrolysis to continue overnight. Without interrupting the current, the vial was unstoppered and the septum, tube, and sides of the vial were washed with distilled water. The septum was replaced and the electrolysis was continued for another 4 hr. The vial was again unstoppered and the electrodes were withdrawn from the solution without interrupting the current. The cathode was rinsed with distilled water while it was being withdrawn to prevent re-solution of copper, dipped into absolute ethanol, and dried for 1 min at 100 °C. The electrode was allowed to stand for 2 hr at room temperature to attain thermal equilibrium and weighed on a microbalance with an accuracy of $\pm 0.002$ mg. The copper was then stripped from the electrode with dilute (1+9) $HNO_3$ after which it was washed, dipped in ethanol, and dried for 1 min at 100 °C. After standing at room temperature for 2 hr, the stripped electrode was weighed on the microbalance. The weight of copper was determined from the difference in weights.

The copper remaining in the electrolyte and washings was determined by the sodium diethyldithiocarbamate method [7] in the following manner: The solution was transferred to a 125 ml separatory funnel and two drops of 0.01 percent thymol blue solution and 5 ml of a 20 percent ammonium citrate solution were added. Dilute ammonium hydroxide (1 + 3) was added until the color of the indicator changed to pale blue ($p$H 9.0–9.2). One milliliter of a 0.1 percent aqueous solution of sodium diethyldithiocarbamate and exactly 5 ml of carbon tetrachloride were then added and the solution was shaken for 2.0 min. The carbon tetrachloride layer, which contained copper diethyldithiocarbamate, was drained into a 1-cm cell. The transmittancy of the carbon tetrachloride solution was measured at 440 nm (m$\mu$) on a Beckman DU Spectrophotometer, and compared to a reference curve.

The total amount of copper present in the sample was calculated from the two determinations. The weight of the electrodeposited copper was corrected for platinum and silver which would have deposited with the copper, and the total weight was corrected for air buoyancy. In a typical determination, the electrodeposited copper amounted to 0.190740 g, while 0.000018 g was found in the residual electrolyte.

This procedure was first applied to the determination of known amounts of copper to evaluate its reliability. Pure copper in the form of rods was obtained commercially. Quantitative spectrographic analysis showed that the copper was about 99.998 percent pure. However, of the impurities found, silver and platinum would electrodeposit with the copper; hence the apparent purity for this purpose was considered to be 99.999 percent.

A sample of the rod weighing about 1 g was pickled successively in dilute HCl and in dilute $HNO_3$, rinsed in distilled water, and finally in ethanol. The sample was dried, weighed on a microbalance to $\pm 0.001$ mg, and transferred to an Erlenmeyer flask which had been weighed on a semi-microbalance along with a rubber septum. The copper was dissolved in dilute nitric acid, diluted to 45 ml with distilled water, and thoroughly mixed. The flask was then stoppered with the septum, allowed to reach thermal equilibrium, and weighed. From the weight of the copper and the weight of the solution, the concentration of copper was calculated. Four weighed samples were withdrawn and the copper determined by the method described.

This procedure was repeated on four additional samples of the copper for a total of 20 determinations. The copper recovered ranged from 99.984 to 100.014 percent of the calculated amounts for samples of from 0.10 to 0.26 g. The standard deviation of an individual determination is estimated to be $1.5 \times 10^{-5}$ g.

Results for the determination of the copper content of the isotope solutions are tabulated in table 1. The standard deviation of the individual determination is estimated to be $2.6 \times 10^{-6}$ g/g sol. Average values of 0.0211654 g Cu(vac)/g sol for solution 63

and 0.0210895 g Cu(vac)/g sol for solution 65 were obtained with a standard deviation of $1.3\times10^{-6}$ g/g sol.

TABLE 1. *Concentration of solution* $Cu^{63}$ [a]

| Sample | Wt. sol. | Wt. Cu [b] | g Cu(vac)/g sol. |
|---|---|---|---|
| | *g* | *g(vac)* | |
| 1 | 5.58000 | 0.118085 | 0.0211622 |
| 2 | 5.48942 | .116189 | .0211660 |
| 3 | 5.66492 | .119903 | .0211659 |
| 4 | 5.95065 | .125960 | .0211674 |
| | | | Ave. 0.0211654 |
| | | | Std error 0.0000013 |
| Concentration of solution $Cu^{65}$ [c] | | | |
| 1 | 5.69855 | 0.120180 | 0.0210896 |
| 2 | 5.66517 | .119486 | .0210913 |
| 3 | 5.77382 | .121754 | .0210873 |
| 4 | 5.72793 | .120800 | .0210896 |
| | | | Ave. 0.0210895 |
| | | | Std error 0.0000013 |

[a] Purity taken as 99.999 percent from spectrographic analysis.
[b] Corrected for Pt and Ag in the copper.
[c] Purity taken as 99.996 percent from spectrographic analysis.

## 2.4. Isotopic Analysis of the Solutions of the Separated Isotopes

The isotopic analysis of the separated isotopes was not done until all the purification chemistry had been completed. To insure against possible bias effects all samples were run at the same total copper signal intensity. Thus, the large ratios encountered in the separated isotope solutions necessitated the use of an ion-multiplier to make the depleted isotope signals measurable.

The isotopic compositions of the separated isotopes used in the preparation of the calibration samples are given in table 2. These results have been corrected for both the discrimination of the ion multiplier and the discrimination from the mode of ionization used, using the average correction factors (cf) given in table 4.

TABLE 2. *Isotopic composition of purified separated copper isotopes used in calibration samples*

| Isotope | Isotopic composition* (Atom %) |
|---|---|
| $Cu^{63}$ | $Cu^{63}=99.8398\pm0.002$ |
| | $Cu^{65}=0.1602\pm.002$ |
| $Cu^{65}$ | $Cu^{63}=0.3575\pm.002$ |
| | $Cu^{65}=99.6425\pm.002$ |

*The limits set on the isotopic composition of the separated isotopes have been expanded to include a liberal estimate of possible bias.

## 2.5. Preparation of the Calibration Samples

Nine calibration samples were prepared by mixing weighed portions of the $Cu^{63}$ solution and the $Cu^{65}$ solution to produce ratios of approximately 0.5 $Cu^{63}$ to 1 $Cu^{65}$ up to approximately 3 $Cu^{63}$ to 1 $Cu^{65}$ on an atomic basis. Calibration samples 1 through 7 and all of the samples for the determination of the copper concentration were withdrawn on the same day. Calibration samples 8 and 9 were withdrawn 3 days later and required a correction in the copper concentration because of a slight loss of water through the rubber septum. The mixing data of the calibration samples is given in table 3. Each calibration sample was analyzed three times, with as many analyses done on the reference sample as the total number of analyses done on the calibration samples.

The calculated isotopic ratio, $\pi$, for each calibration sample was obtained from

$$\pi=\frac{\frac{g_1\ (1-f_1)}{A}+\frac{g_2\ (1-f_2)}{B}}{\frac{g_1 f_1}{A}+\frac{g_2 f_2}{B}}$$

where $A$ and $B$ denote the atomic weights of copper in the $Cu^{63}$ solution and the $Cu^{65}$ solution respectively, and are given as

$A=M_2-(M_2-M_1)\ (1-f_1)=62.93275$
$B=M_2-(M_2-M_1)\ (1-f_2)=64.920642$
$M_1$=nuclidic mass $Cu^{63}$=62.929594
$M_2$=nuclidic mass $Cu^{65}$=64.927786
$g_1$=weight of copper from $Cu^{63}$ solution
$g_2$=weight of copper from $Cu^{65}$ solution
$f_1$=fraction of 65 in $Cu^{63}$ solution=0.001602
$1-f_1$=fraction of 63 in $Cu^{63}$ solution=0.998398
$f_2$=fraction of 65 in $Cu^{65}$ solution=0.996425
$1-f_2$=fraction of 63 in $Cu^{65}$ solution=0.003575

The values of $g_1$, $g_2$, and $\pi$ are tabulated in table 3.

TABLE 3. *Calibration samples*

| Sample | Solution $Cu^{63}$ | | Solution $Cu^{65}$ | | Isotopic ratio $\pi$ |
|---|---|---|---|---|---|
| | Wt. sol. $W_1$ | Wt. Cu $g_1$ | Wt. sol. $W_1$ | Wt. Cu $g_1$ | |
| 1 | 2.86377 | 0.0606128 | 0.99595 | 0.0210041 | 2.97217 |
| 2 | 2.09804 | .0444059 | .91834 | .0193673 | 2.36453 |
| 3 | 2.10181 | .0444856 | .93224 | .0196605 | 2.33361 |
| 4 | 2.13417 | .0451706 | .97065 | .0204705 | 2.27608 |
| 5 | 2.12148 | .0449020 | 1.06498 | .0224599 | 2.06319 |
| 6 | 1.03190 | .0218406 | 1.04034 | .0219403 | 1.03082 |
| 7 | 1.05286 | .0222842 | 2.12004 | .0447106 | .51833 |
| 8 | [a] 2.08309 | .0441042 | [b] 0.95677 | .0201798 | 2.25448 |
| 9 | [a] 2.08161 | .0440729 | [b] 0.97185 | .0204979 | 2.21810 |

Concentration of Solution 63=0.0211654 g Cu(vac)/g Sol
Concentration of Solution 65=0.0210895 g Cu(vac)/g Sol

[a] Withdrawn 3 days after 1 through 7. Concentration of solution changed to 0.0211725 g Cu(vac)/g sol.
[b] Withdrawn 3 days after 1 through 7. Concentration of solution changed to 0.0210916 g Cu(vac)/g sol.

## 3. Results and Discussion

Table 4 summarizes the isotopic abundance ratio $Cu^{63}/Cu^{65}$ measurements for both the calibration samples and the reference sample. Table 5 summarizes the atomic weight calculations for the reference sam-

TABLE 4. *Calculated and observed isotopic ratios of the calibration samples and the observed ratio of the reference sample*

Instr. No. 3

| Mixture | Calc ratio | Obs ratio | CF(Calc/obs) |
|---|---|---|---|
| 1 [a] | 2.9722 | 3.0514 | 0.97402 |
| 2 | 2.3645 | 2.4251 | .97504 |
| 5 | 2.0632 | 2.1188 | .97374 |
| 7 | .51833 | .53244 | .97350 |
| 9 | 2.2181 | 2.2762 | .97449 |
| | | | Avg. .97416 |

Reference sample avg. 2.3039 [b]

Corrected ratio=2.2443

Instr. No. 4

| | | | |
|---|---|---|---|
| 1 | 2.9722 | 3.0131 | 0.98642 |
| 3 | 2.3336 | 2.3661 | .98627 |
| 4 | 2.2761 | 2.3062 | .98694 |
| 6 | 1.0308 | 1.0457 | .98580 |
| 8 | 2.2545 | 2.2876 | .98552 |
| | | | Avg. .98619 |

Reference sample avg. 2.2752

Corrected ratio=2.2437

[a] All calculations were done before rounding off.
[b] Instrument equipped with ion multiplier.

TABLE 5. *Summary calculations of the atomic weight of copper in the reference sample*

| | | |
|---|---|---|
| Corrected isotopic ratio | $Cu^{63}/Cu^{65}$ | =2.2440 ±0.0021* |
| Corrected isotopic composition, atom percent. | $Cu^{63}$ | =69.174±0.020* |
| | $Cu^{65}$ | =30.826±0.020* |
| Nuclidic masses ($C^{12}$=12) | $Cu^{63}$ | =62.929594 ±0.000006 [8] |
| | $Cu^{65}$ | =64.927786 ±0.000006 [8] |
| Atomic weight Cu (unified table, $C^{12}$=12) | | =63.54555 +0.00040* |
| Uncertainty components | | |
| 95% confidence limit of ratio determination. | | ±0.00024 |
| Possible systematic error in composition of separated isotopes. | | ±0.00004 |
| Possible systematic error in synthetic ratios. | | ±0.00012 |
| | | ±0.00040* |

*The indicated uncertainties are overall limits of error based on 95 percent confidence limits for the mean and allowances for effects of known sources of possible systematic error.

ple which was a commercial sample of copper metal. The observed variation in the isotopic ratio for rare secondary minerals makes it necessary to include a variance component for natural variation in the overall uncertainty statement for terrestrial copper. A very large number of mineral samples has been analyzed in an effort to define the limits of variation. The most significant conclusion reached was that a microsample of a secondary mineral might show very large deviations from the average but that all the bulk samples showed little or no variation. If these conclusions are accepted it is not necessary to include the maximum range as the uncertainty in the atomic weight. The value 63.5455 ±0.001 includes a very liberal range of variation for bulk or processed copper. A complete discussion of the effect of the variation on the atomic weight will be published with the mineral survey [4].

---

The authors are indebted to Mrs. Martha Darr for the spectrographic analysis of the separated copper isotopes and the commercial copper, to H. H. Ku for the statistical analysis of the experimental data, and to Oak Ridge National Laboratories for the loan of the separated isotopes.

## 4. References

[1] A. E. Cameron and E. Wichers, J. Am. Chem. Soc. **84,** 4175 (1962).
[2] O. Hönigschmid and T. Johannsen, Z. Anorg. u. Allegem. Chem. **252,** 364 (1944).
[3] R. Ruer and K. Bode, Z. Anorg. u. Allegem. Chem. **137,** 101 (1924).
[4] To be published.
[5] G. E. F. Lundell and J. I. Hoffman, Outlines of Methods of Chemical Analysis, p. 169 (John Wiley & Sons, New York, N.Y., 1938).
[6] L. L. Wilson and S. W. Wilson, Comprehensive Analytical Chemistry, Vol. 1, p. 373 (Elsevier Publ. Co., London, 1962).
[7] E. B. Sandell, Colorimetric Metal Analysis, 3d ed., p. 443 (Interscience Publ. Inc., New York, N.Y., 1959).
[8] F. Everling, L. A. König, J. H. E. Mattauch, and A. H. Wapstra, Nuclear Phys. **18,** 529 (1960).

(Paper 68A6–305)

JOURNAL OF RESEARCH of the National Bureau of Standards—A. Physics and Chemistry
Vol. 68A, No. 6, November–December 1964

# Absolute Isotopic Abundance Ratio and the Atomic Weight of Bromine

Edward J. Catanzaro, Thomas J. Murphy, Ernest L. Garner, and William R. Shields

(August 4, 1964)

An absolute value is obtained for the isotopic abundance ratio of bromine using thermal emission mass spectrometers calibrated for bias by the use of samples of known isotopic composition prepared from nearly pure separated bromine isotopes. The resulting absolute $Br^{79}/Br^{81}$ ratio is 1.02784 ±0.00190 which yields an atomic weight ($C^{12}=12$) of 79.90363 ±0.00092. The indicated uncertainties are overall limits of error based on 95 percent confidence limits for the mean and allowances for the effects of known sources of possible systematic error plus a component to cover possible natural variations in isotopic composition although no provable variations were noted among the $Br^{79}/Br^{81}$ ratios of 29 commercial and natural samples. Mass spectrometric determinations of the atomic weights of bromine and silver give a combining weight ratio of AgBr/Ag=1.740752.

## 1. Introduction

The atomic weights of silver, chlorine, and bromine form the classical basis for establishing atomic weights of many of the elements. Recent mass spectrometric determinations of the atomic weights of silver [1] [1] and chlorine [2] have yielded values of 107.8682 ±0.0010 [2] and 35.45273 $^{+0.00092}_{-0.00097}$, [2] respectively. The present work extends the study to bromine.

A number of mass spectrometric determinations of bromine isotopic abundances have been reported in the literature. Blewett [3], Williams and Yuster [4], White and Cameron [5], and Cameron and Lippert [6] used electron bombardment ion sources and obtained values of $Br^{79}/Br^{81}=1.026$ ±0.026, 1.021 ±0.004, 1.0210 ±0.0020, and 1.0217 ±0.0002, respectively. However, none of these studies included a direct measurement of instrumental bias and, therefore, the resulting ratios were not absolute. White and Cameron [5] recognized that discrepancies between observers and instruments were probably due to mass discrimination occurring in the ion lenses of the sources, but were unable to measure or correct for this discrimination. Cameron and Lippert [6] took care to avoid fractionation during the chemical preparation of their samples, but only asserted that their method of measurement, sublimation of sodium bromide, was free of any instrumental discrimination. They did not attempt to verify this assertion in any manner.

In the present study, both mass spectrometers were calibrated for bias by the use of samples of known isotopic composition, prepared from nearly pure separated bromine isotopes. The measured biases were then used to obtain the absolute $Br^{79}/Br^{81}$ ratio of a reference sample of commercial sodium bromide. In addition, the $Br^{79}/Br^{81}$ ratios of a number of samples of commercial purified bromine and bromide from brines and minerals were also measured.

## 2. Experimental Procedure

### 2.1. Mass Spectrometry

All isotopic measurements were made using two nearly identical solid-source single-focusing mass spectrometers equipped with 68-deg analyser tubes, 60-deg magnet pole pieces and 12-in. radii of curvature. Triple-filament rhenium ribbon (1×30 mils) sources were used and ion currents were measured by means of a vibrating reed electrometer with an expanded-scale recorder. Ratios were measured by varying the magnetic field at constant ion-accelerating voltage.

The bromide was deposited on the sample filaments in the form of ammoniacal solutions of silver bromide. Preliminary experiments showed that AgBr was far superior to NaBr with respect to signal stability during the mass spectrometric analyses. One drop of a AgBr solution containing 3 mg Br/ml (~0.06 mg Br) was deposited on each filament and dried under a heat lamp. To minimize the variability of discrimination, all analyses were made in an identical manner. A strict pattern of filament heating was followed and a set of 10 measurements was made on a growing signal ($3–5\times10^{-13}$ A) between 38 and 52 min after the filaments were turned on. Analyses which did not follow the normal signal-growth pattern were discarded.

[1] Figures in brackets indicate the literature references at the end of this paper.
[2] Overall limit of error based on 95 percent confidence limits for the mean and allowances for effects of known sources of possible systematic error.

### 2.2. Purification of the Separated Isotopes

Electromagnetically separated isotopes in the form of sodium bromide were obtained from the Isotopes Division, Oak Ridge National Laboratory of the Union Carbide Nuclear Company. The $NaBr^{79}$ and the $NaBr^{81}$ were designated Series LM, Lot Number 1391(a) and Series LM, Lot Number 1392(a), respectively. The certificate of analysis accompanying each sample indicated a high degree of cationic purity but did not exclude the possible presence of other halides or pseudohalides. Since the bromide ion concentration of solutions was to be determined by silver coulometry and since the halides iodide and chloride, and pseudo-halides, cyanide and thiocyanate, would react with silver to form insoluble compounds [7], the iostopic samples were further purified to insure the removal of these impurities.

Each separated isotope sample (about 5 g) was divided in half and treated as follows: The sodium bromide (about 2.5 g) was dissolved in a small amount of water and transferred to a 300 ml three-neck distilling apparatus like that described by Murphy, Clabaugh, and Gilchrist [8]. The solution volume was increased to 100 ml and 0.2 ml of redistilled nitric acid was added. Twenty milliliters of dilute ammonium hydroxide (1:9) was added to the receiver flask. The solution was then heated to boiling, and refluxed for 2 hr while a stream of halide-free air was drawn through the system. The heat was then increased and about 10 ml of the solution was distilled into the dilute $NH_4OH$ solution.

This procedure will oxidize iodide to iodine [9] and remove it from solution while only a small amount of bromide is lost. Tests based on the insolubility of silver iodide in ammoniacal solution have shown that when 0.025 mg of iodide ion was added to a solution containing 2.5 g of NaBr and treated as above, the recovery of iodine was complete, so that in terms of the NaBr the iodine concentration in the solution would be less than 0.001 percent. Tests based on the insolubility of silver cyanide have also shown that if cyanide were present, almost all of it would be removed by the above procedure either as hydrogen cyanide or as cyanogen.

Ten milliliters of water and 20 ml of redistilled nitric acid were added to the sodium bromide solution and the solution was refluxed while a stream of halide free air was drawn through the solution. The bromine liberated was slowly distilled into a solution containing a 20 percent excess of the stoichiometric quantity of sodium carbonate and 5 ml of 30 percent hydrogen peroxide. The distillation was continued until only a slight color of bromine remained in the distilland.

Dilute nitric acid (1:5) has been shown to oxidize bromide to bromine quantitatively [8] without oxidizing chloride to chlorine. Chloride analyses [8] of the distillands after removal of the bromine showed that the chloride concentration was less than 0.001 percent in terms of the NaBr present.

After the distillation of bromine was completed, the distillate was heated on a steam bath until the hydrogen peroxide was decomposed. This oxidation by hydrogen peroxide removed any cyanide [10] or thiocyanate [11] that might have distilled with the bromine. Tests, based on the insolubility of silver cyanide and silver thiocyanate, showed that solutions prepared in this manner contained less than 0.001 percent $(CN)^-$ or 0.001 percent $(SCN)^-$ in terms of the NaBr present.

The solution was then transferred to a platinum dish and evaporated to dryness. The dish and contents were covered and heated to 550 °C for ½ hr in an electric furnace to convert any bromate present to bromide. Any nitrate present would be converted to nitrite and cause difficulty in the bromine titration. Therefore, the salt mixture, which contained sodium bromide, sodium nitrite, and the excess sodium carbonate, was dissolved in 50 ml of $H_2O$ and 1 drop of phenolphthalein indicator solution was added. The solution was neutralized to the phenolphthalein end point with (1:9) acetic acid. An equivalent amount of the dilute acetic acid plus a 1-ml excess was then added to neutralize the bicarbonate produced and make the solution slightly acid. Two milliliters of 30 percent hydrogen peroxide was then added and the solution was heated overnight on a steam bath. Under these conditions nitrite is oxidized to nitrate [12] and the prolonged heating destroys the excess peroxide.

Analyses of sodium bromide solutions prepared in the above manner have shown that the solutions contained less than 0.0005 percent bromate ion, less than 0.0005 percent nitrite ion, and less than 0.0005 percent hydrogen peroxide in terms of the sodium bromide present. The bromate test was based on the reaction of bromate with bromide in acid solution to produce bromine which was detected with *o*-tolidine. Nitrite was determined with phenylenediamine [13]. The test for hydrogen peroxide was based on its reaction with titanium to form a colored complex [14].

This purification procedure was repeated on the remaining portions of the separated isotope samples for groups II.

Iodide was not detected in either of the starting isotopic samples. Chloride was found in both the $NaBr^{79}$ and the $NaBr^{81}$ to the extent of 0.13 percent and 0.11 percent, respectively. As stated previously, tests have shown that the purification procedure reduced the chloride content of the sodium bromide to less than 0.001 percent. Cyanide and thiocyanate were not determined, but if they had been present originally, the concentration of each would have been reduced to less than 0.001 percent.

### 2.3. Preparation and Bromide Concentration of Separated Isotope Solutions

The solutions of the purified $NaBr^{79}$ and $NaBr^{81}$ were filtered and transferred to 100 ml volumetric flasks whose necks had been cut off so that only about 1 cm remained. The solutions were diluted to about 65 ml and thoroughly mixed by swirling the flasks for several minutes. Each flask was then sealed with a rubber serum septum and allowed to stand over-

night in the case of a semi-microbalance to insure thermal equilibrium. The flasks and contents were then weighed on the balance to $\pm 0.02$ mg. Samples were withdrawn from each flask by inserting a stainless steel needle attached to a glass hypodermic syringe through the rubber septum and withdrawing the desired amount of solution. A second needle which just punctured the septum served as a vent. The syringe and needle were then washed with distilled water and the washings were combined with the bulk of the sample. The weight of the sample withdrawn was determined from the weight of the flask before and after the withdrawal of solution.

Four samples of from 7 to 9 grams each were withdrawn from each solution by this method. The quantity of bromide in each of these samples was from 2 to 3 meq. Each sample was transferred to a 100 ml beaker and the syringe and needle were washed with distilled water, the washings being caught in the beaker with the bulk of the aliquot. The volume was adjusted to about 15 ml by evaporation on a steam bath.

The bromide ion concentration of each solution was determined by constant-current coulometry using electrically generated silver ions. The end point of the silver titration was determined amperometrically. The details of the method are described by Marinenko and Taylor [15].

This procedure was first applied to solutions prepared from sodium bromide low in iodide and chloride. This sodium bromide was prepared in our laboratory since all of the commercially available sodium bromide was found to be high in chloride content. An excess of redistilled bromine was reacted with sodium carbonate solution. The resulting solution was evaporated to dryness and the mixture of sodium bromide and sodium bromate was heated to 550 °C to convert the bromate to bromide. The sodium bromide was then fused by heating in dry nitrogen to about 800 °C in a tube furnace. The iodide and chloride content of this NaBr was found to be less than 0.001 percent.

Three solutions of sodium bromide were prepared in the approximate concentration of the isotope solutions. Five to six samples each containing from 2 to 3 meq. of bromide ion were withdrawn from each solution and analyzed for bromide ion by the described method.

Data resulting from the analyses of these three preliminary bromide solutions showed that: (a) The meq. of bromide ion found by this method agreed to within 0.1 percent of the meq. calculated, and the assayed percentages were independent of sample size and concentration; and (b) The analyses of the three solutions were of equal precision.

The results of the bromide analyses of the separated isotope solufions are shown in table 1a for Groups I and table 1b for Groups II. Pooling the results of these four sets of analyses with the three described above yields a value of $4.74\times10^{-5}$ meq. Br/g solution as the standard deviation for an individual determination (27 degrees of freedom). The standard error of the mean of four determinations is therefore $2.37\times10^{-5}$ meq. Br/g solution and that of five determinations is $2.12\times10^{-5}$ meq. Br/g solution.

TABLE 1a. *Groups I*

| Sample No. | Wt. Sol | Bromide | Conc Br |
|---|---|---|---|
| Concentration of bromide ion in $NaBr^{79}$ solution | | | |
| | *g* | *meq.* | *meq. Br/g Sol* |
| A | 7.53019 | 2.56406 | 0.340504 |
| B | 8.21278 | 2.79583 | .340424 |
| C | 8.54475 | 2.90845 | .340379 |
| D | 8.26555 | 2.81273 | .340296 |
| E | 7.77453 | 2.64618 | .340365 |
| Mean | | | [a].340394 |
| Concentration of bromide ion in $NaBr^{81}$ solution | | | |
| A | 9.09645 | 2.97587 | 0.327146 |
| B | 8.65398 | 2.83156 | .327197 |
| C | 8.07874 | 2.64328 | .327190 |
| D | 7.81712 | 2.55753 | .327170 |
| Mean | | | [a].327176 |

[a] The standard error of the mean is estimated to be 0.000024 meq/g sol. for the group with four analyses and 0.000021 for the group with five analyses, based on seven groups of data including the sets shown here.

TABLE 1b. *Groups II*

| Sample No. | Wt. Sol | Bromide | Conc Br |
|---|---|---|---|
| Concentration of bromide ion in $NaBr^{79}$ solution | | | |
| | *g* | *meq.* | *meq. Br/g Sol* |
| A | 7.77112 | 2.810027 | 0.361599 |
| B | 7.88535 | 2.851350 | .361601 |
| C | 7.32444 | 2.648832 | .361643 |
| D | 7.73096 | 2.795487 | .361596 |
| Mean | | | [a].361610 |
| Concentration of bromide ion in $NaBr^{81}$ solution | | | |
| A | 7.78525 | 2.74700 | 0.352847 |
| C | 7.78655 | 2.67682 | .352838 |
| D | 7.09924 | 2.50502 | .352857 |
| E | 7.47154 | 2.63715 | .352959 |
| Mean | | | [a].352875 |

[a] The standard error of the mean is estimated to be 0.000024 meq/g sol. based on seven groups of data including the sets shown here.

## 2.4. Isotopic Analyses of the Solutions of the Separated Isotopes

To avoid memory problems, one of the two solutions of the separated isotopes was analyzed on one mass spectrometer and the other solution on the other mass spectrometer. The sources were dismantled and thoroughly cleaned before and after each series of measurements. Blank analyses showed that clean sources yielded no bromine signals.

The isotopic compositions of the separated isotope solutions are given in table 2. The respective $Br^{79}$ and $Br^{81}$ isotopic compositions as reported by ORNL are: "$Br^{79}$", 99.74 $\pm 0.02$ atom percent $Br^{79}$, 0.26 $\pm 0.02$ atom percent $Br^{81}$; "$Br^{81}$", 0.38 $\pm 0.02$ atom

percent $Br^{79}$, 99.62 ±0.02 atom percent $Br^{81}$. The ORNL limits quoted express the precision of the measurements. From known sources of systematic error, the absolute error is estimated by ORNL to be less than 1 percent.

TABLE 2. *Isotopic composition of separated bromine isotopes used in calibration samples*

| Isotope | Isotopic composition [a] (atom %) |
|---|---|
| $Br^{79}$ | $Br^{79}$=99.736<br>$Br^{81}$= 0.264 ±0.008 |
| $Br^{81}$ | $Br^{79}$= 0.386 ±0.008<br>$Br^{81}$=99.614 |

[a] The limits express the maximum uncertainty as estimated from the 95 percent confidence limits of the mass spectrometric determinations and possible errors in the correction factors.

## 2.5. Preparation of the Calibration Samples

Six calibration samples were originally prepared (group I), but the results of sample No. 2 were subsequently discarded when the mass spectrometric data did not conform to the general pattern. In view of this it was considered desirable to prepare a completely new set of six calibration samples (group II).

All calibration samples were prepared by mixing portions of the $Br^{79}$ and $Br^{81}$ solutions, which were withdrawn and weighed in the manner already described. The ratios of $Br^{79}/Br^{81}$ ranged from 1.01 to 1.04 for group I and 0.94 to 1.13 for group II. For each determination, the portions for the calibration samples and the samples for the determination of the bromide concentration were withdrawn on the same day with the exception of sample E of the $Br^{79}$ solution of group I and sample E of the $Br^{81}$ solution of group II which were withdrawn two days after the rest of the group.

Each calibration sample was thoroughly mixed by stirring and 0.5 ml of nitric acid was added. Twenty milliliters of 0.1 *N* $AgNO_3$ solution were added to precipitate the bromide as silver bromide and the solution was allowed to stand overnight in the dark. The solution was filtered through filter paper and the precipitate of silver bromide was washed with dilute (1:500) nitric acid. The paper was carefully folded over the precipitate and both were dried in an electric oven at 110 °C. A weighed portion of the silver bromide was then transferred to a 4 ml screw-cap vial and sufficient concentrated ammonium hydroxide was added so that the resulting solution contained 3 mg of bromide per milliliter of solution.

The isotopic ratio, $\mu$, of each calibration sample was calculated from

$$\mu=\frac{g_1(1-f_1)+g_2(1-f_2)}{g_1f_1+g_2f_2}$$

where

$g_1$=meq. Br from $Br^{79}$ soln
$g_2$=meq. Br from $Br^{81}$ soln
$f_1$=mole fraction of 81 in $Br^{79}$ soln=0.00264
$(1-f_1)$=mole fraction of 79 in $Br^{79}$ soln=0.99736
$f_2$=mole fraction of 81 in $Br^{81}$ soln=0.99614
$(1-f_2)$=mole fraction of 79 in $Br^{81}$ soln=0.00386.

The values of $g$ and $\mu$ are tabulated in table 3a for group I and in table 3b for group II.

TABLE 3a. *Group I—composition of calibration samples*

| Calibration sample No. | $NaBr^{79}$ solution | | $NaBr^{81}$ solution | | Isotopic ratio |
|---|---|---|---|---|---|
| | *wt sol* | *meq.* Br $g_1$ | *wt sol* | *meq.* Br $g_2$ | $\mu$ |
| 1 | 2.20305 | 0.749905 | 2.23035 | 0.729717 | 1.03000 |
| 3 | 2.03553 | .692882 | 2.08166 | .681069 | 1.01972 |
| 4 | 2.07995 | .708003 | 2.11262 | .691199 | 1.02666 |
| 5 | 2.11338 | .719382 | 2.11904 | .693299 | 1.03992 |
| 6 | 2.17520 | .740425 | 2.24607 | .734860 | 1.00999 |

TABLE 3b. *Group II—composition of calibration samples*

| Calibration sample No. | $NaBr^{79}$ solution | | $NaBr^{81}$ solution | | Isotopic ratio |
|---|---|---|---|---|---|
| | *wt sol* | *meq.* Br $g_1$ | *wt sol* | *meq.* Br $g_2$ | $\mu$ |
| 1 | 1.04618 | 0.378309 | 1.08450 | 0.382693 | 0.99104 |
| 2 | 1.09963 | .397637 | 1.09671 | .387002 | 1.02982 |
| 3 | 1.09990 | .397735 | 1.10046 | .388325 | 1.02658 |
| 4 | 1.09030 | .394263 | 1.09721 | .387178 | 1.02068 |
| 5 | 1.18382 | .428081 | 1.07291 | .378603 | 1.13256 |
| 6 | 1.10534 | .399702 | 1.20550 | .425391 | .94230 |

## 2.6. Isotopic Analyses of the Calibration Samples

Although the bromine background signals were completely negligible during the analyses of natural samples, slight memory effects became evident during the analyses of the calibration samples. These samples were run alternatingly with the reference sample and memory effects on the order of 0.2 percent were evident when the calibration sample differed by 10 percent from the reference. To eliminate memory, a uranium sample was run before and after every sample that differed from the reference by more than 1 percent. The very high temperature achieved during the uranium runs served to remove any bromine from the previous analysis.

## 2.7. Natural and Commercial Samples

The reference sample is a commercial sample of sodium bromide designated as NBS Isotopic Reference Sample No. 106. A portion of this sample was converted to silver bromide in the same manner as the calibration samples.

The samples of commercial bromine were reacted with ammonium hydroxide solution and converted to silver bromide in the same manner as the calibration samples after making the solutions acidic with nitric acid.

The sylvites (KCl), carnallites ($KMgCl_3 \cdot 6H_2O$), brines, sea water, and bittern were treated as follows: A measured quantity was dissolved in 500 ml

of $H_2O$ and 1 ml of nitric acid was added. The solution was transferred to a distilling apparatus and, to remove iodine, 50 ml of the solution was distilled into dilute ammonium hydroxide solution. Seventy-five milliliters of nitric acid were then added and the bromine produced was distilled into dilute ammonium hydroxide. Since chloride was the dominant halide in these samples, it was necessary to repeat the oxidation and distillation to free the bromine from chlorine. The bromide concentration in most of these samples ranged from 0.01 percent to 0.1 percent. After the second distillation, the solution was made acidic with nitric acid, converted to silver bromide, and the bromide ion concentration adjusted to 3 mg Br/ml, as in the case of the calibration samples.

The bromyrite sample (AgBr) was dissolved in ammonium hydroxide and the silver was electrodeposited onto a platinum gauze electrode. The solution was made acidic and treated as the above minerals.

## 3. Results and Discussion

Table 4 compares the calculated isotopic ratios of 11 calibration samples with the results obtained on the two mass spectrometers. Two groups of calibration samples were prepared and the sources of both instruments were dismantled and cleaned between the analyses of the two groups. Table 5 shows the results of multiple analyses of the reference sample (12 per mass spectrometer per determination), both uncorrected and corrected for the biases indicated by the calibration samples. The reasons for the differences in bias cannot be quantitatively evaluated, but the major effect appears to be due to slight changes in the alinements of the source parts when they are reassembled after cleaning. In any case, the excellent agreement between all four corrected values of the reference indicates that the calibration method is consistent.

TABLE 4. *Determination of mass spectrometric bias*

| Calibration sample No. | Isotopic ratio, $Br^{79}/Br^{81}$ | | | Correction factor (calc/M.S.) | |
|---|---|---|---|---|---|
| | Calc. | MS-1 | MS-4 | MS-1 | MS-4 |
| **Group I** | | | | | |
| 1 | 1.03000 | 1.02970 | 1.03035 | 1.000301 | 0.999670 |
| 3 | 1.01972 | 1.02055 | 1.02120 | 0.999197 | .998561 |
| 4 | 1.02666 | 1.02820 | 1.02865 | .998512 | .998075 |
| 5 | 1.03992 | 1.04105 | 1.04125 | .998915 | .998723 |
| 6 | 1.00999 | 1.01175 | 1.01235 | .998270 | .997679 |
| Mean | | | | .9990390 | .9985416 |
| **Group II** | | | | | |
| 1 | 0.99104 | 0.99115 | 0.99270 | 0.999899 | 0.998328 |
| 2 | 1.02982 | 1.02960 | 1.03225 | 1.000214 | .997646 |
| 3 | 1.02658 | 1.02735 | 1.02875 | 0.999260 | .997900 |
| 4 | 1.02068 | 1.02125 | 1.02270 | .999442 | .998025 |
| 5 | 1.13256 | 1.13185 | 1.13425 | 1.000627 | .998510 |
| 6 | 0.94230 | 0.94185 | 0.94355 | 1.000478 | .998675 |
| Mean | | | | .9999866 | .9981807 |

TABLE 5. *Observed and corrected values of the $Br^{79}/Br^{81}$ ratio for the reference sample*

| | Observed ratio | Correction factor | Corrected ratio |
|---|---|---|---|
| Group I MS-1 | 1.028792 | 0.9990390 | 1.027807 |
| MS-4 | 1.029592 | .9985416 | 1.028090 |
| Group II MS-1 | 1.027683 | .9999866 | 1.027669 |
| MS-4 | 1.029675 | .9981807 | 1.027803 |
| Mean | | | 1.02784 ±0.00105 [a] |

[a] Uncertainty components:
95 percent confidence limits on ratio determination ±0.00051
Possible error in composition of separated isotopes ±0.00033
Possible error in calibration samples ±0.00021

Table 6 summarizes the bromine isotopic-ratio measurements of samples of commercial bromine and the original bromine source material as supplied by seven major bromine manufacturers in the United States. Table 7 summarizes the results of measurements on a number of mineral samples. The results show that there are no significant isotopic variations among any of the commercial and natural samples. The average $Br^{79}/Br^{81}$ ratio of the 29 samples is displaced from the reference by −0.00048. Most of this shift is due to the mineral samples which yield the lowest ratios. This result is consistent with previous experience at this laboratory on other elements. It may be attributed to a difference in purity between the mineral samples and the reference. In general it is more difficult to obtain standard intensity levels during mass spectrometric analyses of natural samples as compared to reference samples [1] and it was observed that the $Br^{79}/Br^{81}$ ratios obtained in the more difficult (higher filament temperature) analyses were consistently lower than those obtained in the less difficult (lower filament temperature) analyses.

TABLE 6. *Isotopic abundance ratios of bromine from various commercial bromine and bromine source materials relative to reference sample*

| Sample | Source | Average observed ratio of ratios [a] |
|---|---|---|
| Brine, Searles Lake | American Potash & Chemical Corp. | 0.9988 |
| Brine | Arkansas Chemical Co | .9996 |
| Bromine | Arkansas Chemical Co | .9995 |
| Monroe brine | Dow Chemical Co | .9994 |
| Midland bromine, purified | Dow Chemical Co | .9998 |
| Freeport bromine, purified | Dow Chemical Co | .9995 |
| Sea Water | Ethyl-Dow Chemical Co | .9992 |
| Bittern | F. M. C. Corp | .9994 |
| Bromine | F. M. C. Corp | .9990 |
| Brine | Great Lakes Chemical Corp | .9999 |
| Brine | Great Lakes Chemical Corp | .9998 |
| Brine | Great Lakes Chemical Corp | 1.0005 |
| Brine | Great Lakes Chemical Corp | 0.9998 |
| Bromine | Great Lakes Chemical Corp | .9999 |
| Bromine | Great Lakes Chemical Corp | .9998 |
| Bromine | Great Lakes Chemical Corp | 1.0002 |
| Bromine | Great Lakes Chemical Corp | 0.9998 |
| Brine, St. Louis production | Michigan Chemical Corp | 1.0002 |
| Bromine, St. Louis production | Michigan Chemical Corp | 1.0000 |
| Bromine, Manistic production | Michigan Chemical Corp | 0.9994 |
| Bromine, El Dorado production | Michigan Chemical Corp | .9992 |

[a] $(Br^{79}/Br^{81})$ sample/$(Br^{79}/Br^{81})$ reference. The 95 percent confidence limit is ±0.0012.

TABLE 7. *Isotopic abundance ratios of bromine from some minerals relative to reference sample*

| Sample No.[a] | Description | Average observed ratio of ratios [b] |
|---|---|---|
| 62416 | Carnallite, Stassfurt, Germany | 0.9992 |
| 98011 | Carnallite, Barcellona, Spain | .9990 |
| 106869 | Carnallite, New Mexico | .9997 |
| 103518 [c] | Sylvite, Nebra, Germany | .9990 |
| 103518 [c] | Sylvite, Nebra, Germany | .9988 |
| 92665 | Sylvite, New Mexico | .9995 |
| 93472 | Sylvite, Kalusz, Galecia, Poland | .9993 |
| 80263 | Bromyrite, Broken Hill, Australia | .9990 |

[a] U.S. National Museum Catalog numbers.
[b] $(Br^{79}/Br^{81})$ sample/$(Br^{79}/Br^{81})$ reference. The 95 percent confidence limit is $\pm 0.0012$.
[c] Two pieces from the same sample.

The possibility of slight isotopic fractionation during the extraction of the trace amounts of bromine in the natural samples cannot be completely discarded, but is considered extremely unlikely in view of the high recovery techniques used.

A term to cover a possible natural variation of $\pm 0.00085$ (the range of results for the natural samples) in the $Br^{79}/Br^{81}$ ratio has been included in the error attached to the final atomic weight value (tables 8 and 9).

The absolute ratio, $Br^{79}/Br^{81}=1.0274 \pm 0.00105$, for the refererence sample results in the percentage abundances: $Br^{79}=50.686 \pm 0.025$ and $Br^{81}=49.314 \pm 0.025$. The uncertainties are the sum of the 95 percent confidence limits on the ratio determination and the estimated maximum possible errors in the analyses of the separated isotopes and the compositions of the calibration samples. Using the nuclidic masses given by Everling et al. [16], the results yield an atomic weight of 79.90363 $\pm 0.00051$ on the unified scale ($C^{12}=12$). These calculations are summarized in table 8 where the error statements include the effect of possible natural variation to the extent noted previously.

The atomic weight of bromine reported here is significantly different from that accepted by the International Commission on Atomic Weights (1961), 79.909 $\pm 0.002$ ($C^{12}=12$), which was derived by the use of a combining weight for AgBr/Ag=1.740785 and the Commission's value of 107.870 for the atomic weight of silver. Using the herein determined value of 79.90363 for bromine and the silver value of 107.8682 from Shields et al.[1] gives a combining weight ratio AgBr/Ag=1.740752. Table 9 summarizes the atomic weight results on silver, chlorine and bromine obtained in this laboratory using the same mass spectrometers and the same calibration technique. Also shown are the calculated combining weight ratios of AgCl/Ag and AgBr/Ag.

TABLE 8.—*Summary calculation of the atomic weight of bromine*

| | |
|---|---|
| Absolute isotopic ratio | $Br^{79}/Br^{81}=1.02784 \pm 0.00190$ [a] |
| Absolute isotopic composition, Atom percent | $Br^{79}=50.686 \pm 0.047$ [a]<br>$Br^{81}=49.314 \pm 0.047$ [a] |
| Nuclidic masses ($C^{12}=12$) | $Br^{79}=78.918348 \pm 0.000019$ [b]<br>$Br^{81}=80.916344 \pm 0.000037$ [b] |
| Unified atomic weight ($C^{12}=12$) | $=79.90363 \pm 0.00092$ |
| Uncertainty components: | |
| Reference ratio determination | $=\pm 0.00025$ |
| Composition of separated isotopes | $=\pm .00016$ |
| Composition of calibration samples | $=\pm .00010$ |
| Possible natural variations | $=\pm .00041$ |
| Total | $=\pm .00092$ |

[a] The uncertainties are overall limits of error based on 95 percent confidence limits for the mean and allowances for the effects of known sources of possible systematic error (See table 5) plus a component (.00085, in the ratio) to cover possible natural variations in the $Br^{79}/Br^{81}$ ratio.
[b] From ref. [16].

The authors are indebted to George Marinenko for the coulometric titrations of the bromide in the separated isotope solutions and to Hsein H. Ku for the statistical analysis of the experimental data. They also express their appreciation to Dr. George Switzer and the U. S. National Museum for supplying the mineral samples and to the following companies for supplying the bromine and brine samples: American Potash & Chemical Corp., Los Angeles, Calif.; Arkansas Chemicals, Inc., El Dorado, Ark.; The Dow Chemical Co., Midland, Mich.; Ethyl-Dow Chemical Co., Freeport, Tex.; F. M. C. Corporation, Newark, Calif.; Great Lakes Chemical Corp., Filer City, Mich.; Michigan Chemical Corp., Saint Louis, Mich.

TABLE 9.—*Summary of National Bureau of Standards mass spectrometric atomic weight determinations* ($C^{12}=12$) *of silver, chlorine and bromine*

| Element | Absolute isotopic ratio | Nuclidic mass [a] | Atomic weight |
|---|---|---|---|
| Ag [b] | $Ag^{107}/Ag^{109}=1.07597 \pm 0.00135$ | $Ag^{107}=106.904970 \pm 0.000110$<br>$Ag^{109}=108.904700 \pm 0.000110$ | $107.8682 \pm 0.0010$ |
| Cl [c] | $Cl^{35}/Cl^{37}=3.1272 \begin{smallmatrix}+0.0079\\-0.0082\end{smallmatrix}$ | $Cl^{35}=34.9688545 \pm 0.0000028$<br>$Cl^{37}=36.9658959 \pm 0.0000022$ | $35.45273 \begin{smallmatrix}+0.00092\\-0.00057\end{smallmatrix}$ |
| Br | $Br^{79}/Br^{81}=1.02784 \pm 0.00190$ | $Br^{79}=78.918348 \pm 0.000019$<br>$Br^{81}=80.916344 \pm 0.000037$ | $79.90363 \pm 0.00092$ |

Calculated combining weight ratios: AgCl/Ag 1.328667; AgBr/Ag 1.740752

[a] See reference [16].
[b] See reference [1].
[c] See reference [2].

## 4. References


[1] W. R. Shields, E. L. Garner, and V. H. Dibeler, J. Res. NBS **66A** (Phys. and Chem.), 1 (1962).
[2] W. R. Shields, T. J. Murphy, E. L. Garner, and V. H. Dibeler, J. Am. Chem. Soc. **84**, 1519 (1962).
[3] J. P. Blewett, Phys. Rev. **49**, 900 (1936).
[4] D. Williams and P. Yuster, Phys. Rev. **69**, 556 (1946).
[5] J. R. White and A. E. Cameron, Phys. Rev. **74**, 991 (1948).
[6] A. E. Cameron and E. L. Lippert, Jr., Science **121**, 136 (1955).
[7] W. F. Hillebrand, G. E. F. Lundell, H. A. Bright, and J. I. Hoffman, Applied Inorganic Analysis, 2d ed., p. 726 (John Wiley & Sons, New York, N.Y., 1953).
[8] T. J. Murphy, W. S. Clabaugh, and R. Gilchrist, J. Res. NBS **53**, 13 (1954).
[9] E. Abel, Monatsh. **81**, 339 (1950).
[10] O. Masson, J. Chem. Soc. **91**, 1449 (1907).
[11] F. Schuster, Z. anorg. allgem. Chem. 186, **253** (1930).
[12] E. Halfpenny and P. L. Robinson, J. Chem. Soc. **1952**, 928.
[13] R. Uzel, Coll. Czech. Chem. Commun. **5**, 139 (1933).
[14] N. Allen, Ind. Eng. Chem., Anal. Ed. **2**, 55 (1930).
[15] G. Marinenko and J. K. Taylor, J. Res. NBS **67A** (Phys. and Chem.), 31 (1963).
[16] F. Everling, L. A. König, J. H. E., Mattauch, and A. H. Wapstra, Nuclear Phys. **18**, 529 (1960).


(Paper 68A6-306)

JOURNAL OF RESEARCH of the National Bureau of Standards—A. Physics and Chemistry
Vol. 68A, No. 6, November–December 1964

# Optical Properties of Thin Films on Transparent Surfaces by Ellipsometry; Internal Reflection for Film Covered Surfaces Near the Critical Angle

Elio Passaglia and Robert R. Stromberg

(August 5, 1964)

The application of ellipsometry to the determination of the optical properties of thin films on transparent substrates by the use of internal reflection and angles of incidence near the critical angle for total reflection is described and illustrated. Four cases are considered: 1. the angle of incidence, $\theta_i$, is less than either the critical angle for total reflection between the substrate and the film, $\theta_c^{1,2}$, and the critical angle between the substrate and the surrounding medium, $\theta_c^{1,3}$; 2. $\theta_c^{1,3} > \theta_i > \theta_c^{1,2}$; 3. $\theta_c^{1,3} < \theta_i < \theta_c^{1,2}$; and 4. $\theta_c^{1,3} < \theta_i > \theta_c^{1,2}$. For case 1, at certain critical values of film thickness $d$ and refractive index $n_2$, the reflected light may be polarized with its electric vector either entirely in or normal to the plane of incidence. Near these conditions the sensitivity of ellipsometric measurements is extremely high, but the intensity of the reflected light is very low. Except under these conditions the intensity is adequate for experimental measurements, as it is also in case 2. For case 1 it is always possible to determine $n_2$ and $d$ by a single measurement; for case 2 this is possible only for thin films. For cases 3 and 4, and case 2 for thick films, only one of these may be determined. Under these conditions, however, the reflectivity is 100 percent.

## 1. Introduction

The determination of the optical constants of surfaces and the thickness and refractive index of thin films by measurement of the changes in the state of polarization of polarized light upon reflection is based on the well-known equations of Drude [1].[1] The technique for carrying out these measurements is frequently referred to as ellipsometry and has been described in detail elsewhere [e.g., 2, 3, 4].

Most work with ellipsometry has been concerned with studies on metallic surfaces [2, 3], either because of their intrinsic interest or because they form highly reflecting substrates for the study of thin films. However, it is sometimes desirable to measure the properties of thin films on transparent surfaces, in which case the low intensity of the reflected light makes accurate analysis of its state of polarization difficult.

There are two possible systems which would, in general, increase the intensity of the reflected beam over that obtained by direct external reflection from a transparent surface. In one, a thin layer of the transparent material which is to be used as a substrate for the film is placed in intimate contact with a metal, which is used as the reflecting substrate. The transparent material may be placed as a film on a metallic plate, for example by evaporating a film of silica on a metallic substrate in a vacuum evaporator. It is necessary, of course, to determine the optical properties of the metal prior to deposition of the film, and these properties must not change as a result of this deposition. The metal may also be evaporated onto the transparent material. In this case it should be possible to determine the optical properties of the bare metallic surface directly, and, from the other side, the properties of the transparent plate. For this technique the faces of the plate must be sufficiently flat and parallel. This system of a transparent film backed in some manner by a metallic reflecting surface does not differ from the usual system of a metallic reflector with multiple films [5], and will not be discussed further.

A second possible system is one in which it is arranged to have internal reflection at the boundary of the transparent material in question and to use angles near or above the critical angle for total internal reflection. This can be accomplished by constructing a prism of the substrate material or, if other considerations permit, by placing the material in a liquid of higher refractive index. At angles of incidence greater than the critical angle, all the light is reflected and intensity problems are obviated. Although there is total reflection at angles of incidence greater than the critical angle, the beam does penetrate the medium of lower refractive index; this effect has been used to study the infrared spectra of opaque materials [6, 7]. In ellipsometric applications, total reflection permits the use of multiple reflections to increase sensitivity [8], but does lead to the serious limitation that the refractive index and thickness of a thin film may not be determined simultaneously.

[1] Figures in brackets indicate the literature reference at the end of this paper.

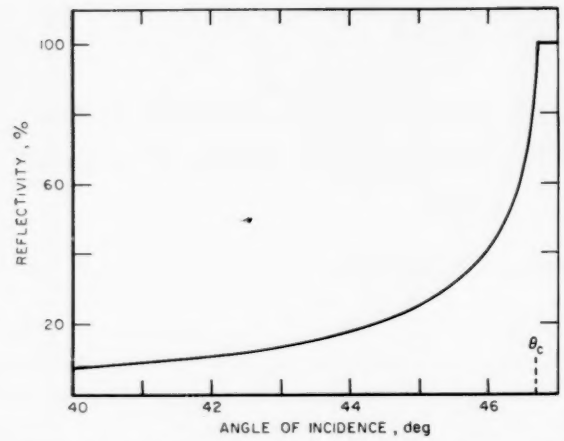


FIGURE 1. *Reflectivity as a function of angle of incidence for internal reflection in the neighborhood of the critical angle.*

The calculations were made using the refractive indexes given in table 1.

At angles between the polarizing angle and the critical angle the intensity of light reflected rises very sharply as the critical angle is approached, and this region may be used quite effectively for ellipsometric studies. For example, the intensity of reflected light as a function of angle of incidence is shown in figure 1 (critical angle=46.68 deg). For an angle of incidence within 0.2 deg of the critical angle, the reflectivity is 60 percent. Although the reflectivity will vary greatly with the thickness and refractive index of any film on the surface, it will be shown that the reflectivity remains quite high for relatively thin films and hence this is a useful region for carrying out ellipsometric measurements on thin films on transparent substrates.

This paper will illustrate the application of ellipsometry to this type of system by presenting detailed calculations of the changes in the state of polarization of light reflected from a transparent surface covered by a transparent film for certain specific values of angles of incidence and refractive indexes. The calculations were carried out by means of the program described by McCrackin and Colson [9] using the IBM 7094 computer.

## 2. Reflection at an Interface

As is well known, $\rho$, the ratio of the reflection coefficient for light polarized with the electric vector in the plane of incidence, $r^p$, to the reflection coefficient for light polarized with the electric vector normal to the plane of incidence, $r^s$, may be represented by the equation

$$\rho=\frac{r^p}{r^s}=\tan\psi e^{i\Delta} \tag{1}$$

where $\tan\psi$ is the ratio of the magnitude of the two coefficients and $\Delta$ is the difference in their phases. For a bare surface $\rho$ is simply the ratio of the Fresnel coefficients. For a semi-infinite medium (which we call the "medium") of refractive $n_3$ separated by a film of refractive index $n_2$ from another semi-infinite medium of refractive index $n_1$ (which we call the "substrate"), the ratio of reflection coefficients for light incident at the $n_1-n_2$ interface from the $n_1$ side is given by the exact Drude equation

$$\tan\psi e^{i\Delta}=\frac{\dfrac{r^p_{12}+r^p_{23}\exp D}{1+r^p_{12}r^p_{23}\exp D}}{\dfrac{r^s_{12}+r^s_{23}\exp D}{1+r^s_{12}r^s_{23}\exp D}} \tag{2}$$

where $r_{12}$ and $r_{23}$ are the Fresnel coefficients at the substrate-film and film-medium interface respectively. $D$ is given by

$$D=-4\pi i n_2\cos\theta_2\, d/\lambda$$

where $\theta_2$ is the angle of incidence at the film-medium interface, $\lambda$ is the wavelength of the light in vacuum, and $i=\sqrt{-1}$. It is clear that if all the parameters in this equation are known but two, say $n_2$ and $d$ (provided $n_2$ is real), then a measurement of $\Delta$ and $\psi$ permits the determination of these two, and the methods for doing this have been described elsewhere [2, 3].

If total reflection occurs, however, $r^p$ and $r^s$ both have a magnitude of unity, so that $\psi$ is always equal to $\pi/4$. This gives only one experimental parameter ($\Delta$) and permits the calculation of only one of the quantities $n_2$ or $d$; the other must be determined by other means. This is the most serious limitation imposed by total internal reflection.

## 3. Parameters of Systems Discussed

We consider only the case in which $n_1$ is greater than both $n_2$ and $n_3$ and all indexes are real. Since light is considered incident at the $n_1-n_2$ interface from the higher refractive index side, internal reflection occurs. We call the angle of incidence $\theta_i$, and for such a system two critical angles must be considered. These are $\theta_c^{1,2}$, the critical angle for total reflection between the substrate and the film, and $\theta_c^{1,3}$, the critical angle for total reflection between the substrate and the surrounding medium. Four cases can then be considered: one in which the angle of incidence, $\theta_i$, is less than either $\theta_c^{1,2}$ or $\theta_c^{1,3}$, two cases in which $\theta_i$ is greater than one of these but less than the other, and the case in which $\theta_i$ exceeds both these critical angles. Note that the critical angle for reflection at the film-medium interface, $\theta_c^{2,3}$, need not be specifically considered, for when $\theta_i=\theta_c^{1,3}$, the angle of incidence at the film-medium interface, $\theta_i^{2,3}$, is equal to $\theta_c^{2,3}$, and if $\theta_i$ is greater or less than $\theta_c^{1,3}$, $\theta_i^{2,3}$ will automatically be greater or less than $\theta_c^{2,3}$.

The parameters of the system chosen for calculation are given in table 1. The values for $n_1$ and $n_3$ arose out of an experimental study reported elsewhere [10]. The index $n_1$ pertains to a leaded glass

prism immersed in a very dilute solution of an organic compound in water ($n=1.337$). The adsorption of this compound onto the glass prism was studied by ellipsometry. Calculations have been carried out for the values of film refractive indexes $n_2$ shown in the table. The value of 1.20, while not easy to achieve experimentally, was chosen merely to illustrate the behavior when $n_2<n_3$.

In all the cases shown we shall be interested in computing the experimentally obtainable quantities $\psi$ and $\Delta$ as a function of film thickness. We shall also be interested in the amount of light reflected, and will consider each case in turn.

TABLE 1. *Parameters of system chosen for calculation* $\lambda=5461$ Å

$n_1=1.8376$ $\theta_s^{1,3}=46.68$ deg
$n_3=1.3370$ $\theta_p^{1,3}=36.05$ deg*

| Case No. | | $\theta_i$, deg | $n_2$ | $\theta_s^{1,2}$, deg | $\theta_p^{1,2}$, deg |
|---|---|---|---|---|---|
| 1 | $\theta_i<\theta_s^{1,2}$<br>$<\theta_s^{1,3}$ | 46.00<br>46.60 | 1.60–1.36<br>1.38–1.36 | 60.7–47.8<br>48.6–47.8 | 41.1–36.5<br>36.9–36.5 |
| 2 | $\theta_i>\theta_s^{1,2}$<br>$<\theta_s^{1,3}$ | 46.00 | 1.200,<br>1.300 | 40.8<br>45.0 | 33.3 |
| 3 | $\theta_i<\theta_s^{1,2}$<br>$>\theta_s^{1,3}$ | 46.70 | 2.00<br>1.60<br>1.40<br>1.35 | 60.7<br>49.6<br>47.2 | 41.1<br>37.3<br>36.3 |
| 4 | $\theta_i>\theta_s^{1,2}$<br>$>\theta_s^{1,3}$ | 46.70<br>50.00<br>50.00 | 1.20<br>1.40<br>1.20 | 40.8<br>49.6<br>40.8 | 33.2<br>37.3<br>33.3 |

*$\theta_p$ denotes the polarizing (Brewester's) angle.

## 4. Case 1, $\theta_s^{1,3}>\theta_i<\theta_s^{1,2}$

In this case, when the angle of incidence is less than either of the two critical angles, some interesting polarization effects occur. This is due to the fact that for certain critical values of thickness and refractive index of the film $r^s$ or $r^p$ may go to zero. When this occurs the reflected light is polarized with its electric vector in the plane of incidence ($r^s=0$) or normal to the plane of incidence ($r^p=0$). The value of tan $\psi$ may therefore be anything from zero ($r^p=0$) to infinity ($r^s=0$). The vanishing of $r^p$ for dielectric films on dielectric substrates is well known [11, 12], and the vanishing of $r^p$ and $r^s$ for dielectric films on metal surfaces has been discussed by Hartman [13] and Mattuck [14]. The conditions for the vanishing of $r^s$ for dielectric films on dielectric substrates have not, to our knowledge, been previously studied. In the appendix there are derived the conditions for the vanishing of $r^s$ and $r^p$. It is shown there that for each case the optical thickness of the film must be such that the phase retardation in the film is an odd multiple of $\pi$, i.e.,

$$\frac{2n_2d\cos\theta_2}{\lambda}=\frac{k}{2} \tag{3}$$

where $k$ is an odd integer. We shall call the thickness necessary to fulfill this condition the "quarter wave thickness." For this thickness $\Delta$ is zero or $\pi$, and if the incident light is linearly polarized, the reflected is also.

In addition to this condition, there is a condition on $n_2$ for the vanishing of $r^s$ or $r^p$. We shall discuss the former case first.

For the vanishing of $r^s$, it is shown in the appendix that $n_2$ must assume a critical value, $n_{2s}$, given by the equation

$$n_{2s}^2=n_1n_3\cos\theta_1\cos\theta_3+n_1^2\sin^2\theta_1 \tag{4}$$

where the symbols have the obvious meanings. For an angle of incidence of 46.00 deg and the other parameters as in table 1, $n_{2s}=1.41542$, and the corresponding thickness from eq (3) is 2700 Å. For these values of the film refractive index and thickness the reflected light will be linearly polarized, but, unlike the condition at Brewster's angle, the electric vector is in the plane of incidence, not normal to it. Thus tan $\psi$ becomes infinite. We shall now discuss the behavior of $\rho$, the ratio of reflection coefficients (see eq (1)) with film thickness for two values of refractive index near the critical index $n_{2s}$.

A polar plot of $\rho$ is given in figure 2 for $n_2$ values of 1.41485 and 1.41600, i.e., slightly lower and slightly higher than $n_{2s}$. The numbers on the curves correspond to film thicknesses. While the curve for $n_2=1.41600$ lies entirely to right of the origin, the curve for $n_2=1.41485$ goes around the origin. (The very large values of tan $\psi$ for these cases make this somewhat hard to see, and therefore, an enlargement of the region around the origin is shown separately. The value of $\psi$ for these curves at zero thickness is, of course, a constant determined by $\theta_i$, $n_1$, and $n_3$.) That is to say, for $n_2$ values above the critical value, as film thickness increases $\Delta$ oscillates between two extreme values, $\Delta_{max}$ and $\Delta_{min}$, symmetrically disposed with respect to the value of $\Delta$ at zero film thickness. For values of $n_2$ less than $n_{2s}$, $\Delta$ assumes all values from zero to $2\pi$.

At the quarter wave thickness the waves reflected from the 2, 3 interface and transmitted into medium 1 are $\pi$ radians out of phase with both the incident wave and the wave reflected from the 1, 2 interface. For $n_2>n_{2s}$ the amplitude of the sum of the $s$ waves reflected from the 2, 3 interface and transmitted into medium 1 is less than the amplitude of the $s$ wave reflected at the 1, 2 interface, and hence the total reflected $s$ wave is in phase with the incident wave. For $n_2<n_{2s}$, the amplitude of the sum of the reflected and retransmitted $s$ waves is greater than the amplitude of the $s$ wave reflected at the 1, 2 interface, and the total reflected $s$ wave is $\pi$ radians out of phase with the incident wave. Thus $\Delta$ at the quarter wave thickness changes from 0 to $\pi$ as $n_2$ goes from above $n_{2s}$ to below.

There is an extremely great dependence of $\Delta$ upon film thickness for values of $n_2$ near the critical refractive index $n_{2s}$ and for film thicknesses near the quarter-wave thickness, i.e., when $\Delta=0$ for $n_2>n_{2s}$ or $\pi$ for $n_2<n_{2s}$. Thus, for example, from the curve for $n_2=1.41600$, a change of thickness from 2688 to 2690 Å produces a change in $\Delta$ of 22 deg. This is a change of 11 deg per angstrom. Clearly, ellipsometric measurements under these conditions are exceedingly sensitive to thickness.

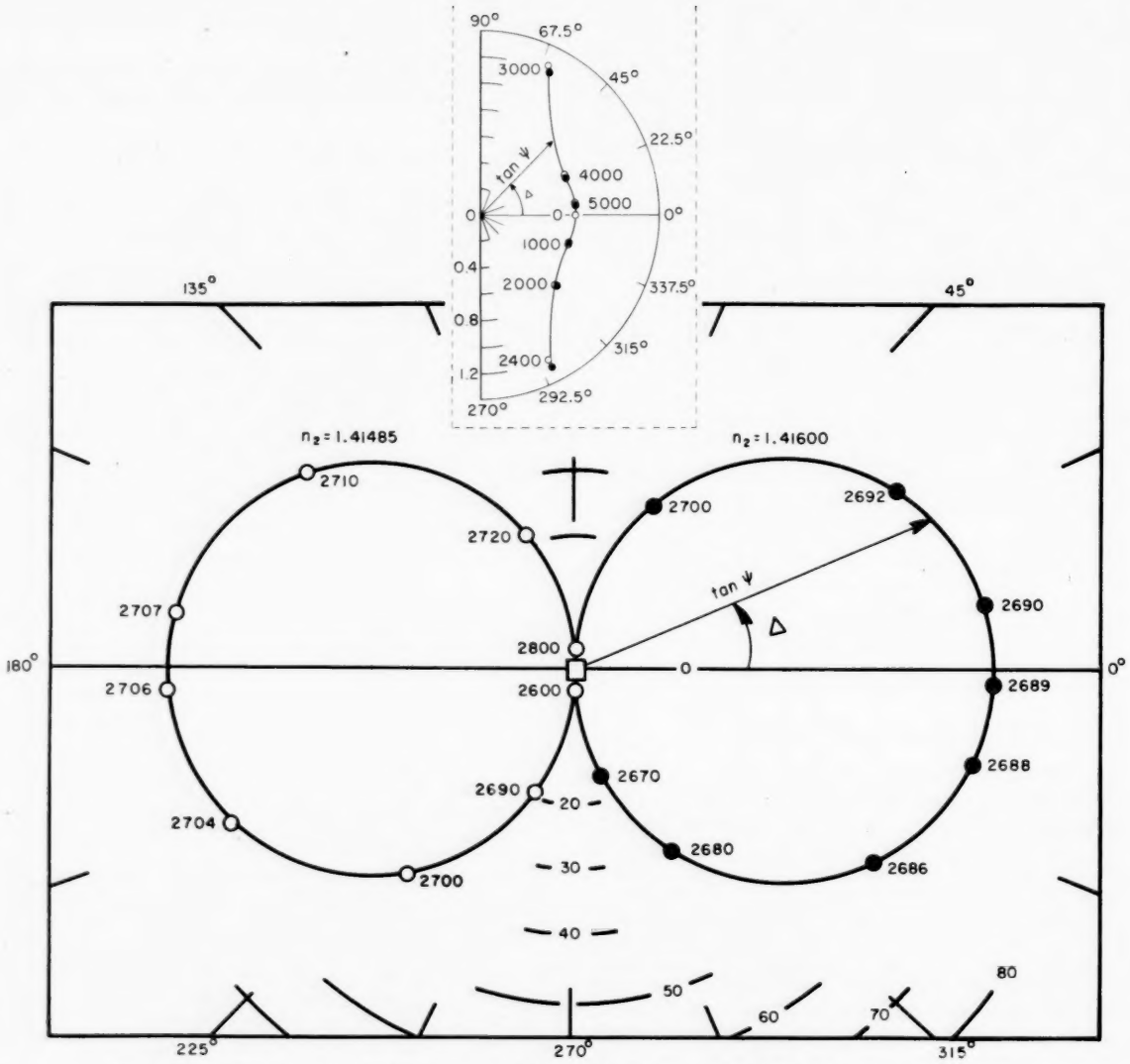


FIGURE 2. *Case 1. A polar plot of $\rho$ for $n_2$ values slightly lower and slightly higher than $n_{2s}$ (see text).*

The insert is an enlargement of the rectangular area at the center. The numbers on the curves correspond to film thickness. ○, $n_2$=1.41485 ●, $n_2$=1.41600

Other parameters as in table 1.

The dependence of $\psi$ on thickness is less easy to see from the figure. The calculations indicate that for a film refractive index of 1.41540, i.e., very close to $n_{2s}$, a change in thickness from 2694 to 2698 Å changes tan $\psi$ from 80 to 1250. This extreme dependence of tan $\psi$ on thickness indicates that the production of accurately linearly polarized light by this method would be a difficult experimental feat. Moreover, the intensity of light reflected under these polarizing conditions is very low, but we shall defer discussion of this until later in this paper.

We shall now discuss the behavior of $\rho$ when $r^p$ vanishes. For this to occur, eq (3) must be obeyed, and in addition there is a condition on $n_2$. As shown in the appendix, the values of $n_2$ necessary to have the $r^p$ vanish, which we call $n_{2p}$, are given by

$$n_{2p}^2=\frac{1}{2}\frac{n_1 n_3}{\cos\theta_1 \cos\theta_3}[1\pm(1-\sin 2\theta \sin 2\theta_3)]^{1/2} \quad (5)$$

There are two values of $n_{2p}$, corresponding to the positive and negative signs, and we call these

$n_{2p}^{+}$ and $n_{2p}^{-}$. For an angle of incidence of 46.00° and $n_1$ and $n_3$ as shown in the table, $n_{2p}^{+}$ is 4.654 and out of the range of our consideration. However, $n_{2p}^{-}$ is 1.3786, and the corresponding thickness from eq (3) is 3487 Å. For these values of thickness and refractive index the reflected light is polarized entirely with its electric vector normal to the plane of incidence, and $\tan\psi=0$.

Figure 3 shows the behavior of $\rho$ with film thickness for $n_2=n_{2p}^{-}$ and two other values near this value (1.36 and 1.3942). For values of $n_2$ less than $n_{2p}^{-}$ (but of course greater than $n_3$) the $\rho$ curve lies between the origin and the value of $\tan\psi$ for the bare surface (fig. 3, $n_2=1.36$). Again $\Delta$ oscillates between two values, $\Delta_{max}$ and $\Delta_{min}$, symmetrically disposed with respect to the value for the bare surface. For $n_2$ equal to $n_{2p}^{-}$, the curve of $\rho$ passes through the origin ($\tan\psi=0$) and $\Delta_{max}$ and $\Delta_{min}$ are $\pi/2$ and $-\pi/2$ respectively (fig. 3, $n_2=1.3786$). For values of $n_2$ larger than $n_{2p}^{-}$ (but smaller than $n_{2s}$) $\Delta$ takes on all values between 0 and $2\pi$ (fig. 3, $n_2=1.3942$).

For the quarter wave thickness and values of $n^2$ between $n_{2p}^{-}$ and $n_{2s}$ the sum of the amplitudes of the waves reflected from the 2,3 interface and transmitted back into medium 1 is greater than the amplitude of the wave reflected from the 1,2 interface for $s$ waves, but less for $p$ waves. Thus the total reflected $s$ wave is $\pi$ radians out of phase with the incident wave. For angles of incidence greater than the polarizing angle the reflected $p$ wave however is in phase [2] and $\Delta$ is therefore $\pi$. For $n_2<n_{2p}^{-}$, however, the sum of the amplitudes of the waves reflected from the 2,3 interface and transmitted back into medium 1 is greater than the amplitude of the wave reflected from the 1,2 interface for both the $s$ and $p$ components. Thus the reflected $s$ and $p$ waves are both $\pi$ radians out of phase with the incident wave and $\Delta$ is zero.

It is now easy to reconstruct the behavior of the reflection coefficient ratio for all values of $n_2$ between $n_1$ and $n_3$. For values of $n_2$ slightly less than $n_1$, such as the $n_2=1.60$ curve in figure 3, the $\rho$ curve lies entirely to the right of the bare-surface point. In this

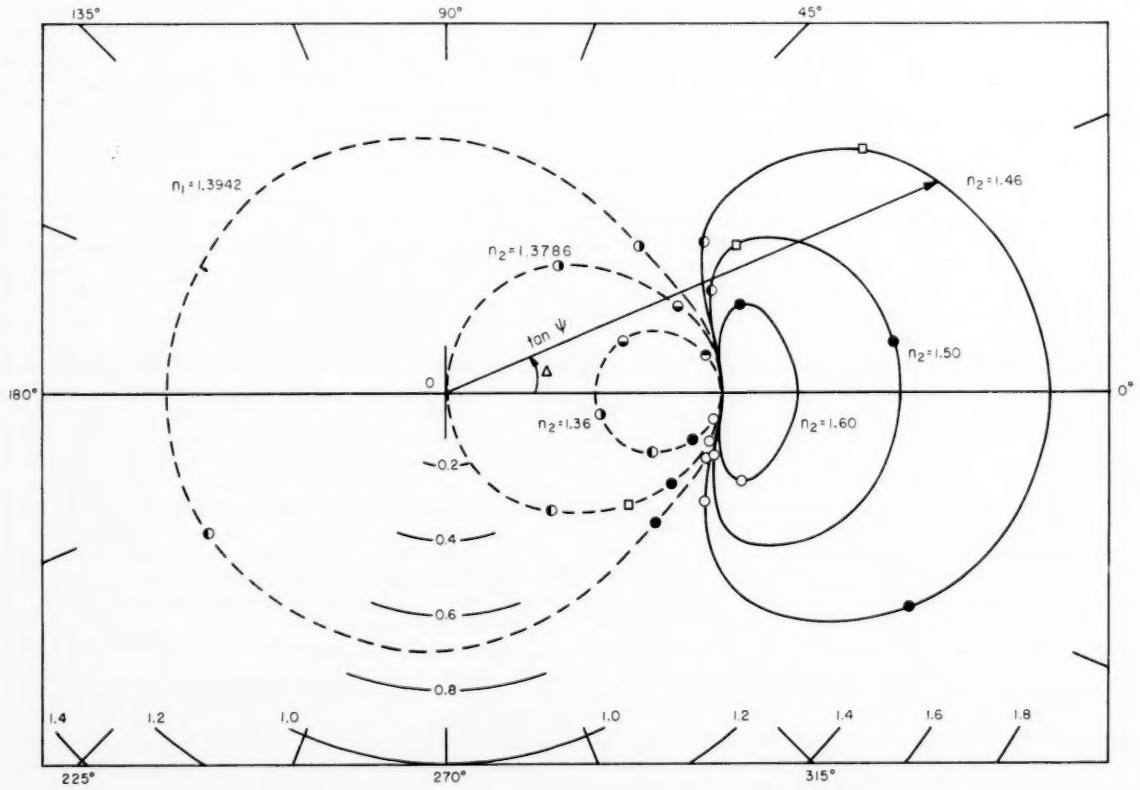


FIGURE 3. *Case 1. Polar plot of $\rho$ for several values of $n_2$ between $n_1$ and $n_3$.*

The three curves drawn with dashed lines represent values of $n_2$ equal to and near $n_{2p}^{-}$. (See text.) The three curves drawn with solid lines represent values of $n_2$ between $n_{2p}^{-}$ and $n_3$. The symbols on the curves correspond to film thicknesses.

○, 1000 Å ●, 2000Å □, 2500Å ◐, 3000Å ◑, 4000 Å ◒, 5000Å ◓, 7000Å

region tan $\psi$ oscillates between a minimum value for the bare surface and a maximum value at the quarter-wave thickness (at which $\Delta=0$) and $\Delta$ in turn oscillates between two values, $\Delta_{max}$ and $\Delta_{min}$. As the refractive index decreases, the maximum value of tan $\psi$ increases, as do $\Delta_{max}$ and $\Delta_{min}$. (fig. 3, $n_2=1.50$ and $n_2=1.46$), approaching infinity and $\pm\pi/2$, respectively as $n_2$ approaches $n_{2s}$ (fig. 2, $n_2=1.416$). For values of $n_2$ less than $n_{2s}$ but greater than $n_{2p}^-$, $\Delta$ takes on all values between zero and $2\pi$, but the maximum value of tan $\psi$ (occurring when $\Delta=\pi$) decreases as $n_2$ becomes progressively lower (fig. 2, $n_2=1.41485$ and fig. 3, $n_2=1.3942$). At some refractive index (equal to 1.3942 in the present case) between $n_{2p}^-$ and $n_{2s}$ the value of tan $\psi$ for $\Delta=\pi$ is equal to the value for the bare surface. As $n_2$ decreases from this value, the value of tan $\psi$ when $\Delta=\pi$ is now less than the value for tbe bare surface, and approaches zero as $n_2$ approaches $n_{2p}^-$. At this point $\Delta$ begins to oscillate between a maximum and minimum value, which are $\pi/2$ for $n_2=n_{2p}^-$. Finally, for $n_2$ between $n_{2p}^-$ and $n_3$ curves such as those for $n_2=1.36$ in figure 3 are obtained, becoming smaller and smaller as $n_2$ approaches $n_3$.

It will be clear that the $\rho$ curves completely cover the plane, those with $n_2>n_{2s}$ covering the half plane to the right of the bare-surface point and those with $n_2<n_{2s}$ covering the half plane to the left of the bare-surface point. Thus every conceivable state of polarization of the reflected light is possible when the incident light is linearly polarized at an azimuth of 45 deg. Linearly polarized light at all possible azimuths is represented by the intercepts on the horizontal axis, and this occurs for the quarter-wave thickness. Circularly polarized light is obtained for that refractive index and thickness for which tan $\psi=1$ and $\Delta=\pm\pi/2$, and so forth. The efficacy of any of these conditions must, however, be determined by calculations such as those carried out for the special cases $n_{2s}$ and $n_{2p}^-$.

The curves of figure 2 and 3, while illustrating the dependence of $\rho$ upon thickness, do not show clearly the dependence of tan $\psi$ and $\Delta$ on thickness. In figure 4 we show how tan $\psi$ varies with $d$ for several values of $n_2$. All these curves are periodic in $2n_2d\cos\theta_2/\lambda$. However, since we have chosen certain critical values of $n_2$, the curves are not as symmetric as those previously described [2]. The values of $n_2$ chosen are as follows: two (1.41485 and 1.41600) close to $n_{2s}$, one (1.3786) at $n_{2p}^-$, one at the value of $n_2$ (1.3942) for which tan $\psi$ at $\Delta=\pi$ is equal to tan $\psi$ for the bare surface, and one value of $n_2$ (1.50) greater than $n_{2s}$. Considering first the case where $n_2=n_{2p}^-$, it will be seen that at $d=3500$ Å, tan $\psi=0$, and hence the reflected light is polarized with the electric vector in the plane of the surface. Similarly, for $n_2$ values slightly lower and slightly higher than $n_{2s}$ (1.41485 and 1.41600, respectively) tan $\psi$ becomes extremely large when the thickness is the quarter-wave thickness. Since the sensitivity (which may be defined as the change of $\psi$ with thickness [3,15]) is the slope of these curves, it will be recognized that $n_2$ values near $n_{2s}$ and thickness values around the quarter-wave thickness give the highest sensitivity. Moreover, the curves for $n_2=1.3786$ and 1.41485 and 1.41600 again show the difficulty of constructing a polarizer using films of these critical refractive indexes; the change of tan $\psi$ with thickness near the proper thickness is almost discontinuous, so that to make a worthwhile polarizer using these effects would be very difficult indeed.

In figure 4 we have also shown the curve for the value of $n_2$ for which tan $\psi$ has the least variation with thickness, with the exception of values of $n_2$ very close to $n_1$ or $n_3$. This is the value of 1.3942, and for this value, tan $\psi$ when $\Delta=\pi$ (the quarter-wave thickness) is equal to the value of tan $\psi$ for the bare surface. As can be seen from figure 3 this $\rho$ curve is almost circular and centered at the origin. The total variation in tan $\psi$ is from 0.743 to 0.650, or, in degrees, from 36.66 to 33.0; this change of 3.7 deg is to be compared with the change of 45 deg obtained for $n_2=n_{2s}$ or $n_2=n_{2p}^-$.

In figures 5 and 6 we illustrate the behavior of $\Delta$ with thickness for the same values of $n_2$ shown in figure 4. For $n_2>n_{2s}$ or $n_2<n_{2p}^-$, $\Delta$ oscillates between two values. This behavior is typified by the curve for $n_2=1.50$ (which is, however, somewhat more asymmetric than previously shown curves) and has been illustrated many times [2]. As $n_2$ approaches $n_{2s}$ from above or $n_{2p}^-$ from below, the curve of $\Delta$ versus thickness becomes more and more asymmetric, finally approaching a discontinuous curve where $n_2=n_{2p}^-$ or $n_{2s}$. This is illustrated by the curves for $n_2=1.3786$ and 1.41600 in figure 5. In these curves as the "half-wave" thickness is passed, $\Delta$ suffers a very sharp change from $-\pi/2$ to $\pi/2$, and since $\psi$ under these conditions is close to either zero or $\pi/2$, the ellipse which represents the polarization of the reflected light goes very rapidly from a very thin ellipse with one sense of rotation to a similar ellipse with the opposite sense of rotation.

The behavior is decidedly different for $n_{2p}^-<n_2<n_{2s}$. Under these conditions $\Delta$ takes on all values from $2\pi$ to 0. This is illustrated in figure 6 for the refractive indices 1.41485 and 1.3942. The value of 1.41485 is slightly less than $n_{2s}$, and the curve of $\Delta$ versus thickness for this value is to be compared with than for $n_2=1.41600$ in figure 5. In the present case, $\Delta$ starts from $2\pi$, approaches $3\pi/2$ as the thickness approaches the quarter-wave value, but then drops almost discontinuously to $\pi/2$ as the thickness becomes greater than the quarter-wave value. The curve for $n_2=1.3942$ illustrates the behavior for intermediate values of $n_2$ between $n_{2p}^-$ and $n_{2s}$. As $n_2$ approaches $n_{2p}^-$, again the curve of $\Delta$ versus thickness becomes more and more asymmetric, approaching a discontinuous curve as $n_2$ approaches $n_{2p}^-$.

We have finally to discuss the intensity of the reflected light for these various situations. This is shown in figure 7 as a function of thickness for the same refractive indexes used for figures 2 to 6. The reflectivity shown here is calculated for "ellipsometric" conditions, i.e., the incident light is linearly polarized at an azimuth of 45 deg to the plane of incidence, and is given by $(r_p^2+r_s^2)/2$. Starting from

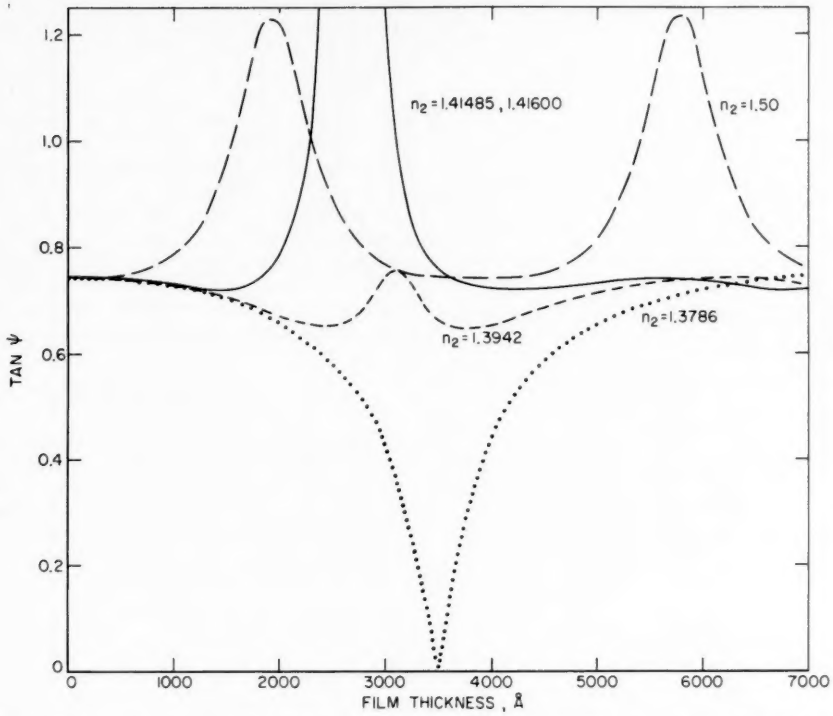


FIGURE 4. *Case 1. Dependence of tan ψ on film thickness for several values of* $n_2$ *shown in figures 2 and 3.*

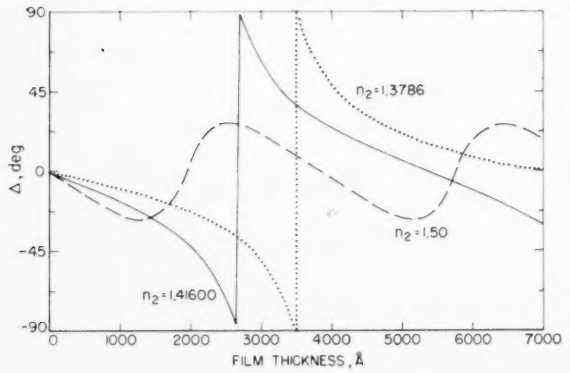


FIGURE 5. *Case 1. Dependence of* $\Delta$ *on film thickness for the three values of* $n_2$ *shown in figure 4 for which* $n_2 \geq n_{2s}$ *or* $n_2 \leq n_{2p}^-$.

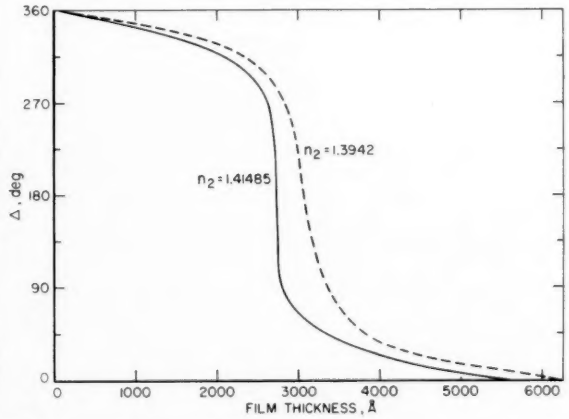


FIGURE 6. *Case 1. Dependence of* $\Delta$ *on film thickness for the two values of* $n_2$ *shown in figure 4 for which* $n_{2p}^- < n_2 < n_{2s}$.

a bare-surface value of 41 percent, the reflectivity drops to a minimum value at the quarter-wave thickness. For $n_2$ close to $n_{2s}$ or $n_{2p}$ this minimum value is very low indeed, being of the order of 2 to 3 percent. With the present values of refractive index for $n_1$ and $n_3$, production of polarized light by such dielectric films would be an inefficient process. More propitious values of $n_1$ and $n_3$ do, however, give higher reflectivity, at least for $n_{2p}^+$ [12]. Increasing the angle of incidence to 46.60 deg (only 0.08 deg less than $\theta_c^{1,3}$) gave $n_{2s}=1.3679$, increased the bare-surface reflectivity to 72.8 percent, but increased the minimum reflectivity to only 3.3 percent. Nevertheless, for films less than about 1000 Å the reflectivity for an angle of incidence of 46.00 deg is 30 percent or greater, and hence the intensity of reflected light is sufficient for experimental measurements under these conditions.

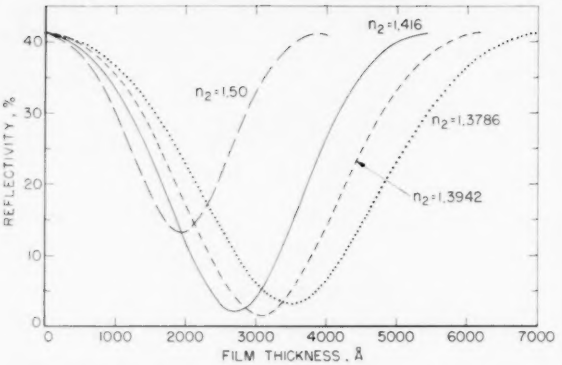


FIGURE 7. *Case 1. Dependence of reflectivity on film thickness for several values of* $n_2$ *shown in figures 2 to 6.*

The reflectivities are calculated for incident light at 45 deg azimuth with respect to the plane of incidence.

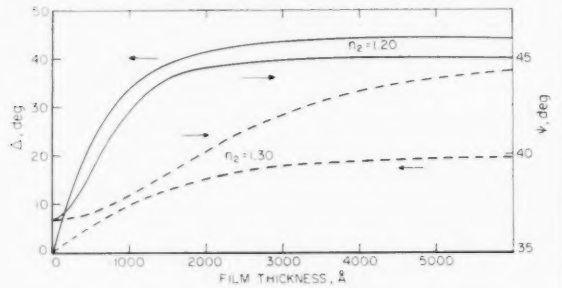


FIGURE 8. *Case 2. Frustrated total reflection.*

Variation of Δ and ψ with film thickness.

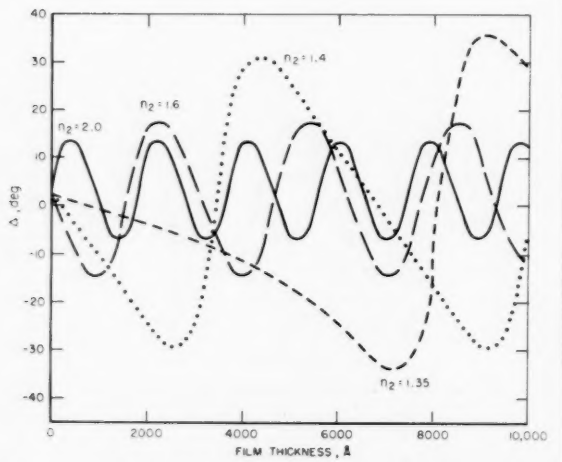


FIGURE 9. *Case 3. Dependence of* Δ *on film thickness for several values of* $n_2$, *including the condition* $n_2 > n_1$.

## 5. Case 2, $\theta_c^{1,3} > \theta_i > \theta_c^{1,2}$

This case is known as "Frustrated Total Reflection" and has already been extensively treated [16]. For this case $n_2$ must be less than $n_3$, and Δ and ψ are shown in figure 8 as a function of film thickness for the two values of $n_2$ given in table 1. For large film thicknesses tan ψ must approach unity, and Δ approaches some value determined by the angle of incidence and the refractive indexes in question. For $n_2$=1.20 this value of Δ is 44 deg, while for $n_2$=1.30 it is 19.5 deg for this angle of incidence (46.0 deg). For very thin films whose refractive index is such as to make the present conditions apply, it is possible to measure thickness and refractive index by a single measurement of Δ and ψ. For the present conditions the minimum reflectivity (occurring when the films are of zero thickness) is 41 percent, and this rises as the film increases in thickness.

## 6. Case 3, $\theta_c^{1,3} < \theta_i < \theta_c^{1,2}$

For this case $n_2 > n_3$, and tan ψ is always unity. The reflectivity is therefore always 100 percent. However, the only experimental parameter which varies is Δ, and this permits only the evaluation of $n_2$ or $d$, but not both; one must be known from other considerations. The behavior of Δ with film thickness is shown in figure 9 for several values of $n_2$. As in case 1, Δ oscillates between maximum and minimum values with a periodicity of $(2\, n_2 d \cos\theta)/\lambda$. However, since tan ψ is always unity none of the interesting polarization effects that occurred in case 1 occur here. As is evident from figure 9, Δ is more sensitive to thickness for those refractive indexes which make $\theta_c^{1,2}$ close to the angle of incidence. The curves of Δ against thickness for these refractive indexes (1.40 and 1.35 in fig. 9) are asymmetric as were the curves in figure 5. We have calculated for this case the behavior of Δ with film thickness for one value of $n_2 > n_1 (n_2 = 2.0)$, and except for the fact that the "phase" of this curve is different from those with $n_2 < n_1$, the behavior is very similar.

## 7. Case 4, $\theta_c^{1,3} < \theta_i > \theta_c^{1,2}$

This is the case which is easiest to achieve in practice [10], for all that it necessitates is that $\theta_i$ be sufficiently high. As in case 3 only Δ varies with film thickness and thus from a single determination of ψ and Δ only the refractive index or thickness of the film may be determined; one must be known from other considerations. Figure 10 shows the result of computations of Δ as a function of film thickness for the three cases shown in table 1. As expected, the curves level off and show none of the periodicity present in cases 1 and 3. It is to be noticed that Δ rises with film thickness for $n_2 < n_3$ and falls for $n_2 > n_3$. Thus it is not strictly correct to say that only thickness or refractive index can be determined; by comparing the value of Δ for the film-covered surface with that for the bare surface one can determine whether the film has a refractive index which is greater or less than the refractive index of the medium 3. Beyond this one cannot in general say from a single measurement.

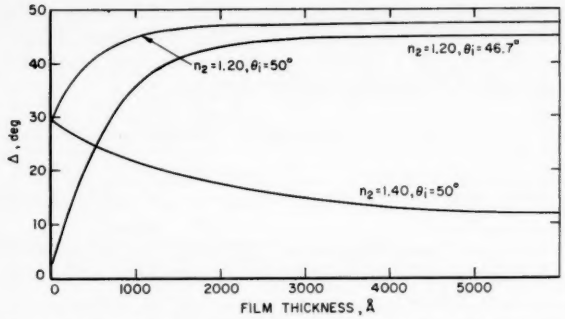


FIGURE 10. *Case 4. Dependence of* $\Delta$ *on film thickness for* $n_2<n_3$ *and* $n_2>n_3$.

## 8. Sensitivity

We have spoken of the desirability in cases 1 and 2 of using an angle of incidence near $\theta^{1,3}_c$ in order to increase reflectivity. There are other criteria, however, which influence the choice of angle of incidence. In case 3 and case 4, in particular, where total reflection occurs, there is the question of experimental sensitivity. This may be defined as the change in $\Delta$ for a given change in film thickness [3, 15], and, for very thin films, a determination of this quantity as a function of angle of incidence leads to an unequivocal result. In figure 11 we show the change in $\Delta$ for a 100 Å film as a function of angle of incidence for $n_2$ values of 1.20, 1.40, and 1.60. Two of the curves span cases 1, 3, and 4, and one spans cases 2 and 4. For each of the curves it is seen that the sensitivity rises as the angle of incidence is lowered. Without considerations of intensity one would conclude that the lowest angle of incidence should be used. However, with an angle of incidence less than $\theta^{1,3}_c$ the conditions are those of case 1 or 2, and reflectivity falls off very rapidly as the angle of incidence is lowered. (The minimum angle of 44° in this graph was chosen to give a reflectivity of about 17 percent for zero film thickness.) Balancing reflectivity against sensitivity one is led to the conclusion that it is always best to work as close to $\theta^{1,3}_c$ as possible. If $\theta_i$ is slightly less than $\theta^{1,3}_c$ then, for thin films such as these, one has the added advantage of having $\psi$ also vary with film thickness. When $n_2>n_3$, choosing $\theta_i$ slightly above $\theta^{1,3}_c$ gives optimum sensitivity and complete reflectivity, although only $\Delta$ varies. While it is not our purpose to pursue the effect of $n_2$ on sensitivity, it will be clear that sensitivity will be zero for $n_2$ equal to $n_1$ or $n_3$, be a maximum for some value of $n_2$ between $n_1$ and $n_3$, and again increase for $n_2>n_1$ or $n_2<n_3$. This is the reason that the curves for $n_2$ of 1.20 and 1.60 in figure 11 are higher than the curve for an $n_2$ of 1.40.

## 9. Appendix

It will be shown that for reflection from a film covered surface either $r^p$ or $r^s$ may be zero, and hence tan $\psi$ may be either zero or infinity.

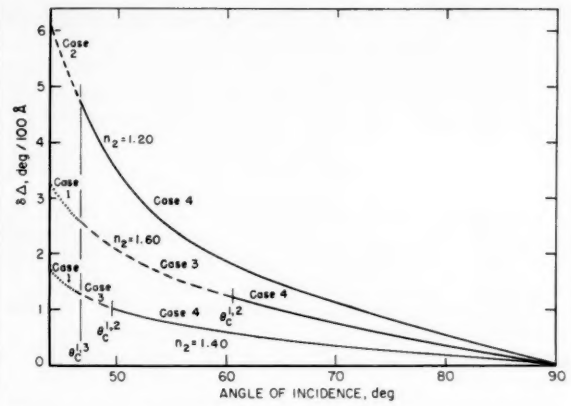


FIGURE 11. *Sensitivity in* $\Delta$ *as a function of* $\theta_i$ *for three values of* $n_2$.

Each of the curves spans at least two cases. Solid line: case 4; — — case 3; - - - case 2; . . . case 1.

The reflection coefficient $r^\nu$, where $\nu$ represents either $s$ or $p$ is given by

$$r^\nu=\frac{r^\nu_{12}+r^\nu_{23}\exp D}{1+r^\nu_{12}r^\nu_{23}\exp D} \tag{A1}$$

where the terms have the same meaning as in eq (2). In order for this reflection coefficient to vanish, two conditions must be met:

$$D=-i\pi;\ \frac{2n_2d\cos\theta_2}{\lambda}=\frac{k}{2} \tag{A2}$$

$$r^\nu_{12}=r^\nu_{23} \tag{A3}$$

where $k$ is an odd integer. For these conditions satisfied and $\nu=p$, $\tan\psi=0$; for $\nu=s$, $\tan\psi$ is infinite. The first state has been studied already [11, 12] but we shall be interested in more detail. We shall discuss each of the two states in turn.

*State 1— vanishing of component with electric vector in plane of incidence*

For this state, $\nu=p$, and the Fresnel coefficients are given by

$$r^p_{ij}=\frac{n_j\cos\theta_i-n_i\cos\theta_j}{n_j\cos\theta_i+n_i\cos\theta_j} \tag{A4}$$

where $\theta_j$ is the angle between the normal to the $i, j$ interface and the ray in medium $j$. Substituting this expression into eq (A3) and simplifying leads to the following equation for $n_{2p}$, the critical value of $n_2$ necessary to make the $p$ component vanish:

$$n^2_{2p}=\frac{1}{2}\frac{n_1n_3}{\cos\theta_1\cos\theta_3}\left[1\pm(1-\sin 2\theta_1\sin 2\theta_3)^{1/2}\right] \tag{A5}$$

This equation has already been derived by Schröder [12] in slightly different form. There are two solu-

tions, which we call $n_{2p}^+$ and $n_{2p}^-$, and we shall investigate certain of their properties.

The critical value $n_{2p}$ is symmetrically dependent upon $n_1$, $n_3$, $\theta_1$, and $\theta_3$. At normal incidence, ($\theta_1=0$, $\theta_3=0$), we obtain the well-known solution [11]

$$n_{2p}^+=(n_1n_3)^{1/2} \tag{A6}$$

for the positive solution, and $n_{2p}^-=0$ for the negative solution. The latter is, of course, inadmissible. For $n_1<n_3$, $\theta_1$ may take values up to $\pi/2$, and as $\theta_1$ approaches $\pi/2$, $n_{2p}^+$ increases without bound. For $n_1>n_3$, $\theta_3$ approaches $\pi/2$ as $\theta_1$ approaches $\theta_c^{1,3}$, the critical angle for total internal reflection, and $n_{2p}^+$ increases without limit as $\theta_1$ approaches $\theta_c^{1,3}$. It may be shown [12] that the behavior of $n_{2p}^+$ as a function of $\theta_1$ is monotonic. Hence, for the positive solution

$$n_{2p}^+\geq(n_1n_3)^{1/2} \tag{A7}$$

the equality sign holding at normal incidence.

For the parameters studied here, i.e., $\theta_1=46°$, $n_1=1.8376$, $n_3=1.337$, $n_{2p}^+=4.654$. For this value of $n_{2p}^+$, $d_o$ is calculated from eq (A1) as 304 Å for $\lambda=5461$ Å.

For the negative solution, $n_{2p}^-=0$ at normal incidence, and becomes $(n_1n_3\sin\theta_3)^{1/2}$ at grazing incidence. The value of $n_{2p}^-$ is always less than $(n_1n_3)^{1/2}$, which in many cases of interest is too low to be realized experimentally. For the present case, at an angle $\theta_1$ of 46°, $n_1=1.8376$ and $n_3=1.337$, $n_{2p}^-=1.3786$, which is easily attainable. For this refractive index, the critical thickness is 3490 Å for $\lambda=5461$ Å, and $r^s=0.25$.

It is of interest to calculate the value of $\theta_i$ for which $n_{2p}^-$ is unity. This, of course, represents the minimum angle of incidence for a given $n_1$ and $n_3$ for which the value of $n_{2p}^-$ is admissible. A certain amount of algebraic manipulation gives

$$\sin^2\theta_1=\frac{n_3^2+n_1^2-2n_1^4n_3^4}{2n_1^2[1-n_1^4n_3^4]}-\frac{[(n_3^2-n_1^2)^2+4n_1^4n_3^4(n_1^2-1)(n_3^2-1)]^{1/2}}{2n_1^2[1-n_1^4n_3^4]}. \tag{A8}$$

Except for the presence of the term $n_1^2$ in the denominator this expression is symmetrical in $n_1$ and $n_3$. Angles of incidence less than the value given by this equation cannot produce linearly polarized light with the electric vector normal to the plane of incidence for the negative solution to eq (A5).

*State 2—vanishing of component with electric vector normal to plane of incidence*

Although mentioned by Schröder [12], this case does not appear to have been studied. Indeed, it has been considered impossible [11]. For this case the Fresnel coefficient is

$$r_{ij}^s=\frac{n_i\cos\theta_i-n_j\cos\theta_j}{n_i\cos\theta_i+n_j\cos\theta_j}. \tag{A9}$$

Substituting this in eq (A3) leads to the following equation for the critical value of $n_2$ for the reflected light to be polarized entirely with its electric vector in the plane of incidence ($n_{2s}$):

$$n_{2s}^2=n_1n_3\cos\theta_1\cos\theta_3+n_1^2\sin^2\theta_1. \tag{A10}$$

In this case there is only one value of $n_{2s}$ which is admissible. At normal incidence we again obtain $n_{2s}=(n_1n_3)^{1/2}$.

Not all combinations of $n_1$, $n_2$, and $n_3$ are possible in this case. To show this we recast eq (A9) into the following form

$$\frac{n_2^2}{n_1^2}=\sin^2\theta_1\left[\frac{1}{\tan\theta_1\tan\theta_3}+1\right]. \tag{A11}$$

Now, if $n_2>n_1$, then

$$\sin^2\theta_1\left[\frac{1}{\tan\theta_1\tan\theta_3}+1\right]>1$$

or

$$\tan\theta_3<\tan\theta_1 \tag{A12}$$

and hence $n_3>n_1$.

A similar calculation for $n_2<n_1$ leads to the condition $n_3<n_1$. An obvious way to satisfy these conditions is for $n_1$, $n_2$, and $n_3$ either to increase or decrease in order. For the case of $n_1=1.337$, $n_3=1.8376$, $\theta_1=46°$ (which is the *opposite* of the direction of propagation treated in the text), direct computation gives $n_2=1.543$ and $d_2=1130$ for $\lambda=5461$. For these values the reflected light is polarized entirely with its electric vector in the plane of incidence. The value of $r^p$ is, however, only 0.032. For the opposite direction of propagation ($n_1=1.8376$, $n_3=1.337$) $n_2=1.41542$.

## 10. References


[1] P. Drude, Ann. Physik. **272,** 532 (1889); ibid **272,** 865 (1889); ibid **275,** 481 (1890).
[2] A. B. Winterbottom, Optical studies of metal surfaces, The Royal Norwegian Scientific Society Report No. 1, 1955 (F. Bruns, Trondheim, Norway).
[3] F. L. McCrackin, E. Passaglia, R. R. Stromberg, and H. L. Steinberg, J. Res. NBS **67A** (Phys. and Chem.), No. 4, 363 (1963).
[4] For a State of the Art, see papers in Ellipsometry in the measurement of surfaces and thin films (Symposium Proceedings), edited by E. Passaglia, R. R. Stromberg, and J. Kruger, NBS Misc. Publ. No. 256 (1964).
[5] F. L. McCrackin and J. P. Colson, ibid, p. 61.
[6] N. J. Harrick, Ann. N. Y. Acad. Sci. **101** Art. 3, 928 (Jan. 1963); J. Phys. Chem. **64,** 1110 (1960).
[7] J. Fahrenfort, Spectrochim. Acta. **17,** 698 (1961).
[8] R. R. Stromberg, E. Passaglia, and D. J. Tutas, J. Res. NBS **67A** (Phys. and Chem.), No. 5, 431 (1963).
[9] F. L. McCrackin and J. Colson, NBS Tech. Note 242 (1964).
[10] D. J. Tutas, R. R. Stromberg, and E. Passaglia, Soc. Plastics Eng. Trans. **4,** 256 (1964).
[11] M. Born and E. Wolf, Principles of Optics, p. 60 (Pergamon Press, New York, N. Y., 1959).
[12] H. Schröder, Optik. **3,** 499 (1948).
[13] R. E. Hartman, J. Opt. Soc. Am. **44,** 192 (1954).
[14] R. D. Mattuck, J. Opt. Soc. Am. **46,** 615 (1956).
[15] R. C. Smith and M. Hacksaylo, see reference 4, p. 83.
[16] T. R. Young and J. M. Fath, see reference 4, p. 349.


(Paper 68A6–307)

JOURNAL OF RESEARCH of the National Bureau of Standards—A. Physics and Chemistry
Vol. 68A, No. 6, November–December 1964

# On the Second-Order Transition of a Rubber

**E. A. DiMarzio***

(July 13, 1964)

The view that the glass transition has a thermodynamic basis is extended to a cross-linked rubber. The elevation of the second-order transition temperature as a function of the number of cross-links is found to be $(T(X)-T(0))/T(0)=KX/1-KX$, where $T(X)$ is the transition temperature for a rubber with degree of cross-linking $X$. The constant $K$ is to first order independent of material. Also a relation involving no adjustable parameter is derived for the ratio of second-order transition temperatures to deformation. It is $T(\lambda)/T(1)=\exp(G(\Sigma\lambda_i^2-3)/2\Delta C_p T_0)$ where $\Delta C_p$ is the value of the specific heat discontinuity per cm³ at the transition and $T_0$ is the temperature at which the modulus $G$ is measured. Available experimental evidence from five separate investigations agrees with these predictions.

## 1. Introduction

All noncrystalline polymers display what at first sight appears to be a second-order transition in the Ehrenfest sense [1]: [1] the temperature and pressure derivatives of both volume and entropy are discontinuous along a line $T(P)$ although the volume and entropy themselves are continuous.

Many believe that this transition is basically a kinetic phenomenon because: (1) the location of the transition can be changed by changing the time scale of the experiment, faster measurements resulting in higher glass temperature, and (2) the measured relaxation times near the transition approach the time scale of the experiment. At temperatures below $T_g$ the relaxation time for certain molecular motions is larger than the time of observation and therefore there is a kinetic "freezing in" of the associated degrees of freedom.

Nonetheless we can state that these glass forming materials have equilibrium properties and ask what they are. One can answer this question experimentally by extrapolating the high temperature behavior of volume and entropy through the glass region. One finds that volumes and entropies smaller than the crystalline values are obtained at finite temperatures [2]. This unacceptable result can be avoided only if the curves level off before they cross the corresponding curves for the crystalline material. This behavior must be postulated even for infinite time scale experiments.

One can also ask what the theoretical predictions of equilibrium properties are. This question has been answered [3, 4] by means of a modified form of the Flory-Huggins lattice model which allows semiflexible chains to stiffen as the temperature is lowered [5]. This theory predicts a second-order transition at the finite temperature point at which the configurational entropy first becomes zero as the temperature of the system is lowered. The theory thus implies that packing difficulties cause the transition [3, 4]. This same lattice model also predicts correctly the existence and behavior of the various kinds of liquid crystals [6]. For these materials also, the extreme difficulty of packing in random arrangement causes the transition behavior [6, 7, 8]. The correct predictions in this case argue for the correctness of the predictions for glasses.

In addition the proposed statistical-mechanical theory correctly predicts the experimental data in those cases to which it has been applied [9]. Specifically, these are the variation of glass temperature with molecular weight and the variation with glass temperature of specific volume [4]. In addition the variation of glass temperature of a copolymer as a function of composition [10], and the variation of glass temperature with diluent [11] have been correctly predicted.

The purpose of this paper is to apply the theory to chemically cross-linked systems (rubbers) and to compare the predictions of the theory with the small amount of available experimental data.

## 2. Relation Between the Transition Temperature and the number of Cross-Links

The criterion of glass formation is that the temperature-dependent configurational entropy become zero. We therefore have for the equation which determines the second-order transition temperature,

$$S_c=S_0+\Delta S_1=0 \tag{1}$$

where $S_0$ is the configurational entropy for an uncross-linked system and $\Delta S_1$ is the change in configurational entropy due to adding cross-links. Now one can immediately see that cross-linking raises the transition temperature because it decreases the configurational entropy over what it would be if there were no added cross-links. A cross-linked polymer on being cooled reaches the $S_c=0$ point at a higher temperature than the corresponding uncross-linked polymer. $S_0$ has been given previously as eq (20) of reference 4. For our purposes we will

*Present address: Polymer Physics Section, National Bureau of Standards, Washington, D.C., 20234; formerly with Bell Telephone Laboratories, Inc., Murray Hill, N.J.

[1] Figures in brackets indicate the literature references at the end of this paper.

use a simplified form obtained when the volume fraction approximation is used with appropriate substitutions from eq (11) and (24).

$$\frac{S_0}{kxN_x}=\ln(1+2e^{-\frac{\Delta\epsilon}{kT}})+f\frac{\Delta\epsilon}{kT}-1+\frac{T\Delta\alpha}{1+2T\Delta\alpha} \tag{2}$$

$$f=2e^{-\frac{\Delta\epsilon}{kT}}/(1+2e^{-\frac{\Delta\epsilon}{kT}}).$$

The left-hand side is the dimensionless entropy per segment, $T$ is the temperature, $\Delta\epsilon$ is the "stiffness energy of the chain," $f$ is the fraction of bonds in upper wells, and $\Delta\alpha(T,P)$ the difference of thermal expansion coefficient for the material above the transition and the value below the transition. Equation 2 is valid for temperatures and pressures resulting in nonnegative values for $S_0/kxN_x$, but the pressure-temperature dependent value of $\Delta\alpha$ must be used. We will discuss actual numerical values of $\Delta\alpha$ later in the paper.

We can easily obtain $\Delta S_1$ by a simple modification of the Flory-Huggins counting scheme. Let us imagine that our system contains but one infinitely long polymer molecule before cross-linking. After cross-linking one can traverse each of the $N_p$ chains between cross-links once and only once by following along the full length of the original molecule. Let us then start at one end of the molecule which we will also assume to be tied to a cross-link and begin the Flory-Huggins counting process. The total number of ways to arrange a chain whose ends are tied down to given cells in the lattice is

$$(\text{F.H.})\left[\frac{b^3}{\pi^{3/2}}\exp(-b^2r^2)d\tau\right],$$

$$b^2=(3/2)/nL^2, \tag{3}$$

where (F.H.) is that value which would obtain if one end were free, and the gaussian form gives the fraction of these conformations which are consistent with the end to end distance $\mathbf{r}$. The quantity $L$ is not the segment length $d$, but is a multiple of it

$$L=cd, \tag{4}$$

and $n$ is the number of these effective lengths.

The element of volume $d\tau$ is necessary because the quantity multiplying it within the brackets is a density. For the time being we restrict the ends to be in a given cell, so that $d\tau$ becomes equal to the volume of a lattice site, $d^3$. For the second chain and each successive chain we have a term identical in form to expression 3. It is evident that after we have laid down the whole molecule we will have for the total number of arrangements consistent with the location of each cross-link to specified cells

$$e^{S_c/k}=e^{S_0/k}\prod_{i=1}^{N_p}\left[\frac{b_i^3}{\pi^{3/2}}\exp(-b_i^2r_i^2)d\tau\right]. \tag{5}$$

In point of fact the junctions are not restricted to particular places on the lattice but can be in any lattice site with probabilities determined by gaussian distributions [12]. For this reason we must assign an effective volume $V(N_p)$ to each of the $N_p/2$ junctions and a corresponding number $V(N_p)/d^3$ of cells which it can occupy. This gives for $\Delta S_1$

$$e^{\Delta S_1/k}=\prod_{i=1}^{N_p}\left[\frac{b_i^3}{\pi^{3/2}}\exp(-b_i^2r_i^2)d\tau\left(\frac{V(N_p)}{d^3}\right)^{1/2}\right]. \tag{6}$$

For the sake of simplicity we will assume that we can replace $n_i$ by $n$, the average number of effective lengths per chain. The effective volume $V(N_p)$ is a quantity whose linear dimensions are proportional to the breadth of the gaussian distribution. According to James and Guth [12] this breadth is proportional to the square root of the average number of effective links between chains. Taking $V(N_p)$ inversely proportional to $b^3$,

$$V(N_p)=A/b^3 \tag{7}$$

and assuming that the chains each have their average mean square lengths, we obtain

$$\frac{\Delta S_1}{k}=-\frac{3}{2}N_p+\frac{3}{4}N_p\ln\left[\left(\frac{d\tau A^{1/2}}{(\pi d)^{3/2}}\right)^{4/3}\Big/\frac{2}{3}nL^2\right]. \tag{8}$$

Using (4) and the fact that the contour length is an invariant, i.e. $(xN_x/N_p)d=nL$, we get [13]

$$\frac{\Delta S_1}{k}=-\frac{3}{2}N_p-\frac{3}{4}N_p\ln c+\frac{3}{4}N_p\ln(A'X) \tag{9}$$

where $X$, the cross-link density, is the number of moles of chains per mole of segments ($X=N_p/xN_x$). Now, $c$ is the same value for all materials at the glass temperature. This is due to the fact that the number of segments in an effective link is a function of the stiffness of the chain, and at their glass temperatures all chains have the same [14] relative stiffness. This value of $c$ is obviously equal to the average number of segments between flexes.

$$c=\frac{1}{f}. \tag{10}$$

The pure number $A'$ has a value which is independent of material since both $d\tau$ and $V(N_p)$ were given in units of $d^3$ which has disappeared from the equation. We therefore have as our eq (11) relating second-order transition temperature to degree of cross-linking [15].

$$\frac{S_c}{kxN_x}=\ln(1+2e^{-\Delta\epsilon/kT})+f\Delta\epsilon/kT-1+\frac{T\Delta\alpha}{1+2T\Delta\alpha}$$

$$-\frac{3}{2}X+\frac{3}{4}X\ln f+\frac{3}{4}X\ln(A'X)=0. \tag{11}$$

The symbol $T$ will be used for glass temperature as well as temperature. No confusion should arise. As it stands eq (11) is presumably valid for all cross-linked polymers. In order to estimate the transition temperature three parameters specific to the material must be known: the number of moles of chains per mole of segments $X$, the stiffness energy $\Delta\epsilon$, and $\Delta\alpha$. As noted above, $A'$ should not depend on material.

Equation 11 includes the effect of pressure, both internal due to cross-links [12], and external. Limiting ourselves to zero external pressure, we can write as an approximation

$$T(X)\Delta\alpha(X)=T(0)\Delta\alpha(0). \tag{12}$$

In words, the glass temperature times $\Delta\alpha$ is a constant independent of amount of cross-linking. Equation (12) is first of all an experimental fact for natural rubber-sulfur vulcanizates [16]. Secondly, even if one were to assume $\Delta\alpha(X)$ a constant then the fourth term of eq (11) would vary with $T$ about ½ as fast as the sum of the first terms, so that even for this extreme case a good first approximation would be to assume $T\Delta\alpha$ constant. Third, it is easy to see from the theory that as $T(X)$ rises due to cross-linking $\Delta\alpha(X)$ must decrease [17]. This phenomenon occurs because of the internal pressure which is built up as the cross-linking density increases. (See eq (3.8), of ref 12.) This sizable internal pressure squeezes out holes (or free volume) and results in a reduction of $\Delta\alpha$. We will therefore assume eq 12 to be true for all rubber systems.

We will approximate the $X$ dependent part of eq 11 by a straight line [15]. In view of the limited amount of experimental data, this is a perfectly adequate approximation, particularly since $X$ (which is the reciprocal of the number of segments per chain) is usually very small in the experiments.

$N_p$ is really equal to the number of effective chains formed when $N_c$ chemical chains are made minus the number of effective chains that exist (due to entanglements) when no chemical chains are made before cross-linking. If one accepts the data of Schaefgen and Flory [18] as typical for all polymers then $N_p=N_c$ to good approximation.

The net results of these developments is that we can replace eq (11) by a simpler relation of wide validity.

$$\ln(1+2e^{-\Delta\epsilon/kT})+f\frac{\Delta\epsilon}{kT}-D+K_1X=0. \tag{13}$$

Here $K_1$ is independent of material and we have absorbed $T(0)\Delta\alpha(0)$ in $D$. The sum of the first two terms in eq 13 is to good approximation linear in $\Delta\epsilon/kT$. Using this fact one can easily express $\Delta\epsilon/k$ in terms of the glass temperature $T(0)$ of the uncrossed-linked material to get from eq (13)

$$\frac{T(X)-T(0)}{T(0)}=\frac{K_2X}{1-K_2X} \tag{14}$$

where $K_2$ is a pure number whose value is to first order independent of material.

There exists in the literature experimental data for variation of glass temperature as a function of number of cross-links for three polymer systems. They are: natural rubber [19], styrene-divinyl benzene copolymers [20, 21] (P.S.), and methyl methacrylate-ethylene glycol dimethacrylate copolymers [22] (P.M.M.). Since the experimental data are given in terms of number of cross-links per gram, we rewrite eq (14) as

$$\frac{T(\chi)-T(0)}{T(0)}=\frac{KM\chi/\gamma}{1-KM\chi/\gamma} \tag{14a}$$

where $\chi$ is the number of cross-links per gram, $M$ is the molecular weight of a residue, and $\gamma$ is the number of flexible bonds (basic units) per residue. Of course $K$ is again independent of material. Perhaps $\gamma$ needs careful definition. It is defined as the number of rotatable bonds per residue which on rotating result in a change in the shape of the molecule. These flexible bonds can occur on side groups as well as in the backbone of the chain. Thus in polymethylmethacrylate $\gamma=4$ and $M/\gamma=25$. For natural rubber $\gamma$ is 3 since the repeat unit carries a double bond and $M/\gamma=22.7$. For polystyrene one can at first sight choose $\gamma$ equal to either 3 or 2 depending on whether or not rotation of the side group is held to cause a change in shape. Since steric hindrances exist it is reasonable to suppose there are two minima 180° apart and that therefore $\gamma=2$, with $M/\gamma=52$. Also, this value agrees with the value for the basic chain unit of Wunderlich [23]. Using these values and the experimental values of $T$ and $\chi$ from references [19–22] we get for values of $K$,

*Evaluation of the constant K*

| | |
|---|---|
| Natural rubber | $K=1.30\times10^{-23}$ |
| P.S. rubber | $K=1.20\times10^{-23}$ |
| P.M.M. rubber | $K=1.38\times10^{-23}$ |

These numbers agree remarkably well with each other and lend support to the contention that $K$ is independent of material.

On the basis of the assumption that all of the cross-linking agent actually cross-links, a linear relation rather than 14a was obtained by others [20, 22]. However, it is reasonable to suppose that at high density some cross-linking sites become immobilized in regions where there are no other such sites. It seems more reasonable to assume, in accordance with theory, that the modulus is proportional to $\chi$ and then evaluate the constant of proportionality by the chemical means at low cross-link density.

Now Martin and Mandelkern [16] have made a careful study of unaccelerated natural rubber-sulfur vulcanizates, and have measured the glass temperature as a function of bound sulfur content. In order for us to make a comparison we must know the relation between number of cross-links and percent

bound sulfur. Gee [24] has made measurements which lead to the relation

$$\frac{10^4}{M_c}=0.2s \tag{15}$$

where $s$ is percent bound sulfur and $M_c$ is molecular weight between cross-links, but his experiments extend only to a bound sulfur content of 7 percent. We will assume that this proportionality holds for larger amounts of bound sulfur [25]. In figure (1) we have plotted the data of Martin and Mandelkern and also fit the curve to this data. It is seen that the agreement is good out to a bound sulfur content of 20 percent. The equation used to fit this data was,

$$\frac{T(X)-T(0)}{T(0)}=\frac{0.085\times10^4/M_c}{1-0.085\times10^4/M_c}, \tag{16}$$

where we have made use of eq (15). Thus as a function of the number of cross-links the data varies as per eq (14) if we assume that modulus is proportional to the number of chains.

The molecular weight between cross-links is a very difficult quantity to obtain. For this reason it is advantageous to express our relation in terms of variations of Young's Modulus ($G\alpha TN_p$). We obtain

$$\Delta T=T(X)-T(0)=K_3V_sM\Delta G/\gamma \tag{17}$$

where $\Delta G$ is the difference in unstretched modulus between a cross-linked system and an uncross-linked system at their transition temperatures, $\Delta T$ is the difference between glass temperatures, and $V_s$ is the specific volume. Again, the coefficient $K_3$ should be independent of material.

In our derivation of eqs (17) and (14), we assumed that the cross-link was such that the two paired residues occupied adjacent sites on the lattice. If the cross-linking material were a long chain polymer we would need to count differently. One can see that the resulting equations are identical in form to eqs 17 and 14. All we need do is reinterpret $T(0)$ as the transition temperature of a linear copolymer formed by stringing together all of the chains into one long chain. $T(0)$ now of course varies as $X$ varies. A formula which adequately predicts the glass temperature of high molecular weight copolymers in terms of glass temperatures of the high molecular weight homopolymers has been given previously [10].

## 3. Relation Between the Transition Temperature and the Degree of Strain in a Rubber

The total configurational entropy for a strained rubber is

$$S_T=S_c+\Delta S_e \tag{18}$$

where $S_c$ has been discussed in section 2 and $\Delta S_e$, which is the change in configurational entropy as a function of strain, has been thoroughly and adequately discussed in the literature. Following Treloar [26] we use

$$\Delta S_e=-\tfrac{1}{2}N_pk(\lambda_1^2+\lambda_2^2+\lambda_3^2-3) \tag{19}$$

where $\lambda_i$ are the stretch ratios. We shall assume no volume changes ($\lambda_1\lambda_2\lambda_3=1$). The isovolume assumption seems to be valid for extension ratios not exceeding five [26]. Thus as a practical measure it is a valid approximation for a dry rubber. However, for a swollen rubber this restriction would have to be relaxed and although this can be done it seems unlikely that the experimental consequences can be tested since, even in a dry rubber, measurements of glass temperature as a function of strain are exceedingly difficult.

We will use for $S_c$

$$S_c=\int\frac{\Delta C_p}{T}\,dT \tag{20}$$

which gives the temperature variation of $S_c$. Here $\Delta C_p$ is the total specific heat per cm$^3$ of sample minus the extrapolated value for the glass.

The relation $S_T=0$ yields for the glass temperature $T(\lambda)$, if we assume $\Delta C_p$ to be a constant,

$$T(\lambda)=T(1)\exp\left(\frac{G}{2\Delta C_pT_0}[\lambda_1^2+\lambda_2^2+\lambda_3^2-3]\right) \tag{21}$$

where $G$ is the Modulus measured at temperature $T_0$. This is our end result.

One can ask why eq (20) was not used for $S_0$ in section 2 rather than eq (2). Had we done this we would have obtained

$$T(X)=T(0)\exp\left(-\frac{K'X}{\Delta C_p}\right) \tag{22}$$

instead of eq (14). The first point is that $\Delta C_p$ at the glass temperature is a constant for all materials [27] when expressed per mole of flexible bonds so that both equations are universal relations. The second point is that as a function of temperature $\Delta C_p$ is not a constant but a decreasing function of $T$ [23, 28]. Over a wide range of temperature one would not expect eq (22) to hold since it was derived assuming $\Delta C_p$ constant. Thus our use of eq (2) is more accurate than assuming $\Delta C_p$ a constant. On the other hand if we are working in a small temperature range as is the case for eq [21] one can assume $\Delta C_p$ a constant.

Equation (21) contains no adjustable parameters and therefore provides a good test of the theory. All of the quantities that appear in eq (21) are independently measurable. Unfortunately the amount of data in the literature is meager and difficult to use for our purposes due to improper accounting of time effects.

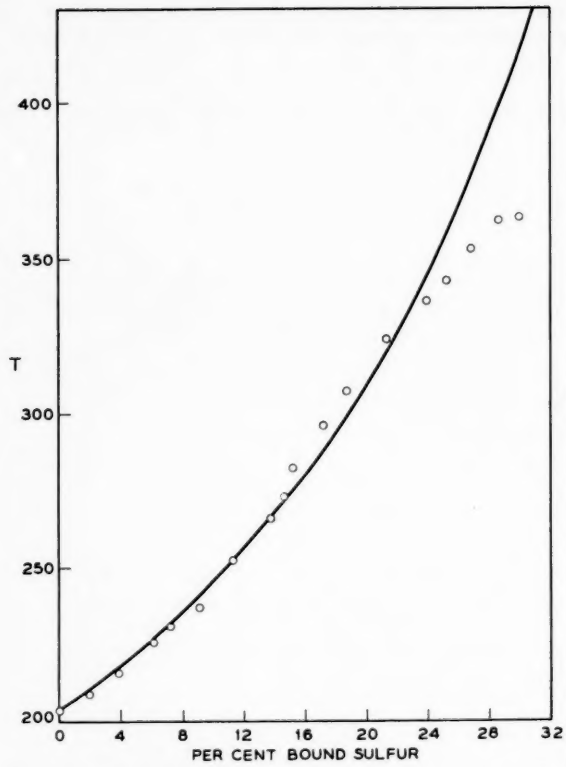


FIGURE 1. *Variation of glass temperature* T *for natural rubber as a function of bound sulfur content.*

The circles are experimental points of Martin and Mandelkern [16] and the line is theoretical.

Because of the nature of the quadratic form in the exponent of eq [21], and of the equation of constraint on the volume any deformation of the rubber from its unstretched state will result in an elevation of the transition temperature. The magnitude of this effect is shown in figure (2) for various values of the quantity $G/2\Delta C_p T_o$ for the case of simple elongation. We have also calculated this quantity for materials used by Gee et al. [29] in some measurements of glass temperature as a function of elongation. The values are 0.0032 for their natural rubber sample, 0.0012 for G.R.S. and 0.0005 for Hycar. The specific heat values were obtained from Wunderlich [23] and the $G$ values were calculated from measurements made on figure (4) of reference (29). The values of $(T(\lambda)-T(0)/T(0)$ measured by Gee are also displayed. In view of the difficulties of the experiment any conclusions must be tentative. It seems however that agreement is satisfactory.

## 4. Discussion

The theory has made two very definite predictions. First, the elevation in transition temperature is proportional to the unstretched Young's Modulus of the rubber, and further the constant of proportionality, $K_3$, is the same for all materials. Second, we have derived a relation with no adjustable parameter between the four independently measurable quantities: glass temperature, modulus, $\Delta C_p$ and $\lambda$. One hopes that more definitive experiments can be carried out in the near future. Further experimental validation of the relations in unison with the previously confirmed predictions would provide strong support for the theory.

However, were an alternative interpretation of the glass transition to predict the same relationships then these equations would carry much less weight. It therefore falls on us to examine the "Critical free volume theory" [30] and the more general "Order parameter theory" [31]. We shall find that the predictions are specific to the "Configurational entropy equals zero" theory.

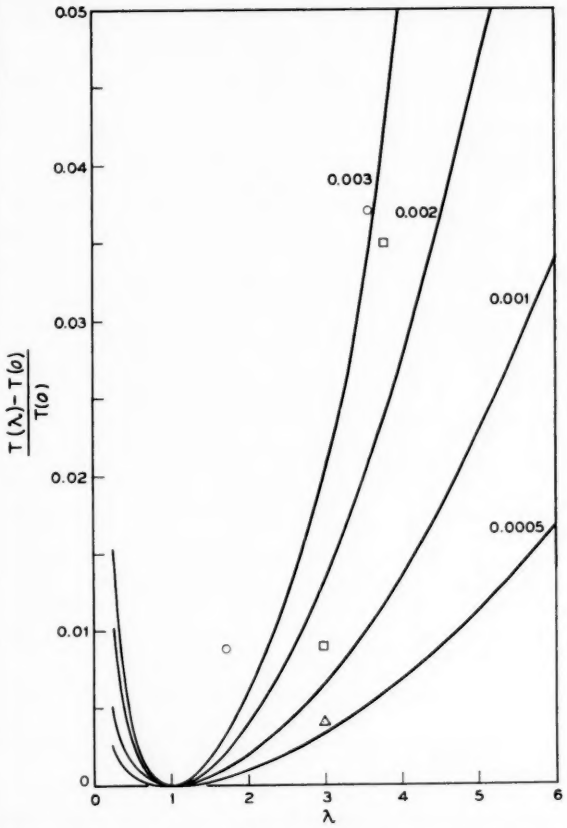


FIGURE 2. *Variation of glass temperature as a function of elongation for various values of* $G/2\Delta C_p T_0 = F$.

○ . . . Experimental points for natural rubber for which $F=0.0032$. □ . . . Experimental points for G.R.S. for which $F=.0.0012$. Δ . . . Experimental point for Hycar for which $F=0.0005$.

### 4.1. Free Volume Theory

If one assumes that the glass forms when the free volume drops to a certain critical value one can

easily derive as an approximation

$$\Delta T=\frac{\Delta\beta}{3\Delta\alpha}\,G \tag{23}$$

where we have used the relation $P=G/3$ of James and Guth [12] and eq (11.42) of reference [30]. Thus while our proportionality constant $K_3$ of eq (17) is to first order independent of material the free volume theory predicts by way of eq (25) a definite first order correlation with compressibility and expansion coefficients. Other free volume approaches are possible [16, 20] which result in equations different from eq (23).

In order to derive a free volume expression for the variation of transition temperature with amount of deformation in a rubber, one has simply to find a relation between free volume and degree of deformation. Since volume changes are to first order zero on stretching a rubber one would expect essentially no change in transition temperature with stretch ratios. In any event one would expect elevation of the transition temperature on compression and depression of transition temperature on elongation to the extent that there are any volume changes. Thus the direction of the effect for the case of simple elongation has opposite sign for the two theories in question.

### 4.2. Order Parameter Theory

The Order Parameter Theory as applied to glasses has been discussed by Davies and Jones [31].

Let us suppose that the Gibbs free energy $G$ of a polymer is dependent not only on $T$ and $P$ but also on an as yet unspecified number of quasi-thermodynamic variables $Z_i$. These variables will, if given enough time, adjust themselves so as to minimize the free energy; i.e.,

$$\frac{\partial G}{\partial Z_i}=0. \tag{24}$$

Thus, at equilibrium one can use eq (24) to eliminate the $Z_i$ in terms of $T$ and $P$ so that *thermodynamic variables are functions only of thermodynamic variables at equilibrium*. For example the entropy is

$$S=-\frac{\partial G}{\partial T}\Big|_p=-\frac{\partial G}{\partial T}\Big|_{p,Z_i}-\sum\frac{\partial G}{\partial Z_i}\frac{\partial Z_i}{\partial T}=S(T,P) \tag{25}$$

One can say that at equilibrium the $Z_i$ are hidden variables.

For nonequilibrium situations eq (24) must be replaced by

$$\frac{\partial G}{\partial Z_i}=\sum\eta_{ij}\dot{Z}_j \tag{26}$$

where the $\eta_{ij}$ are generalized viscosities. Equation (26) assumes small deviations from equilibrium. Now because the $\eta_{ij}$ are temperature dependent there is a range of temperatures for which the $Z_i$ will reach their equilibrium values within the time scale of our experiments, and there is a range of (lower) temperatures for which they will not. Thus, we can say that the $Z_i$ became frozen in at sufficiently small temperatures. If one assumes this transition occurs over a small range of temperatures one has,

$$\Delta S=-\frac{\partial G}{\partial T}\Big|_{p,Z_i}+\frac{\partial G}{\partial T}\Big|_{p,Z_{oi}}=0 \tag{27}$$

at the transition. That is to say, the entropy is continuous across the transition, but since the temperature derivatives are discontinuous we have a kinetically caused second-order transition.

If one uses $\lambda$ instead of $P$ in eq (27) one obtains by implicit differentiation of eq (27) a relation between glass temperatures and strain.

$$\frac{dT}{d\lambda}=-\frac{\dfrac{\partial\Delta S}{\partial\lambda}}{\dfrac{\partial\Delta S}{\partial T}}=\frac{T\dfrac{\partial\Delta f}{\partial T}}{\Delta C_p}. \tag{28}$$

In applying eq (28) all measurements of $f$ must be made from surfaces generated by varying $T$ at constant $\lambda$. Similarly one can think of degree of cross-linking as a thermodynamic variable and obtain,

$$\frac{dT}{dX}=-\frac{T\dfrac{\partial\Delta S}{\partial X}}{\Delta C_p}. \tag{29}$$

Equations (28) and (29) are differential analogs of eqs (14) and (21). They are valid even if the second-order transition has a kinetic basis but they do presuppose that relaxation times are strongly temperature dependent.

These equations do not have the content of eqs (14) and (21) because they do not have a specified form for $\Delta S$. If we assume $\Delta S$ to be total configurational entropy then we do obtain (14) and (21). The above discussion shows that the "configurational entropy equals zero" theory is in some sense a variant of the order parameter theory if $\Delta S$ is itself considered to be an order parameter. For this reason it is proper to point out their differences and similarities.

Both theories assume quasi-thermodynamic variables. In the statistical thermodynamic theory used in this paper the number of empty lattice sites and the fraction of flexed bonds were such variables. At high temperatures both eqs (26) and (24) are applicable to both theories. As we lower the temperature the configurational entropy, $S_c$, becomes zero. At this temperature and for all lower temperatures we have as the equilibrium condition replacing (24),

$$\frac{\partial(G-\mu S_c)}{\partial Z_i}=0, \qquad S_c=0. \tag{30}$$

These equations lead to a second-order transition in the Ehrenfest sense.

Since generalized forces (affinities) are measures of deviations from equilibrium we have in place of eq (26).

$$\frac{\partial(G-\mu S_c)}{\partial Z_i}=\sum \eta_{ij}\dot{Z}_j \qquad (31)$$

Thus the predictions of both theories are the same above the transition and different below. The basis of the transition is thermodynamic in one and kinetic in the other.

It is a conclusion of eq (31) that the temperature derivatives of the $Z_i$ are discontinuous at the transition temperature. Hindsight tells us that this result was not unexpected. After all, for a first-order transition the time dependent quantities show discontinuities as we pass through the transition. In general *the temperature dependence of time dependent quasi-thermodynamic variables shows a discontinuity of the same order as the transition.* We hope to report on some of these aspects at a later date. However, even a cursory examination of the literature shows experimental behavior for relaxation quantities which can be interpreted as showing a change in slope as a function of temperature [32].

---

I thank F. H. Stillinger and W. P. Slichter of the Bell Telephone Laboratories for their constant encouragement and for some helpful suggestions. I also thank E. Passaglia of NBS for helpful criticism of the manuscript.

## 5. References and Notes

[1] P. Ehrenfest, Leiden Comm. Suppl. **756** (1933).
[2] W. Kauzmann, Chem. Revs. **43,** 219 (1948).
[3] J. H. Gibbs, J. Chem. Phys. **25,** 185 (1956).
[4] J. H. Gibbs and E. A. DiMarzio, J. Chem. Phys. **28,** 373 (1958).
[5] P. J. Flory, Proc. Roy. Soc. (London) **A234,** 60 (1956).
[6] E. A. DiMarzio, J. Chem. Phys. **35,** 658 (1961).
[7] L. Onsager, Ann. N.Y. Acad. Sci. **51,** 627 (1949).
[8] P. J. Flory, Proc. Roy. Soc. (London) **A234,** 73 (1956).
[9] In order to compare with experiment it is necessary tentatively to identify the true second-order transition as the actual glass temperature. The possibility that the thermodynamic transition occurs at some constant temperature difference below the observed transition has not been excluded. See, for example, the discussion section of reference [4].
[10] E. A. DiMarzio and J. H. Gibbs, J. Poly. Sci. **40,** 121 (1959).
[11] E. A. DiMarzio and J. H. Gibbs, J. Poly. Sci. **1A,** 1417 (1963).
[12] H. M. James and E. Guth, J. Chem. Phys. **11,** 455 (1943).
[13] Equation (9) is identical in form to eq (15) of a paper by Flory and Rehner, J. Chem. Phys. **11,** 512 (1943). The only difference is in the value for the argument of the logarithm. Our value is $cA'X$, while theirs contain additionally several kinds of localization volumes which occur when one ties together structures formerly free. Thus one could use their equation if one could first explain away the $\Delta\tau$'s. Consider the Flory-Huggins formulas for the configurational entropy of two systems, one of $x$-mers and one of half as many $2x$-mers. Neither of these formulas contain a $\Delta\tau$, yet if we were to calculate the entropy of the $2x$-mers by pairing the $x$-mers we would have introduced a term $N_{2x}\ln(\Delta\tau)$ in our expression for the entropy. Thus it becomes clear that the $\Delta\tau$ is nothing more than a measure of the cell size and that when we use a *lattice model* for our calculation of the configurational entropy of a rubber the $\Delta\tau$ should not appear.
[14] Chain stiffness is the main determinant of the transition. Intermolecular energies have as an effect which is normally small. The quantitative statement is obtained by equating the right hand side of eq 2 to zero.
[15] Were we to have used a "linear" model in which the number of junctions equaled the number of chains the $X$ dependent part of eq (11) would be strictly linear.
[16] G. M. Martin and L. Mandelkern, J. Res. NBS **62,** 141 (1959) RP2944.
[17] The quantitative predictions are made by consideration of eq (11) and a simple extension of eq (11) of reference [4] with its resulting expression for $\Delta\alpha$ analogous to eq (24) of reference [4]. These equations plus the equation of James and Guth (eq (3.8) of ref. 12) relating internal pressure to degree of cross-linking are sufficient to determining both $\Delta\alpha(X)$ and $T(X)$ if $\Delta\alpha(0)$ and $T(0)$ are known.
[18] J. R. Schaefgen and P. J. Flory, J. Am. Chem. Soc. **72,** 689 (1950).
[19] P. Mason, J. Chem. Phys. **35,** 1523 (1961).
[20] T. G. Fox and S. Loshaek, J. Poly. Sci. **15,** 371 (1955).
[21] K. Ueberreiter and G. Kanig, J. Chem. Phys. **18,** 399 (1950).
[22] S. Loshaek, J. Poly. Sci. **15,** 391 (1955).
[23] B. Wunderlich, J. Phys. Chem. **64,** 1052 (1960).
[24] G. Gee, J. Poly. Sci. **2,** 451 (1947).
[25] The linear behavior of the specific volume versus percent bound sulfur curve provides a partial justification of this assumption (see fig. 3 of ref. 16). There are two reasons for this decrease over and above that in the rubber-sulfur mixtures; one is the formation of new chemical bonds, and the other is due to the fact that the large internal pressure compresses the system. According to James and Guth [12] this pressure is ⅓ the modulus and therefore proportional to the number of individual chains. If we assume that the compressability is a constant then at small bound sulfur content the composite linear curve is due to two parts each of which is linear. Since the composite curve continues to be linear above 7 percent bound sulfur we can either assume that the two resolvent curves remain linear or that they are each nonlinear in such a way as to sum up to a linear curve. But the latter alternative would be fortuitous since the individual curves arise from unrelated causes.
[26] L. R. G. Treloar, The Physics of Rubber Elasticity, 2d eidtion, Oxford University Press, (1958).
[27] This has been observed by Wunderlich (ref. 23). The theory also predicts this result since to first order $\Delta C_p$ is a function only of $\Delta\epsilon/kT$ which is a constant at the glass temperature.
[28] G. T. Furukawa and M. L. Reilly, J. Res. NBS **56,** 285 (1956) RP 2676.
[29] G. Gee, P. N. Hartley, J. B. M. Herbert and H. A. Lanceley, Polymer 1, 365 (1960).
[30] J. D. Ferry Viscoelastic Properties of Polymers (John Wiley & Sons, Inc., New York, N.Y., 1961).
[31] R. O. Davies and G. O. Jones, Advances in Physics **2,** 370 (1953).
[32] Examine for example figure 7 from: A. Kovacs, J. Poly. Sci. **30,** 131 (1958).

(Paper 68A6–308)

JOURNAL OF RESEARCH of the National Bureau of Standards—A. Physics and Chemistry
Vol. 68A, No. 6, November–December 1964

# Ionization Constants and Reactivity of Isomers of Eugenol

G. M. Brauer, H. Argentar, and G. Durany

(July 15, 1964)

To determine the scope of the reaction of zinc oxide with isomers of eugenol, the effect of changes in the position of the substituents in the benzene ring on the ionization constants and reactivity of these isomers has been studied.

The ionization constants of eugenol isomers as well as those of newly synthesized allyl- and propenylbenzoic acids were determined by spectrophotometric and potentiometric techniques. The influence of inductive, resonance and steric effects of the substituents on the ionization constants has been discussed and the substituent constant for the Hammett equation $pK_0 - pK = \sigma\rho$ has been calculated. For the 4- and 5- substituted allyl and propenyl derivatives, the Hammett equation is valid.

Vicinal trisubstituted isomers do not harden readily with zinc oxide due to the steric hindrance of the side chain. The unsymmetrically trisubstituted derivatives react rapidly in the presence of zinc acetate. Besides the steric effects of ths substituent groups the rate of the chelation reaction is to a lesser degree dependent on the ionization constants as indicated by the shorter setting time of chavibetol-zinc oxide slurries compared to those containing eugenol.

## 1. Introduction

Mixtures of zinc oxide and 4-allyl-2-methoxyphenol (eugenol) harden to form a product that consists of zinc oxide embedded in a matrix of zinc eugenolate chelate [1].[1] To determine the scope of this reaction it appeared of interest to study how changes of the position of substituent groups in eugenol affect the behavior of the isomers as evidenced by their ionization constants, absorption spectra, hydrogen bonding and reactivity with zinc oxide. The absorption spectra studies will be discussed in a subsequent paper.

## 2. Experimental Procedures and Results

### 2.1. Materials

The eugenol isomers that are commercially available—4-allyl-2-methoxyphenol, 2-methoxy-5-propenylphenol (isochavibetol), and *trans*-2-methoxy-4-propenylphenol (*trans*-isoeugenol)—were redistilled or recrystalized; the final boiling or melting points agreed with those given in the literature.

The synthesis of 3-allyl-2-methoxyphenol, 3-allyl-5-methoxyphenol (chavibetol), 6-allyl-2-methoxyphenol (*o*-eugenol), and 2-methoxy-4-propenylphenol has been described previously [2]. *p*-Allylphenol (chavicol) and *p*-propenylphenol (anol) were synthesized from *p*-allylanisole (estragole) and *p*-propenylanisole (anethole) by demethylation with methyl magnesium iodide. The procedures were similar to those employed by Schöpf and coworkers for the demethylation of 4-allyl-1,2-dimethoxybenzene (methyleugenol) [3]. 2-Methoxy-6-propenylphenol (*o*-isoeugenol) was prepared by the method of Pal'gi [4]. *p*-Allylbenzoic and *p*-propenylbenzoic acids were synthesized from *p*-dibromobenzene through a series of reactions described by Quelet [5, 6].

The *m*-allylbenzoic acid was synthesized by modifying the procedure given by Quelet for the para-isomer [5, 6]. To 5.8 g (0.24 gram atom) of magnesium and a few crystals of iodine, 50 ml of ether was added and the solution was refluxed until the purple color changed to pale green (approximately 30 min). Then 50 g (0.21 mole) of *m*-dibromobenzene in 50 ml of ether was added and the solution refluxed for 2 hr when most of the magnesium had reacted. Allyl bromide (20 ml, 0.24 mole) dissolved in 25 ml of ether was added dropwise with cooling to keep the temperature of the reaction mixture between 5 and 15 °C. After refluxing for 18 hr, the Grignard reagent was decomposed with saturated ammonium chloride adjusted to *p*H 8 with $NH_4OH$, the ether was evaporated, and the residue was steam distilled. Sodium chloride was added to the distillate, the product was separated from the water and dried over calcium chloride. The *m*-bromoallylbenzene containing traces of dibromobenzene distilled at 76–78 °C/6 mm, $n_D^{30} = 1.549$. Yield: 22 g (47%).

The acid was prepared from *m*-bromoallylbenzene as follows: To 0.92 g magnesium (0.038 gram atom) in 25 ml of ether a few crystals of iodine were added and the mixture refluxed until the iodine color disappeared. After addition of 7.0 g (0.0355 mole) *m*-bromoallylbenzene dissolved in 25 ml of ether, the mixture was refluxed for 24 hr, cooled to 5 °C, and dry ice was added over a 4-hr period. The mixture was poured onto crushed ice, 100 ml of 10 percent HCl was added, and the ether layer was separated and extracted with dilute sodium bicarbonate. The extract was acidified and the precipitate extracted with ether. The yellow solid obtained on evaporation of the ether was recrystallized from

[1] Figures in brackets indicate the literature references at the end of this paper.

water and dilute ethanol yielding 0.9 g (16%) of *m*-allylbenzoic acid, mp 61–62 °C.

Anal: Calcd. for $C_{10}H_{10}O_2$: C, 74.05; H, 6.2; neut. equiv. 162.2. Found: C, 74.2; H, 6.3; neut. equiv. 161.1.

By modifying the synthesis given for the para isomer [5, 6], *m*-propenylbenzoic acid was obtained through the following reaction steps:

The *m*-bromophenylmagnesium bromide was prepared as described above. The mixture was cooled to 5 °C and 14 g (0.24 mole) of propionaldehyde in 50 ml of ether was added dropwise with stirring to keep the temperature of the highly exothermic reaction between 5 and 12 °C. The mixture was kept overnight at room temperature and was decomposed with crushed ice. Then 100 ml of 10 percent HCl was added. The water layer was separated and extracted with ether. The ether extracts and original ether layer were combined, dried with anhydrous sodium sulfate, and the ether was evaporated off. On distillation at 123–128 °C/6 mm there was obtained 20 g (44% yield based on *m*-dibromobenzene) 1-(*m*-bromophenyl)-1-propanol, $n_D^{23}=1.5580$.

Anal: Calcd. for $C_9H_{11}OBr$: C, 50.3; H, 5.2. Found: C, 50.9; H, 5.1.

On dehydration of 20.7 g (0.096 mole) 1-(*m*-bromophenyl)-1-propanol by refluxing for 19 hr with 9 g (0.063 mole) $P_2O_5$ in 150 ml of benzene (dried over sodium) there was obtained 6.83 g (36%) 1-(*m*-bromophenyl)propene, bp 92–93 °C/6 mm, $n_D^{28}=1.5855$.

Anal: Calcd. for $C_9H_9Br$: C, 54.85; H, 4.6. Found: C, 54.7; H, 4.4.

The 1-(*m*-bromophenyl)propene (3.0 g, 0.015 mole) was converted to the acid by refluxing it with 0.39 g (0.016 gram atom) magnesium and 25 ml of ether for 3 days and subsequent addition of dry ice. The *m*-propenylbenzoic acid was recovered from the reaction mixture as described in the preparation of *m*-allylbenzoic acid. After recrystallation from acetic acid-water and ethanol-water the colorless needles melted at 104.5–105.5 °C. Yield: 0.5 g (21%).

Anal: Calcd, for $C_{10}H_{10}O_2$: C, 74.05; H, 6.2; neut. equiv. 162.2. Found: C, 74.0; H, 6.3; neut. equiv. 163.1.

### 2.2. Ionization Constants

The thermodynamic ionization constants of eugenol isomers and related phenols were determined spectrophotometrically according to the procedure of Robinson and Biggs [7]. This method depends upon the fact that the ultraviolet absorption spectrum of a weak acid is often markedly dependent on *p*H; that is, in an alkaline solution one obtains the spectrum of the negatively charged anion of the acid whereas in an acidified solution one measures the spectrum of the uncharged molecule of the weak acid. Thus a range of wavelengths can be found in which the anion is highly absorbent and the uncharged molecule shows little if any absorption. All measurements were made with a Beckman DU spectrophotometer thermostated at 25.0 ±0.1 °C. The optical density at a specific wavelength was studied in acidic (0.1*N* HCl) and alkaline (0.1*N* NaOH) media as well as solutions that had been buffered. Buffers used were equimolar mixtures of 0.25*M* or 0.01*M* sodium carbonate and sodium bicarbonate (*p*H=10.020 and 10.112 [8, 9]), 0.1*M* and 0.01939*M* solutions containing sodium acid succinate and sodium chloride (*p*H=4.802 and 4.853 [10] and 0.06*M* sodium acetate and 0.14*M* acetic acid (*p*H=3.875 [11]) at 25 °C. These buffers were chosen since the *p*H of the resulting solutions appeared to be in the neighborhood of the expected *pK* values of the acids.

The negative logarithm of the thermodynamic ionization constant is given by:

$$pK=p\mathrm{H}-\log\frac{\alpha}{1-\alpha}-\log\gamma_{A^-}.$$

The degree of ionization can be calculated from the optical density *D* of the buffered, acidic, and basic solutions.

$$\alpha=(D_{\text{buffer}}-D_{\text{acid}})/(D_{\text{base}}-D_{\text{acid}}).$$

The values of $\gamma_{A^-}$, the activity coefficient of the anion, were obtained from the equation

$$-\log\gamma_{A^-}=[0.5115I^{1/2}/(1+I^{1/2})]-0.2I,$$

where $I$=ionic strength [12]. The values of $-\log\gamma_{A^-}$ were 0.102 and 0.077 for the 0.25*M* and 0.01*M* carbonate and 0.217 and 0.0418 for the 0.100*M* and 0.01939*M* sodium acid succinate-sodium chloride buffer solutions.

The concentration and wavelengths that would be most favorable for the determination of the ionization constant were obtained by scanning the absorption curve of the acidic and basic solution of each phenol in the 270 to 330 mμ region and of the acids in the 230 to 330 mμ region. The concentrations employed varied from $7\times10^{-5}$ to $3.5\times10^{-4}M$.

The propenylbenzoic acids were insoluble in 0.1*N* HCl and thus could not be determined by the spectrophotometric method. The apparent and thermodynamic *pK* values of the propenyl- and allyl-benzoic acids were therefore determined potentiometrically at 25.0±0.1 °C. A 40 ml 1:1 (by volume) abs. ethanol-water solution of the acid of 2.75 to $5.50\times10^{-3}$ molar concentration was titrated in a nitrogen atmosphere with carbonate free (approximately 0.025*N*) 50 percent ethanolic sodium hydroxide employing an automatic constant rate microburette (Sargent, Model C). The change in *p*H was followed using a Radiometer *p*H meter (Model 22) with scale expander which was standardized each day against aqueous 0.05*M* potassium acid phthalate (*p*H=4.010) and Beckman concentrated buffer solution diluted 24 to 1 (*p*H=7.000). The *p*H was measured in the buffer region where the degree of ionization is between 25 and 75 percent and also in the vicinity of the end point. The precise end point was obtained by plotting $\Delta p\mathrm{H}/\Delta$ ml versus

ml of NaOH added and taking as the end point the number of ml of NaOH at which $\Delta\ pH/\Delta$ ml is a maximum. The thermodynamic $pK$ values were calculated using the following equation:

$$pK = pH + \log \frac{C - [Na^+] - [H^+]}{[Na^+] + [H^+]} + \frac{A\sqrt{[Na^+] + [H^+]}}{1 + B\sqrt{[Na^+] + [H^+]}}$$

where

$[Na^+]$ = concentration of the sodium ion
$C = [HA] + [A^-]$ = total concentration of all acid species
$[HA]$ = concentration of the undissociated acid
$[A^-]$ = concentration of the anion of the acid.

The constants $A$ and $B$ depend on the solvent composition and were calculated from the expression given by Bates [13].

$A = 1.825 \cdot 10^6\ (\epsilon T)^{-3/2}$
$B = 1.5\ (78.3/\epsilon)^{1/2}$

where
$T$ = absolute temperature
and

$\epsilon$ = dielectric constant of the solvent which was obtained by interpolation from the values given by Åkerlöf [14].

A Royal computer was used to calculate the $pK$ values. The standard deviation was about 0.004 $pK$ units for one titration and the standard deviation between different runs was within 0.02 $pK$ units.

The degree of ionization and the thermodynamic $pK$ values obtained from the optical density measurements are given in table 1. The $pK$ values are considered to be accurate within $\pm 0.02$ $pK$ units except for *p*-propenylphenol and *m*-allylbenzoic acid since the latter compounds were not stable in the buffered or basic solutions. The $pK$ values of the allyl and propenyl substituted guaiacols increase in the following order: 3-substituted <5-substituted <4-substituted <6-substituted guaiacol.

TABLE 1. *Thermodynamic ionization constants of allyl- and propenyl substituted phenols and benzoic acids*

Solvent: $H_2O$ Temperature: 25.0±0.1 °C

| Compound | Concentration | Wave length | Normality of $Na_2CO_3$-$NaHCO_3$ buffer | $\alpha$ | $pK$ | Avg. $pK$ |
|---|---|---|---|---|---|---|
| | $10^{-4}M$ | $m\mu$ | | | | |
| Phenol | | | | | | 10.00[8] |
| *p*-Allylphenol (Chavicol) | 3.00 | 300 | 0.01 | 0.462 | 10.26 | |
| | 3.00 | 300 | .025 | .452 | 10.21 | 10.23 |
| 3-Allyl-2-methoxyphenol | 3.00 | 290 | .01 | .660 | 9.90 | |
| | 3.00 | 290 | .025 | .617 | 9.92 | 9.92 |
| | 3.00 | 300 | .01 | .653 | 9.91 | |
| | 3.00 | 300 | .025 | .598 | 9.95 | |
| 4-Allyl-2-methoxyphenol (Eugenol) | 2.00 | 300 | .01 | .514 | 10.17 | |
| | 2.00 | 300 | .025 | .458 | 10.20 | 10.19 |
| 5-Allyl-2-methoxyphenol (Chavibetol) | 3.00 | 300 | .01 | .640 | 10.01 | |
| | 3.00 | 300 | .025 | .593 | 10.03 | 10.02 |
| 6-Allyl-2-methoxyphenol (*o*-Eugenol) | 0.70 | 300 | .025 | .363 | 10.37 | |
| | 3.50 | 300 | .01 | .374 | 10.41 | 10.38 |
| | 3.50 | 300 | .025 | .361 | 10.37 | |
| *p*-Propenylphenol (Anol) | 3.00 | 320 | .01 | [a] .438 | [a] 9.8 | |
| | 3.00 | 320 | .025 | [a] .335 | [a] 9.8 | [a] ~9.8 [c] 9.824 |
| 2-Methoxy-4-propenylphenol (Isoeugenol) | 0.70 | 320 | .01 | .679 | 9.86 | |
| | .70 | 320 | .025 | .636 | 9.88 | |
| | .70 | 325 | .01 | .685 | 9.85 | |
| | .70 | 325 | .025 | .643 | 9.87 | 9.88 |
| | 1.00 | 325 | .01 | .652 | 9.92 | [c] 9.875 |
| | 1.00 | 325 | .025 | .644 | 9.87 | |
| 2-Methoxy-5-propenylphenol (Isochavibetol) | 3.00 | 325 | .01 | .665 | 9.89 | |
| | 3.00 | 325 | .025 | .621 | 9.91 | 9.90 |
| 2-Methoxy-6-propenylphenol (*o*-Isoeugenol) | 0.70 | 320 | .025 | .448 | 10.21 | |
| | 2.00 | 320 | .01 | .489 | 10.21 | |
| | 2.00 | 320 | .025 | .453 | 10.20 | 10.20 |
| | 2.00 | 325 | .01 | .491 | 10.20 | |
| | 2.00 | 325 | .025 | .459 | 10.20 | |
| Benzoic acid | | | | | | 4.20[12] |
| *p*-Allylbenzoic acid | 2.00 | 255 | [b] .10 | .782 | 4.36 | |
| | 2.00 | 255 | [b] .01939 | .797 | 4.34 | 4.34 |
| | 2.00 | 260 | [b] .10 | .800 | 4.32 | |
| | 2.00 | 260 | [b] .01939 | .800 | 4.33 | |
| *m*-Allylbenzoic acid | 0.08 | 240 | .06N NaAc + .14N HAc | [a] .519 | [a] 4.33 | [a] 4.32 |
| | .08 | 245 | | .53 | 4.31 | |

[a] Approximate value (±0.1 $pK$ units) since the optical density of the basic and/or buffered solutions changes on standing.
[b] Sodium acid succinate—sodium chloride buffer.
[c] Since completion of this work these recently determined $pK$ values have come to our attention [25].

The presence of an allyl group usually decreases the ionization since this group furnishes electrons to the benzene ring. However, the proximity of an allyl or propenyl group ortho to the hydroxy group hinders the removal of a proton. Thus 6-allyl-2-methoxyphenol and 2-methoxy-6-propenylphenol have lower ionization constants than their respective position isomers. The small magnitude of the inductive effect of the allyl group is indicated by the very slight change in the ionization of 5-allyl-2-methoxyphenol, $pK=10.02$ (where the allyl group is meta to the hydroxyl group and exerts little if any steric and resonance effects) as compared to guaiacol, $pK=9.98$. 3-Allyl-2-methoxyphenol (3-allylguaiacol) has a slightly lower $pK$ value of 9.92. Here again the allyl group is meta to the hydroxyl group, but the proximity of the allyl group to the methoxyl group may cause some electronic interaction. In 4-allyl-2-methoxyphenol the *p*-allyl group supplies electrons to the conjugated system and the $pK$ value of 10.19 is larger than that of 5-allyl-2-methoxyphenol ($pK=10.02$).

Replacement of the allyl group of the position isomers of eugenol by the propenyl group lowers the respective $pK$ values by 0.12 to 0.31. In part the acid strengthening characteristics of the propenyl group (which has a $\pi$ bond conjugated with the benzene ring) especially in the para position are due to the resonance interaction with the phenolic hydroxyl group which increases the stability of the phenoxide ion.

The apparent and thermodynamic ionization constants of the *m*- and *p*-allyl and propenylbenzoic acids in 50 percent ethanol-water are given in table 2. From these values the $\sigma$ values of the Hammett equation $\log (k/k_0)=\sigma\rho$ can be calculated. In this equation, which relates the reactivity of the side chain of an aromatic compound and the nature of the substituent, $k$ and $k_0$ are rate or equilibrium constants for reactions of the meta or para substituted and unsubstituted compound respectively, $\sigma$ is the substituent constant which depends on the nature and position of the substituent and $\rho$ is the reaction constant which depends on the reaction and reaction conditions.

TABLE 2.—*Apparent ionization constants of allyl- and propenylbenzoic acids in 50 percent ethanol*

Temperature: 25.0±0.2 °C

| Acid | $pK$ [b] | | Hammett sigma constant |
|---|---|---|---|
| | Concentration [a] | Thermodynamic | |
| Benzoic Acid | 5.705 | 5.694 ±0.012 [c] | |
| *m*-Allylbenzoic Acid | 5.787 | 5.810 ±0.006 | $\sigma_m=-0.08$ |
| *p*-Allylbenzoic Acid | 5.812 | 5.813 ±0.005 | $\sigma_p=-0.08$ |
| *m*-Propenylbenzoic Acid | 5.765 | 5.765 ±0.020 | $\sigma_m=-0.05$ |
| *p*-Propenylbenzoic Acid | 5.833 | 5.844 ±0.004 | $\sigma_p=-0.10$ |

[a] $pK$ (concentration) $=-\log \frac{C_{A^-}C_{H^+}}{C_{HA}}$.

[b] Average of two or more measurements.

[c] Standard deviation.

The substituent constants for *m*- and *p*-allyl and propenyl groups (table 2) were calculated from the apparent $pK$ values of the benzoic acid derivatives using the $\rho$ value of 1.522 given for the ionization of benzoic acids in 50 percent ethanol [15]. The $\sigma_m$ and $\sigma_p$ values for the allyl group are close to those reported for the $C_2H_5(\sigma_m=-0.04, \sigma_p=-0.15)$ and $n\text{-}C_3H_7(\sigma_p=-0.13)$ groups [16]. Differences in the sigma values for propenyl and allyl groups should be a measure of the increased resonance interaction contributed by the $\pi$ bond of the propenyl substituent which is conjugated with the benzene ring.

The $\sigma_p$ value of the allyl group (−0.14) was the same when calculated from the thermodynamic $pK$ values of the respective substituted benzoic acids and phenols in water. A slightly lower $\sigma_p$ value of −0.08 was obtained from the apparent ionization constant in 50 percent ethanol. Solvation effects may account for this difference of $\sigma_p$ in the two solvents.

Generally, the Hammett equation is not applicable to substituents in the ortho position of the benzene ring. However, previous investigations have shown that for a few reaction series of unsymmetrically trisubstituted compounds, such as 4- and 5- substituted toluic acids [17–19], with the same substituent in the ortho position relative to the reactive group throughout the series, the reaction parameter is constant within experimental error.

Thus for the *o*-methoxyphenol (guaiacol) series the Hammett equation can be written:

$$pK_a^G - pK_a^{RG} = \rho^G\sigma$$

where $pK_a^G$ = −logarithm of the ionization constant of guaiacol

$pK_a^{RG}$ = −logarithm of the ionization constant for the substituted guaiacol

$\rho^G$ = reaction constant for the ionization of the guaiacol derivative.

Although there is hydrogen bonding between the hydroxyl and adjacent methoxyl group in guaiacol, the influence of the ortho methoxyl group on the ionization of the phenolic hydroxyl group is small and of importance only when the coplanarity and resonance of the molecule are concerned [20]. Thus guaiacol, 4-allyl-2-methoxyphenol, and 2-methoxy-4-propenylphenol are only slightly more acidic than phenol, 4-allylphenol, and 4-propenylphenol, respectively (table 3). Furthermore, the sigma values

TABLE 3. *pK values of substituted phenols and the corresponding guaiacols*

| Substituent | $pK_a$ | | $pK_a^{\text{Guaiacol}} - pK_a^{\text{Phenol}}$ | Sigma values | |
|---|---|---|---|---|---|
| | Phenol | Guaiacol | | Phenols $\rho=2.29$[26] | Guaiacols $\rho=2.2$ [b] |
| H | 10.00 [8] [a] | 9.98 [8] | −0.02 | 0.00 | 0.00 |
| 3-Allyl | | 9.92 | | | −.03 |
| 4-Allyl | 10.23 | 10.19 | −.04 | −.10 | −.10 |
| 5-Allyl | | 10.02 | | | −.02 |
| 4-Propenyl | 9.824 [25] | 9.88 | +.06 | +.08 | +.05 |
| 5-Propenyl | | 9.90 | | | +.04 |

[a] Brackets indicate literature reference.

[b] $\rho$ calculated from the $pK$ values of phenol, guaiacol, 4-hydroxymethyl-[20], 4-allyl- and 4-propenyl phenol and guaiacol.

for the 4-allyl- and 4-propenyl group when calculated from the $pK$ values of the respective phenol and guaiacol derivative and unsubstituted compound agree within experimental error.

The above equation does not hold for 3-allyl-2-methoxyphenol since the allyl group in the 3-position will affect the interaction between the methoxyl and the phenol group. The principle of additivity of substituent effects for obtaining the change of the free energies of ionization of 2,3-disubstituted benzoic acids often leads to serious discrepancies between the calculated and observed values [21]. Similar discrepancies should occur for 2,3-disubstituted phenols and even larger differences would be expected for 2,6-disubstituted derivatives (6-allyl-2-methoxyphenol). The propenyl group with a $\pi$ bond conjugated with the double bonds of the aromatic nucleus withdraws electrons from the ring. In *p*-propenylbenzoic acid the $-R$ resonance effect of the propenyl group is transmitted to the para carbon atom of the ring by conjugation, but must be relayed to the acidic $-OH$ group by induction. On the other hand the 4-propenyl group is in direct resonance interaction with phenolic OH.

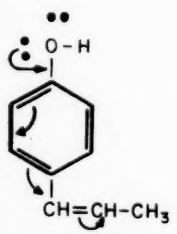


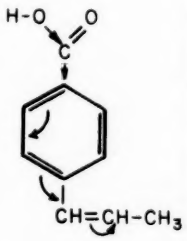


Departures from the Hammett equation have generally been observed for reaction equilibria involving derivatives of anilines and phenols having $-R$ groups *para* to the reaction center. For such reactions a second set of substituent constants somewhat greater than the normal $\sigma$ values and denoted by $\sigma_p^c$ (the superscript $c$ indicating direct conjugation) has been suggested [22]. This agreement of the sigma values derived from *p*-propenylbenzoic acid and from 4-propenyl-2-methoxyphenol should not be expected.

### 2.3. Reaction of the Eugenol Isomers With Zinc Oxide

The four eugenol isomers were mixed with zinc oxide, and zinc oxide containing 1 percent zinc acetate to determine their relative reactivities in the chelating reaction with zinc. Final setting times were determined at 37 °C and 100 percent relative humidity according to American Dental Association Specification No. 9 [23]. Results are given in table 4.

Slurries containing 6-allyl-2-methoxyphenol do not harden and those containing 3-allyl-2-methoxyphenol set only in the presence of zinc acetate. 5-Allyl-2-methoxyphenol mixes, especially those containing zinc acetate harden faster than eugenol mixes. The greatly reduced reactivity of the vicinally substituted isomers as compared to the unsymmetrically substituted ones shows that the chelation reaction is greatly influenced by steric hindrance of the bulky neighboring allyl groups. Studies to determine if substitution of metals with smaller atomic radii than zinc will reduce this steric effect would be of interest.

TABLE 4. *Reactivities of eugenol isomers with ZnO*

| Powder [a] | Liquid [a] | Setting time | |
|---|---|---|---|
| | | Initial set [b] | Final set |
| | | *hr* | *hr* |
| ZnO | 4-allyl-2-methoxyphenol (eugenol). | 3.5 | 23 |
| ZnO+1% $Zn(Ac)_2$ | 4-allyl-2-methoxyphenol | .18 | .35 |
| ZnO | 5-allyl-2-methoxyphenol (chavibetol) | 6.5 | 22 |
| ZnO+1% $Zn(Ac)_2$ | 5-allyl-2-methoxyphenol | .15 | .19 |
| ZnO | 6-allyl-2-methoxyphenol | (c) | (c) |
| ZnO+1% $Zn(Ac)_2$ | 6-allyl-2-methoxyphenol | (c) | |
| ZnO | 3-allyl-2-methoxyphenol | (c) | (c) |
| ZnO+1% Zn $(Ac)_2$ | 3-allyl-2-methoxyphenol | ~90 | ~170 |

[a] Powder-liquid ratio: 1.3 g powder per 0.4 ml liquid.
[b] Initial setting time in hours is the time elapsed from starting the mix to the time when the point of a penetrating instrument such as the point of a Gilmore needle makes only a slight but visible indentation after placing the needle on the material for 5 sec.
[c] Did not harden within 10 days.

Besides steric effects of the substituent groups, the chelation reaction is also dependent to a lesser degree on the ionization constants of the isomers. Thus, 4-allyl-2-methoxyphenol (eugenol) ($pK$=10.19) is somewhat less reactive than 5-allyl-2-methoxyphenol (chavibetol) ($pK$=10.02).

For the reaction of the nucleophilic chelating agents (eugenol or chavibetol) with zinc oxide the reaction constant $\rho$ is likely to be positive. The increased rate of setting of 5-allyl-2-methoxyphenol compared to 4-allyl-2-methoxyphenol would thus be expected since in water the sigma value of the meta allyl- is slightly larger than that of the para allyl group [24]. Results of this study would indicate that synthesis of new chelate cements should be directed towards derivatives with unsymmetrically substituted groups (1,2,4- and 1,2,5- substituted benzene derivatives).

---

The authors thank R. A. Robinson for valuable suggestions and R. W. Morris for assisting in some of the experimental work.

## 3. References

[1] Copeland, H. I., G. M. Brauer, W. T. Sweeney, and A. F. Forziati, J. Res. NBS **55,** 133 (1955).
[2] Brauer, G. M., R. W. Morris, and W. B. Howe, J. Res. NBS **67A,** 265 (1963).
[3] Schöpf, C., E. Brass, E. Jacobi, W. Mocnik, L. Neuroth, and W. Salzer, Ann. **544,** 30 (1940).
[4] Pal'gi, M., J. Gen. Chem. U.S.S.R. **28,** 2278 (1958).
[5] Quelet, R., Bull. Soc. Chim. France [4] **45,** 75 (1929).
[6] Quelet, R., Ibid [4], **45,** 255 (1929).

[7] Robinson, R. A. and A. I. Biggs, Trans. Faraday Soc. **51,** 901 (1955).
[8] Biggs, A. I., Trans. Faraday Soc. **52,** 35 (1956).
[9] Bates, R. G., G. D. Pinching, and E. R. Smith, J. Res. NBS **45,** 418 (1950).
[10] Bates, R. G., and R. Gary, J. Res. NBS **65A,** 495 (1961).
[11] Britton, H. T. S., Hydrogen Ions, 4th ed., D. Van Nostrand Co., Princeton, N.J., Vol. 1, p. 357 (1956).
[12] Robinson, R. A., and R. H. Stokes, Electrolyte Solutions, 2d ed., Academic Press, New York, N.Y. (1959).
[13] Bates, R. G., M. Paabo, and R. A. Robinson, J. Phys. Chem. **67,** 1833 (1963).
[14] Åkerlöf, G., J. Am. Chem. Soc. **54,** 4125 (1932).
[15] McDaniel, D. H., and H. C. Brown, J. Org. Chem. **23,** 420 (1958).
[16] Jaffe, H. H., Chem. Rev. **53,** 191 (1953).
[17] Roberts, J. D., and J. A. Yancy, J. Am. Chem. Soc. **73,** 1011 (1951).
[18] Peltier, D., Bull. Soc. Sci. Bretagne **31,** 7 (1956).
[19] Peltier, D., Bull. Soc. Chim. France **1958,** 994.
[20] Juslén, C. and J. J. Lindberg, Finska Kemistsamf. Medd. **68,** 53 (1959).
[21] Shorter, J. and F. J. Stubbs, J. Chem. Soc. **1949** 1180.
[22] Gould, E. S., Mechanism and Structure in Organic Chemistry, H. Holt and Co., New York (1959), Ch. VII, pp. 199–243.
[23] American Dental Association Specification No. 9 for Dental Silicate Cements. Guide to Dental Materials 1964–1965, American Dental Association, Chicago, Ill. 60611 (1964), p. 107.
[24] Brauer, G. M., H. Argentar, and G. Durany, (unpublished results).
[25] Lindberg, J. J., C. G. Nordström and R. Lauren, Suomen Kem. **35B,** 182 (1962).
[26] Biggs, A. I. and R. A. Robinson, J. Chem. Soc. **1961,** 388.

Paper 68A–309

JOURNAL OF RESEARCH of the National Bureau of Standards—A. Physics and Chemistry
Vol. 68A, No. 6, November–December 1964

# Near Infrared Spectrophotometric Method for the Determination of Hydration Numbers

Richard A. Durst* and John K. Taylor

(July 29, 1964)

The 980 mμ absorption band of water is employed in a new method for the determination of hydration numbers. The decrease in the concentration of "free" water is calculated from the change in absorbance resulting on the addition of an electrolyte. Data are given for chromic chloride and nitrate salts in water-methanol solutions, and an extrapolation is made to give the hydration number in pure water. The results obtained by this technique agree with the values reported using other methods.

## 1. Introduction

Although aqueous electrolyte solutions have been studied in detail for many years, one of the most basic properties of such solutions, the concept of ionic hydration, is still poorly defined. Normally, the effect of the coordinated water molecules is ignored when reactions in aqueous solutions are considered. However, in many cases, this can lead to serious errors in the interpretation of results. The numerous experimental techniques which have been employed to determine hydration numbers give some indication of the widespread influence of ion-solvent interactions. These methods include such phenomena as: transference of ions, freezing and boiling points, vapor pressure, density, compressibility, and refractivity [1],[1] to mention a few. In addition, knowledge of hydration numbers is important for development of a theory of concentrated electrolyte solutions and for the theory of reaction in solution.

## 2. Hydration Number Concept

Part of the difficulty in defining absolute hydration numbers is the indefinite nature of the term "hydration number" itself. It is generally accepted that ions possess two hydration spheres. The primary hydration sphere is made up of those water molecules which are firmly associated with the ion by an electrostatic ion-dipole attraction and have lost their own separate translational degrees of freedom. The secondary hydration sphere contains water molecules which undergo interaction partially with the primary hydration sphere of the ion and partially with the surrounding water structure. This sphere extends an indefinite distance from the ion until it ultimately blends into the bulk water structure. Normally, the secondary hydration is very weak and values found experimentally vary widely depending on the phenomenon observed.

To date, the techniques employed for determining hydration numbers have resulted in values which can be divided into two groups: low values which seem to approximate the primary hydration numbers and considerably larger values corresponding to the primary hydration plus all or part of the secondary hydration sphere. Since it is the primary hydration number which is important as far as the properties of the ionic entity are concerned, the method used must not be so sensitive as to include contributions from the secondary hydration.

The hydration techniques may be further subdivided into those which measure some property of the solvated ions and those which measure some property of the solvent itself. In the former grouping may be included such phenomena as polarography [2, 3], UV-visible spectrophotometry [4], mobility [5], and activity [6] measurements, while the second grouping includes isotope dilution [7], compressibilities [8, 9], and nuclear magnetic resonance [10].

## 3. Technique

The method proposed here is one of the latter type based on the near infrared (NIR) absorption of water. Water exhibits a series of absorption bands in the NIR from about 1 to 3 μ. Using the band peak between 980 mμ and 1020 mμ, which is the third overtone of the OH stretching vibration [11], changes in the free water concentration in solution will be measured when an electrolyte is introduced. The

*Present Address: Dept. of Chemistry, Pomona College, Claremont, Cali
[1] Figures in brackets indicate the literature references at the end of this paper.

change in the free water concentration can then be related to the water tied up in the primary hydration sphere of the ions.

Methanol solutions containing varying amounts of water were prepared for the purpose of calibration. A second identical set of solutions was then prepared containing a known concentration of electrolyte and comparison was made of the water absorption in the 980 to 1020 mμ region. The apparent decrease in the water concentration was attributed to a shift of this absorption band for the water molecules in the hydration sphere of the ions. This shift is caused by the strong interaction of the water dipole with the electric field surrounding the ion. In this region, the water molecules are highly compressed by the strong electrostatic field and, consequently, it is assumed that the OH stretching vibrational energy will be significantly affected. Since the water molecules in the secondary hydration sphere interact very weakly with the hydrated ions, their absorption band closely coincides with the free water band and no separation occurs. Thus the secondary hydration does not cause any apparent water concentration changes.

Since hydrogen bonding in this solvent system causes association to occur, there is the possibility that the absorption changes produced when the electrolyte is added is due to a disassociation effect rather than to hydration. However, it has been demonstrated that the absorption of the water band at 0.96 μ increases with disassociation [12]. Since the effect observed upon the addition of the chromium salts is just the opposite, i.e., a decrease in the absorption, the electrolyte affect on the solvent association can be ruled out as a major factor in this study. To verify this further, it is proposed that a salt such as $NH_4ClO_4$ be used in a subsequent study. This electrolyte should exhibit a hydration number of almost zero and thus not effect the absorption of the water band to any significant extent. In this way, the contribution due to association changes can be evaluated.

It is evident that the number of moles of water in the primary hydration sphere can be calculated from the decrease in the absorption band. This is accomplished by obtaining from the calibration curve the mole percent free water remaining after the salt is added and converting to moles of water. This number is then subtracted from the moles of water originally present to give the total number of moles of hydrating water. This value divided by the moles of electrolyte present must, therefore, be the hydration number of the electrolyte. By choosing an electrolyte composed of a small cation of high charge and a large anion of low charge, the hydration effect may be confined primarily to the cation. If this were not done, the total hydration number of both the cation and anion would be obtained and the individual ionic hydration numbers could not be distinguished.

In order to evaluate the method, chromic ion was selected as the cation since several independent methods [7, 13] have shown this ion to have an inert primary hydration sphere of 6 water molecules. For the preliminary investigation, $CrCl_3 \cdot 6H_2O$ was used. The chloride ion hydration is small, being on the order of 0 to 1 and should not be significant in the dilute water in methanol solutions. Subsequently, the nitrate salt was employed since its hydration is weaker than that of chloride. The best anion in this respect would be perchlorate. However, since this salt is only available with an indefinite number of waters of hydration, it could not be used without causing serious error in the hydration number measured.

Methanol (A.C.S., 99.8% purity) was selected as the solvent since it is completely miscible with water and has a low dielectric constant (31.5 to 32.6 at 25 °C [14]). Because of its low dielectric constant, it will not compete strongly with water ($\epsilon$=78.5 at 25 °C [14]) for the primary solvation sphere of the ion and will be displaced at relatively low water concentrations.

## 4. Apparatus and Procedure

The instrument used in this investigation was a Perkin-Elmer Corp. Spectracord Model 4000A. The methanol-water solutions were placed in 10 cm cells, and the spectra scanned from 1200 to 800 mμ.

In the preliminary work with reagent grade $CrCl_3 \cdot 6H_2O$, the Spectracord was operated as a single-beam spectrophotometer. Using a slit width of 0.40 mm, a series of spectra were recorded for methanol-water solutions from 0.0 to 72.1 mole percent water. Several such spectra superimposed are represented in figure 1. The absorbance of the band peak was plotted versus the water concentration for the purpose of calibration, and this curve is given in figure 2. The transmittance scale was arbitrarily set by instrumental adjustment so that the methanol band at 1020 mμ had a value of approximately 0.80. This was done to bring the methanol-water bands into the more sensitive transmittance region. This technique explains the resulting transmittance greater than 1.00 on either side of the absorption band. Using this scale, the arbitrary transmittance values ($\overline{T}$) obtained were converted into the "absorbance" units ($\overline{A}$) plotted in the empirical working curve given in figure 2.

The solutions containing chromic chloride were then run in the same way giving spectra of the type shown in figure 3. The only differences in the spectra of these solutions and the calibration solutions are the apparent decrease in the water concentration and the rapid cut off at short wavelengths due to chromic ion absorption. By means of the calibration curve, the apparent water concentration of these solutions is measured, and the difference found is attributed to the removal of water from the bulk solution by hydration.

Subsequent work was carried out using chromic nitrate salts and operating the Spectracord in the double beam mode. In these cases, methanol was used as the reference medium while the sample solutions were similar to those used in the case of chromic chloride. By means of the double beam

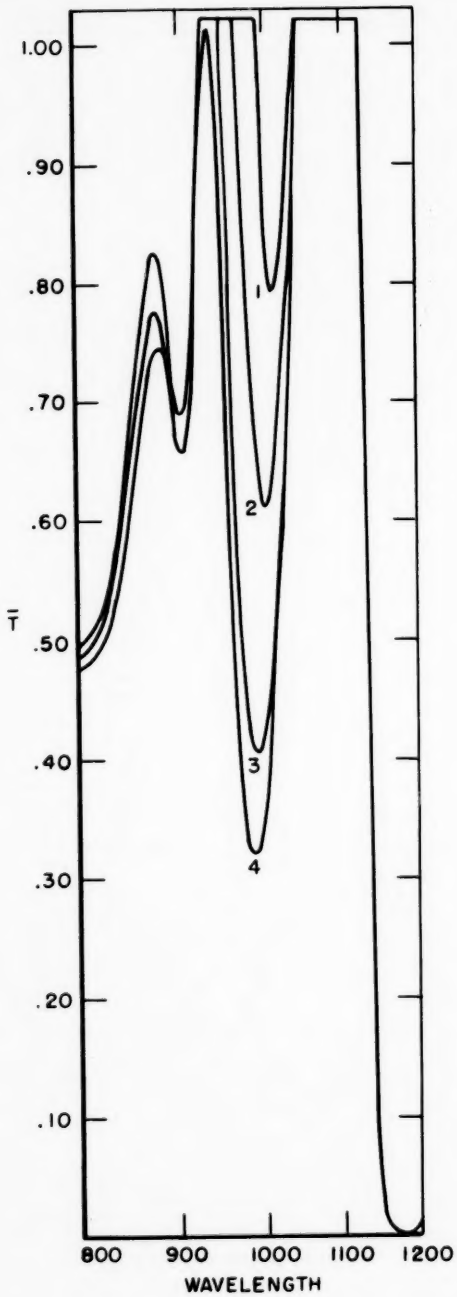


FIGURE 1. $H_2O$ *absorption band in* $H_2O$-$CH_3OH$ *solutions.*

(1) $CH_3OH$
(2) 23.4 mole percent $H_2O$
(3) 43.6 mole percent $H_2O$
(4) 53.8 mole percent $H_2O$

operation, the major portion of the background in the spectra was eliminated as can be seen in figure 4 (curve No. 1). Again, to increase the sensitivity, the transmittance at 1 $\mu$ was arbitrarily set at approximately 0.90 for pure methanol. The calibration spectra and those for the sample solutions were all recorded on the same chart in order to facilitate comparison (fig. 4). In figure 5, the calibration curve is given for the water "absorbance" versus mole percent water in methanol when operating in the double beam mode. By comparison with figure 2, it is seen that the sensitivity of the method is increased by the use of the double beam technique. In all cases, the solutions were rerun several times over the period of a week to ensure equilibration of the aquo complexes. As expected, no changes were noted as a function of time indicating a rapid attainment of equilibrium.

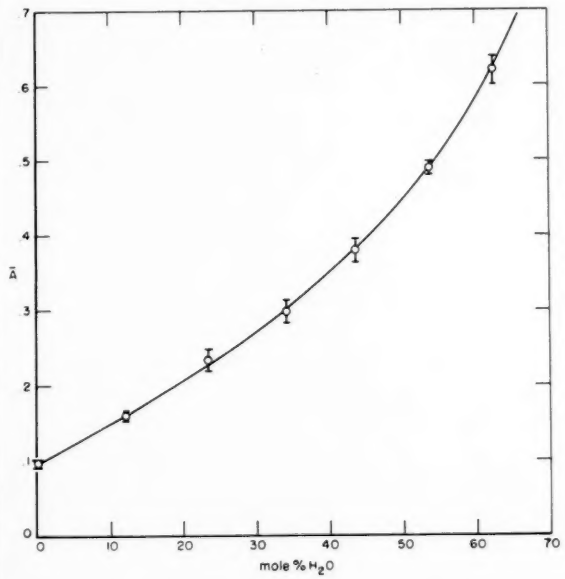


FIGURE 2. *Absorbance of* $H_2O$ *between 980 and 1020 m*$\mu$ *versus mole percent water (single beam operation).*

## 5. Results

### 5.1. Chromic Chloride

The approximately 0.5 *M* $CrCl_3 \cdot 6H_2O$ solutions were prepared containing 0.05 mole of $Cr^{+++}$ in the methanol-water solvents. The water concentration, including the contribution due to the waters of hydration of the salt, was varied from 12.1 to 69.5 mole percent. Data were gathered at seven water concentrations, and the results with the standard deviation of the means are given in table 1. The number of observations reported for each concentration refers to independent measurements on aliquots of a stock solution.

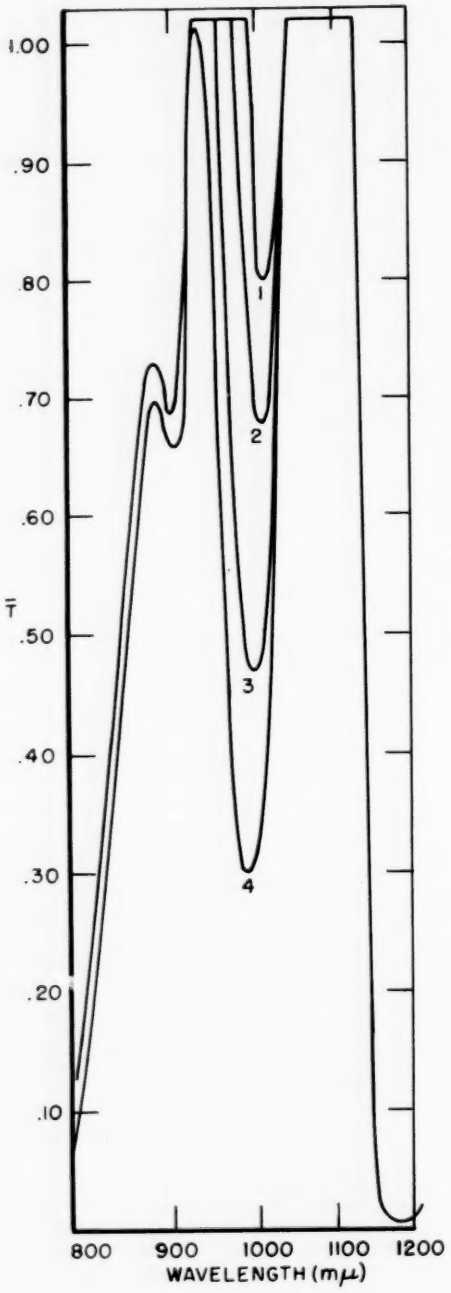


FIGURE 3. $H_2O$ *absorption band in* $H_2O$-$CH_3OH$-$CrCl_3$* *solutions.*

(1) $CH_3OH$
(2) 23.4 mole percent $H_2O$
(3) 43.6 mole percent $H_2O$
(4) 62.5 mole percent $H_2O$

*0.05 mole $CrCl_3$

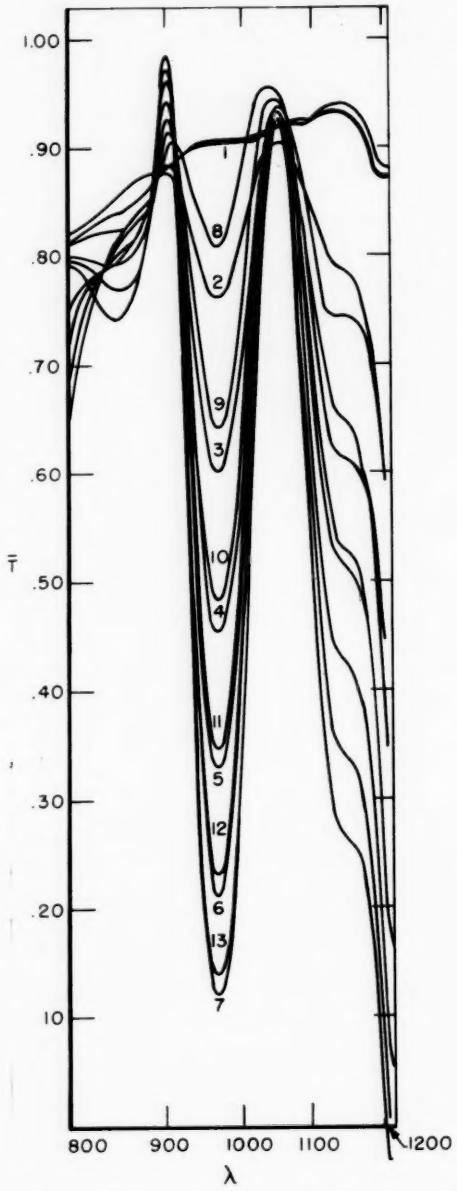


FIGURE 4. $H_2O$ *absorption band in* $H_2O$—$CH_3OH$ *and* $H_2O$—$CH_3OH$—$Cr(NO_3)_3$* *solutions.*

(1) $CH_3OH$
(2) 10 mole percent $H_2O$
(3) 20 mole percent $H_2O$
(4) 30 mole percent $H_2O$
(5) 40 mole percent $H_2O$
(6) 50 mole percent $H_2O$
(7) 60 mole percent $H_2O$
(8) 10 mole percent $H_2O$+$Cr(NO_3)_3$
(9) 20 mole percent $H_2O$+$Cr(NO_3)_3$
(10) 30 mole percent $H_2O$+$Cr(NO_3)_3$
(11) 40 mole percent $H_2O$+$Cr(NO_3)_3$
(12) 50 mole percent $H_2O$+$Cr(NO_3)_3$
(13) 60 mole percent $H_2O$+$Cr(NO_3)_3$

*0.02 mole $Cr(NO_3)_3$

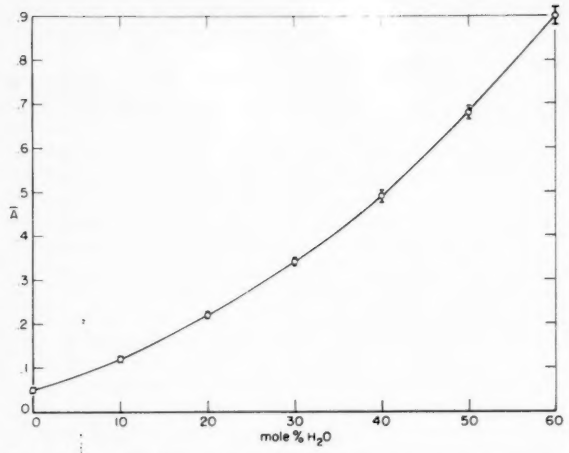


FIGURE 5. *Absorbance of* $H_2O$ *at 980 mμ versus mole percent* $H_2O$ *in* $CH_3OH$ *(double beam operation).*

These seven points lie along a straight line which when extrapolated to 100 mole percent water results in a hydration number for $CrCl_3$ of $5.7_2 \pm 0.1_6$.

This value is the sum of the hydration numbers for chromic and chloride ions. However, since data are taken at lower water concentrations and the degree of chloride ion hydration is small (hyd. No. $=0-1$), the effect of chloride hydration is very likely negligible. Thus, the hydration number found is primarily due to chromic ion hydration.

TABLE 1. $CrCl_3 \cdot 6H_2O$ *results*

| $[Cr^{+++}]$ | Mole percent $H_2O$ | Hydration No. | Number of observations | Standard deviation of the mean |
|---|---|---|---|---|
| *Moles/liter* | | | | |
| 0.59 | 12.1 | 4.7 | 7 | 0.2 |
| .56 | 23.4 | 4.8 | 5 | $.0_8$ |
| .52 | 34.0 | 4.9 | 8 | $.0_5$ |
| .50 | 43.4 | 5.0 | 7 | .1 |
| .50 | 51.8 | 5.1 | 9 | $.1_1$ |
| .50 | 60.4 | 5.3 | 11 | $.1_8$ |
| .50 | 69.5 | 5.4 | 11 | $.1_4$ |

A disadvantage of using chromic chloride is the complication resulting from the formation of chlorochromium complexes. At the concentrations used, only the monochlorochromium complex formation is significant. From the formation constant, $K_{CrCl^{++}} = 0.1$, it is calculated that 0.06 mole of $CrCl^{++}$ is present and, as a first approximation, should lower the accepted hydration number of 6 for noncomplexed chromic ion by about 2.0 percent. This would result in a hydration number of $5.8_8$; a value within the standard deviation of the hydration number experimentally found.

### 5.2. Chromic Nitrate

To avoid the difficulties arising from complex formation, subsequent work was carried out with chromic nitrate salts. Solutions were prepared containing 0.02 mole of reagent grade $Cr(NO_3)_3 \cdot 9H_2O$ in methanol with the water concentration varied from 10 to 50 mole percent. The results of these hydration number determinations are given in table 2.

When the line through these points is extrapolated to 100 mole percent water, the resulting hydration number is $6.6_5 \pm 0.3_4$. This value is higher than expected: possibly due to hydration of the nitrate ion. As in the case of chloride, the nitrate hydration should be small (less than 1), but the larger value for the hydration number of the nitrate salt indicates that its total hydration is greater although weaker than that of the chloride ion and, as will be seen, only becomes significant when the $H_2O$ concentration is relatively high.

TABLE 2. $Cr(NO_3)_3 \cdot 9H_2O$ *results*

| $[Cr^{+++}]$ | Mole percent $H_2O$ | Hydration No. | Number of observations | Standard deviation of the mean |
|---|---|---|---|---|
| *Moles/liter* | | | | |
| 0.24 | 10 | 3.5 | 7 | $0.0_8$ |
| .22 | 20 | 3.5 | 12 | $.1_3$ |
| .21 | 30 | 4.1 | 13 | .1 |
| .20 | 40 | 4.4 | 13 | $.1_2$ |
| .20 | 50 | 4.8 | 13 | $.1_9$ |

Another reagent grade nitrate salt, $Cr(NO_3)_3 \cdot 7\frac{1}{2} H_2O$, was used for the final determination. The solutions were made up to contain 0.04 mole of this salt and water concentrations from 18.7 to 60.0 mole percent. These results are given in table 3.

A line through these points extrapolates to $7.1_6 \pm 0.1_7$ at 100 mole percent water. Again, this value is larger than expected but, as before, is probably due to nitrate hydration and elimination of complexation by the anion which causes a lowering of the hydration number.

TABLE 3. $Cr(NO_3)_3 \cdot 7\frac{1}{2}H_2O$ *results*

| $[Cr^{+++}]$ | Mole percent $H_2O$ | Hydration No. | Number of observations | Standard deviation of the mean |
|---|---|---|---|---|
| *Moles/liter* | | | | |
| 0.44 | 18.7 | 2.5 | 8 | $0.0_7$ |
| .42 | 29.0 | 3.0 | 14 | .1 |
| .40 | 39.3 | 3.6 | 14 | $.0_7$ |
| .40 | 49.7 | 4.2 | 14 | $.0_8$ |
| .40 | 60.0 | 4.9 | 17 | $.0_9$ |

## 6. Discussion and Conclusion

The data for the three salts investigated are plotted in figure 6. Although the chromic salts exhibit large differences in the hydration numbers at low water concentrations, the differences decrease at higher concentrations. That is, at 50 mole percent $H_2O$, all three salts have hydration numbers between 4 and 5 and, at 60 and 70 mole percent $H_2O$, the agreement is even closer. Then, however, at even higher water concentrations, the values again appear to diverge, but since these values are in the extrapolation region of the graph, the actual divergence could be much less.

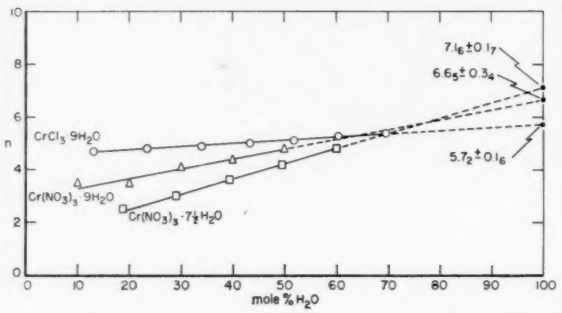


FIGURE 6. *Hydration numbers for chromic salts versus mole percent* $H_2O$.

The large divergence in hydration number values at low water concentrations is to be expected, since in this range, there is a strong competition by the ions present for the small amount of water. Thus it would appear that the chloride ion hydrates more readily than nitrate. This results in the higher apparent hydration number for the chloride salt with respect to the nitrate salts. At higher water concentrations where competition for water is not so strong, the nitrate begins to hydrate and rapidly approaches the chloride salt hydration number. At least three explanations for the increase in the chromic nitrate hydration number over the chromic chloride are possible: (1) the total effective hydration number of nitrate is greater than chloride, (2) the complexation of chromic ion with chloride reduces the number of possible hydration sites around both the chromic and chloride ions, and (3) the extrapolation to 100 mole percent water is invalid and the actual hydration number for the nitrate salts levels off above a concentration of about 60 mole percent of $H_2O$. In the case of (1), it is necessary that the chloride ion hydration be stronger than the nitrate, so that the nitrate hydration is not detected until the water concentration is relatively high. Although it is definitely known that case (2) does occur, the extent to which it lowers the hydration number cannot be predicted with any degree of certainty. Finally, in order to test the effect of case (3), it would be necessary to run chromic nitrate solutions at water concentrations greater than 60 mole percent. However, at these concentrations, the precision of the measurements is extremely low since the method used measures the change in the absorption of free water. Thus it can be seen that any one or combination of these possibilities could be the cause of the divergence in the extrapolated high water concentration region.

The values determined for the chromic ion in the method evaluation experiments further support the results found by other hydration number techniques. The precision of the hydration number values obtained by this technique compares very favorably with those from the existing methods and can be improved with minor modifications. Limitations on the method were set by such factors as the reproducibility of the instrument and errors in the composition of the hydrated salts.

The validity of the extrapolation of the hydration numbers in mixed solvent systems, such as $H_2O$–$CH_3OH$, to pure water can be checked by employing solvents with dielectric constants greater and lesser than that for methanol. This should show any solvent effects on the hydrated ions. Of course, to demonstrate the validity of the extrapolation, the extrapolated value should be independent of the solvent used. A better choice than methanol might have been acetonitrile ($\epsilon$=36.7 at 25 °C [14]) since this solvent does not have an absorption band in the 1 $\mu$ region and there is no complicating OH-type bonding. However, since methanol-water working curves were used, the effects caused by overlapping bands are thereby taken into consideration. Anion and salt concentration effects must also be clarified before the method can be used for any survey of the hydration numbers of diverse ions.

Since it is the concentration of water and not the particular ion which is measured, this method should be applicable to the determination of the hydration numbers of any ions which form relatively inert aquo complexes, i.e., hydrated ions, and do not have interfering absorption bands in the NIR region. Labile or weak aquo complexes probably would not exhibit large enough separation between the complexing and free water bands and only result in broadening the existing free water absorption bands in the NIR. In spite of the limitations noted, the purpose of this preliminary study has been achieved; that of the development of a new, independent method for the determination of primary hydration numbers.

## 7. References


[1] J. O'M. Bockris, Quart. Revs. (London) **3,** 173 (1949).
[2] K. P. Mishchenko and I. S. Pominov, Zhur. Fiz. Khim. **31,** 2026 (1957).
[3] I. S. Pominov, Ibid. **31,** 2184 (1957).
[4] J. Bjerrum and C. K. Jorgensen, Acta Chem. Scand. **7,** 951 (1953).
[5] H. Ulich, Trans. Faraday Soc. **23,** 392 (1927).
[6] P. O. Kosakewich and N. A. Ismailow, Z. Physik. Chem. (Leipzig) **150,** A, 308 (1930).
[7] J. P. Hunt and H. Taube, J. Chem. Phys. **19,** 602 (1951).
[8] A. L. J. Moesveld and H. J. Hardon, Z. physik. Chem. (Leipzig) **155,** A, 238 (1931).
[9] A. Passinski, Acta Physicochim. U.R.S.S. **8,** 385 (1938).
[10] J. A. Jackson, J. F. Lemons, and H. Taube, J. Chem. Phys. **32,** 553 (1960).
[11] W. Kaye, Spectrochim. Acta **6,** 257 (1954).
[12] W. Luck, Berichte Bunsengesellschaft physik. Chem. **67,** 186 (1963).
[13] P. B. D. de la Mare and W. Klyne, Progress in Stereochemistry, V. III (Butterworths, Washington, D.C., 1962).
[14] R. A. Robinson and R. H. Stokes, Electrolyte Solutions (Butterworths, London, 1959).


(Paper 68A6-310)

JOURNAL OF RESEARCH of the National Bureau of Standards—A. Physics and Chemistry
Vol. 68A, No. 6, November–December 1964

# Franck-Condon Factors for the Ionization of $H_2$, HD, and $D_2$

**Morton E. Wacks**

(July 15, 1964)

Franck-Condon factors for the following ionization transitions were computed assuming a Morse potential:

$$H_2\ X^1\Sigma_g^+\ (v=0)\rightarrow H_2^+\ X^2\Sigma_g^+(v=0\rightarrow 15)$$

$$HD\ X^1\Sigma^+\ (v=0)\rightarrow HD^+\ X^2\Sigma^+(v=0\rightarrow 15)$$

$$D_2\ X^1\Sigma_g^+\ (v=0)\rightarrow D_2^+\ X^2\Sigma_g^+(v=0\rightarrow 15).$$

The results are used to interpret several recent ionization experiments which used essentially a monoenergetic ionizing medium. The relative importance of autoionization and direct ionization excitation processes are discussed.

## 1. Introduction

Recently, the use of monoenergetic electrons and photons in the investigation of the ionization of molecules has provided a large amount of information previously obscured by the energy spread of the ionizing medium. This information is contained in the structure of the ionization efficiency curves, i.e., the experimental curves relating the ion current per ionizing particle to the energy of the ionizing particle. In general the gross features of these ionization efficiency curves are related to the electronic transitions involved in the ionization process, while the fine structure observed in these curves is due to transitions involving vibrational excitation within the electronic states and autoionization transitions. Discussion of these finer details of electron or photon ionization of molecules necessitates having the Franck-Condon probabilities for transitions between vibronic states. In the Born-Oppenheimer approximation the probability of a transition is given by

$$P_{ev,e'v'}\sim|\int G_{e,e'}(R,r)\psi_{e,v}(R)\psi_{e',v'}(R)d\tau_R|^2,$$

where $\psi_{e,v}(R)$ and $\psi_{e',v'}(R)$ are the vibrational wave functions for the neutral molecule and ion, respectively [1].[1] If the variation of the perturbation integral $G_{e,e'}$ with $R$ is small, then we have

$$P_{ev,e'v'}\sim|G_{e,e'}(R_e r)|^2\cdot|\int\psi_{e,v}(R)\psi_{e',v'}(R)d\tau_R|^2.$$

Those features of the ionization efficiency curves that are due to transitions to the vibrational levels of the various electronic states of the ion can be described to a good approximation by the vibrational overlap integral with the assumption of appropriate threshold behavior for the ionization process under investigation. For electron impact ionization near threshold $|G_{e,e'}|^2$ varies linearly with the excess energy above threshold [2]. For photoionization it is assumed that the probability near threshold can be approximated by a step function.

## 2. Method

The problems involved in the computation of these integrals have been discussed by Nicholls and coworkers [3]. Under Nicholls' direction a program was prepared at NBS for the 704 electronic digital computer (later modified for the 7094 computer) which will evaluate these integrals for a Morse oscillator. In this method Morse potentials are assumed, each member of the two families of wave functions $\psi_i(i=0\rightarrow v_{\max})$, $\psi_j(j=0\rightarrow v_{\max})$ is computed at 0.01-Å intervals and overlap integrals between all pairs are computed and squared [4]. The computer input data are $\omega_e$, $\omega_e x_e$, $r_e$, $\mu_a$, and $v_{\max}$ for the ground electronic state of the molecule and for each of the electronic states of the ion for which the vibrational transition probabilities are being computed.

## 3. Results

The Franck-Condon probabilities for the transitions,

$H_2\ X^1\Sigma_g^+(v=0)\rightarrow H_2^+\ X^2\Sigma_g^+(v=0\rightarrow 15)$,

$HD\ X^1\Sigma_g^+(v=0)\rightarrow HD^+\ X^2\Sigma_g^+(v=0\rightarrow 15)$,

and

$D_2\ X^1\Sigma_g^+(v=0)\rightarrow D_2^+\ X^2\Sigma_g^+(v=0\rightarrow 15)$

[1] Figures in brackets indicate the literature references at the end of this paper.

were computed using the data of table 1. Tables 2, 3, and 4 present all the vibrational transition probabilities that were computed for these ionization processes. More than 99 percent of the total probability was accounted for in each case.

TABLE 1. *Basic data**

| State | $\omega_e$ | $\omega_e x_e$ | $r_e$ | $\mu_a$ | $v_{max}$ |
|---|---|---|---|---|---|
| | $cm^{-1}$ | $cm^{-1}$ | Å | | |
| HH $X^1\Sigma_g^+$ | 4395.$2_4$ | 117.$90_2$ | 0.$7416_6$ | 0.504066 | 0 |
| HH$^+X^2\Sigma_g^+$ | 2297 | 62. | 1.060 | .503928 | 15 |
| HD $X^1\Sigma_g^+$ | 3817.09 | 94.958 | 0.$7413_6$ | .671917 | 0 |
| HD$^+X^2\Sigma_g^+$ | 1989.5 | 46.5 | 1.06 | .671762 | 15 |
| DD $X^1\Sigma_g^+$ | 3118.$4_8$ | 64.$09_7$ | 0.$7416_4$ | 1.007363 | 0 |
| DD$^+X^2\Sigma_g^+$ | 1624.8 | 31.0 | 1.06 | 1.007217 | 15 |

*The data for the $H_2$, HD, and $D_2$ molecules and the $H_2^+$ ion were obtained from G. Herzberg, The Spectra of Diatomic Molecules (D. Van Nostrand Co., Inc., New York, N.Y. (1950)). The data for the other ionic species were calculated from physical constants and the data of the $H_2^+$ ion.

TABLE 2. *Franck-Condon probabilities* (P) *for the transitions* $H_2X^1\Sigma_g^+$, $v''=0\rightarrow H_2^+X^2\Sigma_g^+$, $v'=0\rightarrow15$.

| $v'$ | $E$ | $\Delta E$ | $P$ | $\Sigma P$ |
|---|---|---|---|---|
| | $eV$ | $eV$ | | |
| 0 | 0.1405 | 0.1405 | 0.0922 | 0.0922 |
| 1 | .4099 | .2694 | .1751 | .2673 |
| 2 | .6639 | .2540 | .1959 | .4632 |
| 3 | .9026 | .2387 | .1700 | .6332 |
| 4 | 1.1258 | .2232 | .1275 | .7607 |
| 5 | 1.3337 | .2079 | .0874 | .8481 |
| 6 | 1.5263 | .1926 | .0566 | .9047 |
| 7 | 1.7034 | .1771 | .0355 | .9402 |
| 8 | 1.8652 | .1618 | .0219 | .9621 |
| 9 | 2.0116 | .1464 | .0134 | .9755 |
| 10 | 2.1427 | .1311 | .0082 | .9837 |
| 11 | 2.2584 | .1157 | .0051 | .9888 |
| 12 | 2.3586 | .1002 | .0032 | .9920 |
| 13 | 2.4436 | .0850 | .0020 | .9940 |
| 14 | 2.5131 | .0695 | .0013 | .9953 |
| 15 | 2.5673 | .0542 | .0008 | .9961 |

$\frac{1}{2}\,h\nu_0(H_2)=2168.1\ cm^{-1}=0.2688\ eV$.

TABLE 3. *Franck-Condon probabilities* (P) *for the transitions* HD $X^1\Sigma_g^+$, $v''=0\rightarrow HD^+\ X^2\Sigma_g^+$, $v'=0\rightarrow15$

| $v'$ | $E$ | $\Delta E$ | $P$ | $\Sigma P$ |
|---|---|---|---|---|
| | $eV$ | $eV$ | | |
| 0 | 0.1219 | 0.1219 | 0.0647 | 0.0647 |
| 1 | .3569 | .2350 | .1416 | .2063 |
| 2 | .5804 | .2235 | .1788 | .3851 |
| 3 | .7924 | .2120 | .1721 | .5572 |
| 4 | .9929 | .2005 | .1408 | .6980 |
| 5 | 1.1818 | .1889 | .1037 | .8017 |
| 6 | 1.3593 | .1775 | .0712 | .8729 |
| 7 | 1.5251 | .1658 | .0467 | .9196 |
| 8 | 1.6795 | .1544 | .0298 | .9494 |
| 9 | 1.8223 | .1428 | .0186 | .9680 |
| 10 | 1.9536 | .1313 | .0116 | .9796 |
| 11 | 2.0734 | .1198 | .0072 | .9868 |
| 12 | 2.1816 | .1082 | .0044 | .9912 |
| 13 | 2.2783 | .0967 | .0028 | .9940 |
| 14 | 2.3635 | .0852 | .0018 | .9958 |
| 15 | 2.4371 | .0736 | .0011 | .9969 |

$\frac{1}{2}\,h\nu_0$ (HD) $=1884.8\ cm^{-1}=0.2337\ eV$.

TABLE 4. *Franck-Condon probabilities* (P) *for the transitions* $D_2X^1\Sigma_g^+$, $v''=0\rightarrow D_2^+\ X^2\Sigma_g^+$, $v'=0\rightarrow15$

| $v'$ | $E$ | $\Delta E$ | $P$ | $\Sigma P$ |
|---|---|---|---|---|
| | $eV$ | $eV$ | | |
| 0 | 0.0998 | 0.0998 | 0.0354 | 0.0354 |
| 1 | .2935 | .1937 | .0950 | .1304 |
| 2 | .4796 | .1861 | .1434 | .2738 |
| 3 | .6580 | .1784 | .1611 | .4349 |
| 4 | .8286 | .1706 | .1507 | .5856 |
| 5 | .9916 | .1630 | .1245 | .7101 |
| 6 | 1.1470 | .1554 | .0943 | .8044 |
| 7 | 1.2946 | .1476 | .0671 | .8715 |
| 8 | 1.4345 | .1399 | .0456 | .9171 |
| 9 | 1.5668 | .1323 | .0300 | .9471 |
| 10 | 1.6914 | .1246 | .0193 | .9664 |
| 11 | 1.8083 | .1169 | .0122 | .9786 |
| 12 | 1.9174 | .1091 | .0077 | .9863 |
| 13 | 2.0190 | .1016 | .0048 | .9911 |
| 14 | 2.1128 | .0938 | .0030 | .9941 |
| 15 | 2.1989 | .0861 | .0019 | .9960 |

$\frac{1}{2}\,h\nu_0$ ($D_2$) $=1543.2\ cm^{-1}=0.1913\ eV$.

## 4. Discussion

The computed values of the vibrational transition probabilities permit a closer look at several ionization experiments. Kerwin and coworkers [5] have examined the ionization efficiency curve of $H_2$ using a monoenergetic electron beam with an energy spread of about 0.03 eV. This permitted the observation of the vibrational states excited in the electron-impact ionization process. The observed vibrational transition probabilities up to the fourth vibrational level of the $H_2^+$ $X^2\Sigma_g^+$ ion are compared in table 5 with the theoretical values of this work and of Krauss and Kropf [6]. They calculated the Franck-Condon factors for the transitions $H_2$ $X^1\Sigma_g^+$, $v=0\rightarrow H_2^+X\,^2\Sigma_g^+$, $v=0\rightarrow5$ and $D_2$ $X^1\Sigma_g^+$, $v=0\rightarrow D_2^+$ $X^2\Sigma_g^+$, $v=0\rightarrow5$, using the data of Richardson [7]. The experimental electron-impact values for the vibrational transition probabilities (obtained with mass analysis of the ionization products) and the previously calculated values compare well with the computed values of this work. Vibrational levels in the electron-impact ionization efficiency curve for $H_2$ were also found by Weingartshofer and Clarke [8]. These appear to follow the predicted trend (table 2) in the relative transition probabilities to the vibrational levels in the $H_2^+$ ion.

TABLE 5. *Comparison of experimental electron-impact vibrational transition probabilities for* $H_2$ *with the theoretical Franck-Condon factors*

| | Vibrational excitation transition, $H_2(X)\rightarrow H_2^+(X)$ | | | | |
|---|---|---|---|---|---|
| | 0-0 | 0-1 | 0-2 | 0-3 | 0-4 |
| Experimental [5] | 0.53 | 0.91 | 1.00 | 0.35 | 0.35 |
| Theoretical: | | | | | |
| (a) | 0.47 | 0.89 | 1.60 | 0.87 | 0.65 |
| (b) | 0.44 | 0.87 | 1.00 | 0.91 | 0.72 |

[a] This work.
[b] Krauss, ref. [6], using the vibrational constants of Richardson, ref. [7].

Dibeler and Reese [9] reported the ionization efficiency curves for $H_2$, HD, and $D_2$, obtained by photoionization followed by mass analysis. The energy spread in their photon beam is 2Å (about 0.03 eV). They observed a difference for the ionization energies of $D_2$ and $H_2$ of 0.04 eV, the value calculated from the data of tables 2 and 4 is 0.0367 eV.

Autoionization phenomena are prevalent in the photoionization efficiency curves for hydrogen and almost completely obscure the vibrational transitions. Autoionization, in general, appears as more or less broadened and asymmetric peaked functions depending upon the lifetimes of the states involved. The resultant photoionization efficiency curve for a molecule in which both autoionization transitions and direct ionization are probable would be composed of a series of steps due to the Franck-Condon vibrational level interaction with peaks due to the autoionization transitions superimposed upon the steps. Krauss [10] discusses the origin of the autoionization peaks and the relative probabilities for the direct ionization and autoionization processes in hydrogen. The autoionization arises from excitation to at least the D, D′, and B″ [11] electronic states of the $H_2$ molecule.

## 5. Conclusion

More detailed knowledge of the autoionization transitions and the predissociation of the electronic states of the molecules and ions is needed to completely determine theoretically the origin of the observed structure in ionization efficiency curves. Since total electronic transition probabilities based upon theoretical considerations are lacking, the complete a priori synthesis of these curves for hydrogen from the computed values of the Franck-Condon factors is not possible. Any complete theoretical discussion and synthesis of the ionization efficiency curves for hydrogen will require not only the prediction of the relative importance of autoionization processes as compared to direct ionization excitation but will also have to account for the dependence of the total electronic transition probabilities upon the medium of excitation.

## 6. References


[1] A. S. Coolidge, H. M. James, and R. D. Present, J. Chem. Phys. **4,** 193 (1936).

[2] D. R. Bates, A. Fundaminsky, J. W. Leech, and H. S. W. Massey, Trans. Roy. Soc. (London) **A243**, 93 (1950); S. Geltman, Phys. Rev. **102,** 171 (1956); R. E. Fox, W. M. Hickman, and T. Kjeldaas, Phys. Rev. **89,** 355 (1953); G. H. Wannier, Phys. Rev. **100,** 1180 (1956).

[3] W. R. Jarmain and R. W. Nicholls, Can. J. Phys. **32,** 201 (1954).

[4] R. W. Nicholls, J. Res. NBS **66A,** 227 (1962).

[5] L. Kerwin, P. Marmet, and E. M. Clarke in Advances in Mass Spectrometry, II, ed. R. M. Elliott (Pergamon Press, London, 1963), pp. 522–526.

[6] M. Krauss and A. Kropf, J. Chem. Phys. **26,** 1776 (1957).

[7] O. W. Richardson, Nuovo cimento **15,** 232 (1938).

[8] A. Weingartshofer and E. M. Clarke, Phys. Rev. Letters **12,** 591 (1964).

[9] V. H. Dibeler and R. M. Reese, Twelfth Annual Conference on Mass Spectrometry and Allied Topics, Montreal, Can. (June 1964) paper No. 44.

[10] V. H. Dibeler, R. M. Reese, and M. Krauss, Proc. 3d Intern. Conf. Mass Spectrometry, Paris, France (1964), to be published.

[11] A. Monfils, Bull. Classe Sci., Acad. roy. Belg. **47,** 816, (1961).


(Paper 68A–311)

JOURNAL OF RESEARCH of the National Bureau of Standards—A. Physics and Chemistry
Vol. 68A, No. 6, November–December 1964

# Calculation of the Geometrical Structure of Some $AH_n$ Molecules

Morris Krauss

(August 4, 1964)

Approximate Hartree-Fock calculations for $H_3$, $CH_2$, $NH_2$, $H_2O$, $H_2O^+$, $BH_4^-$, $NH_4^+$, and $CH_4$ have been used to determine equilibrium angles and internuclear separations. The results are in good agreement with the experimental values where these exist.

Data from these calculations are used to test the usefulness of a partition into one-electron type terms. It is found that the partitioned energies reflect the influence of the other orbitals in such a way as to render a simple interpretation very difficult. For example, the present results predict an equilibrium angle of 119° for $H_2O^+$ which is very unexpected if the usual picture of a nonbonding $b_1$ orbital is accepted.

## 1. Introduction

Perhaps the most widely used scheme for the prediction of molecular shapes is the correlation diagrams proposed by Walsh [1].[1] The simplicity and popularity of the scheme rests on the assumption that the total energy of the molecule is simply the sum of one-electron orbital energies. Substantially, this is equivalent to an extended Hückel calculation as it is usually applied [2]. Hoffmann notes that such a procedure can be valid only if there is a slow variation with distance for the difference between the nuclear-nuclear repulsion and the electron-electron repulsions.

Reliance upon such a fortuitous cancellation or semiempirical parameterization of the problem is not satisfying in two essential respects. In the first place, as noted by Coulson and Neilson [3], there are fundamental theoretical objections to any one-electron model. Secondly, the predictions of the scheme must be treated more cautiously when applied to changes in molecular geometry attendant upon excitation or ionization.

Coulson and Neilson proposed that the apparent simplicity of the partition of the total energy into one-electron terms be retained, nonetheless, for its obvious pedagogic and predictive value. The partition which they devolved upon is a natural one based on the Hartree-Fock molecular orbital approach. The total energy in the Hartree-Fock approximation can be written, for a closed-shell molecule, as

$$E=\sum_i e_i+V_N, \tag{1}$$

[1] Figures in brackets indicate the literature references at the end of this paper.

where $\epsilon_i = E_i + E_r$. $V_N$ is the total nuclear-nuclear repulsion energy, $E_i$ is the expectation value for molecular orbital $i$ of all one-electron potential and kinetic energy operators, and $\epsilon_i$ is the $i$th eigenvalue of the solution of the self-consistent field equations which determine the Hartree-Fock function.

In general, with the exception of $V_N$, these quantities cannot be determined accurately for a general range of molecular cases. The usual method is to expand the Hartree-Fock orbitals as a linear combination of atomic orbitals. Solution of the resultant equations is by an iterative self-consistent field (SCF) procedure [4]. Accuracy of the variational solutions is predicated upon the number and type of basis functions. The total energy of the system is determined by the SCF program precisely by eq (1) or its analog suitably modified for the open-shell case.

Implicit in this approach is the assumption that the geometry of a molecule can be calculated, to a high degree of accuracy, by a self-consistent field one-electron theory which ignores certain types of correlation. This assumption is buttressed by both experimental numerical work with diatomic molecules [5] and theoretical arguments [6].

However, calculations of polyatomic molecules have not been quite as successful. Much of this difficulty probably can be attributed to the approximate integrals that were used in evaluating the necessary matrix elements. The prediction of the equilibrium angle for $AH_2$ molecules with a Hartree-Fock calculation, until recently, was quite problematical.

Higuchi [7] found a rather slow variation of the energy of $NH_2$ with angle in the neighborhood of the experimental value and a minimum of 105°, but the integrals were not evaluated in a consistent fashion. The equilibrium angle calculated by Ellison and Shull [8] was considerably greater than the experimental value. Using approximate integrals, Krauss and Padgett [9] determined the molecular geometry of $CH_2$ which was in poor agreement with experimental results. An accurate configuration interaction calculation by Foster and Boys [10] did not find any better agreement with the experimental equilibrium configuration for either the singlet or triplet ground states of $CH_2$. The total energy, however, is in the neighborhood of the expected Hartree-Fock limit. This emphasizes the relative unimportance of correlation in determining the geometry of a molecule.

SCF results, considerably more accurate than those cited above, have recently been published by Moccia [11]. Using a large number of functions in a one-center expansion, he obtained equilibrium configurations that are in good agreement with the experimental value confirming the impression that the correlation of electrons plays a small role in determining the geometry.

Approximate Hartree-Fock orbitals and energies of the same order as those obtained by Moccia can be obtained readily with Gaussian basis sets. Preliminary results for $CH_4$ and $NH_4^+$ [12] were quite encouraging. Qualitatively interesting results have been reported by Harrison [13], but the number of basis functions that were used for $H_2O$ were insufficient to yield a quantitative result. Extending the basis slightly, however, produced both a large improvement in the total energy and the calculated equilibrium angle. These results indicate that moderately accurate Gaussian SCF results can predict the structures of radicals and ions. Calculations for $H_3$, $CH_2$, $NH_2$, $H_2O$, $H_2O^+$, $BH_4^-$, $NH_4^+$, and $CH_4$ will be reported in this paper.

The SCF results also yield enough data to test the contentions of Coulson and Neilson. It will be seen that the simple one-electron picture is unsatisfactory since the partitioned energies reflect the influence of the other orbitals in a complex fashion. Such conclusions must be qualified by observing that accurate Hartree-Fock values have not been obtained but these results provide a consistent test with functions that do predict a moderately accurate geometry.

## 2. Results of Gaussian Calculations

The SCF calculations follow a standard procedure that has recently been reviewed by Nesbet [4]. Since the open shell is of different symmetry from all other occupied orbitals,

the Nesbet and Roothaan [14] procedures are equivalent and the SCF equations may be solved by the same procedures used for a closed-shell system with a suitably modified $A$ matrix.

For $CH_2$, $^3\Sigma_g^-$, which can be represented

$$(1\sigma_g)^2(2\sigma_g)^2(1\sigma_u)^2\Pi_+\Pi_-$$

the eigenvalues are given by the following expressions

$$\epsilon_{a\sigma_g}=E_{a\sigma_g}+J_{a\sigma_g a\sigma_g}+2J_{1\sigma_g 2\sigma_g}-K_{1\sigma_g 2\sigma_g}+2J_{a\sigma_g 1\sigma_u}-K_{a\sigma_g 1\sigma_u}+2J_{a\sigma_g\Pi}-K_{a\sigma_g\Pi},$$

$$\epsilon_{1\sigma_u}=E_{1\sigma_u}+J_{1\sigma_u 1\sigma_u}+2J_{1\sigma_u 1\sigma_g}-K_{1\sigma_u 1\sigma_g}+2J_{1\sigma_u 2\sigma_g}-K_{1\sigma_u 2\sigma_g}+2J_{1\sigma_u\Pi}-K_{1\sigma_u\Pi},$$

$$\epsilon_{\Pi_\pm}=E_\Pi+\sum_\alpha[2J_{\alpha\sigma_g\Pi}-K_{\alpha\sigma_g\Pi}]+2J_{1\sigma_u\Pi}-K_{1\sigma_u\Pi}+J_{\Pi_+\Pi_-}-K_{\Pi_+\Pi_-},$$

where $E_i$ is the expectation value for the $i$th orbital overall one-electron, potential and kinetic energy, operators, $J_{ij}$ is the Coulomb integral between the $i$ and $j$ orbitals, $K_{ij}$ is the exchange integral between these orbitals, and $\alpha=1$ or 2. The total energy for $CH_2$, $^3\Sigma_g^-$, is then

$$E=\Sigma e_i$$

with

$$e_i=E_i+\epsilon_i.$$

Different expressions are required for $H_3$, which is represented by the configuration

$$(1\sigma_g)^2(1\sigma_u).$$

The eigenvalues are

$$\epsilon_{1\sigma_g}=E_{1\sigma_g}+J_{1\sigma_g 1\sigma_g}-\tfrac{1}{2}K_{1\sigma_g 1\sigma_u}+J_{1\sigma_g 1\sigma_u},$$

$$\epsilon_{1\sigma_u}=E_{1\sigma_u}+2J_{1\sigma_g 1\sigma_u}-K_{1\sigma_g 1\sigma_u},$$

with

$$E=\epsilon_{1\sigma_g}+\tfrac{1}{2}\epsilon_{1\sigma_u}+E_{1\sigma_g}+\tfrac{1}{2}E_{1\sigma_u}.$$

A similar result is obtained for $NH_2$, $^2B_1$, which is represented by the configuration

$$(1a_1)^2(2a_1)^2(1b_2)^2(3a_1)^21b_1$$

where

$$\epsilon_{aa_1}=E_{aa_1}+\sum_\beta[2J_{aa_1\beta a_1}-K_{aa_1\beta a_1}]+2J_{aa_1 1b_2}-K_{aa_1 1b_2}+J_{aa_1 1b_1}-\tfrac{1}{2}K_{aa_1 1b_1},$$

$$\epsilon_{1b_2}=E_{1b_2}+J_{1b_2 1b_2}+\sum_\alpha[2J_{aa_1 1b_2}-K_{aa_1 1b_2}]+J_{1b_1 1b_2}-\tfrac{1}{2}K_{1b_1 b_2},$$

$$\epsilon_{1b_1}=E_{1b_1}+\sum_\alpha[2J_{aa_1 1b_1}-K_{aa_1 1b_1}]+2J_{1b_2 1b_1}-K_{1b_2 1b_1},$$

and

$$E=\sum_\alpha\epsilon_{aa_1}+\epsilon_{1b_2}+\tfrac{1}{2}\epsilon_{1b}+\sum_\alpha E_{aa_1}+E_{1b_2}+\tfrac{1}{2}E_{1b_1}.$$

The use of Gaussian basis functions is recommended for polyatomic calculations because of the ease with which the necessary matrix elements are evaluated (15). However, so many functions are required in order to achieve an accurate Hartree-Fock function that in only five cases, $CH_4$, $NH_4^+$, $BH_4^-$, $CH_2(^3\Sigma_g^-)$, and $H_3$, was an energy obtained that is sufficiently accurate to warrant an analysis of the energy. For all other cases only the angular variation of the approximate energy was considered.

The parameters for the basis orbitals are given in table 1. The tetrahedral orbital parameters were either scaled from the best H atom results of Longstaff and Singer [16] or were varied in a limited manner to minimize the energy. For $H_2O$ the choice of parameters was

dictated by the desire to compare the present results with those reported by Harrison. The parameters for $CH_2$ and $NH_2$ were chosen by reference to various atom results that have been obtained by Huzinaga [17].

In table 2, the eigenvalues, functions and energies for all of the relevant cases are presented. Note that all results are for normalized basis functions. The equilibrium angles and internuclear separations were obtained simply from a quadratic fit and only the three solutions in the neighborhood of the equilibrium are given. Calculated equilibrium angles and distances are compared in table 3 with the experimental values. For the case of $BH_4^-$, $CH_2(^3\Sigma_g^-)$, and $H_3$ a summary of the considerations relevant to determining a bound on the correlation energy are presented in table 4. Finally we have tabulated the quantities, $e_i$, for $CH_2$, $NH_2$, and $H_2O$ in table 5.

TABLE 1a. *Parameters for* $T_D$ *basis orbitals* Nf (x,y,z)exp(−ar²)

| Summetry type | Orbital | f(x,y,z) | Atom | | | |
|---|---|---|---|---|---|---|
| | | | H | B | C | N |
| $a_1$ | 1 | 1 | | 834.54 | 1227.4 | 1695.9 |
| | 2 | 1 | | 128.83 | 189.48 | 261.79 |
| | 3 | 1 | | 33.769 | 49.667 | 68.623 |
| | 4 | 1 | | 13.873 | 20.404 | 28.191 |
| | 5 | 1 | | 5.697 | 8.379 | 11.577 |
| | 6 | 1 | | 2.0393 | 2.999 | 4.144 |
| | 7 | $r^2$ | | 6.08 | 9.5 | 13.68 |
| | 8 | $r^2$ | | 0.832 | 1.3 | 1.87 |
| | 9 | $r^2$ | | .307 | 0.48 | 0.69 |
| $\frac{1}{4}(h_1+h_2+h_3+h_4)$. | 10 | 1 | 5.74 | | | |
| | 11 | 1 | 0.775 | | | |
| | 12 | 1 | .159 | | | |
| $t_1$ | 1 | (x,y,z) | | 9.6 | 15.0 | 21.6 |
| | 2 | (x,y,z) | | 1.92 | 3.0 | 4.32 |
| | 3 | (x,y,z) | | 0.448 | 0.7 | 1. |
| | 4 | (x,y,z) | | .128 | .2 | 0.29 |
| $[\frac{1}{4}(h_1+h_2-h_3-h_4), \frac{1}{4}(h_1-h_2-h_3+h_4), \frac{1}{4}(h_1-h_2+h_3-h_4)]$. | 5 | 1 | 5.74 | | | |
| | 6 | 1 | 0.775 | | | |
| | 7 | 1 | .159 | | | |

TABLE 1b. *Parameters for* $C_{2v}$ *basis orbitals* Nf (x,y,z)exp(−ar²)

| Summetry type | Orbital | f(x,y,z) | Atom | | | |
|---|---|---|---|---|---|---|
| | | | H | C | N | O |
| $a_1$ | 1 | 1 | | 1300 | 2500 | 2500 |
| | 2 | 1 | | 575 | 637.5 | 1090 |
| | 3 | 1 | | 146 | 203 | 276 |
| | 4 | 1 | | 37.3 | 63.5 | 70.4 |
| | 5 | 1 | | 9.42 | 20.2 | 17.8 |
| | 6 | 1 | | 2.39 | 6.35 | 4.51 |
| | 7 | 1 | | 0.608 | 0.7 | 1.15 |
| | 8 | 1 | | .154 | .21 | 0.291 |
| | 9 | z | | 4.78 | 6.89 | 9.38 |
| | 10 | z | | 0.923 | 1.33 | 1.81 |
| | 11 | z | | .178 | 0.257 | 0.35 |
| $\frac{1}{2}(h_1+h_2)$ | 12 | 1 | [a]4.24, 5.74 | | | |
| | 13 | 1 | 0.658, 0.775 | | | |
| | 14 | 1 | 0.148, 0.159 | | | |
| $b_2$ | 1 | y | | 4.78 | 6.89 | 9.38 |
| | 2 | y | | 0.923 | 1.33 | 1.81 |
| | 3 | y | | .178 | 0.257 | 0.35 |
| $\frac{1}{2}(h_1-h_2)$ | 4 | 1 | [a]4.24, 5.74 | | | |
| | 5 | 1 | 0.658, 0.775 | | | |
| | 6 | 1 | 0.148, 0.159 | | | |
| $b_1$ | 1 | x | | 4.78 | 6.89 | 9.38 |
| | 2 | x | | 0.923 | 1.33 | 1.81 |
| | 3 | x | | .178 | 0.257 | 0.35 |

[a] The first column of H parameters were used only for the $H_2O$ calculations.

TABLE 1c. *Parameters for* $D\infty_h$ *basis orbitals* Nf(x, y, z) *exp*(−ar²)($CH_2$)

| Symmetry type | Orbital | f(x, y, z) | Atom | |
|---|---|---|---|---|
| | | | H | C |
| $1\sigma_g$ | 1 | 1 | | 4232.61 |
| | 2 | 1 | | 634.882 |
| | 3 | 1 | | 146.097 |
| | 4 | 1 | | 42.4974 |
| | 5 | 1 | | 14.1892 |
| | 6 | 1 | | 5.14773 |
| | 7 | 1 | | 1.96655 |
| | 8 | 1 | | 0.496241 |
| | 9 | 1 | | .153313 |
| $1/2(h_1+h_2)$ | 10 | 1 | 5.74 | |
| | 11 | 1 | 0.775 | |
| | 12 | 1 | .159 | |
| $1\sigma_u$ | 1 | z | | 18.1557 |
| | 2 | z | | 3.9864 |
| | 3 | z | | 1.14293 |
| | 4 | z | | 0.35945 |
| | 5 | z | | .114595 |
| $1/2(h_1-h_2)$ | 6 | 1 | 5.74 | |
| | 7 | 1 | 0.775 | |
| | 8 | 1 | .159 | |
| | 1 | x | | 18.1557 |
| | 2 | x | | 3.9864 |
| | 3 | x | | 1.14293 |
| | 4 | x | | 0.35945 |
| | 5 | x | | .114595 |

TABLE 1d. *Parameters for* $D\infty_h$ *basis orbitals* Nf ($x^2$ y, z)*exp*(−ar²)($H_3$)

| Symmetry type | Orbital | f(x, y, z) | H |
|---|---|---|---|
| $1\sigma_g$ | | | |
| $\frac{1}{2}(p_A-p_B)$ | 1 | z | 0.8 |
| $\frac{1}{2}(h_A+h_B)$ | 2 | 1 | 22.683 |
| | 3 | 1 | 3.6674 |
| | 4 | 1 | 0.972 |
| | 5 | 1 | .3094 |
| | 6 | 1 | .1209 |
| $h_c$ | 7 | 1 | 22.683 |
| | 8 | 1 | 3.6674 |
| | 9 | 1 | 0.972 |
| | 10 | 1 | .3094 |
| | 11 | 1 | .1209 |
| $1\sigma_u$ | | | |
| $p_z$ | 1 | z | .8 |
| $\frac{1}{2}(p_A+p_B)$ | 2 | z | .8 |
| $\frac{1}{2}(h_A-h_B)$ | 3 | 1 | 22.683 |
| | 4 | 1 | 3.6674 |
| | 5 | 1 | 0.972 |
| | 6 | 1 | .3094 |
| | 7 | 1 | .1209 |

TABLE 2a. $BH_4^-$ *Eigenvalues, eigenvector coefficients, and total energy*

| Internuclear separation (a.u.)[a] | 2.1 | | | 2.3 | | | 2.4 | | |
|---|---|---|---|---|---|---|---|---|---|
| Total energy (a.u.) | −26.9155 | | | −26.9449 | | | −26.9451 | | |
| | $1a_1$ | $2a_1$ | $1t_2$ | $1a_1$ | $2a_1$ | $1t_2$ | $1a_1$ | $2a_1$ | $1t_2$ |
| Eigenvalue | −7.2087 | −0.4625 | −0.1789 | −7.2676 | −0.4434 | −0.1765 | −7.2974 | −0.4347 | −0.1755 |
| Eigenvector: | | | | | | | | | |
| 1 | .0057 | −.0009 | .0118 | .0057 | −.0009 | .0109 | .0057 | −.0009 | .0106 |
| 2 | .0398 | −.0071 | .0848 | .0398 | −.0067 | .0784 | .0398 | −.0066 | .0755 |
| 3 | .1256 | −.0198 | .2701 | .1256 | −.0183 | .2581 | .1257 | −.0177 | .2523 |
| 4 | .2083 | −.0576 | .1569 | .2088 | −.0579 | .1581 | .2089 | −.0583 | .1597 |
| 5 | .4266 | −.1020 | .0980 | .4270 | −.0966 | .0942 | .4271 | −.0943 | .0928 |
| 6 | .3383 | .0436 | .6087 | .3373 | .0561 | .5887 | .3369 | .0618 | .5783 |
| 7 | .0017 | −.0349 | .9952 | .0022 | −.0383 | 1.0300 | .0023 | −.0401 | 1.0459 |
| 8 | .0164 | .2252 | | .0157 | .2273 | | .0154 | .2284 | |
| 9 | −.0027 | .1565 | | −.0021 | .1863 | | −.0019 | .2007 | |
| 10 | .0004 | .0910 | | .0002 | .0847 | | .0002 | .0816 | |
| 11 | .0031 | .4946 | | .0023 | .4715 | | .0020 | .4600 | |
| 12 | .0026 | .6281 | | .0021 | .6586 | | .0019 | .6740 | |

[a] Energy in units of $e^2/a_0=27.21$ eV,
Length in units of $a_0=0.52917\times10^{-8}$ cm.

TABLE 2b. $CH_4$ *Eigenvalues, eigenvector coefficients, and total energy*

| Internuclear separation (a.u.) | 1.9 | | | 2.0665 | | | 2.2 | | |
|---|---|---|---|---|---|---|---|---|---|
| Total energy (a.u.) | −40.1495 | | | −40.1668 | | | −40.1521 | | |
| | $1a_1$ | $2a_1$ | $1t_2$ | $1a_1$ | $2a_1$ | $1t_2$ | $1a_1$ | $2a_1$ | $1t_2$ |
| Eigenvalue | −11.1691 | −0.9803 | −0.5650 | −11.2121 | −0.9421 | −0.5411 | −11.2458 | −0.9147 | −0.5234 |
| Eigenvector: | | | | | | | | | |
| 1 | .0056 | −.0010 | .0142 | .0056 | −.0010 | .0136 | .0056 | −.0010 | .0131 |
| 2 | .0393 | −.0077 | .1005 | .0393 | −.0075 | .0966 | .0393 | −.0075 | .0940 |
| 3 | .1247 | −.0206 | .3378 | .1248 | −.0195 | .3252 | .1248 | −.0189 | .3158 |
| 4 | .2093 | −.0729 | .2612 | .2096 | −.0753 | .2723 | .2098 | −.0773 | .2803 |
| 5 | .4299 | −.1038 | .1021 | .4302 | −.0988 | .0966 | .4303 | −.0958 | .0927 |
| 6 | .3341 | .0922 | .6327 | .3334 | .1026 | .6148 | .3330 | .1095 | .5980 |
| 7 | .0023 | −.0478 | .5911 | .0026 | −.0526 | .6319 | .0028 | −.0561 | .6670 |
| 8 | .0151 | .2871 | | .0146 | .2839 | | .0142 | .2829 | |
| 9 | −.0005 | .3000 | | −.0003 | .3223 | | −.0002 | .3381 | |
| 10 | .0002 | .0942 | | .0002 | .0843 | | .0002 | .0770 | |
| 11 | .0022 | .4549 | | .0017 | .4322 | | .0013 | .4154 | |
| 12 | .0004 | .3612 | | .0004 | .3964 | | .0004 | .4243 | |

TABLE 2c. $NH_4^+$ *Eigenvalues, eigenvector coefficients, and total energy*

| Internuclear separation (a.u.) | 1.8 | | | 1.9464 | | | 2.2 | | |
|---|---|---|---|---|---|---|---|---|---|
| Total energy (a.u.) | −56.4860 | | | −56.5038 | | | −56.4383 | | |
| | $1a_1$ | $2a_1$ | $1t_2$ | $1a_1$ | $2a_1$ | $1t_2$ | $1a_1$ | $2a_1$ | $1t_2$ |
| Eigenvalue | −15.9302 | −1.6026 | −1.0425 | −15.9444 | −1.5418 | −0.9930 | −15.9578 | −1.4487 | −0.9146 |
| Eigenvector: | | | | | | | | | |
| 1 | .0056 | −.0011 | .0161 | .0056 | −.0011 | .0155 | .0056 | −.0011 | .0149 |
| 2 | .0389 | −.0083 | .1189 | .0389 | −.0082 | .1171 | .0389 | −.0083 | .1145 |
| 3 | .1242 | −.0212 | .3815 | .1243 | −.0205 | .3680 | .1243 | −.0198 | .3483 |
| 4 | .2094 | −.0882 | .3439 | .2096 | −.0917 | .3621 | .2098 | −.0963 | .3844 |
| 5 | .4327 | −.1005 | .1045 | .4329 | −.0961 | .0968 | .4330 | −.0922 | .0848 |
| 6 | .3317 | .1241 | .5706 | .3313 | .1330 | .5528 | .3308 | .1445 | .5214 |
| 7 | .0021 | −.0605 | .3198 | .0023 | −.0656 | .3637 | .0025 | −.0719 | .4488 |
| 8 | .0140 | .3177 | | .0136 | .3158 | | .0132 | 3177 | |
| 9 | .0007 | .3963 | | .0008 | .4147 | | .0008 | 4409 | |
| 10 | .0002 | .0874 | | .0002 | .0756 | | .0002 | 0606 | |
| 11 | .0011 | .3980 | | .0009 | .3810 | | .0006 | .3501 | |
| 12 | −.0001 | .2349 | | −.0000$_1$ | .2636 | | .0001 | .3113 | |

TABLE 2d. $CH_2$, $^1A_1$, *Eigenvalues, eigenvector coefficients, and total energy*

| Internuclear separation | 100° | | | | 105° | | | | 110° | | | |
|---|---|---|---|---|---|---|---|---|---|---|---|---|
| $R_{CH}$ = 2.1 (a.u.) Total energy (a.u.) | −38.8017 | | | | −38.8026 | | | | −38.8020 | | | |
| | $1a_1$ | $2a_1$ | $3a_1$ | $1b_2$ | $1a_1$ | $2a_1$ | $3a_1$ | $1b_2$ | $1a_1$ | $2a_1$ | $3a_1$ | $1b_2$ |
| Eigenvalue | −11.3144 | −0.9145 | −0.3934 | −0.5623 | −11.3120 | −0.9095 | −0.3859 | −0.5712 | −11.3095 | −0.9047 | −0.3784 | −0.5793 |
| Eigenvector: | | | | | | | | | | | | |
| 1 | .0036 | −.0006 | .0003 | .0637 | .0036 | −.0006 | .0003 | .0635 | .0036 | −.0006 | .0003 | .0634 |
| 2 | .0062 | −.0011 | .0005 | .3324 | .0062 | −.0011 | .0005 | .3319 | .0062 | −.0011 | .0005 | .3317 |
| 3 | .0477 | −.0088 | .0047 | .3119 | .0477 | −.0088 | .0045 | .3092 | .0477 | −.0089 | .0044 | .3081 |
| 4 | .2098 | −.0398 | .0209 | .0663 | .2098 | −.0400 | .0202 | .0667 | .2098 | −.0402 | .0194 | .0672 |
| 5 | .5740 | −.1394 | .0766 | .5181 | .5739 | −.1401 | .0738 | .5190 | .5739 | −.1408 | .0710 | .5187 |
| 6 | .3339 | −.1577 | .0817 | .4027 | .3339 | −.1586 | .0789 | .3860 | .3339 | −.1595 | .0759 | .3699 |
| 7 | −.0308 | .4535 | −.2430 | | −.0308 | .4561 | −.2350 | | −.0307 | .4586 | −.2265 | |
| 8 | .0209 | .4495 | −.4530 | | .0209 | .4505 | −.4361 | | .0208 | .4502 | −.4196 | |
| 9 | .0027 | .0192 | .0739 | | .0027 | .0183 | .0749 | | .0027 | .0175 | .0759 | |
| 10 | −.0003 | .1183 | .3578 | | −.0002 | .1137 | .3621 | | −.0002 | .1089 | .3663 | |
| 11 | .0040 | .1232 | .4993 | | .0038 | .1176 | .5157 | | .0035 | .1115 | .5316 | |
| 12 | −.0006 | .0536 | .0331 | | −.0006 | .0531 | .0323 | | −.0006 | .0525 | .0313 | |
| 13 | .0047 | .3453 | .2279 | | .0049 | .3439 | .2209 | | .0050 | .3432 | .2138 | |
| 14 | −.0137 | .0560 | .2391 | | −.0137 | .0600 | .2314 | | −.0136 | .0652 | .2245 | |

TABLE 2c. $CH_2$, $^3\Sigma_g^-$, *Eigenvalues, eigenvector coefficients, and total energy*

| Internuclear separation (a.u.) | 1.8 | | | | 1.95 | | | | 2.1 | | | |
|---|---|---|---|---|---|---|---|---|---|---|---|---|
| Total energy (a.u.) | −38.8731 | | | | −38.8936 | | | | −38.8915 | | | |
| | $1\sigma_g$ | $2\sigma_g$ | $1\sigma_u$ | $\pi$ | $1\sigma_g$ | $2\sigma_g$ | $1\sigma_u$ | $\pi$ | $1\sigma_g$ | $2\sigma_g$ | $1\sigma_u$ | $\pi$ |
| Eigen value | −11.2185 | −0.8915 | −0.6886 | −0.3973 | −11.2326 | −0.8635 | −0.6520 | −0.3944 | −11.2456 | −0.8371 | −0.6183 | −0.3920 |
| Eigen vector: | | | | | | | | | | | | |
| 1 | .0012 | −.0002 | .0117 | .0136 | .0012 | −.0002 | .0109 | .0136 | .0012 | −.0002 | .0102 | .0136 |
| 2 | .0093 | −.0018 | .0652 | .0841 | .0093 | −.0018 | .0631 | .0845 | .0093 | −.0017 | .0609 | .0849 |
| 3 | .0454 | −.0087 | .2322 | .2755 | .0454 | −.0086 | .2145 | .2751 | .0454 | −.0085 | .1998 | .2759 |
| 4 | .1544 | −.0320 | .3308 | .5001 | .1545 | −.0312 | .3472 | .4954 | .1545 | −.0307 | .3501 | .4910 |
| 5 | .3583 | −.0805 | .0592 | .3617 | .3584 | −.0795 | .0628 | .3676 | .3584 | −.0786 | .0697 | .3721 |
| 6 | .4365 | −.1515 | .0835 | | .4368 | −.1472 | .0771 | | .4371 | −.1447 | .0718 | |
| 7 | .1478 | −.0562 | .4379 | | .1473 | −.0582 | .4261 | | .1469 | −.0592 | .4177 | |
| 8 | .0032 | .4975 | .3200 | | .0031 | .4974 | .3560 | | .0030 | .4947 | .3899 | |
| 9 | .0006 | .2893 | | | .0005 | .3127 | | | .0005 | .3368 | | |
| 10 | .0003 | .0590 | | | .0002 | .0534 | | | .0001 | .0487 | | |
| 11 | .0014 | .3746 | | | .0011 | .3563 | | | .0009 | .3369 | | |
| 12 | −.0005 | .1620 | | | −.0004 | .1735 | | | −.0003 | .1852 | | |

TABLE 2f. $NH_2$, $^2B_1$, *Eigenvalues, eigenvector coefficients, and total energy*

| Internuclear separation | 95° | | | | | 105° | | | | | 115° | | | | |
|---|---|---|---|---|---|---|---|---|---|---|---|---|---|---|---|
| $R_{NH}$ = 1.95(a.u.) Total energy (a.u.) | −55.4496 | | | | | −55.4537 | | | | | −55.4523 | | | | |
| | $1a_1$ | $2a_1$ | $3a_1$ | $1b_2$ | $1b_1$ | $1a_1$ | $2a_1$ | $3a_1$ | $1b_2$ | $1b_1$ | $1a_1$ | $2a_1$ | $3a_1$ | $1b_2$ | $1b_1$ |
| Eigenvalue | −15.6019 | −1.1341 | −0.4892 | −0.6149 | −0.5049 | −15.5953 | −1.1230 | −0.4709 | −0.6332 | −0.5005 | −15.5879 | −1.1128 | −0.4531 | −0.6486 | −0.4957 |
| Eigenvector: | | | | | | | | | | | | | | | |
| 1 | .0029 | −.0005 | .0003 | .0694 | .0965 | .0029 | −.0006 | .0002 | .0687 | .0962 | .0029 | −.0006 | .0002 | .0682 | .0959 |
| 2 | .0096 | −.0018 | .0008 | .3417 | .4640 | .0096 | −.0019 | .0008 | .3387 | .4622 | .0096 | −.0019 | .0007 | .3368 | .4603 |
| 3 | .0385 | −.0077 | .0036 | .3854 | .6611 | .0385 | −.0077 | .0033 | .3783 | .6628 | .0385 | −.0078 | .0031 | .3762 | .6647 |
| 4 | .1452 | −.0295 | .0133 | .0674 | | .1452 | −.0297 | .0123 | .0688 | | .1452 | −.0299 | .0113 | .0699 | |
| 5 | .3752 | −.0892 | .0423 | .4941 | | .3752 | −.0899 | .0392 | .4968 | | .3752 | −.0904 | .0360 | .4941 | |
| 6 | .5361 | −.1829 | .0841 | .3237 | | .5360 | −.1843 | .0780 | .2938 | | .5360 | −.1855 | .0717 | .2686 | |
| 7 | .0737 | .4764 | −.2295 | | | .0740 | .4799 | −.2140 | | | .0742 | .4830 | −.1969 | | |
| 8 | −.0416 | .4438 | −.3721 | | | −.0422 | .4479 | −.3473 | | | −.0424 | .4488 | −.3240 | | |
| 9 | .0018 | .0164 | .0777 | | | .0018 | .0150 | .0799 | | | .0018 | .0135 | .0819 | | |
| 10 | .0025 | .0966 | .3626 | | | .0023 | .0888 | .3717 | | | .0021 | .0808 | .3805 | | |
| 11 | −.0067 | .1126 | .5052 | | | −.0062 | .1035 | .5331 | | | −.0054 | .0930 | .5593 | | |
| 12 | .0011 | .0507 | .0413 | | | .0011 | .0496 | .0393 | | | .0012 | .0486 | .0367 | | |
| 13 | −.0027 | .2790 | .2625 | | | −.0032 | .2756 | .2428 | | | −.0039 | .2756 | .2245 | | |
| 14 | .0207 | .0223 | .2239 | | | .0215 | .0249 | .2169 | | | .0221 | .0294 | .2100 | | |

TABLE 2g. $H_2O$, $^1A_1$, *Eigenvalues, eigenvector coefficients, and total energy*

| Internuclear separation | 95° | | | | | 105° | | | | | 110° | | | | |
|---|---|---|---|---|---|---|---|---|---|---|---|---|---|---|---|
| $R_{OH}$ = 1.8 (a.u.) Total energy (a.u.) | −75.8384 | | | | | −75.8453 | | | | | −75.8450 | | | | |
| | $1a_1$ | $2a_1$ | $3a_1$ | $1b_2$ | $1b_1$ | $1a_1$ | $2a_1$ | $3a_1$ | $1b_2$ | $1b_1$ | $1a_1$ | $2a_1$ | $3a_1$ | $1b_2$ | $1b_1$ |
| Eigenvalue | −20.5836 | −1.3816 | −0.5794 | −0.6879 | −0.5048 | −20.5757 | −1.3697 | −0.5591 | −0.7061 | −0.4996 | −20.5709 | −1.3638 | −0.5490 | −0.7141 | −0.4967 |
| Eigenvector: | | | | | | | | | | | | | | | |
| 1 | .0033 | −.0007 | .0003 | .0755 | .1002 | .0033 | −.0007 | .0003 | .0745 | .0999 | .0033 | −.0007 | .0002 | .0741 | .0998 |
| 2 | .0059 | −.0011 | .0004 | .3555 | .4529 | .0059 | −.0011 | .0004 | .3517 | .4515 | .0059 | −.0011 | .0004 | .3501 | .4507 |
| 3 | .0451 | −.0095 | .0038 | .4205 | .6696 | .0451 | −.0095 | .0035 | .4122 | .6710 | .0451 | −.0096 | .0034 | .4097 | .6718 |
| 4 | .2016 | −.0433 | .0169 | .0954 | | .2016 | −.0436 | .0156 | .0982 | | .2016 | −.0437 | .0149 | .0993 | |
| 5 | .5711 | −.1601 | .0654 | .4760 | | .5711 | −.1611 | .0604 | .4759 | | .5711 | −.1614 | .0578 | .4740 | |
| 6 | .3461 | −.1675 | .0626 | .2426 | | .3461 | −.1685 | .0579 | .2189 | | .3461 | −.1689 | .0554 | .2092 | |
| 7 | −.0303 | .4886 | −.2007 | | | −.0303 | .4912 | −.1862 | | | −.0303 | .4923 | −.1785 | | |
| 8 | .0184 | .5440 | −.3502 | | | .0185 | .5476 | −.3241 | | | .0186 | .5487 | −.3116 | | |
| 9 | .0021 | .0145 | .0831 | | | .0020 | .0132 | .0854 | | | .0019 | .0125 | .0865 | | |
| 10 | $-.0000_1$ | .0820 | .3761 | | | $.0000_1$ | .0752 | .3856 | | | $.0000_2$ | .0716 | .3901 | | |
| 11 | .0026 | .1050 | .5205 | | | .0023 | .0957 | .5472 | | | .0021 | .0905 | .5594 | | |
| 12 | −.0005 | .0692 | .0627 | | | −.0005 | .0676 | .0593 | | | −.0006 | .0669 | .0573 | | |
| 13 | −.0010 | .2099 | .2769 | | | −.0006 | .2091 | .2491 | | | −.0004 | .2100 | .2371 | | |
| 14 | −.0068 | −.0138 | .1693 | | | −.0072 | −.0131 | .1668 | | | −.0073 | .0127 | .1650 | | |

TABLE 2h. $H_2O^+$, $^2B_1$: *Eigenvalues, eigenvector coefficients, and total energy*

| Internuclear separation | 105° | | | | | 115° | | | | | 125° | | | | |
|---|---|---|---|---|---|---|---|---|---|---|---|---|---|---|---|
| $R_{OH}$=1.9 (a.u.) Total energy (a.u.) | −75.4427 | | | | | −75.4465 | | | | | −75.4462 | | | | |
| | $1a_1$ | $2a_1$ | $3a_1$ | $1b_2$ | $1b_1$ | $1a_1$ | $2a_1$ | $3a_1$ | $1b_2$ | $1b_1$ | $1a_1$ | $2a_1$ | $3a_1$ | $1b_2$ | $1b_1$ |
| Eigenvalue | −21.1628 | −1.8434 | −1.0539 | −1.1732 | −1.1154 | −21.1536 | −1.8323 | −1.0372 | −1.1859 | −1.1096 | −21.1437 | −1.8214 | −1.0211 | −1.1964 | −1.1032 |
| Eigenvector: | | | | | | | | | | | | | | | |
| 1 | .0033 | −.0007 | .0002 | .0841 | .1080 | .0033 | −.0007 | .0002 | .0832 | .1077 | .0033 | −.0007 | .0002 | .0825 | .1074 |
| 2 | .0059 | −.0012 | .0004 | .4009 | .5135 | .0059 | −.0012 | .0003 | .3964 | .5119 | .0059 | −.0012 | .0003 | .3925 | .5102 |
| 3 | .0451 | −.0100 | .0033 | .4721 | .6087 | .0451 | −.0100 | .0029 | .4720 | .6103 | .0451 | −.0100 | .0026 | .4754 | .6122 |
| 4 | .2016 | −.0456 | .0149 | .0607 | | .2016 | −.0458 | .0134 | .0624 | | .2016 | −.0460 | .0119 | .0639 | |
| 5 | .5713 | −.1686 | .0563 | .4126 | | .5713 | −.1693 | .0508 | .4067 | | .5713 | −.1699 | .0449 | .3965 | |
| 6 | .3460 | −.1781 | .0594 | .0951 | | .3460 | −.1790 | .0537 | .0850 | | .3461 | −.1799 | .0475 | .0762 | |
| 7 | −.0303 | .5395 | −.2030 | | | −.0303 | .5424 | −.1837 | | | −.0303 | .5449 | −.1625 | | |
| 8 | .0177 | .5581 | −.2063 | | | .0178 | .5597 | −.1866 | | | .0179 | .5604 | −.1665 | | |
| 9 | .0019 | .0139 | .0939 | | | .0018 | .0125 | .0960 | | | .0017 | .0109 | .0980 | | |
| 10 | $-.0000_4$ | .0775 | .4339 | | | $-.0000_2$ | .0701 | .4435 | | | $.0000_1$ | .0620 | .4527 | | |
| 11 | .0022 | .1084 | .5537 | | | .0019 | .0962 | .5699 | | | .0016 | .0832 | .5849 | | |
| 12 | −.0007 | .0409 | .0382 | | | −.0007 | .0398 | .3500 | | | −.0008 | .0388 | .0312 | | |
| 13 | −.0002 | .1890 | .2065 | | | .0002 | .1912 | .1867 | | | .0005 | .1947 | .1667 | | |
| 14 | −.0070 | −.0438 | .0909 | | | −.0073 | −.0437 | .0843 | | | −.0075 | .0430 | .0769 | | |

TABLE 2i. $H_3$, $^2\Sigma_u^+$: *Eigenvalues, eigenvector coefficients, and total energy*

| Internuclear separation (a.u.) | 1.5 | | 1.6 | | 1.7 | | 1.8 | | 1.9 | |
|---|---|---|---|---|---|---|---|---|---|---|
| Total energy (a.u.) | −1.58123 | | −1.58975 | | −1.59296 | | −1.59215 | | −1.58829 | |
| | $1\sigma_g$ | $1\sigma_u$ | $1\sigma_g$ | $1\sigma_u$ | $1\sigma_g$ | $1\sigma_u$ | $1\sigma_g$ | $1\sigma_u$ | $1\sigma_g$ | $1\sigma_u$ |
| Eigenvalue | −.70835 | −0.36524 | −0.67876 | −0.37499 | −0.65241 | −0.38284 | −0.62878 | −0.38910 | −0.60745 | −0.39403 |
| Eigenvector: | | | | | | | | | | |
| 1 | −.04341 | .05451 | −.04188 | .04980 | −.04055 | .04621 | −.03938 | .04344 | −.03831 | .04128 |
| 2 | .01194 | .01112 | .01153 | .00482 | .01117 | −.00029 | .01085 | −.00451 | .01056 | −.00804 |
| 3 | .06917 | .01508 | .06607 | .01494 | .06344 | .01478 | .06119 | .01461 | .05928 | .01445 |
| 4 | .24285 | .09069 | .23591 | .08995 | .22943 | .08913 | .22333 | .08823 | .21755 | .08725 |
| 5 | .32236 | .32523 | .32278 | .32481 | .32360 | .32275 | .32468 | .31985 | .32582 | .31658 |
| 6 | .12731 | .62984 | .14340 | .62627 | .15885 | .62148 | .17377 | .61579 | .18825 | .60939 |
| 7 | .00861 | .90347 | .00829 | .84821 | .00801 | .80637 | .00775 | .77481 | .00752 | .75126 |
| 8 | .05011 | | .04812 | | .04643 | | .04492 | | .04353 | |
| 9 | .17421 | | .16811 | | .16253 | | .15750 | | .15299 | |
| 10 | .24290 | | .24758 | | .25009 | | .25088 | | .25039 | |
| 11 | .11472 | | .12665 | | .13898 | | .15150 | | .16406 | |

TABLE 3. *Summary of results*

| | $R_e$(a.u.) | | $E_e$(a.u.) |
|---|---|---|---|
| | Calculated | Experimental | |
| $BH_4^-$ | 2.35 | [a] 2.37 | −26.946 |
| $CH_4$ | 2.05 | [b] 2.062 | −40.167 |
| $NH_4^+$ | 1.94 | [c] 1.95 | −56.504 |
| $CH_2$, $^3\Sigma^-_g$ | 2.01 | [d] 1.95 | −38.889 |
| $H_3$ | 1.73 | | −1.593 |

| | $R$ | $\theta_e$ | | |
|---|---|---|---|---|
| | | Calculated | Experimental | |
| $CH_2$, $^1A_1$ | 2.1 | 105°27′ | [d] 103° | −38.803 |
| $NH_2$ | 1.95 | 107°29′ | [e] 103°23′ | −55.454 |
| $H_2O$ | 1.8 | 106°56′ | [f] 104°27′ | −75.845 |
| $H_2O^+$ | 1.9 | 119°23′ | | −75.447 |

[a] P. T. Ford and R. E. Richards, Disc. Faraday Soc. **19,** 230 (1955).
[b] D. P. Stevenson and J. A. Ibers, J. Chem. Phys. **33,** 762 (1960).
[c] H. S. Gutowski, G. E. Pake, and R. Bersohn, J. Chem. Phys. **22,** 643 (1954).
[d] G. Herzberg, Proc. Roy. Soc. (London) **A262,** 291 (1961).
[e] K. Dressler and D. Ramsay, Phil. Trans. Roy. Soc. (London) **A251,** 552 (1959).
[f] G. Herzberg, Infrared and Raman Spectra (D. Van Nostrand Co., New York, 1945), p. 488.

TABLE 4. *Deduction of bound to correlation energy (a.u.)*

| | $BH_4^-$ | $CH_2$, $^3\Sigma^-_g$ | $H_3$ |
|---|---|---|---|
| Calculated Hartree-Fock approximation | −26.946 | −38.895 | −1.593 |
| Heat of atomization | [a] −.550 | [b] −.283 | [c] −.154, [f] −.151 |
| Zero point energy | [a] −.034 | −.02 | [d] −.009 |
| Energy of separated atoms | −26.680 | −38.855 | −1.5 |
| Relativistic correction | [e] −.005 | [e] −.012 | |
| Hartree-Fock energy for separated atoms | −26.529 | −38.689 | −1.499 |
| Hartree-Fock heat of atomization+zero-point energy | −.417 | −.200 | −.094 |
| Upper limit to molecular correlation energy | −.319 | −.28 | −.070, −.067 |

[a] A. P. Altshuller, J. Am. Chem. Soc. **77,** 5455 (1955).
[b] H. Prophet, J. Chem. Phys. **38,** 2345 (1963).
[c] A. Farkas and L. Farkas, Proc. Roy. Soc. **A152,** 124 (1935).
[d] I. Shavitt, J. Chem. Phys. **31,** 1359 (1959).
[e] C. W. Scherr, J. N. Silverman, and F. A. Matsen, Phys. Rev. **128,** 2675 (1962).
[f] R. E. Weston, J. Chem. Phys. **31,** 892 (1959).

TABLE 5. *Partition of molecular energy,* $-\epsilon_i$

| Orbital | $1a_1$ | $2a_1$ | $3a_1$ | $1b_2$ | $1b_1$ |
|---|---|---|---|---|---|
| $H_2O$, $R$=1.7 | | | | | |
| 105° | 53.6388 | 9.3362 | 7.5375 | 7.4739 | 7.6305 |
| 115° | 53.6302 | 9.3115 | 7.5286 | 7.5075 | 7.6183 |
| 125° | 53.6209 | 9.2866 | 7.5233 | 7.5389 | 7.6050 |
| 135° | 53.6111 | 9.2623 | 7.5231 | 7.5669 | 7.5910 |
| $H_2O$, $R$=1.8 | | | | | |
| 95° | 53.5918 | 9.2388 | 7.4249 | 7.2463 | 7.6022 |
| 105° | 53.5838 | 9.2185 | 7.4223 | 7.2693 | 7.5904 |
| 115° | 53.5742 | 9.1965 | 7.4209 | 7.2940 | 7.5767 |
| 125° | 53.5638 | 9.1734 | 7.4241 | 7.3178 | 7.5618 |
| 135° | 53.5525 | 9.1501 | 7.4329 | 7.3391 | 7.5455 |
| 150° | 53.5351 | 9.1162 | 7.4559 | 7.3642 | 7.5205 |
| $H_2O$, $R$=2 | | | | | |
| 105° | 53.4903 | 9.0432 | 7.1825 | 6.9110 | 7.5232 |
| 115° | 53.4797 | 9.0243 | 7.1972 | 6.9198 | 7.5080 |
| 125° | 53.4674 | 9.0030 | 7.2169 | 6.9295 | 7.4905 |
| 135° | 53.4531 | 8.9792 | 7.2449 | 6.9373 | 7.4702 |
| 150° | 53.4299 | 8.9413 | 7.3034 | 6.9435 | 7.4369 |
| $NH_2$, $R$=1.95 | | | | | |
| 95° | 41.0537 | 7.2882 | 5.8303 | 5.7860 | 6.0372 |
| 105° | 41.0469 | 7.2651 | 5.8117 | 5.8195 | 6.0264 |
| 115° | 41.0395 | 7.2420 | 5.7955 | 5.8515 | 6.0146 |
| $CH_2$, $R$=2.1 | | | | | |
| 90° | 30.1910 | 5.6279 | 4.4646 | 4.5631 | |
| 100° | 30.1860 | 5.5980 | 4.4390 | 4.6038 | |
| 105° | 30.1836 | 5.5837 | 4.4267 | 4.6229 | |
| 110° | 30.1810 | 5.5700 | 4.4148 | 4.6412 | |

## 3. Discussion

It is evident that the approximate Gaussian calculations are adequate for the determination of the molecular geometries of first-row hydrides. The greatest discrepancy between the calculated and experimental equilibrium angles is about 5° and the largest error in the equilibrium internuclear separation is 0.05 a.u. This accuracy is of the order of that reported in reference 5, although a more accurate SCF result for $H_2O$ presented by Moccia yields slightly better agreement between the calculated and experimental angle.

The success of the numerical experimentation permits confidence to be placed in the predicted angle for $H_2O^+$, a rather large 119°. This value is totally unexpected from the presumed nonbonding character of the $1b_1$ orbital. Experimental evidence is ambiguous. The

first Rydberg excited state of $H_2O$ has been analyzed (18). Only a small change in angle was observed but it was accompanied by an appreciable increase in the O–H distance. It is usually assumed that the first member of an *np* Rydberg series does not penetrate the core and influence the bonding, but this is not certain.

From Koopman's theorem the vertical ionization potential for $H_2O$, 0.465 a.u., is approximated by the orbital energy 0.500 a.u. However, as noted by Clementi (19), the ionization potential is given by

$$I=-\epsilon-E^+_{RE}+(E_c-E^+_c)+(E_R-E^+_R)+E_{\text{vert}},$$

where $E^+_{RE}$ is the reorganization energy in computing the SCF energy of the ion, $(E_c-E^+_c)$ is the difference in correlation energies between the neutral and ionic species, $(E_R-E^+_R)$ is the difference in relativistic energies between the neutral and ionic species, and $E_{\text{vert}}$ is the internal energy of the ion attendant upon a vertical transition.

$(E_R-E^+_R)$ is very close to zero and for our purposes we shall assume that $E_{\text{vert}}$ is also small enough to be neglected. Then the change in correlation energy can be determined from $E^+_{RE}$, which is approximately $-0.100$ a.u., to be about $-0.065$ a.u. This result is in good agreement with Clementi's [20] estimate of $-0.074$ a.u. for the correlation energy of a pair. In fact, if we use a better estimate of the $CH_4$ correlation energy [21], the correlation energy per bonding pair in $CH_4$ is about $-0.067$ a.u. or less. The fortuitous cancellation of the reorganization energy and the change in correlation energy is the basis for the success of the application of Koopman's theorem to the prediction of ionization potentials.

The results for $H_2O$ were obtained with SCF calculations some 2 eV higher than those reported by Moccia and some 6.5 eV from the Hartree-Fock limit estimated by Moccia. Agreement of estimated and computed pair correlation energies must be considered in this light.

The results for $H_3$ are the most accurate of all those reported. The asymptotic error for three H atoms computed with a five *S*-type Gaussian basis is 0.02 eV and the error in the molecule is probably less than 0.05 eV. Addition of another *p*-type Gaussian improved the total molecular energy by less than 0.01 eV.

Unfortunately, the Hartree-Fock $H_3$ surface is of little value for understanding the kinetics of the $H+H_2$ system since a radical reaction is primarily a correlation problem. There are also complications due to the inaccurate asymptotic behavior of the molecular orbitals. An estimate of the correlation energy cannot be made from the isoelectronic atoms; the intershell correlation is much larger in $H_3$ than in Li due to the appreciable differential overlap in the molecule.

The results for $BH_4^-$ are analogous to those reported for $CH_4$ and $NH_4^+$ and little can be added to the discussion of $BH_4^-$. It should be noted, though, that the experimental heat of atomization is not accurately known and there is a corresponding uncertainty in the bound for the molecular correlation energy.

Evidently, the accuracy for the $^3\Sigma_g^-$ state of $CH_2$ is not comparable to that for the tetrahedral molecules or $H_3$. This is evidenced by the large correlation energy limit in table 4. Although the heat of atomization reported for $CH_2$ may still be too high, the calculated internuclear separation indicates the SCF result for $CH_2$ is still appreciably above the Hartree-Fock limit. For strongly bonded molecules, it would be expected that most excited configurations required to represent the exact function would have larger equilibrium internuclear separations. The Hartree-Fock equilibrium internuclear separation, therefore, should be smaller than the experimental value. The inadequacy of the Gaussian basis for $CH_2$ can be attributed to two main defects: (1) no variation of the orbital exponents was attempted, and (2) *p*-type functions are required on the H atoms.

The final comment is in many ways the most important. A comparison of table 5 with the similar data presented by Coulson and Neilson shows how ill-founded was their expectation that improved molecular wavefunctions would not change their results qualitatively. The behavior of $\epsilon_{3a1}$ in the neighborhood of 105° is not at all similar to that exhibited by the curve for $3_{a1}$ in figure 3 of reference 3. There is little point in examining the differences in detail;

we only need to note that the partitioned energies $e_i$ reflect the influence of the other orbitals in such a way as to render a simple interpretation of these quantities very difficult. The most striking evidence of this effect is the large variation in the $e_{1a1}$ and $e_{1b1}$ even though these molecular orbitals vary only slightly with angle. There is little support for a one-electron type partition of the total energy from the present results.

---

I thank Dr. S. Huzinaga for furnishing me with details of the accurate atom results he has obtained with Gaussian bases. I am also grateful to the Computer Science Center of the University of Maryland for permitting the use of their facilities.

## 4. References

[1] A. D. Walsh, J. Chem. Soc. **1953,** 2260.
[2] R. Hoffmann, J. Chem. Phys. **39,** 1397 (1963).
[3] C. A. Coulson and A. H. Neilson, Discussions Faraday Soc. **35,** 71 (1963).
[4] R. K. Nesbet, Rev. Mod. Phys. **35,** 552 (1963).
[5] Approximate Hartree-Fock calculations of S. Fraga and B. J. Ransil, J. Chem. Phys. **35,** 669 (1961); more accurate results: HF, R. K. Nesbet, J. Chem. Phys. **36,** 1518 (1962); $H_2$ and LiF, A. D. McLean, J. Chem. Phys. **40,** 243 (1964).
[6] R. E. Stanton, J. Chem. Phys. **36,** 1298 (1962); See criticism of this paper by McLean in ref. 5.
[7] J. Higuchi, J. Chem. Phys. **24,** 535 (1956).
[8] F. O. Ellison and H. Shull, J. Chem. Phys. **23,** 2348 (1955).
[9] M. Krauss and A. Padgett, J. Chem. Phys. **32,** 189 (1960).
[10] J. M. Foster and S. F. Boys, Rev. Mod. Phys. **32,** 305 (1960).
[11] R. Moccia, J. Chem. Phys. **40,** 2186 (1964).
[12] M. Krauss, J. Chem. Phys. **38,** 564 (1963).
[13] M. C. Harrison, Quarterly Progress Report, Solid-State and Molecular Theory Group, MIT, October 15, 1963, p. 20.
[14] C. C. J. Roothaan, Rev. Mod. Phys. **32,** 179 (1960).
[15] M. Krauss, J. Research NBS **68B** (Math and Math. Phys.), No. 1, 35 (1964).
[16] J. V. L. Longstaff and K. Singer, **A258,** 421 (1960).
[17] S. Huzinaga, private communication.
[18] J. W. C. Johns, Can. J. Phys. **41,** 209 (1963).
[19] E. Clementi, J. Chem. Phys. **36,** 33 (1962).
[20] E. Clementi, J. Chem. Phys. **38,** 2780 (1963); J. Chem. Phys. **39,** 487 (1963).
[21] B. J. Woznick, J. Chem. Phys. **40,** 2860 (1964).

(Paper 68A6–312)

JOURNAL OF RESEARCH of the National Bureau of Standards—A. Physics and Chemistry
Vol. 68A, No. 6, November–December 1964

# Preparation and Heat of Formation of a Magnesium Oxysulfate

E. S. Newman

(June 10, 1964)

Magnesium oxysulfate, $3Mg(OH)_2 \cdot MgSO_4 \cdot 8H_2O$, was precipitated from metastable aqueous solutions of MgO in $MgSO_4$. The compound forms in solutions containing 12 percent or more of $MgSO_4$, and remains unchanged in solutions containing 10 percent $MgSO_4$, but at lower concentrations is converted to $Mg(OH)_2$. Magnesium hydroxide is not converted to the oxysulfate by nearly saturated $MgSO_4$ solutions in times up to three years. The solubility of the oxysulfate is given in the form of a plot of the basicity and $MgSO_4$ content of magnesium sulfate solutions. The heat of solution of the oxysulfate compound in $HCl \cdot 26.61H_2O$ (2.000 normal at 25 °C) is 68.94 kcal/mole with a standard deviation of 0.23 kcal/mole and its heat of formation from $Mg(OH)_2$, $MgSO_4 \cdot 7H_2O$, and liquid water is $\Delta H = 2.11$ kcal/mole. The corresponding heat of formation from the elements is $\Delta H_f = -1537.9$ kcal/mole.

## 1. Introduction

Magnesium oxychloride and magnesium oxysulfate cements have long been known and used for a variety of purposes, for example as binders in flooring or in insulating materials. In 1952 Newman, Gilfrich, and Wells [1],[1] and in 1955 Newman [2], published the results of thermochemical studies of the system $MgO\text{-}MgCl_2\text{-}H_2O$ at 25 °C. The present paper presents a similar study of the system $MgO\text{-}MgSO_4\text{-}H_2O$ at 25 °C.

In 1957 Demediuk and Cole [3] reviewed the previous work on the system $MgO\text{-}MgSO_4\text{-}H_2O$. In addition, they studied the reactions occurring in the system at $MgSO_4$ concentrations up to saturation and at temperatures from 30 to 120 °C. Four oxysulfates, $5Mg(OH)_2 \cdot MgSO_4 \cdot 3$ or $2H_2O$, $3Mg(OH)_2 \cdot MgSO_4 \cdot 8H_2O$, $Mg(OH)_2 \cdot MgSO_4 \cdot 5H_2O$, and $Mg(OH)_2 \cdot 2MgSO_4 \cdot 3H_2O$ were found, and a diagram was presented showing the conditions of stability of each. Only $3Mg(OH)_2 \cdot MgSO_4 \cdot 8H_2O$, hereafter referred to as the 3:1:8 compound, was found at temperatures below about 35 °C. X-ray powder diffraction patterns of each of the compounds were given.

Recently Adomaviciute and coworkers [4] reported the formula $3Mg(OH)_2 \cdot 2MgSO_4 \cdot 5H_2O$ for the only oxysulfate formed at 20 ±2 °C. These workers gave x-ray patterns also and differential thermal analyses (DTA's), as well as curves showing the solubility of the compound (expressed as grams of titratable MgO per liter) in magnesium sulfate solutions of various concentrations. They found $Mg(OH)_2$ in hardened magnesian cement and, from x-ray and DTA data, suggested the possibility that the formation of oxysulfate occurs in cements only above a $MgSO_4/MgO$ ratio of 0.6.

No thermochemical data for the oxysulfates have been found in the literature. In the present work, only the 3:1:8 compound was found at room temperature, and this paper is concerned with its preparation and the determination of its heat of formation. The heat of reaction of $Mg(OH)_2$, $MgSO_4 \cdot 7H_2O$, and $H_2O$ to form the compound was determined from the heats of solution or dilution of these reactants and of the compound in $HCl \cdot 26.61H_2O$ (2.000$N$ at 25 °C), and the heat of formation was calculated from this heat of reaction and heats of formation taken from the literature [5].

## 2. Materials, Apparatus, and Procedure

### 2.1. Formation of the 3:1:8 Compound

The compound was prepared by precipitation from metastable solutions of MgO in concentrated solutions of $MgSO_4$, or by reaction of the latter with solid MgO. Concentrated aqueous solutions were prepared from distilled water and $MgSO_4 \cdot 7H_2O$ of reagent quality. In some cases the solutions were boiled to remove $CO_2$ and cooled, protected by a $CO_2$ absorption tube, but this procedure was found unnecessary and discontinued. Generally 4 liters of nearly saturated solution was used. Clear metastable solutions of MgO were prepared by shaking the $MgSO_4$ solutions with 30 g of reagent-grade MgO freshly heated at 500 °C. After about 2 hr at room temperature the solutions were filtered and allowed to stand. Precipitation of the 3:1:8 compound began in a few hours and continued slowly for 10 days or more. These concentrated, rather viscous solutions

[1] Figures in brackets indicate the literature references at the end of this paper.

of $MgSO_4$ were slow and difficult to filter and usually retained a few milligrams of material as a hazy suspension. Consequently, and also in order to encourage the formation of larger crystals, less MgO was used (usually 4 g and occasionally as little as 1.5 g), filtration was omitted, the solution was sometimes seeded, and the suspension was stirred continuously with a magnetic stirrer for periods up to two weeks. The precipitate, which in every case gave the x-ray pattern of the 3:1:8 compound, was recovered by filtration, suspended by stirring in methanol, refiltered and washed with more methanol, and dried at room temperature at about 20 mm Hg pressure in vacuum desiccators over saturated $MgCl_2 \cdot 6H_2O$ or $MgSO_4 \cdot 7H_2O$ solution. The former solution maintains air at a relative humidity of 33 percent; the humidity over the latter solution is much higher.

Reagent-quality $MgSO_4 \cdot 7H_2O$ was recrystallized, washed briefly with methanol, crushed to pass a No. 16 sieve, and stored in 1-g quantities in weighing bottles in partial vacuum over saturated $MgSO_4 \cdot 7H_2O$ solution. When the samples reached constant weight, their heats of solution were determined in 2.000 *N* HCl.

### 2.2. Determination of Solubility

In order to obtain information about the solubility and stability of the 3:1:8 compound in $MgSO_4$ solutions at 25 °C, solubility equilibrium was sought from both super- and under-saturation. Several groups of three series of solutions of $MgSO_4$ of differing concentrations were prepared and kept in 1-liter polyethylene bottles as: A, clear unstable solutions of MgO; B, suspensions of 2 g of $Mg(OH)_2$; and C, suspensions of 3:1:8 oxysulfate. The A series was intended to approach equilibrium from supersaturation, and the B and C series, with originally zero concentration of titratable MgO, to approach from under-saturation. These bottles were shaken by hand periodically, and the tests were continued for several years. Later, the three series were prepared and kept in continuous gentle agitation for as long as two years on a 20-in. wheel rotating at about 15 rpm. From time to time the bottles were removed from the wheel and allowed to stand quiescent overnight. Samples of the clear supernatant liquid were taken for titration with standard HCl solution and phenolphthalein indicator, and the solid phases present were examined under a microscope and by x-ray patterns. The basicity obtained by titration was calculated and reported as grams of MgO per liter. When it became evident that little further change in basicity was likely to occur, the solid was recovered by filtration, washed with methanol, and dried at 33 percent rh. X-ray patterns and analysis of some of these precipitates were obtained.

### 2.3. Analyses of Precipitates

In the beginning, analyses were performed by standard methods [6, 7], $SO_3$ being determined by precipitating and weighing as $BaSO_4$, and MgO being determined gravimetrically by the pyrophosphate method. It was found that the $CO_2$, $SiO_2$, $Fe_2O_3+Al_2O_3$ etc., and CaO found by the usual procedures differed little from the blank determinations and were sometimes smaller. Consequently, in the later part of the work $SO_3$ was determined gravimetrically as before, and total MgO was determined as the residue when the sample was ignited to 1200 °C. Tests showed that the results obtained agreed with those obtained by the pyrophosphate method and that $SO_3$ was absent in such heated residues, confirming the work of Schnitzer, Wright, and Hoffman [8] and the results of DTA's showing decomposition of $MgSO_4$ at 1135 °C. The water content was determined by difference. For the later samples to be used in the calorimeter, the material to be analyzed was divided into 0.5-g, 1-g, and 2-g portions in weighing bottles. These samples were equilibrated over $MgSO_4$ or $MgCl_2$ solutions, as described earlier, and weighted periodically. When the weights became essentially constant, the two smaller sized samples were used for analysis, and heat-of-solution determinations of the 2-g samples were begun. Periodic weighing of calorimeter samples was continued until the heat of solution was measured, and the water content at that time calculated from the weight record and the analytical results. In some cases, calorimeter samples which had been held, together with the analytical samples, over one saturated solution were transferred to the in order to change the water content. Earlier calorimeter samples were simply weighed out from a stock bottle of oxysulfate that had been equilibrated at 33 percent rh and analyzed.

### 2.4. Differential Thermal Analyses

Differential thermal analyses were performed with apparatus described elsewhere [9]. Samples of about 0.5 g were used, with alumina as the inert reference material, and a heating rate of about 12 deg/min was maintained. Temperatures of about 1250 °C were reached.

### 2.5. Calorimetric Measurements

Heats of solution were obtained with an isothermal-jacket platinum calorimeter described elsewhere [10]. The electrical-energy equivalent of the calorimeter was determined using instruments calibrated by the Electrical Division of the National Bureau of Standards, the time of heating being controlled by a relay activated by the standard seconds signal. Heats of solution are reported in thermochemical calories of 4.1840 absolute joules. In order to determine the effect of gross changes in the water content of the 3:1:8 oxysulfate on its heat of solution, samples were heated or otherwise dehydrated to various extents and their heats of solution determined. X-ray patterns of some of these partially dehydrated samples were obtained.

## 3. Results and Discussion

### 3.1. Formation and Solubility of the 3:1:8 Oxysulfate

Figure 1 shows, expressed as grams of MgO per liter, the basicity of metastable solutions obtained by shaking MgO for 2 hr with $MgSO_4$ solutions of various strengths. Two hours is about the optimum shaking time for these conditions, since the oxysulfate begins to precipitate soon thereafter. From these solutions this compound was formed in every case if the concentration equaled or exceeded 15 percent of $MgSO_4$. In more dilute solutions, only $Mg(OH)_2$ was formed.

Figure 2 shows the change of concentration of titratable MgO with time for typical solutions of the A, B, and C series. The concentrations for the A series, at first rather high, decreased as the oxysulfate was precipitated. The curves given by Adomaviciute et al., [4] are quite similar. The concentration of MgO in the B and C series rose rapidly from zero initially to a value dependent on the $MgSO_4$ concentration, near which it remained thereafter. These values were approximately those finally reached after longer times by the solutions of the A series.

In figure 3 are plotted the MgO concentrations obtained at 8 months for A, B, and C series kept on the wheel for the full time, plotted as a function of the $MgSO_4$ concentration of the solution (given as percentage $MgSO_4 \cdot 7H_2O$). The scatter of the points was not reduced by longer times. This figure is not a true equilibrium diagram, since x-ray patterns showed that, for instance, $Mg(OH)_2$ remained unchanged even at $MgSO_4 \cdot 7H_2O$ concentrations up to 50 percent where the 3:1:8 compound was precipitated from the A (unstable solution) series, while the oxysulfate remained unchanged in a 20 percent solution although it would not form in solutions containing less than 25 percent.

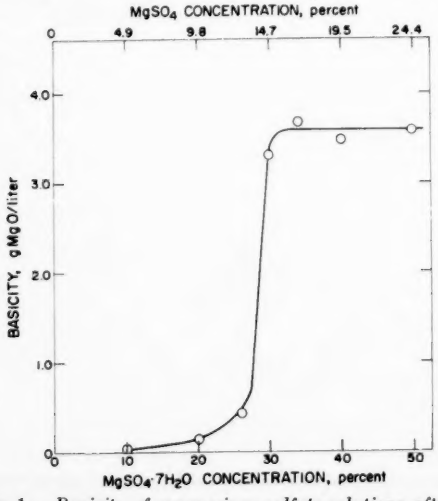


FIGURE 1. *Basicity of magnesium sulfate solutions after 2-hr shaking with an excess of freshly calcined* MgO.

Also plotted in figure 3 are the 6-month results obtained by Adomaviciute et al. [4], at 20±2 °C. These values are generally somewhat lower than the results found in the present work, as might be expected because of the lower temperature. The Russian work is equivalent to the A series of the present investigation. The vertical lines in figure 3 marked "A, 25 °C" and "A, 20 °C" represent the saturation limit of $MgSO_4 \cdot 7H_2O$ [11]. The Russian workers remark on the presence of crystals of this compound in their more concentrated solutions.

It must be pointed out that in the present work only the 3:1:8 oxysulfate and $Mg(OH)_2$ were found to form, while the Russian authors report the composition of the oxysulfate as $3Mg(OH)_2 \cdot 2MgSO_4 \cdot 5H_2O$.

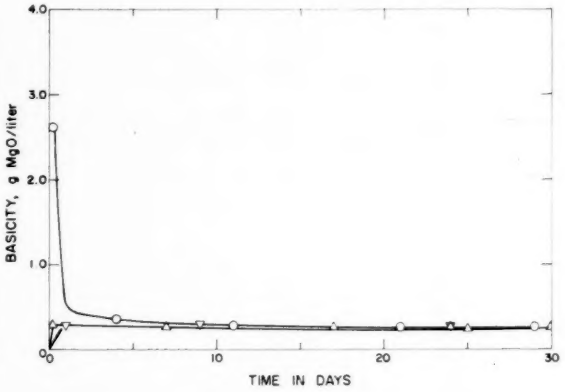


FIGURE 2. *Basicity of magnesium sulfate solutions.*

Concentration of $MgSO_4 \cdot 7H_2O$, 50 percent.
⊙A series, metastable solutions of MgO in $MgSO_4$ solution. No initial solid phase.
△B series, initial solid phase, $Mg(OH)_2$.
▽C series, initial solid phase, $3Mg(OH)_2 \cdot MgSO_4 \cdot 8H_2O$.

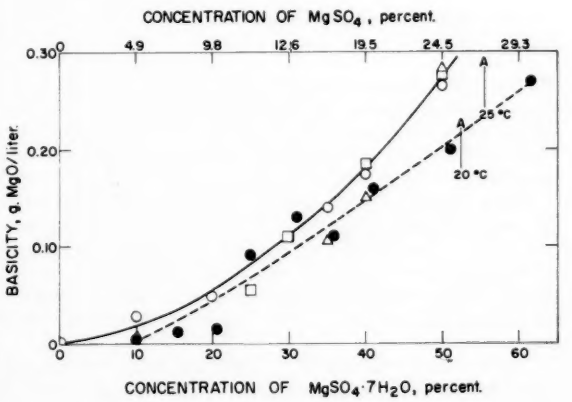


FIGURE 3. *Basicity of magnesium sulfate solutions after 8-months agitation.*

□A series, metastable solution of MgO in $MgSO_4$ aqueous solution. No initial solid phase.
△B series, initial solid phase $Mg(OH)_2$.
▽C series, initial solid phase $3Mg(OH)_2 \cdot MgSO_4 \cdot 8H_2$).
●Data of Adomaviciute, Yanikii, and Vektaris [4]. Lines marked A–20 °C and A–25 °C mark the limit of solubility of $MgSO_4 \cdot 7H_2O$.

TABLE 1. *Heats of solution of magnesium oxysulfate preparations in* HCl·*26.61* $H_2O$

| No. | Composition | | | Molar ratios | | Heat of solution |
|---|---|---|---|---|---|---|
| | MgO | $SO_3$ | $H_2O$ | $MgO/SO_3$ | $H_2O/SO_3$ | |
| | % | % | % | | | J/g |
| 1 | 36.47 | 19.15 | 44.38 | 3.782 | 10.30 | 656.39 |
| | 36.47 | 19.15 | 44.38 | 3.782 | 10.30 | 655.76 |
| 2 | 37.46 | 18.55 | 43.99 | 4.010 | 10.54 | 669.11 |
| | 37.46 | 18.55 | 43.99 | 4.010 | 10.54 | 670.70 |
| | 37.46 | 18.55 | 43.99 | 4.010 | 10.54 | 669.65 |
| | 37.46 | 18.55 | 43.99 | 4.010 | 10.54 | 669.61 |
| | 37.46 | 18.55 | 43.99 | 4.010 | 10.54 | 669.15 |
| 3 | 35.47 | 19.30 | 45.23 | 3.650 | 10.42 | 603.00 |
| | 35.47 | 19.30 | 45.23 | 3.650 | 10.42 | 604.04 |
| | 35.47 | 19.30 | 45.23 | 3.650 | 10.42 | 605.17 |
| 4 | 33.49 | 19.56 | 46.95 | 3.400 | 10.67 | 549.61 |
| | 33.65 | 19.65 | 46.70 | 3.400 | 10.56 | 541.79 |
| | 33.23 | 19.40 | 47.37 | 3.401 | 10.85 | 546.39 |
| | 33.17 | 19.37 | 47.46 | 3.400 | 10.89 | 548.23 |
| 5 | 36.44 | 18.60 | 44.96 | 3.890 | 10.74 | 647.68 |
| | 36.43 | 18.60 | 44.97 | 3.890 | 10.74 | 646.09 |
| | 36.44 | 18.60 | 44.96 | 3.889 | 10.74 | 646.01 |
| 6 | 35.98 | 18.66 | 45.36 | 3.829 | 10.80 | 641.45 |
| | 35.98 | 18.66 | 45.36 | 3.829 | 10.80 | 642.45 |
| | 35.98 | 18.66 | 45.36 | 3.829 | 10.80 | 640.36 |
| 7 | 36.82 | 18.39 | 44.79 | 3.976 | 10.82 | 654.88 |
| | 36.82 | 18.39 | 44.79 | 3.976 | 10.82 | 655.47 |
| 8 | 36.82 | 18.41 | 44.77 | 3.971 | 10.81 | 655.47 |
| 9 | 36.94 | 18.47 | 44.89 | 3.969 | 10.80 | 656.80 |
| | 36.72 | 18.37 | 44.91 | 3.969 | 10.87 | 656.68 |
| 10 | 36.62 | 18.43 | 44.95 | 3.947 | 10.84 | 653.29 |
| | 36.44 | 18.33 | 45.23 | 3.947 | 10.97 | 650.28 |
| | 36.59 | 18.41 | 45.00 | 3.946 | 10.86 | 652.75 |
| | 36.62 | 18.43 | 44.95 | 3.947 | 10.84 | 651.70 |
| | 36.62 | 18.42 | 44.96 | 3.946 | 10.85 | 652.79 |
| | 36.39 | 18.31 | 45.30 | 3.947 | 11.00 | 645.93 |
| | 36.40 | 18.31 | 45.29 | 3.937 | 10.99 | 646.60 |
| | 36.58 | 18.40 | 45.02 | 3.947 | 10.87 | 651.83 |
| | 36.41 | 18.32 | 45.27 | 3.946 | 10.99 | 644.75 |
| 11 | 36.74 | 18.52 | 44.74 | 3.939 | 10.73 | 651.62 |
| | 36.70 | 18.50 | 44.80 | 3.939 | 10.76 | 650.95 |
| | 36.71 | 18.50 | 44.79 | 3.939 | 10.76 | 652.70 |
| | 36.77 | 18.54 | 44.69 | 3.939 | 10.71 | 652.58 |
| | 35.37 | 18.33 | 45.30 | 3.939 | 10.98 | 643.08 |
| | 36.39 | 18.35 | 45.26 | 3.938 | 10.96 | 644.46 |
| | 36.37 | 18.33 | 45.30 | 3.939 | 10.98 | 642.29 |
| | 36.33 | 18.31 | 45.36 | 3.939 | 11.01 | 645.34 |
| | 36.30 | 18.30 | 45.40 | 3.939 | 11.03 | 645.84 |
| | 36.29 | 18.29 | 45.42 | 3.939 | 11.03 | 643.46 |
| | 36.50 | 18.50 | 44.80 | 3.939 | 10.76 | 652.49 |

The present author believes this disagreement to be due to the differing methods of recovering the precipitated oxysulfate. Adomaviciute and coworkers first dried their preparations at a temperature not exceeding 100 °C, *then* washed with methanol, and redried to constant weight. They comment on the incomplete removal of $MgSO_4$ due to incomplete washing. Demediuk and Cole [3] warn that magnesium sulfate hydrates containing less than seven molecules of water are difficultly soluble in methanol and used a procedure designed to avoid their formation.

Magnesium sulfate heptahydrate loses four molecules of water when heated to 106 °C [12], and at temperatures above 68 °C the monohydrate is the stable phase in contact with solution [11]. The 3 : 1 : 8 oxysulfate was found to lose four molecules of water at 105 °C. It would appear that the somewhat variable composition reported by the Russian workers might be formed by a suitable mixture of the probable components $MgSO_4 \cdot nH_2O$ and $3Mg(OH)_2 \cdot MgSO_4 \cdot nH_2O$. On the other hand, the compositions of the present author's preparations, table 1, were not exactly 3 : 1 : 8 either, $Mg(OH)_2$ and $H_2O$ generally being slightly below the proportions of 3 and 8 respectively. It is believed that here, also, incompletely removed magnesium sulfate is largely responsible for the low $Mg(OH)_2/MgSO_4$ ratios. However, a 3.5 g sample of preparation 6 with a ratio of 2.83 (table 1) was stirred with 350 ml of methanol, and the liquid analyzed periodically for $SO_3$. Agitation in methanol for 5 min increased the calculated ratio of the suspended solid to 2.90; no further dissolving of magnesium sulfate from the sample occured in 6 hr. Ample methanol was present to dissolve several grams of $MgSO_4 \cdot 7H_2O$. A small amount of magnesium sulfate may be too strongly bound to the compound for removal with methanol, the true composition may be *slightly* different from 3 : 1 : 8, or the inevitable errors in analysis may be responsible for most of the apparent deviations. Small differences in water content are to be expected, due to variations in attaining vapor-pressure equilibrium between the samples and the atmosphere in which they were kept.

### 3.2. Differential Thermal Analyses

Differential-thermal-analysis curves obtained for three oxysulfate preparations are shown in figure 4. With the aid of oven-heating experiments and x-ray patterns obtained at various stages, the following conclusions were drawn:

Peak A at 100 to 140 °C represents the loss of four molecules of water with the formation of a material giving a different x-ray pattern than does the 3:1:8 oxysulfate. The equivalent oven temperature is about 105 °C.

Peak B at 205 to 230 °C represents the heat effect accompanying the loss of three more molecules of water and the collapse of the structure so that no lines appeared on the x-ray pattern. An oven temperature of 183 °C gave the same result.

Peak C at 430 to 460 °C represents the loss of most of the rest of the water. The x-ray pattern of MgO with a few lines of $MgSO_4$ was obtained. An oven temperature of 425 °C gave the same result. This is the approximate temperature at which $Mg(OH)_2$ loses its water when heated alone.

Peak D at 630 to 645 °C accompanied the loss of a small amount of water and the formation of $MgSO_4$ according to the x-ray pattern. It is this peak, together with x-ray data, on which Adomaviciute and coworkers based their conclusion that the oxysulfate was present in cement samples. Certain forms of magnesium carbonate also show an endothermic reaction in this range. The corresponding oven temperature was 600 °C.

Peaks E and F represent, respectively, a reversible transition of $MgSO_4$ at 1020 to 1028 °C, similar to those found for $CaSO_4$ and $BaSO_4$ at higher temperatures, and the decomposition of $MgSO_4$ to MgO and $SO_3$ at 1118 to 1135 °C.

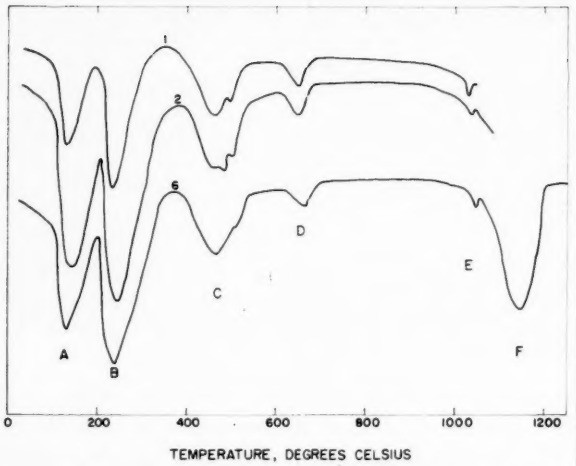


FIGURE 4. *Differential thermal analyses of* $3Mg(OH)_2 \cdot MgSO_4 \cdot 8H_2O$. *Preparations 1, 2, and 6, table 1.*

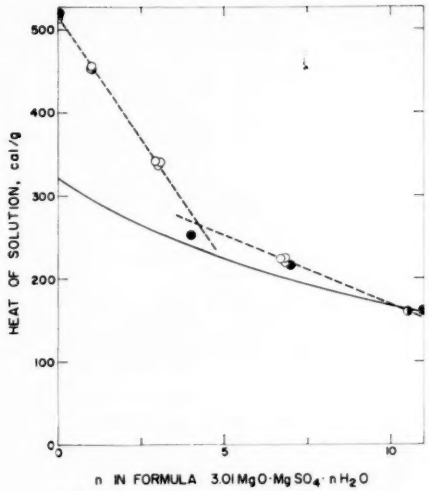


FIGURE 5. *Heats of solution of partially dehydrated magnesium oxysulfate,* $3.01MgO \cdot MgSO_4 \cdot nH_2O$, *in* $HCl \cdot 26.61\ H_2O$.

Open circles, individual experimental values.
Half-closed circle, average of five values for sample 2, table 1.
Closed circles, values calculated for mixtures of indicated composition from individual heats of solution ($\Delta H$) of MgO, $MgSO_3$, $MgSO_4 \cdot H_2O$, $MgSO_4 \cdot 4H_2O$, $MgSO_4 \cdot 7H_2O$, $Mg(OH)_2$, and $H_2O$; −36.67, −15.32, −7.57, +0.70, +8.92, −26.64, and −0.02 kcal/mole, respectively.
Solid line shows values calculated from equation fitted by least squares to 45 points from table 1 and used for computing the heat of solution $3Mg(OH)_2 \cdot MgSO_4 \cdot 8H_2O$. The 11 individual experimental points shown were not used in determining the solid line.

## 3.3. Heats of Solution

In table 1 are listed the measured heats of solutions of 11 preparations of the 3:1:8 oxysulfate. Samples of 2 g were dissolved in 740.00 g of $HCl \cdot 26.61 H_2O$, and in thermochemical calculations the heats of solution of approximately equivalent weights of $Mg(OH)_2$ and $MgSO_4 \cdot 7H_2O$ were used. Details of electrical calibration of the calorimeter have been given elsewhere [13]. The electrical-energy equivalent of the calorimeter was 28,450.5 J/ohm with a standard error of 3.8 J/ohm.

Since the samples listed in table 1 do not conform exactly to the composition of the pure compound $3Mg(OH)_2 \cdot MgSO_4 \cdot 8H_2O$, a three-constant first-degree equation relating the heat of solution to the composition of the sample was fitted to the 45 determinations of table 1 by the method of least squares on an electronic computer. The heat of solution of the compound was determined mathematically from its calculated composition and the coefficients of the equation. It has been more usual to calculate the constitution of samples in terms of the probable impurities, e. g., $3Mg(OH)_2 \cdot MgSO_4 \cdot mH_2O$, $MgSO_4 \cdot nH_2O$, and $Mg(OH)_2$, making assumptions of the values of $m$ and $n$, and compute a corrected heat of solution for each determination in table 1. However, the calculated quantities would themselves be linear in terms of the composition of the samples, so it seemed equally correct to make the computation as described. A heat of solution of 656.22 J/g (156.84 cal/g, 68.94 kcal/mole) was obtained for the predicted value. The standard deviation of this predicted value [14] was 2.21 J/g (0.53 cal/g, 0.23 kcal/mole).

That this type of computation must not be carried too far from the composition region represented by the data is demonstrated by the data shown in figure 5. In this figure are plotted the heats of solution of partially or completely dehydrated portions of sample 2 of table 1 as a function of $n$, the water content in moles per mole of $SO_3$. A single straight line does not fit these data, either a curve or two straight lines intersecting at about $n=4$ giving a much better fit. This value of $n$ would correspond to the composition of a sample constituted of $3Mg(OH)_2$ and $MgSO_4 \cdot H_2O$. The x-ray pattern of such a sample contained no lines, apparently the structure was insufficiently developed. The heats of solution of various mixtures calculated from the individual heats of solution of probable components are plotted as closed circles in figure 5. At $n=0$ and $n=7$ and 11, there is good agreement between the experimental and calculated values. At $n=0$ the agreement is good because the sample as shown by the x-ray pattern does consist of a mixture of MgO and $MgSO_4$ as assumed in calculating the heat of solution, at $n=7$ and 11 the differences are small because of the small heat of reaction of $Mg(OH)_2$ and $MgSO_4 \cdot nH_2O$ to form the oxysulfate. Heats of solution calculated from the equation used to predict the heat of solution of the 3:1:8 oxysulfate agree with the experimental values only in the range $n=10$ to 11. The solid line in figure 5 represents these calculated values. The line is curved because $n$ is not linear with percentage composition. The 11 experimental points shown individually in figure 5 were not used in determining the equation.

An average value for the heat of solution of $MgSO_4 \cdot 7H_2O$ in $HCl \cdot 26.61\ H_2O$ of −151.38 J/g with a standard error of 1.83 J/g was obtained for six determinations. The corresponding $\Delta H$ of solution at 25 °C is +8.92 kcal/mole with a standard error

of 0.11 kcal/mole. These determinations were made in the standard acid charge of 740 g (1.43 moles) of $HCl{\cdot}26.61H_2O$ without prior addition of 0.82 g of $Mg(OH)_2$ (corresponding to a 2-g sample of the 3:1:8 oxysulfate), thereby neglecting the small heat effect due to the presence of 0.014 moles of $MgCl_2$ in the solution.

Taylor and Wells [15] give the value −26.64 kcal/mole for the ΔH of solution of brucite ($Mg(OH)_2$) in 2.085 molal HCl and discuss the dilution corrections necessary to apply to this measurement. Using their values to adjust their result to the final concentrations 0.0198 molal in $MgCl_2$ and 2.0444 molal in HCl used in the present work, a ΔH of solution of −26.65 kcal/mole was obtained and used in following computations.

The partial molal heat content of water in 2.09 molal HCl [16,17] was used to represent the ΔH of solution of water. With these data the following thermochemical equation was written:

$$\begin{array}{lll} 3Mg(OH)_2\,(c, \text{brucite}) + MgSO_4{\cdot}7H_2O(c) + H_2O\,(liq) \rightarrow \\ 3(-26.65) \qquad\qquad +8.92 \qquad\qquad -0.02 \end{array}$$

$$\begin{array}{ll} 3Mg(OH)_2{\cdot}MgSO_4{\cdot}8H_2O\ (c) \\ -68.94 \qquad\qquad \text{kcal/mole.} \end{array}$$

The heat of the indicated reaction is therefore 2.11 kcal/mole. The estimated uncertainty of this result, using the value ±0.01 kcal for brucite given by Taylor and Wells [15] and combining calibration and reaction errors as recommended by Rossini [18], is 0.57 kcal/mole.

## 3.4. Heat of Formation

Using data from the literature [5] for the heats of formation of the compounds from the elements, together with the heat of reaction calculated above, the heat of formation of the 3:1:8 oxysulfate from the elements is calculated to be $\Delta H_f^\circ = -1537.9$ kcal/mole. The uncertainty of this figure in addition to the 0.57 kcal/mole indicated above depends on the uncertainty of the heats of formation used in its computation. The values −221.00, −808.7, and −68.3174 kcal/mole were used for the $\Delta H_f^\circ$ of brucite, magnesium sulfate heptahydrate, and liquid water, respectively.

## Summary

At 25 °C the magnesium oxysulfate compound $3Mg(OH)_2{\cdot}MgSO_4{\cdot}8H_2O$ precipitates spontaneously from metastable solutions of MgO in aqueous $MgSO_4$ solutions more concentrated than 12 percent or may be formed by the reaction of such solutions with solid MgO. The oxysulfate will remain unchanged indefinitely in aqueous solutions containing 10 percent or more of $MgSO_4$, but at lower concentrations is converted to $Mg(OH)_2$. Magnesium hydroxide remains unchanged by exposures to $MgSO_4$ solutions of any concentration up to 25 percent for periods up to three years, but dissolves slightly to give alkalinity to the solutions approximating that finally reached by dissolving MgO and allowing $Mg(OH)_2$ or the oxysulfate compound to precipitate.

The heat of solution of the oxysulfate in $HCl{\cdot}26.61H_2O$ (2.000 *N* at 25 °C) was found to be $\Delta H = -68.94$ kcal/mole with a standard deviation of 0.23 kcal/mole, and that of $MgSO_4{\cdot}7H_2O$ was found to be $\Delta H = +8.92$ kcal/mole with a standard error of 0.11 kcal/mole. The heat of reaction of $Mg(OH)_2$ (brucite), $MgSO_4{\cdot}7H_2O$, and liquid water to form the 3:1:8 compound was found to be, using data from the literature, $\Delta H = +2.11$ kcal/mole. The corresponding heat of formation from the elements was calculated to be $\Delta H_f^\circ = -1537.9$ kcal/mole.

## 5. References

[1] E. S. Newman, J. B. Gilfrich, and L. S. Wells, Heat generation in the setting of magnesium oxychloride cement, J. Res. NBS, **49,** No. 6, 377–83 (Dec. 1952) RP2375.

[2] E. S. Newman, A study of the system magnesium oxide—magnesium chloride—water and the heat of formation of magnesium oxychloride, J. Res. NBS, **54,** No. 6, 347–55 (June 1955) RP2597.

[3] T. Demediuk and W. F. Cole, A study on magnesium oxysulfates, Australian J. Chem. **10,** 287–94 (1957).

[4] B. B. Adomaviciute, J. Yanikii, and B. Vektaris, A study of the system $MgO$-$MgSO_4$-$H_2O$, Lietvos TSR Mokslu Akad. Darbai, Serija B, 2(25)219–25 (1961) (in Russian).

[5] F. D. Rossini, D. D. Wagman, W. H. Evans, S. Levine, and I. Jaffe, Selected values of chemical thermodynamic properties, NBS Circ. 500 (1952).

[6] Federal Test Method Standard No. 158, General Services Admin., Washington, D.C., May 1, 1957.

[7] ASTM Standard C25–58 Standard methods of chemical analysis of limestone, quicklime, and hydrated lime, American Soc. for Testing Materials, Philadelphia, Pa., 1958.

[8] M. Schnitzer, J. R. Wright, and I. Hoffmann. High temperature thermogravimetry of chlorides and sulphates. A study of the application to soils, Anal. Chim. Acta **26,** 371–77 (1962).

[9] E. S. Newman and L. S. Wells, Effects of some added materials on dicalcium silicate. J. Res. NBS **36,** 137–58 (Feb. 1946) RP1696.

[10] H. A. Berman and E. S. Newman, Heat of formation of calcium aluminate monocarbonate at 25 °C. J. Res. NBS, **65A** (Phys. and Chem.), No. 3, 197–207 (May-June 1961).

[11] International Critical Tables, Nat. Res. Council **3,** 228 (McGraw-Hill Book Co., Inc., New York, N.Y., 1933).

[12] Julian Kamecki and Stanislawa Palej, Thermal and thermogravimetric analysis of magnesium sulfate heptahydrate, Roczniki Chemii **29,** 691–704 (1955) (in Polish with English Summary).

[13] H. A. Berman and E. S. Newman, Heat of formation of calcium aluminate monosulfate at 25 °C, J. Res. NBS **67A** (Phys. and Chem.), No. 1, 1–13 (Jan.–Feb. 1963).

[14] Experimental Statistics, Mary Gibbons Natrella, NBS Handbook 91, 6–12. (U.S. Govt. Printing Office, Washington, D.C., 1963.)

[15] K. Taylor and L. S. Wells, Studies of heat of solution of magnesium oxides and hydroxides, J. Res. NBS **21,** 133–49 (Aug. 1938) RP1121.

[16] F. D. Rossini, BS J. Research **9,** 679 (1932) RP499.

[17] E. S. Newman and L. S. Wells, Heats of hydration and transition of calcium sulfate, J. Res. NBS **20,** 825–36 (June 1938) RP1107.

[18] F. D. Rossini, Chem. Rev. **18,** 233 (1936).

(Paper 68A6–313)

JOURNAL OF RESEARCH of the National Bureau of Standards—A. Physics and Chemistry
Vol. 68A, No. 6, November–December 1964

# Heat Capacity of Potassium Borohydride ($KBH_4$) From 15 to 375 °K. Thermodynamic Properties From 0 to 700 °K

George T. Furukawa, Martin L. Reilly, and Jeanette H. Piccirelli*

(August 4, 1964)

The heat capacity of potassium borohydride ($KBH_4$) was determined from about 15 to 375 °K by means of an adiabatic calorimeter. A table of thermodynamic functions was calculated up to 700 °K using the data obtained along with those at high temperatures found in the literature. A solid-solid (order-disorder) transition was observed at 77.16 ±0.02 °K and the entropy change associated with this transition was found to be 2.92 J/deg-mole. A broad transition from about 200 to 450 °K is attributed to a continuation of the order-disorder transition.

## 1. Introduction

The results of heat-capacity investigations on potassium borohydride ($KBH_4$) presented in this paper are a part of the program at the National Bureau of Standards to furnish thermodynamic data on various boron compounds.

Johnston and Hallett [1] [1] reported in their heat-capacity measurements on sodium borohydride ($NaBH_4$) a λ-type solid-phase transition at 189.9 °K with an entropy change of 1.22 cal/deg-mole. (Henceforth the unit of entropy in cal/deg-mole will be abbreviated to e.u.) Stockmayer and Stephenson [2] interpreted this transition as an order-disorder type involving changes in the orientation of the $BH_4^-$ ion group and predicted, on the bases of the heat-capacity data in the neighborhood of the transition and on their previous investigations of ammonium halides ($NH_4Cl$, $ND_4Cl$, and $NH_4I$) [3,4], that the crystal structure of sodium borohydride below the λ point would be tetragonal. Abrahams and Kalnajs [5] found from x-ray diffraction measurements that sodium, potassium, rubidium, and cesium borohydrides have the face-centered cubic structure at room temperature and that sodium borohydride has the body-centered tetragonal structure below the λ point. The results of x-ray measurements of Ford and Powell [6] on sodium and potassium borohydrides at 90 and 293 °K are in agreement with those of Abrahams and Kalnajs [5]. Unfortunately, the measurements of Ford and Powell [6] were not made below the λ point (77.16 ±0.02 °K, obtained in the work presented here) of potassium borohydride.

Stephenson et al. [3,4] obtained between 1.0 and 1.5 e.u. for the entropy of transition at the λ point for ammonium and deutero-ammonium halides. They have interpreted these values, which are close to the theoretical value of Rln2, as arising from an order-disorder transition involving two possible orientations of the $NH_4^+$ tetrahedron in the ammonium halide lattice. Below the λ point all of the $NH_4^+$ tetrahedrons have one orientation and above the λ point they have either of the two orientations. Infrared spectra [7] and neutron diffraction [8,9] measurements on the ammonium halides support the above interpretation.

Stephenson, Rice, and Stockmayer [10] found, from cooling and warming curve investigations, transitions in $KBH_4$ at 76 ±1 °K, $RbBH_4$ at 44 ±3 °K, and $CsBH_4$ at 27 ±1 °K and interpreted these transitions to be the order-disorder type interpreted for the λ transitions in $NaBH_4$ and the ammonium halides. The alkali metal borohydrides have, in contrast with the ammonium halides, the face-centered cubic structure (NaCl) in the region above the λ transition [5]. ($LiBH_4$ has the orthorhombic structure [11].) The ammonium halides exist in the body-centered cubic form (CsCl) in the region above the λ transition and transform by first-order transition into the face-centered cubic form only at higher temperatures [3,9]. From heat-capacity measurements, Shigi [12] found the entropy associated with the transition in $KBH_4$ to be 0.771 e.u. which is considerably lower than the Rln2 or 1.38 e.u. for the order-disorder transition. Shigi [12] ascribed the observation to an order-disorder transition involving $BH_4^-$ ions as interpreted by Stockmayer and Stephenson [2] for the λ transition in $NaBH_4$.

In this paper, the results of new measurements on the heat capacity of $KBH_4$ from 16 to 376 °K are presented. A relatively low heat of λ transition, comparable to that observed by Shigi [12], was obtained. The low-temperature heat-capacity data were compared and anlyzed with the relative enthalpy data (0 to 400 °C) reported by Douglas and Harman [13]. The "broad" transition extending from about 200 to 450 °K is interpreted as a continuation of the order-disorder transition still incomplete at 77.16 °K.

## 2. Apparatus and Method

The heat-capacity measurements were conducted in an adiabatic calorimeter similar in design to that described by Scott et al. [14]. The calorimeter vessel, which was filled externally and sealed by means

*Formerly Jeanette M. Henning.
[1] Figures in brackets indicate the literature references at the end of this paper.

of a specially designed gold-gasket closure [15], was suspended within the adiabatic shield system by means of a linen cord instead of the filling tube shown in the above reference [14]. The design and operation of the calorimeter will be given in detail in a subsequent publication.

The platinum-resistance thermometer used in the measurements was calibrated on the International Practical Temperature Scale of 1948 [16]. The temperatures in degrees Kelvin (°K) were obtained by adding 273.15 deg to the temperatures in degree Celsius (°C). Below 90 °K, the thermometer was calibrated on the NBS–1955 provisional scale which is numerically 0.01 deg lower than the NBS–1939 provisional scale [17]. The resistance measurements were made to the nearest 0.00001 ohm by means of a Mueller bridge and a galvanometer of high sensitivity.

The electrical power introduced into the calorimeter heater (100 ohms of constantan wire) was measured by means of a Wenner potentiometer in conjunction with a volt box, standard resistor, and saturated standard cells. The duration of each heating interval was measured by means of an interval timer of high precision operated on the 60-cycle frequency standard provided at the National Bureau of Standards. The 60-cycle frequency standard is derived from a 100 kc/s quartz oscillator which is stable to 0.5 ppm. The operation of the interval timer was checked periodically with seconds signals also derived from the same 100 kc/s oscillator. The variations were not more than 0.02 sec for any time interval. The heating periods were never less than 2 min.

The observed gross (calorimeter vessel plus sample) heat-capacity values were corrected for curvature wherever significant by a method previously described [18]. The values of net heat capacity (heat capacity of sample only) were obtained by subtracting the values of tare heat capacity (heat capacity of empty calorimeter vessel) from those of the gross heat capacity at the corresponding temperatures. The values of the tare heat capacity at the various temperatures were obtained by four-point Lagrangian interpolation in a table of tare heat-capacity values previously obtained. Corrections were applied for the heat capacity of helium gas and for the small difference in the mass of the calorimeter vessel between the gross and tare measurements. The values of net heat capacity were corrected for the $KBO_2$ impurity and converted to molal basis using the atomic weights based on C–12 [19]. These converted values will be referred to as observed molal heat capacity. Whenever a reference to the energy unit calorie is made, the defined calorie (4.1840 absolute joules) is intended.

## 3. Sample

The potassium borohydride sample used in the investigation was purchased from Metal Hydrides, Inc. The analyses furnished by the supplier showed the sample to contain 99.5 percent of the theoretical hydrogen by a gasometric method and 100.5 and 100.7 percent of the alkali and boron, respectively, by acid-base titration. The supplier believed the sample to have a purity no less than 99.5 percent. The analyses furnished with the sample are summarized in table 1. A portion of the above sample was used for the low-temperature measurements and another portion of the same sample was used by Douglas and Harman [13] in the high-temperature measurements previously reported. After the completion of the measurements, a separate set of chemical analysis was obtained, however, on the portion that was actually used in the low-temperature measurements because of the relatively low stability of the substance.

The sample was received, sealed with paraffin, in a screw-cap jar. The jar was opened approximately two weeks after receipt in an inert atmosphere box containing dry argon and a portion of the sample was transferred without further treatment into a calorimeter vessel. The sample was pumped in the vessel for two days, purged with helium gas several times, and finally sealed wish a small quantity of helium gas. The helium gas serves to increase the rate of temperature equilibrium in the sample during the heat-capacity measurements.

TABLE 1. *Analyses of the potassium borohydride sample*

Gram formula weight=53.94488 g

| Elements | Percentage by weight [a] | |
|---|---|---|
| | Analysis | Theoretical |
| Potassium | 71.2 (flame photometry) | |
| | 72.8 (titration) | 72.49 |
| Boron | 20.2 (titration) | 20.04 |
| Hydrogen | 7.44 (gasometry) | 7.474 |
| Chloride | 0.10 (titration) | |

| Methods | Percentage in weight of $KBH_4$ [b] | |
|---|---|---|
| | Specimen A | Specimen B |
| Hydrogen (by evolution) | 98.69 | 99.12 |
| | 98.73 | 99.12 |
| Boric acid titration | 99.56 | 99.91 |
| | 99.70 | 100.00 |

[a] These values were supplied by the Metal Hydrides, Inc.; the percentages of potassium borohydride, based on potassium (titration), boron, and hydrogen, are 100.4, 100.8, and 99.5, respectively.

[b] These analyses were obtained by R. A. Paulson of the Applied Analytical Research Section of the National Bureau of Standards. Specimen A was sampled from the top and specimen B from the bottom of the storage jar.

After completion of the heat-capacity measurements the purity of the sample was redetermined by hydrogen-evolution analysis and by titration of the boric acid. The analyses were performed by R. A. Paulson of the Applied Analytical Research Section of the Bureau. In the hydrogen analysis, the hydrogen was liberated by hydrolysis with $6N$ hydrochloric acid. The liberated hydrogen gas was swept by nitrogen through an absorber containing Ascarite and Anhydrone to remove any acid and

water. The dried hydrogen gas was then oxidized on copper oxide at 700 °C to water which was absorbed on Anhydrone and weighed. For the boric acid analysis, the sample was first titrated with standard hydrochloric acid to the methyl red end point, and after the addition of several grams of mannitol, was titrated with standard sodium hydroxide to the phenolphthalein end point.

The analyses were not done immediately after the completion of the heat measurements; the composition of the sample investigated is therefore somewhat uncertain. The sample upon removal from the calorimeter vessel was stored in a screw-cap jar in a desiccator containing Drierite and the analyses were performed approximately one year later. Two samples taken from the top of the jar analyzed 98.69 and 98.73 percent by hydrogen analysis and 99.56 and 99.70 percent by titration of the boric acid. Another pair of samples from the bottom of the jar both analyzed 99.12 percent by hydrogen analysis and 99.91 and 100.00 percent by titration of the boric acid. These analyses suggest that the heat-capacity measurements were made on a sample that was at least 99.1 percent $KBH_4$, probably 99.5 percent.

Most literature information indicates that $KBH_4$ is stable, but a test sample exposed continuously for 48 days to the laboratory atmosphere changed in $KBH_4$ content from 98.4 to 96.7 percent according to hydrogen analysis. Considering the analyses given for the sample by the supplier and those obtained approximately one year later, the composition of the sample investigated was taken to be 99.5 percent $KBH_4$ and 0.5 percent $KBO_2$ possibly formed according to the reactions:

$$KBH_4+2H_2O=KBO_2+4H_2 \quad (1)$$

and

$$KBH_4+2O_2=KBO_2+2H_2O. \quad (2)$$

Corrections were made to the observed values of heat capacity on the basis that the heat capacities of $KBH_4$ and $KBO_2$ were additive. Because of the lack of heat-capacity data on $KBO_2$, the corrections were calculated on the basis that the ratio of the heat capacity of $KBO_2$ to $KBH_4$ is the same as that of $NaBO_2$ [20] to $NaBH_4$ [1].

## 4. Experimental Results

### 4.1. Heat Capacity

The observed values of molal heat capacity from about 15 to 375 °K are summarized in table 2 and plotted in figure 1. The heat-capacity curve indicates a broad transition starting from about 200 °K and begins to flatten from about 300 °K. A part of the same transition was observed by Douglas and Harman [13] in their measurements of the enthalpy relative to 273 °K up to 673 °K. Figure 2 shows how the smoothed low-temperature values of heat

TABLE 2. *Observed heat capacity of potassium borohydride*

Gram formula wt=53.94488 g, $T$ deg K=$t$ deg C+273.15

| Run No. | $T$ [a] | $C_p$ [c] | $\Delta T$ [b] |
|---|---|---|---|
| | *Deg K* | *Deg$^{-1}$ Mole$^{-1}$* | *Deg K* |
| 1 | [d] 81. 9262 | 36. 333 | 6. 5263 |
| | 91. 4848 | 40. 047 | 12. 5910 |
| | 103. 4338 | 44. 529 | 11. 3070 |
| | 114. 3040 | 48. 453 | 10. 4333 |
| | 124. 4201 | 51. 861 | 9. 7990 |
| | 134. 6828 | 55. 131 | 10. 7265 |
| | 145. 9480 | 58. 489 | 12. 3533 |
| | 158. 0094 | 61. 922 | 11. 7695 |
| | 169. 5360 | 65. 097 | 11. 2836 |
| | 181. 4994 | 68. 352 | 12. 6433 |
| | 193. 9026 | 71. 710 | 12. 1629 |
| | 205. 8546 | 74. 943 | 11. 7411 |
| | 218. 2744 | 78. 379 | 13. 0987 |
| | 231. 0480 | 81. 848 | 12. 4483 |
| | 243. 6110 | 85. 117 | 12. 6777 |
| | 256. 1038 | 88. 200 | 12. 3081 |
| | 268. 2558 | 90. 902 | 11. 9958 |
| | 280. 5140 | 93. 250 | 12. 5205 |
| | 292. 9078 | 95. 188 | 12. 2673 |
| 2 | 80. 2196 | 35. 680 | 3. 2911 |
| | 85. 2256 | 37. 625 | 6. 7209 |
| | 91. 7576 | 40. 170 | 6. 3431 |
| | 100. 7470 | 43. 526 | 11. 6358 |
| | 110. 1627 | 46. 980 | 7. 1956 |
| | 118. 8492 | 50. 003 | 10. 1775 |
| | 129. 4421 | 53. 488 | 11. 0082 |
| | 141. 2379 | 57. 108 | 12. 5834 |
| | 153. 6396 | 60. 683 | 12. 2201 |
| | 165. 6021 | 64. 029 | 11. 7048 |
| | 177. 0837 | 67. 147 | 11. 2584 |
| | 187. 8338 | 70. 068 | 12. 6470 |
| | 200. 2511 | 73. 443 | 12. 1876 |
| | 212. 2289 | 76. 733 | 11. 7680 |
| | 223. 8089 | 79. 890 | 11. 3920 |
| | 235. 8074 | 83. 109 | 12. 6051 |
| | 248. 2734 | 86. 315 | 12. 3267 |
| | 260. 5716 | 89. 274 | 12. 2698 |
| | 272. 8466 | 91. 918 | 12. 2802 |
| | 285. 2636 | 94. 144 | 12. 5537 |
| | 297. 7020 | 96. 045 | 12. 3231 |
| | 311. 2642 | 97. 892 | 14. 8014 |
| | 325. 9442 | 98. 979 | 14. 5585 |
| | 340. 4102 | 99. 754 | 14. 3736 |
| | 354. 7243 | 100. 05 | 14. 2546 |
| | 368. 9214 | 100. 26 | 14. 1395 |
| 3 | 16. 0784 | 1. 150 | 1. 1323 |
| | 17. 3290 | 1. 474 | 1. 3689 |
| | 18. 9010 | 1. 920 | 1. 7752 |
| | 20. 8022 | 2. 617 | 2. 0273 |
| | 23. 4736 | 3. 672 | 3. 3154 |
| | 26. 3709 | 4. 981 | 2. 4792 |
| | 29. 0787 | 6. 293 | 2. 9364 |
| | 31. 5788 | 7. 543 | 2. 0639 |
| | 33. 9314 | 8. 797 | 2. 6411 |
| | 36. 7419 | 10. 296 | 2. 9800 |
| | 39. 5210 | 11. 806 | 2. 5781 |
| | 42. 6738 | 13. 527 | 3. 7277 |
| | 46. 5295 | 15. 694 | 3. 9836 |
| | 51. 3304 | 18. 471 | 5. 6182 |
| | 56. 3556 | 21. 450 | 4. 4322 |
| | 60. 5536 | 24. 097 | 3. 9637 |
| | 65. 1810 | 27. 221 | 5. 2913 |
| | 70. 9554 | 31. 678 | 6. 2573 |
| | 75. 6252 | 90. 625 | 3. 0824 |
| | 79. 6041 | 44. 427 | 4. 8754 |

See footnotes at end of table.

TABLE 2. *Observed heat capacity of potassium borohydride*—Continued

Gram formula wt=53.94488 g, $T$ deg K=$t$ deg C+273.15

| Run No. | $T$[a] | $C_p$[c] | $\Delta T$[b] |
|---|---|---|---|
| | *Deg K* | *Deg$^{-1}$ Mole$^{-1}$* | *Deg K* |
| 4 | 71. 8152 | 32. 545 | 3. 2608 |
| | 74. 5014 | 35. 330 | 2. 1115 |
| | 76. 3579 | 55. 138 | 1. 6016 |
| | 77. 1587 | Infinity | 0 |
| | 77. 8554 | 67. 049 | 1. 3934 |
| 5 | 68. 2424 | 29. 397 | 5. 2497 |
| | 71. 6737 | 32. 179 | 1. 6130 |
| | 73. 9988 | 34. 714 | 3. 0372 |
| | 76. 3361 | 58. 618 | 1. 6374 |
| | 77. 1626 | 9381. 1 | . 0155 |
| | 78. 0424 | 52. 498 | 1. 7443 |
| | 80. 3469 | 35. 729 | 2. 8646 |
| | 83. 1655 | 36. 789 | 2. 7726 |
| 6 | 317. 3758 | 98. 210 | 14. 8361 |
| | 332. 1227 | 99. 143 | 14. 6578 |
| | 346. 7124 | 99. 653 | 14. 5216 |
| | 361. 4790 | 99. 884 | 15. 0116 |
| | 376. 1383 | 99. 993 | 14. 3070 |
| 7 | 73. 0428 | 33. 675 | 3. 2367 |
| | 75. 7802 | 37. 675 | 2. 2383 |
| | 77. 2337 | 347. 46 | . 6686 |
| | 79. 0754 | 35. 393 | 3. 0149 |

[a] $T$ is the mean temperature of the heating interval.
[b] $\Delta T$ is the temperature interval of heating.
[c] $C_p$ is the observed mean heat capacity over the interval $\Delta T$.
[d] The temperatures given are believed to be accurate to ±0.01 deg K. The figures beyond the second decimal are significant only insofar as small temperature differences are concerned.

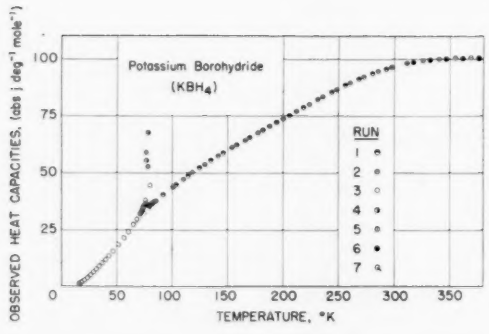


FIGURE 1. *Observed heat capacity of potassium borohydride.*

capacity join with those calculated from the heat-capacity equation:

$$C_p = 0.9999422 \times 4.1840(80.810 - 0.130681T + 1.0217 \times 10^{-4}T^2 - 8{,}303/T) \text{J/deg-mole}, \quad (3)$$

given by Douglas and Harman [13] for the range 273 to 700 °K. (The equation actually given by Douglas and Harman [13] is in cal/deg-mole. The factor 4.1840 for conversion to J/deg-mole was applied to obtain eq (3). The factor 0.9999422 is the ratio of new to old molecular weight of $KBH_4$.) The inflection point is around 460 °K and above this temperature the heat capacity increases "normally."

The values of heat capacity obtained were at helium-gas pressures varying from 50 torr at room temperature to about one-twentieth of this pressure at the lowest temperature and to about 60 torr at the highest temperature. In the case of $KBH_4$ the conversion of its heat capacity from any of the above pressures to 1 atm pressure would make a negligible change. Therefore, all computations and analyses have been carried out as if the measurements were made at constant 1 atm pressure.

### 4.2. Heat of Transition

A solid-phase transition was observed and the transition temperature was estimated from the observed values of the heat capacity to be 77.16 ±0.02 °K. (In this paper, the figure associated with the symbol ± indicates the uncertainty estimated by examining the precision of the measurements and possible sources of systematic errors. The figure has a 50 percent confidence limit.) The apparent heat capacities in this temperature region are given in table 2 and in figure 1. The heat associated with the transition was evaluated by subtracting the enthalpy change calculated from the "normal" heat-capacity curve, shown as a broken line in figure 1, between 65 and 80 °K from the total change obtained for the temperature interval. The total change in enthalpy between 65 and 80° K was determined by summing the various experimental increments of energy introduced to determine the heat capacity over this range. Adjustments were made to the even 65 to 80 °K temperature interval using the observed values of the heat capacity. These results are summarized in table 3 on a molal basis, obtained after subtracting the contribution of the calorimeter vessel to the observed enthalpy increment.

The heat of transition obtained is 225 J/mole (53.8 cal/mole) and the entropy of transition is 2.92 J/deg-mole (0.70 e.u.). These values are in close agreement with 58.4 cal/mole and 0.771 e.u. for the heat and entropy of transition, respectively, reported by Shigi [12] and with the unpublished values 52.8 cal/mole and 0.69 e.u., respectively, obtained by Stull et al. [21].

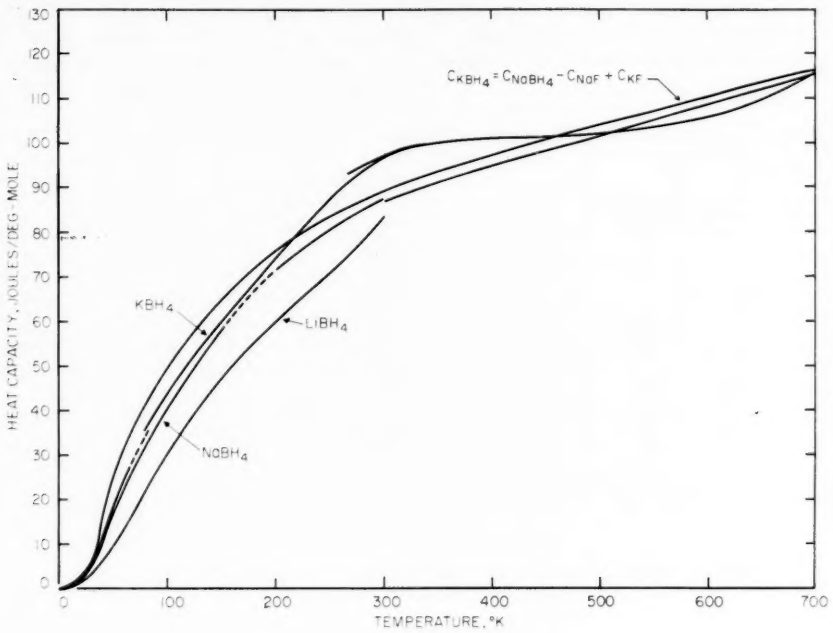


FIGURE 2. *Comparison of heat capacities.*

$KBH_4$, 15° to 375°K, this work.
$KBH_4$, 273° to 673°K, Douglas and Harman [13].
$NaBH_4$, 15° to 300°K, Johnston and Hallett [1].
$NaBH_4$, 273° to 673°K, Douglas and Harman [13].
$C_{KBH_4} = C_{NaBH_4} - C_{NaF} + C_{KF}$, $KBH_4$ (calculated),
$LiBH_4$, 15° to 300°K, Hallett and Johnston [26].

TABLE 3. *Molal enthalpy change of potassium borohydride between 65° and 80 °K. The enthalpy and entropy of transition.*

Gram formula weight = 53.94488 g, °K = t°C + 273.15°
Transition temperature = 77.16 ± 0.02 °K

| Temperature interval | Energy input | Heat capacity correction | $\Delta H$ 65° to 80 °K |
|---|---|---|---|
| °K | J/mole | J/mole | J/mole |
| 62.5354 to 82.0418 | 838.94 | −138.39 | 700.55 |
| 70.1848 to 78.5521 | 499.81 | +201.75 | 701.56 |
| 65.6175 to 81.7792 | 747.64 | −47.20 | 700.44 |
| 71.4244 to 80.5829 | 532.82 | +168.26 | 701.08 |
| Mean | | | 700.91 |
| Standard deviation of the mean [a] | | | ±0.26 |
| Enthalpy change along normal heat capacity curve | | | 475.94 |
| Enthalpy of transition | | | 224.97 |
| Entropy of transition = 2.92 J/deg-mole (0.70 cal/deg-mole) | | | |

[a] Standard deviation of the mean as used above is defined as $[\Sigma d^2/n(n-1)]^{1/2}$; where $d$ is the difference between a single observation and the mean, and $n$ is the number of observations.

### 4.3. Derived Thermodynamic Properties

The values of the observed molal heat capacity were smoothed and combined with the results of the relative enthalpy measurements between 0 and 400 °C reported by Douglas and Harman [13] (see eq (3)) to calculate the thermodynamic functions from 0 to 700 °K. The smoothing method used with the observed low-temperature values of heat capacity involved a combination of analytical and graphical procedures. Several overlapping empirical equations were fitted to the observed values of heat capacity over the range of measurements and the deviations from the empirical equations plotted. Smooth curves were drawn through the deviation points and the values of heat capacity at equally and closely spaced integral temperatures were obtained by combining the values from the empirical equations and the deviation curves. In the regions where the equations overlapped, the values that joined most smoothly were selected. The tabular values were finally checked for smoothness by examining the differences and wherever necessary they were smoothed further by numerical methods [22].

The smoothed low-temperature values of heat capacity were compared with those obtained from the heat-capacity equation (eq (3)) given by Douglas and Harman [13]. The values from the two sets of measurements were found to join best at about 370 °K (see fig. 2) and were smoothed together by a numerical method (a nine-point cubic smoothing procedure) [22]. The enthalpy change between 0 and 100 °C given in the final table of thermodynamic functions (table 5) is 9779 J/mole and the experimental values reported for this temperature interval by Douglas and Harman [13] are 9818 and 9790

J/mole for samples 1 and 2, respectively. The enthalpy increment based on the low-temperature measurements was calculated to be 9776 J/mole.

TABLE 4. *Comparison of thermodynamic functions for potassium borohydride* ($KBH_4$) *with those reported by Douglas and Harman [13].*

Gram formula weight = 53.94488 g, $T$ deg K = $t$ deg C + 273.15
1 defined calorie = 4.1840 joules

| $T$ | This work | | | Douglas and Harman [a] | | |
|---|---|---|---|---|---|---|
| | $C$ | $S$ | $(H_T-H_0^\circ)/T$ | $C$ | $S$ | $(H_T-H_0^\circ)/T$ |
| °K | cal/deg-mole | cal/deg-mole | cal/mole | cal/deg-mole | cal/deg-mole | cal/mole |
| 298.15 | 22.958 | 25.404 | 13.204 | 23.08 | 25.48 | 13.244 |
| 400 | 24.125 | 32.385 | 15.896 | 24.13 | 32.46 | 15.925 |
| 500 | 24.402 | 37.794 | 17.566 | 24.41 | 37.87 | 17.590 |
| 600 | 25.339 | 42.311 | 18.769 | 25.34 | 42.39 | 18.789 |
| 700 | 27.531 | 46.362 | 19.847 | 27.54 | 46.44 | 19.765 |

[a] Gram formula weight used by Douglas and Harman [13] was 53.952 g. Their values were not converted to the new gram molecular weight 53.94488 g. The new molecular weight will lower the values of Douglas and Harman by 0.013 percent, making the variations in the two sets of values smaller.

These values indicate that the low-temperature measurements are on the average in this range about 0.3 percent lower than the average of the two high-temperature measurements. Above about 370 °K, the thermodynamic functions given in table 5 are derived from eq (3) obtained by Douglas and Harman [13]. A few of the values from table 5 are given in table 4 for comparison with those reported by Douglas and Harman. The differences in the values arise primarily from the revised entropy and enthalpy at 298.15 °K given in the present paper. The earlier preliminary entropy and enthalpy values that were furnished Douglas and Harman [13] had not been corrected for the impurities.

The values of heat capacity below the lower limit of measurements (16 °K) were obtained by extrapolation using a Debye heat-capacity function fitted to the experimental values between 16 and 30 °K. The equation used was

$$C = 58.3\ D\left(\frac{250}{T}\right) \text{ J/deg-mole.} \qquad (4)$$

TABLE 5. *Molal thermodynamic functions for potassium borohydride* ($KBH_4$)

Gram formula wt = 53.94488 g, $T$ deg K = $t$ deg C + 273.15

| $T$ | $C_p$ | $(H_T-H_0^\circ)$ | $(H_T-H_0^\circ)/T$ | $(S_T-S_0^\circ)$ | $-(G_T-H_0^\circ)$ | $-(G_T-H_0^\circ)/T$ |
|---|---|---|---|---|---|---|
| Solid phase | | | | | | |
| *deg K* | *deg*$^{-1}$ | *J* | *J deg*$^{-1}$ | *J deg*$^{-1}$ | *J* | *J deg*$^{-1}$ |
| 0.00 | 0.000 | 0.000 | 0.000 | 0.000 | 0.000 | 0.000 |
| 5.00 | .036 | .045 | .009 | .012 | .015 | .003 |
| 10.00 | .290 | .725 | .072 | .097 | .242 | .024 |
| 15.00 | .978 | 3.670 | .245 | .326 | 1.223 | .082 |
| 20.00 | 2.312 | 11.531 | .577 | .769 | 3.853 | .193 |
| 25.00 | 4.327 | 27.928 | 1.117 | 1.493 | 9.388 | .376 |
| 30.00 | 6.733 | 55.468 | 1.849 | 2.490 | 19.238 | .641 |
| 35.00 | 9.356 | 95.617 | 2.732 | 3.723 | 34.680 | .991 |
| 40.00 | 12.059 | 149.14 | 3.728 | 5.148 | 56.787 | 1.420 |
| 45.00 | 14.820 | 216.02 | 4.801 | 6.721 | 86.411 | 1.920 |
| 50.00 | 17.690 | 297.26 | 5.945 | 8.430 | 124.24 | 2.485 |
| 55.00 | 20.625 | 393.02 | 7.146 | 10.253 | 170.90 | 3.107 |
| 60.00 | 23.735 | 503.83 | 8.397 | 12.179 | 226.94 | 3.782 |
| 65.00 | 27.092 | 630.79 | 9.704 | 14.210 | 292.87 | 4.506 |
| 70.00 | 30.5 * | 774.89 | 11.070 | 16.344 | 369.22 | 5.2 5 |
| 75.00 | 33.3 * | 934.45 | 12.459 | 18.545 | 456.42 | 6.086 |
| 77.16 | 34.3 * | 1007.5 | 13.057 | 19.505 | 497.52 | 6.448 |
| 77.16 | 34.3 * | 1232.4 | 15.972 | 22.420 | 497.52 | 6.448 |
| 80.00 | 35.583 | 1331.7 | 16.647 | 23.684 | 562.99 | 7.037 |
| 85.00 | 37.544 | 1514.6 | 17.818 | 25.900 | 686.95 | 8.082 |
| 90.00 | 39.476 | 1707.1 | 18.968 | 28.101 | 821.96 | 9.133 |
| 95.00 | 41.384 | 1909.3 | 20.098 | 30.287 | 967.94 | 10.189 |
| 100.00 | 43.261 | 2120.9 | 21.209 | 32.457 | 1124.8 | 11.248 |
| 105.00 | 45.108 | 2341.8 | 22.303 | 34.613 | 1292.5 | 12.309 |
| 110.00 | 46.922 | 2571.9 | 23.381 | 36.753 | 1470.9 | 13.372 |
| 115.00 | 48.686 | 2811.0 | 24.443 | 38.878 | 1660.0 | 14.435 |
| 120.00 | 50.392 | 3058.7 | 25.489 | 40.986 | 1859.7 | 15.497 |
| 125.00 | 52.048 | 3314.8 | 26.519 | 43.077 | 2069.8 | 16.559 |
| 130.00 | 53.661 | 3579.1 | 27.532 | 45.150 | 2290.4 | 17.618 |
| 135.00 | 55.224 | 3851.3 | 28.528 | 47.205 | 2521.3 | 18.676 |
| 140.00 | 56.733 | 4131.3 | 29.509 | 49.240 | 2762.4 | 19.732 |
| 145.00 | 58.205 | 4418.6 | 30.473 | 51.257 | 3013.7 | 20.784 |

TABLE 5. *Molal thermodynamic functions for potassium borohydride* ($KBH_4$)—Continued

| $T$ | $C_p$ | $(H_T-H_0^\circ)$ | $(H_T-H_0^\circ)/T$ | $(S_T-S_0^\circ)$ | $-(G_T-H_0)$ | $-(G_T-H_0^\circ)/T$ |
|---|---|---|---|---|---|---|
| | | | Solid phase | | | |
| *deg K* | *deg*$^{-1}$ | *J* | *J deg*$^{-1}$ | *J deg*$^{-1}$ | *J* | *J deg*$^{-1}$ |
| 150.00 | 59.643 | 4713.2 | 31.422 | 53.255 | 3275.0 | 21.833 |
| 155.00 | 61.066 | 5015.0 | 32.355 | 55.234 | 3546.2 | 22.879 |
| 160.00 | 62.476 | 5323.9 | 33.274 | 57.195 | 3827.3 | 23.920 |
| 165.00 | 63.858 | 5639.7 | 34.180 | 59.138 | 4118.1 | 24.958 |
| 170.00 | 65.213 | 5962.4 | 35.073 | 61.065 | 4418.6 | 25.992 |
| 175.00 | 66.574 | 6291.9 | 35.954 | 62.975 | 4728.7 | 27.021 |
| 180.00 | 67.941 | 6628.2 | 36.823 | 64.869 | 5048.3 | 28.046 |
| 185.00 | 69.304 | 6971.3 | 37.683 | 66.750 | 5377.4 | 29.067 |
| 190.00 | 70.656 | 7321.2 | 38.533 | 68.616 | 5715.8 | 30.083 |
| 195.00 | 72.001 | 7677.8 | 39.373 | 70.468 | 6063.5 | 31.095 |
| 200.00 | 73.355 | 8041.2 | 40.206 | 72.308 | 6420.5 | 32.102 |
| 205.00 | 74.722 | 8411.4 | 41.031 | 74.137 | 6786.6 | 33.105 |
| 210.00 | 76.108 | 8788.5 | 41.850 | 75.954 | 7161.8 | 34.104 |
| 215.00 | 77.489 | 9172.5 | 42.663 | 77.761 | 7546.1 | 35.098 |
| 220.00 | 78.849 | 9563.3 | 43.470 | 79.558 | 7939.4 | 36.088 |
| 225.00 | 80.229 | 9961.0 | 44.271 | 81.345 | 8341.7 | 37.074 |
| 230.00 | 81.575 | 10366 | 45.068 | 83.123 | 8752.8 | 38.056 |
| 235.00 | 82.883 | 10777 | 45.858 | 84.892 | 9172.9 | 39.034 |
| 240.00 | 84.186 | 11194 | 46.643 | 86.650 | 9601.7 | 40.007 |
| 245.00 | 85.470 | 11619 | 47.423 | 88.400 | 10039 | 40.977 |
| 250.00 | 86.717 | 12049 | 48.196 | 90.139 | 10486 | 41.943 |
| 255.00 | 87.922 | 12486 | 48.963 | 91.868 | 10941 | 42.905 |
| 260.00 | 89.085 | 12928 | 49.724 | 93.587 | 11404 | 43.863 |
| 265.00 | 90.201 | 13376 | 50.477 | 95.294 | 11877 | 44.817 |
| 270.00 | 91.257 | 13830 | 51.222 | 96.990 | 12357 | 45.768 |
| 273.15 | 91.892 | 14119 | 51.688 | 98.052 | 12665 | 46.365 |
| 275.00 | 92.253 | 14289 | 51.960 | 98.674 | 12846 | 46.714 |
| 280.00 | 93.187 | 14752 | 52.687 | 100.34 | 13344 | 47.657 |
| 285.00 | 94.060 | 15221 | 53.406 | 102.00 | 13850 | 48.596 |
| 290.00 | 94.870 | 15693 | 54.114 | 103.64 | 14364 | 49.531 |
| 295.00 | 95.617 | 16169 | 54.811 | 105.27 | 14886 | 50.462 |
| 298.15 | 96.055 | 16471 | 55.244 | 106.29 | 15220 | 51.047 |
| 300.00 | 96.300 | 16649 | 55.497 | 106.89 | 15418 | 51.393 |
| 310.00 | 97.466 | 17618 | 56.832 | 110.07 | 16503 | 53.235 |
| 320.00 | 98.402 | 18598 | 58.117 | 113.18 | 17619 | 55.060 |
| 330.00 | 99.134 | 19585 | 59.350 | 116.22 | 18766 | 56.867 |
| 340.00 | 99.653 | 20580 | 60.528 | 119.18 | 19943 | 58.657 |
| 350.00 | 99.966 | 21578 | 61.651 | 122.08 | 21150 | 60.427 |
| 360.00 | 100.19 | 22579 | 62.718 | 124.90 | 22385 | 62.179 |
| 370.00 | 100.42 | 23582 | 63.734 | 127.65 | 23647 | 63.912 |
| 373.15 | 100.49 | 23898 | 64.044 | 128.50 | 24051 | 64.453 |
| 380.00 | 100.63 | 24587 | 64.702 | 130.33 | 24937 | 65.624 |
| 390.00 | 100.80 | 25594 | 65.626 | 132.94 | 26254 | 67.317 |
| 400.00 | 100.94 | 26603 | 66.507 | 135.50 | 27596 | 68.990 |
| 425.00 | 101.19 | 29130 | 68.540 | 141.62 | 31061 | 73.084 |
| 450.00 | 101.41 | 31662 | 70.360 | 147.41 | 34674 | 77.054 |
| 475.00 | 101.70 | 34201 | 72.002 | 152.90 | 38429 | 80.903 |
| 500.00 | 102.10 | 36748 | 73.496 | 158.13 | 42317 | 84.635 |
| 550.00 | 103.52 | 41885 | 76.154 | 167.92 | 50472 | 91.767 |
| 600.00 | 106.02 | 47118 | 78.530 | 177.03 | 59098 | 98.497 |
| 650.00 | 109.86 | 52509 | 80.784 | 185.66 | 68167 | 104.87 |
| 700.00 | 115.19 | 58129 | 83.041 | 193.98 | 77658 | 110.94 |

*Integration over the temperature interval 65 to 80 deg K is based upon the estimated base line heat capacity. While the distribution of energy in this temperature interval is less accurate, the value of the enthalpy at 80 deg accurately represents the experimentally observed increment over the temperature interval.

$H_0^\circ$ and $S_0^\circ$ are the reference states at absolute zero of temperature.

The thermodynamic functions were calculated from the values of heat capacity according to the following thermodynamic relations:

$$H_T - H_0^c = \int_0^T C dT + \Delta H_{tr} \quad (5)$$

$$S_T - S_0^c = \int_0^T C(dT/T) + \Delta H/T_{tr} \quad (6)$$

$$(G_T - H_0^c) = -\int_0^T (S_T - S_0^c) dT - TS_0^c = (H_T - H_0^c) - T(S_T - S_0^c) - TS_0^c. \quad (7)$$

The functions $(H_T - H_0^c)/T$ and $(G_T - H_0^c)/T$ were obtained by dividing the respective quantities given in eqs (5) and (7) by the corresponding temperatures. The Gibbs energy was calculated using the two equivalent relations given in eq (7) to check the internal consistency of the calculations. The equations were evaluated by step-wise numerical integration and subtabulated using four-point Lagrangian integration coefficients [23] on the IBM 7094 computer at the Bureau.

Between 65 and 80 °K where the solid-phase transition was observed, the thermodynamic functions were calculated on the basis of the "normal" heat-capacity curve shown as a broken line in figure 1. At 77.16 °K the heat and entropy of transition were added in accordance with eqs (5) and (6) and the evaluation continued to the higher temperatures.

### 4.4. Reliability of the Results

The uncertainty in the final smoothed values of heat capacity obtained from the results of the measurements was estimated to be ±0.3 percent. At temperatures below about 50 °K the uncertainty increases because of the decrease in sensitivity of the thermometric method used. At the lowest temperature (16 °K) of the measurements, the uncertainty was estimated to be as much as ±1 percent. A precision of 0.02 percent or better can generally be achieved, however, with the calorimetric system in which the measurements were made. With a stable substance of high chemical and phase purity, and considering possible systematic errors, the accuracy of 0.1 percent or better is expected, except at the lowest temperatures for reasons mentioned above. In the present investigations the uncertainty in the chemical composition of the sample contributed more to the uncertainty of the final values than the uncertainty in the measurements.

The thermodynamic functions derived from the heat capacity are as reliable as the heat capacity. The calculations were performed with an accuracy greater than the precision of the measurements. Some discrepancies may be present in the tabulated thermodynamic functions because of the rounding.

## 5. Discussion of the Results

The λ-type solid-phase transition (transition temperature=189.9 °K, $\Delta S$=1.22 e.u.), observed in $NaBH_4$ by Johnston and Hallett [1], was interpreted by Stockmayer and Stephenson [2] as an order-disorder transition involving two orientations of the tetrahedral $BH_4^-$ ions. Stephenson et al. [10] similarly interpreted the transition found in $KBH_4$ at 76 ±1 °K from cooling and warming curve investigations. The heat capacity investigations on $KBH_4$ presented in this paper show an entropy of transition of 0.70 e.u. at 77.16 °K, which is about one-half of the expected 1.38 e.u. ($R$ ln 2) for completely random arrangement of the $BH_4^-$ tetrahedra between the two orientations. This suggests that the tetrahedra in $KBH_4$ may still remain essentially paired with local ordering just above the transition temper ture From the consideration of the larger lattice parameters of $KBH_4$ relative to those of $NaBH_4$ [5, 6], the interactions between the $BH_4^-$ ions in $KBH_4$ would be expected to be weaker and the rearrangement less hindered. The low entropy increment for the transition in $KBH_4$ indicates, however, that the interactions between the $BH_4^-$ ions are somewhat more complex and involve more than simple interpretations based on lattice parameters.

The heat capacity of $KBH_4$ shown in figure 2 suggests that another "transition" occurs from about 200 °K to as high as 450 °K. This transition is interpreted as the continuation of the order-disorder orientations of the tetrahedral $BH_4^-$ ions. The x-ray diffraction investigations by Ford and Powell [6] show, however, that the crystal structure of $KBH_4$ is the same at 90 and 293 °K. The lower temperature limit of this broad transition is higher than the transition temperature (189.9 °K) found for $NaBH_4$ by Johnston and Hallett [1], which indicates further that the $BH_4^-$ ions in $KBH_4$ interact more than in $NaBH_4$.

The transition at the higher temperatures was expected to contain the remaining 0.7 e.u. The estimation of the entropy contribution of the transition, based on the subtraction from the observed heat capacities the contributions of $C_p - C_v$, lattice vibrations, and internal vibrations and torsional oscillations of the $BH_4^-$ ion, was not satisfactory. For the $C_p - C_v$ and lattice vibration contributions, the heat capacity of KF [24] was taken. For the contributions from internal vibrations in $BH_4^-$, the frequency values given by Altshuller [25] for $NaBH_4$ were used. For the torsional oscillations the value 350 $cm^{-1}$ estimated for $BH_4^-$ in $NaBH_4$ by Stockmayer and Stephenson [2] was used. The sum of the various contributions was found to be considerably lower than the expected heat capacity. The heat capacity of $KBH_4$ is expected to be slightly above that of $NaBH_4$ (see figure 2). For example, at 300 °K the difference between the expected heat capacity and the sum of the heat capacity of KF and the contributions from the internal vibrations in $BH_4^-$ is larger than the classical limit for an oscillator (three degrees of freedom). The results at 400 °K are the same. This

indicates that the frequencies used for the internal vibrations in $BH_4^-$ are too high or that the observed resultant heat capacities are considerably more complex than the simple summation of the contributions given earlier.

The heat capacities obtained from the following relation were found to be fairly satisfactory:

$$C_{KBH_4} = C_{NaBH_4} - C_{NaF} + C_{KF}, \quad (8)$$

where the symbol C represents the heat capacity corresponding to the substance indicated by the subscript [1, 26, 24]. The results are plotted in figure 2 (solid line). The entropy difference in the inteval 200 to 500 °K between the observed values for $KBH_4$ and that calculated according to eq (8) is 1.11 e.u. This value is somewhat larger than the expected value (0.7 e.u.). The calculations based on eq (8) probably yielded heat capacities that are too low. The two values are sufficiently close to suggest that the higher-temperature transition contains the remaining order-disorder transition.

For comparison, heat-capacity measurements should be interesting on the other alkali-metal (Rb and Cs) borohydrides, which have the face-centered cubic crystal structure similar to $KBH_4$ and $NaBH_4$ [5]. Stephenson et al. [10] observed transitions in $RbBH_4$ and $CsBH_4$ in cooling and warming curve investigations. Neither the entropy of these transitions nor the higher-temperature broad transitions have been investigated. Lithium borohydride, $LiBH_4$, which is orthorhombic [11], does not exhibit any transition between 16 and 303 °K [27] similar to those found in $NaBH_4$ or $KBH_4$. (See fig. 2.) A close examination of the $LiBH_4$ data at the upper limit of measurements [27] does, however, show a slight indication of an on-set of a possible transition. The indication may be just a scatter in experimental data. Further measurements on $LiBH_4$ above 300 °K would also be interesting.

(Paper 68A–314)

## 6. References


[1] H. L. Johnston and N. C. Hallett, J. Am. Chem. Soc. **75,** 1467 (1953).
[2] W. H. Stockmayer and C. C. Stephenson, J. Chem. Phys. **21,** 1311 (1953).
[3] C. C. Stephenson, L. A. Landers, and A. G. Cole, J. Chem. Phys. **20,** 1044 (1952).
[4] C. C. Stephenson, R. W. Blue, and J. W. Stout, J. Chem Phys. **20,** 1046 (1952).
[5] S. C. Abrahams and J. Kalnajs, J. Chem. Phys. **22,** 434 (1954).
[6] P. T. Ford and H. M. Powell, Acta Cryst. **7,** 604 (1954).
[7] E. L. Wagner and D. F. Hornig, J. Chem. Phys. **18,** 296, 305 (1950).
[8] H. A. Levy and S. W. Peterson, Phys. Rev. **86,** 766 (1952).
[9] H. A. Levy and S. W. Peterson, J. Am. Chem. Soc. **75,** 1536 (1953).
[10] C. C. Stephenson, D. W. Rice, and W. H. Stockmayer, J. Chem. Phys. **23,** 1960 (1955).
[11] P. M. Harris and E. P. Meibohm, J. Am. Chem. Soc. **69,** 1231 (1947).
[12] T. Shigi, Busseiron Kenkyu **92,** 43 (1956).
[13] T. B. Douglas and A. W. Harman, J. Res. NBS **60,** 117 (1958).
[14] R. B. Scott, C. H. Meyers, R. D. Rands, Jr., F. G. Brickwedde, and N. Bekkedahl, J. Res. NBS **35,** 39 (1945).
[15] G. T. Furukawa, M. L. Reilly, and J. H. Piccirelli, publication pending.
[16] H. F. Stimson, J. Res. NBS **65A,** 139 (1961).
[17] H. J. Hoge and F. G. Brickwedde, J. Res. NBS **22,** 351 (1939).
[18] G. T. Furukawa, D. C. Ginnings, R. E. McCoskey, and R. A. Wilson, J. Res. NBS **46,** 195 (1951)
[19] IUPAC Revises Atomic Weight Values, Chem. Eng. News **39,** 42 (1961).
[20] G. Grenier and E. F. Westrum, Jr., J. Am. Chem. Soc. **78,** 6226 (1956).
[21] D. R. Stull, private communication.
[22] E. T. Whittaker and G. Robinson, The Calculus of Observations. A Treatise on Numerical Mathematics, Fourth Edition, pp. 285–316 (Blackie and Son, London, 1944).
[23] Tables of Lagrangian Interpolation Coefficients (Columbia University Press, New York, 1944).
[24] E. F. Westrum, Jr. and K. S. Pitzer, J. Am. Chem. Soc. **71,** 1940 (1949).
[25] A. P. Altshuller, J. Am. Chem. Soc. **77,** 5455 (1955).
[26] E. G. King, J. Am. Chem. Soc. **79,** 2056 (1957).
[27] N. C. Hallett and H. L. Johnston, J. Am. Chem. Soc. **75,** 1496 (1953).

JOURNAL OF RESEARCH of the National Bureau of Standards—A. Physics and Chemistry
Vol. 68A, No. 6, November–December 1964

# Heat of Combustion and Heat of Formation of Aluminum Carbide

R. C. King and G. T. Armstrong

(August 14, 1964)

The heat of combustion of aluminum carbide ($Al_4C_3$) in oxygen was measured by means of bomb calorimetry. The solid product of the combustion consisted of alpha aluminum oxide and another crystalline form of alumina, which was characterized as delta alumina. The heats of combustion were corrected for the formation of the delta aluminum oxide. The results, when combined with the heats of formation of alpha aluminum oxide and carbon dioxide, yielded $-49.7$ kcal mole$^{-1}$ for the standard heat of formation of aluminum carbide at 298.15 °K with an estimated overall uncertainty of $\pm 1.2$ kcal mole$^{-1}$.

## 1. Introduction

Although several thermodynamic studies have been made on $Al_4C_3$, which is a very stable refractory compound, there exist very few data on the heat of formation. We have, therefore, determined the heat of combustion in oxygen (reaction 1), and have derived the heat of formation.

$$Al_4C_3(s)+6\ O_2(g)=2\ Al_2O_3(s)+3\ CO_2(g). \quad (1)$$

We believe that the most reliable previous study was that of Meichsner and Roth [1][1,2], who also determined the heat of combustion in oxygen by bomb calorimetry. For reaction (1) they reported $\Delta H_{293}=-1047.6\pm 3$ kcal mole$^{-1}$. In a parallel series of experiments they determined the heat of combustion of aluminum, for which they reported $\Delta H_{293}=-392.4\pm 0.4$ kcal mole$^{-1}$. They calculated $\Delta Hf^\circ_{293}$ [$Al_4C_3$]$=-20\pm 3$ kcal mole$^{-1}$.

The heat of combustion of aluminum is very important in establishing the heat of formation of $Al_4C_3$ by this method, because of the presence of aluminum oxide in the products. In the work of Meichsner and Roth it is given added weight by the fact that the latter authors mixed their $Al_4C_3$ with aluminum powder in order to obtain complete combustion. A significant fraction of the total heat they observed was due to the combustion of the free aluminum. The value of the heat of formation of $Al_4C_3$ calculated from their work is therefore very sensitive to the value selected for the heat of formation of $Al_2O_3$.

As a result of later work on the combustion of aluminum, Roth [2] modified the calculations of Meichsner and Roth and obtained $-40$ kcal mole$^{-1}$ for the heat of formation of $Al_4C_3$. If one assumes that the aluminum oxide in their product was corundum ($\alpha-Al_2O_3$), and if a recent value for its heat of formation, $-400.4\pm 0.3$ kcal mole$^{-1}$ [3], is used in recalculating their data, a value of $-48.6$ kcal mole$^{-1}$ is obtained for $\Delta Hf^\circ_{298}$ [$Al_4C_3$]. However, because Meichsner and Roth determined the heat of combustion of aluminum under nearly the same conditions as those under which they determined the heat of combustion of aluminum carbide, it now seems to us that little can be done to improve the calculation they made in their original publication. The principal difficulty in the way of making any further refinement of their original data now seems to be the lack of any detail about the form of $Al_2O_3$ found in the product. They assumed the $Al_2O_3$ to be corundum, but mention no test of their assumption. Because of the presence of a carbonaceous promoter in their reactions, the presence of another form must now be assumed on the basis of the findings described in this paper.

Our work differs from that of Meichsner and Roth in (1) the exclusion of carbonaceous combustion aids from the reaction, (2) the absence of elemental aluminum as a combustion promoter, (3) the absence of water in the combustion bomb, (4) the unambiguous determination of the amount of reaction by measurement of the mass of $CO_2$ formed, and (5) the identification of the crystal forms of the solid combustion product.

The heat of combustion of aluminum carbide has also been measured, and the heat of formation calculated by Berthelot [4], Wöhler and Hofer [5], and Kameyama and Yoshida [6]. The values they reported for the heat of reaction (1) and the heat of formation of $Al_4C_3$ which we have recalculated on the basis of the recent value for $Al_2O_3$ were, respectively, in kcal mole$^{-1}$: Berthelot, $-824$, $-258.9$; Wöhler and Hofer, $-825.1$, $-257.8$; Kameyama and Yoshida, $-991.8$, $-91.2$. These measurements were all made on aluminum carbide samples of relatively low purity. Because of this their work is not considered further, although Kameyama and Yoshida used great care in documenting their measurements.

[1] Figures in brackets indicate the literature references at the end of this paper.
[2] After completion of this manuscript, Mah [40] reported a value for the heat of formation of aluminum carbide, which was also obtained by means of oxygen bomb calorimetry. The value reported for $\Delta Hf^\circ_{298.15}$ [$Al_4C_3$] is $-53.4\pm 2.0$ kcal mole$^{-1}$.

In addition to the calorimetric measurements, several high-temperature equilibrium studies involving aluminum carbide have been made, from which the heat of formation can be calculated. In each case the original calculations required estimates of the values of the thermal functions used for $Al_4C_3$ and, in some cases, for other compounds as well. Recent measurements of the heat capacity by Furukawa et al. [7] permit calculations now to be made using functions based on measurements over much of the temperature range of interest for $Al_4C_3$. In general, we consider the equilibrium studies to be less reliable than the best combustion measurements for calculating the heat of formation. The measured heat of formation and heat capacities can be used to correlate the equilibrium studies. Inconsistencies in the equilibrium data can possibly be used to detect errors of technique or interpretation of the equilibrium measurements. Such a study is presented by Furukawa et al.

The equilibrium studies will be briefly mentioned. Campbell [8] measured the activity of aluminum in $Al_4C_3$ at 920 °C, from which he calculated the free energy of formation of aluminum carbide, $\Delta Gf^\circ_{1193} = -35.8$ kcal mole$^{-1}$. Using thermodynamic data for $Al_4C_3$ based on the heat capacity measurements of Furukawa et al. [7] and recent tabulations of thermal functions for Al(g) and C(s) [9], we calculated $\Delta Hf^\circ_{298}$ [$Al_4C_3$] $= -51.2$ kcal mole$^{-1}$ from Campbell's free energy of formation.

The vapor pressure of aluminum carbide has been measured approximately by Ruff [10] between 1500 and 2300 °K, by Chupka et al. [11] at 2100 °K, and by Meschi and Searcy [12] over the range 1500 to 1800 °K. In the measurement of Ruff the species in the vapor do not appear to be well defined and his pressures are much too high when compared with those of Chupka and of Meschi and Searcy. Chupka et al. found $p = 6 \times 10^{-4}$ atm, from which we can calculate $\Delta Hf^\circ_{298}$ [$Al_4C_3$] $= -91.5$ kcal mole$^{-1}$, assuming the only vapor species present to be Al(g). Taking from Meschi and Searcy the average vapor pressure, $p = 4.2 \times 10^{-6}$ atm at 1600 °K, and assuming that vaporization occurred according to reaction (2) we calculate

$$Al_4C_3(s) = 4Al(g) + 3C(s) \qquad (2)$$

$\Delta H_{1600} = 366.3$ kcal mole$^{-1}$ and $\Delta Hf^\circ_{298}$ [$Al_4C_3$] $= -63.5$ kcal mole$^{-1}$.

Equilibria in the system $Al_4C_3$–$N_2$ were studied by Prescott and Hincke [13]. They assumed that the equilibrium was represented by eq (3),

$$Al_4C_3(s) + 2N_2(g) = 4AlN(s) + 3C(s). \qquad (3)$$

Von Stackelberg et al. [14, 15] pointed out that the more probable reactions were reaction (4) in the nitrogen rich mixture and reaction (5) in the nitrogen lean mixtures and that a distinction could be drawn between these, which would lead to the energy of reaction (6).

$$Al_5C_3N(c) + 2N_2(g) = 5AlN(c) + 3C(c) \qquad (4)$$

$$5Al_4C_3(c) + 2N_2(g) = 4Al_5C_3N(c) + 3C(c) \qquad (5)$$

$$Al_4C_3(c) + AlN(c) = Al_5C_3N(c). \qquad (6)$$

This manner of treating the data has been discussed by Satoh [16] and by Efimenko et al. [17].

If we use the results of the analysis by Efimenko et al., which gives $\Delta H_{298} = 263.2$ kcal mole$^{-1}$ for the enthalpy change of reaction (3), and apply $\Delta Hf^\circ_{298}$ [AlN] $= -76.0$ kcal mole$^{-1}$ recommended by Armstrong and Krieger [18], we find $\Delta Hf^\circ_{298}$ [$Al_4C_3$] $= -40.8$ kcal mole$^{-1}$.

Herstad [19] reported a measurement of equilibrium pressures of Mg vapor in reaction (7) near 1400 °K, and calculation of the free energy of

$$8MgO(s) + Al_4C_3(s) = 2MgAl_2O_4(s) + 3C(s) + 6Mg(g) \qquad (7)$$

formation of aluminum carbide from solid carbon and liquid aluminum at 1400 °K; $\Delta Gf^\circ_{1400} = -220 \pm 1.5$ kcal mole$^{-1}$. Using this value and free energy functions for $Al_4C_3$, Al, and C [7, 9], we calculate $\Delta Hf^\circ_{298}$ [$Al_4C_3$] $= -58.5$ kcal mole$^{-1}$.

Equilibria in the system Al–O–C were studied at high temperatures and the vapor pressures of CO in this system were measured by Prescott and Hincke [20], Brunner [21], and Treadwell and Gyger [22]. These equilibrium studies were used to calculate the heat of formation of $Al_4C_3$ by various workers, before it was realized that the equilibria are complicated by the occurrence of aluminum oxycarbides [23]. More recent equilibrium studies by Cox and Pidgeon [24], by Motzfeldt [25], and by Franck [26] take into account the formation of $Al_4O_4C$ and $Al_2OC$. However, no thermodynamic data have been measured for these compounds. The calculation of the heat of formation of $Al_4C_3$ from the observed equilibrium data requires estimates of the thermal functions of $Al_4O_4C$ and $Al_2OC$, and therefore, we do not consider these equilibria further in this paper.

## 2. Experimental Procedure

### 2.1. Materials

The aluminum carbide sample was supplied by the Aluminum Company of America Research Laboratories. It was prepared by heating a stoichiometric mixture of aluminum and lampblack in an argon atmosphere at 1800 °C. Prior to the present work, this sample had been used for high- and low-temperature heat capacity measurements at the National Bureau of Standards [7]. Specimens from the original sample were spectrochemically and chemically analyzed. After the heat capacity measurements, specimens were again chemically analyzed. The results from the analyses are given in table 1.

TABLE 1. (a) *Qualitative spectrochemical analysis of aluminum carbide sample*

| Element | Percent | Element | Percent |
|---|---|---|---|
| Ag | ? | Mn | 0.0001–0.001 |
| Al | >10 | Ni | .001 – .01 |
| Ca | 0.0001–0.001 | Si | .01 – .1 |
| Cr | .001 – .01 (?) | Ti | .001 – .01 |
| Cu | .001 – .01 | V | .01 – .1 |
| Fe | .1 –1.0 | Zr | .001 – .01 |
| Mg | .001 –0.01 | | |

(b) *Quantitative chemical analyses of aluminum carbide sample*

| Component | Percent by weight | | | | | |
|---|---|---|---|---|---|---|
| | 1a | 1b | 1′ | 2 | 2′ | 3 |
| $Al_4C_3$ | 94.9 | 94.8 | 94.61 | 94.8 | 94.46 | |
| Free Al | 1.2 | 1.3 | 1.25 | 1.0 | 1.00 | |
| Free C | 0.9 | 0.7 | 0.8 | 1.0 | 1.00 | |
| AlN | 1.4 | 1.3 | 1.35 | 1.3 | 1.29 | |
| $Al_2O_3$ | 2.0 | 2.0 | 1.99 | 2.2 | 2.19 | |
| Fe | | | | 0.06 | 0.06 | |
| Total | 100.4 | 100.1 | 100.00 | 100.36 | 100.00 | |
| Total C | 24.65 | 24.43 | 24.48 | 24.73 | 24.64 | 24.57 |

The spectrochemical analysis was performed in the Spectrochemical Section at the National Bureau of Standards. The quantitative analyses 1a, 1b, 2, and 3 were made in the Analysis and Purification Section using methods previously described [7]. Analyses 1a and 1b were made on two specimens before any heat capacity measurements were made. Analyses 2 and 3 were made on two specimens after the sample had been used for high temperature and low temperature heat capacity studies. The fact that the chemical analyses total slightly more than 100 percent may be caused by uncertainties in the analytical methods and small inhomogeneities in the sample. Analysis 1′ is the average of analyses 1a and 1b, normalized to 100 percent. Analysis 2′ is the same as analysis 2, normalized to 100 percent. Analysis 3 was an independent measurement of total carbon, made by combustion of the sample and collection of carbon dioxide as for an organic compound. It was carried out because total carbon dioxide in the product gases was to be used as a measure of the amount of reaction occurring in the calorimetric experiments. The total carbon as listed in column 7 is in excellent agreement with the average of the total carbon in the normalized analyses, columns 4 and 6, but is less than the total carbon calculated from the actual results of these analyses.

The oxygen used in these experiments was of high purity, specified by the manufacturer to contain impurities not exceeding 0.005 percent. Although further purification was probably not necessary for this gas, the oxygen was passed over copper oxide heated to 500 °C to oxidize combustible impurities and through successive columns of ascarite and magnesium perchlorate to remove carbon dioxide and moisture.

## 2.2. Combustion Experiments

The samples were burned in a Dickinson-type calorimeter [27]. The combustion bomb was a commercial calorimeter bomb made of type 20 corrosion resistant alloy steel and equipped with platinum-iridium inlet tube and electrodes. A platinum-iridium support loop, approximately one inch in diameter, was attached to the lower end of the inlet tube.

The combustions were conducted under 30 atm of oxygen. In order to remove the air, the bomb was filled with 10 to 15 atm of oxygen for three times before being filled to the final pressure. The samples were ignited with a fuse wire for which the ignition energy amounted to 22 J.

The definition, 1 cal=4.184 J, was used for expressing the results in calories. All atomic weights were taken from the 1961 Table of Atomic Weights based on carbon 12, adopted by the International Union of Pure and Applied Chemistry [28].

The calorimeter was calibrated with benzoic acid, National Bureau of Standards Sample 39i, which has a certified heat of combustion of 26,434 J $g^{-1}$ (weight in vacuo).

We found it necessary to use different supports for the samples in the calibration experiments and in the aluminum carbide combustions. The benzoic acid pellets were weighed and burned in a small platinum crucible (about 7.5 g). The powdered aluminum carbide samples were weighed in small platinum pans, made from 0.004-in.-thick foil. The samples were burned in these containers on aluminum oxide disks, 0.062 in. thick by 1.25 in. diam. In the bomb the disks were supported on the platinum-iridium loop described above. It was found that a platinum support with a low enough heat capacity to allow complete combustion of benzoic acid melts when aluminum carbide burns on it. On the other hand, incomplete combustion of the benzoic acid occurs if the support is massive enough to prevent melting during the aluminum carbide combustions. The difference is attributed to the fact that most of the heat from a benzoic acid combustion is carried away from the reaction zone by the products of combustion, which are all gases. On the other hand, in the aluminum carbide combustions some of the solid product, aluminum oxide, is in contact with the sample support and retains a large amount of the heat in this location. In all cases the combustion of the carbide was greater than 99.5 percent complete.

The alumina disk container was weighed before and after each aluminum carbide combustion experiment. During the experiment, the disk cracked but remained on the supporting loop. As an extra precaution, the base of the combustion bomb was covered with alumina disks so that the bomb could be cleaned easily if the container disk had shattered during the combustion.

A preliminary test of the behavior of the $Al_4C_3$ sample on exposure to air showed that a gain in weight occurred, which was very gradual at first, and then became increasingly rapid. On the other hand, a sample kept in a desiccator showed no weight

change in the same interval of time. This test, which extended over an interval of 2 months, showed that if, after opening the sealed vial, it was stored in a desiccator, the aluminum carbide could be handled in air for the short time necessary to weigh the combustion sample, and prepare the bomb for a heat measurement, without detriment to the sample. In another preliminary experiment the aluminum carbide was tested for possible reaction in the bomb prior to ignition. A weighed sample was placed in the bomb and all process steps were conducted up to the point of ignition. After 4 hr, the sample was reweighed. No significant weight increase was observed.

The standard calorimeter for the calibration experiments consisted of the calorimeter vessel with stirrer and water, the platinum resistance thermometer, and the combustion bomb with its electrical connections, fuse, platinum crucible, an alumina disk sample support for aluminum carbide, 30 atm of oxygen, 1 ml water, and five alumina disks covering base of the bomb. The water and calorimeter vessel, not including lid, weighed 3670 g. The results for seven calibration experiments are given in table 2.

TABLE 2. *Calibration experiments*

| Experiment No. | $m_s$ | $\Delta R_c$ | $f$ | $q$ | $\Delta\epsilon_i$ | $E_s$ |
|---|---|---|---|---|---|---|
| | *g* | *Ohms* | $\times 10^6$ | *J* | *J ohm*$^{-1}$ | *J ohm*$^{-1}$ |
| 6 | 1.002313 | 0.191495 | −134.25 | 22.24 | 15.5 | 138441.0 |
| 8 | 1.000229 | .191044 | −129.73 | 22.30 | 16.3 | 138479.5 |
| 9 | 1.001456 | .191300 | −129.13 | 22.30 | 16.4 | 138464.4 |
| 15 | 1.000091 | .191031 | −143.38 | 23.20 | 14.1 | 138474.1 |
| 17 | 1.001660 | .191317 | −134.58 | 22.30 | 15.5 | 138480.3 |
| 21 | 1.001504 | .191374 | −140.98 | 22.30 | 14.5 | 138417.7 |
| 22 | 1.000912 | .191257 | −139.41 | 22.30 | 14.7 | 138420.5 |

The calibration experiments were interspersed with measurements on aluminum carbide. In table 2 the columns listed beginning on the left, give the experiment number; the mass (weight in vacuo) of benzoic acid in grams, $m_s$; the corrected resistance thermometer change, $\Delta R_c$; the term $f$ in the factor $1+f$ used to convert the standard energy of combustion of the benzoic acid to actual bomb conditions; the correction for ignition energy and nitric acid formation, $q$; the correction to the energy equivalent of the calorimeter to bring it to that of the standard calorimeter system, $\Delta\epsilon_i$; and the calculated energy equivalent of the standard calorimeter, $E_s$. Seven experiments led to an energy equivalent of 138453.9 J ohm$^{-1}$ with a standard deviation of the mean of 10.4 J ohm$^{-1}$.

The standard calorimeter for the experiments with aluminum carbide differed from that in the calibration experiments only in the omission of water from the bomb in the aluminum carbide experiments.

## 2.3. Examination of the products of the combustion

The products of combustion of the aluminum carbide were examined to determine the quantities of carbon dioxide and nitrogen dioxide formed in the reaction, and to characterize the solid combustion products. Qualitative tests on the gaseous products for NO [29] and CO [30] were negative. The carbon dioxide formed in each experiment was measured by absorption in Ascarite [31]. The nitrogen dioxide formed was determined by absorption on specially purified manganese dioxide [32].

A semi-schematic diagram of the analytical train is given in figure 1. Both the apparatus and

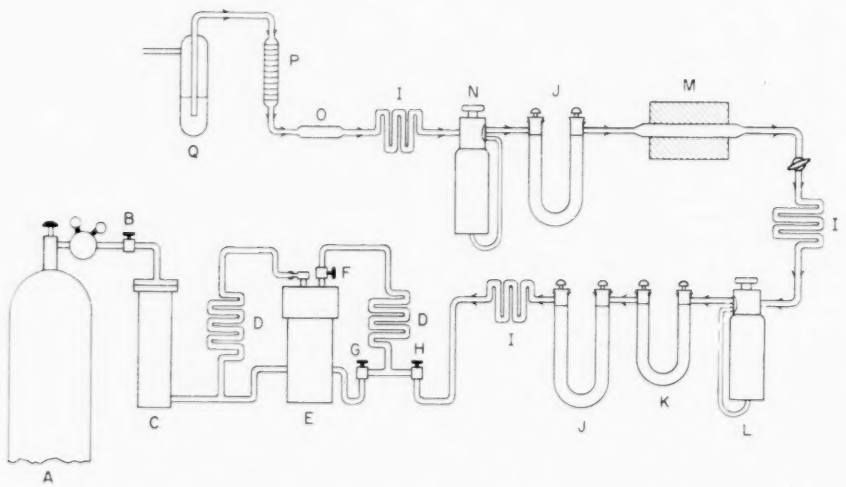


FIGURE 1. *Train for analysis of bomb gases*

(A) Cylinder of high-purity nitrogen, (B) microregulating valve, (C) absorption tube containing Ascarite and magnesium perchlorate, (D) coiled copper tube, (E) combustion bomb, (F) bomb outlet valve, (G) bypass valve, (H) valve, (I) glass tubing coil, (J) drying tube, (K) nitrogen dioxide absorption tube, (L) and (N) carbon dioxide absorbers, (M) furnace, (O) guard tube containing magnesium perchlorate and Ascarite, (P) flowmeter, (Q) bubbler.

analytical procedures are similar in many respects to those used by Prosen and Rossini [33]. *A* is a cylinder of high-purity nitrogen under pressure. The nitrogen passes through a Monel tube, *C*, containing successive layers of Ascarite and magnesium perchlorate. The flow rate of the nitrogen is adjusted with the microregulating valve, *B*. The coiled copper tubes, *D*, lead to the inlet and outlet valves on the combustion bomb, *E*. The valves, *F* and *H*, are used to control the flow rate of gases from the combustion bomb. When the inlet and outlet valves to the bomb are closed, and valves *G* and *H* are open, the train may be flushed with nitrogen, bypassing the combustion bomb. This is often found useful when checking for leaks immediately prior to an analysis. The tube, *J*, contains magnesium perchlorate for removal of moisture. Tube *K*, containing manganese dioxide backed by magnesium perchlorate, absorbs nitrogen dioxide. Carbon dioxide formed in the combustion reaction is absorbed in tube *L*, which contains Ascarite backed by magnesium perchlorate. Any carbon monoxide formed in the combustion is converted to carbon dioxide in the furnace, *M*, and is then dried over magnesium perchlorate in *J*, and absorbed in the tube *N*, which also contains Ascarite backed by magnesium perchlorate. The furnace, *M*, is a tube wound with nichrome and containing a Vycor tube filled with copper oxide which is kept at 500 °C. Tube *O* contains successive layers of magnesium perchlorate and Ascarite to prevent back diffusion of carbon dioxide and moisture from the air. *P* is a float-type flowmeter and *Q* is a bubbler.

During the period immediately preceding the combustion experiment, the absorption tubes, *K*, *L*, and *N*, are flushed, filled with nitrogen, and weighed. The tubes are replaced in the train for the analysis. Immediately after the experiment, the valve, *F*, is attached to the outlet valve on the bomb. After inserting the bomb, the train is flushed with nitrogen by way of the bypass around the bomb for about 10 min and then valve *G* is closed. Valve *H* is opened and the gases are released from the bomb at a rate of about 200 ml $min^{-1}$. When the pressure in the bomb reaches 1 atm, the inlet valve is opened and nitrogen is passed through the bomb at the foregoing rate for 1 hr. The absorption tubes are removed from the train, cleaned, and reweighed. The true mass of the absorbed carbon dioxide was calculated using the method outlined by Rossini [34].

The reproducibility of the weighings of the absorption tubes was 0.0001 to 0.0005 g. In blank experiments in which the same quantity of nitrogen was passed through as in an analysis, no weight changes could be detected outside of these limitations. The accuracy of these analytical procedures was checked from time-to-time by determining the quantity of carbon dioxide produced from the combustion of a sample of benzoic acid. These checks indicated that the analyses were accurate to within $\pm 0.01$ percent for absorption of 3.8 g of carbon dioxide. In the aluminum carbide experiments, the mass of carbon dioxide collected was about 0.77 g. The amount of nitrogen dioxide collected varied from 1.5 to 4.0 mg.

### 2.4. Identification of Solid Product

The solid product from the combustions was characterized by x-ray diffraction on the basis of patterns maintained at the National Bureau of Standards and those published by Newsome et al. [35]. In each experiment a large fraction of the product aluminum oxide was deposited in extremely finely divided form on the wall of the bomb. The remaining alumina, in the form of a fused mass, was on the reaction disk. The alumina on the disk was alpha alumina only, and that on the bomb wall was a different crystalline form, similar to delta alumina. Because all of the alpha aluminum oxide remained on the reaction disk, it was possible to separate the two alumina phases and determine the quantity of each obtained in an experiment.

The x-ray data for the transition [3] alumina obtained in the present study are given in table 3, along with the data obtained by Rooksby [36] and Stumpf [35] for delta alumina. The pattern given by Stumpf was obtained from delta alumina prepared by calcination of pure alpha alumina monohydrate (Böhmite). He has pointed out that delta alumina prepared by this method exhibits slightly diffuse diffraction lines indicative of small crystal size or crystal imperfection [37]. Rooksby investigated several ways of preparing delta alumina and obtained the pattern given here from alumina prepared by calcination of ammonium aluminum sulfate with ammonium molybdate at 950 °C. He found that a more crystalline delta alumina resulted from this method than from the calcination of Böhmite. It will be seen that there are differences between the Rooksby and Stumpf patterns. Even with the variations in the diffraction patterns observed, it is generally acknowledged that delta alumina is a definite crystalline form. However, until the situation is further clarified, a choice cannot be made as to which is the better pattern.

The x-ray pattern for the transition alumina found in this study is more nearly similar to the Rooksby pattern than to that reported by Stumpf. However, it has some features in common with the Stumpf pattern which are lacking in Rooksby's. Each pattern has some distinctive lines.

Foster et al. [23] observed a delta-like alumina in a study of the equilibrium diagram for the $Al_4C_3$—$Al_2O_3$ system. Newsome et al. [35] report that delta alumina can be prepared by fusion together of alumina and aluminum nitride. This indicates that delta alumina is stabilized by nitrogen. These earlier studies suggest that the formation of the delta alumina in this study probably is promoted by the nitrogen and carbon in the aluminum carbide sample.

[3] Newsome et al. [35] designate crystalline forms of alumina, other than alpha alumina, as transition aluminas.

TABLE 3. *X-ray data for finely divided aluminum oxide formed in the combustion bomb*

| Present work | | | Delta $Al_2O_3$ | | | |
|---|---|---|---|---|---|---|
| | | | Rooksby [36] | | Stumpf [35] | |
| $\theta°$ | $d$ | I | d | I | d | I |
| *deg* | *°A* | | *°A* | | *°A* | |
| | | | 7.97 | 8 | | |
| | | | 6.58 | 10 | | |
| 17.42 | 5.08 | 11 | 5.07 | 20 | 5.02 | 30 |
| | | | | | 4.55 | 30 |
| 21.82 | 4.06 | 12 | 4.05 | 20 | 4.07 | 20 |
| 23.60 | 3.76 | 4 | | | | |
| 25.02 | 3.55 | 6 | 3.56 | 7 | | |
| 26.09 | 3.412 | 7 | 3.40 | 10 | | |
| 27.06 | 3.292 | 12 | 3.28 | 15 | | |
| 27.64 | 3.224 | 5 | 3.21 | 10 | | |
| 29.26 | 3.049 | 7 | 3.03 | 10 | | |
| 30.49 | 2.929 | 3 | | | | |
| 31.21 | 2.863 | 6 | | | 2.87 | 40 |
| 31.55 | 2.833 | 8 | | | | |
| 32.04 | 2.791 | 31 | 2.783 | 30 | | |
| 32.74 | 2.732 | 18 | 2.737 | 30 | 2.73 | 80 |
| 34.45 | 2.601 | 47 | 2.593 | 70 | 2.58 | 30 |
| 35.11 | 2.553 | 8 | | | | |
| 36.54 | 2.457 | 62 | 2.457 | 70 | 2.43 | 60 |
| 37.65 | 2.387 | 19 | | | | |
| 38.96 | 2.309 | 36 | 2.311 | 40 | | |
| 39.44 | 2.282 | 36 | 2.277 | 30 | 2.28 | 40 |
| 39.70 | 2.268 | 33 | | | | |
| 41.69 | 2.164 | 13 | 2.156 | 25 | | |
| 44.72 | 2.024 | 3 | | | | |
| 45.70 | 1.983 | 69 | 1.989 | 70 | 1.99 | 80 |
| 46.35 | 1.957 | 37 | 1.950 | 65 | 1.95 | 30 |
| 50.66 | 1.800 | 4 | 1.793 | 7 | 1.91 | 20 |
| 53.84 | 1.701 | 3 | 1.701 | 4 | 1.80 | 20 |
| 56.99 | 1.614 | 12 | 1.616 | 10 | | |
| 57.41 | 1.603 | 11 | 1.602 | 15 | | |
| 59.94 | 1.541 | 11 | 1.543 | 10 | 1.54 | 40 |
| 60.86 | 1.520 | 9 | | | | |
| 61.52 | 1.506 | 20 | 1.507 | 20 | 1.51 | 30 |
| | | | | | 1.49 | 40 |
| 63.57 | 1.462 | 5 | 1.462 | 8 | 1.45 | 30 |
| 64.78 | 1.437 | 3 | | | | |
| 65.87 | 1.418 | 9 | | | | |
| 66.60 | 1.402 | 60 | 1.407 | 60 | 1.40 | 60 |
| 67.13 | 1.393 | 100 | 1.392 | 100 | 1.39 | 100 |
| | | | | | 1.29 | 20 |
| | | | | | 1.26 | 10 |
| 76.23 | 1.247 | 4 | 1.250 | 4 | | |
| 77.16 | 1.235 | 6 | 1.238 | 9 | | |
| 81.24 | 1.183 | 17 | 1.180 | 4 | | |
| 84.92 | 1.141 | 10 | | | 1.14 | 20 |
| 85.20 | 1.137 | 8 | 1.134 | 10 | | |

## 3. Results

### 3.1. Heat Measurements

In table 4 are listed $m_s$, the mass of sample; $m(CO_2)$, the mass of $CO_2$; $\Delta R_c$, the corrected resistance thermometer change; $\Delta e_2$, the correction for the deviation of this calorimeter from the standard calorimeter; and $-\Delta U_B$, the observed energy of reaction at 28 °C.

These include corrections for the combustion of impurities on the basis of analysis 2 (table 1b). In making these corrections, it was assumed that the completeness of combustion of the impurities was the same as that for the aluminum carbide sample, which was calculated from the ratio of the observed to expected amounts of $CO_2$ formed. $q_1$ is the ignition energy; $q_2$, the correction to standard state; and $q_3$, the correction to 25 °C.

TABLE 4. *Heat measurements on aluminum carbide samples*

| Experiment No. | $m_s$ | $m(CO_2)$ | $\Delta R_c$ | $\Delta e_2$ | $-\Delta U_B$ 28 °C |
|---|---|---|---|---|---|
| | *g* | *g* | *Ohm* | *J ohm⁻¹* | *J* |
| 10 | 0.852498 | 0.771016 | 0.178892 | −27.5 | 24763.4 |
| 11 | .851387 | .770745 | .178673 | −27.5 | 24733.1 |
| 12 | .851040 | .764905 | .178031 | −27.5 | 24644.2 |
| 13 | .849675 | .765961 | .178751 | −29.5 | 24743.5 |
| 16 | .851301 | .766513 | .178648 | −28.8 | 24729.4 |
| 18 | .848726 | .765632 | .177593 | −29.8 | 24583.2 |
| 19 | .854470 | .771409 | .179115 | −29.4 | 24793.9 |
| 20 | .850351 | .767780 | .179008 | −29.1 | 24779.2 |

To $\Delta U_B$ were applied corrections listed in table 5.

TABLE 5. *Corrections to combustion data on aluminum carbide*

| Experiment No. | $q_{AlN}$ | $q_{Al}$ | $q_{Fe}$ | $q_C$ | $q_1$ | $q_2$ | $q_3$ | $\Sigma_{corr.}$ |
|---|---|---|---|---|---|---|---|---|
| | *J* | *J* | *J* | *J* | *J* | *J* | *J* | *J* |
| 10 | −137.3 | −264.4 | −3.8 | −279.6 | −22.0 | 5.3 | −4.5 | −706.3 |
| 11 | −136.7 | −264.4 | −3.8 | −279.5 | −22.0 | 5.3 | −4.5 | −705.6 |
| 12 | −136.6 | −262.3 | −3.7 | −277.5 | −22.0 | 5.2 | −4.4 | −701.3 |
| 13 | −137.5 | −262.7 | −3.7 | −277.9 | −22.0 | 5.0 | −4.5 | −703.3 |
| 16 | −136.7 | −262.9 | −3.7 | −278.0 | −22.0 | 5.1 | −4.5 | −702.7 |
| 18 | −137.1 | −262.6 | −3.7 | −277.7 | −22.0 | 5.2 | −4.5 | −702.4 |
| 19 | −136.0 | −264.6 | −3.8 | −279.8 | −22.0 | 5.0 | −4.5 | −705.7 |
| 20 | −135.5 | −263.3 | −3.7 | −278.5 | −22.0 | 5.0 | −4.5 | −702.5 |

In making the correction for the combustion of AlN it was assumed that the AlN burned according to the reactions (8) and (9).

$$AlN(s)+7/4O_2(g)\rightarrow\tfrac{1}{2}Al_2O_3(s)+NO_2(g) \quad (8)$$

$$AlN(s)+3/4O_2(g)\rightarrow\tfrac{1}{2}Al_2O_3(s)+\tfrac{1}{2}N_2(g) \quad (9)$$

Since the $NO_2$ formed was measured, it was possible to obtain the amount of AlN burned in reaction (9) by difference. In both cases, the energies of reaction were calculated using the heats of formation of AlN [18], $Al_2O_3$ [3], and $NO_2$ [38].

Corrections for the energies of combustion of the remaining impurities were made assuming the following reactions, using heat data from the literature [3, 38].

$$Al(s)+\tfrac{3}{4}O_2(g)\rightarrow\tfrac{1}{2}Al_2O_3(s) \quad (10)$$

$$C(s)+O_2(g)\rightarrow CO_2(g) \quad (11)$$

$$Fe(s)+\tfrac{3}{4}O_2(g)\rightarrow\tfrac{1}{2}Fe_2O_3(s) \quad (12)$$

The corrections for the deviation of the gases from the ideal gas law were made according to the procedure outlined by Prosen [39].

The corrected energies of combustion, which are the energies of combustion of aluminum carbide in the original sample, are given in column 2 of table 6.

TABLE 6. *Heat of combustion of* $Al_4C_3$

| Experiment No. | $-q_{Al_4C_3}$ | $CO_2$ (obs/calc) | $\frac{Al_2O_3}{\alpha+\delta}$ | $m_s'$ | $-\Delta U^\circ_{298}$ ($Al_4C_3$) (obs) | $-\Delta U^\circ_{298}$ ($Al_4C_3$) (to $\alpha-Al_2O_3$) |
|---|---|---|---|---|---|---|
| | J | | | g | J $g^{-1}$ | J $g^{-1}$ |
| 10 | 24057.1 | 1.0018 | 0.768 | 0.806580 | 29826.1 | 29947.6 |
| 11 | 24027.5 | 1.0027 | .641 | .806293 | 29800.0 | 29900.6 |
| 12 | 23942.4 | 0.9956 | .456 | .800176 | 29922.0 | 29993.6 |
| 13 | 24040.2 | .9985 | .475 | .801280 | 30002.2 | 30076.8 |
| 16 | 24026.7 | .9973 | .471 | .801857 | 29963.8 | 30037.7 |
| 18 | 23880.8 | .9992 | .517 | .800936 | 29816.1 | 29897.2 |
| 19 | 24088.2 | 1.0000 | .517 | .806976 | 29850.0 | 29931.1 |
| 20 | 24076.7 | 1.0001 | .472 | .803183 | 29976.6 | 30050.7 |
| Mean and standard dev. of the mean, J $g^{-1}$: | | | | | 29894.6 ±30.6 | 29979.4 ±25.4 |
| Mean and std. dev. of the mean, kcal $mole^{-1}$: | | | | | 1028.69 ±1.0 | 1031.5 ±0.9 |

The ratio of $CO_2$ observed to that calculated from analysis 4 is shown in column 3. The observed fraction of delta phase in the alumina formed is given in column 4. The mass of aluminum carbide burned, $m_s'$, was calculated from the observed mass of $CO_2$, corrected for the mass of $CO_2$ originating from the combustion of the free carbon in the original sample. $m_s'$ is considered to be the best measure of the amount of reaction that occurred, because the aluminum carbide was apparently not entirely homogeneous. The lack of homogeneity is suggested by the scatter in the values for $CO_2$ (obs/calc). Values greater than 1.0 can only be accounted for if the percent carbon in the sample burned was greater than that calculated from analysis 4, which showed the highest carbon content of all the analyses. The range of values of the ratio $CO_2$ (obs/calc) is about half the percentage range of values for carbon found in the several analyses of the aluminum carbide sample. The standard energy of combustion of aluminum carbide in J $g^{-1}$ based on $m_s'$, but not corrected for variations observed in $Al_2O_3$ formed, is shown as $-\Delta U^\circ_{298}$ ($Al_4C_3$) in column 6.

As shown in column 4, table 6, delta aluminum oxide constituted a large fraction of the alumina formed in the combustion of the aluminum carbide. To obtain $\Delta H^\circ_{298.15}$ for the combustion of aluminum carbide to alpha alumina only, a correction was applied for the formation of delta alumina.

The energy difference between the delta and alpha aluminas was measured by means of solution calorimetry by Kleppa and Yokokawa.[4] The experiments were carried out by dissolving aluminum oxide samples in a $PbO$–$BaO$–$B_2O_3$ melt at 705 °C. The delta alumina samples used for these experiments were obtained from the combustion of the aluminum carbide in the experiments described in the present work. The alpha alumina studied was obtained from various sources. Some samples were made by heating the delta alumina at 1450 °C, and other samples were of different origin. The solution energies for the alpha alumina from the different sources were in agreement. For the conversion of delta to alpha alumina (reaction 13), these investigators found a value of $\Delta H^\circ = -2.7 \pm 0.4$ kcal $mole^{-1}$.

$$\delta-Al_2O_3=\alpha-Al_2O_3 \qquad (13)$$

The energy of combustion of aluminum carbide to alpha alumina only is $\Delta E_{298,15} = -1031.5 \pm 1.0$ kcal $mole^{-1}$. Conversion to the constant pressure process leads to $\Delta H_{298.15} = -1033.3 \pm 1.0$ kcal $mole^{-1}$. The uncertainty (1.0) is the square root of the sum of the squares of the standard deviation (0.9) in the combustion measurements and the uncertainty (0.4) in the correction for the conversion of delta alumina to alpha alumina.

### 3.2. Heat of Formation of Aluminum Carbide

Combining the heat of combustion for aluminum carbide with $\Delta Hf_{298.15}[CO_2] = -94.05 \pm 0.01$ kcal $mole^{-1}$ [38] and $\Delta Hf^\circ_{298.15}[\alpha-Al_2O_3] = -400.4 \pm 0.3$ kcal $mole^{-1}$ [3], we obtain $\Delta Hf^\circ_{298.15}[Al_4C_3] = -49.7 \pm 1.2$ kcal $mole^{-1}$.

The overall uncertainty (1.2 kcal $mole^{-1}$) of the heat of formation of aluminum carbide is the square root of the sum of the squares of the uncertainty, 0.3 kcal $mole^{-1}$, assigned to the heat of formation of alpha aluminum oxide; 0.01 kcal $mole^{-1}$ for the uncertainty in the heat of formation of carbon dioxide; 1.0 kcal $mole^{-1}$ found for the uncertainty in the heat of combustion of the aluminum carbide to alpha alumina only.

---

The authors thank Professor O. J. Kleppa and Dr. T. Yokokawa of the University of Chicago for carrying out the solution calorimetry experiments. The x-ray diffraction analyses were made by Howard Swanson of the Inorganic Materials Division of the National Bureau of Standards, and the chemical analyses were performed by Rolf Paulson of the Analytical Chemistry Division. Their assistance is also gratefully acknowledged.

This work was supported by the Advanced Research Projects Agency.

## 4. References

[1] A. Meichsner and W. A. Roth, Z. Elektrochem. **40,** 19 (1934).
[2] W. A. Roth, Z. Elektrochem. **48,** 267 (1942).
[3] A. D. Mah, J. Phys. Chem. **61,** 1572 (1957).
[4] M. Berthelot, Compt. Rend. **132,** 281 (1901); Ann. Chim. Phys. [7] **22,** 464 (1901).
[5] L. Wöhler and K. Hofer, Z. anorg. u. allgem. Chem. **213,** 249 (1933).
[6] N. Kameyama and F. Yoshida, Denki Kagaku, **12,** 171 (1944).
[7] G. T. Furukawa, T. B. Douglas, W. G. Saba, and A. C. Victor, J. Res. NBS (Phys. and Chem.), publication pending.
[8] C. S. Campbell, Met. Soc. Conf. **7,** 412 (1962).
[9] W. H. Evans, J. Hilsenrath, and H. W. Woolley, private communication; G. T. Furukawa, M. L. Reilly, J. H. Piccirelli, T. B. Douglas, A. C. Victor, and A. R. Beaudoin, private communication; W. H. Evans, private communication.

[4] O. J. Kleppa and T. Yokokawa (Department of Chemistry and Institute for the Study of Metals, University of Chicago). This work is described in a Letter to the Editor submitted to the Journal of the American Chemical Society.

[10] O. Ruff, Z. Elektrochem. **24,** 157 (1918).
[11] W. A. Chupka, J. Berkowitz, C. F. Giese, and M.G. Ingram, J. Phys. Chem. **62,** 611 (1958).
[12] D. J. Meschi and A. W. Searcy, J. Phys. Chem. **63,** 1175 (1959).
[13] C. H. Prescott and W. B. Hincke, J. Am. Chem. Soc. **50,** 3228 (1928).
[14] M. von Stackelberg, E. Schnorrenberg, R. Paulus, and K. F. Spiess, Z. Physik. Chem. **A175,** 127 (1935).
[15] M. von Stackelberg and K. F. Spiess, Z. Physik. Chem. **A175,** 140 (1935).
[16] S. Satoh, Sci. Papers Inst. Phys. Chem. Research (Tokyo) **34,** 50–59 (1938).
[17] J. Efimenko, R. F. Hampson, R. F. Walker, and T. B. Douglas, private communication.
[18] G. T. Armstrong and L. A. Krieger, private communication.
[19] K. Grjotheim, O. Herstad, and K. Stahl-Johannessen, Z. Anorg. u. allgem. Chem. **327,** 267 (1964).
[20] C. H. Prescott, Jr., and W. B. Hincke, J. Am. Chem. Soc. **49,** 2753 (1927).
[21] R. Brunner, Z. Elektrochem. **38,** 55 (1932).
[22] W. D. Treadwell and A. Gyger, Helv. Chim. Acta **16,** 1214 (1933).
[23] L. M. Foster, G. Long, and M. S. Hunter, J. Am. Ceram. Soc. **39,** 1 (1956).
[24] J. H. Cox and L. M. Pidgeon, Can. J. Chem. **41,** 671 (1963).
[25] K. Motzfeldt, Tek. Ukeblad, 1137 (1962).
[26] W. B. Frank, Aluminum Company of America, private communication.
[27] R. S. Jessup, Precise Measurement of Heat of Combustion with a Bomb Calorimeter, NBS Mono. 7 Feb. 26, 1960.
[28] A. E. Cameron and E. Wichers, J. Am. Chem. Soc. **84,** 4175 (1962).
[29] A. A. Noyes and E. H. Swift, Qualitative Chemical Analysis of Inorganic Substances, p. 368, (The MacMillan Company, N.Y., 1942.)
[30] M. Shepherd, Anal. Chem. **19,** 77 (1947).
[31] R. Goulden, Comprehensive Analytical Chemistry, ed. C. L. Wilson and D. W. Wilson, p. 412, (Elsevier Publ. Co., New York, N.Y., 1960).
[32] R. Belcher and G. Ingram, Anal. Chim. Acta **4,** 401 (1950).
[33] E. J. Prosen and F. D. Rossini, J. Res. NBS **27,** 289 (1941) RP1420.
[34] F. D. Rossini, ch. 4, Experimental Thermochemistry, ed. by F. D. Rossini (Interscience Publishers, Inc., New York, N.Y., 1956).
[35] J. W. Newsome, H. W. Heiser, H. S. Russell, and H. C. Stumpf, Aluminum Company of America, Alcoa Research Laboratories, Tech. Paper No. 10 (revised 1960), pp. 12, 35.
[36] H. P. Rooksby, J. Appl. Chem. **8,** 44 (1958).
[37] H. C. Stumpf, Aluminum Company of America, private communication.
[38] F. D. Rossini, D. D. Wagman, W. H. Evans, S. Levine, and I. Jaffe, Selected Values of Chemical Thermodynamic Properties, NBS Circ. 500 (U.S. Government Printing Office, Washington, D.C., 1952).
[39] E. J. Prosen, ch. 6, Experimental Thermochemistry, ed. F. D. Rossini (Interscience Publishers, Inc., New York, N.Y., 1956).
[40] Allah D. Mah, Heat of Formation of Aluminum Carbide, U.S. Bureau of Mines, Report of Investigations 6415, 1964.

(Paper 68A6–315)

JOURNAL OF RESEARCH of the National Bureau of Standards—A. Physics and Chemistry
Vol. 68A, No. 6, November–December 1964

# Some Elastic Compliances of Single Crystal Rutile From 25 to 1000 °C

S. Spinner and J. B. Wachtman, Jr.

(August 4, 1964)

Young's modulus, as a function of temperature up to 1000 °C, was determined for eight rutile specimens of different crystallographic orientations. From these, the following four elastic compliances or combinations of them were determined as a function of temperature, $s_{11}$, $s_{33}$, $2s_{13}+s_{44}$, and $s_{11}-s_{12}-s_{66}/2$. The method used was the same as had been used in a previous study for rutile at room temperature.

## 1. Introduction

In a previous investigation [1],[1] all the elastic constants of rutile were determined at room temperature by an application of the resonance technique. Briefly, the method of approach consists in determining the mechanical resonance frequencies of both flexural and torsional vibration of a group of cylindrical rods of different orientations of the same type of crystal. Young's and the shear modulus are computed for each bar from these frequencies and from its dimensions and density. Then, from a set of equations given by Nye [2], for instance, relating Young's and the shear modulus to orientation and elastic compliances, one solves for the elastic compliances (since the other parameters, Young's modulus, shear modulus and orientation are known).

The number of equations required in the set, and, hence, also the number of specimens of different orientation, depends upon the number of elastic constants required to completely describe a particular crystal. If more than the minimum number of specimens are available, then, from an overdetermined set of equations, one may obtain an estimate of the precision of measurement of the elastic constants as well as the elastic constants themselves. This has been done for corundum [3] as well as rutile [1].

In this paper, some of the elastic compliances already determined at room temperature for rutile—those arising from the flexural resonance frequencies—are extended to elevated temperatures using the same method of approach. As far as we know, there is no data available on the temperature dependence of any of the elastic properties of rutile.

[1] Figures in brackets indicate the literature references at the end of this paper.

## 2. Experimental Procedure

The method for obtaining resonance frequencies, both at room and elevated temperatures, has already been described [4–6]. However, certain refinements (such as the use of fine wires of phosphor bronze as suspension members) which were developed to obtain torsional resonance for the shorter rutile specimens [1] were not applicable at elevated temperatures. Furthermore, with the glass and wire fibers used at elevated temperatures as suspension members in place of the cotton or silk threads used at room temperature, it was not possible (mainly because of the small cross section of the specimens) to obtain satisfactory torsional resonances even for the longer specimens. Consequently, this investigation is restricted to the flexural resonance frequencies and to those elastic compliances which can be derived from them, as mentioned above.

For this purpose, 8 of the original 16 specimens were used. This included all of the longer ones (which yielded the most reliable values of resonance frequency) and those of the shorter ones having orientations which would be most significant in giving a Young's modulus-orientation relationship. The specimens used, along with their length, mass, and orientation, are given in table 1. The same notation for designating specimens and orientation, as well as most of the other notation used in the previous paper [1] is retained here.

Flexural resonance frequencies for each specimen were determined in steps of about 100 °C, allowing sufficient time for thermal equilibrium to be attained at each temperature. Usually two or three sets of temperature determinations were taken for each specimen. The glass fiber suspensions (which yielded the more reliable results) were used for all the speci-

mens up to the limit of their applicability; from 700 to 800 °C. The wire suspensions gave satisfactory responses with the longer specimens up to the highest temperatures of the furnace, about 1400 °C, but were unsatisfactory for two of the smaller specimens over about 800 °C. Since the changes in elastic compliances were fairly gradual and continuous with temperature, it was felt to be a more accurate procedure to extrapolate the values obtained with the glass suspension for these two specimens up to 1000 °C rather than use the data obtained with the wire suspension.

TABLE 1. *Properties of "single crystal" rutile specimens*

| Specimen number | Mass | Length | End | | Center | | Other end | |
|---|---|---|---|---|---|---|---|---|
| | | | $\theta$ | $\phi$ | $\theta$ | $\phi$ | $\theta$ | $\phi$ |
| | g | cm | All angles in degrees | | | | | |
| **Linde rods** | | | | | | | | |
| 21 | 2.6317 | 13.236 | 12.5<br>12.3 | 2.6<br>2.2 | 12.7 | 2.1 | 14.3<br>14.2 | 1.8<br>1.5 |
| 23 | 2.8205 | 12.168 | 14.0 | 7.3 | 16.1 | 7.0 | 14.8 | 6.3 |
| 24 | 2.3654 | 11.714 | 43.3 | 34.1 | 45.6 | 37.9 | 44.7 | 33.6 |
| 30 | 1.1523 | 5.816 | 58.7 | 24.0 | 58.5 | 24.2 | 59.3 | 23.7 |
| 44 | 15.0251 | 9.848 | 88.8 | 44.1 | 88.4 | 43.4 | 90.0 | 44.5 |
| **NBS rods** | | | | | | | | |
| 49 | 7.1208 | 11.128 | 87.8 | 0.0 | 87.8 | 0.0 | 88.0 | 1.5 |
| 50 | 21.5907 | 17.107 | 88.8 | 5.4 | 89.5 | 5.4 | 90.0 | 5.0 |
| 51 | 16.0263 | 17.634 | 86.2 | 0.4 | 86.2 | 1.0 | 86.8 | 0.9 |

Young's modules at some elevated temperature, $Y_t$, was computed from the resonance frequencies, from the equation

$$Y_t = Y_0 (f_t/f_0)^2 (l_t/l_0)^3 (m_0/m_t)(n_0/n_t)^3. \quad (1)$$

The room temperature value of Young's modulus, $Y_0$, is known from the previous investigation; $f_t$ and $f_0$ are the flexural resonance frequencies at temperature $t$ and room temperature respectively. It should be noted that the ratio, $f_t/f_0$, applies to overtones as well as to the fundamental resonance frequency. This was used for the longer specimens to provide additional points (obtained from overtones as well as the fundamental) during a modulus-temperature run. The points based on overtones also served as an internal check on the consistency of the modulus-temperature relationship. The terms involving $l$, $m$, and $n$ are the correction for thermal expansion. Since the thermal expansion of rutile is anisotropic, the coefficient being about 30 percent larger in the "$c$" or [001] direction than in the "$a$" or [100] direction, it was necessary to take this into account in a manner which has already been described [7]. The length of the long axis of the specimen at temperature $t$ is $l_t$, and $l_0$ is the same dimension at room temperature; similarly for $m$ and $n$, $n$ being the cross-sectional dimension in the direction of flexural vibration and $m$ being the cross-sectional dimension perpendicular to $n$. A more detailed description of the application of this anisotropic thermal expansion correction to rutile is given in the appendix. Actual values of the thermal expansion of rutile in both "$a$" and "$c$" directions were supplied by Richard K. Kirby of the NBS staff. The possibility that certain orientations might change with increasing temperature due to this anisotropic thermal expansion was also considered. However, it was found that even in the extreme case ($t$=1000 °C and $\theta$=45 °C) the change in orientation would be insignificant, i.e., less than ½°.

The scatter of the experimental points of $Y_t$ as a function of temperature, based on repeated runs and (where used) on overtones, about a smooth curve drawn through the points was estimated to be about 5 parts per 1000.

## 3. Results

Values of $1/Y_t$ interpolated from the experimental data at even 100 °C temperature intervals for the 8 specimens measured are shown in table 2. The data at 25 °C are from the previous investigation [1]. The compliances are obtained from eq (6) of [1],

$$1/Y_t = s'_{33} = s_{11}\sin^4\theta + s_{33}\cos^4\theta + (2s_{13}+s_{44})\sin^2\theta\cos^2\theta + \frac{1}{2}\left(s_{12}-s_{11}+\frac{s_{66}}{2}\right)\sin^4\theta\sin^2 2\phi. \quad (2)$$

This equation was solved by computer at each temperature (100 °C, 200 °C . . . 1000 °C) in the same manner as before. It is noted that since 8 specimens are used and 4 coefficients are solved for, an overdetermined set of equations is still available from which, as previously mentioned, one may derive an estimate of the precision of the coefficients from a least square best fit, as well as the coefficients themselves. Table 3 presents the four elastic compliances along with their standard deviations, computed in this manner. The standard deviations of the compliances, especially at the lower temperatures, compare favorably with those computed at room temperature. As might be expected, these standard deviations tend to grow somewhat larger at the higher temperatures. The four coefficients are shown graphically as a function of temperature in figure 1.

Once the compliances are known, they may be resubstituted in equation (6) and "theoretical" or "computed" values of $1/Y_t$ may be solved for at each temperature. The numbers associated with each value of $1/Y_t$ in table 2 represents the difference between these "computed" values and the "experimental" or "observed" values given in the table. Following the same convention as before, a + sign indicates that the experimental value of $1/Y_t$ is larger than the theoretical one and vice versa.

TABLE 2. *Reciprocal of Young's modulus for rutile specimens of various orientations as a function of temperature.*
$1/Y_t = s'_{33}$ in $10^{-13} m^2/N$ ($10^{-13} cm^2$/dyne) at indicated temperature (°C)

| Specimen No. | 25 | 100 | 200 | 300 | 400 | 500 | 600 | 700 | 800 | 900 | 1000 |
|---|---|---|---|---|---|---|---|---|---|---|---|
| 21 | 2.666 | 2.708<br>.0005* | 2.762<br>.0015 | 2.815<br>−.0001 | 2.871<br>−.0003 | 2.927<br>−.0001 | 2.986<br>−.0016 | 3.050<br>−.0011 | 3.108<br>−.0023 | 3.176<br>−.0008 | 3.241<br>−.0016 |
| 23 | 2.690 | 2.731<br>−.0006 | 2.783<br>−.0012 | 2.840<br>−.0013 | 2.895<br>.0009 | 2.950<br>.0005 | 3.011<br>.0016 | 3.072<br>−.0005 | 3.134<br>.0019 | 3.198<br>−.0002 | 3.263<br>−.0004 |
| 24 | 3.047 | 3.092<br>.0003 | 3.147<br>−.0013 | 3.203<br>−.0056 | 3.257<br>−.0029 | 3.314<br>−.0020 | 3.373<br>.0004 | 3.444<br>.0081 | 3.512<br>.0026 | 3.580<br>.0054 | 3.647<br>.0105 |
| 30 | 3.881 | 3.921<br>−.0003 | 3.973<br>.0017 | 4.032<br>−.0070 | 4.074<br>.0035 | 4.125<br>.0024 | 4.175<br>−.0006 | 4.226<br>−.0098 | 4.303<br>−.0032 | 4.364<br>−.0065 | 4.423<br>−.0128 |
| 44 | 2.694 | 2.778<br>.0001 | 2.872<br>−.0002 | 2.960<br>−.0006 | 3.048<br>−.0004 | 3.135<br>−.0003 | 3.223<br>.0001 | 3.320<br>.0011 | 3.408<br>.0003 | 3.501<br>.0007 | 3.597<br>.0019 |
| 49 | 6.777 | 6.777<br>.0016 | 6.779<br>.0009 | 6.798<br>.0093 | 6.800<br>.0022 | 6.820<br>.0017 | 6.846<br>.0016 | 6.877<br>.0014 | 6.922<br>.0058 | 6.964<br>.0006 | 7.047<br>.0212 |
| 50 | 6.650 | 6.651<br>−.0010 | 6.656<br>−.0017 | 6.665<br>−.0057 | 6.681<br>−.0014 | 6.704<br>−.0010 | 6.732<br>−.0010 | 6.769<br>.0027 | 6.812<br>.0036 | 6.859<br>.0018 | 6.911<br>−.0096 |
| 51 | 6.757 | 6.755<br>−.0006 | 6.759<br>.0004 | 6.764<br>−.0054 | 6.777<br>−.0017 | 6.798<br>−.0013 | 6.825<br>−.0005 | 6.855<br>−.0018 | 6.889<br>−.0086 | 6.944<br>−.0009 | 6.998<br>−.0092 |

*Lower number in each box is difference between "observed" value of $1/Y_t$ and "computed" value. Observed values of $1/Y_t$ are given in all cases except at 25° C where computed values from previous investigation [1] are given.

TABLE 3. *Elastic compliances of rutile as a function of temperature in $10^{-12}$ $m^2/N$ ($10^{-13}$ $cm^2$/dyne)*

| Temperature | $S_{11}$ | $S_{33}$ | $2S_{13}+S_{11}$ | $S_{11}-S_{12}-\frac{S_{66}}{2}$ |
|---|---|---|---|---|
| °C | | | | |
| 25 | 6.787 ±.0003* | 2.502 ±.0004 | 6.464 ±.0016 | 8.197 ±.0011 |
| 100 | 6.786 ±.0006 | 2.635 ±.0010 | 6.528 ±.0039 | 8.026 ±.0056 |
| 200 | 6.789 ±.0010 | 2.689 ±.0015 | 6.617 ±.0063 | 7.843 ±.0041 |
| 300 | 6.799 ±.0040 | 2.744 ±.0066 | 6.725 ±.0273 | 7.687 ±.0178 |
| 400 | 6.808 ±.0016 | 2.803 ±.0024 | 6.793 ±.0099 | 7.529 ±.0065 |
| 500 | 6.828 ±.0012 | 2.860 ±.0017 | 6.881 ±.0071 | 7.396 ±.0046 |
| 600 | 6.855 ±.0009 | 2.923 ±.0013 | 6.965 ±.0056 | 7.272 ±.0036 |
| 700 | 6.886 ±.0039 | 2.988 ±.0058 | 7.065 ±.0238 | 7.142 ±.0155 |
| 800 | 6.926 ±.0035 | 3.045 ±.0052 | 7.219 ±.0217 | 7.046 ±.0141 |
| 900 | 6.973 ±.0026 | 3.113 ±.0038 | 7.325 ±.0157 | 6.955 ±.0103 |
| 1000 | 7.036 ±.0088 | 3.181 ±.0131 | 7.414 ±.0540 | 6.890 ±.0353 |

* Standard deviation.

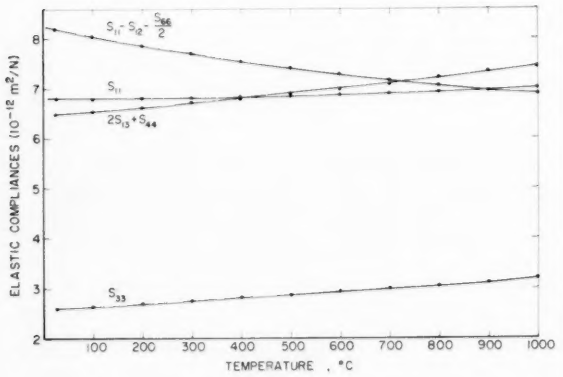


FIGURE 1. *Elastic compliance of rutile as a function of temperature.*

Figure 2 shows the Young's modulus-orientation dependence for rutile at two selected temperatures, 400 °C and 1000 °C, obtained in the same manner as the room temperature curves, which are reproduced from the original study for comparison.

It may be seen from the figure that in addition to the expected decrease in modulus for all orientations with increasing temperature, the anisotropy of the crystal decreases also. For any given value of $\theta$, the change in Young's modulus, as a function of $\phi$, is less at 1000 °C than at 25 °C. Also, for any particular value of $\phi$, the variation in $\theta$ appears to decrease at the higher temperatures, i.e., the lines become flatter.

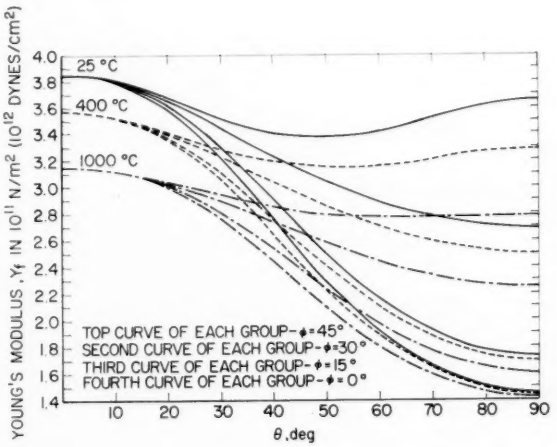
25 °C
400 °C
1000 °C
TOP CURVE OF EACH GROUP-φ=45°
SECOND CURVE OF EACH GROUP-φ=30°
THIRD CURVE OF EACH GROUP-φ=15°
FOURTH CURVE OF EACH GROUP-φ=0°
YOUNG'S MODULUS, $Y_f$ IN $10^{11}$ N/m² ($10^{12}$ DYNES/cm²)
θ, deg

FIGURE 2. *Young's modulus of rutile as a function of orientation at selected temperatures.*

θ is angle of specimen axis with respect to "c" axis of crystal; φ is angle between the projection of specimen axis in (001) plane of crystal, and "a" axis of crystal. (The subscript "f" is retained in $Y_f$ from the previous investigation [1] to indicate the "free" rather than the "pure" modulus.)

## 4. Appendix

The problem is to express eq (1) in terms of the known thermal expansions for rutile for given crystallographic directions. We define these two thermal expansions for the "$c$" and "$a$" directions respectively as $L_{tc}/L_{oc}$ and $L_{ta}/L_{oa}$.

(1) We consider first a "$c$" axis rod, i.e., a specimen of which the long dimension is in the direction of the crystallographic "$c$" axis. For this condition,

$$\frac{l_t}{l_0}=\frac{L_{tc}}{L_{0c}} \text{ and } \frac{m_t}{m_0}=\frac{n_t}{n_0}=\frac{L_{ta}}{L_{0a}}$$

so that equation (1) becomes

$$Y_t=Y_0\left(\frac{f_t}{f_0}\right)^2\left(\frac{L_{tc}}{L_{0c}}\right)^3\left(\frac{L_{0a}}{L_{ta}}\right)^4.$$

(2) We next consider an "$a$" axis rod. In this case, since the thermal expansion of the cross-sectional dimensions are not equal, a specimen having a circular cross section at room temperature will develop a noncircular cross section as the temperature increases. This will give rise to two separate flexural resonance frequencies; one in the direction of the short cross-sectional dimension, the "$a$" direction, and the other in the direction of the long cross-sectional dimension, the "$c$" direction. These two types of vibration are considered separately. For vibrations along the "$a$" direction,

$$\frac{l_t}{l_0}=\frac{L_{ta}}{L_{0a}}, \frac{m_t}{m_0}=\frac{L_{tc}}{L_{0a}}, \text{ and } \frac{n_t}{n_0}=\frac{L_{ta}}{L_{0a}}$$

(since "$n$" is always the dimension in the direction of vibration). Equation (1) then becomes

$$Y_t=Y_0\left(\frac{f_t}{f_0}\right)^2\left(\frac{L_{ta}}{L_{0a}}\right)^3\left(\frac{L_{0c}}{L_{tc}}\right)\left(\frac{L_{0a}}{L_{ta}}\right)^3$$

$$Y_t=Y_0\left(\frac{f_t}{f_0}\right)^2\left(\frac{L_{0c}}{L_{tc}}\right).$$

For vibrations in the "$c$" direction,

$$\frac{l_t}{l_0}=\frac{L_{ta}}{L_{0a}}, \frac{m_t}{m_0}=\frac{L_{ta}}{L_{0a}}, \text{ and } \frac{n_t}{n_0}=\frac{L_{tc}}{L_{0a}}$$

and eq (1) becomes

$$Y_t=Y_0\left(\frac{f_t}{f_0}\right)^2\left(\frac{L_{ta}}{L_{0a}}\right)^3\left(\frac{L_{0a}}{L_{ta}}\right)\left(\frac{L_{0c}}{L_{tc}}\right)^3$$

$$Y_t=Y_0\left(\frac{f_t}{f_0}\right)^2\left(\frac{L_{ta}}{L_{0a}}\right)^2\left(\frac{L_{0c}}{L_{tc}}\right)^3.$$

It is clear that any specimen having its long axis in the (001) plane ($\theta=90°$, $\varphi$ from 0 to 45°) will have the same thermal expansion corrections as the two just given, since the same considerations holding for an "$a$" axis rod would apply.

It also follows from these considerations that rods having their long axis in the (001) plane should develop two noticeably different curves of $(f_t/f_0)^2$ as a function of temperature. This was observed experimentally; however, when the appropriate thermal expansion correction was applied to the points forming each curve (giving $Y_t/Y_0$ as a function of temperature), the two curves were brought into coincidence within experimental error. Conversely, for "$c$" axis rods, it was observed that even if two resonance frequencies were present at room temperature, due to the fact that the cross section was not perfectly circular (at room temperature), nevertheless, the two curves of $(f_t/f_0)^2$ as a function of temperature, based on these two room temperature resonance frequencies, coincided within experimental error. This was further verification of the validity of the thermal expansion corrections.

(3) The final case to be considered is that of a rod having its long axis at some angle, $\theta$, with the "$c$" axis. In this case, since the "$c$" axis does not coincide with any specimen axis ($l$, $m$, or $n$) as has been true in the previous examples, the thermal expansions along $l$, $m$, or $n$ will generally not equal $L_{tc}/L_{oc}$ or $L_{ta}/L_{oa}$, but will lie between these values. The following equation [7] then applies,

$$\frac{Y_t}{Y_0}=\left(\frac{f_t}{f_0}\right)^2\left\{1-\frac{\Delta L_a}{L_a}+\left(\frac{\Delta L_c}{L_c}-\frac{\Delta L_a}{L_a}\right)\right.$$
$$\left.[3\cos^2\theta-\sin^2\theta(1+2\cos^2\psi)]\right\}$$

where $\psi$ is the angle between the direction of vibration and the plane containing the "$c$" axis and the long axis of the rod. If this equation is written for each of the two directions of vibration, and the average of these two equations is taken, the following relationship results:

$$Y_t=Y_0\left(\frac{f_t}{f_0}\right)^2_{\text{ave.}}\left\{1-\frac{\Delta L_a}{\Delta L_a}\right.$$
$$\left.+\left(\frac{\Delta L_c}{L_c}-\frac{\Delta L_a}{L_a}\right)[3-5\sin^2\theta]\right\}.$$

This final equation is also applicable to the specialized orientations previously discussed. It is useful for the case in which the long axis of the rod coincides with the [001] direction or lies in the (001) plane, but in which the direction of vibration does not coincide with a crystallographic axis.

## 5. References


[1] J. B. Wachtman, Jr., W. E. Tefft, and D. G. Lam, Jr., Elastic constants of rutile ($TiO_2$), J. Res. NBS **66A**, (Phys. and Chem.), No. 6, 465–471 (1962).

[2] J. F. Nye, Physical Properties of Crystals (Oxford Univ. Press. London, England, 1957).

[3] J. B. Wachtman, Jr., W. E. Tefft, D. G. Lam, Jr., and R. P. Stinchfield, Elastic constants of synthetic single crystal corundum at room temperature, J. Res. NBS **64A** (Phys. and Chem.), No. 3 213–228 (1960).

[4] S. Spinner and W. E. Tefft, A Method for determining mechanical resonance frequencies and for calculating elastic moduli from these frequencies, Proc. ASTM **61,** 1221–1237 (1961).
[5] J. B. Wachtman, Jr., and D. G. Lam, Jr., Young's Modulus of various refractory materials as a function of temperature, J. Am. Ceram. Soc. **42,** 5, 254 (1959).
[6] Sam Spinner, Temperature dependence of elastic constants of some cermet specimens, J. Res. NBS **65C** (Eng. and Instr.), No. 2, 89–96 (1961).
[7] J. B. Wachtman, Jr., W. E. Tefft, D. G. Lam. Jr., and C. S. Apstein, Exponential temperature dependence of Young's modulus for several oxides, Phys. Rev. **122,** No. 6, 1754–1759 (1961).

(Paper 68A6–316)

JOURNAL OF RESEARCH of the National Bureau of Standards—A. Physics and Chemistry
Vol. 68A, No. 6, November–December 1964

# Energy Dependence of the D-D Reaction Cross Section at Low Energies [1]

J. G. Brennan [2] and J. J. Coyne

(August 11, 1964)

The energy variation of the approach cross section for the D-D reaction is calculated using several different methods. The simplest method assumes strong absorption inside the nuclear surface and uses the WKB approximation. The slope of the Gamow plot is in this case a constant. A strong absorption model, without WKB approximation, leads to negative corrections to this constant slope. A weak absorption model, which seems more applicable, gives both positive and negative corrections, depending on the depth of the nuclear potential. Finally, since the amount of absorption seems important, the effects of varying the absorption are studied using the optical model. The possible influence of the P-waves is also investigated. An experimental study of the energy dependence of the slope of the Gamow plot should give information on the optical potential which one deuteron sees when it approaches another deuteron.

## 1. Introduction

In an earlier treatment [1] [3] of the D-D reaction cross section, the strong energy dependence at low energies was attributed to the effects of the Coulomb and centrifugal barriers on the various angular momentum components of the incident beam. However, the barrier penetration factors were calculated using the WKB approximation for the Coulomb wave functions and retaining only the main energy dependence. If, in addition to these approximations, we also go to the low energy limit, then the energy dependence of the reaction cross section is given by the simple expression

$$\sigma_R = (A/E)\ \exp\ (-BE^{-\frac{1}{2}}) \qquad (1)$$

where $A$ and $B$ are independent of the energy. A plot of the logarithm of $\sigma_R E$ as a function of $E^{-\frac{1}{2}}$ would give a straight line under these approximations. Such a plot is often called a Gamow plot and is frequently used in the analysis of the low energy data.

Looking at the experimental results from three groups [2–4] in the energy region of about 8 to 100 kev (center of mass), Brennan [5] has indicated that the data might suggest an increase in $B$ of eq (1) with energy. Brennan calculated the D-D reaction cross section using a low energy approximation [6] to the small absorption method of Ostrofsky, Breit, and Johnson [7]. In this present paper, the energy dependence of the reaction cross section has been studied under various assumptions suggested by this previous work.

Since retaining only the main energy dependence in the WKB approximation is equivalent to assuming the behavior of the wave function due to scattering from inside the nuclear surface does not affect the energy dependence of the cross section, the reaction cross section was first calculated using the continuum model [8], which assumes complete absorption inside the nucleus and, therefore, does not allow coherent scattering from inside the nuclear surface. The results of this calculation are compared with the results of reference 1. The approach used by Brennan, based on the small absorption model, involves an approximation valid only at low energies. To investigate the validity of this approximation, a second calculation was done, in which this approximation was not made.

Since these two calculations involved models assuming strong and weak absorption, the effects of absorption were studied in a third calculation, using the optical model [9]. An attempt was also made to study the influence of P-waves on the cross section although only S-waves were included in the three main calculations mentioned above.

## 2. General Considerations

In this paper, we are considering the D–D reaction cross section at energies below 1 MeV in the center-of-mass coordinate system. In this low energy region, it is valid to treat the initial kinetic energy as small compared with the energy of the nucleons once they are inside the nucleus. Since the energy dependence of the reaction cross section does not show any of the sharp peaks which are found when there is compound nuclear resonance, we can also assume that there are no resonances to compound nuclear states below 1 MeV.

Under these two assumptions, it is a good approximation to assume that the reaction cross section factors into two parts. The first part, the approach

[1] Work supported by the National Science Foundation and the Defense Atomic Support Agency.
[2] The Catholic University of America, Washington, D.C.
[3] Figures in brackets indicate the literature references at the end of this paper.



743-261—64——9

cross section, contains all of the energy dependence and measures the probability of the bombarding particle getting inside the target mucleus. The second part, the specific nuclear factor, is assumed to be independent of the energy and is related to the probability that, once the bombarding particle gets inside the target nucleus, the system will make a transition from the initial to the final state.

The reaction cross section can also be subdivided into cross sections for reactions initiated by particles with different $l$ values, i.e.,

$$\sigma_R = \sum_l (4/9) P_l \sigma_l \tag{2}$$

where $P_l$ is the specific nuclear factor for initial orbital angular momentum $l$ and $\sigma_l$ is the corresponding approach cross section. The factor 4/9 arises from considerations of spin and symmetry [1]. Following previous treatments [1], we have ignored the contributions from the quintet spin states. In the present treatment, no attempt has been made to calculate the specific nuclear factors, $P_l$. They are assumed independent of the energy, and, therefore, do not affect the energy dependence of $\sigma_R$.

## 3. WKB Approximation and the Continuum Model

The continuum model [8] assumes complete absorption inside the nuclear surface and thus eliminates the effect of coherent scattering from inside the nucleus. The problem of calculating the approach cross section becomes one of calculating a potential barrier transmission coefficient. The approach cross section is related to the transmission coefficient as follows:

$$\sigma_l = \pi \lambda^2 (2l+1) T_l \tag{3}$$

where $\pi\lambda^2(2l+1)$ is the geometric limit and $T_l$ is the transmission coefficient. The transmission coefficients are given in terms of $\Delta_l$ and $S_l$, the penetration and shift factor, by Blatt and Weisskopf [10]. $\Delta_l$ and $S_l$ are, in turn, expressed in terms of the regular and irregular Coulomb wave functions and their derivatives [11].

If the WKB approximation is used for the Coulomb wave functions, and only the main energy dependence is retained, then we have [1]

$$\sigma_l = \exp[-2C_l]$$

$$C_l = \int_R^{r_l} |k_l(r)| dr;$$

$$k_l(r) = \{2\mu/\hbar^2[E - e^2/r - \hbar^2(l+\tfrac{1}{2})^2/2\mu r^2]\}^{\frac{1}{2}} \tag{4}$$

and $r_l$ is the value of $r$ at which $k_l(r)=0$. It should be noted that in excluding all but the most important energy dependence, we have also eliminated all dependence on $U_0$, the depth of the nuclear potential. The approach cross section, calculated using the WKB method, depends only on $R$, the nuclear radius, which we have chosen to be $7\times10^{-13}$ cm throughout this paper. This value of $R$ is the one commonly used in the D-D reaction calculations. Unless $R$ is changed drastically, the only effect of varying $R$ would be to change the height of the potential barrier.

Two calculations have been performed for the S-wave approach cross sections, one using the WKB approximation given by eq (4), the other using exact Coulomb wave functions [12] in the continuum model. In the second calculation, which we shall refer to simply as the continuum model, the dependence on $U_0$ was also retained. Figure 1 gives the slope of the Gamow plot for the WKB calculation and for the continuum model calculations with various well depths. In this figure and in all subsequent graphs of the slope of the Gamow plot, $E_c$ corresponds to the height of the Coulomb barrier, 205.69 keV; the scale marks $a$ and $b$ corresponds to 100 keV and 8 keV, respectively. The depths of the nuclear potentials are given on the curves in MeV. The results of figure 1 were obtained using numerical differentiation and using double interpolation of tabular data [12], good only to four significant

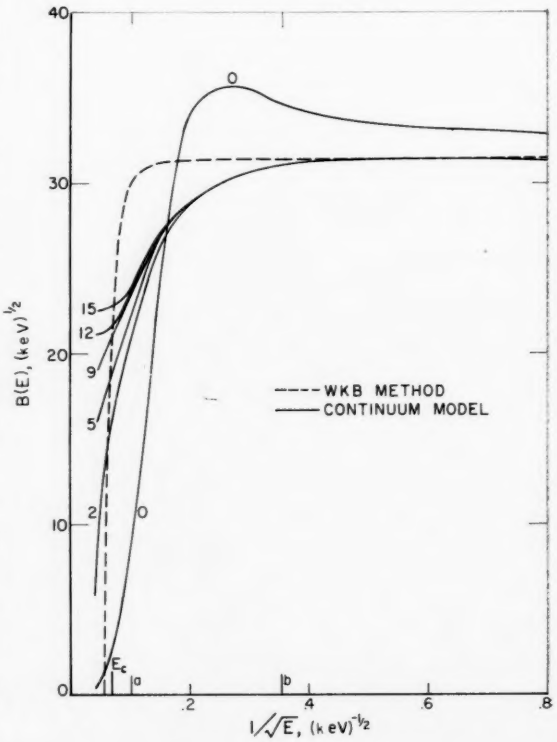


FIGURE 1. B(E) *versus* $E^{-\frac{1}{2}}$, *WKB approximation and the continuum model.*

In this and all subsequent figures, the numbers on the curves are the depths of the nuclear potential in MeV, $E_c$ corresponds to the height of the Coulomb barrier, $a$ corresponds to 100 keV and $b$ to 8 keV.

figures. Consequently the accuracy of the curves shown is only about 10 percent. Except for $U_0=0$, which is certainly an unrealistic value for the depth of the nuclear potential, all of the continuum model curves give negative corrections to the WKB results.

In order to test the importance of higher angular momentum, the WKB calculations were performed also for $l=1$, 2, and 3. If we assume all $l$-waves have the same specific nuclear factors, then, for comparison, we can simply add the cross sections. Figure 2b shows the effect of adding in higher and higher $l$ values, while figure 2a compares the slope of the Gamow plot for $\sigma_0$ with that for $(\sigma_0+\sigma_1)$. Higher $l$-waves were not included in figure 2a because the results were not significantly different in the region of interest. While the addition of the P-waves can cause a positive correction to the slope of the Gamow plot, this correction is very small compared to the correction indicated by experiment. Moreover, in a later and a more accurate calculation involving S- and P-waves, we shall see that the relative importance of higher $l$ values will depend very much on the depth of the nuclear potential.

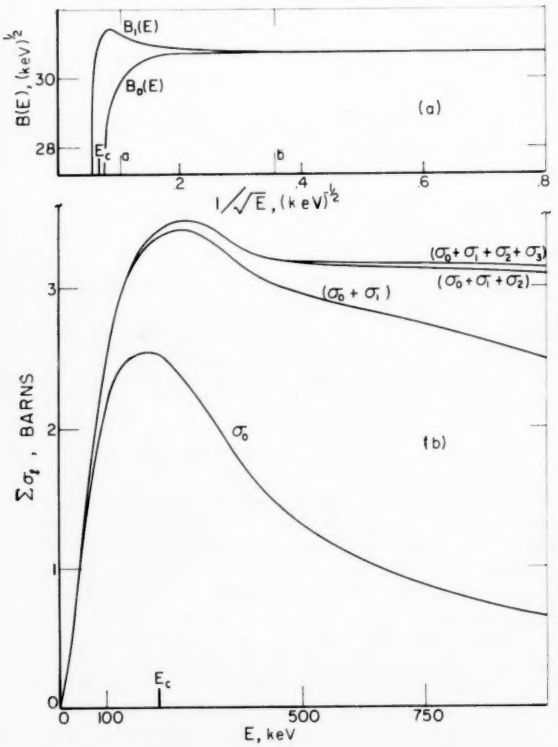


FIGURE 2a. B(E) *versus* $(E)^{-\frac{1}{2}}$ *for* S *waves and for* (S+P) *waves in the WKB approximation.*

FIGURE 2b. $\Sigma\sigma_l$ *versus* E *in the WKB approximation, showing the effects of higher l waves.*

## 4. Small Absorption Approximation

The treatment outlined in the previous section implied complete absorption inside the nucleus, since it ignored the effect of coherent scattering from inside the nucleus. The method described in this section assumes that the absorption is small, in fact so small that its effect on the probability density inside the nucleus can be ignored. This method was first introduced by Ostrofsky, Breit, and Johnson [7] and shall be referred to as the OBJ method. We will assume the absorption probability is the same throughout the nucleus, so that the shape factor for absorption will be one. This, we shall see later, is equivalent to choosing the imaginary part of the optical potential to be a square well. The approach cross section is the integral of the probability density over the nuclear volume divided by the flux of the incident beam. Since, in this method, the approach cross section is really a measure of the probability of being inside the nucleus, the specific nuclear factor is not a "branching ratio" but is related to the absolute probability of absorption.

The wave function inside the nucleus will be a solution for the nuclear potential which has been assumed. Outside the nucleus, the wave function is a linear combination of regular and irregular Coulomb wave functions, chosen so that the wave function and its derivative are continuous at the nuclear surface. With the wave function determined in this way, the approach cross section is given by eq (6) of Ostrofsky, Breit, and Johnson [7]. Using the OBJ method, we have treated only the S-waves, using a square well potential and also a clipped harmonic oscillator potential. The Coulomb wave functions for both calculations were the same as those used for the "continuum model" calculation. The square well calculation was carried out on a Burroughs E101 at the Georgetown College Observatory. The calculation for the harmonic oscillator was done on an IBM 704, located at the U.S. Naval Ordnance Laboratory.

Figure 3 gives Gamow plots for various depths of the nuclear potential. Besides the square well and the oscillator results, we have also included on each graph a plot of the WKB results normalized so that they correspond to the square well results at low energies and zero depth of the nuclear potential. The WKB results are included so that the variation of the curves with the depth of the nuclear potential will be more obvious.

While the results for a given depth may be quite different for the two potentials, the general behavior as a function of $U_0$ is the same. At a given depth the square well will give a curve of a certain shape, which can be duplicated by a harmonic oscillator well of greater depth. As we might suspect, the energy dependence of the low energy reaction cross section will not give us information of the shape of the nuclear potential, but will only indicate what depth must be chosen with a given shape, in order to get the same results.

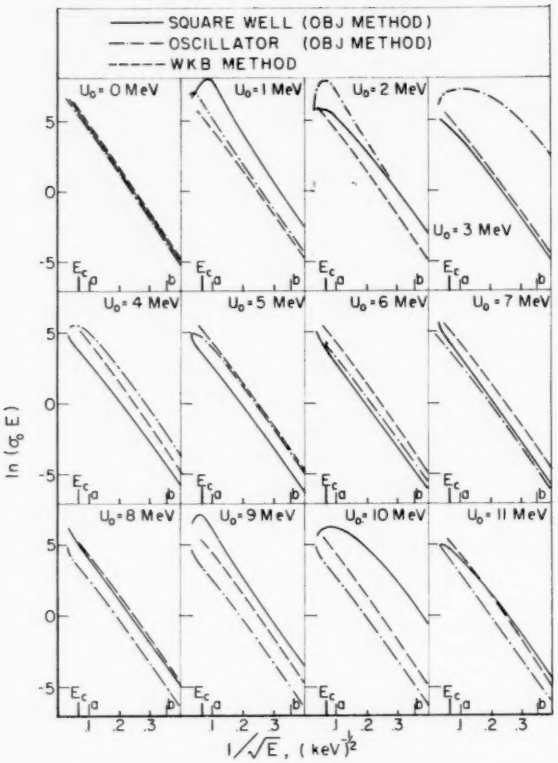


FIGURE 3. *Gàmow plots in the OBJ method for a square well and for a clipped harmonic oscillator nuclear potential, for various values for the depth,* $U_0$.

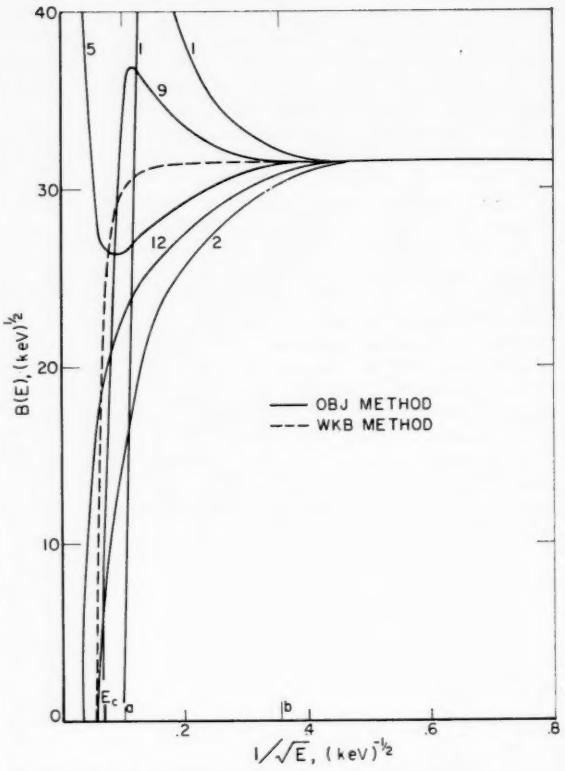


FIGURE 4. B(E) *versus* $E^{-\frac{1}{2}}$ *for a square well in the OBJ method.*

Figure 4 is a graph of the slope of the Gamow plot as a function of $E^{-\frac{1}{2}}$ for a square well of various depths. The WKB results are again included for comparison. This graph should be compared with figure 1 in order to compare the results of the "continuum" model and the OBJ method. The comments about the accuracy of the curves in figure 1 apply equally well to figure 4. However, it is still clear that the OBJ method allows both positive and negative corrections to the WKB result, while the continuum model, for reasonable values of $U_0$, allows only a negative correction.

## 5. Small Absorption Approximation at Very Low Energies

Johnson and Jones [6] have shown that in the low energy limit the approach cross sections of the OBJ method are given by

$$\sigma_l = (q_l/E)(e^{2\pi\eta}-1)^{-1}(1+t_l/\eta^2) \qquad (5)$$

where $\eta = e^2/\hbar v \propto E^{-\frac{1}{2}}$ and $q_l$ and $t_l$ are energy independent quantities, which are functions of the depth of the square well potential.

The expression above was that applied to the D-D reaction cross section by Brennan [5]. He assumed that he was working at low enough energies that only the S-waves were important. If we consider only S-waves, the slope of the Gamow plot is given by

$$d(\ln\sigma E)/dE^{-\frac{1}{2}} = -[(2\mu)^{-\frac{1}{2}}2\pi\hbar/a](1+t_0/\pi\eta^3) \qquad (6)$$

which corresponds to eq (5) of Brennan [5]. The right side of eq (6) is just the slope of the Gamow plot, $B$. The constant corresponds to the WKB result, while the second term includes a correction proportional to $E^{3/2}$. In figure 5 we plot $t_0$ as a function of $U_0^{\frac{1}{2}}$ (the other two curves will be referred to later). We see that the correction term can vary quite a bit depending on the value of $U_0$. Analyzing the available data [2-4], Brennan [5] decided on a value of $U_0$ in the vicinity of 9 MeV.

In order to show comparative results for the OBJ method, and the low energy limit, figure 6 gives the cross sections for both at different values of the depth. If we compare the values of $B$ calcualted, we find that, in general, the low energy limit (6) is valid. However, when $t_0$ is large, the results can differ considerably even at fairly low energies.

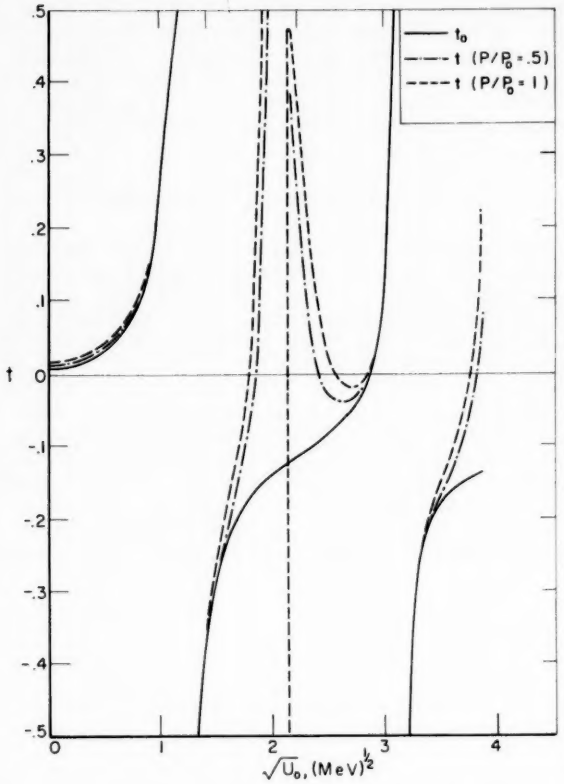


FIGURE 5. $t_0$ *and* t *of equations (6) and (8) versus* $U_0^{\frac{1}{2}}$.

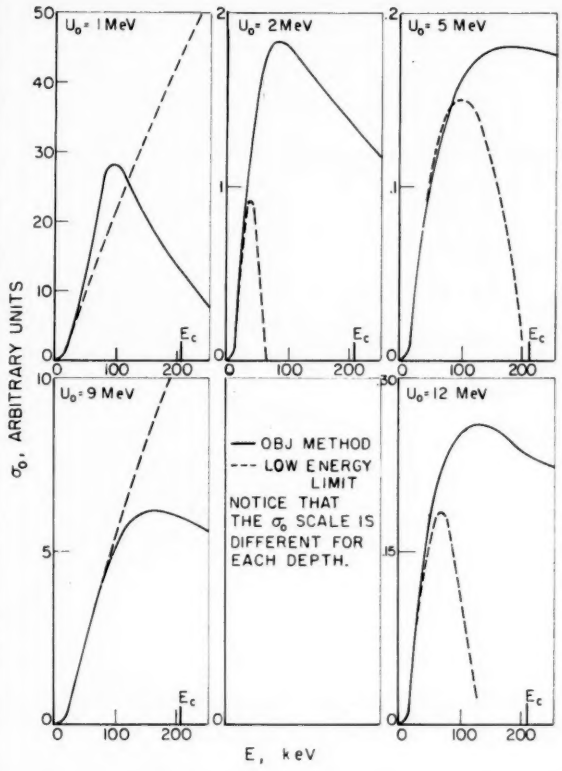


FIGURE 6. $\sigma_0$ *versus* E *for the OBJ method and for the low energy limit, for various values of* $U_0$.

In order to see how important the P-waves could be, the low energy limit (5) was also applied to the P-wave approach cross section. The results, however, are somewhat dependent on the ratio of the specific nuclear factors for the S- and P-waves. Including the P-waves, the total reaction cross section becomes

$$\sigma_R=\frac{4P_0q_0}{9E(e^{2\pi\eta}-1)}\left[1+\frac{t_0}{\eta^2}+\frac{P_1q_1}{P_0q_0}\left(1+\frac{t_1}{\eta^2}\right)\right]. \quad (7)$$

In terms of a Gamow plot this gives

$$d(\ln\sigma E)/dE^{-\frac{1}{2}}=-[(2\mu)^{-\frac{1}{2}}2\pi\hbar/a](1+t/\pi\eta^3) \quad (8)$$

where

$$t=\frac{t_0+(P_1q_1/P_0q_0)t_1}{1+(P_1q_1/P_0q_0)}. \quad (9)$$

The quantity of interest is $t$ and as we see, it is a function of $P_1/P_0$. Figure 5 gives $t$ as a function of $U_0^{\frac{1}{2}}$ for $P_1/P_0=1.0$ and 0.5. Comparing $t$ to $t_0$, we see that the P-wave contribution can be very important or very unimportant, depending on the depth of the nuclear potential. In the vicinity of 9 MeV the P-wave is not very significant.

## 6. Optical Model

The methods for calculating the approach cross sections, which we have treated thus far, are at two extremes. Either we assume that the absorption inside the nucleus is complete or we assume that the absorption is so small that it is negligible compared to the scattering. In order to study the effect of varying the absorption, the S-wave approach cross sections were calculated, using the optical model [9]. The optical model leads to an absorption which is proportional to the probability density inside the nuclear surface. Since, as stated previously, $P_0$, the specific nuclear factor of the OBJ method, is proportional to the absolute probability of absorption, and $V_c$, the imaginary part of the optical potential, is proportional to the absorption in the optical model, the two methods should give the same results for small absorption. Comparing the reaction cross section for the optical model with that for the OBJ method, we find that, in the limit of small absorption,

$$P_0=2V_c/\pi. \quad (10)$$

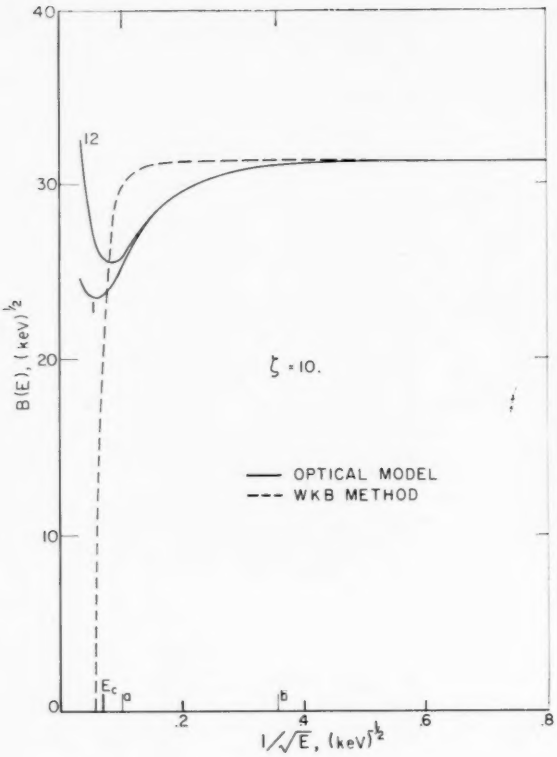


FIGURE 7. B(E) *versus* (E)$^{-½}$, *the optical model.* $\zeta$, *the ratio of the imaginary to the real part of the potential* = 10.

Calculations in the optical model were carried out on the IBM 704 at the National Bureau of Standards. The potential used was a square well of the form $U_0(1+i\zeta)$. However, the Coulomb wave functions used were calculated directly by the computer and, therefore, are probably better than the Coulomb wave functions used in the previous calculations. S-wave approach cross sections were calculated for various values of $U_0$ and $\zeta$. Figures 7 through 11 give $B$, the slope of the Gamow plot as a function of $E^{-½}$. Comparing figure 11 with figure 4, we see that the results for $\zeta=0.0001$ and the OBJ method compare as favorably as we can expect. Calculations were also done for $\zeta=0.0002$, but the cross section results differed from $\zeta=0.0001$ results by only a factor of 2, while the $B$ results coincided in all cases. This indicates that when the absorption is low enough to make $\zeta=0.0001$, the OBJ method is surely a good approximation, i.e., the absorption does not affect the approach cross section.

There is no continuum model equivalent in the optical model, for as the imaginary part of the potential increases, the absorption inside the nucleus increases, but the reflection at the nuclear surface also increases. As the imaginary part of the optical potential approaches very large values the reaction cross section goes to zero. However, a comparison of figures 1 and 7 shows that the shape of the $B$ versus $E^{-½}$ curves is roughly the same for the continuum model and the optical model with large values for $\zeta$.

## 7. Summary and Conclusions

The experimental results for the D-D reaction cross section at low energies are usually given in terms of a straight line on a Gamow plot. Using the WKB method, we have found that the calculated value for $B(E)$, the slope of the Gamow plot, is indeed very close to constant in the energy region from 8 to 100 keV. The "continuum" model, which is the more accurate strong absorption approximation, gives a negative energy dependent correction to the constant value predicted for $B(E)$ by the WKB method. Brennan [5] has pointed out that the experimental results seem to indicate a positive correction to $B(E)$. In addition, theoretical considerations seem to indicate that a weak, rather than

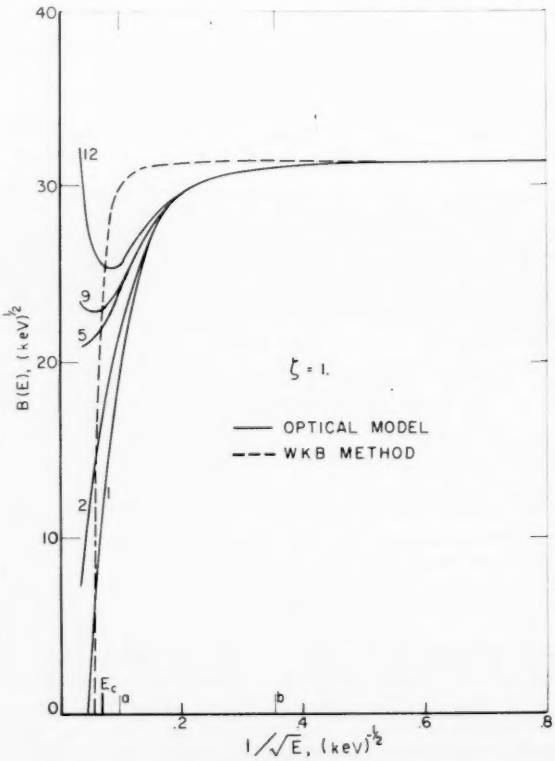


FIGURE 8. B(E) *versus* E$^{-½}$, *optical model,* $\zeta=1$.

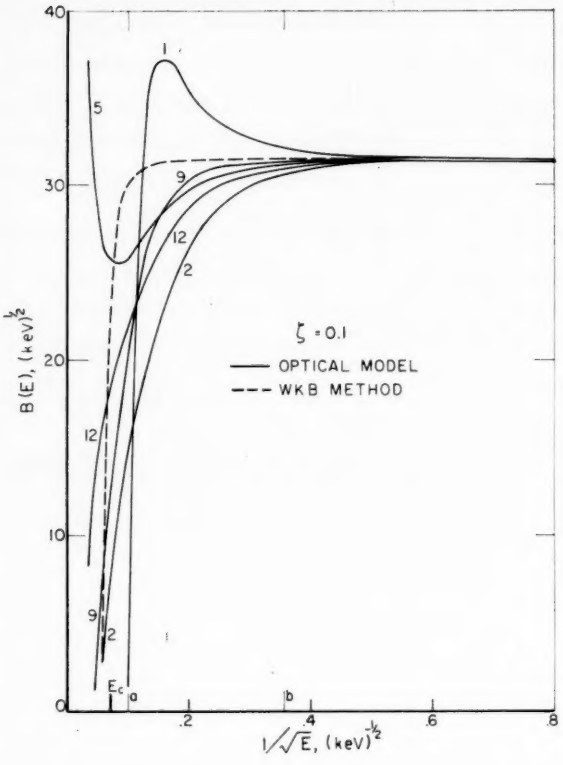


FIGURE 9. B(E) *versus* $E^{-\frac{1}{2}}$, *optical model*, $\zeta = 10^{-1}$.

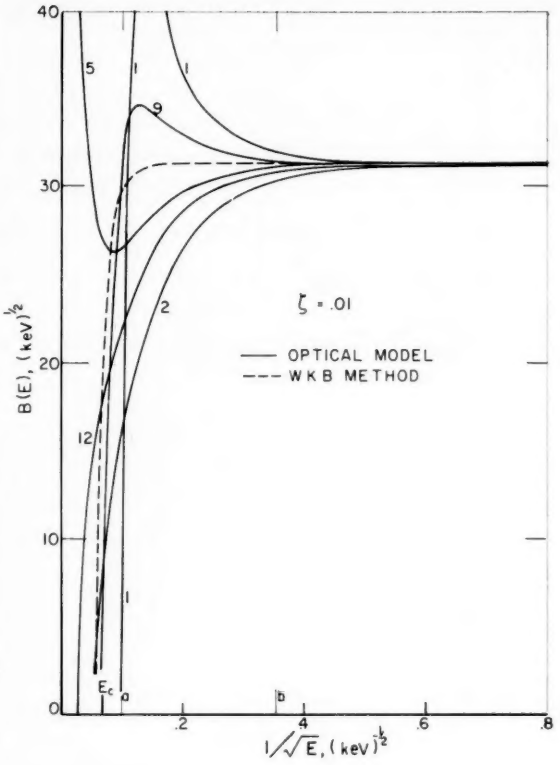


FIGURE 10. B(E) *versus* $E^{-\frac{1}{2}}$, *optical model*, $\zeta = 10^{-2}$.

a strong, absorption model is more applicable to the D-D reaction. Using the OBJ method, which ignores absorption in calculating the approach cross section, we have found that both positive and negative corrections to $B(E)$ are possible. Comparing the results for a square well and a clipped harmonic oscillator nuclear potential, we have found that the approach cross section is not very sensitive to the shape of the nuclear potential.

To study the effects of absorption we have also calculated approach cross sections using the optical model. When the imaginary part of the optical potential becomes small, the optical model results approach the results of the OBJ method, as expected. There is no limit of the optical model which corresponds to the "continuum" model, but as the imaginary part of the optical potential becomes large, the shape of the results approach those of the "continuum" model.

The calculations discussed so far assumed that only the S-waves were important. Using a low energy approximation to the OBJ method, a study was made of the possible influence of P-waves. It was found that the importance of the P-waves was very much a function of the depth chosen for the potential. More accurate experimental results for the total reaction cross section will, we hope, lead to a better knowledge of the energy dependence of $B(E)$, which in turn would tell us more about the optical potential proper to the collision between two deuterons. Also, more accurate studies of the energy dependence of the angular distribution of the reaction products might be used to investigate the influence and importance of the P-waves.

---

The authors express their gratitude to the U.S. Naval Ordnance Laboratory, White Oak, Silver Spring, Md., to the Georgetown College Observatory, Washington, D.C., and to the National Bureau of Standards, Washington, D.C., for the generous use of their computer facilities.

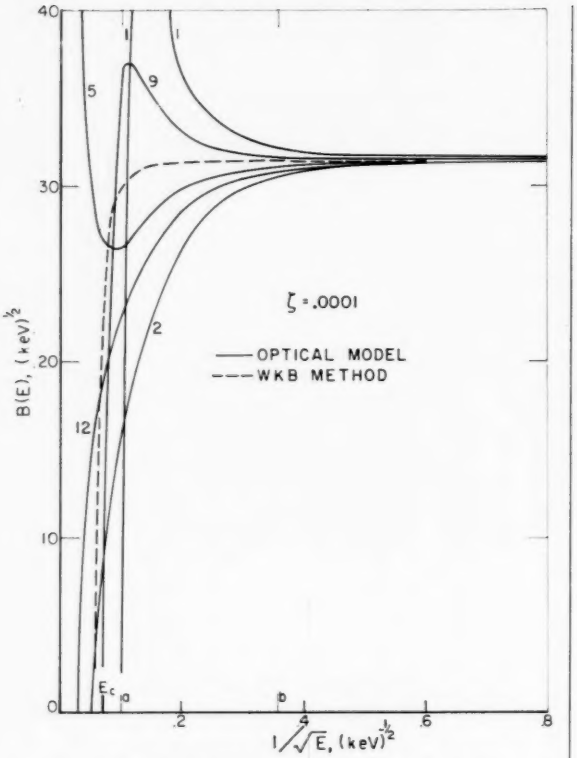


FIGURE 11. B(E) *versus* $E^{-\frac{1}{2}}$, *optical model*, $\zeta = 10^{-4}$.

## 8. References


[1] F. M. Beiduk, J. R. Pruett, and E. J. Konopinski, Phys. Rev. **77,** 622 (1950).
[2] Arnold, Phillips, Sawyer, Stovall, and Tuck, Phys. Rev. **93,** 483 (1954).
[3] Eliot, Roaf, and Shaw, Proc. Roy. Soc. (London) **A216,** 57 (1953).
[4] Davenport, Jeffries, Owen, Price, and Roaf, Proc. Roy. Soc. (London) **A216,** 66 (1953).
[5] J. G. Brennan, Phys. Rev. **111,** 1592 (1958).
[6] J. L. Johnson and H. M. Jones, Phys. Rev. **93,** 1286 (1954).
[7] M. Ostrofsky, G. Breit, and D. P. Johnson, Phys. Rev. **49,** 22 (1936).
[8] H. Feshbach, D. C. Peaslee, and V. F. Weisskopf, Phys. Rev. **71,** 145 (1947).
[9] H. Feshbach, C. E. Porter, and V. F. Weisskopf, Phys. Rev. **96,** 448 (1954).
[10] J. M. Blatt and V. F. Weisskopf, Theoretical Nuclear Physics, p. 360 (John Wiley and Sons, Inc., New York, N.Y., 1957).
[11] Ibid., p. 332.
[12] I. Bloch, M. M. Hull, A. A. Broyles, W. G. Bouricius, B. E. Freeman, and G. Breit, Rev. Mod. Phys. **23,** 147 (1951).


(Paper 68A6–317)

JOURNAL OF RESEARCH of the National Bureau of Standards—A. Physics and Chemistry
Vol. 68A, No. 6, November–December 1964

# Steady-State Response of Silicon Radiation Detectors of the Diffused *p-n* Junction Type to X Rays. I: Photovoltaic Mode of Operation[1]

Karl Scharf and Julian H. Sparrow

(August 13, 1964)

A relation is derived for the photocurrent produced by x rays in silicon radiation detector cells of the *p-n* junction type, giving the dependence of the generated photocurrent on exposure rate, photon energy, and electrical and geometrical parameters of the silicon wafer. Silicon radiation detector cells operated as photovoltaic cells are found to be more sensitive to x rays than silicon solar cells previously investigated, open-circuit voltages being several hundred times larger than those measured in solar cells. The short-circuit current produced by x rays increases with increasing temperature by about 0.3 percent per °C at 25 °C cell temperature. Due to the high zero voltage junction resistance of silicon radiation detector cells, the temperature dependence of the photovoltaic output current increases with increasing load resistance at a smaller rate than that observed in silicon solar cells. The energy dependence of the short-circuit current produced by x rays, measured over a wide range of radiation qualities, is shown to be in good qualitative agreement with calculated values.

## 1. Introduction

In a previous investigation [1] [2] it has been reported that silicon solar cells show a quick and stable photovoltaic response to x and gamma rays and can be used for measurement of exposure rates of such radiations. Since then, several authors investigated the possibility of using silicon solar cells for x- and gamma-ray dosimetry [2,3,4].

Silicon solar cells are photovoltaic cells of the *p-n* junction type specially designed for solar energy conversion. They are made of low resistivity silicon of high impurity concentration and have a narrow depletion region and low cell resistance. In recent years, silicon *p-n* junction type cells have been developed for use in charged particle energy spectroscopy (hereafter referred to as radiation detector cells) which are made of high resistivity silicon. In such cells, the width of the depletion region and the diffusion lengths of minority carriers are much larger than in silicon solar cells. Because of their larger charge collecting volume and higher cell resistance, such cells were expected to have, compared with solar cells, a greater sensitivity for x and gamma rays and better temperature stability when operated as photovoltaic cells.

This paper reports an investigation of the steady-state response of diffused *p-n* junction type silicon radiation detector cells to x rays when operated as photovoltaic cells.[3] Quantitative measurements were made of the dependence of cell sensitivity on exposure rate, cell temperature, and quality of radiation. Furthermore, a theoretical relation was derived for the photocurrent produced by x rays, giving the dependence of the cell sensitivity on quality of radiation, and electrical and geometrical parameters of the silicon wafer.

Measurements reported here were limited to x rays of photon energies less than 250 keV, in order to avoid radiation damage possibly produced by radiations of higher photon energy.

---

[1] Supported in part by the U.S. Atomic Energy Commission.

[2] Figures in brackets indicate the literature references at the end of this paper.

[3] An investigation of the response of such cells to x rays when operated as photodiodes will be reported in a subsequent paper.

## 2. List of Symbols

$I_g$, $J_g$—Generated photocurrent, total (ampere) and density (ampere $cm^{-2}$) respectively.
$(I_g)_{Dr}$, $(J_g)_{Dr}$—Drift component of generated photocurrent, total (ampere) and density (ampere $cm^{-2}$), respectively.
$I_{Df}$, $J_{Df}$—Net diffusion current, total (ampere) and density (ampere $cm^{-2}$) respectively.
$I_j$, $J_j$—Junction leakage current, total (ampere) and density (ampere $cm^{-2}$) respectively.
$(I_j)_V$—Junction leakage current at forward voltage $V$ (ampere).
$I_o$—Diode saturation current in reverse direction (ampere).
$I_s$—Short circuit current (ampere).
$I$—Photovoltaic output current (ampere).
$V_{oc}$—Open-circuit voltage (volt).
$V$—Photovoltage between cell terminals under closed circuit conditions (volt).
$(R_j)_V$—Static junction leakage resistance at forward voltage $V$ (ohm).
$R_L$—Load resistance (ohm).
$q$—Electronic charge (coulomb).
$kT$—Thermal energy (eV).
$\Delta X/\Delta t$—Exposure rate of x rays (R/sec).
$\mu$, $\mu_{en}$—Linear attenuation and linear energy absorption coefficient, respectively, of silicon for x rays ($cm^{-1}$).
$(\mu_{en}/\rho)_{air}$—Mass energy absorption coefficient of air for x rays ($cm^2\ g^{-1}$).
$\epsilon$—Average electron-hole pair production energy (erg).
$g$—Rate of generation of electron-hole pairs due to irradiation ($cm^{-3}\ sec^{-1}$).
$I_R$—Radiation intensity (erg $cm^{-2}\ sec^{-1}$).
$A_c$, $A_R$—Total and irradiated cell area respectively ($cm^2$).
$w$—Width of depletion region (cm).
$d_s$, $d_b$—Widths of $n$-type surface layer and $p$-type base layer, respectively (cm).
$L_p$, $L_n$—Average diffusion lengths of minority carriers (cm).
$\tau_p$, $\tau_n$—Lifetimes of minority carriers (sec).
$D_p$, $D_n$—Diffusion constants of minority carriers ($cm^2\ sec^{-1}$).
$s_p$, $s_n$—Surface recombination velocities of minority carriers (cm $sec^{-1}$).
$p$, $n$—Steady-state concentration of minority carriers ($cm^{-3}$).
$p_n$, $n_p$—Thermal equilibrium concentration of minority carriers ($cm^{-3}$).

## 3. Theoretical Considerations

### 3.1. Basic Equations

Under the photovoltaic mode of operation of a radiation detector cell, a photocurrent is produced in an electrical circuit connected to the cell without application of an external bias voltage. If the cell is irradiated, excess carriers are produced throughout the whole silicon wafer, but only carriers produced inside the junction or depletion region, or minority carriers produced in the bulk of the silicon reaching the junction region by diffusion, are acted upon by the junction field. Holes are driven to the $p$-side and electrons to the $n$-side of the junction, thus producing a voltage difference biasing the cell in the forward direction.

The radiation produced charge carriers separated by the junction field represent the generated photocurrent $I_g$, flowing in the reverse direction of the cell. Under steady-state conditions, the photovoltage $V$ produces a back current equal to $I_g$. Part of it is flowing as the photovoltaic output current $I$ through the external circuit in the reverse direction, the other part is flowing back through the cell as junction current $I_j$ in the forward direction (fig. 14 in appendix). If the load resistance connected across the cell terminals $R_L=0$, the external or short circuit current $I_s$ will reach its maximum value equal to $I_g$. Under open

circuit conditions ($R_L=\infty$), the photovoltage reaches a maximum called the open-circuit voltage $V_{oc}$, and the back current through the cell will be equal to $I_g$.

Several authors [5–9] calculated the photovoltaic output current of a $p$-$n$ junction cell as a function of electrical and geometrical parameters of the cell and quality of radiation, assuming a negligible width of the junction region. Gaertner [10] and Tuzzolino et al. [11] calculated the photocurrent produced in surface barrier cells taking into account the voltage dependent width of the depletion region. All these calculations were made for the photoresponse to visible light, but similar methods of calculation can be applied to the calculation of the photocurrent produced by x rays.

In the case of x rays, secondary high-energy electrons are produced by photon-electron interactions which dissipate their energy by producing low-energy electron-hole pairs in electron-electron collisions. The number of these low-energy charge carriers contributing to the photocurrent is proportional to the *energy* of radiation absorbed and not to the *number* of absorbed photons as in the case of visible light. The average energy required to produce one electron-hole pair by electron-electron collision is approximately 3.5 eV [12], as compared with a threshold energy of approximately 1.1 eV for electron-hole pair production by light. Furthermore, a distinction must be made in the case of x rays between the attenuation coefficient and the energy absorption coefficient of the radiation, the latter determining the amount of absorbed radiation energy converted into electron energy.

For the calculation of the photocurrent produced by x rays, it was assumed that the ionization due to the reabsorption in the silicon wafer of the bremsstrahlung, fluorescence radiation and Compton photon radiation produced in the absorption process of x rays is negligibly small and need not be taken into account. Finally, *true* electronic equilibrium was assumed to exist in the silicon wafer. Under this condition, the energy per unit volume deposited by secondary electrons at a certain point in the charge collecting volume is equal to the entire energy of secondary electrons produced per unit volume by the x rays at this point.

The calculation of the photovoltaic output current produced by x rays in a $p$-$n$ junction cell carried out under the above assumptions, and taking into account the ionization produced inside the depletion region, is given in the appendix. Considering the cell type investigated, it was assumed that the cell consisted of a $p$-type silicon base with a thin $n$-type layer at the irradiated surface.

The result of the calculation can be written as

$$I=I_g-I_j \tag{1}$$

where

$$I_g=\frac{86.9qA_R}{\epsilon}(\Delta X/\Delta t)\frac{(\mu_{en}/\mu)}{(\mu_{en}/\rho)_{\text{air}}}\exp(-\mu d_s)\times\left[1-\left(1-\frac{\mu L_n}{\mu^2L_n^2-1}a_n\right)\exp(-\mu w)+\frac{\mu L_p}{\mu^2L_p^2-1}a\right] \tag{2}$$

$$I_j=A_eq\left[\exp(qV/kT)-1\right]\left(\frac{p_nD_p}{L_p}b_p+\frac{n_pD_n}{L_n}b_n\right) \tag{3}$$

if $I$ and $I_g$ in the reverse direction are taken as positive and $\epsilon$ is given in erg and $\Delta X/\Delta t$ in $R$/sec.

The quantities $a_p$, $a_n$, $b_p$, and $b_n$ given in the appendix (eqs (A.13)) are functions of the geometrical dimensions of the silicon wafer, and of the average diffusion lengths and surface recombination velocities of minority charge carriers. The quantities $a_p$ and $a_n$ are further dependent on the attenuation coefficients of silicon for x rays.

For the $p$-$n$ junction type radiation detector cells considered here, it may be assumed that $d_s/L_p<<1$ and $d_b/L_n>>1$. Under these conditions and assuming small surface recombination at the base contact, approximate values of $a_p$ and $a_n$ can be used as given by eqs (A.20–21). Assuming further the value of $\epsilon=3.5$ eV or $5.61\times10^{-12}$ erg, and expressing $q$ in coulomb, eq (2) can be written as:

$$I_g=2.48\times10^{-6}A_R(\Delta X/\Delta t)\frac{(\mu_{en}/\mu)}{(\mu_{en}/\rho)_{\text{air}}}\exp(-\mu d_s)\times\left[1-\frac{\exp(-\mu w)}{\mu L_n+1}+\frac{\mu d_s}{1+(s_pd_s)/D_p}\right]\text{ampere.} \tag{2a}$$

For values $\mu L_n << 1$, $\mu w << 1$, and $\mu d_s << 1$, and $s_p = 0$, eq (2a) is reduced to the equation given for $I_g$ in a previous paper (eq (19) in ref. [1]) having been derived under the assumption of negligible attenuation of the radiation in the charge collecting volume.

If the cell surface is covered by a contact or any other layer to ensure electronic equilibrium in the cell surface region, the values of $I_g$ obtained from eqs (2) and (2a) have to be multiplied by an attenuation factor exp $(-\mu_c d_c)$ where $\mu_c$ and $d_c$ are the attenuation coefficient and thickness of the surface cover, respectively.

### 3.2. Discussion of Basic Equations

Equation (3) derived from the basic rectifier theory [13] will not be discussed here, but detailed consideration will be given to eq (2) for the generated photocurrent $I_g$ which is of main interest in this investigation.

For the discussion of eq (2), *effective* diffusion lengths may be defined as:

$$L_n' = L_n \frac{a_n}{\mu^2 L_n^2 - 1}; \qquad L_p' = L_p \frac{a_p}{\mu^2 L_p^2 - 1} \tag{4}$$

which determine the electric charge collected by diffusion of electrons and holes from the base and surface layer into the depletion region. The average diffusion lengths $L_n$ and $L_p$ are material constants, but $L_n'$ and $L_p'$ are functions of the same parameters as $a_n$ and $a_p$.

The dependence of the effective diffusion lengths on these parameters is shown in figures 1 to 3. The effective diffusion lengths are given as dimensionless relative values $(L_n'/L_n)$ and $(L_p'/L_p)$, and were calculated by using eqs (A. 13) given in the appendix. The graphs were calculated for photon energies corresponding to effective energies of heavily filtered x rays investigated as given below (table 1).

With increasing ratios of layer thickness to average diffusion length, the effective diffusion lengths increase and approach saturation values for $d_b/L_n > 1$ and $d_s/L_p > 1$ (figs. 1 and 2). With decreasing photon energy, the effective diffusion lengths of minority carriers in the base layer $(L_n'/L_n)$ decrease but increase for those in the surface layer $(L_p'/L_p)$. This increase, however, is offset by the increased attenuation of the radiation in the surface layer taken into account by the factor exp $(-\mu d_s)$ in eq (2). For both types of minority carrier, the effective diffusion lengths are decreased if surface recombination velocity is increased.

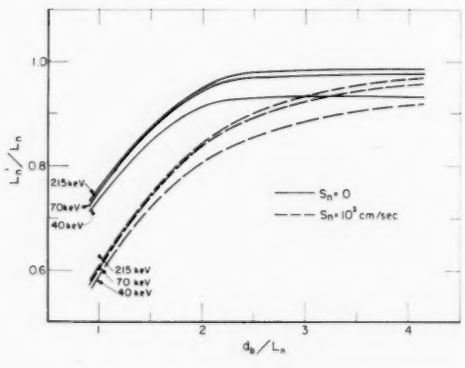


FIGURE 1. *Relative effective diffusion lengths of electrons in the* p-*type silicon base layer* $[L_n'/L_n = a_n/(\mu^2 L_n^2 - 1)]$ *calculated as function of* $d_b/L_n$ *for different photon energies, assuming different values of* $s_n$. $L_n$ *assumed* $= 420\ \mu$.

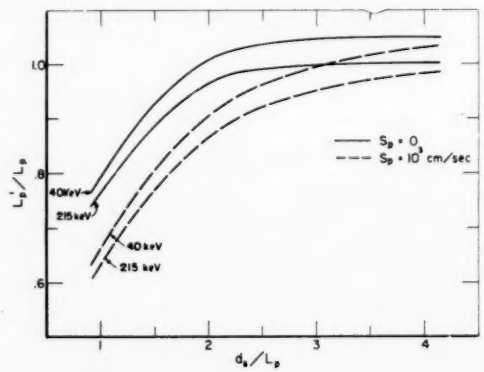


FIGURE 2. *Relative effective diffusion lengths of holes in the* n-*type silicon surface layer* $[L_p'/L_p = a_p/(\mu^2 L_p^2 - 1)]$ *calculated as function of* $d_s/L_p$ *for different photon energies, assuming different values of* $s_p$. $L_p$ *assumed* $= 100\ \mu$.

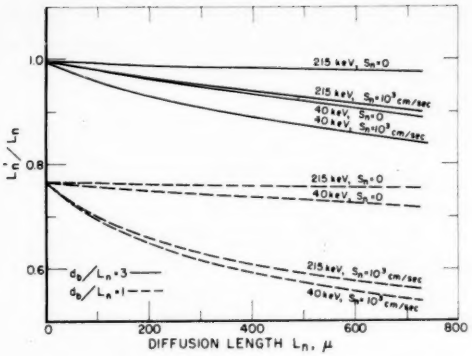


FIGURE 3. *Relative effective diffusion lengths* $L_n'/L_n$ *of electrons in the p-type silicon base layer calculated as function of* $L_n$ *for different photon energies, assuming different values of* $d_b/L_n$ *and* $s_n$.

The widths of the surface layer and the junction region under the photovoltaic mode of operation may be assumed to be small compared with the diffusion lengths of minority carriers. The generated photocurrent $I_g$ will, therefore, mainly consist of minority carriers produced by the radiation in the base layer. For the cell configuration under consideration, $I_g$ will be determined by the effective diffusion length $L_n'$ of electrons produced in the $p$-type base.

Assuming a constant value of $L_n$, $L_n'$ will increase with increasing base layer thickness until $a_n$ reaches a saturation value. A further increase of sensitivity could not be achieved by further increase of the base layer thickness $d_b$, but only by increasing $L_n$. The highest sensitivity would be obtained by increasing $L_n$ as much as possible and increase the base layer thickness so that $a_n$ remains at the saturation value. With increasing $L_n$, the charge collected from the base layer will not increase proportional to $L_n$, but at a smaller rate, dependent on the photon energy and the amount of surface recombination (fig. 3). With increasing $L_n$, $L_n'$ will increase at a smaller rate than $L_n$, i.e., $L_n'/L_n$ will decrease.

Graphs of the energy dependence of the photovoltaic current sensitivity of a $p$-$n$ junction cell calculated by using eq (2) and assuming different values of $L_n$, $d_b/L_n$, and $s_n$ are shown in figures 4 and 5. The photovoltaic current sensitivity is given as the generated photocurrent $I_g$ obtained with an irradiated surface area of 1 cm² at an exposure rate of 1 R/min or $\frac{1}{60}$ R/sec. The calculations were made for monoenergetic x rays, the quality of the radiations being expressed in half-value layers (HVL) of aluminum. Values of $\mu_{en}$ and $\mu$ for silicon were obtained from data given by White Grodstein [14] and Nelms [15]. Values of $(\mu_{en}/\rho)_{air}$ were taken from ICRU reports [16]. Other parameters used in the calculations, but not shown in

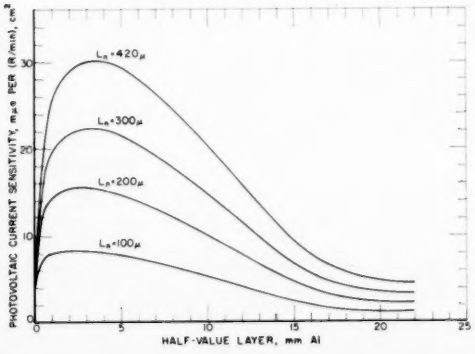


FIGURE 4. *Energy dependence of the short-circuit current obtained at an exposure rate of 1 R/min and 1 cm² irradiated silicon surface, as calculated for different values of* $L_n$, *assuming* $d_b/L_n >> 1$, $s_n=0$.

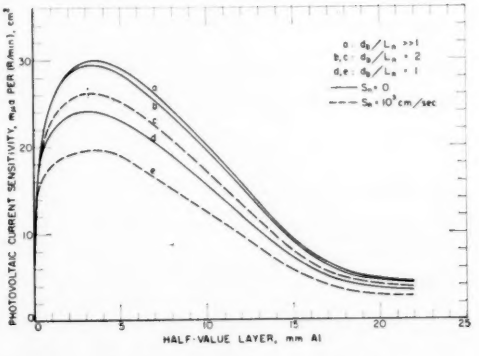


FIGURE 5. *Energy dependence of the short-circuit current obtained at an exposure rate of 1 R/min and 1 cm² irradiated silicon surface as calculated for different values of* $d_b/L_n$ *and* $s_n$, *assuming* $L_n=420$ μ.

figures 4 and 5, were: $d_s=2.0\ \mu$, $d_s/L_p<<1$, $s_p=10^3$ cm/sec, $D_p=10$ cm$^2$/sec, and $D_n=30$ cm$^2$/sec. Considering the small photovoltages obtained with x rays, the junction width $w$ was assumed to be constant for all calculations. Its value was approximately calculated as $w=7.0\ \mu$ by using the relation

$$w=1/3\sqrt{\rho V_o} \tag{5}$$

assuming the resistivity $\rho$ of the $p$-type base layer as 1000 Ω-cm and the barrier voltage $V_o=0.5$ volt.

The photovoltaic current sensitivity is strongly dependent on $L_n$ and increases at all energies nearly linearly with increasing $L_n$ (fig. 4). For $L_n=420\ \mu$, the sensitivity reaches a maximum at an HVL of approximately 3.5 mm Al (34.5 keV) which shifts for $L_n=100\ \mu$ to a HVL of 2.5 mm Al (30 keV). However, the ratio between the maximum value of sensitivity to the sensitivity at a HVL of 21.4 mm Al (200 keV) is nearly the same, approximately 6.5, independent of the parameter $L_n$. The energy dependence is slightly changed, especially at low energies (small HVL) if at constant $L_n$, the base layer thickness or surface recombination is changed (fig. 5). In accordance with the discussion given above, the sensitivity decreases over the whole energy range when the ratio $d_b/L_n$ is decreased or $s_n$ is increased.

### 3.3. Circuit Equations

According to eq (2), the generated photocurrent $I_g$ is proportional to the exposure rate, and measurement of the latter should be based on the measurement of $I_g$ or any other quantity linearly related to it.

Equation (3) can be written in current notation as

$$I_j=I_o\,[\exp\,(qV/kT)-1] \tag{6}$$

from which one obtains from eq (1):

$$I=I_g-I_o\,[\exp\,(qV/kT)-1] \tag{7}$$

$$V=\frac{kT}{q}\ln\left[\frac{I_g-I}{I_o}+1\right]. \tag{8}$$

Here, $V$ is the forward voltage at the junction produced by irradiation. If the series cell resistance consisting of the contact and bulk resistances is negligibly small compared with the load resistance $R_L$, then $V$ is equal to the photovoltage measured between the terminals of the cell

$$V=IR_L. \tag{9}$$

The current $I_s$ measured under short circuit conditions ($R_L=0$, $V=0$) and the voltage $V_{oc}$ measured under open circuit conditions ($R_L=\infty$, $I=0$) are:

$$I_s=I_g \tag{10}$$

$$V_{oc}=\frac{kT}{q}\ln\left(\frac{I_g}{I_o}+1\right). \tag{11}$$

The short circuit current $I_s$, which is equal to $I_g$ and therefore proportional to the exposure rate, can not actually be measured, but only determined by extrapolation of the measured output current to zero load resistance, while quantities directly measurable as $I$, $V$, and $V_{oc}$, are not linearly related to $I_g$. However, under certain conditions, proportionality between $I$ and $I_g$ can be sufficiently approached. Introducing the static junction resistance at the forward junction voltage $V$

$$(R_j)_V=\frac{V}{(I_j)_V},$$

one obtains from eqs (1) and (9)

$$I=I_g-\frac{V}{(R_j)_V}=I_g\left[1+\frac{R_L}{(R_j)_V}\right]^{-1} \tag{12}$$

$$V=(I_j)_V(R_j)_V=(I_g-I)(R_j)_V=IR_L \tag{13}$$

$$V_{oc}=I_g(R_j)_{V_{oc}} \tag{14}$$

The junction resistance is voltage dependent and decreases with increasing forward voltage. Proportionality of the measured values of $I$ and $V$ with $I_g$ or the exposure rate, will be obtained if $(R_j)_V$ is constant or if $R_L/(R_j)_V<<1$.

At small voltages or values of $I_g/I_o<<1$, the junction resistance may be considered as constant, its value being derived from eq (6) as

$$(R_j)_o=\frac{kT}{qI_o}. \tag{15}$$

The resistance $(R_j)_o$, also called the zero voltage junction resistance, is inversely proportional to the reverse saturation current $I_o$. Thus, at small photovoltages as obtained with small exposure rates, the values of $I$, $V$, and $V_{oc}$ may be considered to be proportional to $I_g$ or the exposure rate. For large exposure rates or large $I_g$, proportionality between $I$ or $V$ and the exposure rate can be retained by reducing the load resistance $R_L$, thereby reducing the photovoltage and the ratio $R_L/(R_j)_V$. No such regulation is possible for the open-circuit voltage $V_{oc}$ which at larger values follows a logarithmic dependence on exposure rate (eq (8)).

It is known that eq (6) does not satisfactorily describe the voltage dependence of the measured junction current $I_j$ of a silicon diode [17], but may be considered as an approximation applicable to the operation of photovoltaic cells [8]. Measurements reported here were evaluated by considering the junction leakage current $I_j$ obtained from the current-voltage characteristic measured for small forward voltages. Values of short-circuit currents discussed below were determined either by extrapolating the measured photovoltaic output current $I$ to zero load resistance, or by adding to $I$ the junction current $I_j$, given by the measured current-voltage characteristic of the cell for the respective photovoltage values (eq (1)).

## 4. Experimental Procedure

The silicon radiation detector cells investigated were commercially available encapsulated cells of the diffused $p$-$n$ junction type, provided with a thin protective aluminum layer on the surface. According to the manufacturer's specification, the cells were made of 1000 Ω-cm $p$-type silicon with an $n$-type layer on the sensitive surface. The diffusion depth was approximately 2 $\mu$ and the thickness of the protective aluminum layer approximately 0.5 to 1.0 $\mu$. Cells were exposed to radiation under normal air pressure and were covered with a light-tight paper cover.

The x-ray sources were a 250-kV tube and a 50-kV beryllium-window-type tube with an inherent filtration of approximately 4.0 mm Al and 0.25 mm Be respectively. The x-ray tubes were tungsten target tubes operated by stabilized constant voltage supplies. The different qualities of radiations obtained by using different filtration are shown in table 1. Exposure rates of heavily and moderately filtered x rays were measured by R-meters which had been calibrated for each investigated type of radiation against the NBS standard free-air chamber. Exposure rates of lightly filtered x rays were measured with an NBS free-air chamber.[4]

[4] Exposure rate measurements with the free-air chamber were carried out by Paul Lamperti of the NBS X-Ray Standards Section.

TABLE 1. *Types of radiations investigated*

| kvcp | Approx. inherent filter | Added filter | Target distance | Approx. HVL |
|---|---|---|---|---|
| **Lightly filtered x rays** | | | | |
| | (*mm* Be) | (*mm* Al) | (*cm*) | (*mm* Al) |
| 20 | 0.25 | 0 | 60 | 0.07 |
| 20 | .25 | 0.5 | 60 | .25 |
| 30 | .25 | 0 | 60 | .09 |
| 30 | .25 | 0.5 | 60 | .42 |
| 50 | .25 | 0 | 60 | .12 |
| 50 | .25 | 0.5 | 60 | .64 |
| 50 | .25 | 1.0 | 60 | .93 |

| kvcp | Approx. inherent filter | Added filter | | Approx. HVL |
|---|---|---|---|---|
| | | Al | Cu | |
| **Moderately filtered x rays** | | | | |
| | (*mm* Al) | (*mm*) | (*mm*) | (*mm* Al) |
| 60 | 4.0 | 0 | 0 | 2.79 |
| 75 | 4.0 | 0 | 0 | 3.41 |
| 100 | 4.0 | 1.0 | 0 | 5.05 |
| 150 | 4.0 | 1.0 | 0.25 | 10.1 |
| 200 | 4.0 | 1.0 | 0.5 | 13.2 |
| 250 | 4.0 | 1.0 | 1.0 | 16.2 |

| kvcp | Approx. inherent filter | Added filter | | | Approx. effective energy | Approx. HVL |
|---|---|---|---|---|---|---|
| | | Pb | Sn | Cu | | |
| **Heavily filtered x rays** | | | | | | |
| | (*mm* Al) | (*mm*) | (*mm*) | (*mm*) | (*keV*) | (*mm* Al) |
| 50 | 4.0 | 0.12 | 0 | 0 | 40 | 4.4 |
| 100 | 4.0 | 0.53 | 0 | 0 | 70 | 11.2 |
| 150 | 4.0 | 0 | 1.5 | 4.0 | 120 | 16.8 |
| 200 | 4.0 | 0.7 | 4.0 | 0.6 | 170 | 19.5 |
| 250 | 4.0 | 2.7 | 1.0 | 0.6 | 215 | 21.5 |

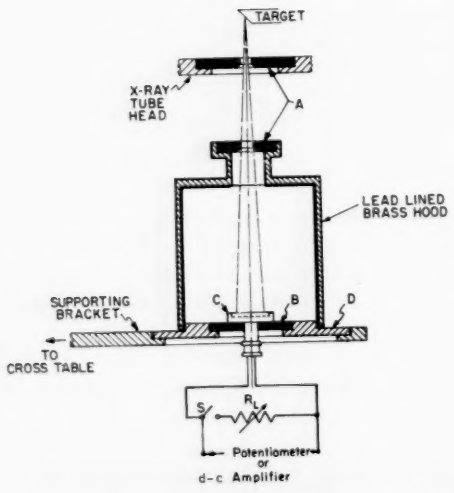


FIGURE 6. *Sketch of mounting of radiation detector cell showing geometry of irradiation.*

(A) Lead diaphragms; (B) Bakelite disk; (C) Silicon radiation detector cell; (D) Lead disk, being removed for measurement of exposure rates in air.

The x-ray beams, if not otherwise stated, were collimated by lead diaphragms mounted in a fixed position relative to the cell. The beam diameter at the cell surface was smaller than the cell area so that no radiation was passing through the cell casing before hitting the sensitive cell surface. The mounting of the cell in the vertical beam of the 250-kV x-ray tube is shown in figure 6. The size and position of the beam spot were checked radiographically. For correct positioning of the cell, the whole fixture was mounted on an adjustable cross-table. For measurements in the horizontal beam of the 50-kV x-ray tube, a holder was used containing the cell and the beam-size defining diaphragm, and mounted on the optical bench used for the low-energy NBS air chamber.

The photovoltaic output current and the open-circuit voltage were measured by a null method with a potentiometer. The photocurrent was determined by measuring the voltage drop over a load resistance of known value.

## 5. Measurements

### 5.1. Exposure Rate Dependence

The exposure rate dependence of the photovoltaic output current $I$ and the open circuit voltage $V_{oc}$ measured on two radiation detector cells of different size is shown in figure 7. The cells were fully irradiated with lightly filtered 30-kV x rays of 0.3 mm Al half-value layer (HVL). The different exposure rates were obtained by changing the x-ray tube current. Due to the strong absorption of the low-energy radiation in the cell casing, the sensitive areas of the two cells may be assumed to be approximately equal to their nominal sensitive free surface areas of 5 $mm^2$ and 2.0 $cm^2$ respectively.

The photovoltaic current of the 5 $mm^2$ cell, measured with a load resistance of $10^5$ Ω is proportional to exposure rates up to $10^5$ R/min, the highest exposure rate investigated. The photocurrent of the larger cell (2.0 $cm^2$) measured with a smaller load resistance of $10^4$ Ω shows a slight deviation from linear response for exposure rates above 2000 R/min. Due to its smaller cell resistance, the condition $R_L/(R_j)_V << 1$ was not fulfilled at the relative high photovoltages, when using a load resistance of $10^4$ Ω. By reducing the load resistance, the linear dependence of the photocurrent could be extended to higher exposure rates, approaching the short-circuit dependence ($R_L=0$) on exposure rate shown in figure 7. The ratio of the photocurrents of the two cells is in good agreement with the ratio of their surface areas which is approximately 40:1.

The open circuit voltages show a nearly linear exposure rate dependence at low exposure rates and follow a logarithmic dependence at higher exposure rates (eq (11)). They are of the same order of magnitude for both cells, and differ at exposure rates of 5000 R/min by only about 15 percent. The open circuit voltage $V_{oc}$ is a function of the ratio $I_g/I_o$, $I_g$ and $I_o$ being proportional to the irradiated and total cell surface respectively. Therefore, for fully

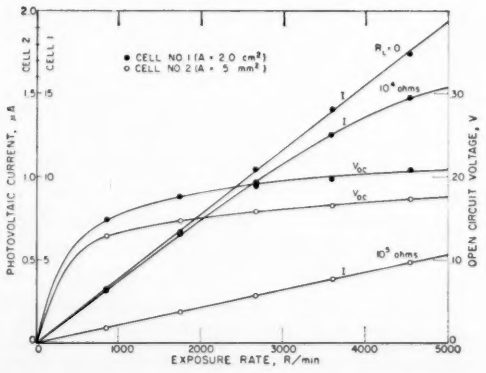


FIGURE 7. *Exposure rate dependence of open-circuit voltage and photovoltaic output current measured with 30-kV lightly filtered x rays of 0.09 mm* Al *HVL.*

irradiated cells of the same type, and the same quality of radiation, $V_{oc}$ should be independent of the cell area. The small difference observed may be explained by some differences in design and structure of the cell.

The response times to irradiation were short, within the response times of the measuring instruments, and no fatigue of the cells was observed during irradiation. At constant temperatures, measurements of the photocurrent were reproducible within one percent. The open-circuit voltage shows a greater noise than the photocurrent and is strongly temperature dependent, making its measurement less accurate.

### 5.2. Temperature Dependence

For measuring the temperature dependence, the detector cells were placed inside a drying oven and fully irradiated through the oven wall consisting of nonmetallic heat insulating material. The oven temperature was thermostatically controlled within $\pm 1$ °C.

The photovoltaic current-voltage characteristic of a silicon radiation detector cell of 2.0 cm² surface area, measured at different temperatures between approximately 25 and 50 °C, is shown in figure 8. These characteristics were measured with 100 kV x rays filtered by 2 mm Al and the oven wall at a constant exposure rate of approximately 50 R/min, and were obtained by changing the load resistance $R_L$. The intercepts of the load lines with the characteristics give the photocurrent and photovoltage at the respective load resistance and temperature. The short circuit current and the open-circuit voltages at different temperatures are given by the intercepts of the characteristics with the current and voltage axis respectively. With increasing temperature, the open-circuit voltage decreases and the short circuit increases slightly. The load lines through the intersections of these characteristics indicate the load resistances required to keep the temperature dependence in the temperature interval considered at a minimum. According to figure 8, the optimum load resistance for the investigated cell with regard to temperature dependence of photocurrent and photovoltage at the exposure rate under consideration is approximately $10^4$ Ω for the temperature interval between 25.6 and 39.2 °C, and about $5\times10^3$ Ω for temperatures between 39.2 and 49.4 °C.

The relative changes of photocurrent and open-circuit voltage with increasing temperature measured on a cell of 5 mm² surface area at the same exposure rate, and using different load resistances, are shown in figure 9. The temperature dependence is qualitatively the same as that shown in figure 8. At 25 °C, the short-circuit current ($R_L=0$) increases by 0.32 percent per °C, and the open-circuit voltage ($R_L=\infty$) decreases by 2.2 percent per °C, with increasing

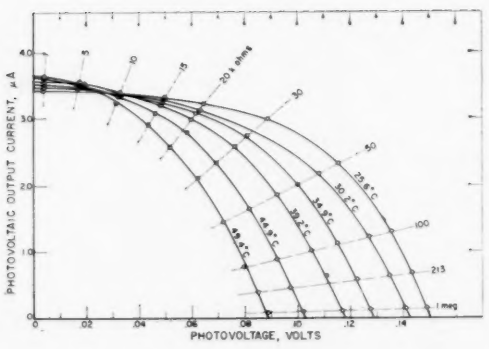


FIGURE 8. *Photovoltaic current-voltage characteristic at different temperatures measured on a silicon radiation detector cell of 2.0 cm² surface area, with indication of load lines for different load resistances.*

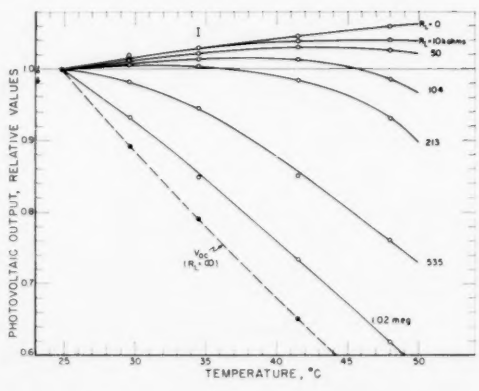


FIGURE 9. *Relative change with temperature of open-circuit voltage and photovoltaic output current measured with different load resistances on a silicon radiation detector cell of 5.0 mm² surface area.*

temperature. For finite load resistances, the temperature dependence of the photocurrent lies between these two extreme values. Due to the larger junction resistance of this cell compared with the cell of 2.0 $cm^2$ surface, the optimum load resistances are of higher values for the smaller cell. For instance, with $R_L = 1.04 \times 10^5\ \Omega$, the photocurrent changes between 25 and 45 °C by less than one percent.

The temperature dependence of the photovoltaic response is mainly due to the temperature dependence of $I_j$. In general, in order to keep the temperature dependence low, the value of the load resistance should be chosen of such a value that the condition $R_L/(R_j)_V << 1$ remains satisfied over the temperature and photovoltage range under investigation.

No definite explanation can be given for the increase of the short-circuit current with increasing temperature. A similar temperature dependence of the short-circuit current produced by visible light, was explained by the displacement of the absorption spectrum of silicon due to a change of the band gap energy [18]. This explanation can apparently not be applied to the short-circuit current produced by x rays. The temperature dependence of the amount of x-ray energy absorbed per unit volume of silicon may be assumed to be negligible. There may exist a temperature dependence of the average energy $\epsilon$ of electron-hole pair production, but the change of band gap energy with change in temperature should be of little influence. The band gap energy accounts for approximately only a third of the value of $\epsilon$ [12], and decreases only by approximately 0.04 percent per °C with increasing temperature [19]. Another explanation could be the decrease of the series cell resistance (bulk and contact resistance), with increasing temperature. As estimated from the forward characteristic of the cell investigated, the cell series resistance was approximately 0.01 percent of the zero voltage junction resistance and could therefore have only a negligible influence on the measured temperature dependence of the short-circuit current. Another explanation would be to assume an increase of the diffusion lengths of minority carriers due to the temperature dependent changes of recombination and trapping rates [20].

### 5.3. Energy Dependence

The energy dependence of the photovoltaic response was measured for heavily, moderately, and lightly filtered x rays (table 1). The photocurrent was determined by measuring the voltage drop over the input resistance of an amplifying d-c microvolt-ammeter serving as load resistance in the cell circuit. The input resistance was variable corresponding to the different measuring ranges of the instrument, so that the input resistance could be chosen small enough to keep the temperature dependence of the photocurrent at a low level. The voltage-amplifying gain at all energies used was 1000, and the amplified voltage drop was measured with a potentiometer with a precision of a few tenths of a percent. The exposure rates were approximately 0.5 to 1.0 R/min for heavily filtered x rays and approximately 5.0 to 50.0 R/min for moderately and lightly filtered radiations. The x-ray beam was collimated as described above.

The charge collecting volume in the radiation detector cell extends from the inside of the silicon up to the irradiated surface. Due to the lack of compensation of charge carried away by high-energy electrons produced in the surface region, the ionization near the surface is only gradually increasing with increasing depth in the silicon until a maximum value is reached at a depth approximately equal to the maximum range of the radiation-produced high-energy electrons. In order to compensate this ionization deficiency and approach electron equilibrium conditions in the surface region, the cell surface was covered with thin layers of aluminum which has an atomic number ($Z_{Al}=13$) close to that of silicon ($Z_{Si}=14$). The photocurrent measured with the cell surface covered with aluminum layers of different thicknesses is shown in figure 10. Covering the silicon surface with aluminum is equivalent to moving the charge-collecting volume deeper into the silicon. The photocurrent shows, therefore, first an increase with increasing layer thickness reaching a broad maximum at a layer thickness equal to the maximum electron range $R$ in aluminum which may be assumed to be approximately the same as in silicon. A further increase of layer thickness reduces the photocurrent due to the attenuation

of the radiation in the aluminum layer which again may be assumed to be approximately equal to that of a silicon layer of the same thickness. The higher the photon energy, the greater the rate of the initial increase of the photocurrent. However, even for 250-kV, heavily filtered x rays ($h\nu_{eff}$=215 keV), the maximum photocurrent was found to be only by a few percent larger than that measured without additional surface layer. Slightly different values, but of the same order of magnitude, were measured with different individual cells of the same type. This indicates that the ionization deficiency in the surface region may be assumed to be small compared with the total charge collected.

The following measurements of the energy dependence of the photovoltaic current were all carried out with the cell surface covered by an aluminum layer 325 $\mu$ thick, equal to the electronic equilibrium thickness for the highest photon energy (250 keV) considered here (fig. 10).

The energy dependence of the photovoltaic current sensitivity of a diffused silicon $p$-$n$ junction cell as measured for different qualities of radiation is shown in figures 11, 12, and 13. The sensitivity is expressed by the short-circuit current measured at an exposure rate of 1 R/min and an irradiated cell surface of 1 cm$^2$. The values of the short-circuit current, assumed to be equal to $I_g$, were derived from the output current $I$, measured at a finite load resistance, using eq (12). All values were corrected for a cell temperature of 22 °C considering the measured temperature dependence of the cell leakage-current and short-circuit current.

Relative values of the photovoltaic current sensitivity for heavily filtered x rays are shown in figure 11 as a function of effective photon energy. The measured currents were corrected for attenuation in the aluminum surface layer, which is very small for these types of radiations. The values of sensitivity are normalized to unity for 250-kV x rays ($h\nu_{eff}$=215 keV), the normalized value having been measured as

$$I_s=4.45\times10^{-9}\ \text{A (R/min)}^{-1}\text{cm}^{-2}.$$

For a comparison of measured and theoretical values, the photovoltaic current sensitivity was calculated according to eq (2a), assuming monoenergetic radiations. All cell parameters except $L_n$ were assumed to be the same as chosen for the calculation of the energy dependence of the current sensitivity shown in figure 4. The value of the diffusion length $L_n$ was determined by solving eq (2a), with $I_g$ given by the short-circuit current measured at 1 R/min and 1 cm$^2$ irradiated cell area, and corrected for attenuation in the aluminum layer. The width $d_b$ of the base layer, assumed to be approximately equal to the total thickness of the silicon wafer, was determined by x-ray radiography [5] as $d_b$=1.4 mm. It was therefore assumed that condition $d_b/L_n >> 1$ was fulfilled and the use of the simplified eq (2a) justified.

Values of $L_n$ calculated in this way from currents measured at different effective energies were not of a constant value, but were slightly increasing with decreasing energy, the value derived from measurements with 250-kV x rays being $L_n$=420 $\mu$.[6] When using this value of $L_n$ for the calculation of the sensitivity at different photon energies, the relative measured values are consequently higher than the calculated ones shown as relative values in figure 11. The ratio of measured to calculated sensitivity reaches a maximum of approximately 1.3 between 70 and 100 keV.

The apparent energy dependence of $L_n$, which should be a constant, shows that an energy dependent factor would have to be included in eqs (2) and (2a), in order to bring measured and calculated sensivity values into agreement. A similar energy dependence of the ratio of measured and calculated sensitivities was observed in a previous investigation of silicon solar cells [1], and was there tentatively explained by a reabsorption of scattered Compton photons.

The photovoltaic current sensitivity measured with moderately and lightly filtered x rays of half-value layers between 0.07 mm Al and 16.0 mm Al is shown in figure 12 (curve b). The

[5] The x-ray photographs of the detector cells were made by L.A. Dobak of the NBS Dosimetry Section.

[6] This value of $L_n$ is in good agreement with that determined by Pfister [21] in a similar way, using monochromatic (characteristic) x rays.

sensitivity reaches a maximum at a HVL of approximately 4.0 mm Al which is only three times larger than its value at 16.0 mm Al HVL. The strong decrease at smaller HVL is partly due to the attentuation of the radiation in the added aluminum layer. Curve a in figure 12 shows the sensitivity obtained by relating the measured photocurrent to the radiation incident on the silicon surface after having passed the aluminum cover layer. The attenuation of the radiation and change of its quality (expressed by the HVL) due to the absorption in the aluminum layer, were obtained from experimentally measured attenuation curves of aluminum, so far as they were available for the types of radiation investigated. The maximum of the attentuation-corrected sensivity is shifted to a HVL of 3.5 mm Al and is approximately 9 percent higher than the maximum sensitivity measured with the aluminum cover.

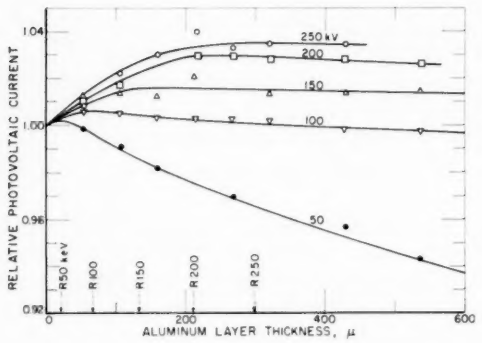


FIGURE 10. *Relative change of photovoltaic output current with increasing thickness of aluminum layer laid on silicon surface as measured with heavily filtered x rays obtained at operating voltages as shown.*

Indicated values of maximum ranges $R$ of electrons in aluminum corresponding to maximum photon energies of radiations investigated agree with layer thicknesses at maximum current values.

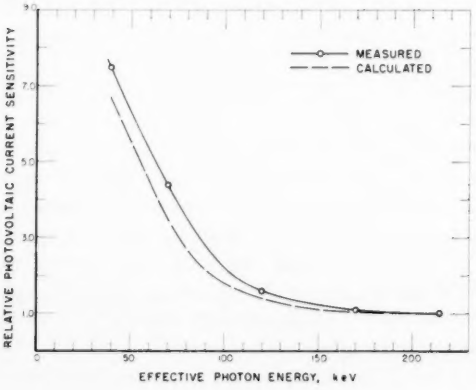


FIGURE 11. *Energy dependence of short-circuit current per R/min and cm² irradiated silicon surface given in relative values as measured with heavily filtered x rays (see table 1) and as calculated for monoenergetic radiations, assuming* $L_n = 420\ \mu$.

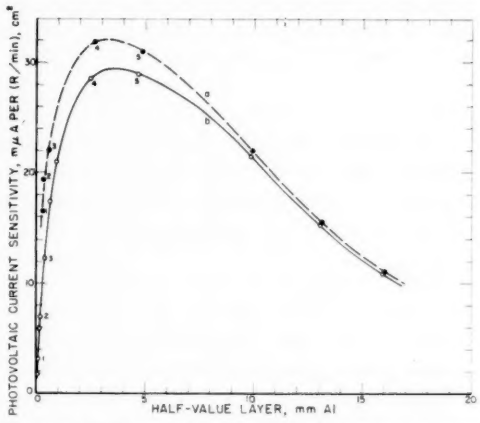


FIGURE 12. *Energy dependence of short-circuit current per R/min and cm² irradiated silicon surface measured with moderately and lightly filtered x rays (see table 1):*

○, as measured with the silicon surface covered with a 325-μ-thick aluminum layer; ●, corrected for attenuation and change of quality of radiation in the aluminum surface layer. Numbers shown near points indicate corresponding measured and corrected values.

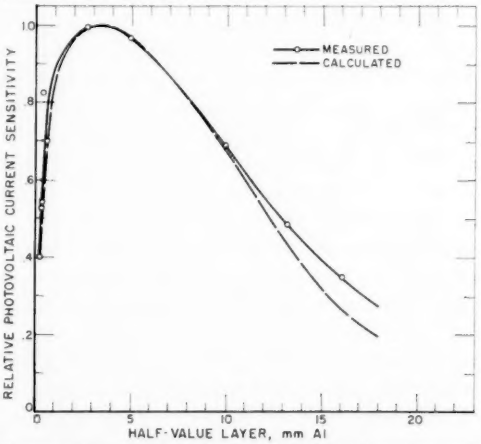


FIGURE 13. *Energy dependence of short-circuit current per R/min and cm² irradiated silicon surface given in relative values as measured with moderately and lightly filtered x rays (see table 1) and as calculated for monoenergetic radiations, assuming* $L_n = 420\ \mu$.

Measured values shown were corrected for attenuation in the aluminum surface layer.

A good qualitative agreement is obtained when comparing sensitivities measured with moderately and lightly filtered x rays and values calculated for monoenergetic radiations. Measured sensitivities corrected for attenuation in the aluminum surface layer, and values calculated assuming a constant $L_n$=420 $\mu$ are shown in figure 13. These sensitivities are given as relative values, normalized to unity at their peak values which are $3.2\times10^{-8}$ A and $3.0\times10^{-8}$ A per R/min and cm$^2$ irradiated surface for the measured (fig. 12) and calculated sensitivity (fig. 4) respectively. The greater discrepancies between measured and calculated sensitivities at larger HVL are apparently due to the low energy components of the broad spectrum of radiations obtained with moderate and light filtration.

Taking into account that several simplifying assumptions were made in the derivation of eqs (2) and (2a), the energy dependence of the short-circuit current calculated for monoenergetic x rays, and the energy dependence measured with nonmonochromatic radiations may be considered to be in satisfactory qualitative agreement.

## 6. Conclusions and Summary

A relation has been derived for the photocurrent produced by x rays in silicon radiation detector cells of the *p-n* junction type, giving its dependence on exposure rate, quality of radiation, and electrical and geometrical parameters of the silicon crystal. This relation should be useful for designing a dosimeter using a silicon cell of predetermined performance characteristic.

Silicon radiations detector cells of the diffused *p-n* junction type show a quick and stable response to x rays like silicon solar cells, but have a larger sensitivity. The short-circuit current $I_s$ per cm$^2$ irradiated cell surface, and the open-circuit voltage $V_{oc}$ extrapolated for a fully irradiated surface produced by heavily filtered 100-kV x rays at an exposure rate of 1 R/min were measured at a cell temperature of 22 °C as follows:

| | $I_s$ | $V_{oc}$ |
|---|---|---|
| Silicon solar cell: | $2.96 \times 10^{-9}$ A/cm$^2$, | $4.12 \times 10^{-5}$ V |
| Silicon radiation detector cell: (covered with a 325-$\mu$-thick aluminum layer) | $1.92 \times 10^{-8}$ A/cm$^2$, | $2.91 \times 10^{-2}$ V |

The short-circuit current $I_s$ is proportional to the irradiated surface area and exposure rate. However, the open-circuit voltage $V_{oc}$, which is independent of the cell area in the case of a fully irradiated surface, shows a nonlinear dependence on exposure rates in radiation detector cells, even at rather low values of the order of a few R/min. According to eqs (14) and (15), the value of $V_{oc}$ may be approximated by a linear function of $I_g$, if $I_g/I_o << 1$. The saturation current $I_o$ in radiation detector cells is much smaller than in solar cells. Thus, due to the larger value of the ratio $I_g/I_o$, a nonlinear dependence of $V_{oc}$ will become apparent in radiation detector cells at much smaller exposure rates than in solar cells. For this reason, and because of the large temperature dependence of $V_{oc}$, measurements of the exposure rates should be based rather on the measurement of the photocurrent $I$ obtained with a suitable load resistance than on the measurement of $V_{oc}$, except in the case of very small exposure rates.

The measurement of the photovoltaic current can be carried out with high precision, especially when using d-c amplification. The standard deviation of 10 measurements, each being the average of a set of five readings, carried out with heavily filtered 100-kV x rays at an exposure rate of 1 R/min on different days, and at temperatures varying between 20 and 23 °C, was 0.96 percent. The standard deviations for each set of readings made at constant temperature were between 0.1 and 0.3 percent.

The larger current sensitivity of radiation detector cells is apparently due to the larger diffusion length of minority carriers in the high-resistivity base layers of such cells. The high values of $V_{oc}$ observed in radiation detector cells, being several hundred times larger than in solar cells, can be explained by the increased photocurrent and their much larger zero voltage

leakage resistance. This large leakage resistance makes it also possible to use larger load resistances than with solar cells, thereby producing larger photovoltages, without producing a great change in the temperature dependence of the photocurrent. This is especially important for the measurement of small photosignals requiring sensitive instruments of high impedance.

Proportionality between photocurrent and exposure rate was obtained with radiation detector cells up to the highest level investigated of approximately 5000 R/min. The lower limit of the range of measurement of exposure rates was not established, but may be assumed to be dependent on the inherent noise of the photocurrent or photovoltage, and of the noise level of instrumentation used. Under conditions for which temperature dependence of the photocurrent is of less importance, large load resistances could be used, thereby obtaining photovoltages approaching open-circuit voltage values. At an exposure dose of 1 R/min, the open-circuit voltage is, as shown above, of the order of several millivolts. With a noise level of the photosignal of a few microvolts, it should be possible to measure exposure rates of 1 R/hr with sufficient accuracy.

The energy dependence of the short-circuit current measured over a wide range of photon energies, is in good qualitative agreement with calculated values. In particular, the energy dependence measured with heavily filtered x rays of effective photon energies between 40 and 215 keV is similar to that measured on silicon solar cells in this energy range [1]. The photocurrent reaches a maximum value for x rays of low HVL, approximately at 3.5 mm Al for the cells investigated. Around this maximum, the energy dependence is rather small. The value of the photocurrent spreads by only about 10 percent when the HVL of the radiation is changed from 2 mm Al to 7 mm Al. It has been shown by theoretical considerations, that the shape of the energy dependence curve can be changed by changing electrical and geometrical cell parameters determining the photovoltaic current sensitivity of the cell.

It may be concluded from this investigation that the use of silicon radiation detector cells of the *p-n* junction type for x-ray exposure rate measurements is preferable to that of silicon solar cells when operated as photovoltaic cells. A further improvement in sensitivity and performance characteristic of such cells could be achieved by designing silicon cells specially suited for x-ray measurement. The width of the *n*-type surface layer in such cells should be increased, thereby increasing sensitivity, and shape and encapsulation should be of such design that the energy dependence should be reduced, and directional dependence and radiation scattering inside the cell be kept at a minimum.

## 7. Appendix

The total nonequilibrium current passing through the *p-n* junction under the photovoltaic mode of operation consists, as indicated in figure 14, of: (a) The drift current $(I_g)_{Dr}$ due to

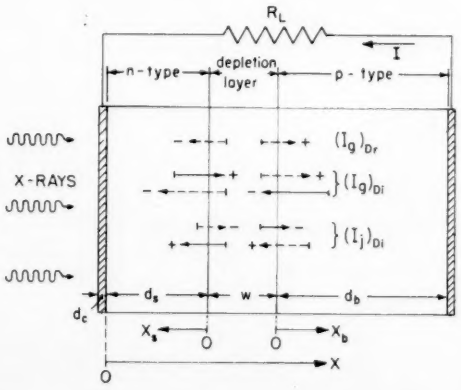


FIGURE 14. *Drift and diffusion currents of electrons and holes in a* p-n *junction cell when operated as a photovoltaic cell.*

Currents of carriers entering or leaving the depletion layer as minority carriers are shown in solid lines.

the electron-hole pairs produced by the radiation in the depletion region and separated by the electric junction field. (b) The diffusion current $(I_g)_{Di}$ of minority charge carriers produced by the radiation in the $n$-type and $p$-type layers of the silicon wafer reaching the depletion region by diffusion. Both $(I_g)_{Dr}$ and $(I_g)_{Di}$ are flowing in the reverse current direction of the cell, forming together the generated photocurrent $I_g$. (c) The diffusion current $(I_j)_{Di}$ in the forward current direction due to the photovoltage $V$ produced by irradiation if the load resistance $R_L>0$.

The photovoltaic output current $I$ is obtained by adding the different currents passing through a certain section of the circuit which is conveniently chosen at one of the junction edges. If it is assumed that thermal generation and recombination of carriers inside the depletion region can be neglected, then all carriers entering the junction on one side will leave it on the other side without change in carrier density. Electron and hole currents at both junction edges will be the same, making it possible to sum up current components calculated at different sides of the junction.

Calculating the drift current $(I_g)_{Dr}$ and the net diffusion current

$$I_{Di}=(I_g)_{Di}-(I_j)_{Di}$$

separately, one obtains the photovoltaic output current

$$I=(I_g)_{Dr}+I_{Di}. \tag{A.1}$$

In the following calculation the radiation is assumed to be monoenergetic and incident on the $n$-type surface layer of the cell in the positive $x$-direction perpendicular to the junction (fig. 14).

(a) *Drift current density.* The generation rate of charge carriers produced by the radiation at a distance $x$ inside the silicon wafer is

$$g(x)=g_s \exp(-\mu x) \tag{A.2}$$

if $g_s$ is the carrier generation rate at the silicon surface which is the number of electron-hole pairs produced per cubic centimeter per second in a thin layer of thickness $dx$ at the irradiated silicon surface.

Assuming total charge collection of charge carriers produced by the radiation inside the junction region, one obtains

$$(J_g)_{Dr}=q\int_{x=d_s}^{x=(d_s+w)} g(x)dx=[(qg_s/\mu)\exp(-\mu d_s)][1-\exp(-\mu w)] \tag{A.3}$$

The drift current is flowing in the positive $x$-direction, which is, as assumed, in the reverse current direction of the cell.

(b) *Diffusion current density.* Assuming that there is no charge carrier recombination in the junction region, the total diffusion current is calculated as the sum of diffusion currents of holes and electrons entering or leaving the junction region as minority carriers.

$$J_{Di}=J(p)_{Di}+J(n)_{Di} \tag{A.4}$$

or

$$J_{Di}=-qD_p\left(\frac{dp}{dx}\right)_{x=ds}+qD_n\left(\frac{dn}{dx}\right)_{x=(d_s+w)}. \tag{A.5}$$

Introducing new variables (fig. 14)

$$x_s=d_s-x \text{ and } x_b=x-(d_s+w), \tag{A.6}$$

one obtains

$$J_{Di}=qD_p\left(\frac{dp}{dx_s}\right)_{x_s=0}+qD_n\left(\frac{dn}{dx_b}\right)_{x_b=0}. \tag{A.6a}$$

The values of $\left(\frac{dp}{dx_s}\right)$ and $\left(\frac{dn}{dx_b}\right)$ are obtained by solving the continuity equations for electrons and holes under steady-state conditions.

$n$-region:

$$D_p \frac{d^2p}{dx_s^2} - \frac{p-p_n}{\tau_p} + g(x_s) = 0 \tag{A.7}$$

$p$-region:

$$D_n \frac{d^2n}{dx_b^2} - \frac{n-n_p}{\tau_n} + g(x_b) = 0 \tag{A.7a}$$

where

$$g(x_s) = g(x_s)_o \exp(\mu x_s) \tag{A.8}$$

$$g(x_b) = g(x_b)_o \exp(-\mu x_b) \tag{A.8a}$$

if $g(x_s)_o$ is $g(x_s)$ at $x_s = 0$, and $g(x_b)_o$ is $g(x_b)$ at $x_b = 0$.

The following boundary conditions were used for solving the continuity eqs (A.7 and A.7a), assuming surface carrier-recombination on the surface and base contact of the silicon wafer:

$n$-side:

$$x_s = 0;\ p = p_n \exp(qV/kT) \tag{A.9}$$
$$x_s = d_s;\ \frac{dp}{dx_s} = -\frac{s_p}{D_p}(p-p_n).$$

$p$-side:

$$x_b = 0;\ n = n_p \exp(qV/kT) \tag{A.10}$$
$$x_b = d_b;\ \frac{dn}{dx_b} = -\frac{s_n}{D_n}(n-n_p).$$

Using the relations

$$L_n = \sqrt{D_n \tau_n};\ L_p = \sqrt{D_p \tau_p} \tag{A.11}$$

one obtains as a result of the calculation for the diffusion currents:

$$J(p)_{Di} = g(x_s)_o \frac{qL_p}{\mu^2 L_p^2 - 1} a_p - \frac{qp_n D_p}{L_p} b_p [\exp(qV/kT) - 1] \tag{A.12}$$

$$J(n)_{Di} = g(x_b)_o \frac{qL_n}{\mu^2 L_n^2 - 1} a_n - \frac{qn_p D_n}{L_n} b_n [\exp(qV/kT) - 1] \tag{A.12a}$$

The factors $a_p$, $a_n$, $b_p$, and $b_n$ are given by the following equations where $S_p = (s_p L_p)/D_p$, and $S_n = (s_n L_n)/D_n$:

$$a_p = \frac{(\mu L_p + S_p)\exp(\mu d_s) - \sinh(d_s/L_p) - S_p \cosh(d_s/L_p)}{\cosh(d_s/L_p) + S_p \sinh(d_s/L_p)} - \mu L_p$$

$$a_n = \mu L_n - \frac{(\mu L_n - S_n)\exp(-\mu d_b) + \sinh(d_b/L_n) + S_n \cosh(d_b/L_n)}{\cosh(d_b/L_n) + S_n \sinh(d_b/L_n)} \tag{A.13}$$

$$b_p = \frac{\sinh(d_s/L_p) + S_p \cosh(d_s/L_p)}{\cosh(d_s/L_p) + S_p \sinh(d_s/L_p)}$$

$$b_n = \frac{\sinh(d_b/L_n) + S_n \cosh(d_b/L_n)}{\cosh(d_b/L_n) + S_n \sinh(d_b/L_n)}.$$

Using eq (A.2) one can substitute in eqs (A.12) and (A.12a):

$$g(x_s)_o = g_s \exp(-\mu d_s) \tag{A.14}$$

$$g(x_b)_o = g_s \exp[-\mu(d_s+w)]. \tag{A.14a}$$

For x rays of the intensity $I_R$

$$g_s = \frac{I_R \mu_{en}}{\epsilon} \tag{A.15}$$

or assuming the energy required to produce an ion pair in air as $W=33.7$ eV [16] one obtains

$$g_s = \frac{86.9\mu_{en}}{\epsilon(\mu_{en}/\rho)_{air}} (\Delta X/\Delta t) \tag{A.16}$$

if $\epsilon$ is given in erg and $\Delta X/\Delta t$ in R/sec.

The total output current is obtained as the sum of the drift and diffusion currents as given by eqs (A.3) and (A.12). Summing up the radiation dependent parts separately, the photocurrent $I$ is obtained as

$$I = J_g A_R - J_j A_c = I_g - I_j \tag{A.17}$$

if $A_R$ is the irradiated and $A_c$ the total cell surface area and

$$J_g = (86.9q/\epsilon)(\Delta X/\Delta t)\frac{(\mu_{en}/\mu)}{(\mu_{en}/\rho)_{air}} \exp(-\mu d_s) \times \left\{ [1-\exp(-\mu w)] + \frac{\mu L_p}{\mu^2 L_p^2 - 1} a_p + \frac{\mu L_n \exp(-\mu w)}{\mu^2 L_n^2 - 1} a_n \right\} \tag{A.18}$$

$$J_j = q[\exp(qV/kT) - 1]\left(\frac{p_n D_p}{L_p} b_p + \frac{n_p D_n}{L_n} b_n\right). \tag{A.19}$$

The terms in the braces of eq (A.18) indicate the separate current contributions by carriers produced in the junction region, and in the surface and base layer of the silicon wafer respectively.

Equations (A.13) for $a_p$, $a_n$, $b_p$, and $b_n$ can be simplified by using approximations applicable under certain conditions:

(1) Surface layer: $d_s << L_p$; $\mu d_s << 1$; $\sinh(d_s/L_p) \sim \frac{d_s}{L_p}$; $\cosh\frac{d_s}{L_p} \sim 1$

$$a_p = \frac{d_s}{L_p}\left[\frac{\mu^2 L_p^2 - 1}{1 + (s_p d_s/D_p)}\right] \tag{A.20}$$

$$b_p = \frac{(d_s/L_p) + S_p}{1 + S_p(d_s/L_p)}.$$

(2) Base layer: $d_b >> L_n$; $\sinh(d_b/L_n) \sim \cosh(d_b/L_n)$

$$a_n = (\mu L_n - 1)\left[1 - \frac{(\mu L_n - S_n)\exp(-\mu d_b)}{(\mu L_n - 1)(1+S_n)\cosh(d_b/L_n)}\right] \tag{A.21}$$

$$b_n = 1.$$

For small values of $S_n$ or $S_n = 0$, a condition applicable for an ohmic contact, one can assume

$$a_n = \mu L_n - 1. \tag{A.21a}$$

## 8. References


[1] K. Scharf, Bull. Am. Phys. Soc. (Series 2) **3,** No. 4, 261 (1958); J. Res. NBS **64A,** 297 (1960).
[2] J. W. Moody, G. L. Kendall, and R. K. Willardson, Nucleonics **16,** No. 10, 101 (1958).
[3] J. Calkins, Nucleonics **20,** No. 1, 70 (1962).
[4] W. Rosenzweig, Rev. Sci. Instr. **33,** 379 (1962).
[5] R. L. Cummerow, Phys. Rev. **95,** 16 (1954).
[6] R. Wiesner, Halbleiterprobleme (ed. W. Schottky) **3,** 59 (1956).
[7] G. L. Bir and G. E. Pikus, Soviet Phys.-Tech. Phys. **2,** 419 (1957).
[8] M. Wolf, Proc. IRE **48,** 1246 (1960).
[9] J. J. Loferski and J. J. Wysocki, RCA Review **22,** 38 (1961).
[10] W. W. Gärtner, Phys. Rev. **116,** 84 (1959).
[11] A. J. Tuzzolino, E. L. Hubbard, M. A. Perkins, and C.Y. Fan, J. Appl. Phys. **33,** 148 (1962).
[12] W. Shockley, Solid State Electr. **2,** 35 (1961).
[13] W. Shockley, Bell Syst. Tech. J. **28,** 435 (1949).
[14] G. White Grodstein, NBS Circ. 583 (1957).
[15] A. T. Nelms, NBS Circ. 542 (1953).
[16] Physical Aspects of Irradiation, Recommendations of the International Commission on Radiological Units and Measurements, NBS Handb. 85 (1964).
[17] C. Sah, R. N. Noyce, and W. Shockley, Proc. IRE **45,** 1228 (1957).
[18] M. B. Prince and M. Wolf, J. Brit. Radio Engrs. **18,** 583 (1958).
[19] F. J. Morin and J. P. Maita, Phys. Rev. **96,** 28 (1954).
[20] M. Lax, Phys. Rev. **119,** 1502 (1960).
[21] H. Pfister, Z. angew. Phys. **15,** 407 (1963).


(Paper 68A6–318)

JOURNAL OF RESEARCH of the National Bureau of Standards—A. Physics and Chemistry
Vol. 68A, No. 6, November–December 1964

# Intercomparison of High-Energy X-Ray Intensity Measurements

John S. Pruitt and Steve R. Domen

(August 14, 1964)

This paper describes experimental comparison of the sensitivity of the NBS P2–4 ionization chamber and a replica of Wilson's Quantameter. The sensitivity ratios are used to compare calorimetric measurements of total x-ray beam energy made at the NBS and in the USSR between 20 and 90 MeV. The agreement is within the combined errors, but the source of an apparent 2 percent systematic difference has not been found.

## 1. Introduction

Several ionization chambers of various design have been calibrated in recent years to determine the total energy transported by a high-energy x-ray beam [1].[1] In general, these calibrations depend on $k_o$, the maximum photon energy, and although there have been some direct intercomparisons of different chambers when they have been calibrated in the same energy range, the task of intercomparisons of the measurements of different laboratories is by no means complete. The purpose of this paper is to report on comparison measurements made at the National Bureau of Standards between our standard chamber, P2–4 [2], and a Quantameter [3], a replica of the instrument which has been calorimetrically calibrated between 15 and 90 MeV by Komar, Kruglov, and Lopatin of the Academy of Sciences in the U.S.S.R. [4]. Despite the fact that the comparison was not direct, in the sense that a replica Quantameter was used, the profits have been severalfold. The agreement is a partial verification of the measurements of both laboratories, as well as of the energy dependence of these two chambers. Furthermore, the measurements of Komar, Kruglov, and Lopatin, when transferred to P2–4, have considerably reduced the uncertainty in its calibration.

## 2. The Ionization Chambers

Figure 1 is a schematic cross section of the Quantameter, an instrument which sums the ionization produced in twelve air cavities between 1-cm-thick copper plates. It is not large enough to absorb all of the secondary electrons, but compensates for the few percent leaking out the sides and back with peripheral air cavities and an oversize cavity at the rear. The internal cavities are alternately 2 mm and 1 mm thick, so that the measured ionization is proportional to a Simpson's rule approximate integration of the total ionization produced in a semi-infinite copper medium. The advantage of this design is that the chamber calibration (joules incident per coulomb collected) should be almost independent of $k_o$, since the ratio of cavity ionization to locally absorbed energy is known to vary very slowly with photon energy. This is apparently quite true for $k_o$ greater than about 100 MeV, but the data presented below indicates that the Simpson's rule approximation breaks down at lower $k_o$.

Figure 2 is a schematic cross section of P2–4, a chamber which measures ionization produced at a depth of 27 g/cm$^2$ in a medium of 2024 Dural (nominally 93.4% Al, 4.5% Cu, 1.5% Mg, and 0.6% Mn). Its design is based on the empirical fact that transition curves (cavity ionization as a function of depth) in water for $k_o$ between 10 and 40 MeV exhibit a common crossover point when normalized to include unit area [5], which implies that with proper selection of a front wall thickness it is possible to construct a chamber whose calibration is almost independent of $k_o$ over this energy range. Evidence presented below shows this to be true, although the calibration changes more rapidly with $k_o$ above about 100 MeV.

## 3. Experimental Arrangement and Method

Figure 3 is a schematic diagram of the apparatus used in the comparison measurements. X rays from the NBS 180 MeV synchrotron successively passed through the donut wall (4.1 g/cm$^2$ of Pyrex), a 0.3-in.-diam. beam forming aperture in a 12-in. lead block, a 4-in. lead baffle designed to stop stray secondary electrons and x rays without intercepting the main x-ray beam, an ionization chamber monitor (3.4 g/cm$^2$ of Al), and a second nonintercepting 4-in. lead baffle, before bombarding either P2–4 or the Quantameter. These two chambers were alternately

[1] Figures in brackets indicate the literature references at the end of this paper.

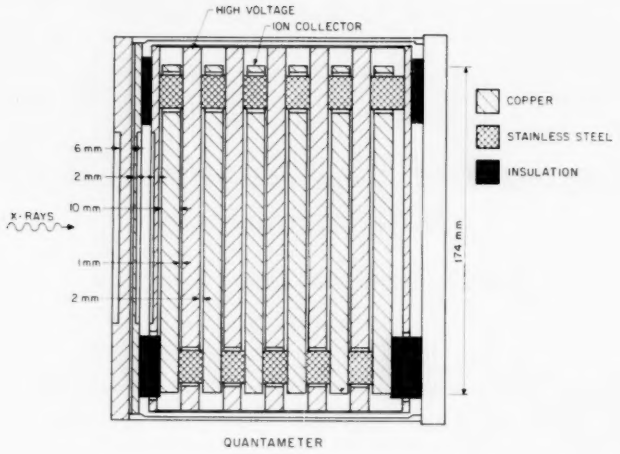


FIGURE 1. *Ionization collection sector of a copper Quantameter.*

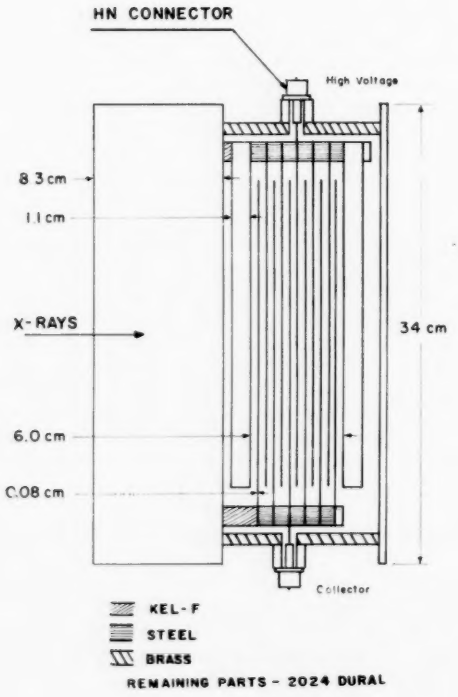


FIGURE 2. *Ionization collection sector of a Dural P2 chamber.*

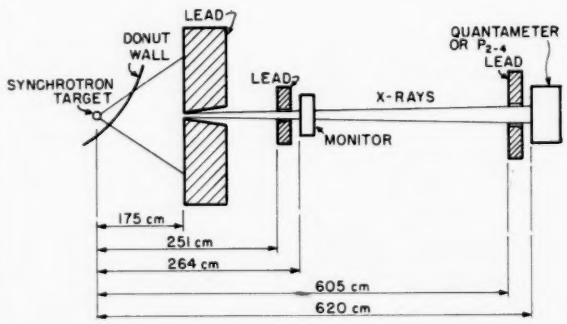


FIGURE 3. *Experimental arrangement for chamber intercomparisons.*

placed in the same position, and the ratio of their sensitivities per unit monitor response was determined at a variety of $k_o$.

The quantameter was used both with the recommended filling of 760 mm of argon plus 40 mm of carbon dioxide [3], and filled with air at atmospheric pressure. P2–4 was always open to the atmosphere. The sensitivities of the air-filled chambers were corrected to 20 °C, 760 mm.

Ionization measurements were made for both the monitor and the comparison chamber with Townsend balance circuits, using polystyrene capacitors to collect the charge, potentiometers to supply and measure the bucking voltages, and vibrating reed electrometers as null detectors.

## 4. Results and Corrections

The measured ratios of P2–4 sensitivity to Quantameter sensitivity are listed as a function of $k_0$ in table 1. The replica Quantameter had been constructed according to Wilson's original design, but when it was assembled, the air-cavity thicknesses were found to differ from the design dimensions by 0.03 to 0.08 mm with an average of 0.055 mm. If all of the cavities had been too thick (or too thin) by 0.055 mm, the measured sensitivity would have been in error by about 3.5 percent, but the Quantameter design is such that dimensional errors tend to cancel, and cavities which are too thick alternate with cavities which are too thin.

TABLE 1. *Ratio of P2–4 sensitivity (20 °C, 760 mm) to Quantameter sensitivity with* $A+CO_2$ *filling (20 °C, 800 mm) and with air filling (20 °C, 760 mm)*

| $k_0$ | Filling | |
|---|---|---|
| | $A+CO_2$ | Air |
| *MeV* | | |
| 15 | ------- | 3.120 |
| 20 | 1.951 | 3.106 |
| 25 | 1.949 | 3.093 |
| 30 | 1.940 | 3.079 |
| 35 | 1.934 | 3.081 |
| 40 | 1.936 | 3.082 |
| 45 | 1.940 | 3.092 |
| 50 | 1.937 | 3.098 |
| 55 | ------- | 3.110 |
| 60 | 1.951 | 3.114 |
| 70 | 1.957 | 3.130 |
| 90 | 1.970 | 3.150 |
| 110 | 1.971 | 3.150 |
| 130 | 1.955 | 3.128 |
| 150 | 1.936 | 3.101 |
| 170 | 1.908 | 3.063 |

A correction for these deviations was calculated with the help of transition curves for copper obtained from Marshall, Rosenfeld, and Wright [6] at $k_0$= 46 MeV, and from Kruglov [7] at $k_0$=85 MeV. These were used to determine the relative contribution of each cavity to the total ionization, and it was found that the replica Quantameter sensitivity was higher than the design value, but only by 0.1 percent at each energy. Transition curves for lead [8] and for 2024 Dural [9], which cover a wider energy range, were used to show that the sensitivity correction caused by errors in the air-cavity thicknesses would have varied from 0.06 percent at 25 MeV to 0.17 percent at 170 MeV if the plates had been lead (of the same g/cm$^2$ thickness), and from 0.03 percent at 25 MeV to 0.05 percent at 170 MeV if they had been Dural. The correction for copper should be between these extremes, and was finally taken as 0 for $k_0<45$ MeV and 0.1 percent for larger $k_0$.

During the comparison measurements it was found that the ends of the bolts holding together the quantameter (not shown in fig. 1) collected enough charge from ionized air behind the chamber to raise the measured sensitivity by as much as 0.67 percent. This correction is included in the $A+CO_2$ ratios of table 1, which were obtained before this was discovered, and it was avoided in the measurements with air filling by covering these studs with rubber caps.

## 5. Quantameter Calibrations

TABLE 2. *Quantameter calibration (joules/coulomb) with* $A+CO_2$ *filling (20 °C, 800 mm) and with air filling (20 °C, 760 mm).*

| $k_0$ | Filling | | Uncertainty |
|---|---|---|---|
| | $A+CO_2$ | Air | |
| (*MeV*) | | | |
| 20 | $8.12\times10^5$ | $12.92\times10^5$ | ±2.4% |
| 26 | 8.00 | 12.70 | 2.7 |
| 31 | 7.99 | 12.69 | 1.8 |
| 36 | 7.95 | 12.66 | 1.5 |
| 41 | 7.92 | 12.61 | 2.1 |
| 45 | 7.80 | 12.43 | 1.8 |
| 50 | 7.74 | 12.36 | 1.8 |
| 60 | 7.69 | 12.27 | 1.8 |
| 70 | 7.56 | 12.08 | 2.7 |
| 90 | 7.49 | 11.97 | 2.7 |
| 110 | 7.58 | 12.10 | 2.7 |
| 130 | 7.46 | 11.92 | 1.5 |
| 150 | 7.40 | 11.85 | 1.8 |
| 170 | 7.39 | 11.85 | 1.8 |

Table 2 is a list of the Quantameter calibrations obtained by multiplying the corrected ratios of table 1 by the calorimetric calibrations of P2–4 measured earlier in this laboratory [2, 8], with uncertainties equal to those of the P2–4 calibrations plus 0.3 percent for these ratios and corrections. The calibrations are plotted as a function of $k_0$ in figure 4, which shows that in general, they agree with those of Komar et al. to within the stated errors. There is also agreement that the calibration increases with decreasing $k_0$ at these energies. The calibrations obtained at higher energies by comparing the $A+CO_2$ filled Quantameter with a thick-walled Cornell ionization chamber [1] indicate that the energy dependence does indeed disappear with increasing $k_0$.

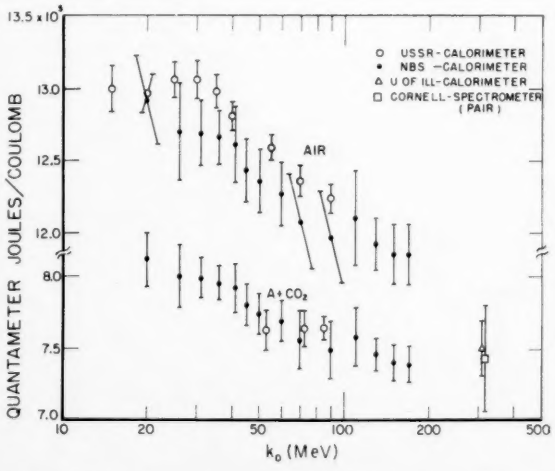


FIGURE 4. *Quantameter calibration in joules/coulomb.*

## 6. P2–4 Calibrations

TABLE 3. *P2–4 calibration (joules/coulomb) at 20 °C. 760 mm*

| $k_0$ | joules/coulomb | Uncertainty |
|---|---|---|
| (*MeV*) | | |
| 15 | $4.17\times10^5$ | ±1.5% |
| 20 | 4.18 | 1.3 |
| 25 | 4.22 | 1.2 |
| 30 | 4.24 | 1.3 |
| 35 | 4.21 | 1.2 |
| 40 | 4.16 | 1.1 |
| 53 | 3.93 | 2.1 |
| 55 | 4.05 | 1.0 |
| 70 | 3.95 | 1.2 |
| 72 | 3.90 | 1.9 |
| 85 | 3.88 | 1.3 |
| 90 | 3.89 | 1.1 |

Table 3 is a listing of the P2–4 calibrations obtained by dividing the corrected ratios of table 1 into the Quantameter calibrations of Komar, et al [4]. They are plotted in figure 5 along with all other known P2–4 calibrations [1]. There are enough of these to warrant some statistical manipulation, and they have consequently been fitted to a curve of the type:

$$\text{P2–4 calibration}=\sum_{i=0}^{4} a_i\chi^i, \text{ joules/coulomb}$$

where $\chi=9.80\ \log_{10}\ (k_0(\text{MeV})/43.2)$

with uncertainties expressed as:

$$\Delta(\%)=\sum_{i=0}^{4}\delta_i\chi^i.$$

The $a_i$ and $\delta_i$ are listed in table 4. The $a_i$ were obtained by least squares, with each calibration weighted with a factor equal to the inverse square of its uncertainty. The $\delta_i$ were calculated using Gauss' law for combining errors. The two curves of figure 5 represent the extreme predictions of this formula. There is no guarantee that the true P2–4 calibration lies between these curves, since they were obtained statistically, using weights which include both statistical and systematic uncertainties, but the good agreement between the calibrations obtained in several laboratories by several means supports this view.

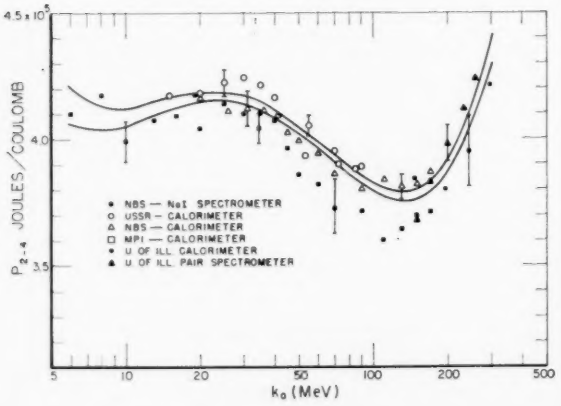


FIGURE 5. *P2–4 calibration in joules/coulomb.*

## 7. Comments

The NBS Quantameter calibrations of figure 4 agree with those of Komar et al. to within the combined uncertainties, but there is indication of a systematic discrepancy of about 2 percent between the measurements of these two laboratories. In each case, the original calibrations were made with calorimeters of about the same design, and an obvious place to look for systematic differences is in the corrections made to the calorimeter data for leakage of secondary photons and electrons. In the NBS case, this correction was based on scintillation measurements of backscattering plus photographic determinations of energy leaking from the other surfaces [8]. The Soviet correction is presumably based on ionization chamber measurements described earlier by Kruglov and Lopatin [10], which are presented in a form well suited for comparison. Their measurements indicate that for a 9-cm-diam 7.5 cm lead cylinder, such as we used, they would expect a leakage flux of 5.3 percent of the incident energy at $k_0=50$ MeV, and 5.1 percent at 85 MeV, while our own measurements indicate 5.4 percent at each of these energies. This difference is both too small and in the wrong direction to explain the 2 percent discrepancy.

TABLE 4. *Coefficients in "*P2−4 joules/coulomb$=\sum_{i=0}^{4}a_i\chi^i$*," and in "*$\Delta(\%)=\sum_{i=0}^{4}\delta_i\chi^i$*," where* $\chi=9.80\ \log_{10}\ (k_0(MeV)/43.2)$

| $i$ | $a_i$ | $\delta_i$ |
|---|---|---|
| 0 | $4.077\times10^5$ | 0.39 |
| 1 | −.0650 | −.017 |
| 2 | −.00971 | .0001 |
| 3 | .001187 | −.00009 |
| 4 | .0001809 | .000243 |

The only other plausible source of a 2 percent systematic difference is the Quantameter dimensions, which should be controlled very carefully because of the thin air-cavity dimensions. A direct comparison of the two Quantameters would certainly help to clear up the reasons for this difference.

After these intercomparisons had been completed, it was found that Komar et al., have calibrated a replica P2 chamber [11] and have also found a difference of about 2 percent between the NBS and Soviet calibrations.

The authors thank the operators of the NBS synchrotron for their help with these intercomparisons.

## 8. References

[1] Methods of Experimental Physics, Vol. V, Pt. B, Sec. 2.8.2.4., ed. L. Marton (Academic Press, New York, N.Y., 1963).
[2] John S. Pruitt and Steve R. Domen, NBS Mono. 48 (1962).
[3] R. R. Wilson, Nuclear Instr. **1,** 101 (1957).
[4] A. P. Komar, S. P. Kruglov, and I. V. Lopatin, Dok. Akad. Nauk SSSR **145,** 309 (1962) [Soviet Phys.-Dok. **7,** 653 (1963)]; A. P. Komar and S. P. Kruglov, Zh. Tekh. Fiz. **30,** 1369 (1960) [Soviet Phys.–Tech. Phys. **5,** 1299 (1961)].
[5] Bernard Zendle, private communication.
[6] L. Marshall, A. H. Rosenfeld, and S. C. Wright, Phys. Rev. **83,** 305 (1951).
[7] S. P. Kruglov, Zh. Tekh. Fiz. **31,** 1451 (1961) [Soviet Phys.–Tech. Phys. **6,** 1060 (1962)].
[8] J. S. Pruitt and S. R. Domen, J. Res. NBS **66A** (Phys. and Chem.), 371 (1962).
[9] The data from which figure 16 in reference [2] was taken.
[10] S. P. Kruglov and I. V. Lopatin, Zh. Tekh. Fiz. **32,** 1399 (1962) [Soviet Phys.–Technical Phys. **7,** 1031 (1963)].
[11] A. P. Komar, S. P. Kruglov, and I. V. Lopatin, Zh. Eksper. i Teoret. Fiz. **45,** 825 (1963).

(Paper 68A6–319)



743 261–64——11

JOURNAL OF RESEARCH of the National Bureau of Standards—A. Physics and Chemistry
Vol. 68A, No. 6, November–December 1964

# Publications of the National Bureau of Standards*

## Selected Abstracts

**Handbook of mathematical functions with formulas, graphs, and mathematical tables,** Ed. M. Abramowitz and I. A. Stegun, *NBS Applied Math. Series 55, (June 1964), $6.50.*
This publication not only combines the material found in all former reference volumes on the subject; it additionally expands the work of past authors by increasing the number of functions covered, presenting more extensive numerical tables, and giving larger collections of mathematical properties of the tabulated functions. It also provides comparatively simple methods of obtaining values of functions outside the tabulated range.
As a result of scientific advances and, especially, the increasing use of automatic computers, a greater variety of functions and a higher accuracy of tabulation are now in demand by users of mathematical functions. The *Handbook* includes rational approximation formulas for all the functions, tailored to the modern computer and tables useful for a pre-programming survey of the access to a computer; for the researcher who does not, and who must do his own computations, they are, of course, indispensable. Subjects covered are included by the following chapter headings: Mathematical Constants; Physical Constants and Conversion Factors; Elementary Analytical Methods; Elementary Transcendental Functions-Logarithmic, Exponential, Circular, and Hyperbolic Functions; Exponential Integral and Related Functions; Gamma Function and Fresnel Integrals; Legendre Functions; Bessel Functions of Integer Order; Bessel Functions of Fractional Order; Integrals of Bessel Functions; Struve Functions and Related Functions; Confluent Hypergeometric Functions; Coulomb Wave Functions; Hypergeometic Functions; Jacobian Elliptic Functions and Theta Functions; Elliptic Integrals; Weierstrass Elliptic and Related Functions; Parabolic Cylinder Functions; Mathieu Functions; Spheroidal Wave Functions; Orthogonal Polynomials; Bernoulli and Euler Polynomials, Riemann Zeta Functions; Combinatorial Analysis; Numerical Interpolation, Differentiation, and Integration; Probability Functions; Miscellaneous Functions; Scales of Notation, and Laplace Transforms.

**Infrared spectra of NF, NCl, and NBr,** D. E. Milligan and M. E. Jacox, *J. Chem. Phys.* **40,** *No. 9, 2461–2466 (May 1, 1964).*
The infrared spectra of $FN^3$, $ClN^3$, and $BrN^3$ suspended in Ar and $N^2$ matrices have been observed at 4° and at 20° K. Ultraviolet photolysis of these systems results in the appearance of absorptions assigned to the free radicals NF, NCl, and NBr. Evidence is presented for the matrix deactivation of NBr to its ground $^3\Sigma^-$ state. Slow photolytic decomposition of NCl and NBr has been observed. Possible mechanisms are discussed for the origin of a green phosphorescence identified as resulting from N atoms trapped in the matrix.

**Optical studies at high pressures,** L. S. Whatley, E. R. Lippincott, A. Van Valkenburg, and C. E. Weir, *Science* **144,** *No. 3621, 968–976 (May 22, 1964).*
The development of a miniaturized high-pressure cell which is useful to pressures of 150 kbar and fits easily into the small sample areas of commercial optical equipment has greatly facilitated optical studies at high pressures. With this cell the nature and optical characteristics of polymorphic changes in transparent solids and liquids have been investigated. A microscope spectrophotometer with which absorption spectra of small areas of the compressed sample can be obtained has been devised. A camera attachment provides a convenient means of recording the visual observations. X-ray diffraction powder patterns have been recorded for low- and high-pressure forms of several substances, and new high-pressure forms have been discovered in some cases. The wide range of problems in which the cell is applicable, its miniature size, and the relative simplicity of the experimental techniques involved in its use make the development of the diamond cell a marked advance in high-pressure technology.

**Refractive properties of barium fluoride,** I. H. Malitson, *J. Opt. Soc. Am.* **54,** *No. 5, 628–632 (May 1964).*
Refractive properties of barium fluoride are discussed. The refractive index, $n$, was determined at 25 °C for 46 measured wavelengths from 0.2652$\mu$ in the ultraviolet to 10.346 in the infrared. The dispersion equation

$$n^2-1=\frac{0.643356\lambda^2}{\lambda^2-(0.057789)^2}+\frac{0.506762\lambda^2}{\lambda^2-(0.10968)^2}+\frac{3.8261\lambda^2}{\lambda^2-(46.3864)^2},$$

where $\lambda$ is expressed in microns was found to fit the measured values with an average absolute residual of $1.91\times10^{-5}$. A tentative average thermal coefficient of index $dn/dt$ for the measured spectral range is $-12\times10^{-6}$/°C. Dispersive quantities which indicate the expected relative dispersion, chromatic aberration, and the effect of index on resolution are graphically presented. A review of transmittance data from the literature is also presented.

**Statistical model for the beta zirconium hydrides,** T. B. Douglas, *J. Chem. Phys.* **40,** *No. 8, 2248–2257 (Apr. 15, 1964).*
After consideration of the known structure of $ZrH_2$, it is postulated that the non-stoichiometric "beta" (bcc) Zr–H phases have four symmetrical hydrogen sites on each face of the unit cell, with simultaneous occupancy restricted to pairs not closer than twice the van der Waals radius of hydrogen. The configurational problem is solved for all concentrations by a simple process of building up the lattice, after making tests of the amount of detail required for accurate solutions in one and two dimensions. The total entropy, when decreased by the corresponding configurational entropy, corresponds to values of the hydrogen vibration frequency averaging 1440 $cm^{-1}$ and showing no consistent trend with temperature or with a four-fold change in concentration. A semi-empirical energy model is constructed on the postulate that zirconium bonded to no hydrogen is "abnormally stable," and the two energy parameters are derived from the experimental data. The agreement with the curves derived from thermodynamic data is fairly good for the partial molal entropy and energy of hydrogen, and excellent for the hydrogen equilibrium pressures.

**Optical constants of thin films from the characteristic electron energy losses,** *R. E. LaVilla and H. Mendlowitz, J. Phys.* **25,** *114–118 (Jan. Feb. 1964).*
A method for obtaining the optical constants by employing the correlation between the characteristic electron energy absorption spectrum of a substance with its optical properties is described. This method is applied to a study of the optical properties in the far ultraviolet of aluminum, a metal, and of polystyrene, an organic compound. The information that is derived by this method lends itself to a study of the optical oscillator strengths.

**Thermodynamics of solutions of deuterium chloride in heavy water from 5 to 50°,** R. Gary, R. G. Bates, and R. A. Robinson, *J. Phys. Chem.* **68,** *1186–1190 (1964).*
The standard e.m.f. of the cell $D_2$ (g. 1 atm.), DCl in $D_2O$, AgCl; Ag has been determined from 5 to 50°. At 25° the

standard e.m.f. is lower by 9.78 mv. (on the molality scale) or 4.31 mv. (on the mole fraction scale) than the standard e.m.f. of the corresponding cell with a hydrogen electrode and a solution of hydrochloric acid in ordinary water. Thermodynamic quantities have been calculated for the reaction

$$1/2\ D_2\ (g.) + HCl\ (in\ H_2O) = 1/2\ H_2(g.) + DCl\ (in\ D_2O).$$

At 25°, $\Delta G$ is 418 j. mole$^{-1}$, $\Delta H°$ is $-611$ j. mole$^{-1}$, and $\Delta S°$ is $-3.5$ j. deg.$^{-1}$ mole$^{-1}$, when all four substances are in the standard state on the mole fraction scale. The mean ionic activity coefficient and relative partial molal enthalpy of DCl at molalities from 0.01 to 0.05 in heavy water have been obtained and are compared with those for HCl in $H_2O$. The activity coefficient of DCl in $D_2O$ is slightly smaller than that of HCl in $H_2O$ at the same molality; at $m=0.05$, $t=25°$, the difference in log $\gamma\pm$ is 0.0022.

**Direct quantitative analysis of photomicrographs by a digital computer,** G. A. Moore, *Photo. Sci. Eng.* **8,** *No. 3, 152–161 (May–June 1964).*

A program on the National Bureau of Standards SEAC Computer directly accepts photomicrographs or other pictures as the information input. Commands in English format cause compilation of operational orders as required to carry out modifications or analyses of the pictures. The 28 operations now functional include lineal and area analyses of whole pictures, sorting out of individual coherent objects, and determining 15 parameters of each. Special photographic precautions are necessary to supply only truthful information to the computer. Studies of complex niobium-tin superconductors and dispersed particle structures are shown. Probable applicability to biological problems and to photographic emulsions is considered.

**Superconductivity in semiconducting $SrTiO_3$,** J. R. Schooley, W. R. Hosler, and M. L. Cohen, *Phys. Rev. Letters* **12,** *474 (1964).*

Superconducting transitions have been observed in three specimens of strontium titanate, a semiconductor. The specimens were reduced to approximately $10^{20}$ charge carriers $(cc)^{-1}$ and showed degeneracy at liquid helium temperatures. Four-lead d.c. resistance measurements showed that the transitions are complete within less than 0.1 °K at about 0.26 °K. and that $H_c$ is a few kilo-oersted. A.c. magnetic susceptibility measurements indivate that a bulk diamagnetism is present and that the first critical field is less that one oersted.

**An engineering method for calculating protection afforded by structures against fallout radiation,** C. Eisenhauer, *NBS Mono. 76 (July 2, 1964), 20 cents.*

This report is a discussion of the technical assumptions underlying the methods currently recommended by the Office of Civil Defense (OCD) for calculating protection afforded by structures against fallout radiation. It discusses methods for calculating the contributions from radioactive sources on the roof and on the ground surrounding a simple one-storied building. It shows in detail how each technical chart in the OCD Professional Manual is derived from basic data on radiation penetration developed by Dr. L. V. Spencer. Charts from the Professional Manual and relevant curves from Spencer's work are included in this report in order to make it self-contained.

**Shielding for high-energy electron accelerator installations,** *NBS Handbook 97 (July 1, 1964), 30 cents.*

This publication is intended to give a summary of the presently available data required to calculate the shielding for high-energy, high-intensity electron-accelerator installations. The report is not intended to present specific, all-inclusive recommendations since it is not felt that at the present time the "state of the art" has progressed to the point where such recommendations are feasible. This publication is aimed at outlining the present state of our knowledge about the factors governing the shielding required in the vicinity of these accelerators. The recommendations that are made have to do primarily with a procedure to be followed in establishing the required amount of shielding.

**Absolute temperatures determined from measurements of the velocity of sound in helium gas,** G. Cataland and H. H. Plumb, *Proc. Advisory Committee on Thermometry to the Intern. Bureau of Weights and Measures, 6th Session, p. 175 (Sept. 26–27, 1962).*

At 20 °K and below, the measurement of the speed of sound in helium gas appears to yield a more accurate determination of absolute temperatures than has been previously realized. In an ideal gas, the speed of sound is directly proportional to the square root of the absolute temperature; for a real gas, corrections must be made which involve virial coefficients of the gas expressed in a pressure expansion. Because these corrections increase with pressure, it is desirable that velocity measurements for absolute temperature determinations be conducted at the lowest practical pressures, where a real gas approaches the state of an ideal gas.

An acoustical interferometer has been used as a measuring instrument, and absolute temperature determinations at 2 °K and 20 °K have been investigated. The temperature, measured acoustically, at 2 °K is three millidegrees higher than the temperature associated with the $T_{58}$ helium vapor pressure scale; at 20 °K, it is within 10 millidegrees of the equilibrium hydrogen vapor pressure-temperature scale of Woolley, Brickwedde and Scott. The work is being continued to determine an absolute temperature scale below 20 °K.

**Some results and problems in calibrating the NBS photoelectric pyrometer of 1961,** R. D. Lee, *Proc. Advisory Committee Thermometry to the Intern. Bureau Weights and Measures, 6th Session, pp. 79–90 (Sept. 26–27, 1962).*

The realization of the International Practical Temperature Scale (IPTS) above 1063 °C has been accomplished in the past with a disappearing filament optical pyrometer. Photoelectric means of detecting the equality of spectral radiance along the same principles of the visual optical pyrometer have been demonstrated to be considerably more precise, and this increased precision has been accomplished with a narrower spectral bandpass.

In the past few years photoelectric pyrometers have been developed at the National Bureau of Standards (NBS) and at other national standards laboratories. Some progress has been made toward the realization of the IPTS with the NBS pyrometer. This paper reports on the preliminary results and problems observed in this work.

**Metastable levels in the continuum and the independent particle model,** F. Prats and U. Fano, *Proc. IIIrd Intern. Conf. Physics of Electronic and Atomic Collisions, London, England, pp. 600–605 (July 22–26, 1963).*

Resonances in scattering processes and the related metastable levels of atoms, molecules or ions, which decay by autoionization, predissociation or Auger effect, are generally classified by quantum numbers of an independent particle model. This model often affords only a quantitatively very poor initial approximation, and one may wonder how to define operationally meaningful concepts, such as decay rates and line shapes, so that they be independent of the initial approximation. This definition can be achieved in terms of a reaction matrix or, equivalently, in terms of the matrix of the residual interaction in an intermediate representation which is obtained from the independent-particle states by a process of partial, or "preliminary", diagonalization.

**Approximations to the pair correlation function for a hard-sphere fluid,** M. Klein, *Phys. Fluids* **7,** *No. 3, 391–401 (Mar. 1964).*

The equation of state for hard spheres as predicted by a number of approximations to the pair correlation function are compared with each other and with a reference isotherm. The reference isotherm is given by the five known virial coefficients for $\rho a^3$ 0.5, by the molecular dynamics calculations of Alder and Wainwright for $\rho a^3 > 0.7$, and by a graphical interpolation between the two for 0.5 $\rho a^3$ 0.7. The approxi-

mations considered are the chain, watermelon, convolution-hypernetted chain, and Percus-Yevick approximation. The solutions to the integral equation of the convolution-hypernetted chain approximation can be used to define a sequence of diagrammatic approximations to the pair correlation function according to the number of parallel branches included. We shall designate these as the approximations $n=1, 2, \ldots$, etc. according to the number of branches included. We have found both the chain and watermelon approximations to yield equations of state which are only slight improvements over the linear correction to the ideal gas law. The equation of state of the convolution-hypernetted chain approximation was found to be a qualitatively good first approximation to the reference isotherm in our earlier work. We have now found the $P$–$Y$ theory to be a further improvement over this for hard spheres in agreement with the results of Hoover and Poirier for hard cubes and of Broyles for several densities of the Lennard-Jones (12,6) gas. We have found the approximation $n=2$ to yield an equation of state in excellent quantitative agreement with the reference isotherm for densities up to 0.707 times the close packed density.

The sequence of approximations which starts with the chain approximation and ends with the CHNC approximation appears to be part of a uniform approach to the reference isotherm. At the same time, the representations of the known virial coefficients associated with each of these approximations do not approach the correct virial coefficients in a uniform fashion. It would thus appear that the sequence of infinite sums (i.e. over chains, etc.) forms an approximation scheme whose meaning cannot be found from an examination of the usual density series.

**Effect of pressure in the radiolysis and photolysis of methane,** P. Ausloos, R. Gorden, Jr., and S. T. Lias, *J. Chem. Phys.* **40,** *No. 7, 1854–1860 (Apr. 1, 1964).*

The photolysis and radiolysis of equimolar $CH_4$-$CD_4$ mixtures was investigated as a function of pressure. The fact that, in the presence of NO, the ethane fraction consists entirely of $C_2D_6$, $C_2D_4H_2$, $C_2H_4D_2$, and $C_2H_6$ in comparable amounts indicates that $CH_2$ and $CD_2$ are produced. The relative yield of these ethanes which are formed by insertion of methylene into methane increases with pressure in both the photolysis and radiolysis. In the radiolysis, the $G$ value reaches a value of $0.35 \pm 0.1$ at pressures above 15 atmospheres. Information about the effect of pressure on the production of the methyl ion was obtained by investigating the radiolysis of $CH_4$-iso-$C_4D_{10}$ and $CD_4$-$C_3H_8$ mixtures from 1.5 cm to 130 atmospheres. The data indicate that there is a gradual decrease of the methyl ion yield with increase in pressure while the parent ion yield increases with increase in pressure to a pressure of at least 15 atmospheres.

**Intense resonance line sources for photochemical work in the vacuum ultraviolet region,** H. Okabe, *J. Opt. Soc. Am.* **54,** *No. 4, 478–481 (Apr. 1964).*

A simple, completely sealed, discharge resonance lamp operated by 2450 mc/sec microwave power is described which emits atomic lines of sufficient intensity to be useful as a photochemical light source.

When a water impurity is present in the lamp, many emission lines appear in the region of wavelength from 1500 to 2000 A. These impurity lines can be effectively removed by means of a getter or by a suitable cold trap. The pressures of pure Xe or Kr in the resonance lamp, required to give maximum intensity (approximately $5 \times 10^{14}$ quanta/sec), are 0.7 mm and 1.0 mm, respectively. The presence of a CO impurity does not affect the intensity of the resonance lines. After passing through a 1 mm LiF window, the intensity of the Xe resonance line at 1295 A is about 2 percent of that at 1470 A and the intensity of the Kr line at 1165 A is about 28 percent of that at 1236 A. A mixture of the rare gas and He gives more intense light than the pure gas. Lyman alpha (1216 A) line from excited atomic hydrogen and a group of lines at 1743–45 A from excited atomic nitrogen may be used as a photochemical light source.

**Constants of the interpolation formula for platinum resistance thermometers,** J. L. Riddle, *Proc. Advisory Committee Thermometry to the Intern. Bureau Weights and Measures, 6th Session, pp. 198–201 (Sept. 26–27, 1962).*

Values of the constants in the interpolation formula for a large number of thermometers recently submitted to the National Bureau of Standards for calibration are summarized. All thermometers suitable as standards which were received over a period of about one year during 1959 and 1960 are included. Limitations on such constants can serve either to make the International Practical Temperature Scale (IPTS) more precisely defined or to reduct the number of calibration points required for application over limited temperature ranges.

## Other NBS Publications

**J. Res. NBS 68C (Eng. and Instr.), No. 4 (Oct.–Dec. 1964), 75 cents.**

Theory of mirror spectrographs. I. Astigmatic illumination of plane gratings and prisms. K. D. Mielenz.

Theory of mirror spectrographs. II. General theory of focal surfaces and slit curvatures. K. D. Mielenz.

Theory of mirror spectorgraphs. III. Focal surfaces and slit curvature of Ebert and Ebert-Fastie spectrographs. K. D. Mielenz.

Heat flow in a right circular cylinder with arbitrary temperature boundary conditions—applications to the determination of thermal conductivity. D. R. Flynn.

Digitized phasemeter. W. S. Epstein.

Active and passive direct-reading ratio sets for the comparison of audio-frequency admittances. R. D. Cutkosky.

Review of methods for the excitation of atomic and ionic spectra by means of high-frequency discharges and sliding sparks. Lennart Minnhagen.

Standards for the calibration of $Q$-meters 50 kHz to 45 MHz. R. N. Jones.

X-ray measurement of residual strains in individual grains of polycrystalline aluminum. C. J. Newton.

Ferrimagnetic resonance measurements using IF substitution techniques. W. E. Case, R. D. Harrington, and L. B. Schmidt.

A Pienkowsky-type calibration scheme for 5211Σ1 weight series using two knife-edge direct-reading balances. H. S. Peiser.

Reference tables for the Platinel II thermocouple. L. O. Olsen and P. D. Freeze.

Effects of cathodic currents on the corrosion of an aluminum alloy. W. J. Schwerdtfeger.

Photooxidation of asphalts in the presence of ozone. J. R. Wright and P. G. Campbell.

Designs for temperature and temperature gradient compensated capacitors smaller than ten picofarads. R. D. Cutkosky.

**Radio Sci. J. Res. NBS/USNC–URSI, 68D, No. 11, (Nov. 1964), $1.00.**

Interaction of an antenna with a hot plasma and the theory of resonance probes. J. A. Fejer.

Observations of earth-ionosphere cavity resonances and their interpretation in terms of a two-layer ionosphere model. F. W. Chapman and D. Llanwyn Jones.

On the theory of reflection of electromagnetic waves from the interface between a compressible magnetoplasma and a dielectric. J. R. Wait.

Propagation over plane earth through an exponential atomsphere. I. H. Gerks and R. M. Anderson.

Propagation in nonuniform waveguides with impedance walls. R. L. Gallawa.

Some approximate formulas concerning the reflection of electromagnetic waves from a stratified semi-infinite medium. R. Burman.

A VLF timing experiment. A. H. Morgan and O. J. Baltzer.

Phase and time variations in VLF propagation over long distances. D. D. Crombie.

Geometrical optics convergence coefficient for whistler propagation. G. McK. Allcock.

Errors induced by the atmosphere in microwave range measurements. H. B. Janes and M. C. Thompson.

Some features of Es-ionization of the equatorial ionosphere. P. Bandyopadhyay and H. Montes.

A note on the insulated loops antenna immersed in a conducting medium. J. R. Wait and K. P. Spies.

Observation and analysis of transequatorial propagation. J. A. Thomas and B. A. McInnes.

**Radio Sci. J. Res. NBS/USNC–URSI, 68D, No. 12, (Dec. 1964), $1.00.**

Experiment on the constancy of the velocity of electromagnetic radiation. P. Beckmann and P. Mandics.

Measurement of the phase velocity of VLF propagation in the earth-ionosphere waveguide. F. K. Steele and C. J. Chilton.

Wave hop theory of long distance propagation of low-frequency radio waves. L. A. Berry.

Wave propagation in a compressible ionosphere. Part I. S. R. Seshadri.

Wave propagation in a compressible ionosphere. Part II. S. R. Seshadri.

Spatial properties of the amplitude fading of continuous HF radio waves. J. Ames.

Physical properties of the polar winter mesosphere obtained from low-frequency propagation and partial reflection studies. J. S. Belrose, L. R. Bodé, and L. W. Hewitt.

Reply to the "Remarks by Donald H. Menzel With Reference to Bailey's Comments on Solar Electric Fields." V. A. Bailey.

---

Tables of chemical kinetics homogeneous reactions (Supplementary tables) NBS Mono. 34, Vol. 2 (July 1, 1964), $2.75.

Line parameters and computed spectra for water vapor bands at 2.7$\mu$, D. M. Gates, R. F. Calfee, D. W. Hansen, and W. S. Benedict, NBS Mono. 71, (Aug. 3, 1964), $2.00.

Examination of farm milk tanks. A manual for weights and measures officials, M. W. Jensen, NBS Handb. 98, (May 22, 1964), 35 cents.

Foreign-lanuage and English dictionaries in the physical sciences and engineering. A selected bibliography 1952 to 1963, T. W. Marton, NBS Misc. Publ. 258 (July 24, 1964), $1.25.

Selection of camera filters for color photography, C. S. McCamy, NBS Misc. Publ. 259, (June 26, 1964), 5 cents.

Standard reference materials: Preparation of NBS white cast iron spectrochemical standards, R. E. Michaelis and L. L. Wyman, NBS Misc. Publ. 260–1, (June 19, 1964), 30 cents.

Quarterly radio noise data December 1962; January, February 1963, W. Q. Crichlow, R. T. Disney, and M. A. Jenkins, NBS Tech. Note 18–17 (May 21, 1964), 50 cents.

Absolute photometry of the light of the night sky. The zenith intensity of Haleakala (latitude N 20.7°) and at Fritz peak (latitude N 39.9°), F. E. Roach and L. L. Smith, NBS Tech. Note 214 (June 29, 1964), 35 cents.

Percentage points of the beta distribution, L. E. Vogler, NBS Tech. Note 215 (May 30, 1964), 25 cents.

Computation of Hankel functions, L. A. Berry, NBS Tech. Note 216 (June 12, 1964), 20 cents.

A bibliography of thermophysical properties of argon from 0 to 300 °K, L. A. Hall, J. G. Hurst, and A. L. Gosman, NBS Tech. Note 217 (June 12, 1964), 55 cents.

Average power dissipated in a diode swept along its reverse characteristic, H. A. Schafft, NBS Tech. Note 240 (Apr. 30, 1964), 20 cents.

Calculations for comparing two-point and four-point probe resistivity measurements on rectangular bar-shaped semiconductor samples, L. J. Swartzendruber, NBS Tech. Note 241 (June 1, 1964), 25 cents.

A fortran program for analysis of ellipsometer measurements and calculation of reflection coefficients from thin films, F. L. McCrackin and J. P. Colson, NBS Tech. Note 242 (May 27, 1964), 30 cents.

Survey of multiply charged ions, F. L. Mohler, NBS Tech. Note 243 (May 27, 1964), 10 cents.

An international comparison of voltage-transformer calibrations to 350 kv, F. K. Harris, W. C. Sze, N. L. Kusters, O. Petersons, and W. J. M. Moore, IEEE Trans. Commun. and Elec. No. 70, 13–19 (Jan. 1964).

The quest for design data, R. B. Stewart, Symp. The Role Cryogenics is Playing in Expanding Mechnical Engineering, Am. Soc. Refrigerating and Air Conditioning Engineers, New York, N.Y., Feb. 11–14, 1964, pp. 13–24 (1964).

A coaxial adjustable sliding termination, W. E. Little and J. P. Wakefield, IEEE Trans. Microwave Theory Tech. **MTT–12**, No. 2, 247–248 (Mar. 1964).

Effect of blowing variables on durability of coating grade asphalts, S. H. Greenfeld, Indust. & Eng. Chem. Prod. Res. & Dev. **3,** pp. 158–164 (June 1964).

*Q* Meter measurements up to 260 MHZ, M. G. Broadhurst (Proc. Conf. Electric Insulation) 1963 Annual Report, Natl. Acad. Sci.-Natl. Res. Council Publ. 1141, pp. 77–80 (1964).

Satellite scintillation observations at Boulder, Colorado, J. L. Jespersen and G. Kamas, J. Atmospheric Terrest. Phys. **26,** 457–473 (1964).

The reaction of methyl radicals with dimethylmercury, R. E. Rebbert and P. Ausloos, J. Am. Chem. Soc. **86,** No. 10, 2068–2069 (May 20, 1964).

The performance of point level sensors in liquid hydrogen, D. A. Burgeson, W. G. Pestalozzi, and R. J. Richards (Proc. 1963 Cryogenic Eng. Conf., Univ. Colorado and National Bureau of Standards, Boulder, Colo., Aug. 19–21, 1963), Book, Advances in Cryogenic Engineering **9,** Paper G–5, pp. 416–422 (Plenum Press Inc., New York, N.Y. 1963).

On associated ions in polyelectrolytes and trapped Browian trajectories, J. L. Jackson and S. R. Coriell, J. Chem. Phys. **40,** No. 5, 1460–1461 (Mar. 1, 1964).

He-Ne laser with perpendicular end windows, K. D. Mielenz, K. F. Neffen, and K. Gillilland, J. Opt. Soc. Am. Letter to Editor **3,** No. 6, p. 785 (June 1964).

Functions for the calculation of entropy, enthalpy, and internal energy for real fluids using equations of state and specific heats, J. G. Hust and A. L. Gosman (Proc. 1963 Cryogenic Eng. Conf., Univ. Colorado and National Bureau of Standards, Boulder, Colo., Aug. 19–21, 1963), Book, Advances in Cryogenic Engineering **9,** Paper D–8, 227–233 (Plenum Press, Inc., New York, N.Y., 1964).

Physical processes in the *D* region of the ionosphere, G. C. Reid, Rev. Geophys. **2,** No. 2, 311–333 (May 1964).

Observation of FeO in absorption by flash heating and kinetic spectroscopy, A. M. Bass, N. A. Kuebler, and L. S. Nelson, J. Chem. Phys. **40,** No. 10, 3121–3122 (May 15, 1964).

Computer simulation of traffic on nine blocks of a city street, M. C. Stark, (Proc. 41st Annual Meeting Highway Research Board, Jan. 8–12, 1962), Highway Res. Board Bull. 356, Publ. 1051, p. 40 (Natl. Acad. Sci.-Natl. Res. Council, Wash., D.C., 1962).

One man's opinion—a common language (nomenclature for rubbers), R. D. Stiehler, Rubber World **148,** No. 3, 119 (June 1963).

Long-lived effects in the *D* region after the high-altitude nuclear explosion of July 9, 1962, A. H. Brady, D. D. Crombie, A. G. Jean, A. C. Murphy, and F. K. Steele, J. Geophys. Res. **69,** No. 9, 1921–1924, (May 1, 1964).

Some remarks concerning non-reciprocity in radio propagation, J. R. Wait, IEEE Trans. Ant. Prop. **AP–12,** No. 3, 372–373 (May 1964).

Synthesis of diatomic radicals, H. E. Radford, J. Chem. Phys. **40,** No. 9, 2732–2733 (May 1, 1964).

The effective area of a guarded electrode, J. I. Lauritzen, Jr., (Proc. Conf. Electric Insulation) 1963 Annual Report, Natl. Acad. Sci.- Natl. Res. Council Publ. 1141, pp. 67–73 (1964).

On the measurement of radom chain scission by stress relaxation, H. Yu, Polymer Letter **2,** 631–635 (1964).

The listing of sudden ionospheric disturbances, J. V. Lincoln, Planet. Space Sci. **12,** 419–434 (1964).

Evidence of a stratified echoing region at 150 kilometers in the vicinity of the magnetic equator during daylight hours, B. B. Balsley, J. Geophys. Res. **69,** No. 9, 1925–1930 (May 1, 1964).

Electrical resistances of wires of low temperature-coefficient of resistance useful in calorimetry (10° K–380° K), G. T. Furukawa, M. L. Reilly, and W. G. Saba, Rev. Sci. Instr. **35,** No. 1, 113–114 (Jan. 1964).

Introduction, V. J. Johnson, Am. Soc. Refrigerating and Air Conditioning Engineers, Symp., The Role Cryogenics

is Playing in Expanding Mechanical Engineering at the semi-annual meeting of the Am. Soc. of Heating, Refrigerating and Air-Conditioning Engineers, New York, N.Y., Feb. 11–14, 1963, pp. III–IV (1964).

Measurement of the cross section for elastic scattering of slow electrons by hydrogen atoms, W. L. Wiese, VIth Intern. Conf. Ionization Phenomena in Gases I, 5–8 (Paris, 1963).

Mass spectrometric study of the isotopic exchange rate of oxygen atoms with $O^2$, NO, and $NO_2$, J. T. Herron and F. S. Klein, J. Chem. Phys. **40,** No. 9, 2731 (May 1, 1964).

Growth twins and branching of electrodeposited copper dendrites, F. Ogburn, J. Electrochem. Soc. **11,** No. 7, 870–872 (July 1964).

Ultrasonically induced nuclear spin transitions in antiferromagnetic $KMnF_3$ A. B. Denison, L. W. James, J. D. Currin, W. H. Tantilla, and R. J. Mahler, Phys. Rev. Letters **12,** 244–245, (1964).

Techniques for using the air-gap method for the precise determination of the dielectric constant and loss angle of solid disk specimens, A. H. Scott, (Proc. Conf. Electric Insulation) 1963 Annual Report, Natl. Acad. Sci.-Natl. Res. Council Publ. 1141, pp. 74–76 (1964).

Low-temperature infrared study of intermediates in the photolysis of HNCO and DNCO, M. E. Jacox and D. E. Milligan, J. Chem. Phys. **40,** No. 9, 2457–2460 (May 1, 1964).

$N_2+$ oscillators strength from arc spectroscopic measurements using an analog computer, J. B. Shumaker, Jr. (Proc. Sixth Intern, Symp. Ionization Phenomena in Gases VII, No. **15,** 311–313 (1963).

Ixiolite and other polymorphic types of $FeNbO_4$, R. S. Roth and J. L. Waring, Am. Mineralogist **49,** 242–246 (Mar.–Apr. 1964).

Separation and determination of zirconium in zirconia-yttria mixtures by precipitation with cupferron, E. J. Maienthal and J. K. Taylor, Anal. Chem. **36,** 1286–1287 (June 1964).

Analysis of the frost phenomena on a cryo-surface, R. V. Smith, D. K. Edmonds, E. G. F. Brentari, and R. J. Richards, (Proc. 1963 Cryogenic Eng. Conf. Univ. Colorado and National Bureau of Standards, Boulder, Colo., Aug. 19–21, 1963), Book, Advances in Cryogenic Engineering **9,** Paper B-7, pp. 88–97 (Plenum Press Inc., New York, N.Y., 1964).

Free subgroups and normal subgroups of the modular group, M. Newman, Ill. J. Math. **8,** No. 2, 262–265 (June 1964).

The operating characteristics of Zener reference diodes and their measurements, W. G. Eicke, Jr., ISA Trans. **3,** No. 2, 93–99 (Apr. 1964).

Four critical fields in superconducting indium lead alloys, S. Gygax, J. L. Olsen, and R. H. Kropschot, Phys. Letters **8,** No. 4, 228–230 (1964).

The correlation of thermodynamic properties of cryogenic fluids, R. B. Stewart and K. D. Timmerhaus (Proc. 1963 Cryogenic Eng. Conf., Univ. Colorado and National Bureau of Standards, Boulder, Colo., Aug. 19–21, 1963), Book, Advances in Cryogenic Engineering 9, Paper A-3, 20–27 (Plenum Press Inc. New York, N.Y., 1964.)

Modern methods of analysis for the design of cryogenic equipment and processes, T. R. Strobridge and D. B. Mann, Symp., The Role Cryogenics is Playing in Expanding Mechanical Engineering, Am. Soc. Refrigerating and Air Conditioning Engineers, New York, N.Y., Feb. 11–14, 1963 pp. 26–37 (1964).

Survey of current NBS work on properties of parahydrogen, R. D. Goodwin, D. E. Diller, W. J. Hall, H. M. Roder, L. A. Weber, and B. A. Younglove, (Proc. 1963 Cryogenic Eng. Conf., Univ. Colorado and National Bureau of Standards, Boulder, Colo., Aug. 19–21, 1963), Book, Advances in Cryogenic Engineering **9,** Paper D–9, 234–242 (Plenum Press Inc., New York, N.Y., 1964).

The calorimeter and its influence on the development of chemistry, G. T. Armstrong, J. Chem. Educ. **41,** 297 (June 1964).

Presidential address before the Electrochemical Society meeting, Toronto, Canada, May 5, 1964, W. J. Hamer, J. Electrochem. Soc. **III,** No. 7, 145C–147C (July 1964).

Precise determination of the area of guarded electrodes for accurate dielectric measurements on solid-disk specimens, W. P. Harris, (Proc. Conf. Electric Insulation) 1963 Annual Report, Natl. Acad. Sci.-Natl. Res. Council Publ. 1141, p. 71 (1964).

Open-probe thermocouple control of radio-frequency heating, A. W. Ruff, Jr., Rev. Sci. Instr. **35,** No. 6, 760–761 (June 1964).

A new steady-state calorimeter for measuring heat transfer through cryogenic insulation, D. R. Beck, F. Kreith, and R. H. Kropschot (Proc. 1963 Cryogenic Eng. Conf. Univ. Colorado and National Bureau of Standards, Boulder, Colo., Aug. 19–21, 1963), Book, Advances in Cryogenic Engineering **9,** Paper B–4, 64–70 (Plenum Press Inc., New York, N.Y., 1964).

Surface currents in type II superconductors, S. Gygax and R. H. Kropschot, Phys. Letters **9,** No. 2, p. 91, (Apr. 1, 1964).

A preliminary study of the orifice flow characteristics of liquid nitrogen and liquid hydrogen discharging into a vacuum, J. A. Brennan (Proc. 1963 Cryogenic Eng. Conf., Univ. Colorado and National Bureau of Standards, Boulder Colo., Aug. 19–21, 1963), Book, Advances in Cryogenic Engineering 9, Paper E–6, p. 292–303, (Plenum Press, Inc., New York, N.Y., 1964).

Sieve techniques for obtaining small amounts of narrowly classified particles, C. M. Hunt and A. R. Woolf, Mater. Res. Std. Tech. Note 4, No. 7, 364 (July 1964).

Preliminary thermodynamic properties of neon, R. D. McCarty and R. B. Stewart (Proc. 1963 Cryogenic Eng. Conf. Univ. Colorado and National Bureau of Standards, Boulder Colo., Aug. 19–21, 1963), Book, Advances in Cryogenic Engineering **9,** Paper D–1, 161–167 (Plenum Press Inc., New York, N.Y., 1963).

The effect of coulomb collisions on incoherent scattering of radio waves by a plasma, D. T. Farley, Jr., J. Geophys. Res. **69,** No. 1, 197–200 (Jan. 1, 1964).

On the connection between the theories of collisions and of atomic spectra, U. Fano and F. Prats, Proc. Nat. Acad. Sci. India, **XXXIII,** Part IV, 553–562 (1963).

Electromagnetic scattering from a radially inhomogeneous sphere, J. R. Wait, J. Appl. Phys. Sec. B, **10,** 441–450 (Jan. 7, 1963).

An approach to the classification of electromagnetic surface waves, J. R. Wait, Book, Radio Waves and Circuits by S. Silver, Pt. 1, pp. 86–95 (Elsevier Publ. Co., Princeton, N.J., 1963).

Mass spectrometry, R. M. Reese and F. N. Harllee, Anal. Chem. **36,** No. 5, 278R–295R (April 1964).

Colorimetry in parafoveal fields I. Color-matching functions, I. Nimeroff, J. Opt. Soc. Am. **54,** No. 6, 824–832 (June 1964).

Colorimetry in parafoveal fields II. Additivity failure, I. Nimeroff, J. Opt. Soc. Am. **54,** No. 6, 833–838 (June 1964).

An experimental 350-kv, 1-picofarad air capacitor, A. E. Peterson, IEEE Trans. Commun. Elec. No. **71,** 129–131 (Mar. 1964).

The association of plane-wave electron-density irregularities with the equatorial electro jet, K. L. Bowles, J. Geophys. Res. **68,** No. 9, 2503–2525 (May 1, 1963).

Some results of the energy-dependent Milne problem for thermal neutrons and light gases, C. Eisenhauer, Nucl. Sci. Eng. **19,** 95–101 (1964).

Nitrogen NMR chemical shifts in the azide ion, R. A. Forman, J. Chem. Phys. **39,** No. 9, 2393 (Nov. 1, 1963).

Exact Faxén solution for centrifugation when sedimentation depends linearly on concentration, I. H. Billick and G. H. Weiss, Nature **201,** No. 4922, 912–913 (Feb. 29, 1964).

$4f^3$ and $4f^2\,5d$ configurations of doubly ionized praseodymium (Pr III), R. E. Trus, J. Opt. Soc. Am. **54,** No. 5, 651–657 (May 1964).

Distillation analysis, R. T. Leslie and E. C. Kuehner, Anal. Chem. **36,** 56R (Apr. 1964).

The second industrial revolution (Spanish translation), A. T. McPherson, Rev. Centro Estud. Ing. **132,** No. 669, 348–354 (1963).

A comparison of the $TA_1$ and the NBS—A atomic time scales, J. Bonanomi, P. Kartaschoff, J. Newman, J. A. Barnes, and W. R. Atkinson, Proc. IEEE **52,** No. 4, 439 (Apr. 1964).

Jet thinning device for preparation of $Al_2O_3$ electron microscope specimens, N. J. Tighe, Rev. Sci. Instr. **35,** No. 4, 520–521 (Apr. 1964).

Nuclear magnetic resonance in lead alloys, R. J. Snodgrass and L. H Bennett, Phys. Rev. **134,** No. 5A, A1294 (June 1, 1964).

Radar echoes from Venus at 50 Mc/sec, W. K. Klemperer, G. R. Ochs, and K. L. Bowles, Astron. J. **69,** No. 1 (1316) 22–28 (Feb. 1964).

On the theory of Schumann resonances in the earth-ionosphere cavity J. R. Wait, Can. J. Phys. **42,** 575–582 (Apr. 1964).

Absorption spectra of diatomic molecules in liquid and crystalline rare gases, G. L. Pollack and A. A. Pollack (Proc. 14th Annual Mid-America Spectroscopy Symp. Chicago, Ill., May 20–23, 1963), Book, Developments in Applied Spectroscopy **3,** 376–382 (Plenum Press, New York, N.Y., 1964) ed. J. E. Foreette and E. Lanterman.

A note on some quadrature formulas for the interval $(-\infty, \infty)$, S. Haber, Math, Computation **18,** No. 86, 313–314 (Apr. 1964).

Comments by J. R. Wait on the paper "Obstacle gain and shadow loss," by G. H. Crenier, to the Editor of Microwave J. **6,** No. 7, 83 (July 1963).

Microwave standards and measurements, a progress review 1960–1963, R. W. Beatty, IEEE Trans. Instr. Meas. **IM–12,** No. 3, 134–138 (Dec. 1963).

Absence of pronounced quadrupole effects in the nuclear resonance of $In^{115}$ in a non-cubic environment, L. H. Bennett and R. J. Snodgrass, Phys. Rev. **134,** No. 5A, A1290 (June 1, 1964).

Kinetics and mechanism of the low-cubic to hexagonal phase transformation of silver iodide, J. Phys. Chem. **68,** No. 5, 1111–1113 (1964).

On the concentrations of vibrationally excited $O_2$ formed in the flash photolysis of $NO_2$, A. M. Bass and D. Garvin, J. Chem. Phys. **40,** No. 6, 1772–3 (Mar. 15, 1964).

Energy, temperature, and organisms, D. M. Gates, Sci. Teacher **31,** No. 4 (May 1964).

Some aspects of the coordination chemistry of boron, T. D. Coyle and F. G. A. Stone, Progr. Boron Chem. **1,** 83–166 (1964).

The relation between VLF propagation and *D*-layer characteristics, J. R. Wait, IEEE Trans. Ant. Prop. **AP–12,** No. 2 (Mar. 1964).

**Publications for which a price is indicated are available by purchase from the Superintendent of Documents, U.S. Government Printing Office, Washington, D.C., 20402 (foreign postage, one-fourth additional). Reprints from outside journals and the NBS Journal of Research may often be obtained directly from the authors.*

JOURNAL OF RESEARCH of the National Bureau of Standards—A. Physics and Chemistry
Vol. 68A, No. 6, November–December 1964

# INDEX TO VOLUME 68A

January to December 1964


## A

*Abramowitz, S., H. P. Broida,* The O-2transition of CO in condensed oxygen, nitrogen, and argon ... 331
Absolute light scattering photometer: II. Direct determination of scattered light from solutions ... 87
Absolute isotopic abundance ratio and the atomic weight of bromine ... 593
Absolute isotopic abundance ratio and the atomic weight of a reference sample of copper ... 589
Absorption spectrum, infrared, of nitrous oxide ($N_2O$) from 1830 $cm^{-1}$ to 2270 $cm^{-1}$ ... 79
Acenaphthylene, ionic polymerization of, stereoregularity ... 165
Acidity, in methanol-water solvents ... 305
Acids, dissociation of, in methanol-water solvents at 25 °C ... 305
Action of water on calcium aluminoferrites ... 453
Adsorption and desorption of polystyrene on chrome surface, rates ... 391
Aldehydes and aldoses-*1-t* with sodium chlorite, mechanism for oxidation. Tritium-labeled compounds. XI ... 301
Aldoses-*1-t* and aldehydes with sodium chlorite, mechanism for oxidation. Tritium-labeled compounds. XI ... 301
Aldoses-*1-t* with bromine, isotope effects in the oxidation of. Tritium-labeled compounds. X ... 145
Aluminoferrites, calcium reaction with water ... 453
Aluminum carbide, heat of combustion and heat of formation ... 661
Ammonium sulfate mixtures, crystallization of anhydrous copper sulfate from sulfuric acid ... 313
Anhydrous copper sulfate, crystallization of, from sulfuric acid-ammonium sulfate mixtures ... 313
Aqueous solution at 25 °C, ionization constants of the six dichloroanilines and the six dichlorophenols ... 159
*Argentar, H., G. M. Brauer, G. Durany,* Ionization constants and reactivity of isomers of eugenol ... 619
*Armstrong, G. T., R. C. King,* Heat of combustion and heat of formation of aluminum carbide ... 661
Aromatization of inositol derivatives ... 287
Atomic spectra, W II ... 207
Atomic weight determination and absolute isotopic abundance ratio of bromine ... 593
Atomic weight determination, copper, and absolute isotopic abundance ... 589

## B

*Bates, R. B., E. F. Sager, R. A. Robinson,* Medium effects on the dissociation of weak acids in methanol-water solvents at 25 °C ... 305
*Beverly, W. B., V. Spiegel, Jr.,* Fast neutron dose measurements for a D–D source in water ... 1
Bismuth esquioxide, polymorphism. II. Effect of oxide additions on the polymorphism of $Bi_2O_3$ ... 197
Bismuth sesquioxide, polymorphism—pure $Bi_2O_3$ ... 189
Borates, crystalline inorganic, infrared spectra ... 465
*Brauer, G. M., H. Argentar, G. Durany,* Ionization constants and reactivity of isomers of eugenol ... 619
*Brennan, J. G., J. J. Coyne,* Energy dependence of the D–D reaction cross section at low energies ... 675
*Broida, H. P., S. Abramowitz,* The O-2 transition of CO in condensed oxygen, nitrogen, and argon ... 331
Bromine, absolute isotopic abundance ratio and the atomic weight ... 593
Bromine, aldoses-*1-t* with, isotope effects in the oxidation of. Tritium-labeled compounds. X ... 145
*Burley, G.,* X-ray investigation of strain in cold-worked silver iodide ... 355

## C

Calcium aluminoferrite hydrates ... 453
Calcium aluminoferrites, reaction with water ... 453
Calcium aluminosilicate hydrate ... 449
Calorimetric properties of some alkali pentaborate hydrates from 15 to 370° K ... 381
Calculation of the geometrical structure of some $AH_n$ molecules ... 635
Calculation of the higher order dipole-dipole effect in paramagnetic crystals ... 113
*Canty, G., W. M. Story,* Stereoregularity in ionic polymerization of acenaphthylene ... 165
$2CaO \cdot Al_2O_3 \cdot SiO_2 \cdot H_2O$, hydrothermal preparation ... 449
$4CaO \cdot 3Al_2O_3 \cdot 3H_2O$, x ray diffraction pattern ... 449
*Carlson, E. T.,* Action on water on calcium aluminoferrites ... 453
——, Hydrothermal preparation of a gehlenite hydrate ... 449
*Carrera, N. J., R. F. Walker, E. R. Plante,* Vapor pressures of ruthenium and osmium ... 325
*Catalan, M. A., W. F. Meggers, O. Garcia-Riquelme,* The first spectrum of manganese, Mn I ... 9
*Catanzaro, E. J., T. J. Murphy, E. L. Garner, W. R. Shields,* Absolute isotopic abundance ratio and the atomic weight of bromine ... 593
*Caul, H. J., B. W. Mulligan, S. D. Rasberry, B. F. Scribner,* X-ray spectrometric analysis of noble metal dental alloys ... 5
Compressibility of natural rubber at pressures below 500 $kg/cm^2$ ... 259
Copolymer with lamellar morphology ... 269
Copper, absolute isotopic abundance ratio and atomic weight of reference sample ... 589
*Coyne, J. J. J. G. Brennan,* Energy dependence of the D–D reaction cross section at low energies ... 675
Crystal point defects, trapped, relaxation modes of, the three-neighbor model in NaCl ... 425
Crystalline inorganic borates, infrared spectra ... 465
Crystallization of anhydrous copper sulfate from sulfuric acid ammonium sulfate mixtures ... 313
Crystals, polymer, dislocations ... 513
Cyclic polyhydroxy ketones II. *xylo*-Trihydroxycyclohexenediolic acid and keto-inositols ... 287

## D

D–D reaction, energy dependence at low energies ... 675
D–D source in water, fast neutron dose measurements ... 1
Density measurements of silicon ... 529
Dental alloys, noble metal, X-ray spectrometric analysis ... 5
Dependence of mechanical relaxation on morphology in isotactic polypropylene ... 519
Detection of lattice deformation and recovery in epsilon phase silver tin alloys ... 317
Deuterium isotope ... 1
*Dibeler, V. H., R. W. Reese,* Mass spectrometric study of photoionization. I. Apparatus and initial observations on acetylene, acetylene-$d_2$, benzene, and benzene-$d_6$ ... 409
Dichloroanilines and dichlorophenols, six, in aqueous solution at 25 °C, ionization constants ... 159
Dichlorophenols and dichloroanilines, six, in aqueous solution at 25 °C, ionization constants ... 159
Dielectric behavior of the film formed on mica cleaved in moist air ... 173
Dielectric losses and surface conductivity of dielectrics in parallel plane test capacitors, on the measurement ... 185
Dielectrics in parallel plane test capacitors, on the measurement of dielectric losses and surface conductivity ... 185
*Diller, D. E., R. D. Goodwin, H. M. Roder, L. A. Weber,* Second and third virial coefficients for hydrogen ... 121
*DiMarzio, E. A.,* On the second order transition of a rubber ... 611
Dipole-dipole effect in paramagnetic crystals, calculation of the highest order ... 113
Dislocations in polymer crystals ... 513
Dissociation constants, in methanol-water solvents at 25 °C ... 305
Dissociation constants of the six dichloroanilines and the six dichlorophenols in aqueous solution at 25 °C ... 159
*Domen, S. R., J. S. Pruitt,* Intercomparison of high energy x-ray intensity measurements ... 703
Dose measurements, fast neutron, for a D–D source in water ... 1
Double-bond structure, some changes in, during the vulcanization of natural rubber ... 499
*Durany, G., G. M. Brauer, H. Argentar,* Ionization constants and reactivity of isomers of eugenol ... 619
*Durst, R. A., J. K. Taylor,* Near infrared spectrophotometric method for the determination of hydration numbers ... 625

## E

*Eby, R. K.,* A copolymer with lamellar morphology ... 269
Effect of pressure and temperature upon the optical dispersion of benzene, carbon tetrachloride, and water ... 489
Ellipsometry, transparent surfaces by, optical properties of thin films; internal reflection for film covered surfaces near the critical angle ... 601
Energy dependence of the D–D reaction crass section at low energies ... 675
Energy levels of W II ... 207
Ether, perfluorophenyl, and related polymers ... 277
Eugenol isomers, ionization constants and reactivity ... 619

## F

Fast neutron dose measurements for a D–D source in water ... 1
*Fataidi, A. J., H. S. Isbell,* Cyclic polyhydroxy ketone II. *xylo*-Trihydroxycyclohexenediolic acid and keto-inositols ... 287
Films, thin, optical properties of, on transparent surfaces by ellipsometry; internal reflection for film covered surfaces near the critical angle ... 601
First spectrum of manganese, Mn I ... 9
Forbidden lines, probabilities of, transition ... 61
Fractionated high and low molecular weight polyisobutylene, thermal degradation ... 153
Franck-Condon factors for the ionization of $H_2$, HD, and $D_2$ ... 631
Franck-Condon factors to high vibrational quantum numbers III: CN ... 75
Franck-Condon factors to high vibrational quantum numbers IV: NO band systems ... 535
*Franklin, A. D., A. Shorb, J. B. Wachtman, Jr.,* Relaxation modes of trapped crystal point defects, the three-neighbor shells model in NaCl ... 425
*Frenkel, L.,* On the measurement of dielectric losses and surface conductivity of dielectrics in parallel plane test capacitors ... 185
——, *S. Ruthberg,* Dielectric behavior of the film formed on mica cleaved in moist air ... 173
*Furukawa, G. T., M. L. Reilly, J. H. Piccirelli,* Calorimetric properties of some alkali pentaborate hydrates from 15 to 370 °K ... 381

Page

*Furukawa, G. T. M., L. Reilly, J. H. Piccirelli,* Heat capacity of potassium borohydride ($KBH_4$) from 15 to 375 °K. Thermodynamic properties from 0 to 700 °K ..... 651

——, ——, ——, *M. Tenebaum,* Thermodynamic properties of some methylphosphonyl dihalides from 15 to 335 °K ..... 367

G

*Garcia-Riguelme, O., M. A. Katalan, W. F. Meggers,* The first spectrum of managnese, Mn I ..... 9

*Garner, E. L., E. J. Catanzaro, T. J. Murphy, W. R. Shields,* Absolute isotopic abundance ratio and the atomic weight of bromine ..... 593

——, *W. R. Shields, T. J. Murphy,* Absolute isotopic abundance ratio and the atomic weight of a reference sample of copper ..... 589

*Garstang, R. H.,* Transition probabilities of forbidden lines ..... 61

Gehlenite hydrate, hydrothermal preparation ..... 449

Glass, standard soda-lime-silica, viscosity ..... 439

Glass temperature, variation of, with pressure in polypropylene ..... 273

Glass transition in a rubber ..... 611

*Goodwin, R. D., D. E. Diller, H. M. Roder, L. A. Weber,* Second and third virial coefficients for hydrogen ..... 121

*Grant, W. H., E. Passaglia, R. R. Stromberg,* Rates of adsorption and desorption of polystyrene on chrome surface ..... 391

*Gruzensky, P. A.,* Crystallization of anhydrous copper sulfate from sulfuric acid-ammonium sulfate mixtures ..... 313

H

Halides, some alkali, lattice parameters and lattice energies of high-pressure polymorphs ..... 105

*Hawkins, E. G., A. Napolitano,* Viscosity of a standard soda-lime-silica glass ..... 439

1962 $He^3$ scale of temperatures. I. New vapor pressure comparison ..... 547

1962 $He^3$ scale of temperatures. II. Derivation ..... 559

1962 $He^3$ scale of temperatures. III. Evaluation and status ..... 567

1962 $He^3$ scale of temperatures. IV. Tables ..... 579

Heat capacity of potassium borohydride ($KBH_4$) from 15 to 375 °K. Thermodynamic properties from 0 to 700 °K ..... 651

Heat of combustion and heat of formation of aluminum carbide ..... 661

Heat of formation of a magnesium oxysulfate, preparation ..... 645

Heats of solution, transition, and formation of three crystalline forms of metaboric acid ..... 127

Heats of sublimation of ruthenium and osmium ..... 325

*Henins, I.,* Precision density measurement of silicon ..... 529

*Hicho, G. E., R. M. Waterstrat,* Detection of lattice deformation and recovery in epsilon phase silver-tin alloys ..... 317

High-energy x-ray intensity measurements, intercomparison ..... 703

High-pressure microscopy of the silver and cuprous halides ..... 97

High vibrational quantum numbers IV, NO band systems, Franck-Condon factors ..... 535

*Hubbard, W. D., S. P. Wasik,* Light-scattering measurements of solutions of some quaternary ammonium salts ..... 359

Hydrate, gehlenite, hydrothermal preparation ..... 449

Hydration numbers, near infrared spectrophotometric method for the determination ..... 625

Hydrogen, second and third virial coefficients ..... 121

Hydrothermal preparation of a gehlenite hydrate ..... 449

I

Infrared absorption spectrum of nitrous oxide ($N_2O$) from 1830 $cm^{-1}$ to 2270 $cm^{-1}$ ..... 79

Infrared spectra of the crystalline inorganic borates ..... 465

Intercomparison of high-energy x-ray intensity measurements ..... 703

Ionization constants and reactivity of isomers of eugenol ..... 619

Ionization constants, in methanol-water solvents ..... 305

Ionization constants of the six dichloroanilines and the six dichlorophenols in aqueous solution at 25 °C ..... 159

Ionization of $H_2$, HD, and $D_2$, Franck-Condon factors ..... 631

Inositol derivatives ..... 287

*Isbell, H. S., A. J. Fatiadi,* Cyclic polyhydroxy ketones II. *xylo*-Trihydroxycyclohexenediolic acid and keto-inositols ..... 287

——, *L. T. Sniegoski,* Tritium-labeled compounds X. Isotope effects in the oxidation of aldoses-*l*-*t* with bromine ..... 145

——, ——, Tritium-labeled compounds XI. Mechanism for the oxidation of aldehydes and aldoses-*l*-*t* with sodium chlorite ..... 301

Isotope effects in the oxidation of aldoses-*l*-*t* with bromine, tritium-labeled compounds X ..... 145

Iterative unfolding procedure ..... 401

K

*Keith, H. D., E. Passaglia,* Dislocations in polymer crystals ..... 513

Keto-inositols and *xylo*-trihydroxycyclohexenediolic. Cyclic polyhydroxy ketone II ..... 287

*Kilday, M. V., E. J. Prosen,* Heats of solution, transition, and formation of three crystalline forms of metaboric acid ..... 127

*King, R. C., G. T. Armstrong,* Heat of combustion and heat of formation of aluminum carbide ..... 661

*Krauss, M.,* Calculation of the geometrical structure of some $AH_n$ molecules ..... 635

L

Lamellar morphology, a copolymer ..... 269

Lattice deformation and recovery, detection of, in epsilon phase silver-tin alloys ..... 317

Lattice parameters and lattice energies of high-pressure polymorphs of some alkali halides ..... 105

*Levin, E. M., R. S. Roth,* Polymorphism of bismuth sesquioxide. I. Pure $Bi_2O_3$ ..... 189

——, ——, Polymorphism of bismuth sesquioxide. II. Effect of oxide additions on the polymorphism of $Bi_2O_3$ ..... 197

Page

Light-scattering measurements on solutions of some quaternary ammonium salts ..... 359

*Linnig, F. J., E. J. Parks, J. E. Stewart,* Some changes in double-bond structure during the vulcanization of natural rubber ..... 499

M

Magnesium oxysulfate, preparation and heat of formation ..... 645

*Maki, A. G., E. K. Plyler, E. D. Tidwell,* Infrared absorption spectrum of nitrous oxide ($N_2O$) from 1830 $cm^{-1}$ to 2270 $cm^{-1}$ ..... 79

Manganese, Mn I, the first spectrum ..... 9

*Martin, G. M., E. Passaglia,* Dependence of mechanical relaxation on morphology in isotactic polypropylene ..... 519

——, ——, Variation of glass temperature with pressure in polypropylene ..... 273

——, *L. A. Wood,* Compressibility of natural rubber at pressures below 500 $kg/cm^2$ ..... 259

Mass spectrometric study of photoionization. I. Apparatus and initial observations on acetylene, acetylene-$d_2$, benzene, and benzene-$d_6$ ..... 409

*Mc Intyre, D.,* An absolute light scattering photometer: II. Direct determination of scattered light from solutions ..... 87

——, *J. H. O'Mara, S. Straus,* Thermal degradation of fractionated high and low molecular weight polyisobutylene ..... 153

Medium effects, of methanol on dissociation of acids ..... 305

Medium effects on the dissociation of weak acids in methanol-water solvents at 25 °C ..... 305

*Meggers, W. F., M. A. Catalan, O. Garcia-Riquelme,* The first spectrum of mangenese, Mn I ..... 9

*Meijer, P. H. E.,* Calculation of the higher order dipole-dipole effect in paramagnetic crystals ..... 113

Metaboric acid, three crystalline forms of, heats of solution, transition, and formation ..... 127

Metallographic characterization of an NBS spectrometric low-alloy steel standard ..... 343

Methanol-water solvents, dissociation of acids ..... 305

Methylphosphonyl chlorofluoride, thermodynamic properties of, from 15 to 335 °K ..... 367

Methylphosphonyl dichloride, thermodynamic properties of, from 15 to 335 °K ..... 367

Methylphosphonyl difluoride, thermodynamic properties of, from 15 to 335 °K ..... 367

Methylphosphonyl dihalides, thermodynamic properties of, from 15 to 335 °K ..... 367

Mica cleaved in moist air, dielectric behavior of film formed ..... 173

*Michaelis, R. E., H. Yakowitz, G. A. Moore,* Metallographic characterization of an NBS spectrometric low-alloy steel standard ..... 343

Microscopy, high pressure, of the silver and cuprous halides ..... 97

*Moore, G. A., R. E. Michaelis, H. Yakowitz,* Metallographic characterization of an NBS spectrometric low-alloy steel standard ..... 343

Morphology in isotactic polypropylene, dependence of mechanical relaxation ..... 519

Morphology, lamellar, a copolymer ..... 269

*Mulligan, B. W., H. J. Caul, S. D. Rasberry, B. F. Scribner,* X-ray spectrometric analysis of noble metal dental alloys ..... 5

*Murphy, T. J., E. J. Catanzaro, E. L. Garner, W. R. Shields,* Absolute isotopic abundance ratio and the atomic weight of bromine ..... 593

——, *W. R. Shields, E. L. Garner,* Absolute isotopic abundance ratio and the atomic weight of a reference sample of copper ..... 589

N

*Napolitano, A., E. G. Hawkins,* Viscosity of a standard soda-lime-silica glass ..... 439

Natural rubber, some changes in double-bond structure during vulcanization ..... 499

Near infrared spectrophotometric method for the determination of hydration numbers ..... 625

Neutron dose measurements, fast, for a D-D source in water ..... 1

*Newman, E. S.,* Preparation and heat of formation of a magnesium oxysulfate ..... 645

*Nicholls, R. W.,* Franck-Condon factors to high vibrational quantum numbers III: CN ..... 75

——, Franck-Condon factors to high vibrational quantum numbers IV: NO band systems ..... 535

Nitrous oxide ($N_2O$), infrared absorption spectrum of, from 1830 $cm^{-1}$ to 2270 $cm^{-1}$ ..... 79

Noble metal dental alloys, x-ray spectrometric analysis ..... 5

O

O–2 transition of CO in condensed oxygen, nitrogen, and argon ..... 331

*O'Mara, J. H., D. McIntyre, S. Straus,* Thermal degradation of fractionated high and low molecular weight polyisobutylene ..... 153

On the measurement of dielectric losses and surface conductivity of dielectrics in parallel plane test capacitors ..... 185

On the second-order transition of a rubber ..... 611

Optical properties of thin films on transparent surfaces by ellipsometry; internal reflection for film covered surfaces near the critical angle ..... 601

Osmium and ruthenium, vapor pressures ..... 325

Oxidation of inositol with nitric acid ..... 287

P

P2-4—Quantameter intercomparison ..... 703

Parallel plane test capacitors, on the measurement of dielectric losses and surface conductivity of dielectrics ..... 185

Paramagnetic crystals, calculation of the higher order dipole-dipole effect ..... 113

*Parks, E. J., J. Linnig, J. E. Stewart,* Some changes in double-bond structure during the vulcanization of natural rubber ..... 499

*Passaglia, E., H. D. Keith,* Dislocation in polymer crystals ..... 513

——, *G. M. Martin,* Dependence of mechanical relaxation on morphology in isotactic polypropylene ..... 519

——, ——, Variation of glass temperature with pressure in polypropylene ..... 273

Page

*Passaglia, E., R. R. Stromberg,* Optical properties of thin films on transparent surfaces by ellipsometry; internal reflection for film covered surfaces near the critical angle ... 601
——, ——, *W. H. Grant,* Rates of adsorption and desorption of polystyrene on chrome surface ... 391
Pentaborate hydrates, alkali, calorimetric properties of some ... 381
Perfluorophenyl ether and related polymers ... 277
Photometer, an absolute light scattering. II. Direct determination of scattered light from solutions ... 87
Photovoltaic mode of operation of steady-state response of silicon radiation detectors to x rays ... 683
*Piccirelli, J. H., G. T. Furukawa, M. L. Reilly,* Calorimetric properties of some alkali pentaborate hydrates from 15 to 370 °K ... 381
——, ——, ——, Heat capacity of potassium borohydride ($KBH_4$) from 15 to 375 °K. Thermodynamic properties from 0 to 700 °K ... 651
——, ——, ——, *M. Tenebaum,* Thermodynamic properties of some methylphosphonyl halides from 15 to 335 °K ... 367
*Piermarini, G. J., C. E. Weir,* Lattice parameters and lattice energies of high-pressure polymorphs of some alkali halides ... 105
*Plante, E. R., N. J. Carrera, R. F. Walker,* Vapor pressures of ruthenium and osmium ... 325
*Plyler, E. K., E. D. Tidwell, A. K. Maki,* Infrared absorption spectrum of nitrous oxide ($N_2O$) from 1830 $cm^{-1}$ to 2270 $cm^{-1}$ ... 79
Polyisobutylene, fractionated high and low molecular weight, thermal degradation ... 153
Polymer crystals, dislocations ... 513
Polymer, rates of adsorption of polystyrene ... 391
Polymerization, ionic, of acenaphtylene, stereoregularity ... 165
Polymers, related, and perfluoropbenyl ether ... 277
Polymorphism of bismuth sesquioxide. I. Pure $Bi_2O_3$ ... 189
Polymorphism of bismuth sesquioxide. II. Effect of oxide additions on the polymorphism of $Bi_2O_3$ ... 197
Polymorphs of some alkali halides, lattice parameters and lattice energies of high pressure ... 105
Polypropylene, isotactic, dependence of mechanical relaxation on morphology ... 519
Polypropylene, variation of glass temperature with pressure ... 273
Polystyrene on chrome surface, rates of adsorption and desorption ... 391
Potassium borohydride, heat capacity from 15 to 375 °K; thermodynamic properties from 0 to 700 °K ... 651
Precision density measurement of silicon ... 529
Preparation and heat of formation of a magnesium oxysulfate ... 645
Pressures below 500 $kg/cm^2$, compressibility of natural rubber ... 259
Probabilities of forbidden lines, transition ... 61
*Prosen, E. J., M. V. Kilday,* Heats of solution, transition, and formation of three crystalline forms of metaboric acid ... 127
*Pruitt, J. S., S. R. Domen,* Intercomparison of high-energy x-ray intensity measurements ... 703
*Pummer, W. J., L. A. Wall,* Perfluorophenyl ether and related polymers ... 277


## Q


Quantameter-P2-4 intercomparison ... 70


## R


*Rasberry, S. D., B. W. Mulligan, H. J. Caul, B. F. Scribner,* x-ray spectrometric analysis of noble metal dental alloys ... 5
Rates of adsorption and desorption of polystyrene on chrome surface ... 391
Reaction cross section, energy dependence of the D–D ... 675
Reactivity and ionization constants of isomers of eugenol ... 619
*Reese, R. W., V. H. Dibeler,* Mass spectrometric study of photoionization. I. Apparatus and initial observations on acetylene, acetylene-$d_2$, benzene, and benzene-$d_6$ ... 409
*Reilly, M. L., G. T. Furukawa, J. H. Piccirelli,* Calorimetric properties of some alkali pentaborate hydrates from 15 to 370 °K ... 381
——, ——, ——, Heat capacity of potassium borohydride ($KBH_4$) from 15 to 375 °K. Thermodynamic properties from 0 to 700 °K ... 651
——, ——, ——, *M. Tenebaum,* Thermodynamic properties of some halides from 15 to 335 °K ... 367
Relaxation modes of trapped crystal point defects, the three-neighbor shells model in NaCl ... 425
*Roberts, T. R., R. H. Sherman, S. G. Sydoriak,* The 1962 $He^3$ scale of temperatures. III. Evaluation and status ... 567
——, ——, ——, The 1962 $He^3$ scale of temperatures. IV. Tables ... 579
——, *S. G. Sydoriak, R. H. Sherman,* The 1962 $He^3$ scale of temperatures II. Derivation ... 559
*Robinson, R. A.,* Ionization constants of the six dichloroanilines and the six dichlorophenols in aqueous solution ... 159
——, *E. E. Sager, R. G. Bates,* Medium effects on the dissociation of weak acids in methanol-water solvents at 25 °C ... 305
*Roder, H. M., R. D. Goodwin, D. E. Diller, L. A. Weber,* Second and third virial coefficients for hydrogen ... 121
*Roth, R. S., E. M. Levin,* Polymorphism of bismuth sesquioxide. I. Pure $Bi_2O_3$ ... 189
——, ——, Polymorphism of bismuth sesquioxide. II. Effect of oxide additions on the polymorphism of $Bi_2O_3$ ... 197
Rubber, natural, at pressures below 500 $kg/cm^2$, compressibility ... 259
Rubber, on the second-order transition ... 611
*Ruthberg, S., L. Frenkel,* Dielectric behavior of the film formed on mica cleaved in moist air ... 173
Ruthenium and osmium, vapor pressures ... 325
Rutile, single crystal, some elastic compliances of, from 25 to 1000 °C ... 669


## S


*Sager, E. E., R. A. Robinson, R. G. Bates,* Medium effects on the dissociation of weak acids in methanol-water solvents at 25 °C ... 305
*Schamp, H. W. Jr., R. M. Wazler, C. E. Weir,* Effect of pressure and temperature upon the optical dispersion of benzene, carbon tetrachloride, and water ... 489
*Scharf, K., J. H. Sparrow,* Steady-state response of silicon radiation detectors of the diffused P–N junction type x rays. I. Photovoltaic mode of operation ... 683
*Schroeder, R. A., C. E. Weir,* Infrared spectra of the crystalline inorganic borates ... 465
*Scribner, B. F., B. W. Mulligan, H. J. Caul, S. D. Rasberry,* X-ray spectrometric analysis of noble metal dental alloys ... 5
Second and third virial coefficients for hydrogen ... 121
Second spectrum of tungsten (W II) ... 207
*Sherman, R. H., T. R. Roberts, S. G. Sydoriak,* The $He^3$ scale of temperatures. III. Evaluation and status ... 567
——, *S. G. Sydoriak,* The 1962 $He^3$ scale of temperatures. I. New vapor pressure comparisons ... 547
——, ——, *T. R. Roberts,* The 1962 $He^3$ scale of temperatures. II. Derivation ... 559
——, ——, ——, The 1962 $He^3$ scale of temperatures. IV. Tables ... 579
*Shields, W. R., E. J. Catanzaro, T. J. Murphy, E. L. Garner,* Absolute isotopic abundance ratio and the atomic weight of bromine ... 593
——, *T. J. Murphy, E. L. Garner,* Absolute isotopic abundance ratio and the atomic weight of a reference sample of copper ... 589
*Shorb, A., A. D. Franklin, J. B. Wachtman, Jr.,* Relaxation modes of trapped crystal point defects, the three-neighbor shells model in NaCl ... 425
Silicon, precision density measurement ... 529
Silicon, radiation detectors, response to x rays ... 683
Silver and cuprous halides, high pressure mocroscopy ... 97
Silver iodide, cold-worked, x-ray investigation of strain ... 355
Silver-tin alloys, detection of lattice deformation and recovery in epsilon phase ... 317
*Sniegoski, L. T., H. S. Isbell,* Tritium-labeled compounds. X. Isotope effects in the oxidation of aldoses-1-t with bromine ... 145
——, ——, Tritium-labeled compounds. XI. Mechanism for the oxidation of aldehydes and aldoses-*1-t* with sodium chlorite ... 301
Sodium chlorite, reactions with aldehydes and aldoses-*1-t* ... 301
Some changes in double-bond structure during the vulcanization of natural rubber ... 499
Some elastic compliances of single crystal rutile from 25 to 1000 °C ... 669
*Sparrow, J. H., K. Scharf,* Steady-state response of silicon radiation detectors of the diffused P–N junction type of x rays. I. Photovoltaic mode of operation ... 683
Spectrophotometric method, near infrared, for the determination of hydration numbers ... 625
Spectrum, infrared absorption, of nitrous oxide ($N_2O$) from 1830 $cm^{-1}$ to 2270 cm ... 79
*Spiegel, V. Jr., W. B. Beverly,* Fast neutron dose measurements for a D–D source in water ... 1
*Spinner, S., J. B. Wachtman, Jr.,* Some elastic compliances of single crystal rutile from 25 to 1000 °C ... 669
Steady-state response of silicon radiation detectors of the diffused P–N junction type of x rays. I. Photovoltaic mode of operation ... 683
Stereoregularity in ionic polymerization of acenaphthylene ... 165
*Stewart, J. E., F. J. Linnig, E. J. Parks,* Some changes in double-bond structure during the vulcanization of natural rubber ... 499
*Story, V. M., G. Canty,* Stereoregularity in ionic polymerization of acenaphthylene ... 165
*Straus, S., D. McIntyre, J. H. G'Mora,* Thermal degradation of fractionated high and low molecular weight polyisobutylene ... 153
*Stromberg, R. R., W. H. Grant, E. Passaglia,* Rates of adsorption and desorption of polystyrene on chrome surface ... 391
——, *E. Passaglia,* Optical properties of thin films on transparent surfaces by ellipsometry; internal reflection for film covered near the critical angle ... 601
*Sydoriak, S. G., T. R. Roberts, R. H. Sherman,* The 1962 $He^3$ scale of temperatures. II. Derivation ... 559
——, ——, ——, The 1962 $He^3$ scale of temperatures. III. Evaluation and status ... 567
——, *R. H. Sherman,* The 1962 $He^3$ scale of temperatures. I. New vapor pressure comparisons ... 547
——, ——, *T. R. Roberts,* The 1962 $He^3$ scale of temperatures. IV. Tables ... 579


## T


*Taylor, J. K., R. A. Durst,* Near infrared spectrophotometric method for the determination of hydration numbers ... 625
*Tenebaum, M., G. T. Furukawa, M. L. Reilly, J. H. Piccirelli,* Thermodynamic properties of some methylphosphonyl dihalides from 15 to 335 °K ... 367
Thermal degradation of fractionated high and low molecular weight polyisobutylene ... 153
Thermodynamic properties of potassium borohydride from 0 to 375 °K; heat capacity from 15 to 700 °K ... 651
Thermodynamic properties of some methylphosphonyl dihalides from 15 to 335 °K ... 367
Three-neighbor shells model in NaCl, relaxation modes of trapped crystal point defects ... 425
*Tidwell, E. D., E. K. Plyler, A. G. Maki,* Infrared absorption spectrum of nitrous oxide ($N_2O$) from 1830 $cm^{-1}$ to 2270 $cm^{-1}$ ... 79
Transition probabilities of forbidden lines ... 61
Tritium-labeled compounds. X. Isotope effects in the oxidation of aldoses-*1-t* with bromine ... 145
Tritium-labeled compounds. XI. Mechanism for the oxidation of aldehydes and aldoses-*1-t* with sodium chlorite ... 301
Tungsten (W II), second spectrum ... 207


## U


*Uhlig, R. P.,* An iterative unfolding procedure ... 401


## V


*Van Valkenburg, A.,* High pressure microscopy of the silver and cuprous halides ... 97
Vapor pressure comparison, 1962 $He^3$ scale of temperatures ... 547
Vapor pressures of ruthenium and osmium ... 325
Variation of glass temperature with pressure in polypropylene ... 273
Virial coefficients, second and third, for hydrogen ... 121
Viscosity of a standard soda-lime-silica glass ... 439
Vulcanization of natural rubber, some changes in double-bond structure ... 499

## W


Page

*Wachtman, J. B., Jr., A. D. Franklin, A. Shorb,* Relaxation modes of trapped crystal point defects, the three-neighbor shells model in NaCl ..... 425
——, *S. Spinner,* Some elastic compliances of single crystal rutile from 25 to 1000 °C ..... 669
*Wacks, M. E.,* Franck-Condon factors for the ionization of $H_2$, HD, $D_2$ ..... 631
*Walker, R. F., N. J. Carrera, E. R. Plante,* Vapor pressures of ruthenium and osmium ..... 325
*Wall, L. A., W. J. Pummer,* Perfluorophenyl ether and related polymers ..... 277
*Wasik, S. P., W. D. Hubbard,* Light-scattering measurements on solutions of some quaternary ammonium salts ..... 359
Water, a D–D source in, fast neutron dose measurements ..... 1
*Waterstrat, R. M., G. E. Hicho,* Detection of lattice deformation and recovery in epsilon phase silver tin alloys ..... 317
*Waxler, R. M., C. E. Weir, H. W. Schamp, Jr.,* Effect of pressure upon the optical dispersion of benzene, carbon tetrachloride, and water ..... 489
*Weber, L. A., R. D. Goodwin, D. E. Diller, H. M. Roder,* Second and third virial coefficients for hydrogen ..... 121
*Weir, C. E., G. J. Piermarini,* Lattice parameters and lattice energies of high-pressure polymorps of some alkali halides ..... 105
Page
*Weir, R. A. Schroeder,* Infrared spectra of the crystalline inorganic borates. 465
——, *R. M. Waxler, H. W. Schamp, Jr.,* Effect of pressure and temperature upon the optical dispersion of benzene, carbon tetrachloride, and water .. 489
*Wood, L. A., G. M. Martin,* Compressibility of natural rubber at pressures below 500 kg/cm$^2$ ..... 259


## X


X-ray intensity measurements, high-energy intercomparison ..... 703
X-ray investigation of strain in cold-worked silver iodide ..... 355
X-ray spectrometric analysis of noble metal dental alloys ..... 5
*xylo*-Trihydroxycyclohexenediolic acid and keto-insitols. Cyclic polyhydroxy ketones II ..... 287


## Y


*Yakowitz, H., R. E. Michaelis, G. A. Moore,* Metallographic characterization of an NBS spectrometric low-alloy steel standard ..... 343




U.S. GOVERNMENT PRINTING OFFICE: 1964

(Continued from back cover)


| | Page |
|---|---|
| Heat of combustion and heat of formation of aluminum carbide. R. C. King and G. T. Armstrong. | 661 |
| Some elastic compliances of single crystal rutile from 25 to 1000 °C. S. Shinner and J. B. Wachtman, Jr. | 669 |
| Energy dependence of the D–D reaction cross section at low energies. J. G. Brennan and J. J. Coyne. | 675 |
| Steady-state response of silicon radiation detectors of the diffused $p$–$n$ junction type to $x$ rays. I. Photovoltaic mode of operation. Karl Scharf and Julian H. Sparrow. | 683 |
| Intercomparison of high-energy [illegible] intensity measurements. John S. Pruitt and Steve R. Domen. | 703 |
| Publications of the National Bureau of Standards. | 709 |
| Index to volume 68A. Physics and Chemistry, January to December 1964. | 715 |

...ERSITY MICROFILMS
313 NORTH FIRST STREET
ANN ARBOR, MICHIGAN
SJR-A-OCT

UNITED ...
GOVERNMENT P...
DIVISION OF ...
WASHINGTON, D.C. 20402

OFFICIAL BUSINESS

JOURNAL OF RESEARCH of the National Bureau of Standards Vol. 68A, No. 6 November–December 1964
A. Physics and Chemistry

## Contents

| | Page |
|---|---|
| The 1962 $He^3$ scale of temperatures. I. New vapor pressure comparisons. S. G. Sydoriak and R. H. Sherman. | 547 |
| The 1962 $He^3$ scale of temperatures. II. Derivation. S. G. Sydoriak, T. R. Roberts, and R. H. Sherman. | 559 |
| The 1962 $He^3$ scale of temperatures. III. Evaluation and status. T. R. Roberts, R. H. Sherman, and S. G. Sydoriak. | 567 |
| The 1962 $He^3$ scale of temperatures. IV. Tables. R. H. Sherman, S. G. Sydoriak, and T. R. Roberts. | 579 |
| Absolute isotopic abundance ratio and the atomic weight of a reference sample of copper. William R. Sheilds, Thomas J. Murphy, and Ernest L. Garner. | 589 |
| Absolute isotopic abundance ratio and the atomic weight of bromine. Edward J. Catanzaro, Thomas J. Murphy, Ernest L. Garner, and William R. Sheilds. | 593 |
| Optical properties of thin films on transparent surfaces by ellipsometry; internal reflection for film covered surfaces near the critical angle. Elio Passaglia and Robert R. Stromberg. | 601 |
| On the second-order transition of a rubber. E. A. DiMarzio. | 611 |
| Ionization constants and reactivity of isomers of eugenol. G. M. Brauer, H. Argentar, and G. Durany. | 619 |
| Near infrared spectrophotometric method for the determination of hydration numbers. Richard A. Durst and John K. Taylor. | 625 |
| Franck-Condon factors for the ionization of $H_2$, HD, and $D_2$. Morton E. Wacks. | 631 |
| Calculation of the geometrical structure of some $AH_2$ molecules. Morris Krauss. | 635 |
| Preparation and heat of formation of a magnesium oxysulfate. E. S. Newman. | 645 |
| Heat capacity of potassium borohydride ($KBH_4$) from 15 to 375 °K. Thermodynamic properties from 0 to 700 °K. George T. Furukawa, Martin L. Reilly, and Jeanette H. Piccirelli. | 651 |

(Continued on inside of back cover)

Library of Congress Catalog Card Number: 62-37059

For sale by the Superintendent of Documents, U.S. Government Printing Office, Washington, D.C., 20402. Price $1.00 (single copy)
Subscription price: $4 a year; 75 cents additional for foreign mailing.
UNITED STATES GOVERNMENT PRINTING OFFICE, WASHINGTON : 1964